Controlled Radical Polymerization: Mechanisms

Controlled Radical Polymerization: Mechanisms

Krzysztof Matyjaszewski, Editor

Carnegie Mellon University
Pittsburgh, Pennsylvania

Brent S. Sumerlin, Editor

University of Florida
Gainesville, Florida

Nicolay V. Tsarevsky, Editor

Southern Methodist University
Dallas, Texas

John Chiefari, Editor

CSIRO
Melbourne, Victoria, Australia

Sponsored by the
ACS Division of Polymer Chemistry

American Chemical Society, Washington, DC

Distributed in print by Oxford University Press

The paper used in this publication meets the minimum requirements of American National Standard for Information Sciences—Permanence of Paper for Printed Library Materials, ANSI Z39.48n1984.

Foreword

The ACS Symposium Series was first published in 1974 to provide a mechanism for publishing symposia quickly in book form. The purpose of the series is to publish timely, comprehensive books developed from the ACS sponsored symposia based on current scientific research. Occasionally, books are developed from symposia sponsored by other organizations when the topic is of keen interest to the chemistry audience.

Before agreeing to publish a book, the proposed table of contents is reviewed for appropriate and comprehensive coverage and for interest to the audience. Some papers may be excluded to better focus the book; others may be added to provide comprehensiveness. When appropriate, overview or introductory chapters are added. Drafts of chapters are peer-reviewed prior to final acceptance or rejection, and manuscripts are prepared in camera-ready format.

As a rule, only original research papers and original review papers are included in the volumes. Verbatim reproductions of previous published papers are not accepted.

ACS Books Department

Preface

This book and the following volume are addressed to chemists and polymer scientists interested in radical processes, and especially in controlled/living radical polymerization. They summarize the most recent advances in the field, including mechanistic, materials, and applications aspects.

These two volumes comprise the topical reviews and specialists' contributions presented at the American Chemical Society (ACS) Symposium on *Controlled Radical Polymerization* that was held in San Francisco, CA, August 10-14, 2014, which was the meeting place of the very first symposium of the series in 1997. The most recent San Francisco meeting was a sequel to several previous ACS Symposia on controlled/living radical polymerization held in San Francisco, California (1997), New Orleans, Louisiana (1999), Boston, Massachusetts (2002), Washington, DC (2005), Philadelphia, Pennsylvania (2008), and Denver, Colorado (2011). The work presented at those symposia was summarized in the ACS Symposium Series Volume 685: *Controlled Radical Polymerization*, Volume 768: *Controlled/Living Radical Polymerization: Progress in ATRP, NMP and RAFT*, Volume 854: *Advances in Controlled/Living Radical Polymerization*, Volume 944: *Controlled/Living Radical Polymerization: From Synthesis to Materials*, Volume 1023: *Controlled/Living Radical Polymerization: Progress in ATRP*, Volume 1024: *Controlled/Living Radical Polymerization: Progress in RAFT, DT, NMP and OMRP*, Volume 1100: *Progress in Controlled Radical Polymerization: Mechanisms and Techniques*, and Volume 1101: *Progress in Controlled Radical Polymerization: Materials and Applications*. The San Francisco 2014 meeting was very successful with 93 lectures and a similar number of posters presented. This level of participation illustrates a continuous growth in comparison to the San Francisco meeting (32 lectures), the New Orleans meeting (50 lectures), the Boston meeting (80 lectures), the Washington meeting (77 lectures), the Philadelphia meeting (90 lectures) and the Denver meeting (96 lectures).

The 37 chapters submitted for publication in the ACS Symposium series could not fit into one volume, and therefore we were asked by ACS to divide the contents into two volumes. Similar to the volumes originating from the Denver meeting, these two volumes are dedicated to mechanisms and techniques (17 chapters and 358 pages) and materials and applications (20 chapters and 345 pages).

The first chapter in this volume provides an overview of the current status of controlled/living radical polymerization (CRP) systems. The following three chapters discuss important issues relevant to all radical polymerization methods. The mechanistic and kinetic aspects of ATRP are the subject of the next five

chapters, followed by degenerative transfer and more complex mechanisms (including "hybrid" processes), which are discussed in the ensuing eight chapters.

The accompanying volume contains 20 chapters on various materials aspects and applications of materials prepared by controlled/living radical polymerization techniques, including structures with controlled macromolecular architectures and functionalities, as well as hybrid materials and biomaterials, and one final chapter dealing with polymer characterization.

Thirty-seven chapters published in two volumes show that there have been significant developments in CRP over the last 15 years. New systems have been discovered; substantial progress has been achieved in understanding the mechanism and kinetics of reactions involved in all CRP systems. As a result of these advances, significant progress has been made towards developing a comprehensive relationship between molecular structure and macroscopic properties. Several commercial applications of CRP were announced at the San Francisco meeting, and it is anticipated that new products made by CRP will soon be on the market.

Krzysztof Matyjaszewski
Department of Chemistry
Carnegie Mellon University
4400 Fifth Avenue
Pittsburgh, PA 15213

Brent S. Sumerlin
George & Josephine Butler Polymer Research Laboratory
Center for Macromolecular Science & Engineering
Department of Chemistry
University of Florida
Gainesville, FL 32605-7200

Nicolay V. Tsarevsky
Department of Chemistry and Center for Drug Discovery, Design, and Delivery in Dedman College
Southern Methodist University
3215 Daniel Avenue
Dallas, TX 75275

John Chiefari
Commonwealth Scientific and Industrial Research Organisation (CSIRO)
Manufacturing Flagship
Private Bag 10
Clayton South, Victoria, 3169
Australia

Editors' Biographies

Krzysztof Matyjaszewski

Krzysztof Matyjaszewski is the J.C. Warner University Professor of Natural Sciences at Carnegie Mellon University. He developed Cu-based atom transfer radical polymerization and other controlled radical polymerization processes that were commercialized in the U.S., Europe, and Japan (17 signed licenses). He has co-authored 880 publications, co-edited 17 books, and holds 51 U.S. patents as well as132 international patents. Matyjaszewski received the 2013 Inaugural AkzoNobel North America Science Award, the 2011 Wolf Prize in Chemistry, and the 2009 Presidential Green Chemistry Award in addition to seven honorary degrees.

Brent S. Sumerlin

Brent Sumerlin is an associate professor in the department of chemistry at the University of Florida. His research interests include stimuli-responsive polymers, dynamic-covalent materials, and biological applications of synthetic polymers. He has been named a Kavli Fellow (Frontiers of Science, National Academies of Sciences), an Alfred P. Sloan Research Fellow, and a Gerald J. Ford Research Fellow. He has received an NSF CAREER Award, the ACS Leadership Development Award, and the Journal of Polymer Science Innovation Award. He is also a Fellow of the Royal Society of Chemistry.

Nicolay V. Tsarevsky

Nicolay V. Tsarevsky is an assistant professor of chemistry at Southern Methodist University in Dallas, TX. His interests include polymerization techniques, catalysis, functional materials, the chemistry of hypervalent iodine compounds, as well as the history of science and science education. He has published 78 peer-reviewed papers and book chapters, co-authored one textbook and co-edited three books, and is the co-inventor on several patents.

John Chiefari

John Chiefari is a research leader in CSIRO's Manufacturing Flagship. He is a co-inventor and co-developer of the RAFT process, which has been commercialized with products in the U.S., Europe, Australia, and Japan. He is currently managing CSIRO's research activities to extend the utility of the RAFT

process and to explore new application areas in the biomedical, agricultural, personal care, and industrial chemical fields.

Chapter 1

Controlled Radical Polymerization: State-of-the-Art in 2014

Krzysztof Matyjaszewski*

Center for Macromolecular Engineering, Department of Chemistry, Carnegie Mellon University, 4400 Fifth Avenue, Pittsburgh, Pennsylvania 15213, United States
***E-mail: km3b@andrew.cmu.edu**

Recent trends in controlled radical polymerization are presented. They include new methods of improving chain end functionality, sequence control and systems with external stimuli to control polymerization rate and pattern on surface initiated systems. Mechanistic aspects of atom transfer radical polymerization in the presence of zerovalent copper are discussed in more detail. These systems follow closely SARA (supplemental activators and reducing agents) ATRP, where >99% of the activation of alkyl halides proceeds with Cu^I species and less than 1% with Cu^0, which acts as supplemental activator and reducing agent. Unexpectedly, the same scenario operates in aqueous media, due to a very high values of activation rate constants with Cu^I and slow activation with Cu^0.

Introduction

Controlled/living radical polymerization (CRP) or reversible-deactivation radical polymerization (RDRP, as recommended by IUPAC) is among the most rapidly expanding areas of chemistry and polymer science (*1–4*).

The dynamic equilibria in CRP systems can be reached in two ways: via reversible deactivation of propagating radicals to form dormant species that can be intermittently re-activated either in the presence of a catalyst, as in atom transfer radical polymerization, ATRP (*5–9*), or spontaneously, as in stable radical mediated polymerization, SRMP (typically mediated by aminoxyl radicals or organometallic species) (*10–13*). Other systems employ

degenerate transfer between propagating radicals and dormant species. Typical examples of degenerate transfer radical polymerization, DTRP, include reversible addition-fragmentation chain transfer polymerization, RAFT, iodine transfer radical polymerization and processes with tellurium or bismuth derivatives (*14–19*). Generally, in DTRP, an external source of radicals is necessary but dormant species can also be activated by a Cu-based catalyst, without generation of new chains (*20*). In a similar way, iodine transfer may progress in a catalyzed manner using variety of organic catalysts (*21*). RAFT kinetics is similar to conventional RP but may be accompanied by retardation, depending on the nature of radicals and transfer agents. ATRP and SRMP follow persistent radical effect kinetics (*22*). However, there are some new ATRP systems, operating at ppm amounts of Cu catalysts in the presence of reducing agents (ARGET) or radical initiators (initiators for continuous activators regeneration, ICAR) that follow the same kinetics as conventional RP or RAFT (*23*).

Figure 1 presents the cumulative number of papers published on ATRP, SMRP and RAFT during the last 20 years. The growth in the number of publications in all areas of CRP reflects the increasing interest in this field. This is accompanied by an increase in the number of patent applications and symposia partially or entirely devoted to CRP (*24–31*).
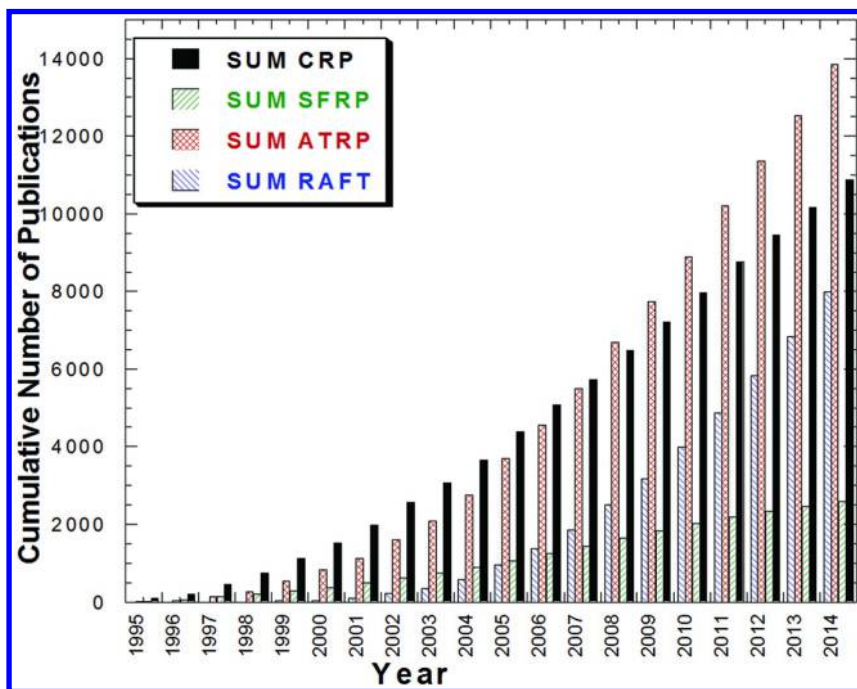

Figure 1. Results of SciFinder Search on various CRP systems as of December 20, 2014. Detail explanation of terms is provided in the text.

Figure 1 illustrates the results of a recent SciFinder Scholar search using the following terms:; *ATRP* or *atom transfer radical polymn* ("SUM ATRP", this search does not include terms such as metal mediated or metal catalyzed (living) radical polymerization or single electron transfer living radical polymerization; *NMP* or *SFRP* or *nitroxide mediated polymn* or *stable free polymn* ("SUM SFRP") and RAFT ("SUM RAFT")). The latter two terms were refined with terms *radical polymn* and "*polymer* or *polymn*", respectively, since the search coincides with other common chemical terms such as *N-methylpyrrolidone* or *raft-associated proteins*. In summary, over 25,000 papers have been published on various CRP systems since 1995 and ca. 14,000 on ATRP alone.

CRP has many advantages over ionic and standard radical polymerization procedures but also inherate some limitations originating from the particular nature of radical intermediates. These includes limited stereochemical control and unavoidable radical termination. The same rate of polymerization (in a conventional process or any CRP), indicates the same radical concentration leading to a similar concentration of terminated chains. However, essentially all chains are terminated in conventional RP, whereas in CRP, the fraction of terminated chains is between 1 and 10%. The remaining chains are in the dormant state, capable of reactivation, functionalization, chain extension to form block copolymers, etc. One of the main challenges in CRP is to minimize the fraction of the terminated chains or maximize chain end functionality at a sufficient polymerization rate. The fraction of dead chains increases with polymerization rate, conversion and targeted molecular weight (MW) and depends critically on the ratio of rate coefficients of propagation and termination (k_p/k_t). Thus, under comparable conditions (rate, MW, conversion), chain end functionality is best preserved in polymerization of acrylates or acrylamides (highest k_p/k_t), in polar and viscous media, at higher temperature and also in confined media (*32*). This research direction is among the most rapidly developing in CRP (*33–35*).

Radical copolymerization is characterized by reactivity ratios much smaller than observed in ionic copolymerization. This enables synthesis of many statistical copolymers and also facilitates synthesis of block and gradient copolymer by CRP. However, it also makes the synthesis of periodic copolymers more difficult. Nevertheless, significant progress has been made in synthesis and analysis of sequence controlled copolymers (*36–40*) which often requires use of special monomer pairs (such styrene, maleimide) or use of preformed dimers or trimers can potentially be expanded to include solid supported synthesis.

Kinetics of RP can be affected by temperature, pressure, catalysts and additives, as reportedt for ATRP, RAFT and NMP, but also by some other external stimuli such as electricity or light (*41–46*). Recently, the effect of photochemical activation on ATRP, RAFT and NMP has been explored and used to control both polymerization rate and patterned growth from surfaces (*47–49*).

Very recently, photochemistry was applied to ATRP in the presence of organic catalysts such as derivatives of perylene and phenothiazine (*50, 51*). It is interesting to observe that phenothiazine is used as a very efficient inhibitor of polymerization of acrylic acid but N-phenyl phenothiazine (*52*) is an excellent photocatalysts in polymerization of methacrylates (*51*).

Novel organic/inorganic hybrid materials and bioconjugates prepared by CRP are among the most rapidly developing areas of polymer science. This is related to the development of new and previously unreachable properties present in polymer hybrids with inorganics and biomolecule components. In the former case, polymers grown from nanoparticles or flat surfaces, dramatically change particles stability, dispersibility and thermomechanical properties, in addition to tremendously enhancing lubricity, antifouling or antibacterial properties (53–61). Hybrids with proteins or nucleic acids increase stability of proteins in harsh environments, (including temperature, pH, and salts) assist in delivery of genes, and can be used in advanced drug delivery (45, 62–71).

In separate chapters in this volume, recent advances in the mechanistic and synthetic aspects of nitroxide mediated polymerization and RAFT are discussed by Gigmes and Moad, respectively. Therefore, in the remaining part of this chapter, some important mechanistic details of ATRP will be discussed. The main focus is on ATRP in the presence of zerovalent copper, as this is a controversial issue and may require some clarifications.

CRP in the Presence of Cu^0

Traditional ATRP obeys the persistent radical effect (22) and often requires catalyst concentrations in the range of 0.1 mol% vs. monomer in order to reach high conversion. However, in the past decade several new methods were developed that provide well-controlled polymerizations, in the presence of ppm amounts of Cu catalyst and various reducing agents (72, 73). These reducing agents continuously regenerate the activator complex and compensate for radical termination (74–76). In continuous activator regeneration (ICAR) ATRP these processes employ the same radical initiators as in RAFT (23), whereas in electrochemically mediated ATRP (77), or photochemically mediated ATRP no initiator based chains are formed (78–81). In activators regenerated by electron transfer (ARGET) ATRP, benign sulfites, ascorbic acid, and zerovalent metals are used (72, 82). Zero valent metals such as Fe^0 and Cu^0 were first used in CRP in 1997 (83, 84). With the development of ARGET ATRP it is now recognized that they can act not only as reducing agents for regeneration of Cu^I from Cu^{II}, formed as by-product of radical termination in addition to acting as supplemental activators by direct reaction with alkyl halides. This process was later termed SARA ATRP (for supplemental activator and reducing agent) (85). Use of Cu^0 provides some advantages, due to low concentrations of the soluble Cu species, simple removal and reuse of unreacted solid Cu^0 and control of the polymerization rate by the amount of ligand and the surface area of Cu^0 (86–88). Various well-defined polymers with complex architecture, such as multiblock copolymers, stars, branched, end functional were prepared using Cu^0 (89–93).

Mechanistically, the SARA ATRP process occurs in the same manner as any other ATRP procedure, by intermittent activation of dormant alkyl halides by Cu^I and deactivation of growing radicals by Cu^{II}. In addition, Cu^0 serves as both a supplemental activator for alkyl halides and reducing agent for the Cu^{II} via comproportionation (*87*). In SARA ATRP, the contribution of disproportionation to the kinetics of the polymerization is small and alkyl halide activation occurs exclusively by inner sphere electron transfer (ISET) by reaction with either Cu^I or Cu^0 (*87, 94–96*).

However, a very different mechanism for the polymerization using exactly the same components in exactly the same concentrations (monomer, initiator, ligand and Cu^0) was postulated and termed single-electron transfer living radical polymerization (SET-LRP) (*97*). In SET-LRP, alkyl halides were proposed to be exclusively activated by Cu^0 via outer sphere electron transfer (OSET), Cu^I should not activate alkyl halides, instead it was envisioned to undergo instantaneously disproportionate to Cu^0 (the exclusive activator) and Cu^{II}, and there should be minimal comproportionation to retain suitable concentrations of activator (Cu^0) and deactivator (*86, 97, 98*). The reactions involved in SARA ATRP and SET-LRP are shown in Scheme 1 (*99*).
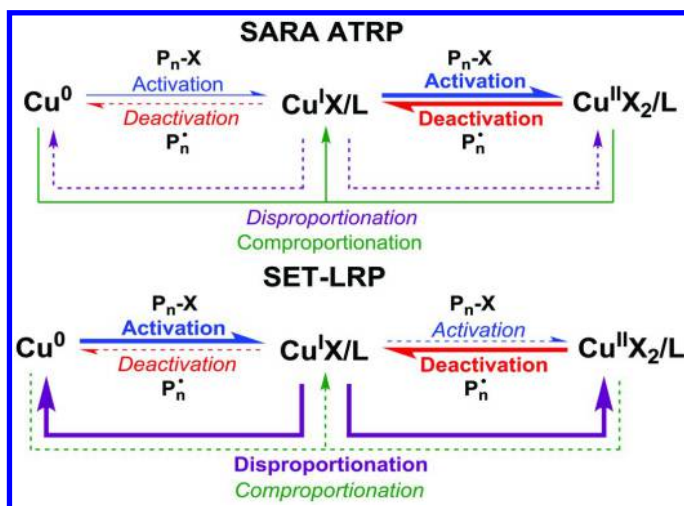
Scheme 1. The mechanism of SARA ATRP (top) and SET-LRP (bottom). Bold arrows indicate major reactions, solid arrows represent supplemental reactions and dashed arrows reactions that can be neglected. Cu^0, Cu^IX/L and $Cu^{II}X_2/L$ represent a Cu^0, Cu^I and Cu^{II} species without particular speciation. In the activation reactions, the radical products are omitted for clarity, and in the deactivation reaction the alkyl halide products are also omitted. All radicals propagate and terminate. Reproduced with permission from reference (99). Copyright (2014) Royal Society of Chemistry.

It is clear from Scheme 1 that the SARA ATRP and SET-LRP mechanisms use the same components and involve exactly the same reactions, but with very different contributions. The fundamental differences between SARA ATRP and SET-LRP can be summarized as follows:

- How alkyl halides are activated: by Cu^I (*87*, *95*, *100*) or Cu^0 (*101*)? Are alkyl halide activated by inner sphere electron transfer (*102*, *103*) or outer sphere electron transfer (*97*)?
- Does disproportionation (*86*, *97*, *98*) or comproportionation (*87*, *94*, *104*) dominate during polymerization?

Quantification of the rates of all the involved reactions enables one to define the role of Cu^I, either it acts as an activator or as a participant in immediate disproportionation and also determine whether Cu^0 participates in the reaction as a supplemental activator and reducing agent (*87*, *95*, *96*, *104*) or the major activator of alkyl halides (*101*)?

The evaluation of contributions of particular reaction pathways was performed under polymerization relevant conditions, in media consisting of monomer (typically methyl acrylate or oligo(ethylene oxide) methyl ether acrylate) and solvents (typically DMSO or water), with very active Cu complexes formed with tris(pyridylmethyl)amine (TPMA) or tris(2-(dimethylamino)ethyl)amine Me_6TREN ligands, and alkyl halides modelling dormant species, such a methyl 2-bromopropionate (MBP) or oligo(ethylene oxide) methyl ether 2-bromopropionate (OEOBP). Kinetic measurements were performed for isolated systems and then modelled using kinetic simulations taking into consideratiom the contributions of all involved reactions. The competition between two or more involved parallel reactions can suppress or enhance their contributions depending on rate constants and concentrations of the involved reagents.

Activation Kinetics

In pure DMSO, the apparent activation rate coefficient of MBP, measured by stopped flow, is very large and the reaction is completed within 1 s when using mM concentration of Cu^I/Me_6TREN and MBP, $k_{a1} = 320$ M^{-1} s^{-1} (*95*). In the presence of monomer, MA/DMSO 2/1 (v/v), the value was slightly lower $k_{a1} = 200$ M^{-1} s^{-1} (*95*).

In aqueous media, activation of alkyl halides was much faster, as measured by cyclic voltammetry (CV) (*105*). Evaluation of the total catalysis procedure showed that OEOBP is activated by Cu^I/Me_6TREN with a rate coefficient of $k_{a1} = 6.6 \times 10^5$ M^{-1} s^{-1} in pure water and $k_{a1} = 2.5 \times 10^4$ M^{-1} s^{-1} in 18 wt% OEOA/82 wt% H_2O.

A summary of all Cu^I activation rate coefficients is given in Table 1.

Table 1. Activation rate coefficients of alkyl halides by Cu^I/L

Alkyl Halide	Ligand	Solvent	k_{a1}^{app} $(M^{-1} s^{-1})$	Ref.
MBrP	Me$_6$TREN	DMSO	3.2×10^2	(95)
MBrP	Me$_6$TREN	MA/DMSO 2/1 (v/v)	2.0×10^2	(95)
OEOBrP	Me$_6$TREN	H$_2$O	6.6×10^5	(104)
OEOBrP	Me$_6$TREN	OEOA/ H$_2$O 18/82 (wt/wt)	2.5×10^4	(104)

Due to the heterogeneous nature of the Cu^0, the rate coefficients were based on the ratio of the surface area of Cu^0 wire to the total reaction volume, using the dimensions of cm s^{-1}. Activation of alkyl halides by Cu^0 in DMSO was relatively slow and required ca. 10,000 s to reach completion, vs 1s for Cu^I. In aqueous systems the disparity between the activity of Cu^0 and Cu^I was even larger. The rate coefficient of activation of OEOBrP by Cu^0 with Me$_6$TREN $k_{a0}^{app} = 4.0 \times 10^{-6}$ cm s^{-1} in water, which is 50 times smaller than for MBrP in DMSO (104). In fact, to match the activity of just 10^{-6} M of Cu^I/Me$_6$TREN in 18 wt% OEOA in water, 3 km of Cu^0 wire with diameter 0.25 mm would be required in 10 mL volume. A summary of the activation rate coefficients of alkyl halides by Cu^0 with different ligands and reaction media is listed in Table 2.

Table 2. Activation rate coefficients of alkyl halides by Cu^0.

Alkyl Halide	Ligand	Solvent	k_{a0}^{app} $(cm\ s^{-1})$	Ref.
MBrP	Me$_6$TREN	DMSO	1.8×10^{-4}	(95)
MBrP	Me$_6$TREN	MA/DMSO 1/1 (v/v)	1.0×10^{-4}	(95)
MBrP	TPMA	MA/DMSO 1/1 (V/V)	5.8×10^{-5}	(95)
OEOBrP	Me$_6$TREN	H$_2$O	4.0×10^{-6}	(104)
OEOBrP	Me$_6$TREN	OEOA/H$_2$O 18/82 (wt/wt)	1.0×10^{-5}	(104)

In the SET-LRP model, the "nascent" Cu^0 as activator of the alkyl halides was postulated to form via disproportionation of Cu^I, giving Cu^{II} and Cu^0 (97). The "lifting" and "decanting" experiments (101) showed that the polymerization rate was reduced by a factor of 10 when the Cu^0 wire was lifted out of the solution (101). This 10 fold reduction of the rate indicates that the surface area of the newly produced "nascent" Cu^0 should be ca. 1% of the original surface area of the wire, due to the dependence of the polymerization rate on the square root of surface area of Cu^0 (106).

Nature of the Electron Transfer, ISET vs. OSET

The main difference between the activation of alkyl halides in SARA ATRP and SET-LRP is the nature of the electron transfer. In SARA ATRP an inner sphere electron transfer (ISET) is assumed while in SET-LRP an outer sphere electron transfer was postulated (*87, 97, 103, 107*). According to Marcus theory (*108*) the ISET process (SARA) is favoured by almost 15 kcal mol^{-1}, corresponding to ISET being 10^{10} faster than OSET (*102*). These predictions were confirmed by comparing activation kinetics of some alkyl halides by species acting as OSET donors, typically aromatic radical anions, and the activation kinetics of alkyl halides by Cu^I complexes with amine ligands (*109*), showing that Cu^I complexes react by an ISET mechanism with rate coefficients 7-10 orders of magnitude larger than k_{act} of OSET donors of the same standard potential. Interestingly activation of RX by Cu^0 also occurs by ISET 10^9 times faster than by OSET (*87*).

Disproportionation and Comproportionation Kinetics

Using spectroscopic methods, the kinetics and thermodynamics of disproportionation and comproportionation were quantified in several solvents, as shown in Table 3. In DMSO, the disproportionation half-life is 44 h. The formation of Cu^0 and Cu^{II} could be faster when a ligand is added to Cu^I species, resulting in electron transfer between Cu^I coordinated by solvent and Cu^I/Me$_6$TREN.

Table 3. Comproportionation and disproportionation rate coefficients for the Cu^I/Me$_6$TREN complex measured in DMSO, MA/DMSO = 2/1 (v/v) and OEOA/H$_2$O = 18/82 (wt/wt).

Medium	k_{comp}^{app} (cm s^{-1})	k_{disp}^{app} (cm s^{-1})	K_{disp}^L	Ref.
DMSO	9.0×10^{-4}	2.0×10^{-5}	2.2×10^{-2}	*(94)*
MA/DMSO 2/1 (v/v)	3.5×10^{-3}	3.1×10^{-6}	8.9×10^{-4}	*(94)*
OEOA/H$_2$O 18/82 (wt/wt)	2.4×10^{-5}	5×10^{-4}	22	*(104)*

In aqueous media, disproportionation of Cu^I/Me$_6$TREN complexes is thermodynamically favoured, because the equilibrium constant is greater than 1. However, activation of alkyl halides by Cu^I is also strongly accelerated and while these reactions will compete and the fastest reaction should dominate. In water, in the absence of alkyl halides, disproportionation is relatively fast and a Cu^0 precipitate is quickly formed. However, when Cu^{I}Br and Me$_6$TREN are added to a solution of an alkyl halide in water no Cu^0 precipitate was formed and a continuous increase in the concentration of Cu^{II}/Me$_6$TREN species was observed (*104*). Thus, the activation of the alkyl halides by Cu^I species is kinetically preferred. Although disproportionation is thermodynamically favoured, it is very slow due to a the presence of a very low concentration of Cu^I, as dictated

by the dominant ATRP equilibrium. This is in clear contrast to the case with pre-disproportionation of Cu^I in the monomer solution in the absence of alkyl halides.

Contribution of Various Reactions

There are 3 competing equilibria in an ATRP when it is conducted in the presence of Cu^0. The first one involves classical ATRP reactions, where Cu^I/L activates an alkyl halide generating a radical and $Cu^{II}X/L$ complex, and a reverse reaction where $Cu^{II}X/L$ deactivates a radical regenerating the Cu^I/L complex and a dormant alkyl halide. The second one is activation of alkyl halides by Cu^0, giving radicals and Cu^IX/L, as well as its reverse reaction of radical deactivation by Cu^IX/L giving Cu^0 and an alkyl halide. The third one is the disproportionation process, where two Cu^I species form Cu^0 and Cu^{II}, and the reverse comproportionation reaction, where Cu^0 and Cu^{II} react to give two Cu^I species. Within this series of competing equilibria, the equilibrium with the fastest kinetics is established first, while the reaction with slowest dynamics may not equilibrate within a reasonable time frame.

Kinetic simulations, using the rate coefficients from Tables 2-4 for each reaction step in DMSO, the polymerization medium of MA/DMSO = 2/1 (v/v), and the typical aqueous polymerization medium of $OEOA/H_2O$ = 18/82 (wt/wt) were used to evaluate and compare the reaction rates (in M s^{-1}) at 80% conversion of alkyl halide for the DMSO system, or 80% monomer conversion for the MA/DMSO = 2/1 (v/v) and $OEOA/H_2O$ = 18/82 (wt/wt) systems, as shown in Table 4.

Table 4 confirms that the dominant reactions are the basic ATRP reactions; Cu^I mediated activation of alkyl halides and Cu^{II} mediated deactivation of radicals are fastest, well balanced and maintain an ATRP equilibrium. Activation of alkyl halides by Cu^0 and comproportionation occur approximately 10^3 times slower and follow the SARA mechanism, Cu^0 acts as a supplemental activator and reducing agent. Disproportionation and radical deactivation by Cu^I proceed at a rate several orders of magnitude slower than the ATRP reactions. Interestingly, although disproportionation is thermodynamically favored in water, it is kinetically suppressed due to the presence of the very low Cu^I concentration dictated by very large values for the ATRP equilibrium constant.

Analysis of the kinetic data of polymerization of acrylic monomers in the presence of Cu^0 under typical conditions clearly indicates that Cu^I species are more than 1000 times more active than Cu^0, and activation proceeds by an ISET mechanism, which is $\sim 10^9$ times faster than activation by OSET. The Cu^I species activate alkyl halides $> 10^6$ times faster than they could disproportionate in both DMSO and mixtures of monomer and H_2O. It should be noted that both mechanisms refer to the same polymerization process with the same components. However, due to their vastly different assumptions, they cannot bothbe valid and contribute to the final CRP. This is similar to the competition between different mechanisms, such as the S_N1 and S_N2 reactions. They give almost the same transformation of atoms, but through very different mechanisms. In the same way, the names SET-LRP and SARA ATRP should not be used if the assumptions

underlying the mechanism are not backed up by experimental data. The SET-LRP could hypothetically operate for some other systems, where OSET would be faster than ISET and activation of dormant species faster by Cu^0 than by Cu^I and disproportionation faster than comproportionation and faster than activation by Cu^I, but that should to be first experimentally verified.

Table 4. Summary of reaction rates for reactions between radicals, alkyl halides and Cu species in all relevant oxidation states. The rate were determined in DMSO, MA/DMSO = 2/1 (v/v) and OEOA/H₂O = 18/82 (wt/wt).[a]

Rate[b]	DMSO (95)	MA/DMSO 2/1 (v/v) (96)	OEOA/H₂O 18/82 (wt/wt) (104)
R_{a1} (M s^{-1})	1×10^{-4}	6×10^{-3}	3×10^{-5}
R_{d1} (M s^{-1})	1×10^{-4}	6×10^{-3}	3×10^{-5}
R_{a0} (M s^{-1})	6×10^{-8}	1×10^{-6}	1×10^{-8}
R_{d0} (M s^{-1})	1×10^{-12}	1×10^{-9}	2×10^{-16}
R_{comp} (M s^{-1})	6×10^{-7}	2×10^{-7}	1×10^{-9}
R_{disp} (M s^{-1})	1×10^{-11}	2×10^{-10}	7×10^{-14}

[a] All rates are at 80% conversion of alkyl halide for the DMSO system, or 80% monomer conversion for the MA/DMSO = 2/1 (v/v) and OEOA/H₂O = 18/82 (wt/wt) systems.   [b] R_{a1} is the rate of alkyl halide activation by Cu^I, R_{d1} is the rate of radical deactivation by Cu^{II}, R_{d0} is the rate of radical deactivation by Cu^I, R_{a0} is the rate of alkyl halide activation by Cu^0, R_{comp} is the rate of comproportionation, and R_{disp} is the rate of disproportionation.

ATRP in Water

Several well-controlled Cu mediated polymerizations have been performed in water and protic media (*98, 105, 110–112*). These polymerizations have traditionally been a challenge, due to the low binding constant between Cu^{II} species and halide anions. In pure water, the association constant $K_X^{II} = 4.4$ M^{-1} has been measured for Cu^{II}/Me₆TREN binding a bromide anion (*113, 114*). This value is higher in 18 wt% OEOA/H₂O due to the lower polarity of the medium, $K_X^{II} = 14$ M^{-1} (*104*). Two strategies can be implemented to overcome this challenge. The traditional strategy has been to use a high concentration of Cu catalyst, ca. 10,000 ppm, to make the absolute concentrations of the Cu^{II}X/L complex high enough to provide efficient deactivation (*98, 110*). The second strategy is to use low concentration of Cu^{II} species but add an excess of halide anions. Thus, the equilibrium will be shifted significantly towards Cu^{II}X/L (*111*). This strategy has been also applied to provide a successful polymerization in the presence of ammonium halides, Cu^0 and < below100 ppm of initial CuBr₂/L species. Well controlled ICAR or ARGET ATRP can be carried out in water with the concentration of Cu/TPMA complex as a low as 30 ppm (*115*).

Aqueous ATRP is characterized by very large equilibrium constants leading to high radical concentrations and enhanced radical termination. The appropriate level of control can be achieved by either using less active catalysts (e.g. based on bipyridine) or using more active catalysts in the oxidatively stable state such as CuBr$_2$/TPMA that are continuously reduced to the activator with a slow dosing of reducing agent, such as ascorbic acid (115) or by applying electrochemistry. Under such conditions various bioconjugates were successfully prepared (110).

Photochemically Mediated ATRP

Highly active and air-sensitive Cu^I/L complexes are generally used in ATRP systems with low ppm Cu catalysts. Very often the polymerization starts from air-stable Cu^{II}/L species that are initially reduced to activating Cu^I/L species in the presence of radical initiators (ICAR) or organic/inorganic reducing agents (ARGET). The reduction process continues during the entire polymerization and provides an excellent tool for the regeneration of activators lost in radical termination. Mild reducing agents are used, or controlled dosing of more active agents, to provide the required reduction rate and appropriate concentration of radicals. The reduction can be also accomplished by physical means such as electrical current or light. The advantage of both of these systems is that they can be fine-tuned externally by changing electrical potential or light intensity. Light has been used to mediate ATRP under various conditions, in the presence of photoinitiators, photocatalysts, direct breaking of the alkyl-(pseudo)halogen bond and also photoreduction of the Cu^{II}/L species (78–81, 116, 117). In an ATRP several species can absorb in the UV-visible region and can generate radicals alone or in a combination with other reagents and participate in a photoreduction process (118).

Contributions of several pathways in photochemically mediated ATRP of methyl acrylate were evaluated using 392 nm irradiation in the presence of TPMA and Me$_6$TREN ligands. The dominant mode of Cu^I/L activator (re)generation (>90%) is the photochemically mediated reduction of Cu^{II} complexes by electron donors. Simple addition of triethylamine or an excess of Me$_6$TREN or TPMA ligand provide available amines that can serve as electron donors. Cu^{II}/L species absorb strongly in UV/VIS and the excited species are reduced to Cu^I/L species and, concurrently, free amines are oxidized to the corresponding radical cation, which can initiate a new chain after proton transfer. The second most significant step (~ 5%) is the synergistic radical generation between alkyl halide species and the electron donor. Other processes such as direct photochemical cleavage of the alkyl halide, photochemical radical generation from the ligand, or ligand with monomer are minor reactions with lower contributions (<1%). Relative contributions may, of course change, depending on the structure of the involved reagents, light wavelength and intensity. Nevertheless, kinetic simulations revealed that the main role of these photochemical reactions is to supplement radicals lost to termination, and that control over the polymerization is governed by the classical ATRP activation and deactivation reactions proceeding by the inner sphere electron transfer mechanism (118). This may change in the presence

of organic photocatalysts, which can under excitation produce very strongly reducing species that can plausibly participate in the outer sphere electron transfer processes. Light may effect some slow ATRP processes such as ICAR. For example, in a 392 nm photoreactor of intensity 0.9 mW/cm^2 at 0.2 equiv with respect to ATRP initiator, the contribution of photochemical processes to the overall polymerization is ca. 15% (*119*). Ambient laboratory lighting of intensity 0.3 mW/cm^2 (fluorescent light at a distance 1 m from the reaction flask) has negligible influence on the rate of polymerization in ICAR ATRP but can enhance the reaction at shorter distances (*120*).

Outlook

In this chapter, the main emphasis was on the new ATRP systems and confirming the mechanistic details of ATRP in the presence of zerovalent metals, light and in aqueous media. These techniques offer an excellent tool for synthesis of polymers with precisely controlled architecture. However, very siginificant advances have been also made in RAFT and SFRP, as presented by Moad and Gigmes in other chapters in this volume. Thus, some of the challenges discussed 3 years ago are now overcome and CRP progressively moves to commercialization. Nevertheless, detailed kinetic and mechanistic studies will provide the information required to design and prepare various well-defined polymers for many targeted advanced applications.

Acknowledgments

References

1. Matyjaszewski, K., Davis, T. P. Eds. *Handbook of Radical Polymerization*; Wiley-Interscience: Hoboken, 2002.
2. Goto, A.; Fukuda, T. *Prog. Polym. Sci.* **2004**, *29*, 329–385.
3. Braunecker, W. A.; Matyjaszewski, K. *Prog. Polym. Sci.* **2007**, *32*, 93–146.
4. Destarac, M. *Macromol. React. Eng.* **2010**, *4*, 165–179.
5. Matyjaszewski, K.; Xia, J. *Chem. Rev.* **2001**, *101*, 2921–2990.
6. Kamigaito, M.; Ando, T.; Sawamoto, M. *Chem. Rev.* **2001**, *101*, 3689–3745.
7. Matyjaszewski, K.; Tsarevsky, N. V. *Nat. Chem.* **2009**, *1*, 276–288.
8. Pintauer, T.; Matyjaszewski, K. *Encycl. Radicals Chem., Biol. Mater.* **2012**, *4*, 1851–1894.
9. Matyjaszewski, K.; Tsarevsky, N. V. *J. Am. Chem. Soc.* **2014**, *136*, 6513–6533.
10. Bertin, D.; Gigmes, D.; Marque, S. R. A.; Tordo, P. *Chem. Soc. Rev.* **2011**, *40*, 2189–2198.
11. Nicolas, J.; Guillaneuf, Y.; Lefay, C.; Bertin, D.; Gigmes, D.; Charleux, B. *Prog. Polym. Sci.* **2013**, *38*, 63–235.

12. Poli, R.; Allan, L. E. N.; Shaver, M. P. *Prog. Polym. Sci.* **2014**, *39*, 1827–1845.
13. Allan, L. E. N.; Perry, M. R.; Shaver, M. P. *Prog. Polym. Sci.* **2012**, *37*, 127–156.
14. Moad, G.; Thang, S. H. *Aust. J. Chem.* **2009**, *62*, 1379–1381.
15. Gregory, A.; Stenzel, M. H. *Prog. Polym. Sci.* **2012**, *37*, 38–105.
16. Ahmed, M.; Narain, R. *Prog. Polym. Sci.* **2013**, *38*, 767–790.
17. Ohtsuki, A.; Goto, A.; Kaji, H. *Macromolecules* **2013**, *46*, 96–102.
18. Matyjaszewski, K.; Gaynor, S.; Wang, J.-S. *Macromolecules* **1995**, *28*, 2093–2095.
19. Yamago, S. *Chem. Rev.* **2009**, *109*, 5051–5068.
20. Kwak, Y.; Nicolay, R.; Matyjaszewski, K. *Macromolecules* **2008**, *41*, 6602–6604.
21. Lei, L.; Tanishima, M.; Goto, A.; Kaji, H.; Yamaguchi, Y.; Komatsu, H.; Jitsukawa, T.; Miyamoto, M. *Macromolecules* **2014**, *47*, 6610–6618.
22. Fischer, H. *Chem. Rev.* **2001**, *101*, 3581–3610.
23. Matyjaszewski, K.; Jakubowski, W.; Min, K.; Tang, W.; Huang, J.; Braunecker, W. A.; Tsarevsky, N. V. *Proc. Natl. Acad. Sci. U. S. A.* **2006**, *103*, 15309–15314.
24. Matyjaszewski, K., Ed. *Controlled Radical Polymerization*; ACS Symposium Series 685; American Chemical Society: Washington, DC, 1998 (Proceedings of a Symposium at the 213th National Meeting of the American Chemical Society, held 13−17 April 1997, in San Francisco, CA).
25. Matyjaszewski, K., Ed. *Controlled/Living Radical Polymerization. Progress in ATRP, NMP, and RAFT*; ACS Symposium Series 768; American Chemical Society: Washington, DC, 2000 (Proceedings of a Symposium on Controlled Radical Polymerization held on 22−24 August 1999, in New Orleans, LA).
26. Matyjaszewski, K., Ed. *Advances in Controlled/Living Radical Polymerization*; ACS Symposium Series 854; American Chemical Society: Washington, DC, 2003 (ACS Symposium held 15−18 August 2002, in Boston, MA),.
27. Matyjaszewski, K., Ed. *Controlled/Living Radical Polymerization: From Synthesis to Materials*; ACS Symposium Series 944; American Chemical Society: Washington, DC, 2006 (ACS Symposium held in 2005 in Washington, DC).
28. Matyjaszewski, K., Ed. *Controlled/Living Radical Polymerization: Progress in ATRP*; ACS Symposium Series 1023; American Chemical Society: Washington, DC, 2009.
29. Matyjaszewski, K., Ed. *Controlled/Living Radical Polymerization: Progress in Progress in RAFT, DT, NMP and OMRP*; ACS Symposium Series 1024; American Chemical Society: Washington, DC, 2009.
30. Matyjaszewski, K., Sumerlin, B., Tsarevsky, N. V., Eds. *Progress in Controlled Radical Polymerization: Mechanisms and Techniques*; ACS Symposium Series 1100; American Chemical Society: Washington, DC, 2012.
31. Matyjaszewski, K., Sumerlin, B., Tsarevsky, N. V., Eds. *Progress in Controlled Radical Polymerization: Materials and Applications*; ACS

Symposium Series 1101; American Chemical Society: Washington, DC, 2012.

32. Zhong, M.; Matyjaszewski, K. *Macromolecules* **2011**, *44*, 2668–2677.

33. Gody, G.; Maschmeyer, T.; Zetterlund, P. B.; Perrier, S. *Nat. Commun.* **2013**, *4*, 3505–3509.

34. Zetterlund, P. B.; Gody, G.; Perrier, S. *Macromol. Theory Simul.* **2014**, *23*, 331–339.

35. Gody, G.; Maschmeyer, T.; Zetterlund, P. B.; Perrier, S. *Macromolecules* **2014**, *47*, 3451–3460.

36. Lutz, J. F.; Ouchi, M.; Liu, D. R.; Sawamoto, M. *Science* **2013**, *341*.

37. Lutz, J. F. *Acc. Chem. Res.* **2013**, *46*, 2696–2705.

38. Lutz, J. F.; Sumerlin, B.; Matyjaszewski, K. *Macromol. Rapid Commun.* **2014**, *35*, 122.

39. Colquhoun, H.; Lutz, J.-F. *Nat. Chem.* **2014**, *6*, 455–456.

40. Mutlu, H.; Lutz, J.-F. *Angew. Chem., Int. Ed.* **2014**, *53*, 13010–13019.

41. Leibfarth, F. A.; Mattson, K. M.; Fors, B. P.; Collins, H. A.; Hawker, C. J. *Angew. Chem., Int. Ed.* **2013**, *52*, 199–210.

42. Magenau, A. J. D.; Strandwitz, N. C.; Gennaro, A.; Matyjaszewski, K. *Science* **2011**, *332*, 81–84.

43. Magenau, A. J. D.; Bortolamei, N.; Frick, E.; Park, S.; Gennaro, A.; Matyjaszewski, K. *Macromolecules* **2013**, *46*, 4346–4353.

44. Fors, B. P.; Poelma, J. E.; Menyo, M. S.; Robb, M. J.; Spokoyny, D. M.; Kramer, J. W.; Waite, J. H.; Hawker, C. J. *J. Am. Chem. Soc.* **2013**, *135*, 14106–14109.

45. Xu, J.; Jung, K.; Corrigan, N. A.; Boyer, C. *Chem. Sci.* **2014**, *5*, 3568–3575.

46. Shanmugam, S.; Xu, J.; Boyer, C. *Macromolecules* **2014**, *47*, 4930–4942.

47. Treat, N. J.; Fors, B. P.; Kramer, J. W.; Christianson, M.; Chiu, C.-Y.; Read de Alaniz, J.; Hawker, C. J. *ACS Macro Lett.* **2014**, *3*, 580–584.

48. Li, B.; Yu, B.; Huck, W. T. S.; Liu, W.; Zhou, F. *J. Am. Chem. Soc.* **2013**, *135*, 1708–1710.

49. Li, B.; Yu, B.; Huck, W. T. S.; Zhou, F.; Liu, W. *Angew. Chem., Int. Ed.* **2012**, *124*, 5182–5185.

50. Miyake, G. M.; Theriot, J. C. *Macromolecules* **2014**, *47*, 8255–8261.

51. Treat, N. J.; Sprafke, H.; Kramer, J. W.; Clark, P. G.; Barton, B. E.; Read de Alaniz, J.; Fors, B. P.; Hawker, C. J. *J. Am. Chem. Soc.* **2014**, *136*, 16096–16101.

52. Mosnacek, J.; Nicolay, R.; Kar, K. K.; Fruchey, S. O.; Cloeter, M. D.; Harner, R. S.; Matyjaszewski, K. *Ind. Eng. Chem. Res.* **2012**, *51*, 3910–3915.

53. Trefonas, P.; Thackeray, J. W.; Sun, G.; Cho, S.; Clark, C.; Verkhoturov, S. V.; Eller, M. J.; Li, A.; Pavía-Jiménez, A.; Schweikert, E. A.; Wooley, K. L. In *Proceedings of SPIE - The International Society for Optical Engineering*; 2013; Vol. 8682.

54. Rungta, A.; Natarajan, B.; Neely, T.; Dukes, D.; Schadler, L. S.; Benicewicz, B. C. *Macromolecules* **2012**, *45*, 9303–9311.

55. Li, Y.; Tao, P.; Viswanath, A.; Benicewicz, B. C.; Schadler, L. S. *Langmuir* **2013**, *29*, 1211–1220.

56. Li, J.; Wang, L.; Benicewicz, B. C. *Langmuir* **2013**, *29*, 11547–11553.

57. Wang, L.; Chen, Y. P.; Miller, K. P.; Cash, B. M.; Jones, S.; Glenn, S.; Benicewicz, B. C.; Decho, A. W. *J. Chem. Soc., Chem. Commun.* **2014**, *50*, 12030–12033.

58. Kobayashi, M.; Matsugi, T.; Saito, J.; Imuta, J. I.; Kashiwa, N.; Takahara, A. *Polym. Chem.* **2013**, *4*, 731–739.

59. Kobayashi, M.; Takahara, A. *Polym. Chem.* **2013**, *4*, 4987–4992.

60. Ishikawa, T.; Takenaka, A.; Kikuchi, M.; Kobayashi, M.; Takahara, A. *Macromolecules* **2013**, *46*, 9189–9196.

61. Hui, C. M.; Pietrasik, J.; Schmitt, M.; Mahoney, C.; Choi, J.; Bockstaller, M. R.; Matyjaszewski, K. *Chem. Mater.* **2014**, *26*, 745–762.

62. Shrestha, R.; Shen, Y.; Pollack, K. A.; Taylor, J. S. A.; Wooley, K. L. *Bioconjugate Chem.* **2012**, *23*, 574–585.

63. Broyer, R. M.; Grover, G. N.; Maynard, H. D. *J. Chem. Soc., Chem. Commun.* **2011**, *47*, 2212–2226.

64. Matsumoto, N. M.; González-Toro, D. C.; Chacko, R. T.; Maynard, H. D.; Thayumanavan, S. *Polym. Chem.* **2013**, *4*, 2464–2469.

65. Maynard, H. D. *Nat. Chem.* **2013**, *5*, 557–558.

66. Oh, S. S.; Lee, B. F.; Leibfarth, F. A.; Eisenstein, M.; Robb, M. J.; Lynd, N. A.; Hawker, C. J.; Soh, H. T. *J. Am. Chem. Soc.* **2014**, *136*, 15010–15015.

67. Averick, S. E.; Dey, S. K.; Grahacharya, D.; Matyjaszewski, K.; Das, S. R. *Angew. Chem., Int. Ed.* **2014**, *53*, 2739–2744.

68. Averick, S. E.; Paredes, E.; Dey, S. K.; Snyder, K. M.; Tapinos, N.; Matyjaszewski, K.; Das, S. R. *J. Am. Chem. Soc.* **2013**, *135*, 12508–12511.

69. Cho, H. Y.; Averick, S. E.; Paredes, E.; Wegner, K.; Averick, A.; Jurga, S.; Das, S. R.; Matyjaszewski, K. *Biomacromolecules* **2013**, *14*, 1262–1267.

70. Averick, S. E.; Paredes, E.; Irastorza, A.; Shrivats, A. R.; Srinivasan, A.; Siegwart, D. J.; Magenau, A. J.; Cho, H. Y.; Hsu, E.; Averick, A. A.; Kim, J.; Liu, S.; Hollinger, J. O.; Das, S. R.; Matyjaszewski, K. *Biomacromolecules* **2012**, *13*, 3445–3449.

71. Pelegri-O'Day, E. M.; Lin, E.-W.; Maynard, H. D. *J. Am. Chem. Soc.* **2014**, *136*, 14323–14332.

72. Jakubowski, W.; Matyjaszewski, K. *Angew. Chem., Int. Ed.* **2006**, *45*, 4482–4486.

73. Tsarevsky, N. V.; Matyjaszewski, K. *Chem. Rev.* **2007**, *107*, 2270–2299.

74. Abreu, C. M. R.; Mendonça, P. V.; Serra, A. C.; Popov, A. V.; Matyjaszewski, K.; Guliashvili, T.; Coelho, J. F. J. *ACS Macro Lett.* **2012**, *1*, 1308–1311.

75. Guliashvili, T.; Mendonça, P. V.; Serra, A. C.; Popov, A. V.; Coelho, J. F. J. *Chemistry – Europ. J.* **2012**, *18*, 4607–4612.

76. Wang, Y.; Zhong, M.; Zhang, Y.; Magenau, A. J. D.; Matyjaszewski, K. *Macromolecules* **2012**, *45*, 8929–8932.

77. Magenau, A. J. D.; Bortolamei, N.; Frick, E.; Park, S.; Gennaro, A.; Matyjaszewski, K. *Macromolecules* **2013**, *46*, 4346–4353.

78. Tasdelen, M. A.; Uygun, M.; Yagci, Y. *Macromol. Chem. Phys.* **2010**, *211*, 2271–2275.

79. Mosnáček, J.; Ilčíková, M. *Macromolecules* **2012**, *45*, 5859–5865.

80. Konkolewicz, D.; Schröder, K.; Buback, J.; Bernhard, S.; Matyjaszewski, K. *ACS Macro Lett.* **2012**, *1*, 1219–1223.

81. Fors, B. P.; Hawker, C. J. *Angew. Chem., Int. Ed.* **2012**, *51*, 8850–8853.

82. Jakubowski, W.; Min, K.; Matyjaszewski, K. *Macromolecules* **2006**, *39*, 39–45.

83. Matyjaszewski, K.; Coca, S.; Gaynor, S. G.; Wei, M.; Woodworth, B. E. *Macromolecules* **1997**, *30*, 7348–7350.

84. Matyjaszewski, K.; Gaynor, S. G.; Coca, S. In *PCT International Application*; Carnegie Mellon University, U.S.A.\; WO 9840415, 1998, p 230.

85. Zhang, Y.; Wang, Y.; Matyjaszewski, K. *Macromolecules* **2011**, *44*, 683–685.

86. Rosen, B. M.; Percec, V. *Chem. Rev.* **2009**, *109*, 5069–5119.

87. Konkolewicz, D.; Wang, Y.; Zhong, M.; Krys, P.; Isse, A. A.; Gennaro, A.; Matyjaszewski, K. *Macromolecules* **2013**, *46*, 8749–8772.

88. Harrisson, S.; Couvreur, P.; Nicolas, J. *Polym. Chem.* **2011**, *2*, 1859–1865.

89. Boyer, C.; Soeriyadi, A. H.; Zetterlund, P. B.; Whittaker, M. R. *Macromolecules* **2011**, *44*, 8028–8033.

90. Boyer, C.; Derveaux, A.; Zetterlund, P. B.; Whittaker, M. R. *Polym. Chem.* **2012**, *3*, 117–123.

91. Matyjaszewski, K.; Pyun, J.; Gaynor, S. G. *Macromol. Rapid Commun.* **1998**, *19*, 665–670.

92. Wang, W.; Zhao, J.; Zhou, N.; Zhu, J.; Zhang, W.; Pan, X.; Zhang, Z.; Zhu, X. *Polym. Chem.* **2014**, *5*, 3533–3546.

93. Boyer, C.; Zetterlund, P. B.; Whittaker, M. R. *J. Polym. Sci., Part A: Polym. Chem.* **2014**, *52*, 2083–2098.

94. Wang, Y.; Zhong, M.; Zhu, W.; Peng, C.-H.; Zhang, Y.; Konkolewicz, D.; Bortolamei, N.; Isse, A. A.; Gennaro, A.; Matyjaszewski, K. *Macromolecules* **2013**, *46*, 3793–3802.

95. Peng, C.-H.; Zhong, M.; Wang, Y.; Kwak, Y.; Zhang, Y.; Zhu, W.; Tonge, M.; Buback, J.; Park, S.; Krys, P.; Konkolewicz, D.; Gennaro, A.; Matyjaszewski, K. *Macromolecules* **2013**, *46*, 3803–3815.

96. Zhong, M.; Wang, Y.; Krys, P.; Konkolewicz, D.; Matyjaszewski, K. *Macromolecules* **2013**, *46*, 3816–3827.

97. Percec, V.; Guliashvili, T.; Ladislaw, J. S.; Wistrand, A.; Stjerndahl, A.; Sienkowska, M. J.; Monteiro, M. J.; Sahoo, S. *J. Am. Chem. Soc.* **2006**, *128*, 14156–14165.

98. Zhang, Q.; Wilson, P.; Li, Z.; McHale, R.; Godfrey, J.; Anastasaki, A.; Waldron, C.; Haddleton, D. M. *J. Am. Chem. Soc.* **2013**, *135*, 7355–7363.

99. Konkolewicz, D.; Wang, Y.; Krys, P.; Zhong, M.; Isse, A. A.; Gennaro, A.; Matyjaszewski, K. *Polym. Chem.* **2014**, *5*, 4396–4417.

100. Matyjaszewski, K.; Tsarevsky, N. V.; Braunecker, W. A.; Dong, H.; Huang, J.; Jakubowski, W.; Kwak, Y.; Nicolay, R.; Tang, W.; Yoon, J. A. *Macromolecules* **2007**, *40*, 7795–7806.

101. Levere, M. E.; Nguyen, N. H.; Sun, H.-J.; Percec, V. *Polym. Chem.* **2013**, *4*, 686–694.

102. Lin, C. Y.; Coote, M. L.; Gennaro, A.; Matyjaszewski, K. *J. Am. Chem. Soc.* **2008**, *130*, 12762–12774.

103. Isse, A. A.; Gennaro, A.; Lin, C. Y.; Hodgson, J. L.; Coote, M. L.; Guliashvili, T. *J. Am. Chem. Soc.* **2011**, *133*, 6254–6264.

104. Konkolewicz, D.; Krys, P.; Góis, J. R.; Mendonça, P. V.; Zhong, M.; Wang, Y.; Gennaro, A.; Isse, A. A.; Fantin, M.; Matyjaszewski, K. *Macromolecules* **2014**, *47*, 560–570.

105. Bortolamei, N.; Isse, A. A.; Magenau, A. J. D.; Gennaro, A.; Matyjaszewski, K. *Angew. Chem., Int. Ed.* **2011**, *50*, 11391–11394.

106. Nguyen, N. H.; Rosen, B. M.; Lligadas, G.; Percec, V. *Macromolecules* **2009**, *42*, 2379–2386.

107. Tang, W.; Kwak, Y.; Braunecker, W.; Tsarevsky, N. V.; Coote, M. L.; Matyjaszewski, K. *J. Am. Chem. Soc.* **2008**, *130,* 10702–10713.

108. Marcus, R. A. *J. Chem. Phys.* **1956**, *24*, 966–978.

109. Isse, A. A.; Bortolamei, N.; De Paoli, P.; Gennaro, A. *Electrochim. Acta* **2013**, *110*, 655–662.

110. Averick, S.; Simakova, A.; Park, S.; Konkolewicz, D.; Magenau, A. J. D.; Mehl, R. A.; Matyjaszewski, K. *ACS Macro Lett.* **2012**, *1*, 6–10.

111. Zhang, Y. Z.; Wang, Y.; Peng, C. H.; Zhong, M. J.; Zhu, W. P.; Konkolewicz, D.; Matyjaszewski, K. *Macromolecules* **2012**, *45*, 78–86.

112. Simakova, A.; Averick, S. E.; Konkolewicz, D.; Matyjaszewski, K. *Macromolecules* **2012**, *45*, 6371–6379.

113. Golub, G.; Lashaz, A.; Cohen, H.; Paoletti, P.; Andrea, B.; Valtancoli, B.; Meyerstein, D. *Inorg. Chim. Acta* **1997**, *255*, 111–115.

114. Tsarevsky, N. V.; Pintauer, T.; Matyjaszewski, K. *Macromolecules* **2004**, *37*, 9768–9778.

115. Simakova, A.; Averick, S. E.; Konkolewicz, D.; Matyjaszewski, K. *Macromolecules* **2012**, *45*, 6371–6379.

116. Anastasaki, A.; Nikolaou, V.; Zhang, Q.; Burns, J.; Samanta, S. R.; Waldron, C.; Haddleton, A. J.; McHale, R.; Fox, D.; Percec, V.; Wilson, P.; Haddleton, D. M. *J. Am. Chem. Soc.* **2014**, *136*, 1141–1149.

117. Kwak, Y.; Matyjaszewski, K. *Macromolecules* **2010**, *43*, 5180–5183.

118. Ribelli, T. G.; Konkolewicz, D.; Bernhard, S.; Matyjaszewski, K. *J. Am. Chem. Soc.* **2014**, *136*, 13303–13312.

119. Ribelli, T. G.; Konkolewicz, D.; Pan, X.; Matyjaszewski, K. *Macromolecules* **2014**, *47*, 6316–6321.

120. Zhang, T.; Chen, T.; Amin, I.; Jordan, R. *Polym. Chem.* **2014**, *5*, 4790–4796.

Chapter 2

Radical Ring-Opening Polymerization: Molecular Designs, Polymerization Mechanisms, and Living/Controlled Systems

Takeshi Endo* and Atsushi Sudo

Molecular Engineering Institute, Kinki University, Kayanomori 11-6, Iizuka, Fukuoka 820-8555, Japan
*E-mail: tendo@moleng.fuk.kindai.ac.jp

Radical ring-opening polymerization (radical ROP) has emerged as a useful tool for synthesizing polymers with main chains containing heteroatoms, which are difficult to be obtained by the chain polymerization of vinyl monomers. In this chapter, the structural characteristics of the cyclic monomers that can undergo radical ROPs, their respective polymerization mechanisms, their copolymerizations with conventional vinyl monomers for synthesizing degradable polymers, and their living/controlled radical ROPs for synthesizing functional materials are described.

Introduction

To date, a wide variety of cyclic monomers such as epoxides and lactones and other heterocyclic compounds have been developed. Ring-opening polymerizations (ROPs) have yielded functional polymers consisting of carbon-hetero atom bonds; such polymers cannot be obtained by the addition polymerizations of vinyl monomers (*1–4*). Various initiators and catalysts have been developed to allow for the precise control of these ROPs (*5–10*).

The rational design of cyclic compounds makes it possible to achieve their radical ROPs (*11–13*). As is the case with the ionic ROPs of heterocyclic monomers, radical ROPs can also yield polymers with hetero atom-containing main chains. In addition, the potential applicability of radical ROPs for copolymerizations with vinyl monomers is a highly attractive feature.

Figure 1 shows several cyclic monomers, which have been categorized by structure type. It has been reported that cycloalkanes, cyclic ethers, and a few other heterocyclic compounds are monomers that can undergo radical ROPs. A common structural feature of these cyclic monomers is that they all have a carbon-carbon double bond. This double bond is necessary as a radical acceptor in order for the radical ROPs to occur. In addition to exhibiting this feature, the monomers must meet three other requirements. First, the monomers should possess distorted ring structures that promote their respective ring-opening reactions. Second, their ring-opening reactions should be accompanied by isomerization processes that yield thermodynamically more favored functional groups. Finally, these ring-opening reactions should be promoted by the stabilization of the corresponding radical species.
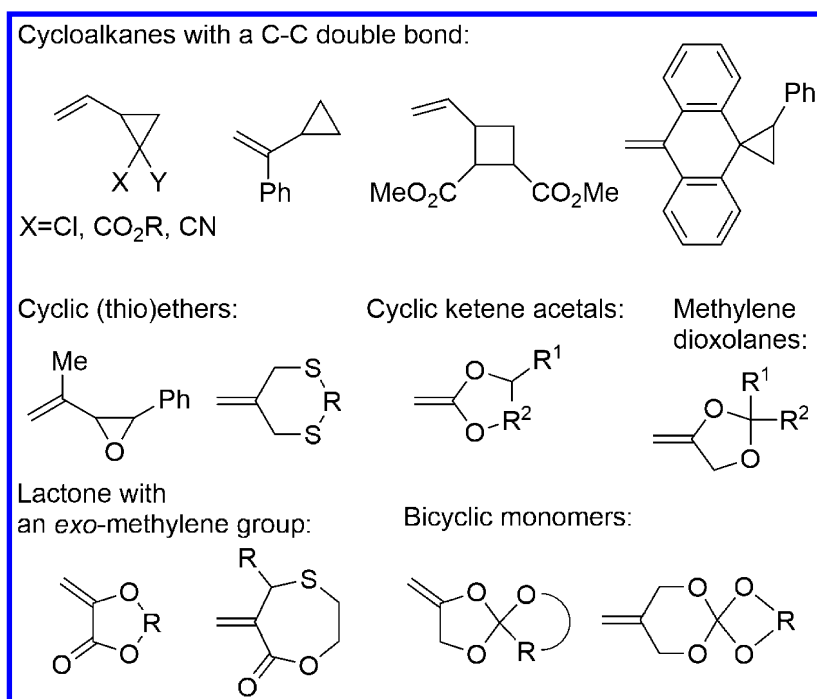

Figure 1. Cyclic monomers capable of undergoing radical ring-opening polymerizations.

For a more detailed explanation, we chose the radical ROP of a cyclopropane derivatives as an example; the ROP process is depicted in Figure 2 (*11*). The first step in the process is the addition reaction of a radical species to the vinyl group. This step is followed by the ring-opening reaction of the highly distorted three-membered ring, leading to the formation of a radical stabilized by the substituents X and Y, which are selected from phenyl, ester, and cyano groups. At the same time, the formation of a thermodynamically more stable internal olefin also promotes the ring-opening reaction.
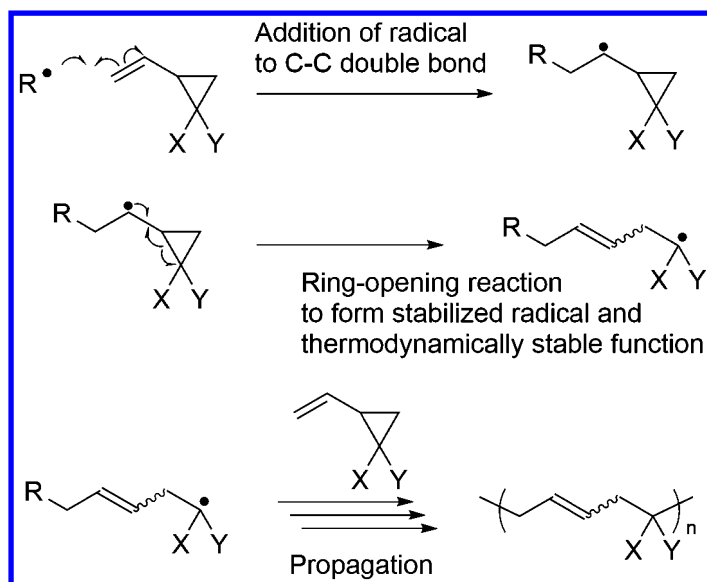
Figure 2. Fundamental molecular design of radically polymerizable cyclic monomers.

In this chapter, the structural characteristics of the cyclic monomers that can undergo radical ROPs are described; further, the characteristics are correlated to their respective polymerization mechanisms. Their copolymerizations with conventional vinyl monomers are also described, as are a few living/controlled radical ROPs that have been developed recently.

Radical ROPs of Cycloalkanes

As described in Introduction, vinyl cyclopropanes bearing functional groups such as halogens, esters and cyano groups can undergo radical ROPs (*14–18*). In comparison to the large volume shrinkage that accompanies the chain-growth polymerizations of vinyl monomers such as styrene derivatives, acrylates, and methacrylates, the volume shrinkage in the case of the radical ROPs of these vinyl cyclopropanes is much smaller, indicating their potential applicability as shrinkage-free adhesives and void-free sealants (*19*). The main chain of the resulting polymers has carbon-carbon double bonds, which can potentially act as reactive sites for polymer reactions.
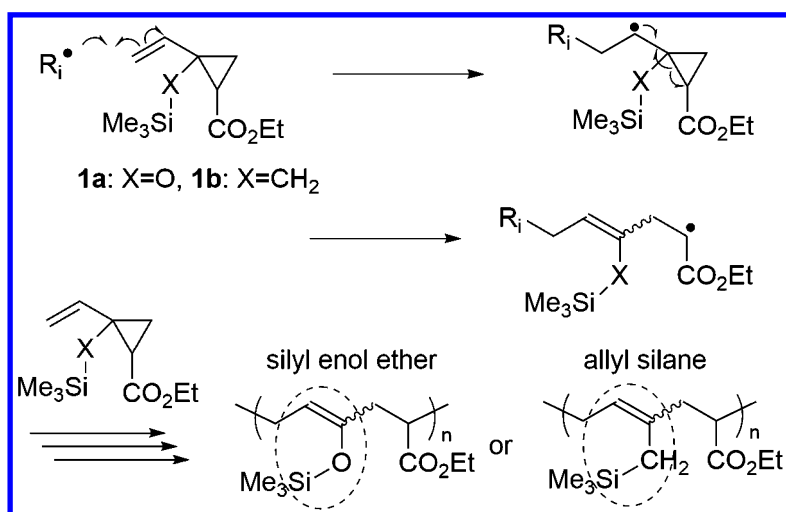
Figure 3. Radical ROP of vinylcyclopropane with a siloxyl moiety.

Another design of a cyclopropane derivative that undergoes radical ROP is based on a combination of styrene and cyclopropane moieties (Figure 4) (*22*). In the monomer **2**, the styrene moiety acts as an acceptor of radicals, forming a radical stabilized by the phenyl group. Then, the cyclopropyl moiety undergoes the ring-opening reaction to yield an acyclic radical species. Although the formed radical is not stabilized, the styrene part in the monomer captures this highly active radical immediately, suppressing the termination and chain transfer reactions.

The cyclopropane **3**, which contains a dihydroanthracene moiety, undergoes radical ROP efficiently (Figure 5) (*23*). An *exo*-methylene group gets attached on the dihydroanthracene moiety and can accept radical species. After the addition of a radical by the methylene group, the dihydroanthracene moiety is transformed into an anthracene group, resulting in a radical stabilized with a phenyl group. This aromatization process and the release of the distortion energy of the cyclopropane ring are the driving forces that promote the ROP process.

In addition to cyclopropane derivatives, the cyclobutane derivative 4 can also undergo radical ROPs (Figure 6) (*24*). The addition of a radical species to the vinyl group is followed by the ring-opening reaction of the cyclobutane ring and the release of the ring-distortion energy of the four-membered ring. The resulting radical is stabilized by the adjacent ester group; this promotes the ring-opening reaction.
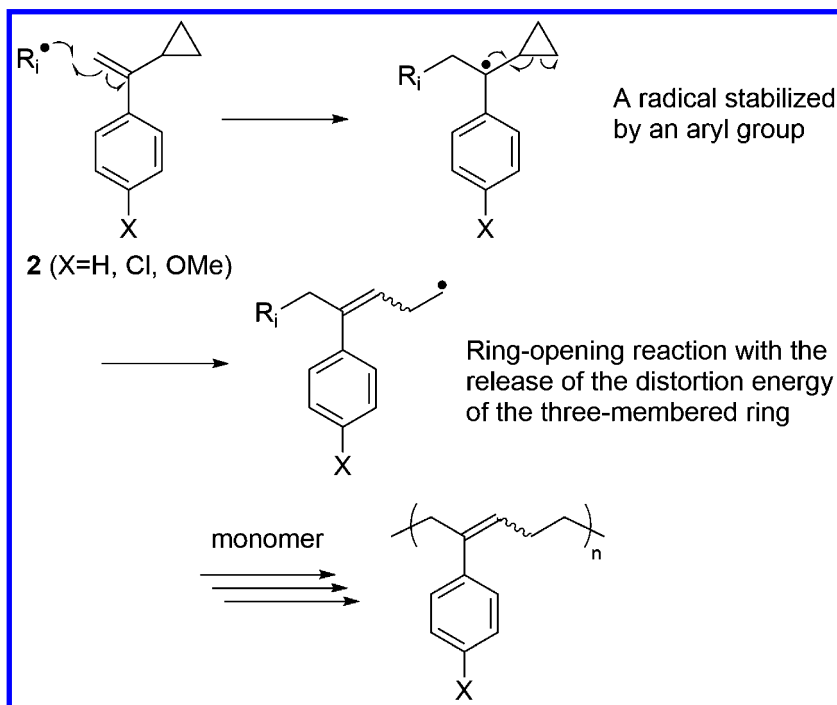

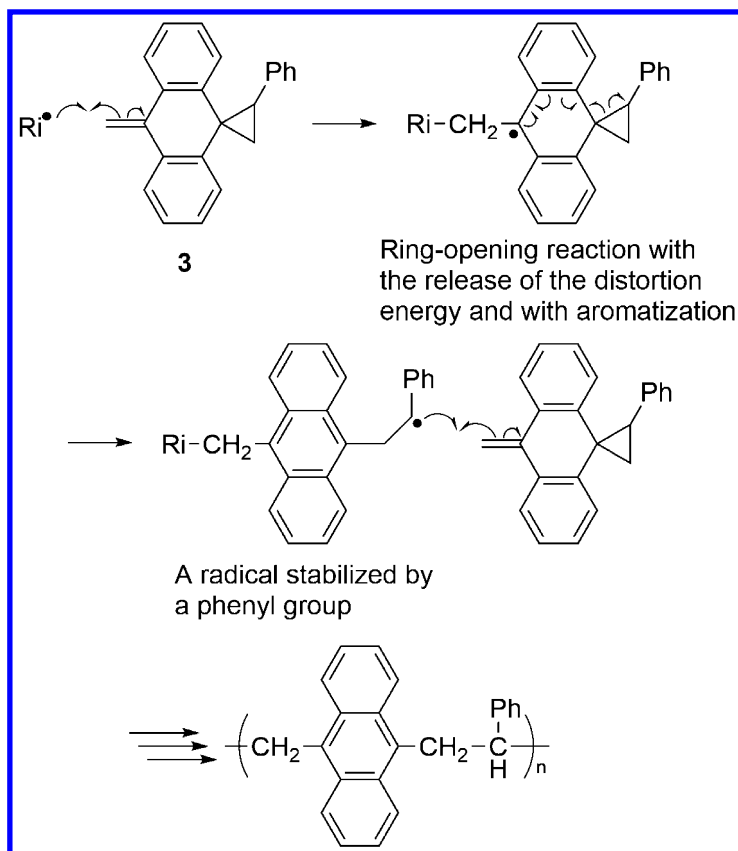*Figure 4. Radical ROP of (1-phenyl)ethenylcyclopropane.*

Figure 5. Radical ROP of cyclopropane with a dihydroanthracene moiety.
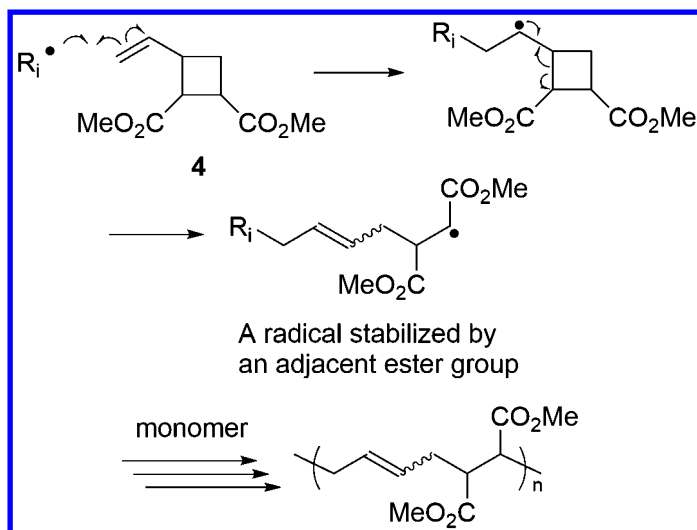

Figure 6. Radical ROP of vinyl cyclobutane.

Radical ROPs of Cyclic Ethers and Sulfides

Three-membered cyclic ethers (i.e., oxiranes) can undergo cationic and anionic ROPs but not radical ROPs. However, the attachment of a vinyl group that serves as a radical acceptor allows one to synthesize radically polymerizable oxiranes. Figure 7 shows the radical ROP of 2-phenyl-3-vinyloxirane (**5**) (*25–27*). The first step of the process is the addition of the radical species to the vinyl group of the monomers. This reaction is followed by the ring-opening reaction of the three-membered ring, which is driven by the release of the distortion energy of the three-membered ring. The resulting radical is stabilized by the phenyl group; this stabilization of the radical is essential for the ring-opening reaction of the oxirane ring to occur.
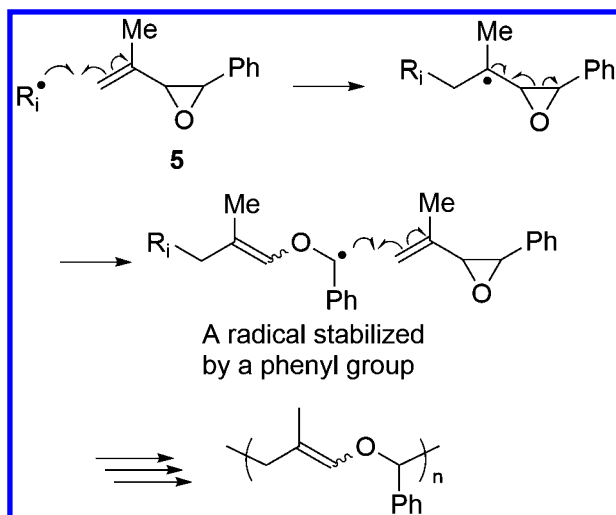

Figure 7. Radical ROP of vinyl oxirane.

The methylene oxetane **6**, shown in Figure 8, can be regarded not only as a cyclic monomer but also as a vinyl ether-type monomer. Consequently, this monomer undergoes not only radical ROP but also the chain-growth radical polymerization of the C-C double bond (*28*). The resulting polymer consists of ketone-containing units and oxetane-containing units in a 4:6 ratio. The *exo*-methylene group accepts a radical, which is transformed into a primary alkyl radical. The formed radical is not stabilized and is thus relatively difficult to form; however, the formation of a thermodynamically stable ketone group can drive the ring-opening reaction.
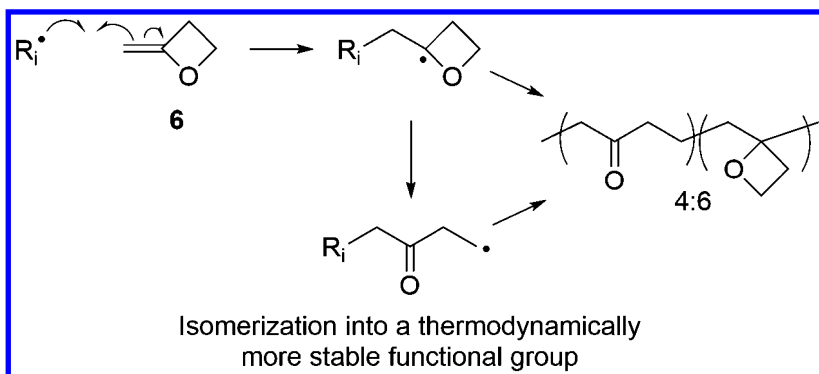
Figure 8. Radical ROP of exo-methylene oxetane.

The five-membered cyclic ether 7, which has an *exo*-methylene group, is a monomer that can undergo radical ROP (Figure 9) (*29*). The radically induced ring-opening reaction is promoted by two factors: 1) the formation of a thermodynamically stable ketone group and 2) the formation of a relatively stable benzyl radical-type chain end.
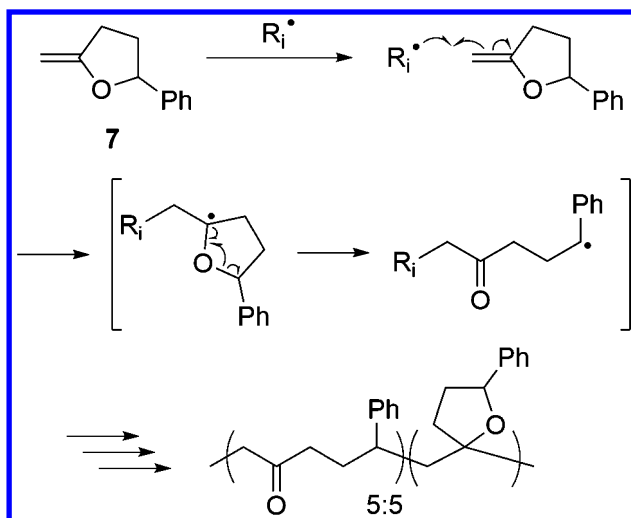

Figure 9. Radical ROP of exo-methylene tetrahydrofuran.

On the other hand, an analogous compound with a six-membered cyclic ether-like structure does not undergo ROP, but its *exo*-methylene group undergoes chain-growth radical polymerization.

Cyclic allylic sulfides are cyclic monomers that undergo radical ROPs (Figure 10) (*30–32*). Those with seven- and eight-membered rings, such as **8** and **9**, are polymerizable. In a meanwhile, a six-membered one is not reactive under the same conditions presumably because of the smaller distortion energy of six-membered ring than those of seven- and eight-membered rings. The bifunctional cyclic allylic sulfide **10** has also been used as a monomer for synthesizing a cross-linked polymer. These monomers have been designed on the basis of the high reactivity of allyl sulfides in various radical reaction systems. The ROPs yield the corresponding polysulfides, which bear C-C double bonds in their main chains.
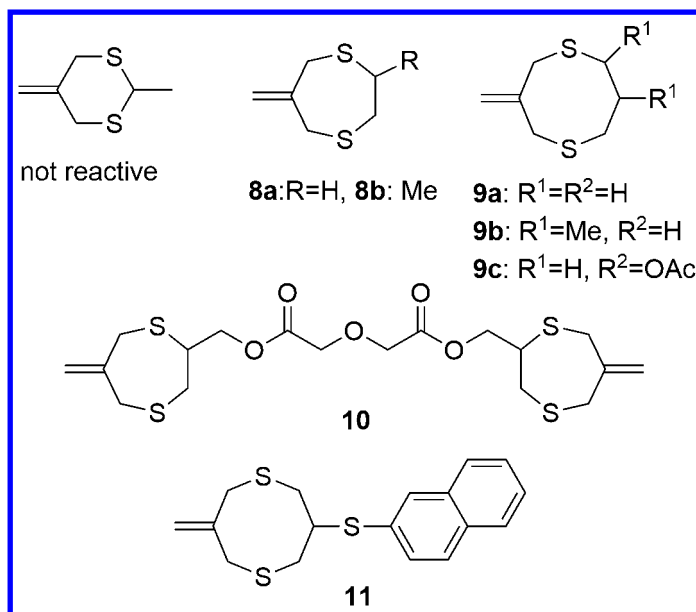

Figure 10. Cyclic allylic sulfides.

As shown in Figure 11, the first step in the process is the addition of a radical to the *exo*-methylene group of the monomer, which leads to the formation of a radical at the β-position of the sulfur atom. This cyclic radical undergoes the ring-opening reaction, which results in the formation of a new acyclic allyl sulfide and thiyl radical. In general, thiyl radicals react readily with carbon-carbon bonds without undergoing hydrogen abstraction, a process that can cause various side reactions. The radical ROP of the seven-membered cyclic allyl sulfide proceeds smoothly at 70 °C, yielding the corresponding polysulfide, whose weight-average molecular weight is higher than 600,000. Similarly, monomers with eight-membered ring also undergo radical ROPs readily.
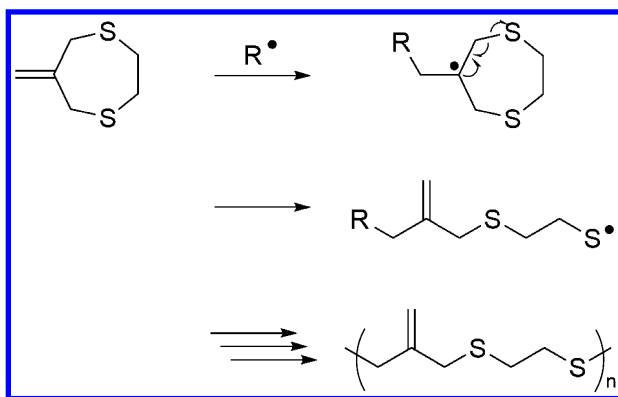
Figure 11. Radical ROP of a seven-membered cyclic allylic sulfide with an exo-methylene group.

The main chains of the resulting polymers have acyclic allylic sulfide moieties, which can accept radical species, leading to chain transfers and the formation of macrocyclic polymers. These mechanistic viewpoints as well as the corresponding polymerization kinetics have been studied in detail (*33*, *34*).

One of the advantages of subjecting these cyclic allylic sulfides to radical ROPs is that the resulting shrinkage in volume is low (*31*, *32*). The volume shrinkages that accompany the ROPs range from 1.4% to 2.4% and are much smaller than those that follow the radical polymerizations of vinyl monomers.

Another advantage is that the high sulfur contents of the resulting polymers should allow for the development of materials with high refractive indexes. A monomer bearing a naphthylthio moiety, namely, **11**, whose reflective index is high as 1.686, also undergoes radical ROP while exhibiting a volume shrinkage of only 0.02%. It has been successfully used as a holographic data storage media (*35*).

Radical ROP of Cyclic Ketene Acetals

Cyclic ketene acetals, a class of highly nucleophilic cyclic monomers, have been developed as they undergo efficient cationic ROPs. However, these monomers also undergo radical ROP. The ROPs yield the corresponding polyesters. As a result, their degradable nature has been a focus of extensive research (*36*, *37*). As a typical example, Figure 12 depicts the radical ROP of the five-membered cyclic ketene acetal **12** (*38*). In this case, the *exo*-methylene group is the radical acceptor. The ring-opening reaction is accompanied by the formation of an acyclic ester linkage, which is thermodynamically much more stable than the original cyclic acetal. In addition, the resulting radical is stabilized by the adjacent phenyl group, and this stabilization process contributes to the ring-opening reaction.
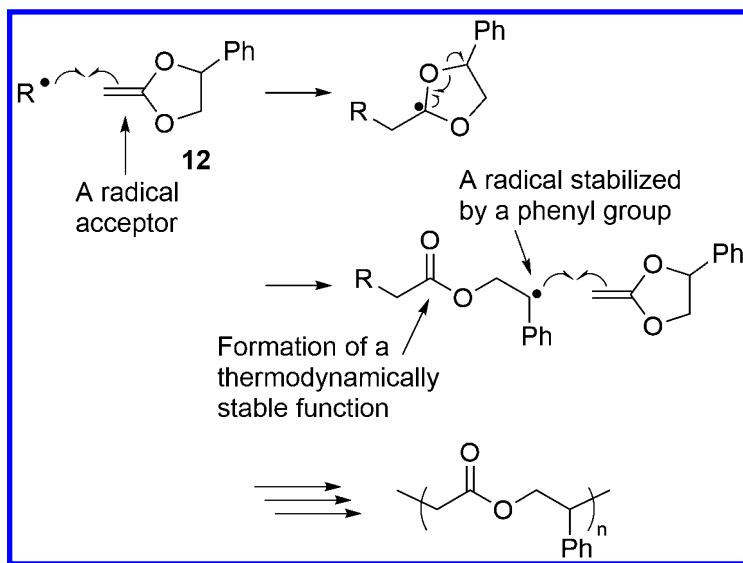
Figure 12. Radical ROP of a cyclic ketene acetal.

In addition to five-membered cyclic ketene acetals, a few six- and seven-membered ones undergo radical ROPs too (Figure 13) (*39–43*). The radical ROP behavior of cyclic ketene acetals depends on two parameters: their ring size and substituents. These monomers can undergo not only ROPs but also vinyl polymerization. In this context, the "ring-opening efficiency" is defined as the following ratio: number of units formed by ring-opening polymerization/total number of units, including those formed by vinyl polymerization. With respect to the polymerizations of the five-, six-, and seven-membered cyclic ketene acetals without substituents, the corresponding ring-opening efficiencies are 83, 85, and 100%, respectively, implying that the degree of ring distortion is a critical parameter. On the other hand, by introducing substituents such as alkyl and phenyl groups, the ring-opening efficiency can be improved to 100% regardless of ring size, presumably owing to the effects that these substituents have on the ring-opening reaction by stabilizing the radicals formed at the chain end. The ketene acetals **13** and **14** are the ones used most commonly for copolymerizations with vinyl monomers, as shown later. In addition, the seven-membered cyclic ketene acetal **15**, which bears a C-C double bond in the ring, also undergoes radical ROP (*44*). The eight-membered cyclic ketene acetal **16** also undergoes radical ROP to yield the corresponding poly(ester-ether), which is more biodegradable than the polyester obtained by the radical ROP of **13** (*45*).
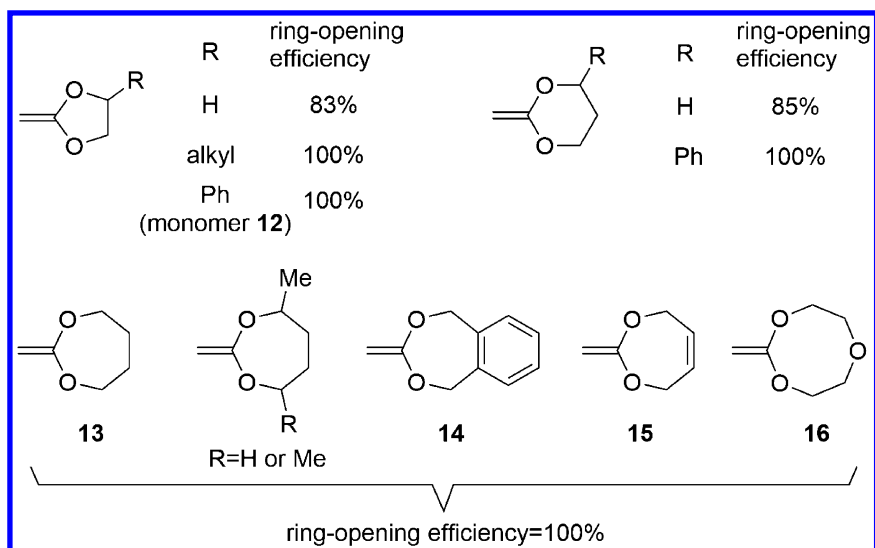
Figure 13. Cyclic ketene acetals that undergo radical ROPs.

The polymers formed by the radical ROPs of cyclic ketene acetals without chain transfer are polyesters that are the synthetic equivalents of the polyesters formed by the ionic ROPs of lactones. Detailed studies on the structure of the polymer obtained by the radical ROP of 2-methylene-1,3-dioxepane (**13**) have revealed that the polymer is not a perfectly linear one but contains branches, which are formed by hydrogen transfer during the propagation stage (*46*). Owing to the presence of such a branched structure, the polymer does not have crystalline domains. In contrast, the polyester synthesized by the ionic ROP of ε-caprolactone does.

Radical ROP of 4-Methylene-1,3-dioxolane

The radical polymerization of 4-methylene-1,3-dioxolane involves three polymerization modes (Figure 14) (*47–51*): The first one is the chain-growth radical polymerization of the *exo*-methylene group. The second one is the ROP. Finally, the third one is another mode of the ROP, yielding polyketone; this is accompanied by the elimination of the corresponding carbonyl compounds.
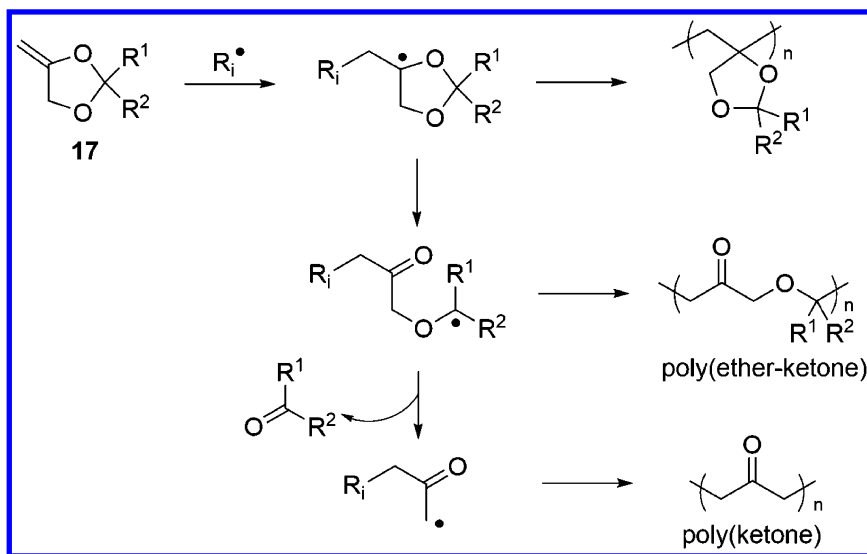
Figure 14. Radical polymerization of 4-methylene-1,3-dioxolane.

Methylene dioxolane, which has two phenyl groups at the 2-position ($R^1=R^2=Ph$), selectively undergoes radical ROP in the third mode at 120 °C (*47*). The ROP proceeds with the elimination of benzophenone, resulting in the corresponding polyketone. The high selectivity is attributable to the smooth ring-opening reaction of the five-membered ring, which is driven by the formation of a stable diphenyl methyl radical. When the polymerization is performed at lower temperatures (60–100 °C), the resulting polymer contains a dioxolane ring (*48*). When one of the two substituents at the 2-position is replaced by H or an alkyl group, vinyl polymerization accompanies the ROP (*49*, *50*). The introduction of an electron-donating group at the para position of the phenyl ring accelerates the polymerization process (*51*). For example, the monomer bearing 4-cyanophenyl groups ($R^1=R^2=4$-cyanophenyl) does not undergo polymerization at 60 °C while using azobisisobutyronitrile (AIBN) as an initiator; in contrast, the monomer bearing 4-methoxyphenyl groups ($R^1=R^2=4$-methoxyphenyl) undergoes polymerization readily under the same conditions.

Radical ROP of α-*exo*-Methylene Lactones

The cyclic lactones **18**, which bear an *exo*-methylene group at the α-position, have been designed so that 1) the acrylate-type structure of the monomer can accept radicals and 2) the resulting radical species can be transformed into a benzyl radical. By virtue of this molecular design, six-membered lactones can undergo radical ROPs readily to give the corresponding polymer, which bears an α-ketoester linkage in the main chain and exhibits photodegradability (Figure 15) (*52, 53*). In addition to five-membered lactones, the six-membered analogue **19** also undergoes radical ROP (*54*).
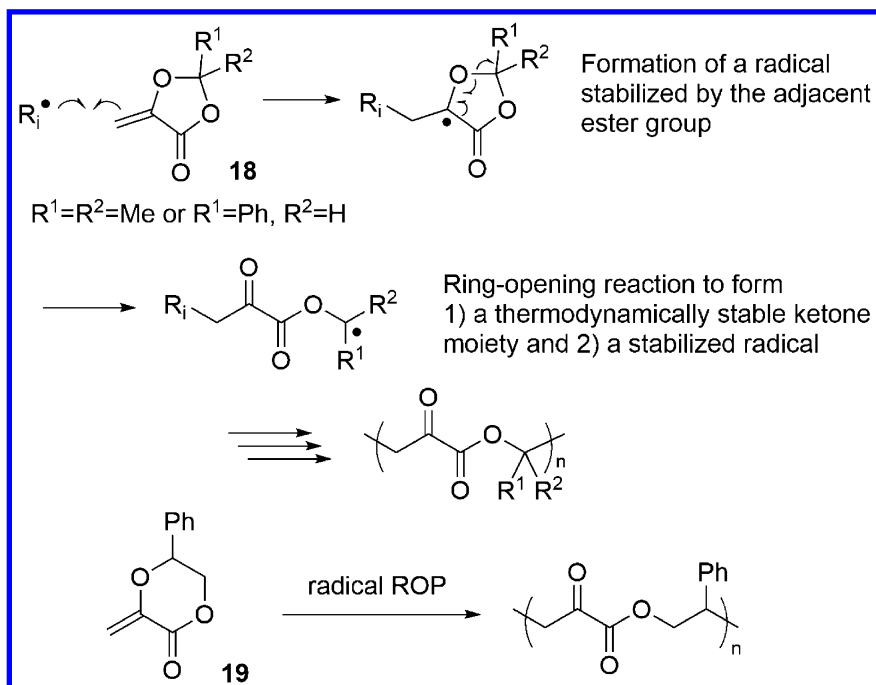

Figure 15. Radical ROP of a cyclic α-alkoxyacrylate.

The seven-membered cyclic lactone **20**, which has an *exo*-methylene group and a sulfur atom, also undergoes radical ROP (Figure 16) (*55, 56*). The addition of a radical species to the *exo*-methylene group is owing to the formation of a radical that is stabilized by the neighboring ester group. Then, the ring-opening reaction of the seven-membered ring takes place to yield a thiyl radical, which is readily added to the *exo*-methylene group of another molecule of the monomer.
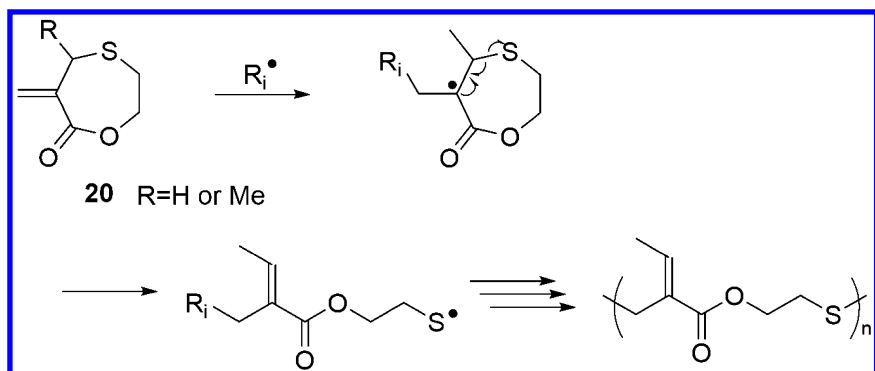
Figure 16. Radical ROP of an exo-methylene seven-membered lactone bearing a sulfur atom in the ring.

Radical ROPs with Double-Ring Opening of Bicyclic Monomers

The molecular designs of bicyclic monomers that can undergo radical ROPs through a cascade of the ring-opening reactions involving the two cyclic structures expand the applicability and range of radical ROPs. Combining vinylcyclopropane and seven-membered cyclic acetal moieties gives the monomer **21**, which undergoes double-ring-opening polymerization (Figure 17) (*57*). Although the resulting polymer is contaminated by a few other units such as those formed by vinyl polymerization and the ring-opening polymerization of the vinylcyclopropane part without the ring opening of the cyclic acetal part, the pathway dominating the system is the double-ring-opening polymerization. This process yields the corresponding polyester, which contains C-C double bonds in the main chain. The high ring-distortion energy of the seven-membered ring is essential for the double-ring-opening polymerization to occur.
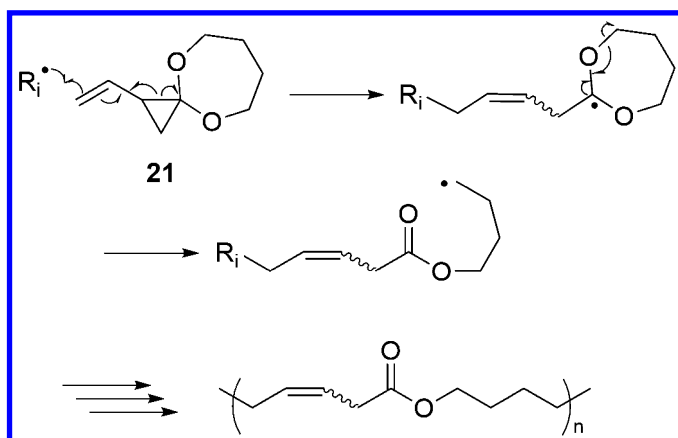

Figure 17. Radical ROP of vinylcyclopropane, which has a spiroketal structure.

Another interesting combination is that of vinyl oxirane and cyclohexane moieties to form the spirobicyclic monomer **22** (Figure 18) (*58*). As is the case with other cyclic monomers that undergo radical ROPs, this spirobicyclic monomer accepts radical species at its vinyl group. The radical formed by this process is transformed into an oxy radical via the ring-opening reaction of the oxirane ring. The successive ring-opening reaction of the six-membered ring is assisted by the formation of a benzyl radical. The resulting polymer has an α,β-unsaturated ketone structure in the main chain, which can be used as an electrophilic reactive group for the functionalization of the polymer.
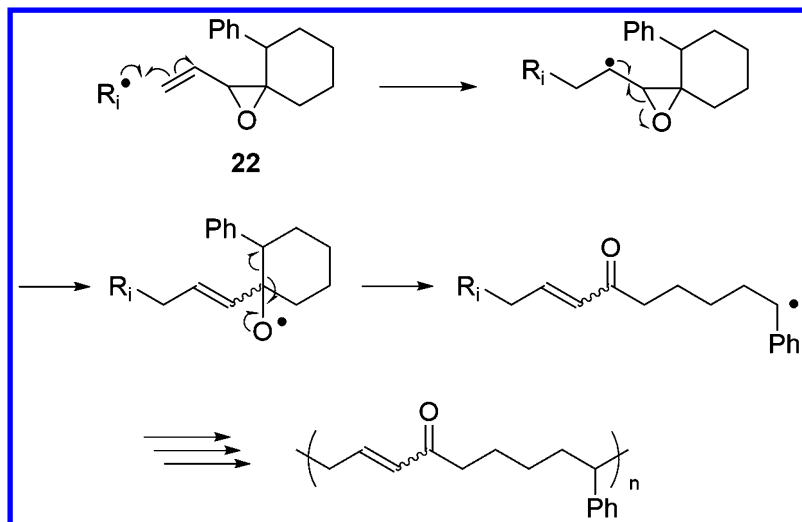

Figure 18. Radical ROP of vinyloxirane, which has a spirocyclic structure.

Spiroorthocarbonates (SOCs) and spiroorthoesters (SOEs) are cyclic monomers that can undergo cationic ROPs. Their cationic polymerizations are accompanied by volume expansion, because the highly compact structures of the monomers are transformed into acyclic ones that occupy much more space. These "volume-expandable monomers" can be employed as sealants and adhesives that do not exhibit the voids and cracks caused by the volume shrinkage that occurs during the polymerization of conventional monomers.

SOC, which contains an *exo*-methylene group, undergoes radical ROP through double-ring-opening reactions, yielding the corresponding polycarbonate (Figure 19) (*59*). In the case of the polymerization of a monomer bearing a six-membered cyclic acetal moiety, the degree of volume expansion is reported to be 4.5%. These monomers are potentially applicable as volume-expandable monomers that can copolymerize with conventional vinyl monomers to suppress volume shrinkage.
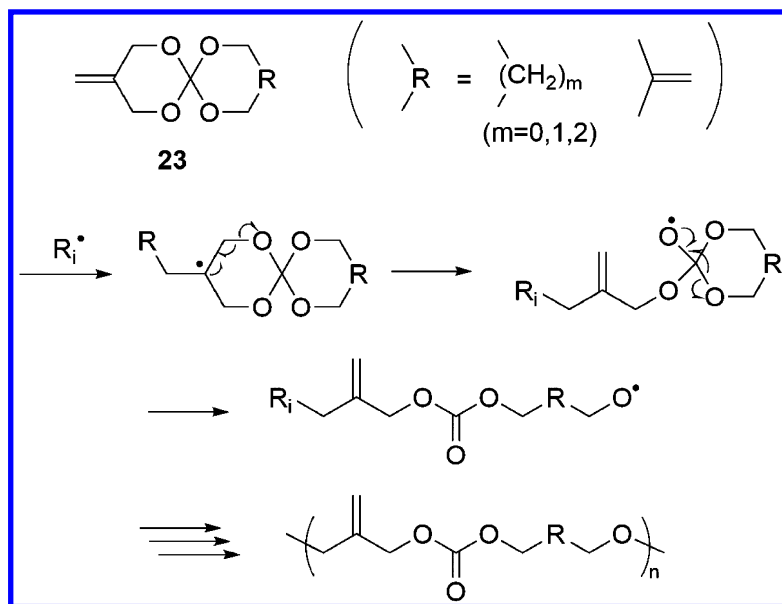

Publication Date (Web): May 1, 2015 | doi: 10.1021/bk-2015-1187.ch002

Figure 19. Radical ROP of a spiroorthocarbonate with an exo-methylene group.

The SOEs **24** and **25**, which bear an *exo*-methylene group and consist of a five-membered ring acetal ring (ring A) and a cyclic ether (ring B), also undergo radical ROP (Figure 20) (*60–62*). After the addition of a radical species to the *exo*-methylene group, ring A undergoes the ring-opening reaction, resulting in a ketone moiety. The second ring-opening reaction, that is, the ring-opening reaction of ring B, results in an ester moiety. The formation of these thermodynamically stable functional groups drives the radical ROP of these SOEs bearing an *exo*-methylene group.

Radical Copolymerizations of Cyclic Monomers with Vinyl Monomers

The distinctive advantage of radical ROP over ionic ROP is that it can be used to copolymerize cyclic monomers with vinyl monomers bearing different functional groups (Figure 21). Owing to statistic copolymerization, the functional groups formed by the radically induced ring-opening reactions of cyclic monomers are distributed randomly in the main chains of the copolymers. Owing to the presence of such functional groups in the main chains, the copolymers become degradable (*36, 37, 63, 64*). The hydrolysis, biodegradation, and photoscission of the copolymers obtained by the radical copolymerizations of vinyl monomers and cyclic monomers have been studied intensively.
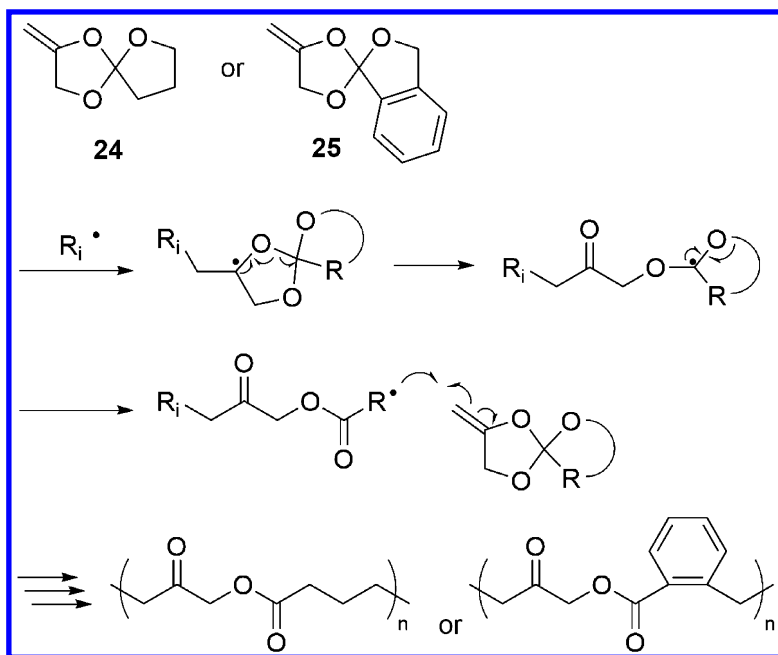
Figure 20. Radical ROP of an exo-methylene spiroorthoester via double-ring-opening reactions.
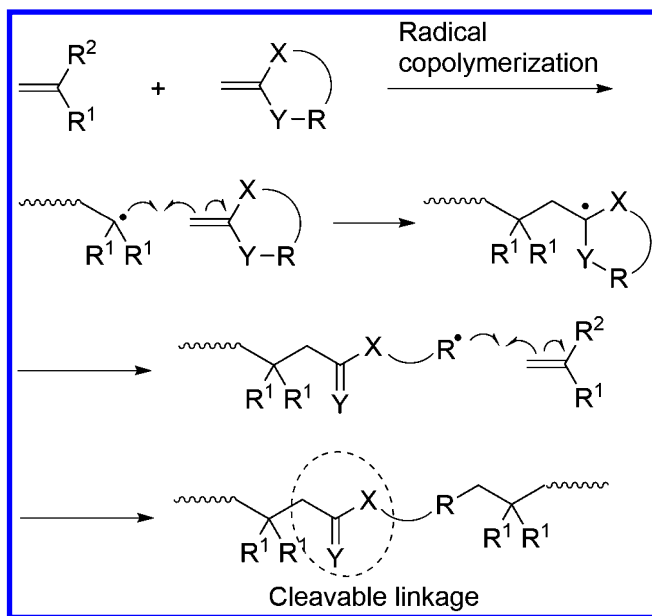

Figure 21. Radical copolymerization of vinyl monomers with cyclic monomers that can undergo ROPs.

Cyclic ketene acetals are the comonomers that have been investigated the most intensively so far. For example, the five-membered cyclic ketene acetal with a phenyl group **15** undergoes radical copolymerization with various vinyl monomers (Figure 22) (*65*). During copolymerization with methyl methacrylate (MMA), the composition of the copolymers can be controlled efficiently such that it lies in the range of 9:91 to 82:18, by varying the feed ratio of the monomers. This is a useful method for synthesizing degradable polymers bearing ester linkages in the main chains, which were derived from the cyclic monomers.
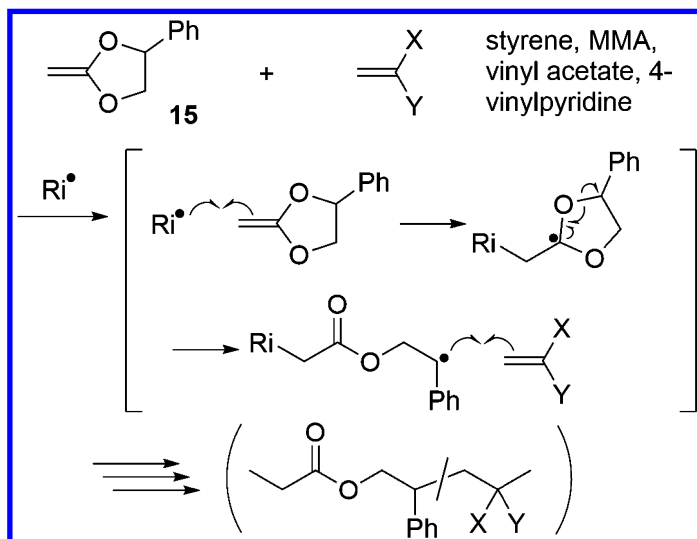

Figure 22. Radical copolymerization of a five-membered cyclic ketene acetal with vinyl monomers.

Seven-membered cyclic ketene acetals have been used as comonomers for synthesizing various copolymers based on combinations with a variety of vinyl monomers (Figure 23). The copolymerizations of such acetals with styrene (*66, 67*), methyl acrylate (*68*), methyl methacrylates (*69*), and vinyl acetate (*70*) have been reported. Further, the degradability of the main chains of some of the copolymers has also been studied (*67, 68, 70*). Copolymerizations with highly polar and hydrophilic monomers such as vinylphosphonic acid and N-isopropylacrylamide have also been studied, as these copolymers are expected to exhibit improved biodegradability (*71, 72*). A three-component copolymerization process involving a cyclic ketene acetal, maleic anhydride, and poly(ethylene glycol diacrylate) and the subsequent hydrolysis of the anhydride moiety incorporated in the copolymer results in a biodegradable hydrogel (*73*). Copolymerization with fluoroalkenes proceeds in the opposite manner, yielding hydrophobic and degradable polymers (*74*). Recently, methods for designing and synthesizing various biodegradable copolymers for biomedical applications, such as drug delivery and DNA transfection, have been investigated extensively.

Successful methods that use seven-membered cyclic ketene acetals have been reported (*75–78*).
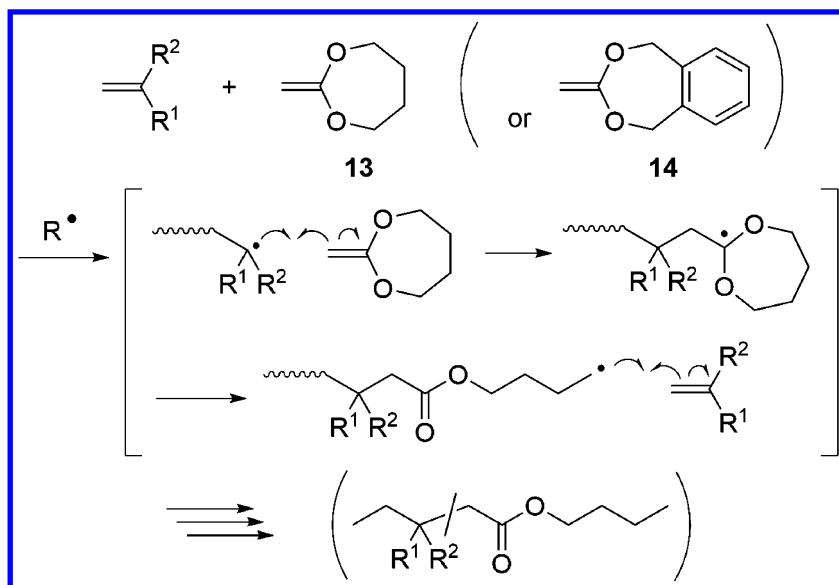

Figure 23. Radical copolymerization of a seven-membered cyclic ketene acetal with vinyl monomers.

The copolymerizations of a five-membered cyclic acetal bearing an *exo*-methylene group with vinyl monomers have been also reported (Figure 24) (*79*). Owing to the ring-opening reaction of the five-membered cyclic acetal with the releasing benzophenone, units bearing a ketone moiety can be incorporated into the copolymers. The copolymerizations with vinyl pyrrolidone, styrene, and vinyl acetate proceed through the ring-opening reaction of the cyclic acetal, while that with MMA is accompanied by the vinyl polymerization of the *exo*-methylene group.

Since ketone groups can undergo photoinduced reactions (i.e., Norrish-type reactions), copolymers with ketone groups in the main chain are potentially photodegradable. The copolymerization of a cyclic acetal with *O*-protected 4-hydroxystyrenes results in the corresponding polystyrene derivatives, which bear ketone moieties in the main chains (Figure 25) (*80*). Upon the irradiation of ultraviolet (UV) radiation on the copolymers, their main chains degrade efficiently into oligomers. This photodegradability as well as the acid-labile nature of the protective groups in the side chains makes these copolymers potentially employable as photoresist materials.
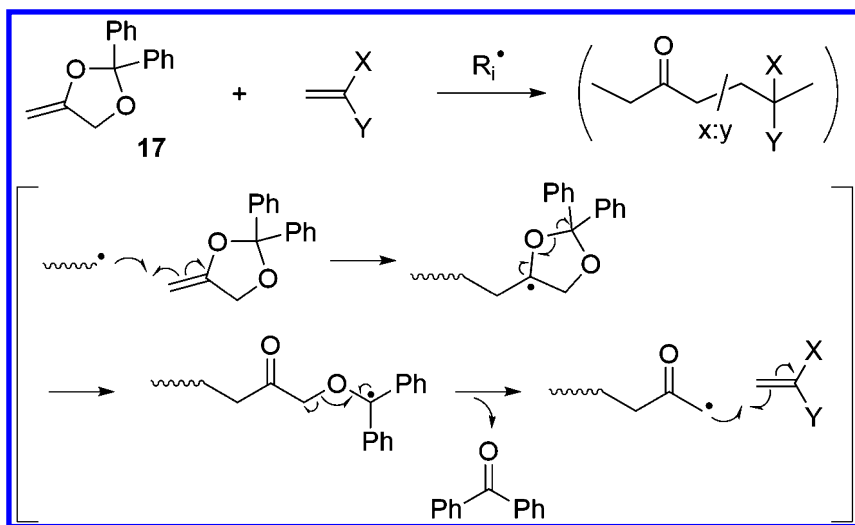
Figure 24. Radical copolymerization of exo-methylene dioxolane with vinyl monomers.
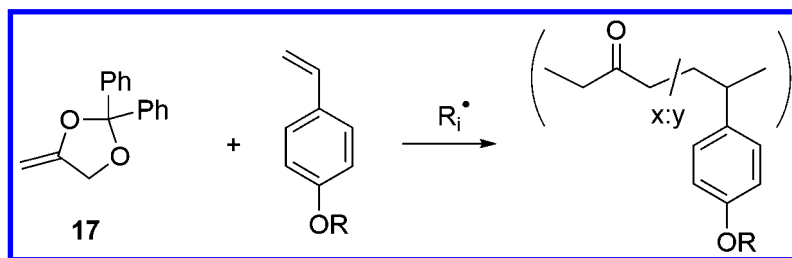
Figure 25. Radical copolymerization of exo-methylene dioxolane for the synthesis of photodegradable polystyrene derivatives.

A seven-membered cyclic lactone with an *exo*-methylene group and a sulfur atom also undergoes radical copolymerization with styrene (Figure 26) (*81*). The ring-opening reaction gives a thiyl radical, which can react readily with acrylates and styrene, allowing for the successful copolymerizations of the cyclic monomer and these vinyl monomers.

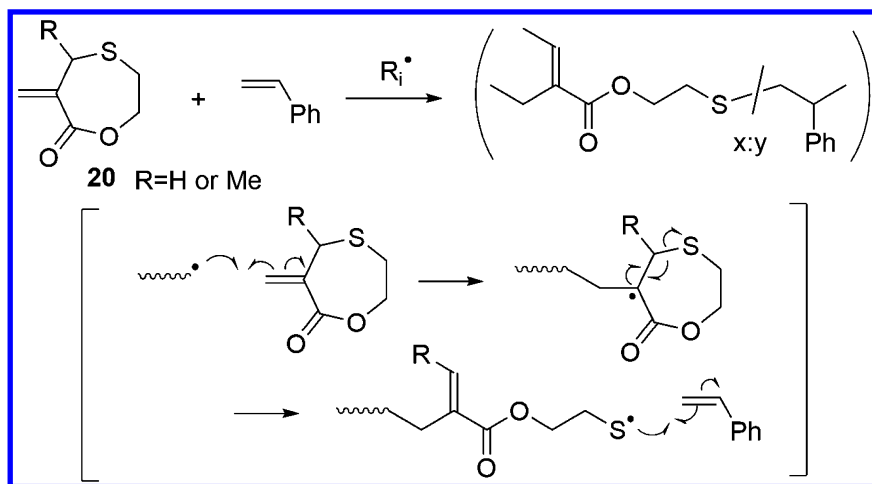*Figure 26. Radical copolymerization of exo-methylene lactone with vinyl monomers.*

Living/Controlled Radical ROP

Recent developments in the field of living/controlled radical polymerization now allow one to synthesize polymers with defined molecular weights, shapes, and terminal structures from a wide range of vinyl monomers (*82–86*). Using the techniques developed so far, various functional polymer architectures have been constructed successfully (*87–90*). Recently, the techniques developed for the living/controlled polymerizations of vinyl monomers have been applied to the living/controlled radical ROPs of cyclic monomers, leading to the successful syntheses of well-defined polymers having main chains completely different from those of polymers obtained from vinyl monomers. In addition, the statistic copolymerization of cyclic monomers with vinyl monomers in a living/controlled fashion yields the corresponding copolymers such that they have precisely controlled chain lengths and terminal structures.

The control of the radical ROP of vinyl cyclopropanes has been achieved by using nitroxide-mediated polymerization (NMP) (*91*) and atom-transfer radical polymerization (ATRP) (*92, 93*). Through the ATRP-type radical ROP of vinylcyclopropane 26, one can obtain the corresponding polymer such that it exhibits a narrow molecular weight distribution (Mw/Mn = 1.11) (Figure 27). In addition, the ATRP-type copolymerization of **26** with MMA has also been reported (*93*). In contrast to the radical ROP of vinylcyclopropane with MMA, which is accompanied by the formation of a cyclic moiety to yield a polymer without a C-C double bond (*94*), the use of the ATRP technique permits the synthesis of a polymer with a C-C double bond in the main chain.
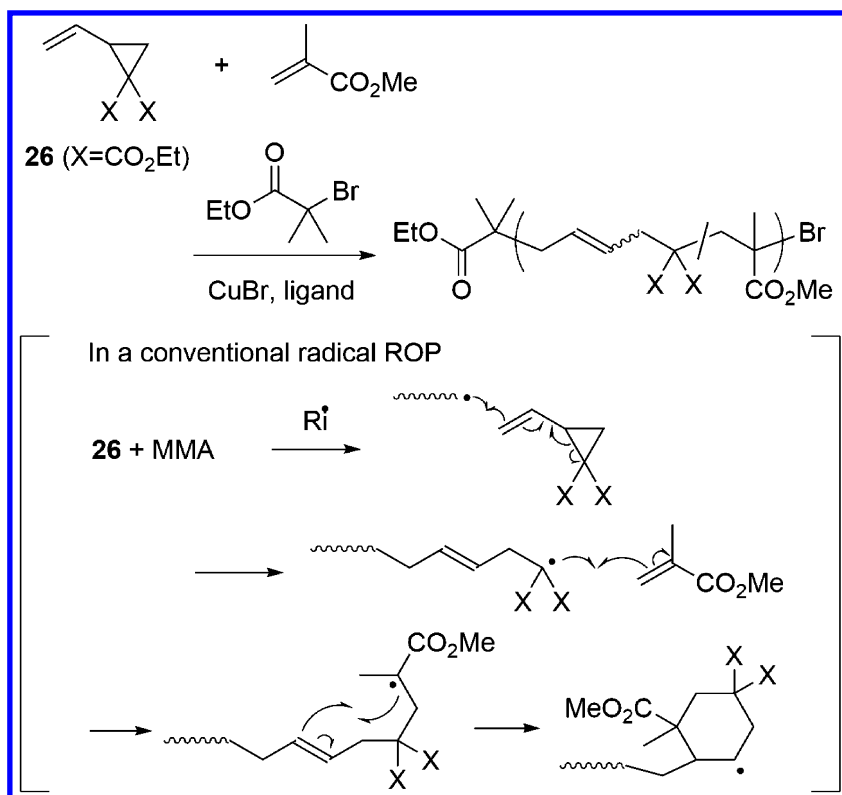
Figure 27. ATRP-type homopolymerization of vinylcyclopropane and the copolymerization of vinylcyclopropane with MMA.

The radical ROP of 10-methylene-9,10-dihydroanthryl-9-spirocyclopropane (**3**) can be successfully controlled using the reversible addition-fragmentation chain transfer (RAFT) technique (Figure 28) (*95*). The resulting polymer has a predictable molecular weight and a narrow molecular weight distribution. The RAFT polymerizations of analogous monomers bearing halophenyl and pyridyl groups have been reported as well (*96, 97*). The resulting polymers can be functionalized through the reactions of the halophenyl and pyridyl groups in the side chains.

Several systems for the living/controlled radical ROPs of seven-membered cyclic ketene acetals have been reported. These systems are based on the NMP, ATRP, and RAFT techniques. The radical ROP of 2-methylene-1,3-dioxepane (**13**) in the presence of 2,2,6,6-tetramethyl-1-piperidinyloxy (TEMPO) results in the corresponding polyesters, which have narrow molecular weight distributions (Figure 29) (*98*). Feeding the second portion of the monomer to the polyester bearing an alkoxyamine moiety at the terminal and then heating the mixture results in the extension of the polyester chain. This demonstrates the living nature of the system.
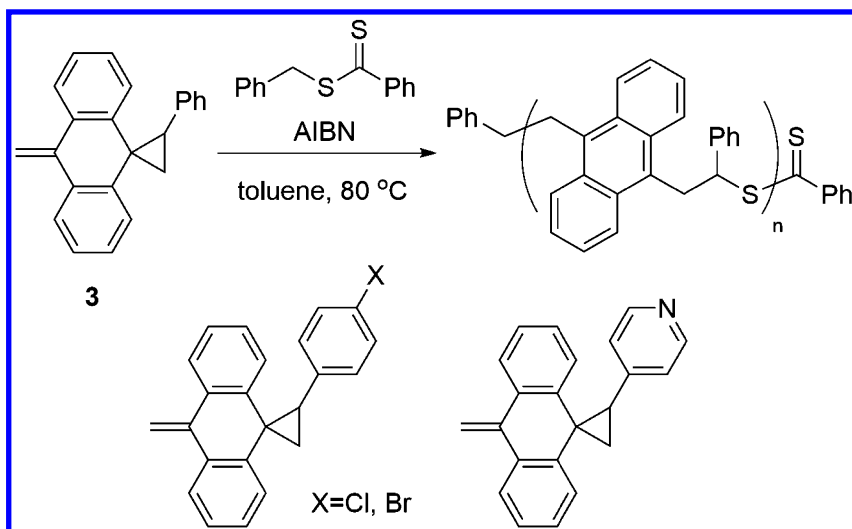
Figure 28. Reversible addition-fragmentation chain transfer (RAFT) polymerization of cyclopropanes bearing an exo-methylene dihydroanthracene moiety.
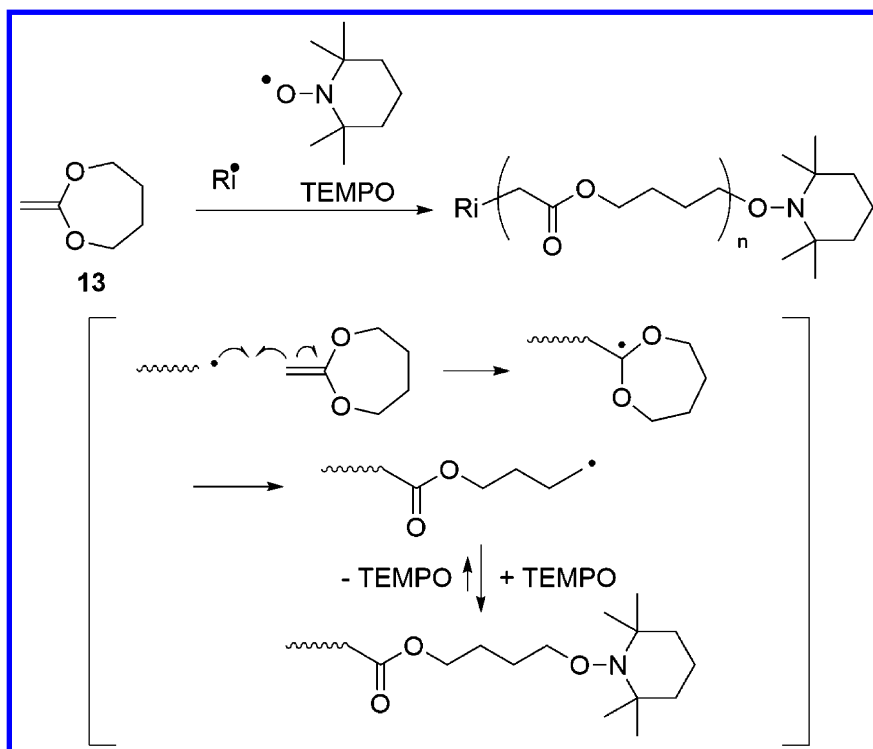

Figure 29. Controlled radical ROP of a cyclic ketene acetal mediated by a nitroxyl radical.

5,6-Benzo-2-methylene-1,3-dioxepane (**14**) also undergoes nitroxide-mediated controlled ROP (Figure 30) (*99*). This system allows for block copolymerization with styrene (*99*) and statistic copolymerization with vinyl monomers such as methacrylate with an oligo(ethylene glycol) chain (*100*). The latter yields a hydrophilic comb-like polymer with hydrolysable ester linkages in the main chain.
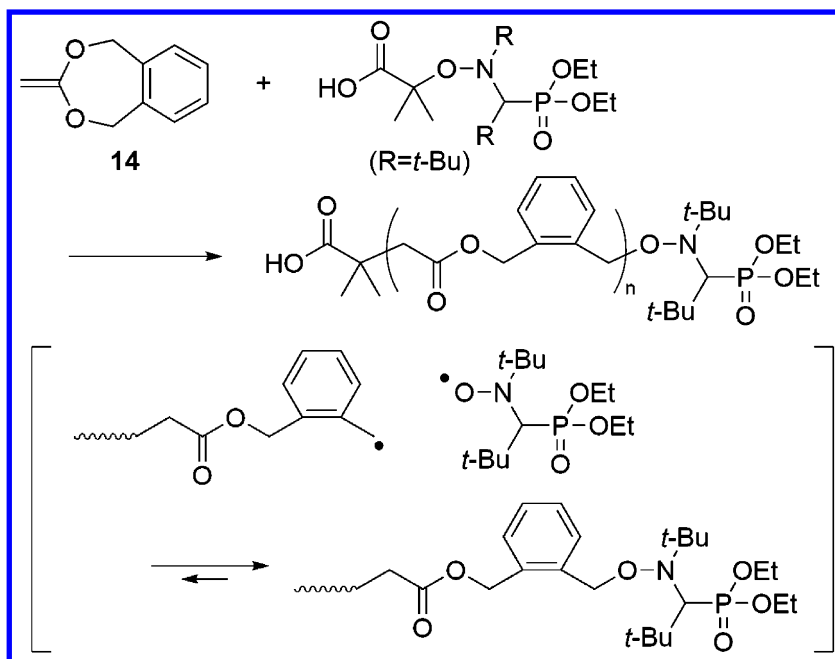

Figure 30. Controlled radical ROP of a cyclic ketene acetal mediated by a nitroxyl radical.

ATRP is also a useful technique for the controlled radical ROP of the seven-membered cyclic ketene acetal **14** (Figure 31) (*101*). The polymerization proceeds in a controlled manner. That is to say, the plot for the corresponding first-order kinetics is a linear one. The resulting polymer is a telechelic polyester: the initiating end is derived from the α-bromo ester used as the initiator and the propagating end has a benzyl bromide-type structure. The molecular weight increases linearly with the rate of monomer conversion, and the molecular weight distribution is narrow. The use of macroinitiators bearing a bromo-functionalized chain end allows for the precise synthesis of block copolymers composed of a vinyl polymer segment and a polyester segment that is formed by the radical ROP of a cyclic ketene acetal (*102*). The statistic copolymerization of **14** and styrene, which can be controlled by the ATRP technique, yields the corresponding copolymers, which bear cleavable ester linkages in their main chains (*103*). A detailed study of the polymer structure revealed that the polymer is not a perfectly linear one but has short branches because of intramolecular chain transfer.

The development of biocompatible and biodegradable materials based on the ATRP-type copolymerizations of **14** is of great interest (*104*, *105*). The ATRP technique also allows for the graft polymerization of **14** from a bromo-ester-type initiator immobilized on the surface of silicon oxide (*106*). The degradability of the grafted chains would be an advantage for the development of functional coatings for biorelated applications.
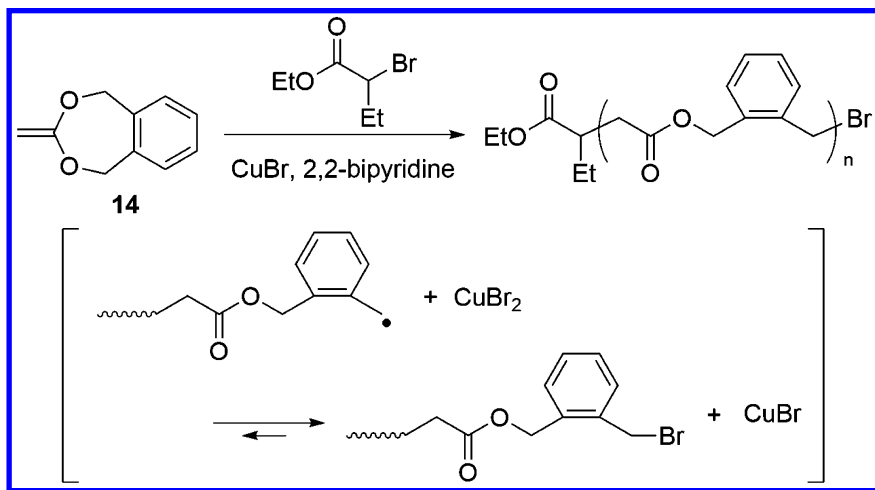

Figure 31. ATRP-type living/controlled radical ROP of a cyclic ketene acetal.

Another reliable tool for controlling the radical ROP of cyclic ketene acetals is RAFT. The radical ROP of **14** is mediated by a dithioester, yielding the corresponding polyester, which bears a dithioester moiety at the chain end (Figure 32) (*107*). The ROP exhibits first-order kinetics and there is a linear relationship between the molecular weight and the monomer conversion rate, demonstrating the living nature of the ROP. The molecular weight distribution is much narrower than that of the polymer obtained by ROP without the addition of the dithioester.

In addition, the copolymerization of 2-methylene-1,3-dioxepane (**13**) with vinyl acetate, which can be controlled by adding a xanthate as a chain transfer agent, has also been reported (Figure 33) (*108*). The resulting copolymers, poly(vinyl acetate)s with ester linkages distributed randomly in the main chains, were degradable under basic conditions. In place of vinyl acetate, other vinyl monomers such as *N*-vinylpyrrolidone, *N*-vinylpiperidone, and vinyl chloroacetate can be also used as the comonomers. Block copolymerization has also been demonstrated using a poly(*N*-vinylpyrrolidone) bearing a xanthate moiety at the chain end as a macroinitiator. Through the copolymerization of 2-methylene-1,3-dioxepane with vinyl acetate and using a small amount of divinyl adipate as a cross-linker in the presence of the macroinitiator, a hyperbranched block copolymer that aggregates into nanoparticles can be synthesized.
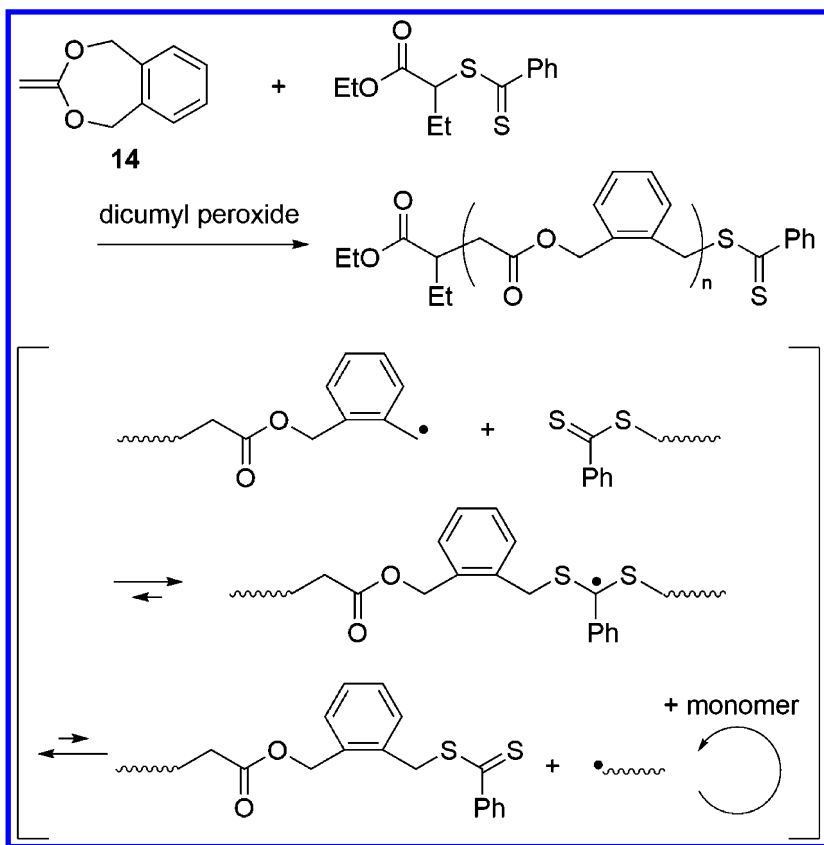
Figure 32. Controlled radical ROP of a cyclic ketene acetal mediated by a dithioester.
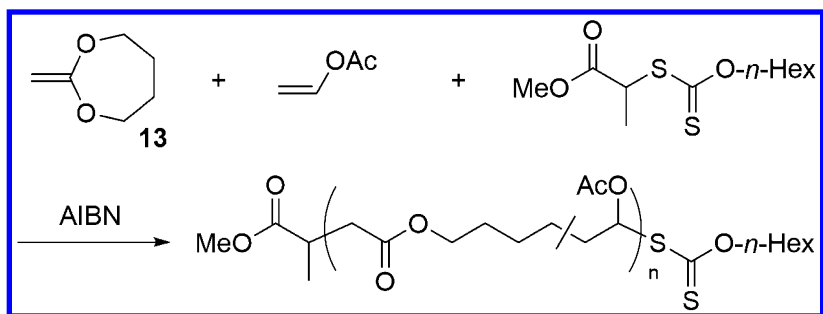
Figure 33. Controlled radical copolymerization of a cyclic ketene acetal with vinyl acetate, mediated by a xanthate.

The controlled radical ROP of a bicyclic monomer through a double-ring-opening reaction has been reported (Figure 34) (*109*). A spiroorthoester bearing an *exo*-methylene group was used as the monomer. When this radical ROP was performed in the presence of TEMPO, the polymerization proceeded in a living fashion, leading to the formation of the corresponding polymers, which had predictable molecular weights and narrow molecular weight distributions. The main chain, which consisted of an ester linkage and a ketone moiety, was potentially degradable by hydrolysis or photolysis.

Figure 34. Nitroxyl radical-mediated radical ROP of a spiroorthoester bearing an exo-methylene group.

Summary

Radical ROP is expected to become a useful tool for synthesizing polymers with main chains containing heteroatoms, which cannot be obtained by the chain polymerization of vinyl monomers. In addition, recent advances in "living"/controlled radical polymerization techniques allow for the control of radical ROPs, resulting in the synthesized polymer chains having predictable molecular weights. For this purpose, NMP, RAFT, and ATRP are the most convenient systems. F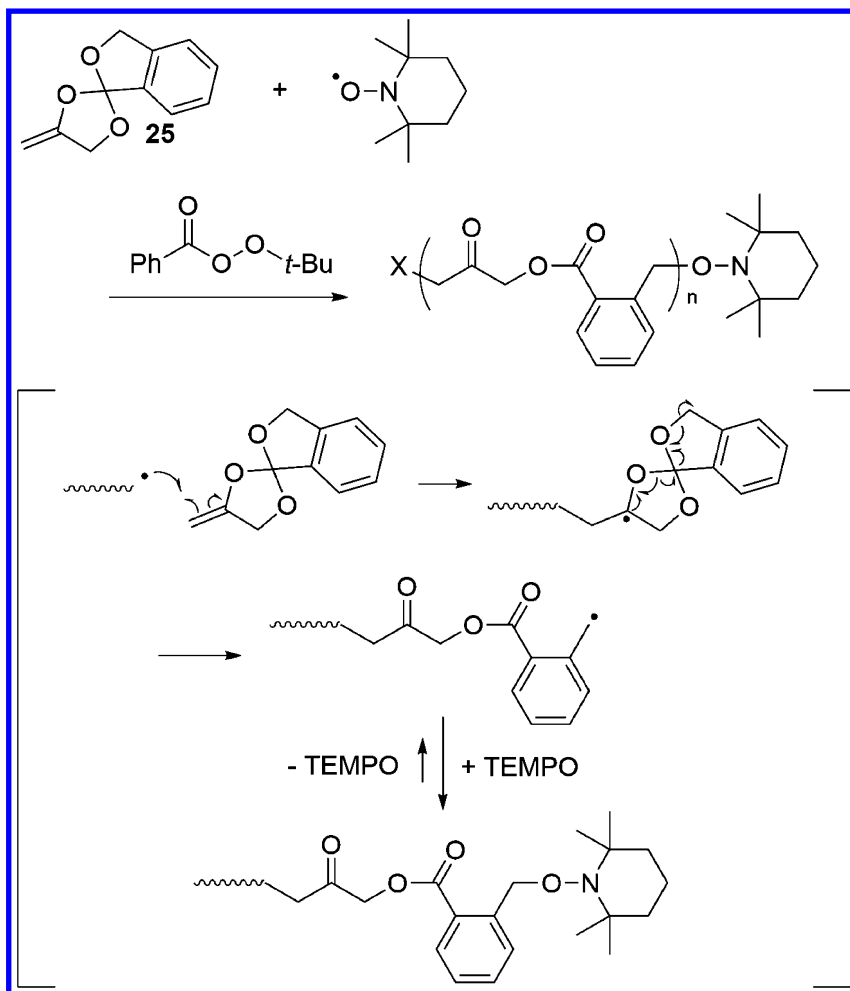urthermore, one of the features of radical ROP that has attracted much attention is that it permits radical copolymerizations with a wide range of conventional vinyl monomers such as styrenics, acrylics, and methacrylics. Through these copolymerizations, various functional groups derived from cyclic monomers can be incorporated into the resulting main chains, which can be hydrolysable and photodegradable. A proper understanding of the mechanisms underlying the radical ROPs described herein should lead to new molecular designs for cyclic monomers. Further, the development of their controlled ROPs will result in the synthesis of novel polymer materials with wide applicabilities.

References

1. Endo, T.; Nagai, D. *Macromol. Symp.* **2005**, *226*, 79–86.
2. Manners, I. *J. Organomet. Chem.* **2011**, *696*, 1146–1149.
3. Nuyken, O.; Pask, S. D. *Polymers* **2013**, *5*, 361–403.
4. Duda, A.; Kubisa, P.; Lapienis, G.; Slomkowski, S. *Polimery* **2014**, *59*, 9–23.
5. Ajellal, N.; Carpentier, J.-F.; Guillaume, C.; Guillaume, S. M.; Helou, M.; Poirier, V.; Sarazin, Y.; Trifonov, A. *Dalton Trans.* **2010**, *39*, 8363–8376.
6. Guillaume, S. M. *Eur. Polym. J.* **2013**, *49*, 768–779.
7. Brocas, A.-L.; Mantzaridis, C.; Tunc, D.; Carlotti, S. *Prog. Polym. Sci.* **2013**, *38*, 845–873.
8. Brown, H. A.; Waymouth, R. M. *Acc. Chem. Res.* **2013**, *46*, 2585–2596.
9. Hunley, M. T.; Orski, S. V.; Beers, K. L. *ACS Symp. Ser.* **2013**, *1144*, 43–57.
10. Mespouille, L.; Coulembier, O.; Kawalec, M.; Dove, A. P.; Dubois, P. *Prog. Polym. Sci.* **2014**, *39*, 1144–1164.
11. Bailey, W. J.; Endo, T. *J. Polym. Sci., Polym. Symp* **1978**, *64*, 17–26.
12. Bailey, J.; Chou, J. L.; Feng, P. Z.; Kuruganti, V.; Zhou, L. L. *Acta Polym.* **1988**, *39*, 335–41.
13. Sanda, F.; Endo, T. *J. Polym. Sci., Part A: Polym. Chem.* **2001**, *39*, 265–276.
14. Endo, T.; Watanabe, M.; Suga, K.; Yokozawa, T. *J. Polym. Sci., Part A: Polym. Chem.* **1987**, *25*, 3039–3048.
15. Endo, T.; Watanabe, M.; Suga, K.; Yokozawa, T. *J. Polym. Sci., Part A: Polym. Chem.* **1989**, *27*, 1435–1438.
16. Endo, T.; Watanabe, M.; Suga, K.; Yokozawa, T. *Makromol. Chem.* **1989**, *190*, 691–696.
17. Endo, T.; Suga, K. *J. Polym. Sci., Polym. Chem. Ed.* **1989**, *27*, 1831.
18. Moszner, N.; Zeuner, F.; Volkel, T.; Rheinberger, V. *Macromol. Chem. Phys.* **1999**, *200*, 2173–2187.

19. Sanda, F.; Takata, T.; Endo, T. *Macromolecules* **1995**, *28*, 1346–1355.
20. Mizukami, S.; Kihara, N.; Endo, T. *J. Am. Chem. Soc.* **1994**, *116*, 6453–6454.
21. Sanda, F.; Takata, T.; Endo, T. *Macromolecules* **1993**, *26*, 5748–5754.
22. Sanda, F.; Murata, J.; Endo, T. *Macromolecules* **1997**, *30*, 160–162.
23. Cho, I.; Song, K. Y. *J. Polym. Sci., Part A: Polym. Chem.* **1994**, *32*, 1789–1791.
24. Hiraguri, Y.; Endo, T. *J. Polym. Sci., Part C: Polym. Lett.* **1989**, *27*, 333–337.
25. Endo, T.; Kanda, N. *J. Polym. Sci., Polym. Chem. Ed.* **1985**, *23*, 1931–1938.
26. Koizumi, T.; Nojima, Y.; Endo, T. *J. Polym. Sci., Part A: Polym. Chem.* **1993**, *31*, 3489–3492.
27. Koizumi, T.; Moriya, O.; Urata, Y.; Nojima, Y.; Endo, T. *Polym. J.* **1995**, *27*, 757–761.
28. Sidney, L. N.; Shaffer, S. E.; Bailey, W. J. *ACS Polym. Prepr.* **1981**, *22*, 373–374.
29. Cho, I.; Gong, N.S. *Polymer (Korea)* **1985**, *9*, 503–509.
30. Evans, R. A.; Rizzardo, E. *Macromolecules* **1996**, *29*, 6983–6989.
31. Evans, R. A.; Rizzardo, E. *Macromolecules* **2000**, *33*, 6722–6731.
32. Evans, R. A.; Rizzardo, E. *J. Polym. Sci., Part A: Polym. Chem.* **2001**, *39*, 202–215.
33. Harrisson, S.; Davis, T. P.; Evans, R. A.; Rizzardo, E. *Macromolecules* **2000**, *33*, 9553–9560.
34. Phelan, M.; Aldabbagh, F.; Zetterlund, P. B.; Yamada, B. *Macromolecules* **2005**, *38*, 2143–2147.
35. Choi, K.; Chon, J. W. M.; Gu, M.; Malic, N.; Evans, R. A. *Adv. Funct. Mater.* **2009**, *19*, 3560–3566.
36. Bailey, W. J.; Kuruganti, V. K.; Angle, J. S. *ACS Symp. Ser.* **1990**, *433*, 149–60.
37. Agarwal, S. *Polym. Chem.* **2010**, *1*, 953–964.
38. Cho, I.; Gong, M. S. *J. Polym. Sci., Polym. Lett. Ed.* **1982**, *20*, 361–364.
39. Bailey, W. J.; Ni, Z.; Wu, S.-R. *J. Polym. Sci., Polym. Chem. Ed.* **1982**, *20*, 3021–3030.
40. Bailey, W. J.; Wu, S.-R.; Ni, Z. *Makromol. Chem.* **1982**, *183*, 1913–1920.
41. Bailey, W. J.; Ni, Z.; Wu, S.-R. *Macromolecules* **1982**, *15*, 711–714.
42. Schulze, T.; Klemm, E. *Angew. Makromol. Chem.* **1995**, *229*, 123–132.
43. Hiraguri, Y.; Aiba, S. *J. Macromol. Sci., Part A: Pure Appl. Chem.* **2014**, *51*, 582–588.
44. Plikk, P.; Tyson, T.; Finne-Wistrand, A.; Albertsson, A.-C. *J. Polym. Sci., Part A: Polym. Chem.* **2009**, *47*, 4587–4601.
45. Hiraguri, Y.; Katase, K.; Tokiwa, Y. *J. Macromol. Sci., Part A: Pure Appl. Chem.* **2005**, *A42*, 901–907.
46. Jin, S.; Gonsalves, K. E. *Macromolecules* **1997**, *30*, 3104–3106.
47. Hiraguri, Y.; Endo, T. *J. Am. Chem. Soc.* **1987**, *109*, 3779–3780.
48. Hiraguri, Y.; Endo, T. *J. Polym. Sci., Part A: Polym. Chem.* **1989**, *27*, 2135–2138.

49. Pan, C.-Y.; Wu, Z.; Bailey, W. J. *J. Polym. Sci., Part C: Polym. Lett.* **1987**, *25*, 243–248.

50. Hiraguri, Y.; Endo, T. *J. Polym. Sci., Part A: Polym. Chem.* **1989**, *27*, 4403–4411.

51. Hiraguri, Y.; Sugizaki, T.; Endo, T. *Macromolecules* **1990**, *23*, 1–5.

52. Bailey, W. J.; Feng, P. *Polym. Prepr.* **1987**, *28*, 154–155.

53. Feng, P. *Chinese J. Polym. Sci.* **1992**, *10*, 350–355.

54. Feng, P. *Chinese J. Polym. Sci.* **1993**, *11*, 153–157.

55. Evans, R. A.; Moad, G.; Rizzardo, E.; Thang, S. H. *Macromolecules* **1994**, *27*, 7935–7937.

56. Phelan, M.; Aldabbagh, F.; Zetterlund, P. B.; Yamada, B. *Polymer* **2005**, *46*, 12046–12056.

57. Sanda, F.; Takata, T.; Endo, T. *Macromolecules* **1994**, *27*, 1099–1111.

58. Koizumi, T.; Ando, T.; Kojima, T.; Endo, T. *Macromolecules* **1998**, *31*, 9096–9098.

59. Endo, T.; Bailey, W. J. *J. Polym. Sci., Polym. Chem. Ed.* **1975**, *13*, 2525–2530.

60. Endo, T.; Bailey, W. J. *J. Polym. Sci., Polym. Lett. Ed.* **1980**, *18*, 25–27.

61. Pan, C.; Lu, S.; Bailey, W. J. *Makromol. Chem.* **1987**, *188*, 1651–1658.

62. Han, Y.- K.; Choi, S.- K. *J. Polym. Sci., Polym. Chem. Ed.* **1983**, *21*, 353–364.

63. Bailey, W. J.; Endo, T.; Gapud, B.; Lin, Y. N.; Ni, Z.; Pan, C. Y.; Shaffer, S. E.; Wu, S. R.; Yamazaki, N.; Yonezawa, K. *J. Macromol. Sci., Chem.* **1984**, *A21*, 979–995.

64. Bailey, W. J.; Kuruganti, V. K. *Polym. Mater. Sci. Eng.* **1990**, *62*, 971–975.

65. Endo, T.; Yako, N.; Azuma, K.; Nate, K. *Makromol. Chem.* **1985**, *186*, 1543–1548.

66. Morris, L. M.; Davis, T. P.; Chaplin, R. P. *Polymer* **2000**, *42*, 495–500.

67. Xu, J.; Liu, Z.-L.; Zhuo, R.-X. *J. Appl. Polym. Sci.* **2007**, *103*, 1146–1151.

68. Sun, L. F.; Zhuo, R. X.; Liu, Z. L. *J. Polym. Sci., Part A: Polym. Chem.* **2003**, *41*, 2898–2904.

69. Roberts, G. E.; Coote, M. L.; Heuts, J. P. A.; Morris, L. M.; Davis, T. P. *Macromolecules* **1999**, *32*, 1332–1340.

70. Undin, J.; Illanes, T.; Finne-Wistrand, A.; Albertsson, A.-C. *Polym. Chem.* **2012**, *3*, 1260–1266.

71. Jin, S.; Gonsalves, K. E. *Macromolecules* **1998**, *31*, 1010–1015.

72. Ren, L.; Agarwal, S. *Macromol. Chem. Phys.* **2007**, *208*, 245–253.

73. Tokiwa, Y. *J. Macromol. Sci., Part A: Pure Appl. Chem.* **2006**, *43*, 1021–1027.

74. Borkar, S.; Sen, A.; Shallenberger, J. R. *J. Polym. Sci., Part A: Polym. Chem.* **2006**, *44*, 1225–1232.

75. Zhang, Y.; Zheng, M.; Kissel, T.; Agarwal, S. *Biomacromolecules* **2012**, *13*, 313–322.

76. Jin, Q.; Maji, S.; Agarwal, S. *Polym. Chem.* **2012**, *3*, 2785–2793.

77. Zhang, Y.; Aigner, A.; Agarwal, S. *Macromol. Biosci.* **2013**, *13*, 1267–1275.

78. Cai, T.; Chen, Y.; Wang, Y.; Wang, H.; Liu, X.; Jin, Q.; Agarwal, S.; Ji, J. *Macromol. Chem. Phys.* **2014**, *215*, 1848–1854.

79. Hiraguri, Y.; Endo, T. *J. Polym. Sci., Part C: Polym. Lett.* **1989**, *27*, 1–4.

80. Ishikawa, T.; Morino, K.; Sudo, A.; Endo, T. *J. Polym. Sci., Part A: Polym. Chem.* **2011**, *49*, 5142–5151.

81. Chaumont, P.; Asgarzadeh, F.; Colombani, D.; Arotcarena, M.; Baudouin, A. *Macromol. Chem. Phys.* **1998**, *199*, 2577–2582.

82. Braunecker, W. A.; Matyjaszewski, K. *Prog. Polym. Sci.* **2007**, *32*, 93–146.

83. Ouchi, M.; Terashima, T.; Sawamoto, M. *Chem. Rev.* **2009**, *109*, 4963–5050.

84. Yamago, S. *Chem. Rev.* **2009**, *109*, 5051–5068.

85. Kamigaito, M. *Polym. J.* **2011**, *43*, 105–120.

86. Moad, G.; Rizzardo, E.; Thang, S. H. *Aust. J. Chem.* **2012**, *65*, 985–1076.

87. Nicolas, J.; Mantovani, G.; Haddleton, D. M. *Macromol. Rapid Commun.* **2007**, *28*, 1083–1111.

88. Le D., B.; Nicolas, J. *Polym. Chem.* **2010**, *1*, 563–598.

89. Kakwere, H.; Perrier, S. *Polym. Chem.* **2011**, *2*, 270–288.

90. Terashima, T. *Polym. J.* **2014**, *46*, 664–673.

91. Sanda, F.; Miyagawa, T.; Endo, T. *Macromol. Chem. Phys.* **1999**, *200*, 1089–1093.

92. Singha, N. K.; Kavitha, A.; Sarker, P.; Rimmer, S. *Chem. Commun.* **2008**, *26*, 3049–3051.

93. Ata, S.; Mal, D.; Singha, N. K. *RSC Adv.* **2013**, *3*, 14486–14494.

94. Sanda, F.; Takata, T.; Endo, T. *Macromolecules* **1994**, *27*, 3982–985.

95. Mori, H.; Masuda, S.; Endo, T. *Macromolecules* **2006**, *39*, 5976–5978.

96. Mori, H.; Tando, I.; Tanaka, H. *Macromolecules* **2010**, *43*, 7011–7020.

97. Nakabayashi, K.; Inoue, S.; Abiko, Y.; Mori, H. *Macromolecules* **2013**, *46*, 4790–4798.

98. Wei, Y.; Connors, E. J.; Jia, X.; Wang, C. *J. Polym. Sci., Part A: Polym. Chem.* **1998**, *36*, 761–771.

99. Tardy, A.; Delplace, V.; Siri, D.; Lefay, C.; Harrisson, S.; Pereira, B. F. A.; Charles, L.; Gigmes, D.; Nicolas, J.; Guillaneuf, Y. *Polym. Chem.* **2013**, *4*, 4776–4787.

100. Delplace, V.; Tardy, A.; Harrisson, S.; Mura, S.; Gigmes, D.; Guillaneuf, Y.; Nicolas, J. *Biomacromolecules* **2013**, *14*, 3769–3779.

101. Yuan, J.-Y.; Pan, C.-Y.; Tang, B. Z. *Macromolecules* **2001**, *34*, 211–214.

102. Yuan, J.-Y.; Pan, C.-Y. *Eur. Polym. J.* **2002**, *38*, 1565–1571.

103. Wickel, H.; Agarwal, S. *Macromolecules* **2003**, *36*, 6152–6159.

104. Lutz, J.-F.; Andrieu, J.; Uezguen, S.; Rudolph, C.; Agarwal, S. *Macromolecules* **2007**, *40*, 8540–8543.

105. Siegwart, D. J.; Bencherif, S. A.; Srinivasan, A.; Hollinger, J. O.; Matyjaszewski, K. *J. Biomed. Mater. Res., Part A* **2008**, *87A*, 345–358.

106. Riachi, C.; Schuwer, N.; Klok, H.-A. *Macromolecules* **2009**, *42*, 8076–8081.

107. He, T.; Zou, Y.-F.; Pan, C.-Y. *Polym. J.* **2002**, *34*, 138–143.

108. Hedir, G. G.; Bell, C. A.; Ieong, N. S.; Chapman, E.; Collins, I. R.; O'Reilly, R. K.; Dove, A. P. *Macromolecules* **2014**, *47*, 2847–2852.

109. Jia, X.; Li, M.; Han, S.; Wang, C.; Wei, Y. *Mater. Lett.* **1997**, *31*, 137–139.

Chapter 3

Effects of Ionization on Tacticity and Propagation Kinetics in Methacrylic Acid Polymerization

Benjamin B. Noble and Michelle L. Coote*

Research School of Chemistry, Australian National University, Canberra ACT 2601, Australia
*E-mail: michelle.coote@anu.edu.au

Theoretical calculations have been performed to model the propagation kinetics and ionization behavior of methacrylic acid (MAA) from first principles. The pK_a values of various COOH groups of chemical species with direct relevance to MAA polymerization have also been calculated. At a given temperature, syndiotacticity increases with solvent polarity and ionization, and herein we show that accurate quantum chemistry can correctly account for these effects and explain their origin in terms of the changing structure of the charged propagating species.

Introduction

The objective of synthetic polymer chemistry is to control the assembly of macromolecules to facilitate alterations to their microstructure and bulk properties. Over the last few decades, living radical polymerization has revolutionized polymer synthesis by allowing precise control of most aspects of polymer microstructure. Unfortunately, these approaches by themselves have no influence on polymer stereochemistry (tacticity), which is usually poorly regulated. Despite being the focus of many pioneering investigations over the last 60 years, the synthesis of stereoregular polymers via radical polymerization has remained enormously challenging (*1*). Since the first attempts to control stereochemistry in radical polymerization in the 1950s, a broad array of strategies

have been developed (Scheme 1), with notable success in some monomer systems (*1*). However, many of these approaches are difficult and expensive to implement, while others have a relatively narrow scope or are simply unable to replicate the high stereoselectivity that can be achieved in contemporary anionic and coordination polymerization. Some of the most effective (and elegant) strategies, such as stereoregular templating (*2–4*), are impractical and could not be readily applied to grams scale polymer synthesis. The strategy that is best able to balance the competing demands of effectiveness and practicality is monomer modification to incorporate bulky (*5–8*), chiral (*9, 10*) and ionic auxiliaries (*11–20*).

Scheme 1. Different strategies for stereocontrol in radical polymerization.

Methacrylic acid (MAA) is a particularly intriguing system for which a variety of polymer tacticities can be targeted depending on pH, countercation identity and solvation conditions. The synthesis of poly(MAA) and its derivatives is of interest more broadly for applications as diverse as pH selective carriers for drug delivery (*21*) to radiological protection (*22*) and reinforcing agents for rubber (*23*). In this work we use quantum chemistry, in addition to drawing on previous experimental work, to explore the propagation kinetics in the radical polymerization of non-ionized and ionized methacrylic acid (MAA).

Previous Experimental Studies of MAA

The radical polymerisation of MAA in bulk and toluene at 60 °C affords polymer with a syndiotactic triad fraction (*rr*) of 45% and 51%, respectively (*24, 25*). Solvation in polar solvents increases this syndiotactic tendency. For instance, in water at 45 °C and DMF at 60 °C, polymer with an *rr* of 64% and 65%, respectively is formed (*17, 20*). Syndiotacticity can be further enhanced by performing polymerizations at reduced temperatures. For instance, the

polymerization of MAA in 2-methylcyclohexanol at 0 °C and isopropyl alcohol at −78 °C afforded polymer with an *rr* of 92% and 95%, respectively (*24*, *26*). More than 60 years ago, it was erroneously reported that methacrylate anions cannot undergo radical polymerization (*27*). It was later clarified that the radical initiator used in this study, hydrogen peroxide, was ineffective at high pH and it was subsequently verified with appropriate initiators that ionized methacrylic acid can undergo radical polymerization; although both propagation and termination are significantly inhibited (*28*, *29*). In addition, Bovey noted that the resultant polymer stereochemistry is pH dependent, with syndiotacticity increasing at high pH (*12*). Since these initial reports, the propagation kinetics of ionized acrylic and methacrylic acid in aqueous conditions has been the subject of a number of pioneering investigations. Kabanov and coworkers found that in addition to pH, the identity of the neutralizing agent also influenced resultant polymer stereochemistry (*13*, *14*). More recently, Gramain found the radical polymerization of the tetramethyl and tetraethyl ammonium methacrylate in aqueous conditions also yielded highly syndiotactic polymer (*16*). Rizzardo et al. used methacrylate salts and water-soluble RAFT agents to synthesize syndiotactic-rich polymer with a low polydispersity and designer end-groups (*17*). The majority of these ionized MAA studies have been performed in aqueous conditions and have found that syndiotactic-rich polymer is formed. Results from these various studies are summarized in Table 1, where it is clear that the tacticity of poly(MAA) can vary significantly depending on the polymerization conditions and the ionization state of the COOH moieties; understanding and modeling these results, is the aim of the present work.

Theoretical Background

Stereochemistry in radical polymerization is determined by the relative orientation of the terminal and penultimate side-chains during monomer addition (Scheme 2). The steric bulk of the penultimate unit blocks monomer addition to the cis-face of the planar radical and thus addition occurs exclusively at the trans-face. Hence, the conformations of the polymer terminus can be classified as either pro-*meso* or pro-*racemo* based on the relative orientation of the terminal and penultimate side-chains with respect to the macromolecular backbone. These configurations can interconvert via rotation of the terminating main-chain C-C bond (indicated by the blue arrow in Scheme 2), without disrupting conjugation between the radical and the terminal side-chain. Thus, it would be reasonably anticipated that these conformers would rapidly equilibrate prior to propagation and hence their concentration would depend only on their thermodynamic stability rather than the rate of their formation. Provided this occurs, tacticity is determined by the relative concentrations of the pro-*meso* and pro-*racemo* conformations and their relative reactivity to monomer addition. Hence, predicting tacticity from first principles requires at least a tetrameric transition state model of the polymer system.

Table 1. Illustrative examples highlighting the effect of solvents and countercations (or neutralizing agents) on the resultant poly(MAA) stereochemistry

Cation	Solvent	T (°C)	Tacticity (%)				Ref
			mm	mr	rr	r	
None[a]	bulk	60	9	46	45	68	(24)
None[a]	toluene	60	8	41	51	71	(25)
None[a]	water	45	4	33	64	81	(17)
None[a]	DMF[b]	60	5	30	65	80	(20)
None[a]	MCH[c]	0	>1	18	82	91	(26)
None[a]	i-PrOH	−78	>1	5	95	98	(24)
H_3N^+i-Bu	water	60	>1	12	87	93	(13, 14)
NH_4^+	water	60	>1	17	83	92	(13, 14)
NMe_4^+	water	60	4	17	79	88	(16)
NEt_4^+	water	60	4	16	80	88	(16)
NEt_4^+	water	5	>1	8	92	96	(16)
Na^+	water	60	5	34	61	77	(13, 14)
Ca^{2+}	water	60	6	36	58	76	(20)

[a] None denotes unionized methacrylic acid.   [b] N,N-dimethylformamide.
[c] 2-methylcyclohexanol.
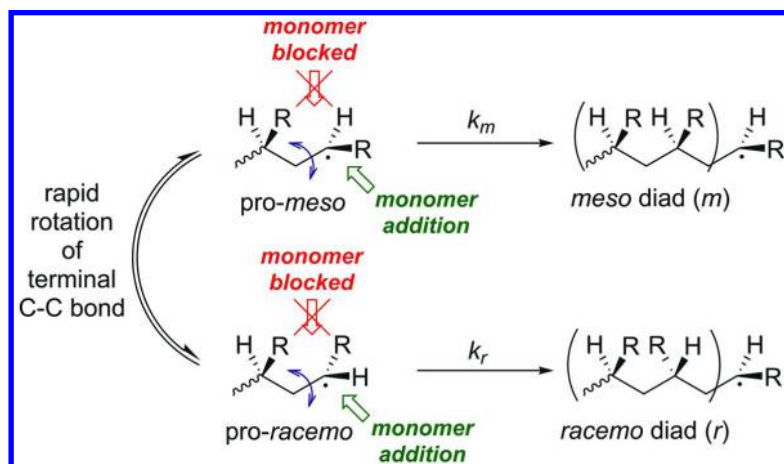
Scheme 2. The mechanism of tacticity determination in free-radical polymerization of a mono-substituted alkene, $H_2C=CHR$. The blue arrow indicates the terminal chain bond.

The authors of earlier computational studies of acrylic and methacrylic acid (*30*), and methyl methacrylate (*31*), have failed to properly appreciate these mechanistic subtleties. Both studies erroneously modelled tacticity by calculating the rate of formation of (trimeric) pro-*meso* and pro-*racemo* conformations. However, as these conformations can interconvert, their concentration is not under kinetic control and thus the rate of their formation is completely irrelevant to the prediction of tacticity. Moreover, both of these studies attempted to predict tacticities, which are diastereoselectivities, using transition structures that only possessed a single stereogenic center.

To avoid such erroneous computational modeling of tacticity, and to properly explain the effect of stereocontrol agents, it is of critical importance that this mechanism is clarified and its subtleties are appreciated. The rational improvement of existing polymerization procedures relies on an adequate understanding of the structure and reactivity of the propagating species. Thus, improving existing stereocontrol is dependent on identifying the underlying mechanism of stereoselection and understanding both its complexities and limitations. In this work, we aim to clarify the propagation kinetics of non-ionized and ionized MAA, using accurate state-of-the-art quantum chemical calculations. First, we examine the propagation kinetics of non-ionized MAA, using quantum chemistry to predict propagation rate coefficients and tacticities from first principles. We utilize these calculations to demonstrate the correctness of the qualitative mechanism presented in Scheme 2 and so clarify the complexities surrounding tacticity determination in radical polymerization. Secondly, we examine the ionization behaviour of model systems relevant to MAA polymerizations and explore the effects of ionization on propagation kinetics.

Computational Procedures

We have used the high-level composite *ab initio* G3(MP2,CC) method (*32*) to calculate propagation barriers, rotational barriers and reaction energies for uncharged dimeric MAA systems. In cases where the either the reactant, transition state or product was anionic, we have (consistently) applied the modified G3(MP2,CC)(+) method. For larger trimeric and tetrameric systems (where these methods are infeasible), we have employed an ONIOM inspired approximation (*33*, *34*), with UMP2/GTMP2Large used to model remote substituent effects. For pK_a calculations on unimeric models (and isobutyric acid), we have used the highly accurate CCSD(T)-F12a approximation (*35*) in conjugation with the VTZ-F12 optimized F12 basis set (*36*). The highly efficient CCSD(T)-F12 approximations afford significantly more accurate results than normal CCSD(T) calculations with a comparable basis set. For instance, the CCSD(T)-F12a approximation in conjugation with a standard AVTZ basis set, has been shown to deliver mean absolute deviations of only 1 kJ mol^{-1} from benchmark CCSD(T)/CBS data for a diverse test set of reaction energies; giving better performance than CCSD(T)/AV5Z (*35*). For pK_a calculations on the larger dimeric and trimeric models (where such high-level calculations are infeasible) we

have used the G3(MP2-CC) (+) and UMP2/GTMP2Large methods, respectively, in conjunction with an ONIOM inspired approximation (*33*, *34*).

Throughout this work we have used M06-2X/6-31+G(d,p) geometries and appropriately scaled frequencies (*37*) to obtain accurate gas-phase free-energies (*38*). Rotational saddle points were identified by performing a relaxed scan around the dihedral of interest and further optimizing the identified approximate saddle point geometry without any constraints at M06-2X/6-31+G(d,p). Except where otherwise noted, solvation free energies were calculated using the COSMO-RS model (*39–41*). Additionally, a small number of calculations were performed on unimeric systems (see text) with the SMD model (*42*) for comparative purposes. The ADF package (*43*) was used to compute COSMO-RS solvation free energies on gas-phase structures at the BP/TZP level of theory (as it was parameterized for), and the remaining parameters were kept as default values (*44*). SMD calculations were performed using Gaussian 09 (*45*), at the M06-2X/6-31+G(d,p) level of theory, with all other parameters kept as their defaults. All standard *ab initio* molecular orbital theory and density functional theory (DFT) calculations were carried out using Gaussian 09 (*45*), with the exception of CCSD(T) and CCSD(T)-F12a calculations, which were performed using Molpro 2012 (*46*, *47*). We note that similar methodology has been previously shown to predict accurate values for the kinetics and thermodynamics of a wide range of reactions, including propagation (*48–50*).

Propagation Kinetics of Non-Ionized Methacrylic Acid

Equilibration of Polymer Conformations

The first question we need to investigate is whether the concentrations of the pro-*meso* and pro-*racemo* radicals can rapidly interconvert on the timescale of a propagation step or not (see Figure 1). As noted above, if they can, then their concentrations depend only on their relative free energies, rather than the kinetics of their formation, and tacticity predictions can be simplified accordingly (see Scheme 2). To demonstrate that pro-*racemo* and pro-*meso* conformations can rapidly interconvert, the rotational Gibbs free energy barriers around the terminal chain bond (indicated θ in Figure 1) were calculated. For linear conformations, this barrier was found to be very modest; only 17 - 18 kJ mol^{-1} (depending on the solvation conditions) relative to the global minimum conformation. Unsurprisingly, this barrier was larger in helical conformations; increasing to 27 - 28 kJ mol^{-1}. In addition, the barrier for the conversion of linear and helical conformations (indicated φ in Figure 1) was also examined. This barrier was found to range between 20 - 25 kJ mol^{-1}, depending on other conformational aspects of the polymer terminus. In contrast to these very modest rotational barriers, the Gibbs free energy barrier for propagation in typical radical polymerizations ranges from 45 - 60 kJ mol^{-1} (depending on the monomer system, temperature, solvation conditions etc.). These results unequivocally demonstrate that both pro-*meso*/ pro-*racemo* and linear/ helical conformations can equilibrate prior to propagation; as such rotations would be several orders of magnitude faster than propagation.
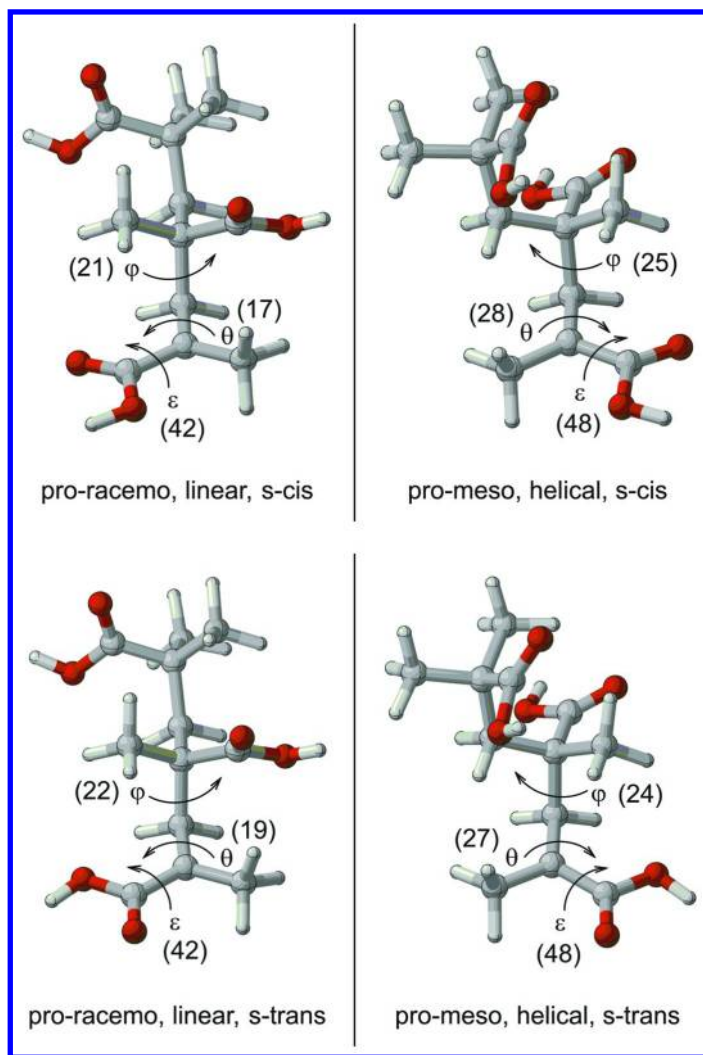
Figure 1. The geometries of the lowest energy pro-racemo and pro-meso conformations of s-cis and s-trans type radicals. Various rotations are indicated (θ, φ and ε), with their corresponding Gibbs free energy barrier (in kJ mol^{-1}) relative to the global minimum conformation stated in parentheses.

The only high energy rotation that would be expected in poly(MAA) systems is around the terminal COOH group (indicated ε in Figure 1). This rotation, which converts s-cis to s-trans radicals (and vice versa), disrupts conjugation between the COOH group and the C-centered radical. This rotational barrier was found to be more comparable to propagation, around 42 - 48 kJ mol^{-1} depending other conformational aspects of the polymer terminus. Collectively, these results indicate that the only aspect of polymer conformation that could be under some kinetic control is the population of s-cis/ s-trans radicals.

Importance of Explicit Solvent Interactions

COOH moieties have a well-known tendency to form 6 membered cyclic H-bonded dimers in non-polar solvents. To investigate the stability of these H-bonded dimers for MAA, the Gibbs free energy for their formation was calculated from first principles. In the gas phase the H-bonded dimer is (unsurprisingly) quite stable; by around 20 kJ mol^{-1} compared to separated monomer units. In water the H-bonded dimer is unstable and solvation of the component MAA units is significantly more favorable; by around 15 kJ mol^{-1}. This suggests that COOH dimerization in aqueous conditions is negligible and so should not be considered for studies of propagation kinetics. In bulk MAA, COOH dimer formation is predicted to be slightly unfavorable (by 0.4 kJ mol^{-1}). However, we should note that applying continuum solvation corrections in bulk monomer may not accurately describe the tendency of COOH groups to form dimers. Indeed, as Deglmann noted, dimerization would decrease the effective polarity of the solvent mixture (*51*). This reduction in polarity would make the formation hydrogen bonded dimers more energetically favorable, causing further dimerization of COOH groups (and further reduction in solvent polarity) until an equilibrium point is reached. It is quite unclear if COSMO-RS (or indeed any other continuum solvent model) can properly account for the dynamic nature of these effects and to what extent these effects are implicitly accounted for by the solvent model. Thus, it is difficult to accurately determine the dimerization energy of COOH moieties in bulk MAA, although it seems likely that some portion of the solution would form dimers.

Propagation Kinetics and Tacticity

As the rotational barrier around the terminal COOH group is comparable to the range of typical barriers for propagation, it is somewhat unclear if s-cis and s-trans radicals can completely equilibrate or if their concentration might be under some kinetic control. Thus, the propagation of s-cis and s-trans type radicals was considered separately. While our prior calculations suggest that a significant portion of the COOH units of MAA exist as dimers in bulk solution, unfortunately we found that the computational cost associated with modelling these dimers in kinetic calculations was prohibitive. As such, we calculated the predicted kinetics without any explicit treatment of COOH dimers in the respective chemical models of propagation. A potential energy surface (PES) for propagation of s-trans type trimer radicals (in bulk and aqueous solution) is depicted in Figure 2. A very similar surface is observed for s-cis radicals, although both *meso* and *racemo* propagation barriers were slightly larger (by around 3 kJ mol^{-1}) on account of their slightly more stable reagent conformers and slightly less stable transition structures. However, the predicted stereoselectivities were found to be fairly independent of the conformation of the terminal COOH group, varying by less than 0.5 kJ mol^{-1} between the s-cis and s-trans surfaces.
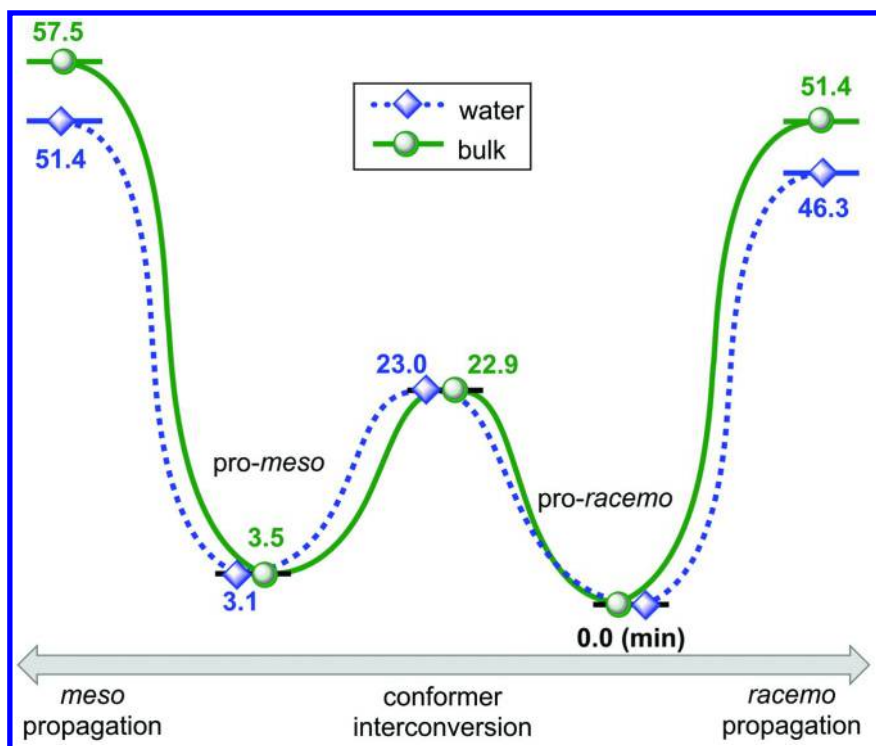
Figure 2. The potential energy surface (in kJ mol⁻¹) for the propagation of an s-trans MAA trimer in bulk (green line) and aqueous solution (blue line) at 25 °C. The rotational barriers for the interconversion of the lowest energy s-trans pro-racemo and pro-meso conformation are also indicated for comparison.

Given the barrier for s-cis to s-trans conversion is close to that for propagation, it is somewhat unclear if s-cis and s-trans type conformations would be able to fully equilibrate prior to propagation. However, these calculations suggest that s-cis/s-trans radicals possess nearly identical stereoselectivity, although their reactivity difference may have some effect on the absolute propagation rate. In any case, the s-cis/s-trans equilibration is still around 4-8 kJ mol⁻¹ more favorable than propagation at the present level of theory and so for the purposes of this work we have assumed that they do equilibrate on the timescale of a propagation step. Thus, we have calculated an effective barrier using the lowest energy reagent conformation and the lowest energy transition state conformations, regardless of the conformation of the radical. The theoretically calculated propagation rate coefficients and tacticities are given in Table 2, with corresponding experimental values shown for comparison (*52*, *53*).

Table 2. A comparison of theoretical and experimentally derived propagation rate coefficients (k_p), Arrhenius parameters (E_a and A) and tacticity.[a]

Solvent	Bulk		Water	
	Theory	Exp	Theory	Exp
log k_p	3.68	4.76	4.55	3.73
E_a	15.0	16.1 ± 1.6	10.0	15.0 ± 0.3
log A	6.31	5.58	6.30	6.44
tacticity (r)	91%	68%	87%	81%

[a] log k_p and log A given in L·mol^{-1}·s^{-1}, E_a is given in kJ mol^{-1}. Experimental values taken from references (*17*), (*24*), (*52*) and (*53*).

Comparing the theoretical predictions with experiment in Table 2, we note that there is reasonable agreement, to within an order of magnitude, in the k_p across both solvent systems. The theoretical results also correctly predict that k_p increases by roughly an order of magnitude in aqueous solution compared to in bulk MAA. The Arrhenius parameters show a somewhat larger deviation, but are still within the expected range for a first principles prediction of a rate coefficient, particularly in such a highly solvent sensitive system. The activation energy (E_a) in water was found to be around 5 kJ mol^{-1} below the experimental value, although the respective frequency factors (A) were in reasonable agreement. Conversely, for bulk MAA, E_a agreed well with experiment, while A was overestimated by around an order of magnitude. The calculated results correctly predict an increase in propagation rate coefficient of around an order of magnitude moving from bulk to water, but assign this increase to enthapic rather than entropic effects. While this latter result is contrary to the experimental data, it is not surprising given the use of continuum solvent models for both systems. Continuum solvent models attempt to describe solvation, which is a very complex phenomenon, using a variety of physical approximations. Such models can recreate the average effect of solvation reasonably well; however they may not adequately describe more subtle explicit interactions, such as the dynamic hydrogen bonding effects, expected in these systems. The present results highlight that continuum models can predict variations in reactivity quite well, but need to be employed cautiously in systems were explicit solute solvent interactions are present.

The theoretical predictions of tacticity presented in Table 2 agree qualitatively with experiment; correctly predicting the modest syndiotactic preference of MAA. Quantitatively, tacticity is well predicted in aqueous solutions; with the 6% discrepancy from experiment corresponding to an error of only 1 kJ mol^{-1} in the stereoselectivity. In addition to the tacticities reported in Table 2, we predicted tacticities of $r = 95\%$ in methyl cyclohexanol at 0 °C and $r = 99\%$ in isopropyl alcohol at −78 °C. These tacticities were also in good agreement with experimental values of 91% and 98%, respectively. This level of agreement corresponds to a consistent overestimation of the syndiotactic selectivity (relative to experiment)

on the order of 1 kJ mol⁻¹, which is reasonably minor in the context of a quantum chemical calculation. However, the tacticity prediction in bulk deviated by 23% from the experimental value, which corresponds to an error of around 4 kJ mol⁻¹ in the stereoselectivity. As tacticity is dependent on the relative energy difference of quite similar reactions, large amounts of intrinsic error cancellation would be expected and so such a large deviation is quite surprising. It is likely that this deviation originates from a failure to consider explicit COOH dimers when modelling propagation in bulk. Such interactions would increase the effective steric bulk of the COOH groups. This increase in the steric bulk of the side-chains would be expected to alter the underlying stereoselectivity of propagation, thereby decreasing syndioselectivity in a manner analogous to bulky methacrylates (*54*). While explicitly modeling solvent interactions around the COOH groups would likely improve the agreement with the experimentally determined parameters, such considerations would be computationally prohibitive at the high levels of theory used here, and are beyond the scope of the present work.

In contrast to the present results, the previous theoretical study (*30*) that (incorrectly) equated the rate of formation of pro-*meso* and pro-*racemo* conformations to tacticity, would have concluded that poly(MAA) is slightly isotactic; as transition states leading to pro-*meso* conformations were found have lower electronic energies than the corresponding pro-*racemo* structures. This inference is completely contrary to experimental data, further demonstrating the importance of modelling stereoselectivity with an appropriate chemical model and a kinetically correct mechanistic scheme (in addition to choosing sufficiently accurate theoretical procedures).

Polymerization of Ionized Methacrylic Acid

Having examined the non-ionized MAA systems, we now consider the effects of deprotonation of the propagation kinetics. While the radical polymerization of ionized MAA has attracted significant interest, the exact structure of the propagating species under different conditions remains quite speculative. It is well known that for the monomeric species the degree of ionization is identical to degree of neutralization. However, this correlation is not valid for the polymeric species because of differing pK_a values (and thus differing degrees of ionization at a particular p*H*) and because of the accumulation of countercations on surface of the polyanion (*53*). These differing pK_a values may lead to an exchange of protons and/or countercations between the COO⁻ groups of the monomer and the polymer terminus (*53*). Thus, the precise structure of the polymer terminus, which is likely influenced by the identity of the countercation, degree of ionization and ionic strength, may also vary with conversion. These complexities make the experimental analysis of ionized MAA polymerizations extremely difficult and hence it is not possible to unambiguously determine and validate different kinetic models of propagation.

Clearly it would be desirable to clarify the structure of the polymer terminus in ionized conditions and the mechanism of propagation. However, determining the acidity of all the relevant COOH groups in an MAA polymerization is

difficult or even impossible with experimental techniques. While measuring the pK_a values of isolated MAA monomer and poly(MAA) is straightforward, it is generally not possible to apply similar experimental methodology to the polymer terminus because of the very low concentration of radical chain-ends in the polymerising medium. As radicals are known to influence the stability of conjugated (*55*) and even remarkably non-conjugated anions (*56*), it cannot be assumed that the COOH moieties of the polymer terminus would be deprotonated in an analogous manner to the main chain. This is a situation where theoretical chemistry can provide meaningful insights into the underlying structure of the polymer terminus, which is inaccessible from direct experiments.

pK_a Values of Poly(MAA)

To clarify the protonation structure of the polymer terminus under different conditions, the pK_a values of various model systems were calculated from first principles using a proton exchange approach. Isobutyric (*57*), glutaric (*22*) and tricarballylic acid (*22*) were selected as reference acids for monoprotic, diprotic and triprotic systems, respectively. Prior to discussing these pK_a values, the accuracy of the unimeric pK_a predictions was rigorously examined. We note the excellent agreement (to within 0.5 pK_a units) between the predicted pK_a values (see Figure 3) and the experimentally determined values of 4.65 for methacrylic acid (*58*) and 5.03 for chain (pivalic acid) (*59*). To assess the influence that the continuum solvation model has on these values, we tested the use of an alternative model, SMD. The absolute pK_a values predicted with SMD were found to be consistently below those predicted by COSMO-RS; Mon: 4.0, Chain: 5.0 and Rad: 6.9. These discrepancies are reasonably systematic and do not significantly affect the relative pK_a values of the unimeric models. These results suggest that the predicted pK_a values are fairly insensitive to choice of the continuum solvent model and so very high accuracy could be anticipated. Having confirmed the high accuracy of the predicted pK_a values, we will now discuss their origin and significance in more detail.

Interestingly, the calculated pK_a values in Figure 3 indicate that the COOH group conjugated to the carbon radical is significantly less acidic than the COOH groups of either the monomer or a model polymer chain segment. These differences were found to originate entirely from their respective gas-phase acidities and can be rationalized by considering the effect of cross-conjugation between the C-centred radical and the COOH/ COO$^-$ group. When the COOH is protonated, the C-centred radical can be delocalized on the carbonyl O atom. However upon deprotonation, this resonance is inhibited by the competing delocalization of the O anion in the COO$^-$ group. Hence, deprotonation disrupts the delocalization of the radical and is thus significantly more unfavourable than in the comparable non-radical systems. This qualitative rationale is supported by M06-2X/6-31+G(d,p) spin densities, which indicate that the C-centred radical is relatively delocalized in the protonated structure (0.84) and significantly more localized in the deprotonated structure (0.96).
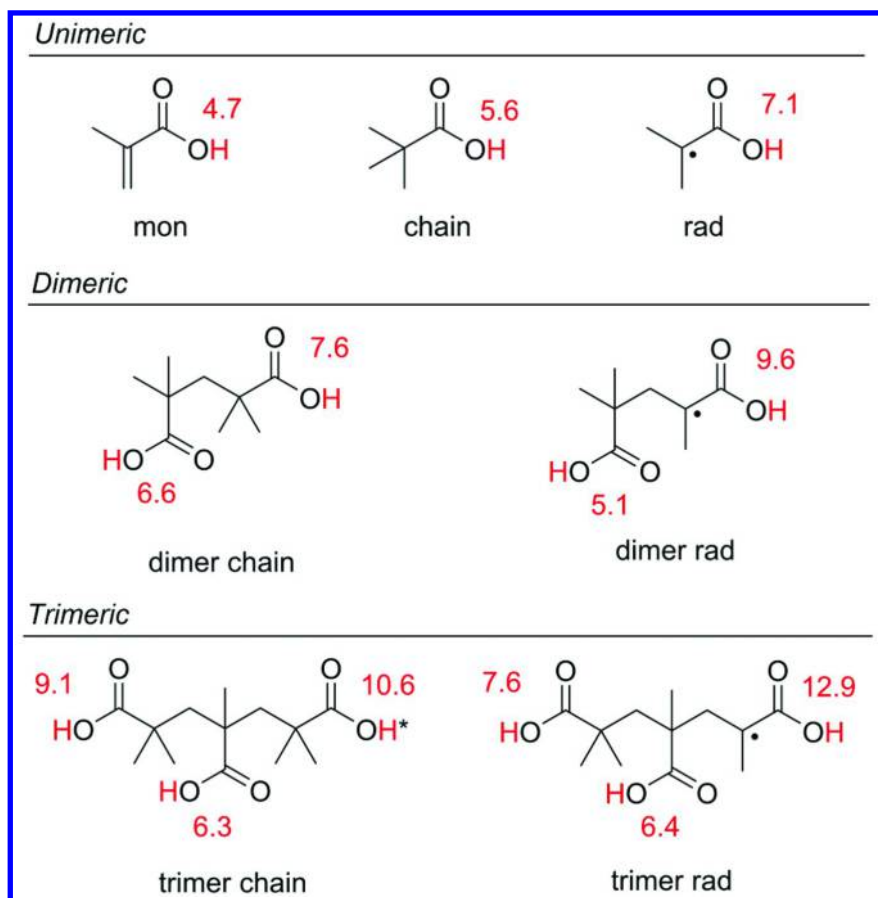
*Figure 3. pK_a values of various unimeric, dimeric and trimeric models relevant to MAA polymerization. * Indicates that the respective proton is transferred to the adjacent COO[−] group prior to deprotonation (see text).*

Having established the influence of the conjugated substituent on COOH acidity, larger and more realistic dimeric and trimeric models were considered. Recently, it was reported that some types of distonic radical anions show remarkable stability compared with analogous non-radical species (*56*). Thus, we sought to examine if such stabilization could increase the acidities of remote COOH groups of the poly(MAA) terminus. Indeed, we found that the penultimate COOH unit of the dimer radical model is more acidic than the comparable dimer chain system. However in contrast, the pK_{a1} value for the penultimate COOH moiety in the trimer radical system was very similar to the corresponding dimer and trimer chain. Thus, it appears that long-range stabilizing interactions in these poly(MAA) distonic radical anions are negligible, which would be anticipated on the basis of the relatively high localization (and thus low polarizability) of

the C-centred radical and the high dielectric constant of the aqueous reaction medium (*56*). Instead, the relatively low pK_{a1} in the dimer radical compared to the chain systems probably results from the different stabilities of the intramolecular H-bonds that are formed upon ionization. A similar effect was observed in the trimeric systems, with pK_{a2} of the trimer radical being significantly below that of the corresponding trimer chain model.

Given the significant influence of the (conjugated) substituent on the unimeric pK_a values, it is interesting to contrast the successive ionization behaviour of the trimer chain and trimer radical systems. In the trimer chain system, the first ionization occurs at the central COOH moiety. As anticipated, the second ionization is accompanied by a proton transfer, which protonates the central COO$^-$ at the expense of the remaining terminal COOH group. This proton transfer reduces electrostatic repulsion by maximising the separation between the two resultant COO$^-$ groups. As expected, an analogous proton transfer also occurs in the respective triprotic reference acid, Tricarballylic acid. However, in the trimer radical system no proton transfer occurs between the first and second ionization steps. Remarkably, deprotonating the COOH conjugated to the terminal radical is so unfavourable that ionization of the adjacent (penultimate and antepenultimate) COOH groups occurs instead.

Given that Deglmann and co-workers have performed similar calculations on acrylic acid (AA) (*51*), it is worth briefly comparing their results with the present MAA systems. In the AA systems, Deglmann noted no significant differences between the pK_a values of the COOH moieties of acrylic acid, with all solution-phase acidities differing by less than 1 pK_a unit. We confirmed this earlier computational result with our high level theory (CCSD(T)-F12a/VTZ-F12//M06-2X/6-31+G(d,p) and COSMO-RS solvation corrections), which affords predicted pK_a values of 3.6 for AA monomer, 4.6 for a unimeric AA radical and 4.8 for unimeric AA chain (which is also the reference acid). The results indicate that the cross-conjugation in AA systems is much weaker than in the corresponding MAA models reported in this work.

Ionization of Polymerizing Methacrylic Acid Solutions

These theoretical pK_a values provide a foundation on which to predict the ionization behaviour of polymerizing MAA solutions. However, we should note that these theoretically predicted pK_a values implicitly assume infinite dilution of solutes and hence zero ionic strength. Clearly, the ionic strength of actual polymerizing MAA solutions is non-zero and at high ionic strength Debye shielding would significantly influence these pK_a values. While the monovalent salts of MAA are strong electrolytes, the corresponding salts of poly(MAA) are weak polyelectrolytes and thus the ionic strength of a polymerizing solution decreases with an increase in monomer conversion. As such, the Debye length would depend on the initial monomer concentration and increase with conversion over the course of a polymerization. While incorporating the effects of ionic strength into first principles pK_a predictions is not straightforward, its influence

on speciation can be understood more qualitatively by comparing the Debye length (κ^{-1}) of different solutions to the separation between the COO$^-$ moieties of the polymeric systems. We should emphasize that it is our aim is to explore the polymerization of MAA under a diverse range of conditions and not simply the high ionic strength/ low conversion regimes relevant to PLP-SEC experiments.

At high ionic strengths, Debye shielding would likely screen repulsion between the adjacent COO$^-$ groups on the polymer terminus and chain. Thus, direct conjugation effects would likely be the largest influence on the acidities of the different COOH moieties and hence the ionization behavior would probably be best described by the unimeric pK_a values. Even under the high ionic strength regime, the variable acidity of the COOH groups significantly affects speciation between pH = 4 to 8 (see Figure 4). For instance, at pH = 6, most of the COOH groups of the monomer (95%) and the polymer chain (71%) would be ionized, compared with only a small fraction of polymer terminus (7%). At lower ionic strength, Debye shielding would no longer screen repulsion between the adjacent COO$^-$ groups on the polymer terminus and polymer chain. As such, the pK_a values of the polymer terminus and main-chain would be influenced by the ionization state of the nearest adjacent COOH/COO$^-$ group(s). Thus, the tendency or the polymer terminus to ionize would be described by the pK_{a2} of the dimer radical model, while the ionization of the polymer chain would be described first by the pK_{a1} and then subsequently by the pK_{a3} value of the trimer chain model. The larger variation in the COOH acidities would lead to a more dramatic speciation difference with pH (see Figure 4).

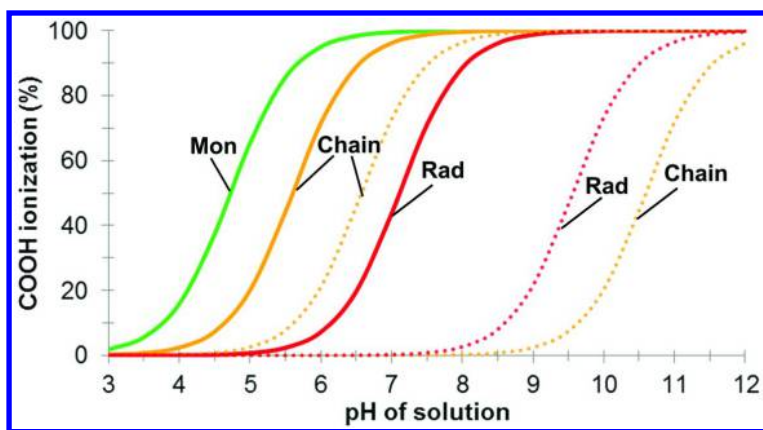*Figure 4. The effect of pH on the ionization of COOH moieties of the polymer radical (Red), main chain (yellow) and monomer (green). Solid lines indicate the predicted speciation using unimeric pK$_a$ values, which is relevant at high ionic strength (I). Dashed lines indicate the speciation predicted by dimer radical (pK$_{a2}$) and trimer chain (pK$_{a1}$ and pK$_{a3}$) values, which is relevant at lower I.*

Effect of Ionization on the Propagation Kinetics

Having established the relative acidities of the COOH groups in a MAA polymerization, the effects of deprotonation on propagation were examined using progressively ionized models. These models neglect any explicit interactions between the polymer terminus and countercations. Nevertheless, these calculations are expected to provide a reasonable, albeit imperfect model for systems with large diffuse countercations, such as $^+NMe_4$ and $^+NEt_4$. In addition to neglecting explicit countercation effects, we should again emphasize that such quantum chemical calculations implicitly assume solvation at infinite dilution and so completely neglect Debye shielding effects. To minimize inaccuracies incurred from the use of continuum solvent models, the barriers and reaction energies for the ionized systems were calculated via a Hess's law thermocycle using experimentally referenced solution-phase acidities and the fully protonated data as a reference. This approach implicitly corrects for errors arising from the treatment of intramolecular H-bonds and anionic systems with continuum solvation models.

Prior to considering larger oligomer systems, the kinetic effects of ionization of the COOH groups were examined using a relatively small dimer transition state model (See Figure 5). Upon ionization of the monomer, the barrier to propagation increases significantly (by around 7 kJ mol^{-1}) as the incoming methacrylate anion hydrogen bonds to the terminal COOH group. This H-bond was found to be very short (~1.4 Å) and in the gas-phase C-C bond formation was followed by rapid hydrogen transfer to the new terminal COO$^-$ group. Ionization of the monomer was found to have no significant effect on the thermodynamic favorability of addition. Remarkably, this hydrogen bonded transition structure can itself be used to qualitatively explain kinetic effects observed in experimental PLP-SEC studies. In these studies, a decrease in both E_a and A is observed with increasing monomer ionization. We speculate that these decreases could be caused by the formation of a strong hydrogen bond (upon ionization) between the radical chain-end and incoming monomer. Such a bond would likely stabilize the transition structure enthapically and so lower E_a but would also significantly increase its rigidity and so also decrease A. Ionization of both COOH groups dramatically increases the barrier for propagation (by more than 20 kJ mol^{-1} compared to the fully protonated structure) and also significantly reduces its thermodynamic favorability. As argued quite intuitively in classic studies of ionized MAA propagation, these effects are readily attributable to the electrostatic repulsion between the adjacent COO$^-$ groups of the monomer and radical. However, as discussed by Buback and co-workers, electrostatic repulsion between COO$^-$ groups does not play a significant role in PLP-SEC experiments, which are performed at high ionic strength where repulsive interactions are adequately screened (*53*).
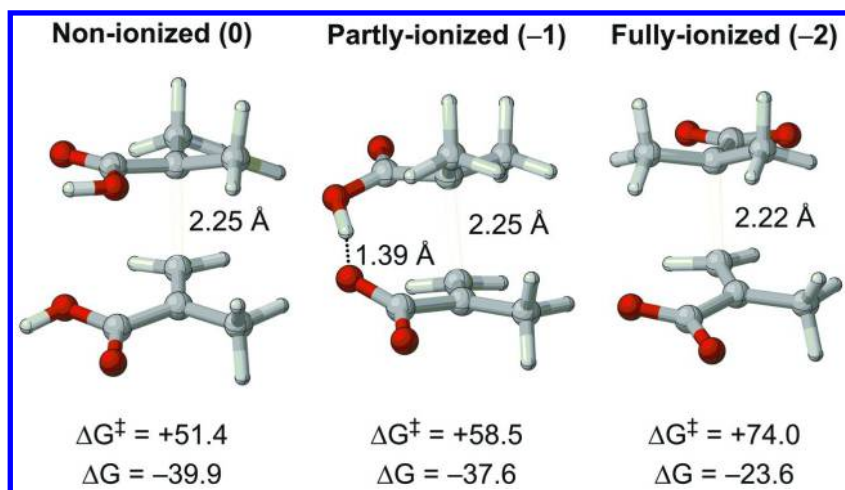
Figure 5. A comparison of progressively ionized dimeric transition structures (charge given in parenthesis), respective aqueous barriers and corresponding reaction energies (in kJ mol⁻¹) at 25 °C. Forming C-C bond and H-bond distances are indicated.

These calculations suggest that at high pH, under conditions where adjacent COO^- repulsion is not adequately screened (i.e., low ionic strength), addition of methacrylate anions to the ionized radical terminus would be very slow. This does not necessarily preclude propagation completely, as countercation condensation may still facilitate some chain growth. While reports of propagation rates coefficients for ionized MAA at low ionic strength are rare, it is interesting to compare the results of Sontag and co-workers (*60*) to the present calculations and PLP-SEC studies. Using ESR, Sontag estimated the propagation rate for ionized MAA at high pH at very low ionic strengths, finding a k_p of 15 L mol⁻¹ s⁻¹ (*60*). Interestingly this value is around a factor of 30 smaller than a comparable value determined at high ionic strengths by Buback and co-workers, using PLP-SEC experiments (*53*). While this difference may simply reflect uncertainties in the ESR determined rate coefficient, it could also be indicative of ionic strength effects on propagation rate. Indeed, Sontag and co-workers also found that under such high pH low ionic strength conditions, poly(MAA) showed an enhanced tendency to depropagate and bimolecular termination was retarded, presumably because of electrostatic repulsion between the ionized polymer termini (*60*).

To allow rough predictions of stereoselectivity under ionized conditions, monomer addition via this hydrogen bonded transition state was examined for trimeric radicals. The geometries of the lowest energy syndiotactic and isotactic transition states for the addition of ionized monomer to trimeric poly(MAA) are shown in Figure 6. The predicted stereoselectivity for these additions is r = 93% at 25 °C, increasing from r = 89% for the corresponding non-ionized reaction. Interestingly, these results suggest that even ionizing the monomer notably increases the stereoselectivity of propagation. While further ionization of these propagating isotactic and syndiotactic polymer chains could also be investigated in a similar manner, we found the computational cost associated with these predictions was prohibitive. It is also unclear if such predictions of tacticity and propagation rate would be relevant to any practical systems and so correlating these predictions with experimental data would be very difficult. As such, we limit our focus to the present mono-anionic transition states, which are expected to provide reasonable chemical models, even at high ionic strength.
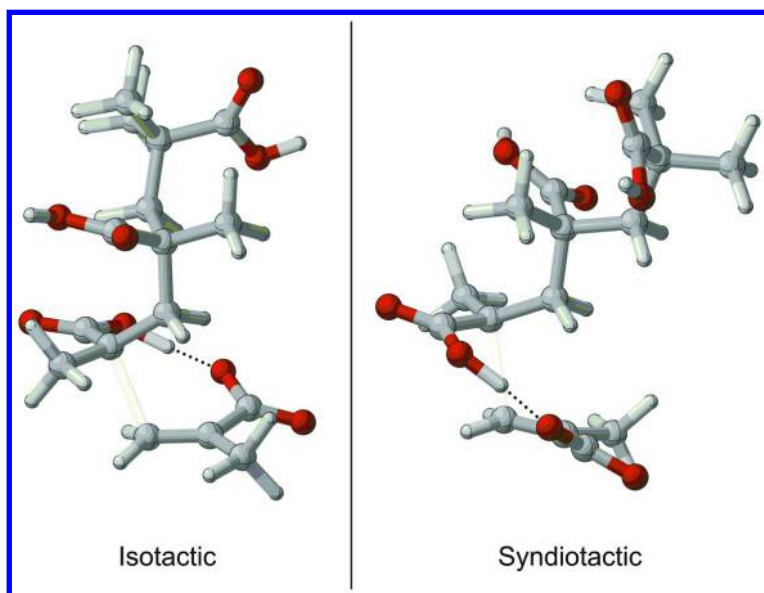
Figure 6. The geometries of the lowest energy transition states leading to isotactic (meso) and syndiotactic (racemo) addition of ionized monomer to a poly(MAA) trimer.

Conclusions

Returning now to the experimental data of Table 1, where it is clear that a given temperature, syndiotacticity increases with solvent polarity and ionization, we note that accurate quantum chemistry can correctly account for these effects and explain their origin (see Figure 7). In particular, in an ionized MAA

polymerization the formation of hydrogen bonds in the transition states between the incoming monomer and radical leads to an increased syndiotactic tendency. Ionization of the COOH groups of the polymer chain itself would likely increase this syndiotactic selectivity further, although under high ionic strength conditions the resultant electrostatic repulsion may be at least partly screened by Debye shielding. In bulk MAA polymerizations, the syndiotactic tendency is lowered because hydrogen bonding of the side chains with the monomer increases the effective bulk of the side chain creating helical structures in which steric repulsion favours an isotactic tendency in a manner analogous to bulky methacrylates. Moreover, on the basis of the transition structures of the ionized and partially ionized species, we can also tentatively attribute countercation dependencies in the stereoselectivity of ionized MAA to the structure of the charged species. Large diffuse cations such as $^+NMe_4$ and $^+NEt_4$ would not be expected to interact strongly with the propagating polymer terminus and hence highly syndiotactic polymer would be formed. In contrast, smaller and more charged cations such as Ca^{2+} would likely chelate to $COOH/COO^-$ groups around the polymer terminus and such chelation would likely increase the isotacticity of the polymer.
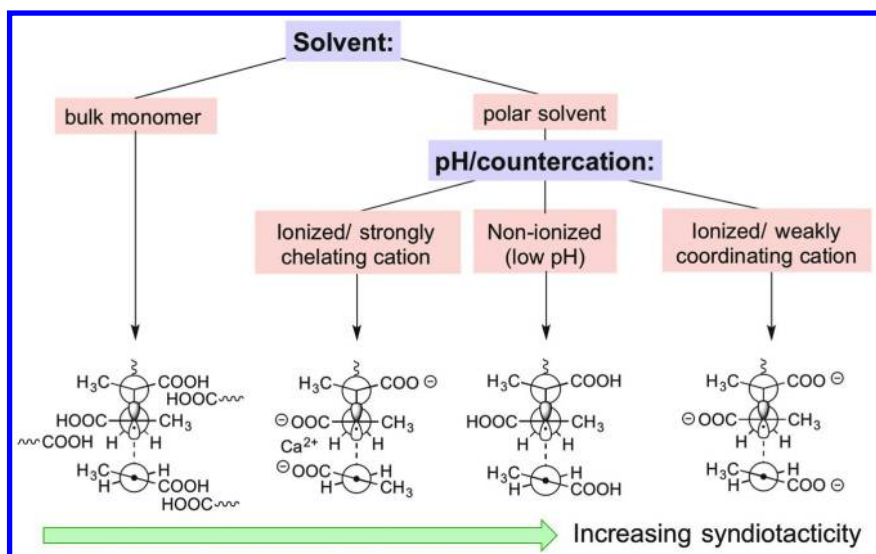
Figure 7. Mechanistic interpretation of stereocontrol in methacrylic acid polymerization.

Acknowledgments

References

1. Satoh, K.; Kamigaito, M. *Chem. Rev.* **2009**, *109*, 5120–5156.
2. Serizawa, T.; Hamada, K.-I.; Akashi, M. *Nature* **2004**, *429*, 52–55.
3. Hamada, K.-I.; Serizawa, T.; Akashi, M. *Macromolecules* **2005**, *38*, 6759–6761.
4. Serizawa, T.; Akashi, M. *Polym. J.* **2006**, *38*, 311–328.
5. Nakano, T.; Mori, M.; Okamoto, Y. *Macromolecules* **1993**, *26*, 867–868.
6. Nakano, T.; Matsuda, A.; Okamoto, Y. *Polym. J.* **1996**, *28*, 556–558.
7. Nakano, T.; Shikisai, Y.; Okamoto, Y. *Polym. J.* **1996**, *28*, 51–60.
8. Nakano, T.; Satoh, Y.; Okamoto, Y. *Polym. J.* **1998**, *30*, 635–640.
9. Porter, N. A.; Allen, T. R.; Breyer, R. A. *J. Am. Chem. Soc.* **1992**, *114*, 7676–7683.
10. Wu, W.-X.; McPhail, A. T.; Porter, N. A. *J. Org. Chem.* **1994**, *59*, 1302–1308.
11. Fukuda, H.; Diem, T.; Stefely, J.; Kezdy, F. J.; Regen, S. L. *J. Am. Chem. Soc.* **1986**, *108*, 2321–2327.
12. Bovey, F. A. *J. Polym. Sci., Part A: Polym. Chem.* **1963**, *1*, 843–848.
13. Popov, V. G.; Topchiev, D. A.; Kabanov, V. A.; Kargin, V. A. *Vysokomol. Soedin., Ser. A* **1972**, *14*, 117–130.
14. Kabanov, V. A.; Topchiev, D. A.; Karaputadze, T. M.; Mkrtchian, L. A. *Eur. Polym. J.* **1975**, *11*, 153–159.
15. Kabanov, V. A.; Topchiev, D. A.; Karaputa, T *J. Polym. Sci., Part C: Polym. Symp.* **1973**, *42*, 173–183.
16. Chovino, C.; Gramain, P. *Macromol. Chem. Phys.* **1996**, *197*, 1411–1418.
17. Rizzardo, E.; Chen, M.; Chong, B.; Moad, G.; Skidmore, M.; Thang, S. H. *Macromol. Symp.* **2007**, *248*, 104–116.
18. Nakano, T.; Okamoto, Y. *ACS Symp. Ser.* **1998**, *685*, 451–462.
19. Ishigaki, Y.; Takahashi, K.; Fukuda, H. *Macromol. Rapid Commun.* **2000**, *21*, 1024–1027.
20. Kaneko, Y.; Iwakiri, N.; Sato, S.; Kadokawa, J. I. *Macromolecules* **2008**, *41*, 489–492.
21. Zhang, J.; Peppas, N. A. *Macromolecules* **1999**, *33*, 102–107.
22. Pomogailo, A. D.; Dzhardimalieva, G. I.; Kestelman, V. N. *Macromolecular Metal Carboxylates and Their Nanocomposites*; Berlin: Springer, 2010; p 156.
23. Samui, A. B.; Dalvi, V. G.; Chandrasekhar, L.; Patri, M.; Chakraborty, B. C. *J. Appl. Polym. Sci.* **2006**, *99*, 2542–2548.
24. Lando, J. B.; Semen, J.; Farmer, B. *Macromolecules* **1970**, *3*, 524–527.
25. Ishitake, K.; Satoh, K.; Kamigaito, M.; Okamoto, Y. *Polym. Chem.* **2012**, *3*, 1750–1757.
26. Lando, J. B.; Litt, M.; Kumar, N. G.; Shimko, T. M. *J. Polym. Sci., Part C: Polym. Symp.* **1974**, *44*, 203–208.
27. Katchalsky, A.; Blauer, G. *Trans. Faraday Soc.* **1951**, *47*, 1360–1370.
28. Pinner, S. H. *J. Polym. Sci.* **1952**, *9*, 282–285.
29. Blauer, G. *J. Polym. Sci.* **1953**, *11*, 189–192.

30. Degirmenci, I.; Ozaltın, T. F.; Karahan, O.; Van Speybroeck, V.; Waroquier, M.; Aviyente, V. *J. Polym. Sci., Part A: Polym. Chem.* **2013**, *51*, 2024–2034.

31. Degirmenci, I.; Eren, S.; Aviyente, V.; De Sterck, B.; Hemelsoet, K.; Van Speybroeck, V.; Waroquier, M. *Macromolecules* **2010**, *43*, 5602–5610.

32. Henry, D. J.; Sullivan, M. B.; Radom, L. *J. Chem. Phys.* **2003**, *118*, 4849–4860.

33. Coote, M. L.; Krenske, E. H.; Izgorodina, E. I. *Macromol. Rapid Commun.* **2006**, *27*, 473–497.

34. Izgorodina, E. I.; Brittian, D. R. B.; Hodgson, J. L.; Krenske, E. H.; Lin, C. Y.; Namazian, M.; Coote, M. L. *J. Phys. Chem. A* **2007**, *111*, 10754–10768.

35. Knizia, G.; Adler, T. B.; Werner, H.-J. *J. Chem. Phys.* **2009**, *130*, 054104.

36. Peterson, K. A.; Adler, T. B.; Werner, H.-J. *J. Chem. Phys.* **2008**, *128*, 084102.

37. Alecu, I. M.; Zheng, J.; Zhao, Y.; Truhlar, D. G. *J. Chem. Theory Comput.* **2010**, *6*, 2872–2887.

38. Zhao, Y.; Truhlar, D. G. *Theor. Chem. Acc.* **2008**, *120*, 215–241.

39. Klamt, A. *J. Phys. Chem.* **1995**, *99*, 2224–2235.

40. Klamt, A.; Jonas, V.; Bürger, T.; Lohrenz, J. C. W. *J. Phys. Chem. A* **1998**, *102*, 5074–5085.

41. Klamt, A. *COSMO-RS: from quantum chemistry to fluid phase thermodynamics and drug design*; Elsevier Science Ltd.: Amsterdam, The Netherlands, 2005.

42. Marenich, A. V.; Cramer, C. J.; Truhlar, D. G. *J. Phys. Chem. B* **2009**, *113*, 6378–6396.

43. *ADF2012 COSMO-RS, SCM, Theoretical Chemistry*; Vrije Universiteit: Amsterdam, The Netherlands, http://www.scm.com.

44. Pye, C. C.; Ziegler, T.; van Lenthe, E.; Louwen, J. N. *Can. J. Chem.* **2009**, *87*, 790–797.

45. Frisch, M. J.; Trucks, G. W.; Schlegel, H. B.; Scuseria, G. E.; Robb, M. A.; Cheeseman, J. R.; Scalmani, G.; Barone, V.; Mennucci, B.; Petersson, G. A.; Nakatsuji, H.; Caricato, M.; Li, X.; Hratchian, H. P.; Izmaylov, A. F.; Bloino, J.; Zheng, G.; Sonnenberg, J. L.; Hada, M.; Ehara, M.; Toyota, K.; Fukuda, R.; Hasegawa, J.; Ishida, M.; Nakajima, T.; Honda, Y.; Kitao, O.; Nakai, H.; Vreven, T.; Montgomery, J. A., Jr.; Peralta, J. E.; Ogliaro, F.; Bearpark, M.; Heyd, J. J.; Brothers, E.; Kudin, K. N.; Staroverov, V. N.; Kobayashi, R.; Normand, J.; Raghavachari, K.; Rendell, A.; Burant, J. C.; Iyengar, S. S.; Tomasi, J.; Cossi, M.; Rega, N.; Millam, M. J.; Klene, M.; Knox, J. E.; Cross, J. B.; Bakken, V.; Adamo, C.; Jaramillo, J.; Gomperts, R.; Stratmann, R. E.; Yazyev, O.; Austin, A. J.; Cammi, R.; Pomelli, C.; Ochterski, J. W.; Martin, R. L.; Morokuma, K.; Zakrzewski, V. G.; Voth, G. A.; Salvador, P.; Dannenberg, J. J.; Dapprich, S.; Daniels, A. D.; Farkas, Ö.; Foresman, J. B.; Ortiz, J. V.; Cioslowski, J.; Fox, D. J. *Gaussian 09*, Revision D.01; Gaussian, Inc.: Wallingford, CT, 2009.

46. Werner, H. J.; Knowles, P. J.; Knizia, G.; Manby, F. R. *WIREs Comput. Mol. Sci.* **2012**, *2*, 242–253.

47. Werner, H.-J.; Knowles, P. J.; Knizia, G.; Manby, F. R.; Schütz, M.; Celani, P.; Korona, T.; Lindh, R.; Mitrushenkov, A.; Rauhut, G.; Shamasundar, K. R.; Adler, T. B.; Amos, R. D.; Bernhardsson, A.; Berning, A.; Cooper, D. L.; Deegan, M. J. O.; Dobbyn, A. J.; Eckert, F.; Goll, E.; Hampel, C.; Hesselmann, A.; Hetzer, G.; Hrenar, T.; Jansen, G.; Köppl, C.; Liu, Y.; Lloyd, A. W.; Mata, R. A.; May, A. J.; McNicholas, S. J.; Meyer, W.; Mura, M. E.; Nicklass, A.; O'Neill, D. P.; Palmieri, P.; Peng, D.; Pflüger, K.; Pitzer, R.; Reiher, M.; Shiozaki, T.; Stoll, H.; Stone, A. J.; Tarroni, R.; Thorsteinsson, T.; Wang, M. *MOLPRO*, version 2012.1, a package of ab initio programs, see http://www.molpro.net.
48. Izgorodina, E. I.; Coote, M. L. *Chem. Phys.* **2006**, *324*, 96–110.
49. Lin, C. Y.; Izgorodina, E. I.; Coote, M. L. *Macromolecules* **2010**, *43*, 553–560.
50. Noble, B. B.; Coote, M. L. *Int. Rev. Phys. Chem.* **2013**, *32*, 467–513.
51. Deglmann, P.; Müller, I.; Becker, F.; Schäfer, A.; Hungenberg, K.-D.; Weiß, H. *Macromol. React. Eng.* **2009**, *3*, 496–515.
52. Beuermann, S.; Buback, M.; Hesse, P.; Lacík, I. *Macromolecules* **2005**, *39*, 184–193.
53. Lacík, I.; Učňová, L.; Kukučková, S.; Buback, M.; Hesse, P.; Beuermann, S. *Macromolecules* **2009**, *42*, 7753–7761.
54. Degirmenci, I.; Noble, B. B.; Lin, C. Y.; Coote, M. L., The Mechanism of Stereoregulation in Free-Radical Polymerization of Bulky Methacrylates. In *Progress in Controlled Radical Polymerization: Mechanisms and Techniques*; ACS Symposium Series; American Chemical Society: Washington, DC, 2012; Vol. 1100, pp 15−32.
55. Ho, J.; Coote, M. L.; Easton, C. J. *Aust. J. Chem.* **2011**, *64*, 403–408.
56. Gryn'ova, G.; Coote, M. L. *J. Am. Chem. Soc.* **2013**, *135*, 15392–15403.
57. Kortum, G.; Vogel, W.; Andrussow, K. *Dissociation Constants of Organic Acids in Aqueous Solution*; International Union of Pure and Applied Chemistry; Butterworth: London, 1961; p 245.
58. Serjeant, E. P.; Dempsey, B. *Ionisation constants of organic acids in aqueous solution*; Pergamon: New York, 1979.
59. Dean, J. A. *Handbook of Organic Chemistry*; New York: McGraw-Hill, 1987; p 884.
60. Ulanski, P.; Bothe, E.; Hildenbrand, K.; von Sonntag, C. *Chem. - Eur. J.* **2000**, *6*, 3922–3934.

Chapter 4

ESR Investigations of Radicals by Various Magnetic Resonance Techniques with the Aid of ATRP

Atsushi Kajiwara*

Department of Materials Science, Nara University of Education, Takabatake-cho, Nara 630-8528, Japan
***E-mail: kajiwara@nara-edu.ac.jp**

This chapter illustrates how each elementary process of radical polymerizations can be examined by various magnetic resonance techniques. The reactions of radicals formed during radical polymerizations were investigated by various types of electron spin resonance (ESR) spectroscopic technique. High pressure ESR measurements provided ESR spectra of radicals formed during high pressure polymerizations up to 600 bar. The high-pressure ESR spectra provided information not only on structure of the propagating radicals but also on the molecular dynamics of the radicals under high pressure. Time-resolved ESR technique can investigate initial stage of radical polymerizations and the alternating copolymerization of styrene with maleic anhydride was examined. The results indicated that the first radical addition to the monomers occurred without selectivity. A combination of atom transfer radical polymerizations (ATRP) with ESR was developed just after development of ATRP. In this study, model precursor polymers were prepared by ATRP and radical migration reactions from model propagating radicals to mid-chain radicals were examined to determine both dependencies on chain lengths and side groups of acrylates.

Introduction

The developments of various kinds of controlled radical polymerization technique has allowed the synthesis of polymers with a wide variety of architectures which were extremely difficult or almost impossible to be prepared by other polymerization procedures. Each elementary step of the controlled radical polymerizations is considered to be the same to that in conventional radical polymerizations which means information on the elementary steps of conventional radical polymerizations is essential for development of deeper understanding of mechanisms of controlled radical polymerizations.

Electron spin resonance (ESR) spectroscopy can be utilized to observe each reaction step directly (*1–4*). Results of the ESR observation of these radical reactions during conventional radical polymerizations should be useful in providing a deeper understanding of the mechanisms of controlled radical polymerizations. Direct observations of radicals during actual radical polymerizations can be achieved using various ESR spectroscopic techniques. Propagating radicals in actual radical polymerizations can be observed by steady-state ESR (SS ESR) (*2, 4*). Time-resolved ESR (TR ESR) can be applied to the observation of the initial stage of the polymerization process, especially the first addition reaction of an initiator to a monomer resulting in formation of chain initiating radicals in actual radical polymerizations (*5–13*). TR ESR spectroscopy provides not only estimations of addition rate constants and activation energy of radical addition reactions in initiation reactions of radical homo-polymerization reactions (*14, 15*), but allows investigation of the initial step of alternating copolymerizations. The combination of results from both SS and TR ESR spectroscopy could be a strong tool for detailed examination of the mechanism of the alternating copolymerizations.

Radical termination reactions are usually very difficult to evaluate by SS ESR spectroscopy due to the time resolution of this method, SS ESR observation of radical polymerizations under high pressure would provide various information on termination reactions indirectly (*16, 17*). Termination reaction is usually too fast to observe by SS ESR technique. On the other hand, Buback *et al.* have investigated the radical termination reaction by single pulse-pulsed laser polymerization-electron paramagnetic resonance (SP-PLP-EPR) technique. The technique have much higher time-resolution than SS ESR and can conduct kinetic study of the radical termination reactions (*18–21*).

As discussed below a combination of ESR and atom transfer radical polymerization (ATRP) provided significant new information on the properties of radicals in radical polymerizations, e. g. dependency of chain length, dynamics, and reactivity (hydrogen transfer) of the propagating radicals (*22–27*).

In this research work, the elementary processes of conventional radical polymerizations were investigated in combination with various kinds of ESR spectroscopies and precursor polymers prepared by ATRP. The initiation reaction was examined by TR ESR, radical migration reaction during radical polymerizations of acrylates were evaluated by a combination of SS ESR/ATRP methods, and information on termination reactions were obtained by SS ESR under high pressure polymerizations.

Results and Discussion

High-Pressure ESR

Radical polymerizations under high-pressure have been conducted for both conventional and controlled radical polymerizations such as ATRP and RAFT (*28–31*) and it has been determined that propagation rate constants (k_p) are increased and termination rate constants (k_t) are decreased under high pressure. Buback and co-workers have also examined pressure effect on radical polymerizations extensively (*32–37*). They spent many years to clarify what happened during radical polymerizations under pressure.

As a result, molecular weight of the resulting polymers increased with increasing propagating radical concentrations. Indeed high pressure polymerizations were used for preparation of polymers with extremely high molecular weights that cannot be realized under ambient pressure. Although many results of polymerizations under high pressure have been reported, as far as I know, no one has observed the ESR spectra of actual propagating radicals under high pressure.

A specially designed pressure-proof quartz ESR cell (6 mm o.d. and 1 mm i.d.) for high pressure measurements has been developed by Sueishi *et al* (*16*, *17*). Up to 1 k bar pressure can be applied to this cell during photo-irradiation measurements. Since polymerizations under various pressures can be observed in this cell from ambient pressure to 1 k bar, pressure dependency of the spectra and molecular weights of the resulting polymers can be examined.

Figures 1a-1c show the pressure dependent ESR spectra of propagating radicals of *tert*-butyl methacrylate (*t*BMA) (Figure 1e) under 1, 300, and 600 bar initiated with di-*tert*-butyl peroxide (*t*BPO) under irradiation. For comparison, the ESR spectrum of propagating radicals of *t*BMA observed in typical ESR cell under ambient pressure is also shown (Figure 1d) which has a very similar ESR spectrum to that under 1.013 bar. Two kinds of spectroscopic difference were observed at higher pressure. One is S/N ratio. ESR spectra at higher pressure apparently showed better S/N ratio suggesting a higher concentration of radicals. The other is that intensities and linewidths of the inner spectroscopic lines, indicated by asterisk, increased with increasing pressure. Such a spectroscopic change implies that molecular motion of propagating radicals is restricted under high pressure, which is usually observed only in polymerizations in very viscous media. The hyperfine splitting constants are almost the same under various pressures indicating that the electronic structures of the propagating radicals were not influenced under 600 bar pressure. Propagating radical concentrations increased with increasing pressure as shown in Figure 1f.

SEC elution diagrams of resulting polymers after ESR measurements under 1, 300, and 600 bar are shown in Figure 2. Molecular weights (*M*n), molecular weight distributions (*M*w/*M*n) and conversions of the resulting polymers were shown in the figure caption of Figure 2. The intensities of the peaks at the lower molecular weight side were normalized in the Figure 2. A bimodal feature was observed in the diagrams and relative intensities at higher molecular weight side were increased with increasing pressure. Molecular weights of the polymers at higher molecular weight side were almost twice larger than those at lower

molecular weight side. One interpretation of the bimodal feature in the diagrams is a pressure effect. The higher molecular weight peak would be due to polymers terminated by coupling and the other peak would be due to polymers terminated by disproportionation. The ratio of polymers at higher molecular weight side were 42% and 16% at 600 bar and 1 bar respectively. The increase in the ratio under higher pressure indicates relieving the pressure effect by decreasing the numbers of molecules. The explanation looks reasonable in the present stage. Detailed structural analysis of these polymers would clarify the origin of the bimodal diagrams in the further investigations. Pressure effects on molecular weights and termination mechanisms can be examined without observation of ESR spectra. On the other hand, detection of ESR spectra under high pressure would provide deeper understanding of the pressure effects. These present results are the beginnings of ESR study of high-pressure radical polymerizations. Based on the ESR spectra of tBMA under pressure, kinetic parameters such as propagation rate constants (k_p) would be estimated. Moreover, this method can be applied to an investigation of the pressure effects on radical migration reactions during acrylate polymerizations. Pressure effects on TR ESR spectroscopy is also considered to be very interesting as a future project.
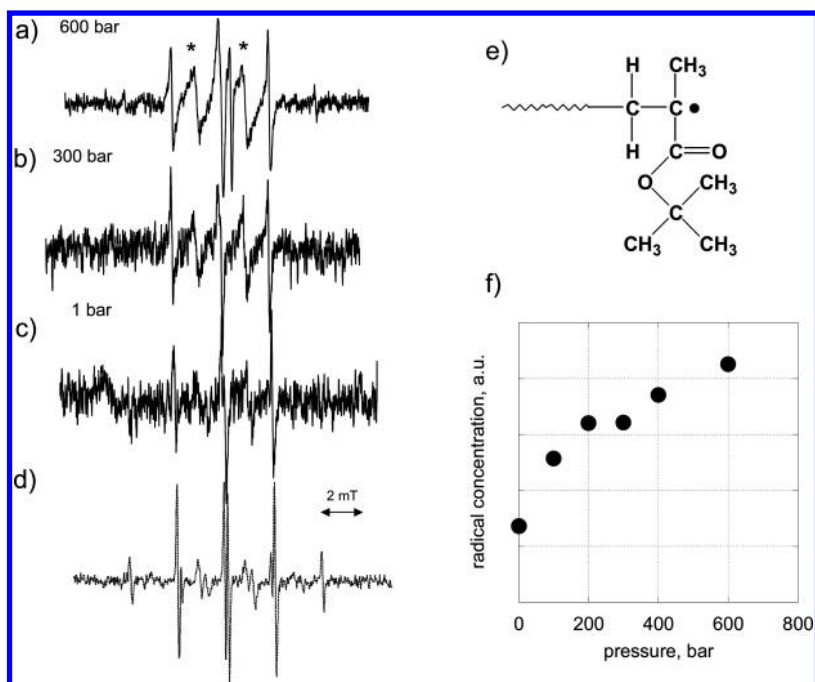
Figure 1. SS ESR spectra of propagating radicals of tBMA under high pressure at 25℃ along with structure of the radical and a plot of pressure dependent radical concentrations. (a) 600 bar, (b 300 bar, (c) 1 bar, (d) 1 bar using typical ESR cell (o.d. 5 mm), (e) structure of propagating radical, and (f) plot of radical concentrations under pressure.
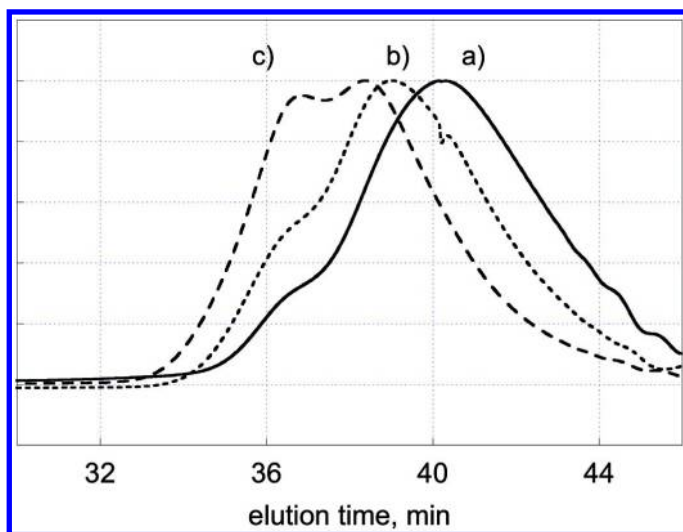
Figure 2. SEC elution diagrams of polymers prepared under high pressure polymerizations. Peaks are normalized at lower molecular weight peak (right hand side of bimodal peaks). (a) 1 bar, (b) 300 bar, and (c) 600 bar. (1 bar: conv. 20% Mn = 1810, Mw/Mn = 2.17, 300 bar: conv. 33% Mn = 5850, Mw/Mn = 2.45, 600 bar: conv. 40% Mn = 7990, Mw/Mn = 2.41).

Alternating Co-Polymerization

TR ESR spectroscopy can exclusively observe the first radical addition reaction of a radical, generated from an initiator to a monomer. Laser pulse generated spin polarized radicals relaxed to a thermally stable state with Boltzmann distribution and the relaxation process can be observed as ESR signals. 2,4,6-trimethylbenzoyl diphenylphosphine oxide (TMDPO) has a carbon-phosphorous bond that can be homolytically cleaved by a 355 nm laser pulse (*10*). The left hand side of Figure 3 shows the formation of both the resulting carbon- and phosphorous-centered radicals from TMDPO.

Both C- and P-centered radicals are spin polarized but the P-centered radical addition to monomer is faster than that of C-centered radical. Spin polarization of the P-centered radical is transferred to the chain initiating radical formed by an addition reaction of P-centered radical to a first monomer unit. Thus, polarization and relaxation of the chain initiating radicals can be detected in the ESR signal by TR ESR spectroscopy. The transferred spin polarization will relax within 2-3 µsec which is before second radical addition. That is why the first radical addition reaction is selectively observed. This method has been applied to the polymerizations of (meth)acrylates, styrenes, dienes and other monomers for estimation of addition rate constants and activation energies (*13–15*).
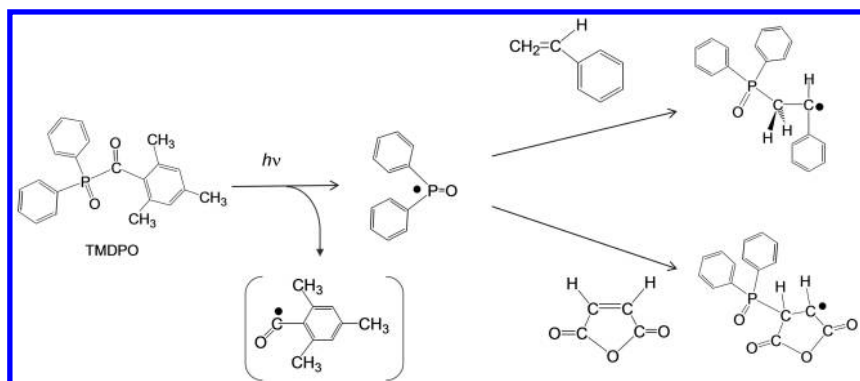
Figure 3. First radical addition reactions of alternating copolymerization of styrene and maleic anhydride initiated with TMDPO under photo-irradiation.

In this research work, TR ESR spectroscopy has been applied to investigation of the initiation mechanism of an alternating copolymerization of styrene and maleic anhydride. In a previous study, SS ESR spectroscopy demonstrated that the maleic anhydride terminal radical was predominant radical species during the propagation processes using a reversible addition fragmentation chain-transfer (RAFT) agent as a spin trapping agent (*38*). This time, the initiation step of the alternating copolymerization was examined. When copolymerization systems, with both styrene and maleic anhydride present, were examined by TR ESR overlapped signals of those styrene and maleic anhydride were observed as shown in Figure 4c indicating that P-centered radical added to the each monomer just like as in homo-polymerization even in a co-polymerization system. When the ratios of styrene and maleic anhydride were varied with ratios of St:MAnh = 1:0.5, 1:1, 1:2, 1:5, and 1:10, spectroscopic intensities of TR ESR signals of styrene were increased with increasing the relative ratio of styrene. Although, in principle, TR ESR spectroscopy does not provide quantitative results, we can state that first radical addition of the P-centered radical to the monomers was done without any selectivity. The reactivity of the radical addition reaction of the each monomer seemed to be determined by the individual reactivity of the each monomer.

There was no clear observation due to some kinds of interaction between styrene and maleic anhydride while the potential formation of a charge transfer complex that had been discussed in such alternating copolymerization systems (*39*).

Judging from the results of both previous and present study, an alternating copolymerization of styrene with maleic anhydride is initiated with no selectivity but is propagated in alternating manner probably from second monomer addition, and the maleic anhydride radical is predominant during propagation steps. High pressure polymerization, as described in this chapter, may provide more detailed information on the predominant terminal radicals by examination of pressure effects on termination reactions.
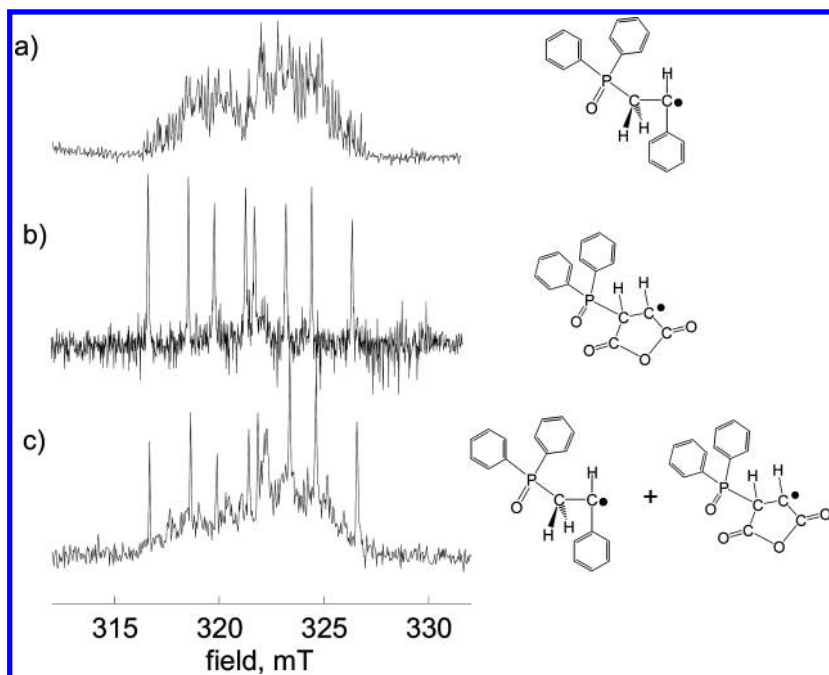
*Figure 4. TR ESR spectra of radical polymerizations at 25°C. (a) styrene only,
(b) maleic anhydride only, and (c) styrene and maleic anhydride (1:1). Estimated
structures of chain initiating radicals are shown at right hand side of the spectra.*

Chain Length Dependence on Chain Transfer in Acrylate Polymerizations

Radicals in actual radical polymerization systems can be observed directly
by SS ESR spectroscopy. During actual radical polymerizations of acrylates,
both propagating and mid-chain radicals can be observed. Mid-chain radicals are
formed by intramolecular radical transformation reaction through a 1,5-hyrodogen
shift mechanism.

Various kinds of radical precursors with pre-determined structures can be
prepared by ATRP (*40*, *41*) and a combination of ESR and ATRP techniques were
employed to form radicals with pre-determined structures. The radicals were
generated from the precursors by reactions with organotin compounds (*42*) and
were observed by SS ESR spectroscopy. With this combination of techniques,
various dependencies like chain length dependence, side-group dependence, and
monomer sequence dependence can be investigated.

In this chapter the results of examination of side group and chain length
dependencies on 1,5-hydrogen shift reactions using model radicals with
pre-determined structures of acrylates are reported. Model radical precursors
of ethyl acrylate and dodecyl acrylate with DP = 10 and 30 were prepared by
ATRP. Size exclusion chromatography (SEC) elusion diagrams of these radical
precursors are shown in Figure 5. Model propagating radicals were generated
by reactions with organotin compounds and were observed by ESR at various

temperatures (Figure 5). At -30ºC, only ESR spectra of model propagating radicals were observed. When the temperature was higher than 0ºC, overlapped signals of model propagating and mid-chain radicals were recorded. The relative ratio of propagating and mid-chain radicals can be estimated by double integration of the spectra. The ESR spectrum of the model propagating radical of oligoDoA (DP = 30) at 30ºC is shown as an example on the lower right had side of Figure 5. This is an overlapped spectrum of the model propagating radical (*) and mid-chain radical (+) signals. The plot of the ratio of mid-chain radicals of DoA of DP = 10 (●) and 30 (○) at different temperatures is shown in Figure 6. When the results for DP = 30 is compared with those of DP = 10, it is observed that radical migration is faster or easier for radicals formed from a polymer with a DP = 30. As far as I know, this is the first experimental evidence for chain length dependence of the rate of radical migration reactions in acrylate radical polymerizations.

Model radical precursors of EA were also prepared and it was observed that DoA model propagating radicals showed faster or easier radical migration reactions than EA radicals. This tendency was also observed in an ESR study of actual radical polymerizations of DoA and EA. In summary, both dependencies on chain lengths and side groups can be evaluated by a combination of ATRP-ESR method. Indeed Buback found that DoA showed faster or easier radical migrations than *t*BA in actual radical polymerizations (*43*). This present study provided quantitative results on chain lengths and side group dependencies.
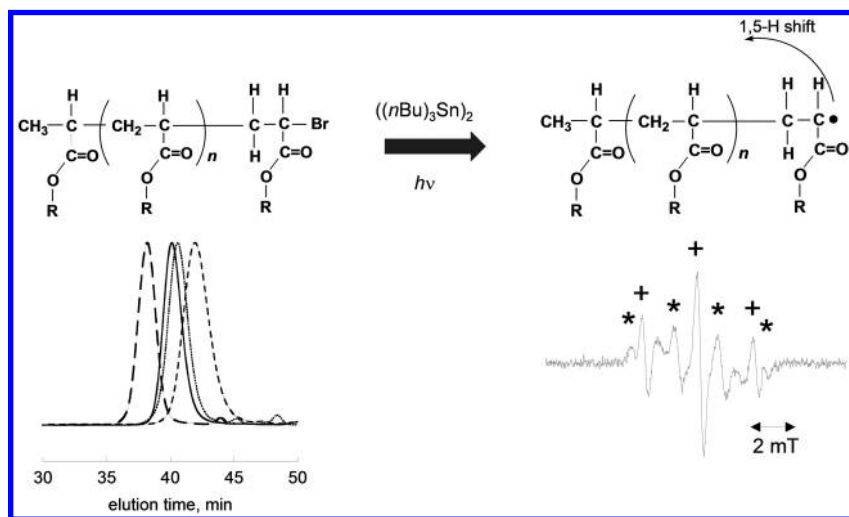
Figure 5. Generation of model radicals from model radical precursors with elusion diagrams of the precursors and SS ESR spectrum of one model radical at 30ºC. In the elusion diagrams, from left to right, DoA (DP = 30, dashed line), EA (DP = 30, solid line), DoA (DP = 10, dotted line), and EA (DP = 10, broken line). An asterisk (*) and plus (+) in ESR spectrum indicate signals of model propagating radicals and mid-chain radicals, respectively.
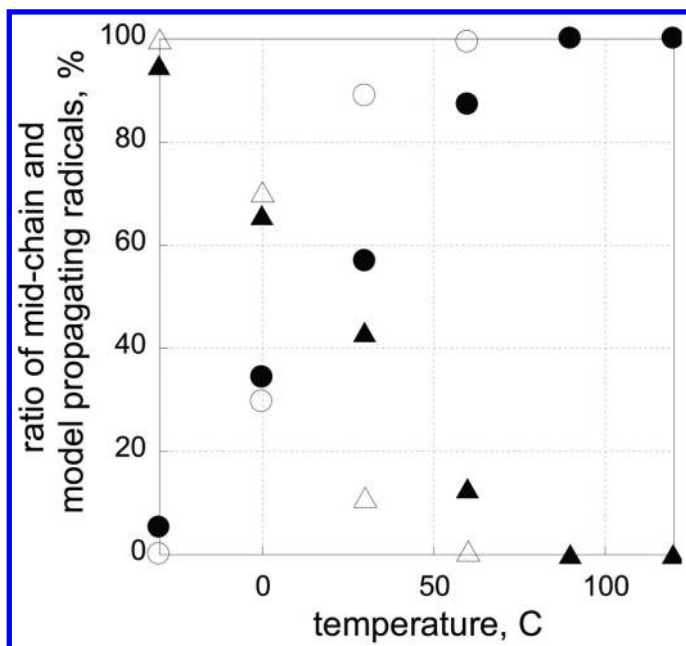
Figure 6. Plot of temperature dependent change of ratio of model propagating radicals and mid-chain radicals of oligoDoA (DP = 30) (open triangle for model propagating radical and circle for mid-chain radical), and (DP = 10)(closed triangle for model propagating radical and circle for mid-chain radical).

Conclusion

The elementary processes that occur in radical polymerization reactions were directly observed by application of various kinds of magnetic resonance techniques. High pressure ESR study showed structure and molecular dynamics of propagating radicals in the polymerization of *t*BMA under pressure and the successful observation of ESR spectra under pressure would enable us to determine kinetic parameters such as propagation rate constants (k_p) directly using propagating radical concentrations estimated from the spectra. An investigation of the pressure effects on radical migration reactions during acrylate polymerizations would also be possible.

TR ESR spectroscopy provided information on the selectivity of the first radical addition of a radical to a monomer in an alternating copolymerization of styrene and maleic anhydride. There was no observed selectivity in this first addition reaction of phosphorous centered radical to a mixture of styrene and maleic anhydride. Both chain initiating radicals of styrene and maleic anhydride were observed as overlapped spectra. In addition there was no evidence of formation of a donor-acceptor complex in the spectra.

A combination of SS ESR/ATRP demonstrated the chain length and side group dependencies on the nature of radical migration reaction during acrylate polymerizations. ATRP can provide model radical precursors with

well-defined structures and SS ESR observation of actual radicals participating in polymerizations of various kinds of acrylates show spectroscopic change due to radical migration reactions from propagating radicals to mid-chain radicals including dependencies on side groups and chain lengths. Each dependency of side group and chain length can be examined separately by the SS ESR/ATRP combination method.

The findings in this chapter can provide experimental evidence that should lead to a deeper understanding what happens during radical polymerizations.

Experimental

High Pressure SS ESR

High pressure SS ESR spectra were measured using a JEOL JES RE-2X ESR spectrometer equipped with a universal cavity. A specially designed high-pressure ESR cell developed by Sueishi *et al*. was used. *t*BMA (1.50 g, 1.0 x 10^{-2} mol) and *t*BPO (0.30 g, 2.0 x 10^{-3} mol) were dissolved in toluene (1.50 g) to make a stock solution. A mixture of 50 μL was taken from the stock solution to put into a high-pressure ESR cell. After appling the pressure, photo-initiated polymerization was conducted under irradiation using Ushio USD-500D (500 W) ultra-high pressure mercury lamp. After the measurements, pressures of the samples were measured again at the pressure pump with a gauge.

SS ESR/ATRP Combination Method

Model radical precursors were synthesized by atom transfer radical polymerization (ATRP) using a molar excess of initiator compared to monomer, in presence of a Cu^{I}/Cu^{II}PMDETA complex. The obtained products were purified by reprecipitation and column chromatography. Purity and molecular weights of the purified materials were confirmed using SEC, ^{1}H NMR, and electron spray ionization mass spectroscopy. Model radicals were generated by a reaction of the radical precursors with organotin compounds under irradiation. The generated radicals were observed by ESR spectroscopy by means of a JEOL JES RE-2X ESR spectrometer equipped with a universal cavity. Measurement temperature was controlled by a JEOL DVT2 variable-temperature accessory. ESR measurements were mainly performed in mesitylene at 150 and 120 °C and in toluene at 90, 60, 30, 0, -30 and -60 °C. Spectroscopic simulation was carried out by a JEOL IPRIT data analysis system.

TR ESR Spectroscopy

Diphenyl(2,4,6-trimethylbenzoyl)phosphine oxide (TMDPO, Aldrich) was purified by recrystallization from ethanol before use. Acrylates were purified by distillation just before use. A toluene or benzene solution of TMDPO (0.1 M) containing various concentrations of monomers was taken in an ESR sample cell. Laser pulses were irradiated by using a Q-switched Nd:YAG laser (Spectra Physics Quantaray DCR-2) operated at the third harmonic (10 mJ/flash at 355

nm with a 6-ns fwhm). For the measurements of the time-resolved ESR, a JEOL JES RE-2X spectrometer, equipped with a WBPA2 wide band pre-amplifier, was operated without magnetic field modulation, and the data were stored in a Tektronix TDS520A digital oscilloscope. Magnetic fields at resonance signals were determined by an Echo Electronics ES-FC5 NMR field meter. Measurement temperature was controlled by a JEOL DVT2 variable-temperature accessory. Data analysis was conducted by CIDEP software provided by JEOL Ltd.

Size Exclusion Chromatography (SEC)

Molecular weights and molecular weight distributions were estimated using a TOSOH CCP&8020 series GPC system with TSK-gel columns. Lenear combination of two $G2000H_{HR}$ and two GMH_{XL} colums was employed. Polystyrene standards were used to calibrate the columns.

Acknowledgments

References

1. Fischer, H. *Adv. Polym. Sci.* **1968**, *5*, 463–530.
2. Kamachi, M. *Adv. Polym. Sci.* **1987**, *82*, 207–275.
3. Yamada, B.; Westmoreland, D. G.; Kobatake, S.; Konosu, O. *Prog. Polym. Sci.* **1999**, *24*, 565–630.
4. Kamachi, M.; Kajiwara, A. *Macromolecules* **1996**, *29*, 2378–2382.
5. Weil, J. A.; Bolton, J. R. *Electron Paramagnetic Resonance*, 2nd ed.; Wiley: Hoboken, NJ, U.S.A., 2007
6. Trifunac, A. D.; Thurnauber, M. C. In *Time-Domain Electron Spin Resonance*; Kevan, L., Schwartz, R. N., Eds.; Wiley: New York, NY, U.S.A., 1979; pp 107−152.
7. Atkins, P. W.; McLauchlan, K. A. In *Chemically Induced Magnetic Polarization*; Lepley, A. R., Closs, G. L., Eds.; Wiley-Interscience: New York, NY, U.S.A., 1973; pp 41−93.
8. Sumiyoshi, T.; Henne, A.; Lechtken, P.; Schnabel, W. *Z. Naturforsch.* **1984**, *A39*, 434–436.
9. Sumiyoshi, T.; Schnabel, W. *Polymer* **1985**, *26*, 141–146.
10. Kamachi, M.; Kuwata, K.; Sumiyoshi, T.; Schnabel, W. *J. Chem. Soc., Perkin Trans. 2* **1988**, 961−965.
11. Mizuta, Y.; Morishita, N.; Kuwata, K. *Chem. Lett.* **1999**, 311–312.
12. Kajiwara, A.; Konishi, Y.; Morishima, Y.; Schanbel, W.; Kuwata, K.; Kamachi, M. *Macromolecules* **1993**, *26*, 1656–1658.

13. Kamachi, M.; Kajiwara, A.; Saegusa, K.; Morishima, Y. *Macromolecules* **1993**, *26*, 7369–7371.
14. Kajiwara, A. *Macromol. Rapid Commun.* **2009**, *30*, 1975–1980.
15. Kajiwara, A. In *Progress in Controlled Radical Polymerization: Mechanisms and Techniques*; Matyjaszewski, K., Ed.; ACS Symposium Series 1100; American Chemical Society: Washington, DC, 2012; pp 33−46.
16. Sueishi, Y.; Miyazono, K.; Iwamoto, S.; Kotake, Y. *Chem. Phys. Lett.* **2009**, *474*, 153–157.
17. Sueishi, Y.; Tobisako, H.; Kotake, Y. *J. Phys. Chem. B* **2004**, *108*, 12623–12627.
18. Bath, J.; Buback, M.; Hesse, P.; Sergeeva, T. *Macromolecules* **2010**, *43*, 4023–4031.
19. Buback, M.; Müller, E.; Russel, G. T. *J. Phys. Chem. A* **2006**, *110*, 3222–3230.
20. Buback, M.; Egorov, M.; Junkers, T.; Panchenko, E. *Macromol. Chem. Phys.* **2005**, *206*, 333–341.
21. Buback, M.; Egorov, M.; Junkers, T.; Panchenko, E. *Macromol. Rapid Commun.* **2004**, *25*, 1004–1009.
22. Kajiwara, A.; Maeda, K.; Kubo, N.; Kamachi, M. *Macromolecules* **2003**, *36*, 526–528.
23. Kajiwara, A; Nanda, A. K.; Matyjaszewski, K. *Macromolecules* **2004**, *37*, 1378–1385.
24. Kajiwara, A.; Matyjaszewski, K. In *Advanced ESR Methods in Polymer Research*, Wiley Interscience: 2006; Chapter 5, pp 101−132.
25. Kajiwara, A. In *Controlled/Living Radical Polymerization*; Matyjaszewski, K., Ed.; ACS Symposium Series 944; American Chemical Society: Washington, DC, 2006; Chapter 9, pp 111−124.
26. Kajiwara, A. *Macromol. Symp.* **2007**, *248*, 50–59.
27. Kajiwara, A. In *Controlled/Living Radical Polymerization: Progress in ATRP*; Matyjaszewski, K., Ed.; ACS Symposium Series 1023; American Chemical Society: Washington, DC, 2009; Chapter 4, pp 49−59.
28. Arita, T.; Buback, M.; Jenssen, O.; Vanna, P. *Macromol. Rapid Commun.* **2004**, *25*, 1376–1381.
29. Rzayev, J.; Penelle, J. *Angew. Chem., Int. Ed.* **2004**, *43*, 1691–1694.
30. Arita, T.; Kayama, Y.; Ohon, K.; Tsujii, Y.; Fukuda, T. *Polymer* **2008**, *49*, 2426–2429.
31. Kwiatkowski, P.; Jurczak, J.; Pietrasik, J.; Jakubowski, W.; Mueller, L.; Matyjaszewski, K. *Macromolecules* **2008**, *41*, 1067–1069.
32. Beuermann, S.; Buback, M.; Schmaltz, C. *Ind. Eng. Chem. Res.* **1999**, *38*, 3338–3344.
33. Buback, M.; Degener, B. *Makromol. Chem.* **1993**, *194*, 2875–2883.
34. Buback, M. *Makromol. Chem.* **1990**, *191*, 1575–1587.
35. Buback, M. *Angew. Chem., Int. Ed.* **1991**, *30*, 1654–1656.
36. Buback, M.; Hippler, H.; Schweer, J.; Vögele, H.-P. *Makromol. Chem. Rapid Commun.* **1986**, *7*, 261–265.
37. Buback, M. *Makromol. Chem* **1980**, *181*, 373–382.

38. Du, F.-S.; Zhu, M.-Q.; Guo, H.-Q.; Zi-Chen Li, Z.-C.; Li, F.-M.; Kamachi, M.; Kajiwara, A. *Macromolecules* **2002**, *35*, 6739–6741.
39. Tsuchida, E.; Tomono, T. *Makromol. Chem.* **1971**, *141*, 265–298.
40. Wang, J.-S.; Matyjaszewski, K. *J. Am. Chem. Soc.* **1995**, *117*, 5614–5615.
41. Wang, J.-S.; Matyjaszewski, K. *Macromolecules* **1995**, *28*, 7901–7910.
42. Giese, B.; Damm, W.; Wetterich, F.; Zeitz, H.-G. *Tetrahedron Lett.* **1992**, *33*, 1863–1865.
43. Buback, M. *Macromol. Symp.* **2009**, *275−276*, 90–101.

Chapter 5

Catalyst Activity in ATRP, Determining Conditions for Well-Controlled Polymerizations

Dominik Konkolewicz*,[1,2] and Krzysztof Matyjaszewski*,[1]

[1]Department of Chemistry, Carnegie Mellon University, 4400 Fifth Ave., Pittsburgh PA, 15213
[2]Department of Chemistry and Biochemistry, Miami University, 651 E High St., Oxford, OH 45056
***E-mail: d.konkolewicz@miamiOH.edu; km3b@andrew.cmu.edu**

This chapter uses kinetic simulations to determine the general trends between the activity of a catalyst and its ability to create well controlled polymers by both Normal and ICAR ATRP. The general trend observed is that in Normal ATRP, where the Cu is not regenerated in the reaction, the activity of the catalyst must be carefully tuned so that the polymerization rate is rapid enough to form polymer in a reasonable time frame, but not so active that radical termination dominates the reaction. In contrast, polymers synthesized by ICAR ATRP are generally better controlled with more active catalysts. This is because the more active catalyst can activate chains with lower Cu^I concentrations, leaving more Cu^{II} to deactivate propgating radicals and increase the number of reversible activation/deactivation cycles.

Introduction

Reversible deactivation radical polymerization (RDRP) methods have lead to a vast range of new polymers and materials since their discovery in last two decades (*1, 2*). In all cases, RDRP reactions control the polymer architecture through an equilibrium between dormant and active chains (*2, 3*). RDRP methods allow polymers to be synthesized with control over polymer structure comparable to ionic polymerizations, with tolerance to functional groups and impurities similar to conventional radical polymerization (*4*). Nitroxide mediated polymerization

(NMP) (*5*, *6*), atom transfer radical polymerization (ATRP) (*7–9*), and reversible addition-fragmentation chain transfer polymerization (RAFT) (*10*, *11*) are the three most commonly used RDRP techniques. ATRP is a particularly useful technique, since it can polymerize a wide range of monomers under relatively mild conditions (*9*, *12*).

In ATRP, control over the polymeric architecture is gained through a reversible activation of an alkyl halide to a radical, which gives the ATRP equilibrium (*9*, *12*). In ATRP, a low oxidation state transition metal complex, most often Cu^I, activates the alkyl halide species to generate an alkyl radical and the transition metal in a higher oxidation state, most often Cu^{II} (*2*). This alkyl radical can propagate with monomer for a short period of time, before being deactivated back to an alkyl halide by the transition metal in a higher oxidation state (*2*). In this way, the low oxidation state complex acts as the activator of alkyl halides, and the high oxidation state complex is the deactivator complex. A reaction which starts with the activator complex, monomer and alkyl halide, is termed Normal ATRP, or Normally initiated ATRP. It has many advantages, such as compatibility with various monomers (*9*, *13*). However, due to unavoidable termination events, radical terminatation leads to the irreversible build of the deactivator complex, by the persistent radical effect (*12*, *14*). Therefore, Normal ATRP requires high concentrations of the activator catalyst, typically in excess of 1000 parts per million (ppm), to ensure a reasonable rate of polymerization (*15*).

One approach that can be used to overcome the high concentrations of catalyst needed in Normal ATRP is to continually regenerate the activator complex, by reducing the deactivator complex (*16*). The continuous reduction of the deactivator allows the catalyst to be used at concentrations < 100 ppm (*16*). A summary of the core ATRP reaction, and the process of activator regeneration is shown in Scheme 1. There are several ways that the activator regeneration can be achieved, including: the use of conventional radical initiators, as is done in initiator for continuous activator regeneration (ICAR) ATRP (*16*, *17*); chemical reducing agents, as is done in activators regenerated by electron transfer (ARGET) ATRP (*18*, *19*); electrochemically as is done in *e*ATRP (*20*, *21*); using zerovalent metals or sulfites as supplemental activators and reducing agent (SARA) ATRP (*22–24*); or photochemically as is done in photoATRP (*25–27*).
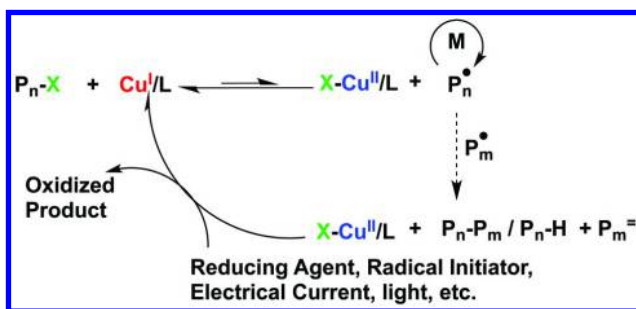
Scheme 1. Core ATRP activation deactivation process, and the regeneration of the activator by the continuous reduction of the deactivator complex. In this case, Cu^I and Cu^{II} complexes are used.

One key parameter in all ATRP processes is the ATRP equilibrium constant (K_{ATRP}), given by

$$K_{ATRP} = \frac{[Cu^{II}][R^{\cdot}]}{[Cu^{I}][RX]}$$

where [R] is the concentration of radicals, [X-Cu^{II}] is the deactivator concentration, [Cu^{I}] is the activator concentration, and [RX] is the alkyl halide concentration (*12*). The ATRP equilibrium constant is known to govern the rate of polymerization in Normal ATRP (*12*), although its role in ATRP with activator regeneration is less clear. Both the monomer type and the structure of the catalyst can affect the ATRP equilibrium constant. The goals of this chapter are to use kinetic simulations to investigate the relationship between the activity of the catalyst and the polymerization outcomes for 5 catalysts. In all cases an acrylic monomers are considered, although similar trends are expected for other monomers. Both Normal and ICAR ATRP conditions are considered.

The Kinetic Model

A total of 6 ligands are considered, 5 have been used in ATRP reactions. These ligands are shown in Scheme 2: 1,1,4,7,10,10-Hexamethyltriethylenetetramine (HMTETA), N^1,N^1,N^2,N^2-tetrakis(pyridin-2-ylmethyl)ethane-1,2-diamine (TPEDA), tris(pyridylmethyl)amine (TPMA), tris[2-(dimethylamino)ethyl]-amine (Me$_6$TREN) and tris((4-methoxy-3,5-dimethylpyridin-2-yl)methyl)-amine (TPMA*). TPMA*^{N} is a proposed ligand with activity 1000 times larger than the activity of TPMA*. All ligands are shown in Scheme 2. Although TPMA*^{N} ligand has not been used in ATRP, it is consistent with TPMA substituted with dimethylamino groups para to the pyridinic nitrogens (2-((bis((4-(dimethylamino)pyridin-2-yl)methyl)amino)methyl)-*N*,*N*-dimethyl-pyridin-4-amine). Based on cyclic voltammetry data on substituted bipyridine Cu complexes, the dimethylamino groups showed a similar increase in activity (*28*). Furthermore, Karlin et al. (*29*) showed that the tris(*p*-dimethylaminopyridine) substituted TPMA Cu complex was approx. 200 mV, more reducing than the tris(*p*-methoxypyridine). This would correspond to approximately 3 orders of magnitude increase in the activity of the dimethylamino substituted TPMA compared to the methoxy substituted TPMA (*30*). In all cases, an acrylate like chain end was considered, and the activities of the small molecule initiator (similar to methyl 2-bromopropionate) and polymer were assumed to be the same.

The reactions in Scheme 3 were used to describe all reactions. The reaction was the same for normal ATRP or ICAR ATRP, except that the additional azo initiator (I$_2$) dissociation reaction was added. It should be noted that speciation is not considered in this chapter, and instead apparent rate coefficients are used (*22*). The use of apparent rate coefficients also extends to radical termination, implying that diffusional limitations on termination are also applied as an average across all chain-lengths, etc. Table 1 gives the rate coefficients for the standard radical reactions.
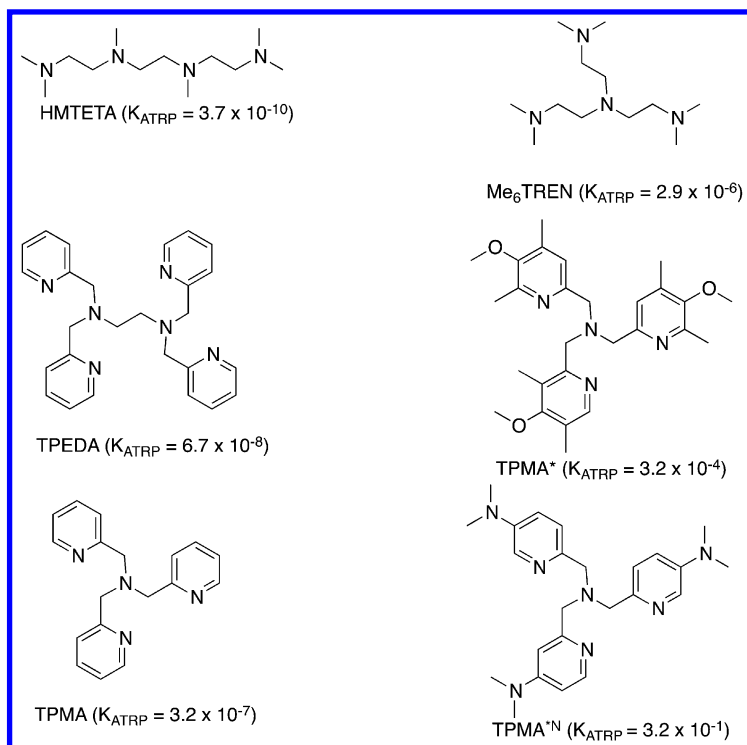
Scheme 2. The structure of the ligand used to make the activator catalyst Cu^I/L and deactivator complex X-Cu^II/L. Here TPMA*^N is a proposed ligand whose activity is 1000 times larger than TPMA*. The equilibrium constant is for temperatures near room temperature.

The rate coefficients for the radical reactions are given in the below table, based on literature data. The value of $k_{p,I}$ was determined by multiplying the ratio of $k_{p,I}/k_p$ at 42 °C by k_p at 25 °C (*31*, *32*). Reactions 11 through 16 represent the formation of dead chains.

Additionally, the rate coefficients for ATRP specific reactions of activation and deactivation reactions are given below in Table 2. These parameters are determined from measurements in acetonitrile for the HMTETA, TPEDA, TPMA, Me$_6$TREN and TPMA* based catalysts. For the TPMA*^N based catalyst the value of k_d was assumed to be the same as for TPMA*, and the value of k_a was increased by a factor of 1000. However, in practice, the value of k_d is expected to be lower for the more active catalyst.

For the initiator fragments, the scaling was more complicated. 2,2′-Azobis(4-methoxy-2.4-dimethyl valeronitrile) (V-70) gives a tertiary nitrile radical and assumed to have similar reactivity as the isobutyronitrile (IBN) radical. Due to the presence of side groups on V-70, it is possible that V-70 derived radicals will be even more ATRP active, with potentially lower rates of V-70 derived radicals addition to monomer. The original data is from Pintauer et al. (*37*) for chloro-isobutronotrile. 2,2′-Bipyridine (Bpy), TPMA and Me$_6$TREN were used

to estimate the rate coefficients for deactivation and activation of isobutyronitrile radicals and bromo-isobutyronitrile respectively with each catalyst. Interestingly the IBN-Cl has essentially the same reactivity with TPMA and Me$_6$TREN. The activation rate constants were scaled from 60 °C to 25 °C using the activation energy of 28.1 kJ/mol which is from the work of Seeliger et al. for 2-bromopropionitrile (BrPN) (*38*). The ATRP equilibrium constant (K_{ATRP}) was decreased by a factor of 1.5 (*16*). The reactivity of the chloro group was converted to the reactivity of the bromo-group. In this case k$_d$ was assumed to be the same, but k$_a$ was rescaled by the ratio of the k$_a$ for 2-bromopropionitrile (BrPN) to2-chloropropionitrile (ClPN) (this ratio is 50) taken from the data of Tang (*30*). Finally, the solvent effect (factor of 0.8) is accounted for using the data of Braunecker et al. (*39*) This gives the k$_a$ and k$_d$ for isobutyronitrile bromide (IBN-Br) with Bpy, TPMA and Me$_6$TREN. For more active ligands (TPMA*, TPMA*^{N}) the reactivity is taken to be the same as for Me$_6$TREN (which is almost the same as for TPMA). For less active ligands (HMTETA, TPEDA) the data were scaled from Bpy in the case of HMTETA by applying the ratio of k$_a$ for BrPN with ligand of interest:bpy and same for k$_d$. This gives the following table of activities for the IBN-Br interacting with different catalysts, as shown in Table 3.

Simulation Results

Having established these rate coefficients, it is possible to predict the key experimental parameters measured in a polymerization, conversion, number averaged molecular weight (or degree of polymerization) and the dispersity (M$_w$/M$_n$).

Simulations of Normal ATRP

Initially Normal ATRP conditions are investigated. Here the Cu^I is added at the start of the reaction, but is not regenerated throughout the process, so termination events lead to the irreversible accumulation of Cu^{II} by the persistent radical effect. Figure 1 shows the semi-logarithmic kinetic plot for Normal ATRP with each catalyst. An interesting conclusion to be drawn is that increasing catalyst activity, or higher K_{ATRP}, initially leads to an increase in the polymerization rate. In the case of the polymerization of acrylate monomers, the polymerization rate increased with the catalyst activity until the catalyst based on Me$_6$TREN, however, the more active catalysts of TPMA* and TPMA*^{N} did not increase the rate of polymerization further. In fact the TPMA*^{N} based system lead to no polymerization. This is initially counterintuitive, since the more active catalyst should lead to a higher rate of radical generation, higher radical concentration and faster polymerization. However, with the highly active catalysts, radicals are generated at such a high rate that the termination reactions dominate the system, and in a relatively short time, the vast majority of the activator complex is oxidized to the deactivator complex. A similar effect has been observed by Malmstrom et al. (*40*) and Matyjaszewski et al. (*36*)

$$RX + CuX \xrightarrow{k_a} R^\bullet + CuX_2 \tag{1}$$

$$R^\bullet + CuX_2 \xrightarrow{k_d} RX + CuX \tag{2}$$

$$I_2 \xrightarrow{k_{azo}} I^\bullet \tag{3}$$

$$IX + CuX \xrightarrow{k_{a,I}} I^\bullet + CuX_2 \tag{4}$$

$$I^\bullet + CuX_2 \xrightarrow{k_{d,I}} IX + CuX \tag{5}$$

$$R^\bullet + M \xrightarrow{k_p} P(1)^\bullet \tag{6}$$

$$I^\bullet + M \xrightarrow{k_{p,I}} P(1)^\bullet \tag{7}$$

$$P(j)^\bullet + M \xrightarrow{k_p} P(j+1)^\bullet \tag{8}$$

$$P(j)^\bullet + CuX_2 \xrightarrow{k_d} P(j)X + CuX \tag{9}$$

$$P(j)X + CuX \xrightarrow{k_a} P(j)^\bullet + CuX_2 \tag{10}$$

$$R^\bullet + R^\bullet \xrightarrow{k_{t0}} D \tag{11}$$

$$P(j)^\bullet + R^\bullet \xrightarrow{k_{t0}} D(j) \tag{12}$$

$$R^\bullet + I^\bullet \xrightarrow{k_{t0}} D \tag{13}$$

$$I^\bullet + I^\bullet \xrightarrow{k_{t0}} D \tag{14}$$

$$P(j)^\bullet + I^\bullet \xrightarrow{k_{t0}} D(j) \tag{15}$$

$$P(j)^\bullet + P(k)^\bullet \xrightarrow{k_t} D(j+k) \tag{16}$$
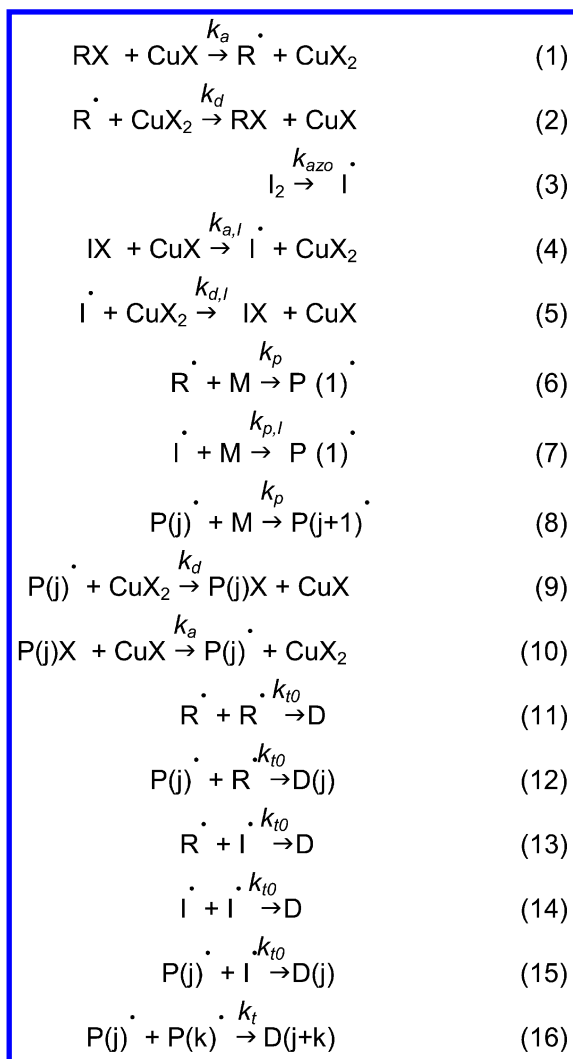
Scheme 3. List of all reactions used in the Normal and ICAR ATRP simulations.

Table 1. The rate coefficients for the intrinsic radical reactions for MA with V-70 at 25 °C.

Rate coefficient	Value	References
k_p (MA)	15600 M^{-1} s^{-1}	(31)
$k_{p,I}$ (MA)	245 M^{-1} s^{-1}	(31, 32)
k_{t0} (MA)	1×10^9 M^{-1} s^{-1}	(33)
k_t (MA)	1×10^8 M^{-1} s^{-1}	(34)
k_{azo} (V-70)	8.9×10^{-6} s^{-1}	(35)

Table 2. The rate coefficients for the ATRP activation deactivation processes for various catalysts with methyl 2-bromopropionate (MBrP) at 22 °C.[a]

Catalyst	k_a (M^{-1} s^{-1})	k_d (M^{-1} s^{-1})
HMTETA	8.6×10^{-3}	2.3×10^7
TPEDA	6.6×10^{-1}	9.9×10^6
TPMA	3.8×10^0	1.2×10^7
Me$_6$TREN	2.8×10^1	9.6×10^6
TPMA*	3.8×10^3	1.2×10^7
TPMA*N	3.8×10^6	1.2×10^7

[a] This is taken as being sufficiently close to 25 °C, that no additional scaling was performed. The rate coefficients for HMTETA, TPEDA, TPMA, Me$_6$TREN were taken from the work of Tang et al. (30) The ATRP equilibrium constant (K_{ATRP}) for TPMA* was taken from the work of Schröder et al. (36), and the values of k_d and k_a were in good agreement with the value obtained experimentally. The k_a and k_d for TPMA*N were estimated to ensure that the TPMA*N based catalyst was 1000 times more active than the TPMA* based catalyst with a hypothetical preservation of the the same rate constant if deactivation. This is based on the fact that as the K_{ATRP} is increased, deactivation rate coefficients typically decrease significantly less than activation rate coefficient increases (30). Therefore, for the TPMA*N based catalyst, the k_d is assumed to be the same as for TPMA*, even though it is likely to be slightly smaller.

Table 3. The rate coefficients for the ATRP activation deactivation processes for various catalysts with IBN-Br at 25 °C. Scaling as outlined earlier.

Catalyst	$k_{a,I}$ (M^{-1} s^{-1})	$k_{d,I}$ (M^{-1} s^{-1})
HMTETA	7.8×10^3	1.5×10^8
TPEDA	1.2×10^5	2.2×10^7
TPMA	7.2×10^5	2.6×10^7
Me$_6$TREN	7.1×10^5	2.5×10^7
TPMA*	7.2×10^5	2.6×10^7
TPMA*^{N}	7.2×10^5	2.6×10^7
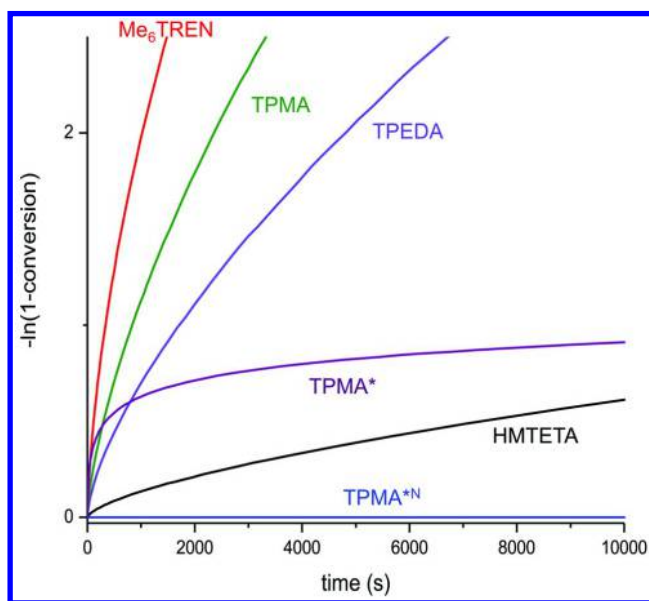
Figure 1. First order kinetic plot for the normal ATRP of MA with different catalysts under the conditions: [M]:[RX]:[CuX]:[CuX$_2$]=200:1:0.2:0 in 50% (v/v) solvent, with the temperature of 25 °C.

In addition to the kinetic data it is also important to consider, the ability of the catalyst to control the polymerization. Figure 2 displays the evolution of number averaged degree of polymerization (DP$_n$) with conversion for all 5 catalysts that lead to appreciable conversion. Therefore, the TPMA*^{N} catalyst is not included, since the polymerization did not proceed to even 5% conversion. The top figure compares the evolution of the DP$_n$ for HMTETA to TPEDA, and the bottom figure compares the polymerization with all catalysts, except those based on HMTETA and TPMA*^{N}.
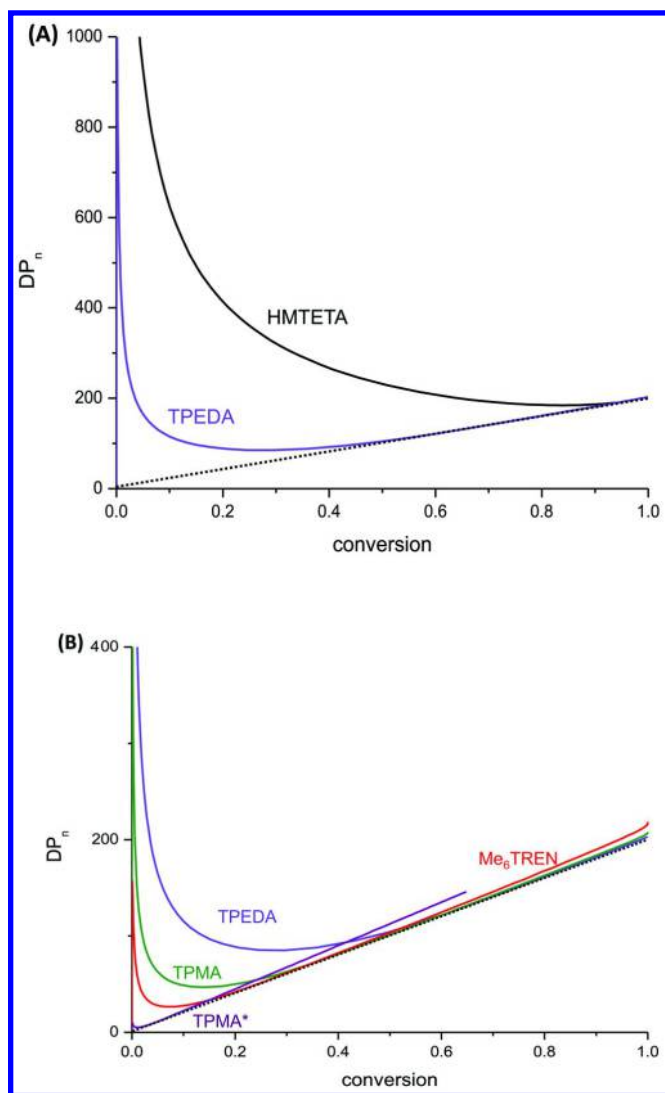
Figure 2. Evolution of DP$_n$ with conversion for (A) HMTETA and TPEDA, and (B) all catalysts except HMTETA for the normal ATRP of MA with different catalysts. Conditions: [M]:[RX]:[CuX]:[CuX$_2$]=200:1:0.2:0 in 50% (v/v) solvent, with the temperature of 25 °C. Theoretical chain length based on full initiation is given as the dashed black line.

It is important to note that in all cases the polymerization ultimately reached close to full initiation, with good agreement between the simulated and theoretical chain length, although the less active catalysts lead to slower initiation. In the case of TPMA or TPEDA, acceptable initiation was reached by conversions of 0.2 and 0.4 respectively. Me$_6$TREN reached close to full initiation at a conversion of 0.1, and TPMA* reached essentially complete initiation within a few percent

conversion. In contrast, HMTETA required monomer conversion of 0.9 to approach the theoretical molecular weight. Although in practice HMTETA is able to control acrylic monomers effectively, temperature, initial presence of deactivator and other parameters should be adjusted to ensure the reaction creates well-controlled polymers.

A third parameter investigated is the uniformity of chains, measured by the M_w/M_n ratio. As seen in Figure 3, the uniformity of chains follows the same trends as initiation efficiency. In fact, the lower catalytic activity, leading to slower initiation in this system is the primary cause of the less uniform chains. Although the fact that the more active catalysts form higher concentrations of the deactivator complex (as a consequence of higher termination rates) also contributes to the lower dispersity in the more active catalysts.
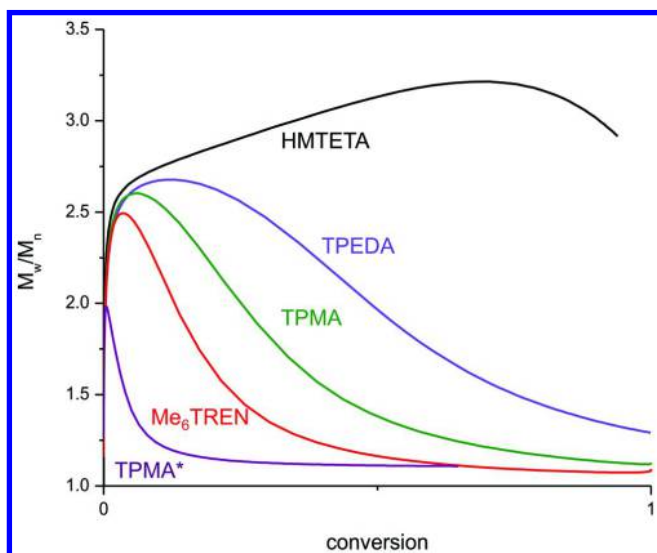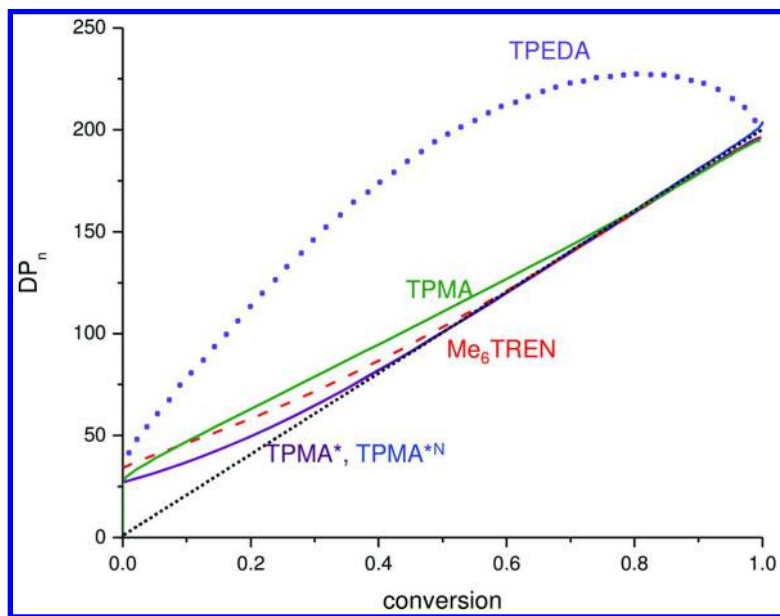

Figure 3. Evolution of M_w/M_n with conversion for the normal ATRP of MA with different catalysts. Conditions: [M]:[RX]:[CuX]:[CuX₂]=200:1:0.2:0 in 50% (v/v) solvent, at a temperature of 25 °C.

Finally, the ratio of Cu^{II} (deactivator) to total Cu was compared for all polymerizations that reached appreciable conversion. This is proportional to the dead chain fraction in Normal ATRP, by the persistent radical effect, with the scaling factor being the ratio of the amount of Cu^{II} formed during the reaction to the initial amount of the initiator (*41*). As shown in Figure 4, with the more active catalyst, Cu is more rapidly oxidized. Therefore, as predicted from Figure 1, more active catalysts lead to more rapid formation of the Cu^{II} complex.
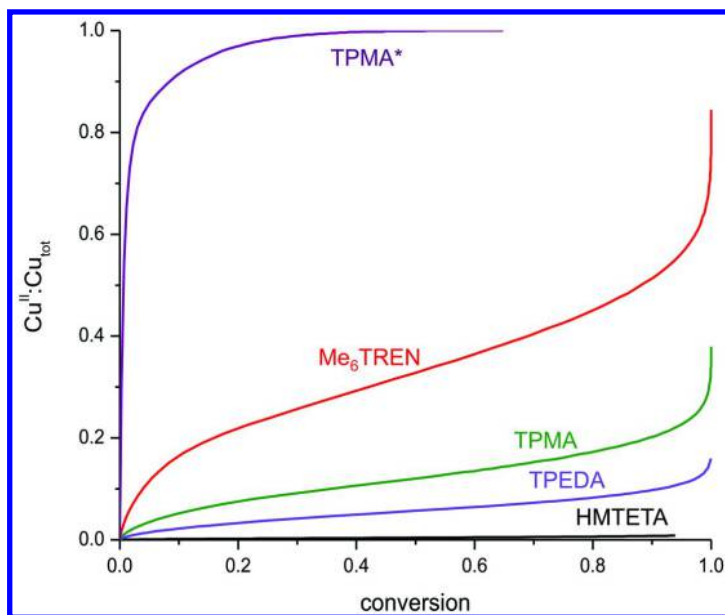
Figure 4. The ratio of Cu^{II} (deactivator) to total Cu ratio in Normal ATRP of MA with different catalysts. Conditions: [M]:[RX]:[CuX]:[CuX$_2$]=200:1:0.2:0 in 50% (v/v) solvent, at a temperature of 25 °C.

The key conclusions that can be drawn from Figures 1-4 are that in Normal ATRP the rate of polymerization increases with the ATRP equilibrium constant up to a certain point. Beyond this optimal activity, the overall polymerization rate decreases since the rate of radical generation and termination is so high that a large fraction of activator complex and polymer chains are lost, and unable to participate in polymerization. Therefore, there was a short period of very high polymerization rate, followed by a relatively low polymerization rate throughout. As long as the catalyst does not lead to excessive termination, a more active catalyst leads to better initiation efficiency and lower dispersity throughout the polymerization.

Simulations of ICAR ATRP

It is also of interest to compare these Normal ATRP results to those of ICAR ATRP, as a model system that uses activator regeneration. ICAR ATRP is chosen since the rate coefficients for all relevant reactions are either known, or can be estimated by scaling known rate coefficients by known factors. In all simulations, the radical initiator of V-70 was assumed, since it decomposes at a non-trivial rate at 25 °C. It should be noted that in the Normal ATRP simulations 1000 ppm of Cu was used, while in these ICAR simulations only 50 ppm of Cu was used, both measured as a molar ratio of Cu to monomer.

Figure 5 shows the semi-logarithmic kinetic plot for all catalysts studied, and indicates that the ultimate rate of polymerization does not depend on the catalyst activity, since all systems had the same steady state slope of the semi-logarithmic kinetic plot. Instead the rate of polymerization is dictated by the balance of radicals generated by dissociation of the radical initiator, and radical loss due to termination (*15*). However, the less active catalysts TPEDA and HMTETA had a significant induction period that was not present in the highly active catalysts such as TPMA* and TPMA*^{N}, and less significant for Me$_6$TREN and TPMA.
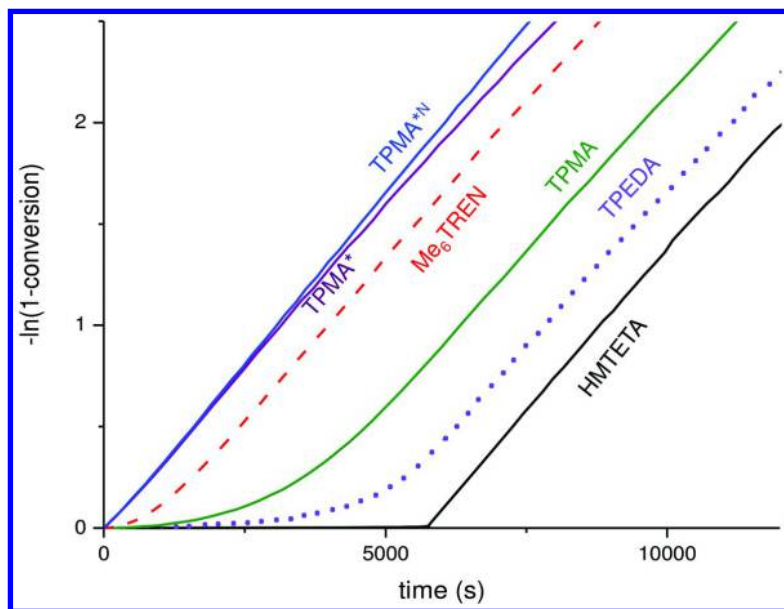
Figure 5. First order kinetic plot for ICAR ATRP of MA with different catalysts. Conditions: [M]:[RX]:[V-70]:[CuX$_2$]=200:1:0.2:0.01 in 50% (v/v) solvent, at a temperature of 25 °C.

It is important to also determine the control over the polymers properties such as uniformity of chains and average chain length in these ICAR ATRP simulations. As seen in Figure 6, the more active catalysts lead to faster initiation and better control over the polymers number average degree of polymerization. HMTETA was not shown in these simulations since the initiation efficiency and its ability to control the molecular weight was very poor. All catalysts, except for TPEDA, gave polymers with molecular weight growing linearly, or close to linearly with conversion, once the conversion exceeded 0.4 (or 40%). In addition, by a conversion of 0.5 the DP$_n$ of all polymer except for the polymer synthesized with the TPEDA catalyst is close to the predicted chain length (dashed black line). In contrast, TPEDA initially gives a very high molecular weight, and the molecular weight only approached the theoretical value after a conversion of 0.8. These results clearly indicate that more active catalysts are desirable for ATRP with catalyst regeneration. This result is expected, since a more active catalyst

is able to initiate chains more effectively, even with low concentrations of the activator.

Figure 6. Evolution of DP_n with conversion for ICAR ATRP of MA with different catalysts. Conditions: $[M]:[RX]:[V-70]:[CuX_2]=200:1:0.2:0.01$ in 50% (v/v) solvent, at a temperature of 25 °C. The predicted DP_n assuming complete and exclusive initiation by the RX initiator is give by the black dashed line.

Similarly, Figure 7 shows the evolution of dispersity (M_w/M_n) with conversion. As expected, based on Figure 6, the catalysts that were more active, lead to lower dispersities. In fact, the most active catalysts TPMA* and TPMA*N lead to very low dispersities at high conversion. In contrast, TPMA leads to polymers with dispersity around 1.4 at high conversion and 1.6-1.7 and a conversion of 0.6, consistent with literature data (*16*). TPEDA leads to a very complex evolution of M_w/M_n, in all cases the dispersity is between 2 and 2.6, it initially increases due to the slow and incomplete initiation and formation of chains with variable chain length. Between a conversion of 0.3 and 0.8 the dispersity decreases slowly, due to the predominant growth of the already formed chains with some contribution from slow initiation of the small molecule alkyl halide to give polymer chains. Finally, above a conversion of 0.8 the dispersity increases again due to the completion of initiation and formation of new much shorter chains. Overall, it is clear that the more active catalysts lead to polymers with lower dispersity. However, there is negligible difference between TPMA* and TPMA*N, and in fact the deactivation rate coefficient of the more active catalyst should be somewhat lower, which would lead to an increase in the dispersity.
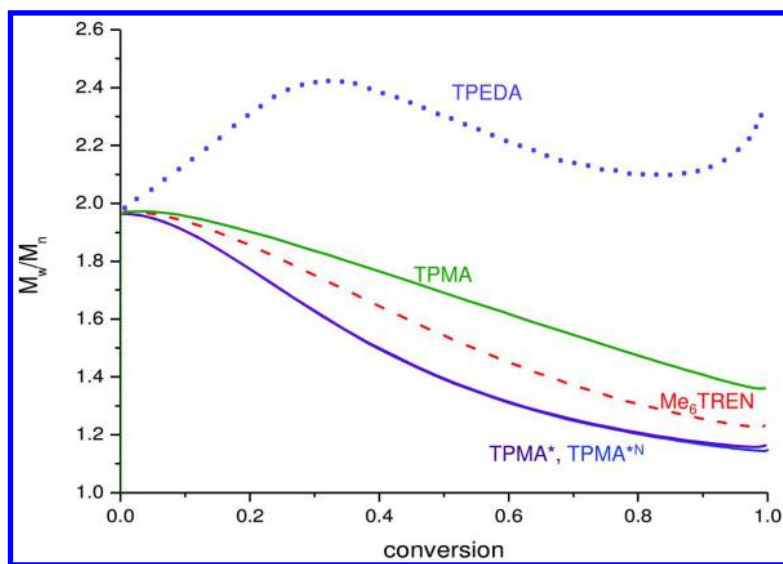
Figure 7. Evolution of M_w/M_n with conversion for ICAR ATRP of MA with different catalysts. Conditions: [M]:[RX]:[V-70]:[CuX$_2$]=200:1:0.2:0.01 in 50% (v/v) solvent, at a temperature of 25 °C.

Finally, it is important to examine the fraction of Cu that is in the deactivator, and consequently as the activator. Figure 8 shows the fraction of Cu that is Cu^{II} for each catalyst, including the HMTETA based catalyst. As expected the more active catalysts such as TPMA* and TPMA*^{N} have essentially all the Cu in the Cu^{II} deactivator state. This allows efficient deactivation of the radical. In contrast, the less active catalyst such as TPMA have only about one third of the Cu as Cu^{II}, implying that the transient radical lifetime is longer and chains are less uniform. Finally TPEDA has only 1 out of 10 Cu in the Cu^{II} state, and HMTETA has almost no Cu in the deactivator state. This leads to very high chain lengths, since there is virtually no Cu^{II} available to deactivate radicals. This leads to an important point of distinction between Normal ATRP and ATRP with activator regeneration. In Normal ATRP, to a good approximation the radical concentration is determined by the ATRP equilibrium constant and the externally added ratio of Cu^{I} to Cu^{II}. In well-controlled Normal ATRP the ratio of Cu^{I} to Cu^{II} does not change dramatically as the reaction progresses, especially if some Cu^{II} is added at the start of the reaction. In contrast, in ICAR ATRP, and other ATRPs that utilize activator regeneration, the radical concentration is determined from the balance of radicals generated, for instance by the decomposition of a radical initiator, and radicals lost to termination. Once this radical concentration is established, the ratio of Cu^{I} to Cu^{II} is determined by the ATRP equilibrium constant, the radical concentration and the alkyl halide concentration. Therefore, polymerizations with active catalysts will have the Cu^{I} to Cu^{II} ratio shifted far towards the Cu^{II} deactivator, while less active catalysts have more Cu^{I} present during polymerization.
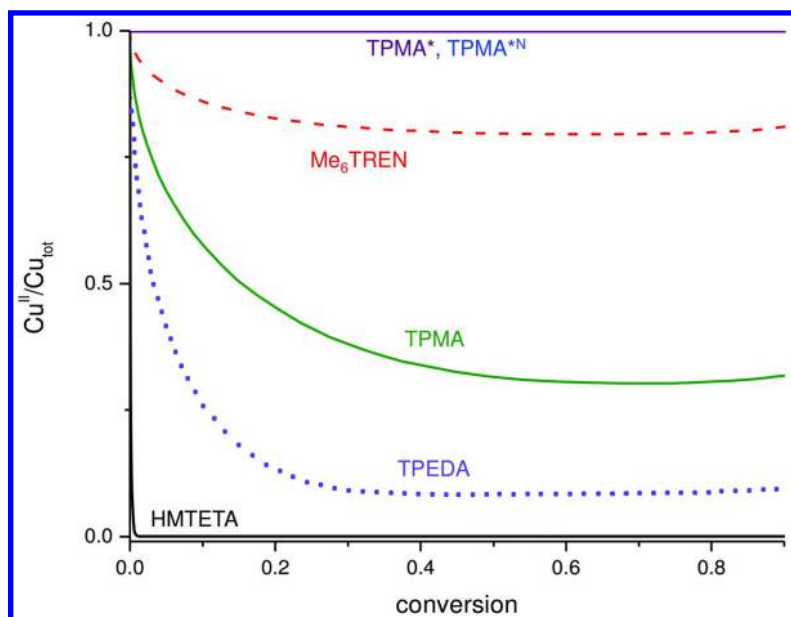
Figure 8. Evolution of The Cu^{II} (deactivator) to total Cu ratio with conversion for ICAR ATRP of MA with different catalysts. Conditions: [M]:[RX]:[V-70]:[CuX$_2$]=200:1:0.2:0.01 in 50% (v/v) solvent, at a temperature of 25 °C.

Conclusions

Simulations were performed for Normal and ICAR ATRP. Based on the key findings in this chapter, conditions must be carefully chosen for Normal ATRP. The nature of the catalyst must be properly selected for the monomer to be polymerized in a controlled fashion. The catalyst must be sufficiently active to allow the reaction to proceed at a reasonable rate, but if the catalyst is too active, the reaction will not reach high conversion since radical termination will dominate in the initial phase. ICAR ATRP is less sensitive, and in principle more active catalyst will lead to as good, if not better control over the polymerization. However, side reactions such as catalytic radical termination (*42*, *43*) and lower deactivation rates for highly active catalysts (*30*), could lead to a decrease in performance with highly active catalysts. Nevertheless, the general conclusion is that Normal ATRP requires a catalyst that is carefully tuned to the activity of the monomer, while ICAR ATRP, and other ATRP processes with activator regeneration, are better controlled with more active catalysts.

Acknowledgments

References

1. Goto, A.; Fukuda, T. *Prog. Polym. Sci.* **2004**, *29*, 329–385.
2. Braunecker, W. A.; Matyjaszewski, K. *Prog. Polym. Sci.* **2007**, *32*, 93–146.
3. Konkolewicz, D.; Krys, P.; Matyjaszewski, K. *Acc. Chem. Res.* **2014**, *47*, 3028–3036.
4. Moad, G.; Solomon, D. H. *The chemistry of free radical polymerization*, 2nd ed.; Elsevier: Amsterdam, 2006.
5. Georges, M. K.; Veregin, R. P. N.; Kazmaier, P. M.; Hamer, G. K. *Macromolecules* **1993**, *26*, 2987–8.
6. Nicolas, J.; Guillaneuf, Y.; Lefay, C.; Bertin, D.; Gigmes, D.; Charleux, B. *Prog. Polym. Sci.* **2013**, *38*, 63–235.
7. Kato, M.; Kamigaito, M.; Sawamoto, M.; Higashimura, T. *Macromolecules* **1995**, *28*, 1721–3.
8. Wang, J.-S.; Matyjaszewski, K. *J. Am. Chem. Soc.* **1995**, *117*, 5614–15.
9. Matyjaszewski, K. *Macromolecules* **2012**, *45*, 4015–4039.
10. Chiefari, J.; Chong, Y. K.; Ercole, F.; Krstina, J.; Jeffery, J.; Le, T. P. T.; Mayadunne, R. T. A.; Meijs, G. F.; Moad, C. L.; Moad, G.; Rizzardo, E.; Thang, S. H. *Macromolecules* **1998**, *31*, 5559–5562.
11. Moad, G.; Rizzardo, E.; Thang, S. H. *Aust. J. Chem.* **2012**, *65*, 985–1076.
12. Matyjaszewski, K.; Xia, J. *Chem. Rev.* **2001**, *101*, 2921–2990.
13. Matyjaszewski, K.; Tsarevsky, N. V. *J. Am. Chem. Soc.* **2014**, *136*, 6513–6533.
14. Fischer, H. *Chem. Rev.* **2001**, *101*, 3581–3610.
15. Tsarevsky, N. V.; Matyjaszewski, K. *Chem. Rev.* **2007**, *107*, 2270–2299.
16. Matyjaszewski, K.; Jakubowski, W.; Min, K.; Tang, W.; Huang, J. Y.; Braunecker, W. A.; Tsarevsky, N. V. *Proc. Natl. Acad. Sci. U. S. A.* **2006**, *103*, 15309–15314.
17. D'Hooge, D. R.; Konkolewicz, D.; Reyniers, M.-F.; Marin, G. B.; Matyjaszewski, K. *Macromol. Theory Simul.* **2012**, *21*, 52–69.
18. Jakubowski, W.; Matyjaszewski, K. *Angew. Chem., Int. Ed.* **2006**, *45*, 4482–4486.
19. Jakubowski, W.; Min, K.; Matyjaszewski, K. *Macromolecules* **2006**, *39*, 39–45.
20. Magenau, A. J. D.; Strandwitz, N. C.; Gennaro, A.; Matyjaszewski, K. *Science* **2011**, *332*, 81–84.
21. Magenau, A. J. D.; Bortolamei, N.; Frick, E.; Park, S.; Gennaro, A.; Matyjaszewski, K. *Macromolecules* **2013**, *46*, 4346–4353.
22. Konkolewicz, D.; Wang, Y.; Zhong, M.; Krys, P.; Isse, A. A.; Gennaro, A.; Matyjaszewski, K. *Macromolecules* **2013**, *46*, 8749–8772.
23. Percec, V.; Barboiu, B.; van der Sluis, M. *Macromolecules* **1998**, *31*, 4053–4056.
24. Abreu, C. M. R.; Mendonça, P. V.; Serra, A. n. C.; Popov, A. V.; Matyjaszewski, K.; Guliashvili, T.; Coelho, J. F. J. *ACS Macro Lett.* **2012**, *1*, 1308–1311.
25. Tasdelen, M. A.; Uygun, M.; Yagci, Y. *Macromol. Chem. Phys.* **2010**, *211*, 2271–2275.

26. Konkolewicz, D.; Schröder, K.; Buback, J.; Bernhard, S.; Matyjaszewski, K. *ACS Macro Lett.* **2012**, *1*, 1219–1223.

27. Ribelli, T. G.; Konkolewicz, D.; Bernhard, S.; Matyjaszewski, K. *J. Am. Chem. Soc.* **2014**, *136*, 13303–13312.

28. Magenau, A. J. D.; Kwak, Y.; Schröder, K.; Matyjaszewski, K. *ACS Macro Lett.* **2012**, *1*, 508–512.

29. Zhang, C. X.; Kaderli, S.; Costas, M.; Kim, E.-i.; Neuhold, Y.-M.; Karlin, K. D.; Zuberbühler, A. D. *Inorg. Chem.* **2003**, *42*, 1807–1824.

30. Tang, W.; Kwak, Y.; Braunecker, W.; Tsarevsky, N. V.; Coote, M. L.; Matyjaszewski, K. *J. Am. Chem. Soc.* **2008**, *130*, 10702–10713.

31. Buback, M.; Kurz, C. H.; Schmaltz, C. *Macromol. Chem. Phys.* **1998**, *199*, 1721–1727.

32. Heuts, J. P. A.; Russell, G. T. *Eur. Polym. J.* **2006**, *42*, 3–20.

33. Smith, G. B.; Russell, G. T.; Heuts, J. P. A. *Macromol. Theory Simul.* **2003**, *12*, 299–314.

34. Johnston-Hall, G.; Monteiro, M. J. *J. Polym. Sci., Part A: Polym. Chem.* **2008**, *46*, 3155–3173.

35. Dixon, K. W. Decomposition rates of organic free radical initators. In *Polymer Handbook*, 4th ed.; Brandrup, J., Immergut, E. H., Grulke, E. A., Eds.; John Wiley and Sons: New York, 1999; p II/8.

36. Schröder, K.; Mathers, R. T.; Buback, J.; Konkolewicz, D.; Magenau, A. J. D.; Matyjaszewski, K. *ACS Macro Lett.* **2012**, 1037–1040.

37. Balili, M. N. C.; Pintauer, T. *Inorg. Chem.* **2010**, *49*, 5642–5649.

38. Seeliger, F.; Matyjaszewski, K. *Macromolecules* **2009**, *42*, 6050–6055.

39. Braunecker, W. A.; Tsarevsky, N. V.; Gennaro, A.; Matyjaszewski, K. *Macromolecules* **2009**, *42*, 6348–6360.

40. Bergenudd, H.; Jonsson, M.; Malmström, E. *Macromol. Theory Simul.* **2011**, *20*, 814–825.

41. Wang, Y.; Zhong, M.; Zhang, Y.; Magenau, A. J. D.; Matyjaszewski, K. *Macromolecules* **2012**, *45*, 8929–8932.

42. Wang, Y.; Soerensen, N.; Zhong, M.; Schroeder, H.; Buback, M.; Matyjaszewski, K. *Macromolecules* **2013**, *46*, 683–691.

43. Schröder, K.; Konkolewicz, D.; Poli, R.; Matyjaszewski, K. *Organometallics* **2012**, *31*, 7994–7999.

<center>**Chapter 6**</center>

Tris(2-pyridylmethyl)amine Based Ligands in Copper Catalyzed Atom Transfer Radical Addition (ATRA) and Polymerization (ATRP)

<center>**Tomislav Pintauer***</center>

<center>**Department of Chemistry and Biochemistry, Duquesne University, 308 Mellon Hall, 600 Forbes Avenue, Pittsburgh, Pennsylvania 15282, United States**
***E-mail: pintauert@duq.edu**</center>

Copper complexes with tris(2-pyridylmethyl)amine (TPMA) ligand are currently among the most active catalysts in atom transfer radical addition (ATRA) and polymerization (ATRP) reactions that utilize reducing agents. Both processes originated from well-known Kharasch addition in which polyhalogenated compounds were added to alkenes via free-radical means. The main focus of this article is to review structural and mechanistic aspects of ATRA and ATRP reactions catalyzed by copper complexes with TPMA ligand. Special emphasis will be placed on recently developed substituted TPMA based ligands that contain electron donating groups.

Introduction and Background

Historical Perspectives

Tris(2-pyridylmethyl)amine (TPMA or TPA) is a widely used neutral tripodal nitrogen based ligand that has been complexed to a wide variety of transition metals. The original synthesis of TPMA reported in 1967 involved alkylation of picolylamine by picolyl chloride (*1*). A more efficient route through reductive amination of 2-pyridinecarboxaldehyde using sodium triacetoxyborohydride as the reducing agent was discovered in 1998 (Scheme 1) (*2*).

Currently, the Cambridge Crystallographic Database contains over 1100 structures of TPMA complexes with metals spanning from group 1 to 13 of

the periodic table, including many cases from the lanthanide and actinide series (Figure 1). Some representative examples are shown in Figure 2 (*3–9*). TPMA contains both σ-donating tertiary amine and π-accepting pyridyl groups and it is an excellent chelator that typically coordinates to a transition metal in a tetradentate fashion (*10–13*). However, in some cases tridentate coordination resulting from pyridyl arm dissociation has also been observed (*10*, *14*, *15*).
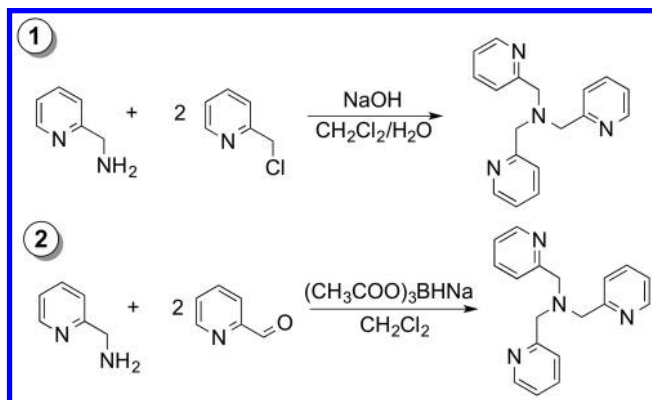
Scheme 1. Synthetic routes for the preparation of tris(2-pyridylmethyl)amine (TPMA).
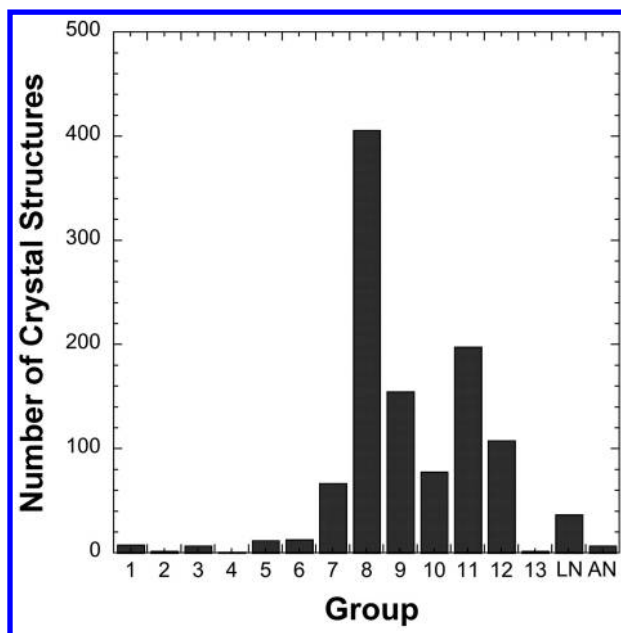
Figure 1. A plot of a number of crystal structures containing TPMA ligand vs. group number in the periodic table. LN and AN correspond to lanthanide and actinide series, respectively.
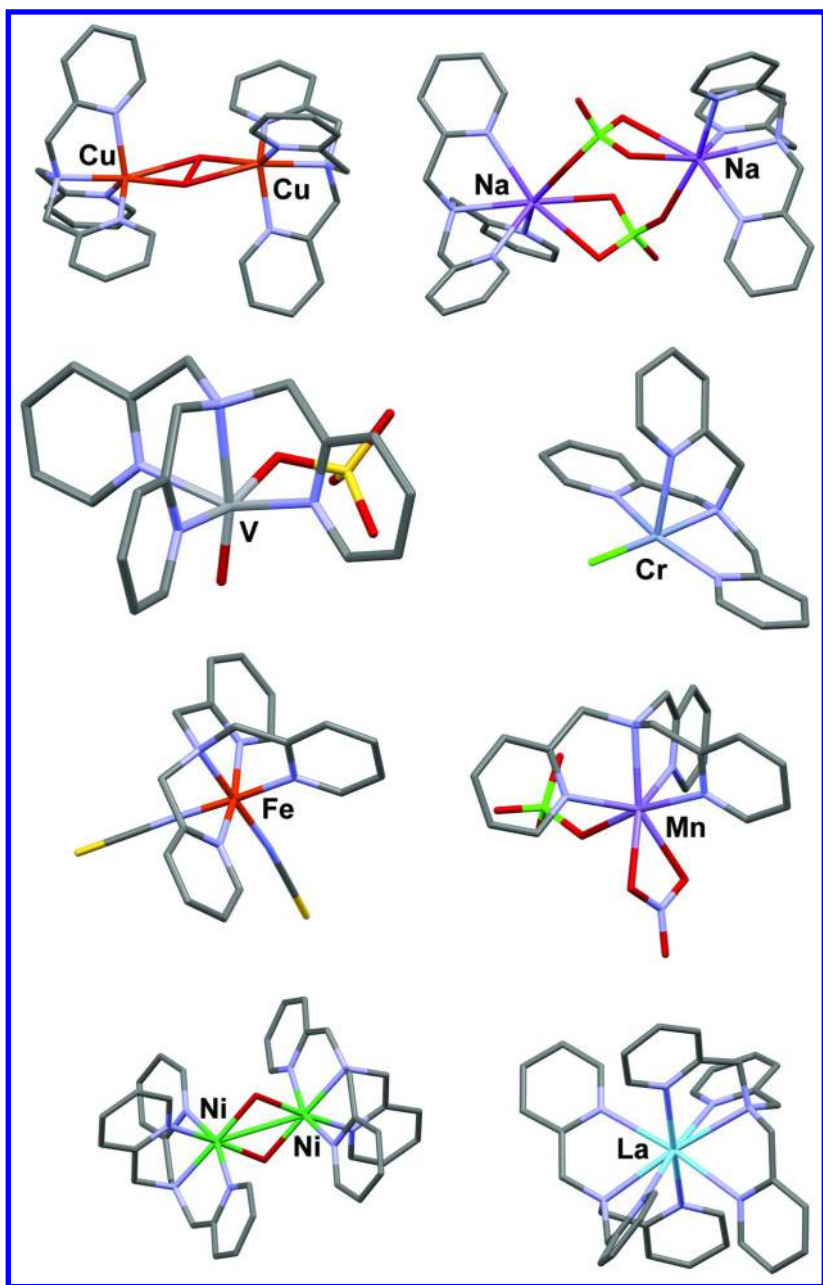
Figure 2. Selected molecular structures of metal complexes containing TPMA ligand (3–9).

Catalysis with Transition Metal Complexes Containing TPMA Ligand

During the past two decades, TPMA has received a considerable attention as a ligand of choice for many transition metal catalyzed reactions. For example, it is widely used as a chelator in copper and/or iron complexes that mimic certain metalloenzymes of relevance to oxygen activation (*12*, *16–25*). Furthermore, a number of metal complexes with TPMA have also been shown to be active in C-H and O-O activation of small molecules (*26–32*), as well as [3+2] azide-alkyne cycloaddition (*33–38*).

Lastly, copper complexes with TPMA are currently among the most active catalysts in atom transfer radical addition (ATRA) (*13*, *39*, *40*) and polymerization (ATRP) reactions (*41–43*). Both processes originated from well-known Kharasch addition in which polyhalogenated compounds were added to alkenes via free-radical means (*13*, *39*, *40*). Recent studies have also indicated that TPMA is a superior complexing ligand in ATRA (*13*, *33*, *40*, *44–54*) and ATRP (*49*, *55–58*) that utilize reducing agents. The role of a reducing agent in both systems is to continuously regenerate the activator species (copper(I) complex) from the corresponding deactivator (copper(II) complex). The latter one accumulates in the system as a result of unavoidable and often diffusion controlled radical-radical termination reactions. As a result, both processes can be conducted very efficiently using ppm amounts of the catalyst (*49*). As indicated in Scheme 2,in the case of ARGET and ICAR ATRP, the ATRP equilibrium ($K_{ATRP}=k_a/k_d$) is controlled by a fast and reversible homolytic cleavage of C-(pseudo)halogen bond in a redox reaction with a copper(I) catalyst, yielding well-defined halogen-capped polymers. Concequently, ATRP provides a very versatile tool for the preparation of polymers with predefined functionalities, compositions and architectures (*59–62*). Alternative approaches to catalyst regeneration that are not shown in Scheme 2 include recently reported e-ATRP, photo-ATRP and SARA ATRP.
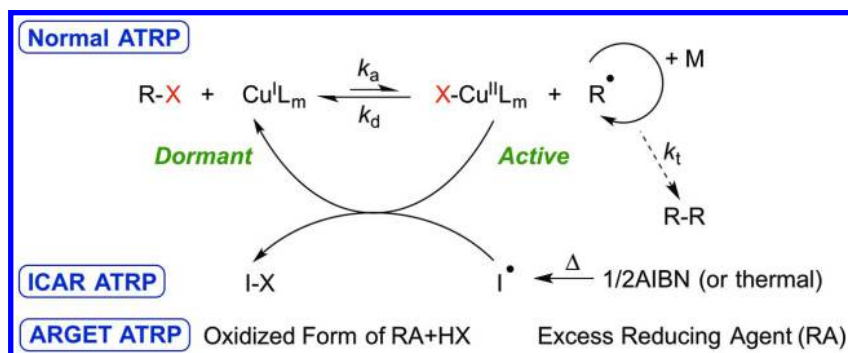
Scheme 2. Representation of ATRP equilibrium.

Methods Commonly Used To Determine Activity of Copper Complexes in ATRA and ATRP

The equilibrium constant for atom transfer ($K_{ATRP \text{ or } ATRA}=k_a/k_d$) provides critical information about the position of dynamic equilibrium between dormant

and active species during polymerization or addition. The relative magnitude of K_{ATRP} can be easily accessed from the kinetics using $\ln([M]_o/[M]_t)$ v.s. t plots, which provide values for the apparent equilibrium constant $K_{ATRP}^{app}=K_{ATRP}/[Cu^{II}]$. More accurate values can be obtained from model studies using modified analytical solution of the persistent radical effect (*63*) originally developed by Fischer (*64–66*) and Fukuda (*67*). It is very important to note that it is not possible to determine from K_{ATRP} alone whether the polymerization will be controlled; fast activation and even more importantly fast deactivation are required to achieve good control over polymer molecular weights and molecular weight distribution. Therefore, precise measurements of the activation (k_a) and deactivation (k_d) rate constants should be used for correlation with catalyst, alkyl halide and monomer structures.

Activation rate constants (k_a) in ATRA/ATRP are typically determined from model studies in which copper(I) complex is reacted with alkyl halide in the presence of radical trapping agents such as TEMPO (*68–70*). Rates are determined by monitoring the rate of disappearance of alkyl halide in the presence of large excess of the activator (Cu^I/L) and TEMPO. Under such pseudo-first order conditions, the activation rate constant can be calculated from $\ln([RX]_o/[RX]_t)$ v.s. t plots (slope=$-k_a[Cu^I/L]_o$).

Deactivation rate constants (k_d) have been much less studies in ATRA/ATRP. The principal reason is the lack of experimental techniques for measuring relatively fast deactivation processes (10^7-10^9 M^{-1}s^{-1}). One of the methods includes the clock reaction in which the generated radical are simultaneously trapped with TEMPO and the deactivator or copper(II) complex (*69*).

Apart from independently measuring $K_{ATRA\ or\ ATRP}$, k_a and k_d, electrochemical measurements are commonly used to predict the activity of copper complexes in ATRA or ATRP (*50, 61, 71–76*). Generally, for a given alkyl halide, $K_{ATRA\ or\ ATRP}$ can be directly correlated with $E_{1/2}$ values, provided that the halidophilicity of the metal complex remains constant. As a result, for copper complexes with neutral nitrogen based ligands commonly used in ATRA and ATRP, a linear correlation between $\ln(K_{ATRP})$ and $E_{1/2}$ values is typically observed (*63, 74, 77*).

Another method of predicting the activity of copper complexes in ATRA or ATRP is to directly compare the stability constants of Cu^{II} and Cu^I complexes with the particular ligand (β^{II} and β^I, respectively, Eq. [1]). Both β^{II} and β^I

$$\beta^m = \frac{[Cu^m L_n]}{[Cu^m][L]^n}; m=I\ or\ II, n=1\ or\ 2 \qquad [1]$$

should be large enough in order to eliminate or suppress possible concurrent reactions such as coordination of monomer and/or polymer, which are typically present in large excess relative to the catalyst. Generally, a copper complex with a low reduction potential should be more stable in its oxidized form (i.e. Cu^{II} should be more stable than Cu^I) in order to achieve high catalytic activity (*75, 76*). For the case of relatively stable 1:1 copper complexes, the ratio of stability constants can be calculated from the readily available reduction potentials using Eq. [2], where $E^{o'}_{Cu^{II}/Cu^I}$ corresponds to a standard reduction potential for the Cu^{II}/Cu^I couple in the absence of a coordinating ligand (*78–81*).

$$\ln \frac{\beta^{\mathrm{II}}}{\beta^{\mathrm{I}}} = \frac{F}{RT}\left(E^{\mathrm{o'}}_{\mathrm{Cu^{II}/Cu^{I}}} - E^{\mathrm{o'}}_{\mathrm{Cu^{II}L/Cu^{I}L}}\right) \qquad [2]$$

Unfortunately, Eq. [2] only provides the ratio and not the specific stability constants for the respective oxidation states. While this ratio may increase with more active catalysts, it is not directly known whether this is a result of an increase in β^{II} or a decrease in β^{I}. However, another quantity, namely $\beta^{\mathrm{II}}/(\beta^{\mathrm{I}})^2$ ratio, can be readily obtained from disproportionation studies as previously reported in the literature (57, 71). Utilizing the reaction between Cu^0 and $[Cu^{II}/L][OTf]_2$ (L=complexing ligand), the equilibrium constant, K_{disp}, can be determined and consequently $\beta^{\mathrm{II}}/(\beta^{\mathrm{I}})^2$. Finally, using these two experimentally determined ratios ($\beta^{\mathrm{II}}/\beta^{\mathrm{I}}$ and $\beta^{\mathrm{II}}/(\beta^{\mathrm{I}})^2$), the individual stability constants β^{I} and β^{II} can be calculated. It is important to note that both the electrochemical and disproportionation studies need to be conducted in the same solvent for accurate and consistent results. As indicated in Table 1, more reducing copper(I) complexes indeed have higher values for both K_{ATRP} and the ratio of stability constants ($\beta^{\mathrm{II}}/\beta^{\mathrm{I}}$).

Table 1. Correlations between K_{ATRP}, redox potential ($E_{1/2}$) and stability constants (β^{I} and β^{II}) for copper complexes with neutral nitrogen based ligands commonly used in ATRA and ATRP.

Cu^IBr/L^a	$E_{1/2}$ (V)	K_{ATRP}	β^{I}	β^{II}	$\beta^{\mathrm{II}}/\beta^{\mathrm{I}}$
bpy	0.035	3.9×10^{-9}	8.9×10^{12}	4.5×10^{13}	5.1
HMTETA	-0.025	8.4×10^{-9}	1.0×10^{11}	4.0×10^{12}	40
PMDETA	-0.075	7.5×10^{-8}	$<1.0\times10^8$	1.4×10^{12}	$>1.4\times10^4$
TPMA	-0.245	9.6×10^{-6}	7.9×10^{12}	3.9×10^{17}	4.9×10^4
Me$_6$TREN	-0.300	1.5×10^{-4}	6.3×10^8	2.7×10^{15}	4.3×10^6

[a] All values were taken from Refs. (75) and (77). Stability constants (β^{I} and β^{II}) were measured in aqueous medium. K_{ATRP} values were determined in CH_3CN at 22±2 °C for ethyl-2-bromoisobutyrate. $E_{1/2}$ values were measured in CH_3CN and are relative to SCE.

Furthermore, an increase in $\beta^{\mathrm{II}}/\beta^{\mathrm{I}}$ ratio for a particular ligand is mostly the result of an increase in the stability constant of the copper(II) relative to copper(I) complex (63, 75, 77, 82–86).

Development of Highly Active Copper Complexes for ATRA and ATRP

With the recent discovery indicating that the reducing agents can significantly reduce the amount of copper complexes in ATRA and ATRP (49), a significant effort has been devoted towards development of more active catalysts that could be used at even lower concentrations, and potentially enable single additions and controlled radical polymerization of α-olefins. In the case of ATRA, the complexity of challenges behind future catalytic design is depicted in

Figure 3, which shows the values of the equilibrium constant for atom transfer ($K_{ATRA}=k_a/k_d$) for a variety of alkyl halides using currently among the most active Cu^I(TPMA)X (X=Br or Cl) complexes (*45*, *46*). Clearly, K_{ATRA} spans several orders of magnitude, which is mainly the result of large differences in C-X bond dissociation energies. Furthermore, since the rate of alkene consumption in ATRA is directly proportional to the product of addition rate constant (k_{add}) and K_{ATRA}, one can compare the reaction times and catalyst loadings for other alkyl halides to currently the most active CBr$_4$, which has been extensively studied in our laboratories (*44–46*, *54*, *87*). For example, the addition of CBr$_4$ to 1-octene in the presence of reducing agents using 5 ppm of the catalyst is completed within 3 h at 60 °C, yielding the monoadduct in greater than 96% yield (*45*). Under identical reaction conditions and assuming that k_{add} stays constant, ATRA with CCl$_4$, 2-chloropropionitrile (**7**) and bromoethane (**14**) would require 63, 6.8×10^4 and 8.8×10^9 ppm of copper, respectively, in order to be completed in 3 hours (bottom plot in Figure 3). Alternatively, if the catalyst concentration was kept at 5 ppm, ATRA with the same alkyl halides would take 38 hours, 1800 days and nearly one million years, respectively (top plot in Figure 3). Similar conclusions can also be drawn for mechanistically similar ATRP. Clearly, a search for a better and more efficient catalysts could be beneficial for both processes.
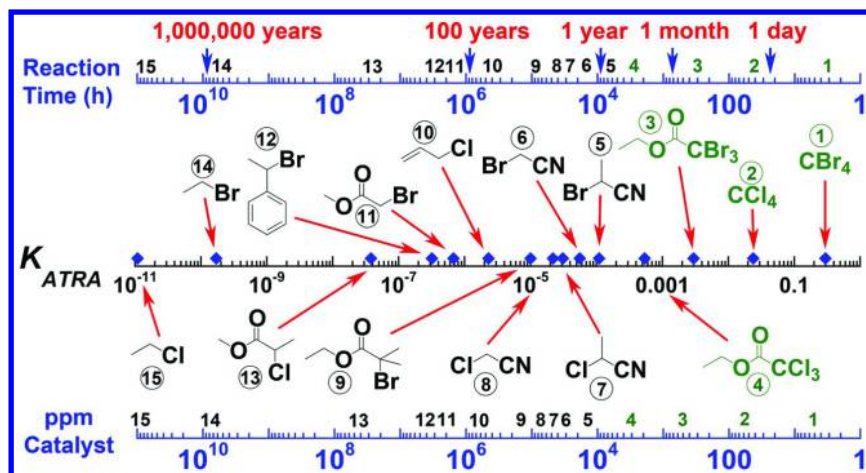
Figure 3. ATRA equilibrium constants (K_{ATRA}) for various initiators with Cu^I(TPMA)X (X=Br or Cl) in CH$_3$CN at 22 °C. Top: time required to reach 99% conversion with 5 ppm of catalyst. Bottom: catalyst concentration in ppm required to reach 99% conversion in 3 hours. Values for K_{ATRA} were taken from Refs. (63, 74) and (44). Calculations were based on the assumption that the kinetics are not governed by other processes such as reduction.

Recent advances in this area of research are significantly focused on modifying the existing ligand frameworks, which can be used to tailor electronic properties of the copper(I) center. One way to increase the reduction potential of copper(I) complex is through systematic incorporation of electron donating groups

(EDGs) to ligands that are already active in ATRA or ATRP. This approach indeed seems to be justified, as demonstrated in a recent study which showed that EDGs in the *para*-substituted 2,2′-bipyridine ligands can significantly enhance catalytic activity in ATRP (*88*). In a related work, inspired by the synthetic modifications of TPMA ligand for copper catalyzed oxygen activation (*89*) and iron mimicking site for methane monooxygenase (*90*), even more active $Cu^{II}X_2$/TPMA*3 (X=Br or Cl, TPMA*3= tris((4-methoxy-3,5-dimethylpyridin-2-yl)methyl)amine) *in situ* system was discovered containing a total of nine EDGs (*91*). This catalyst attained excellent polymerization results in photoATRP (*92–94*) of acrylates and emerged as one of the most active ATRP systems nowadays. Furthermore, it also elucidated the interplay between ATRP, organometallic mediated radical polymerization (OMRP) and catalytic termination pathways for the first time (*95*).

As evident from the discussion above, further development and catalytic activity of transition metal complexes containing modified TPMA ligands could provide invaluable and important information to various research fields ranging from inorganic, bioinorganic to organic/polymer chemistry. The main focus of this article is to review structural and mechanistic aspects of ATRA and ATRP reactions catalyzed by copper complexes with tris(2-pyridylmethyl)amine ligand and its derivatives containing electron donating groups.

Structural Features of Copper(I and II) Complexes with TPMA Ligand

Solid State Studies

Currently, copper complexes with neutral tetradentate tris(2-pyridylmethyl)amine) (TPMA) ligand are among the most active and versatile catalysts for ATRP/ATRA/ATRC reactions that utilize reducing agents (*13*, *36*, *40*, *47*, *50*). In the solid state, copper(II) complexes with the general formula $[Cu^{II}(TPMA)X][Y]$ (X=Cl^-, Br^- and Y=Cl^-, Br^-, ClO_4^-, BPh_4^- or PF_6^-) are typically distorted trigonal bipyramidal in geometry, and the counterion has negligible effect on the structure of $[Cu^{II}(TPMA)X]^+$ cation (Table 2 and Figure 4), which acts as a deactivator during the catalytic cycle (Scheme 2) (*10*).

On the contrary, the structures of the corresponding Cu^I complexes or activators are strongly dependent not only on the counterion, but also on neutral auxiliary ligands (*10*). For example, partial dissociation of one of the pyridyl arms in TPMA is typically not observed when small auxiliary ligands such as CH_3CN, Cl^- or Br^- are coordinated to the copper(I) center, but will occur with the larger ones such as PPh_3 or 4,4′-dipyridyl.

Furthermore, depending on the counterion, dimerization in the solid state can also be observed. So far, all structurally characterized copper(I) complexes with TPMA ligand adopt a distorted tetrahedral geometry, with the exception of $[Cu^I(TPMA)][BPh_4]$, which is trigonal pyramidal due to stabilization via a long cuprophilic interaction with a bond length of 2.8323(12) Å (Figure 5).

Table 2. Structural Comparison of [Cu^{II}(TPMA)X][Y] Complexes (X=Br⁻ or Cl⁻, Y=Cl⁻, Br⁻, ClO₄⁻).

parameter[a]	X=Cl⁻, Y=Cl⁻	X=Br⁻, Y=Br⁻	X=Cl⁻, Y=ClO₄⁻
Cu-N$_{ax}$	2.0481(14)	2.040(3)	2.0413(15)
Cu-N$_{eq}$	2.0759(8)	2.073(2)	2.1115(16)
Cu-N$_{eq}$	2.0759(8)	2.073(2)	2.0567(16)
Cu-N$_{eq}$	2.0759(8)	2.073(2)	2.0292(16)
Cu-X	2.2369(4)	2.3836(6)	2.2390(5)
τ	1.0	1.0	1.0

[a] Bond lengths are given in angstroms (Å) and angles in degrees (deg). τ parameter is calculated as $\tau=(\varphi_1-\varphi_2)/60$, where φ_1 and φ_2 are the largest and second largest N-Cu^{II}-N(X) bond angles, τ=1 (regular trigonal bipyramidal geometry) and τ=0 (regular square pyramidal geometry.
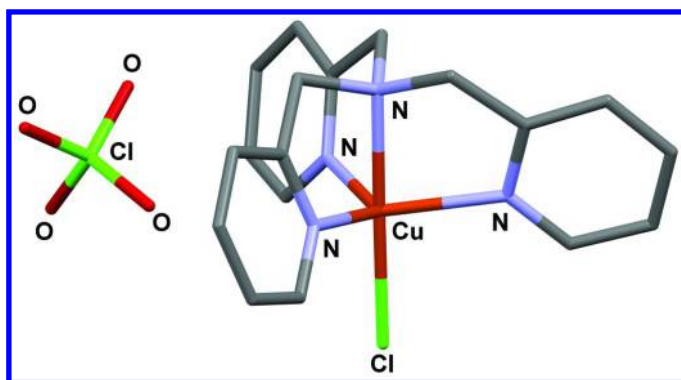
Figure 4. Molecular structure of [Cu^{II}(TPMA)Cl][ClO₄] (10). H atoms have been omitted for clarity.

Solution Studies

Variable temperature ^{1}H NMR spectroscopy is typically used to probe structures of copper(I) complexes with TPMA ligand in solution. This technique has been used to examine the structures of Cu^I(TPMA)Br (*45*) and Cu^I(TPMA)Cl (*46*, *96*) complexes, which were found to be highly symmetrical and monomeric in solution, as indicated by chemically equivalent pyridine rings (Figure 6a). A very similar ^{1}H NMR spectrum was also observed for [Cu^I(TPMA)(CH₃CN)][BPh₄].
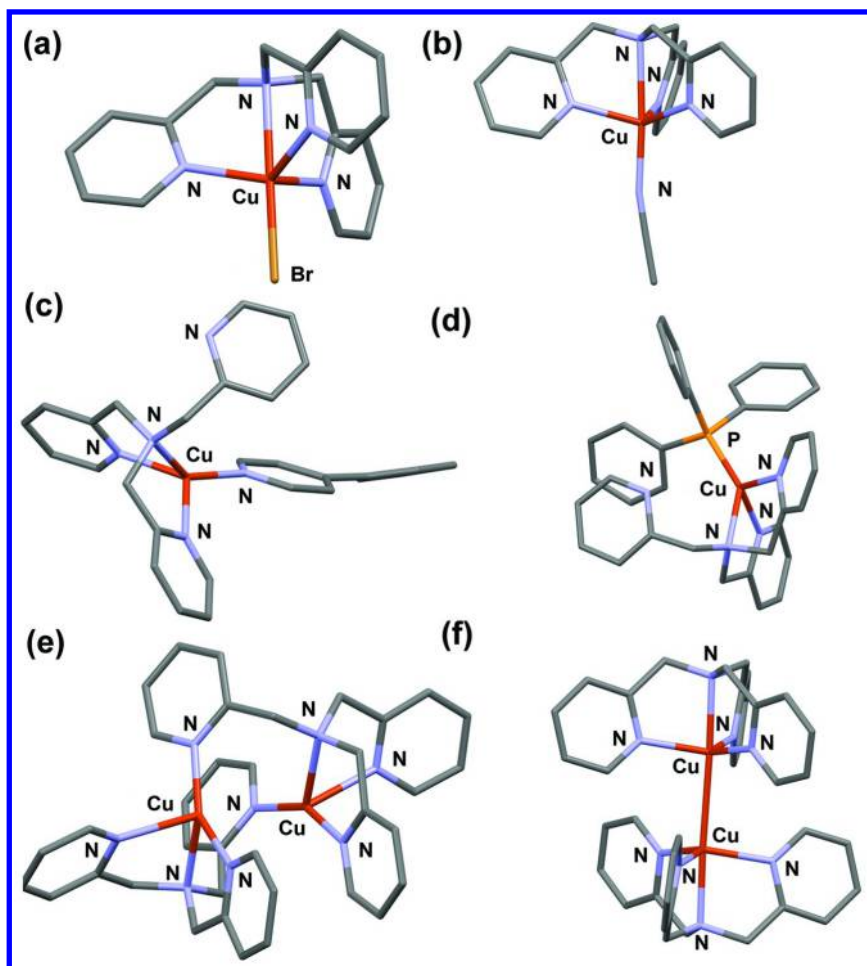
Figure 5. Molecular structures of Cu^I(TPMA)Br (a), [Cu^I(TPMA(CH$_3$CN))][BPh$_4$] (b), [Cu^I(TPMA)(4,4'-bpy)][BPh$_4$] (c), [Cu^I(TPMA)(PPh$_3$)][BPh$_4$] (d), [Cu^I(TPMA)]$_2$[ClO$_4$]$_2$ (e) and [Cu^I(TPMA)][BPh$_4$] (f) (10, 45, 46). H-atoms and counterions have been omitted for clarity.
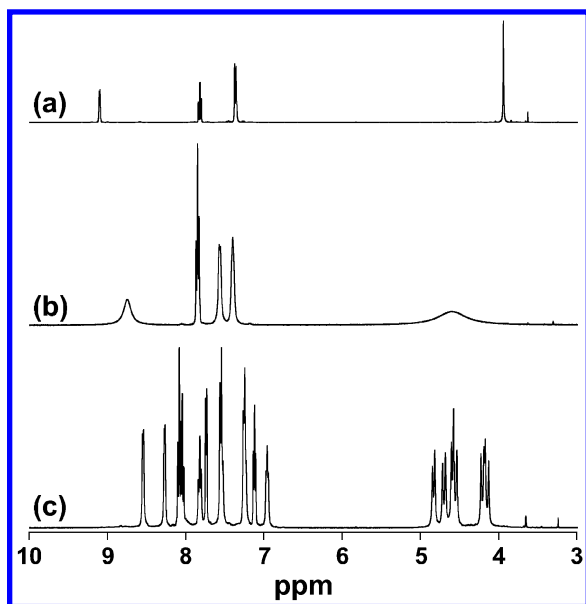
Figure 6. ^1H NMR spectra (400 MHz, $(CD_3)_2CO$) of $[Cu^I(TPMA)Br]$ at 180K (a), $[Cu^I(TPMA)][ClO_4]$ at 298K (b), and $[Cu^I(TPMA)]_2[ClO_4]_2$ at 185K (c). Reproduced with permission from reference (10). Copyright 2010, American Chemical Society.

In $[Cu^I(TPMA)(CH_3CN)][BPh_4]$, a singlet for acetonitrile was shifted downfield by approximately 1.6 ppm in acetone-d_6 upon cooling from 298 K to 180 K, indicating a deshielding effect as a result of coordination (*10, 87*). On the other hand, $[Cu^I(TPMA)]_2[ClO_4]*CH_3OH$, exhibited four broad resonances at room temperature similar to $Cu^I(TPMA)Br$, suggesting the structure was also monomeric (Figure 6b). Interestingly, upon cooling to 185K, evidence for dimer formation consistent with the solid state structure was clearly observed by the emergence of three sets of unequal peaks between 8.54 and 6.95 ppm for the pyridyl and 4.82 and 4.17 ppm for the methylene protons (Figure 6c). When the same complex was dissolved in acetonitrile-d_3, only peaks corresponding to the monomer were observed, indicating the formation of $[Cu^I(TPMA)(CD_3CN)][ClO_4]$. Similarly, at room temperature $[Cu^I(TPMA)][BPh_4]$ also exhibited a monomeric structure resembling $[Cu^I(TPMA)(CH_3CN)][BPh_4]$. However, upon cooling to 180K, the peaks associated with the dimer formation clearly emerged in relatively equal proportions relative to the monomer. Therefore, it is likely that for $[Cu^I(TPMA)][BPh_4]$, an equilibrium between the monomer and dimer exists in solution as shown in Scheme 3.
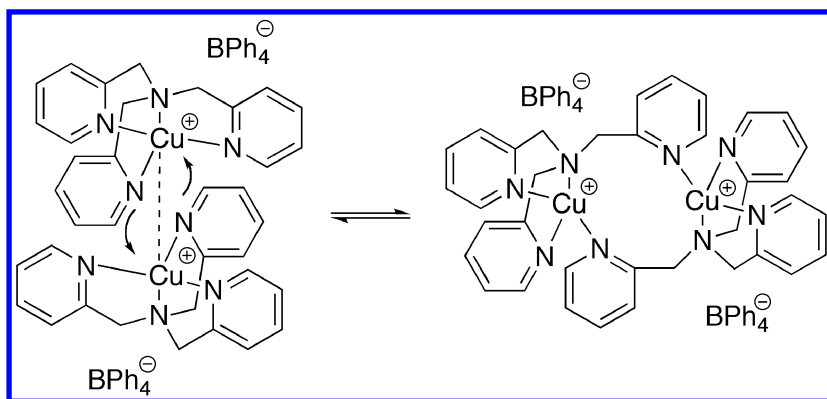
Scheme 3. Proposed equilibrium between monomeric [Cu^I(TPMA)][BPh₄] and dimeric [Cu^I(TPMA)]₂[BPh₄]₂ in the absence of a coordinating solvent.

Scheme 3. Proposed equilibrium between monomeric [Cu^I(TPMA)][BPh$_4$] and dimeric [Cu^I(TPMA)]$_2$[BPh$_4$]$_2$ in the absence of a coordinating solvent.

Structural Features of Copper(I and II) Complexes with Substituted TPMA Based Ligands

Solid State Studies

Substituted TPMA based ligands, particularly those containing electron-donating groups, are a relatively new class of ligands that were reported in the mid-2000s (Scheme 4) (*89*, *90*). The motivation towards development of synthetic methodologies for modification was largely driven by research in the area of copper catalyzed oxygen activation (*12*, *18–21*, *25*, *97*). Recently, copper complexes with TPMA based ligands containing 4-methoxy-3,5-dimethyl substituted pyridine arms (TPMA*1-*3) were also successfully utilized in ATRA and ATRP reactions (Scheme 4) (*91*, *98*).

Structural features of transition metal complexes with TPMA modified ligands containing 4-methoxy-3,5-dimethyl substituted pyridine arms are relatively unexplored. Since the first reported ligand synthesis, only one molecular structure of iron (III) complex appeared in the literature (*90*) .

Very recently, crystal structures of six novel copper(I and II) complexes with TPMA*1, TPMA*2 and TPMA*3 ligands were reported (*98*). Their structural features are briefly discussed in the following sections.
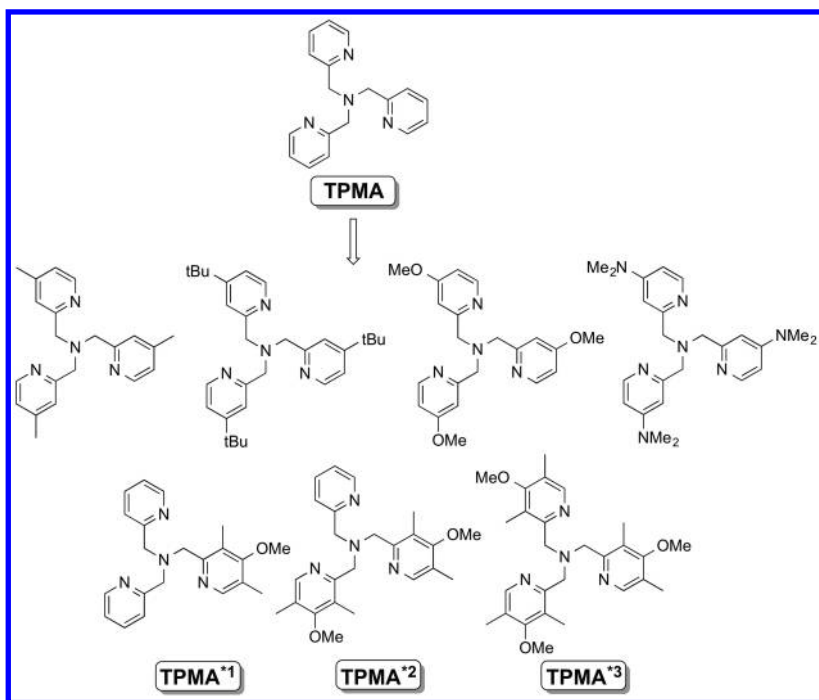
Scheme 4. Examples of TPMA based ligands containing electron-donating groups (89–91).

In the solid state, Cu^I(TPMA*1)Br , Cu^I(TPMA*2)Br and Cu^I(TPMA*3)Br complexes were found to be distorted tetrahedral in geometry and contained coordinated bromide anions (Cu^I-Br=2.3511(10) Å, 2.5025(3) Å and 2.5045(6) Å, respectively, Figure 7). Pseudo coordination of the aliphatic nitrogen atom to copper(I) center was observed in Cu^I(TPMA*2)Br (Cu^I-N=2.4190(19) Å) and Cu^I(TPMA*3)Br (Cu^I-N=2.406(3) Å) complexes, similarly to previously isolated Cu^I(TPMA)Br (Cu^I-N=2.4397(14) Å) (*45*). On the other hand, pyridine arm dissociation occurred in Cu^I(TPMA*1)Br complex (Cu^I-N$_{py}$= 3.494(3)) Å). Regardless of the number of 4-methoxy-3,5-dimethyl substituted pyridine arms in TPMA*2 and TPMA*3 complexes, two of the Cu^I-N$_{py}$ bonds were nearly identical (2.083±0.012 Å), whereas the third one either increased (TPMA*3: Cu^I-N$_{py}$=2.116(3) Å) or decreased (TPMA*2: Cu^I-N$_{py}$=2.0452(17) Å). Lastly, significant ligand arm twisting was observed in Cu^I(TPMA*3)Br complex when compared to Cu^I(TPMA)Br, which was found to be nearly C$_3$-symmetric in the solid state.

Copper(II) complexes that are generated during ATRA and ATRP processes are essential for the deactivation step (i.e. reversible halogen atom abstraction from a copper(II) complex by radicals to generate dormant alkyl halide species and a copper(I) complex, Scheme 1) (*49*, *50*, *71*). [Cu^{II}(TPMA*^{1})Br][Br], [Cu^{II}(TPMA*^{2})Br][Br] and [Cu^{II}(TPMA*^{3})Br][Br] complexes were synthesized by reacting Cu^{II}Br$_2$ with the stoichiometric amounts of substituted TPMA based ligand. Crystals suitable for X-ray analysis were obtained in dichloromethane by slow diffusion of *n*-pentane. The corresponding molecular structures are shown in Figure 8.

All three complexes deviated from the ideal trigonal bipyramidal geometry observed in previously characterized [Cu^{II}(TPMA)Br][Br] (*45*). This can easily be seen from the corresponding τ values (τ=1 for regular trigonal bipyramidal geometry and τ=0 for regular square pyramidal geometry) (*99*, *100*), which generally decreased in the order [Cu^{II}(TPMA)Br][Br] (τ=1) > [Cu^{II}(TPMA*^{1})Br][Br] (τ=0.92) > [Cu^{II}(TPMA*^{3})Br][Br] (τ=0.77) > [Cu^{II}(TPMA*^{2})Br][Br] (τ=0.72)). The average Cu^{II}-N$_{eq}$ bond distances increased on going from [Cu^{II}(TPMA*^{1})Br]Br] (2.055(3) Å) to [Cu^{II}(TPMA*^{2})Br][Br] (2.078(8) Å) and [Cu^{II}(TPMA*^{3})Br][Br] (2.084(5) Å) complexes, and were not equal when compared to [Cu^{II}(TPMA)Br][Br] (2.073(15) Å). Generally, two Cu^{II}-N$_{eq}$ bond lengths were either longer (TPMA*^{1}: 2.063(3) Å v.s. 2.040(2) Å) or shorter (TPMA*^{2}: 2.050(7) Å v.s. 2.136(4) Å and TPMA*^{3}: 2.052(4) Å v.s. 2.149(3) Å). Furthermore, Cu^{II}-Br bond length in [Cu^{II}(TPMA*^{1})Br]Br] (2.3852(3) Å) and [Cu^{II}(TPMA*^{2})Br][Br] (2.3814(7) Å) were similar to [Cu^{II}(TPMA)Br][Br] (2.3836(6) Å), but slightly decreased in [Cu^{II}(TPMA*^{3})Br][Br] (2.3740(5) Å). Additionally, particularly in the case of [Cu^{II}(TPMA*^{2})Br][Br] and [Cu^{II}(TPMA*^{3})Br][Br], the presence of methoxy and methyl groups in the pyridine rings caused significant ligand arm twisting. Lastly, the crystal structures of copper(II) complexes with substituted TPMA based ligands were stabilized by π-π stacking interactions between pyridine rings and/or a series of weak C-H---C and dipole C-H---O interactions.

Solution Studies

Structural features of copper(I) complexes with substituted TPMA based ligands were also investigated in solution using variable temperature ^{1}H NMR spectroscopy. Cu^I(TPMA*^{1})Br, Cu^I(TPMA*^{2})Br and Cu^I(TPMA*^{3})Br complexes were found to be more fluxional than previously investigated Cu^I(TPMA)Br and Cu^I(TPMA)Cl (*46*, *96*). Furthermore, the structures of all three complexes were not consistent with the solid-state discussed above. At low temperature, Cu^I(TPMA*^{1})Br was found to be symmetrical and monomeric.

Lastly, dissociation of either unsubstituted pyridine and/or 4-methoxy-3,5-dimethyl substituted pyridine arms was observed in Cu^I(TPMA*^{2})Br and Cu^I(TPMA*^{3})Br (Figure 9) complexes.
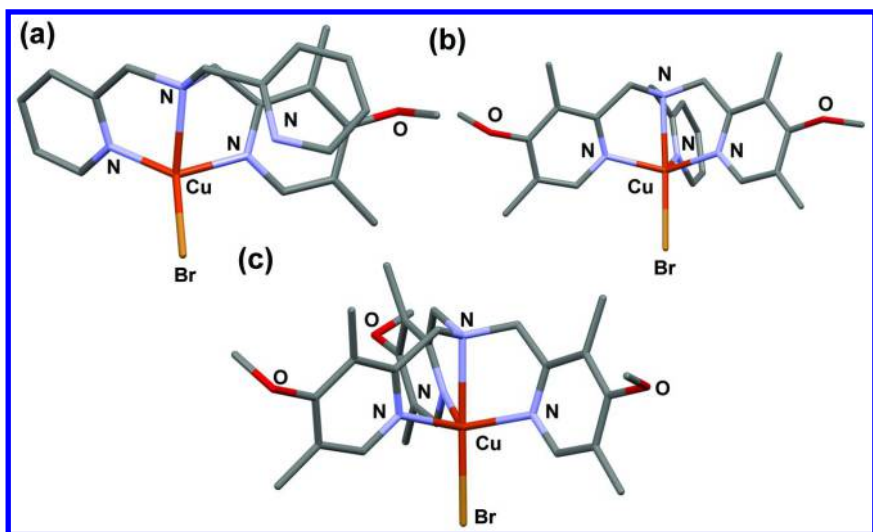
Figure 7. Molecular structures of Cu^I(TPMA^1)Br (a), Cu^I(TPMA*^{2})Br (b) and Cu^I(TPMA*^{3}) (c) complexes (98). H-atoms have been omitted for clarity.*
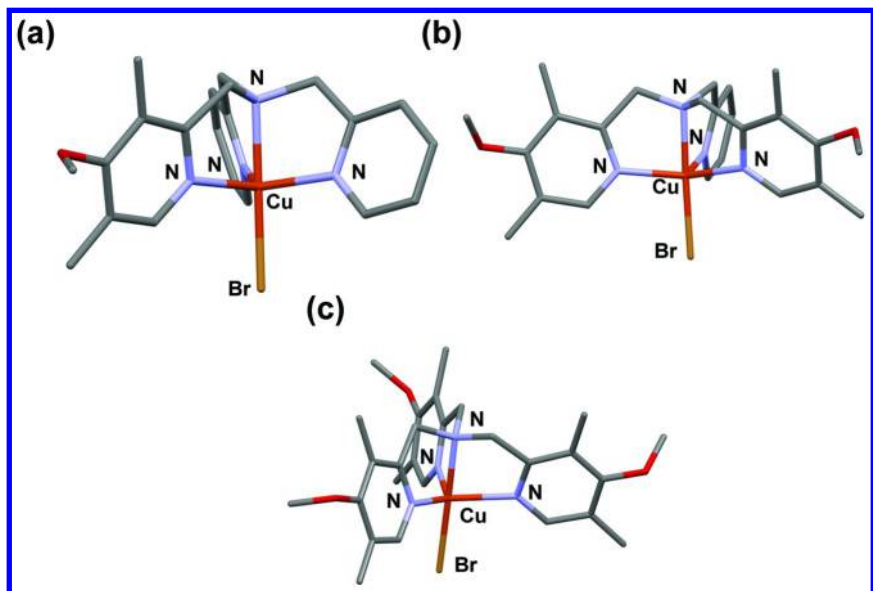
Figure 8. Molecular structures of [Cu^{II}(TPMA^1)Br][Br] (a), [Cu^{II}(TPMA*^{2})Br][Br] (b) and [Cu^{II}(TPMA*^{3})Br][Br] (c) shown with 30% probability displacement ellipsoids. H-atoms and bromide counterion have been omitted for clarity (98).*
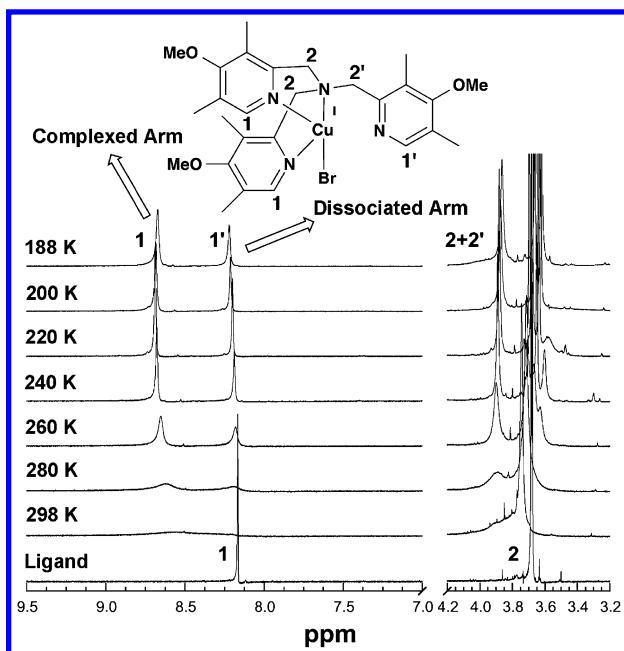
Figure 9. Variable temperature ^1H NMR spectra (400 MHz, $(CD_3)_2CO$) of $Cu^I(TPMA*^3)Br$ complex in the aromatic and methylene regions. Reproduced with permission from reference (98). Copyright 2014, American Chemical Society.

Electrochemical Studies and Stability Constants for Copper Complexes with Substituted TPMA Based Ligands

As mentioned in the introduction section, electrochemical measurements are commonly used to predict the activity of copper complexes in atom transfer radical processes, namely ATRA and ATRP (*50, 61, 71–76*). Generally, for a given alkyl halide, the equilibrium constant for atom transfer ($K_{ATRP}=k_a/k_d$) can be directly correlated with $E_{1/2}$ values provided that the halidophilicity of the metal complex ($X^- + [Cu^{II}L_m]^{2+} \rightleftharpoons [Cu^{II}L_mX]^+$, K_X, X=Br or Cl) remains constant. As a result, for copper complexes with neutral nitrogen based ligands commonly used in ATRA or ATRP, a linear correlation between $\ln(K_{ATRP})$ and $E_{1/2}$ values is typically observed (*63, 74, 77*). The electrochemical data (relative to SCE) for copper complexes with substituted TPMA ligands are given in Table 3.

Table 3. Cyclic Voltammetry Data for Copper Complexes with TPMA Based Ligands in Acetonitrile.

Complex[a]	$E_{1/2}$ (mV)	ΔE_p (mV)	i_{pa}/i_{pc}	$\beta_{Br}^{II} / \beta_{Br}^{I}$
[Cu^I(TPMA)Br][Br]	-240	93	1.08	2.5×10^4
[Cu^I(TPMA^{*1})Br][Br]	-310	84	0.96	1.2×10^4
[Cu^I(TPMA^{*2})Br][Br]	-360	86	0.95	6.9×10^3
[Cu^I(TPMA^{*3})Br][Br]	-420	79	1.18	1.3×10^4
[Cu^I(TPMA)][OTf]$_2$	22	86	0.94	
[Cu^I(TPMA^{*1})][OTf]$_2$	-69	104	0.78	
[Cu^I(TPMA^{*2})][OTf]$_2$	-133	120	0.83	
[Cu^I(TPMA^{*3})][OTf]$_2$	-177	108	1.20	

[a]Potentials are reported relative to SCE and were measured under the same electrochemical cell conditions.

All copper complexes display a single quasireversible redox behavior with i_{pa}/i_{pc} varying from 0.95 to 1.18 and peak separations of less than 90 mV at a scan rate of 100 mV/s. Interestingly, a nearly stepwise decrease ($E\sim60$ mV) of $E_{1/2}$ values (TPMA (-240 mV) > TPMA*1 (-310 mV) > TPMA*2 (-360 mV) > TPMA*3 (-420 mV)) is observed on going from [Cu^{II}(TPMA)Br][Br] to [Cu^{II}(TPMA^{*3})Br][Br], clearly indicating that the presence of electron donating groups in the 4 (-OMe) and 3,5 (-Me) positions of the pyridine rings in TPMA increases the reducing ability of the corresponding copper(I) complexes. Similar trends were observed previously in the case of copper complexes containing tris-4-substituted (-^{t}Bu, -Me, -MeO and -NMe$_2$) TPMA (*89*) and 4,4′-subsituted (-Me, -MeO and -NMe$_2$) bipyridine (*88*) based ligands. Furthermore, cyclic voltammograms for the copper(II) triflate complexes with substituted TPMA based ligands also followed the similar trend, with the exception that the $E_{1/2}$ values are less negative by $\sim250-275$ mV (Table 3). The diminished reducing potential originates from the differences in Cu^{II} stability constants as discussed below (*45, 83, 84, 101*).

Another method for predicting the activity of copper catalysts in ATRP is to compare the overall stability constants (as opposed to step formation constants) of the Cu^{II} and Cu^I complexes with the particular ligand (β^{II}: Cu^{II} + mL $\rightleftharpoons$ Cu^{II}L$_m$ and β^I: Cu^I + mL $\rightleftharpoons$ Cu^{I}L$_m$, respectively), since the equilibrium constant for atom transfer, K_{ATRP}, directly correlates with the ratio β^{II}/β^I (vide supra, Eq. [2]). The stability constants (β_L^{II} and β_L^I) for the complexation of TPMA, TPMA^{*1}, TPMA^{*2} and TPMA^{*3} ligands to copper(I and II) triflate complexes in dimethylformamide at 25 °C are summarized in Table 4. The stability constant β^I remains nearly constant for all ligands, while β^{II} increases nearly 2300 times from TPMA to TPMA^{*3}. Therefore, the trend observed in redox potentials discussed above clearly indicate that the TPMA based ligands induce a stronger influence towards the stabilization of the copper(II) oxidation state (logβ^I=13.40.2, logβ^{II}=19.3 (TPMA^{*1}), 20.5 (TPMA^{*2}) and 21.5 (TPMA^{*3})). Electrochemical data, stability constants and previously established linear correlation between ln(K_{ATRP}) and $E_{1/2}$ values (*50, 77*) indicate that copper complexes with TPMA^{*1}, TPMA^{*2} and TPMA^{*3} ligands should have the equilibrium constant for atom

transfer (K_{ATRP}) approximately 10, 100 and 1000 times larger than TPMA. Indeed, for Cu^I(TPMA*3)Br complex, the equilibrium constant for atom transfer ($K_{ATRP}=k_a/k_d=8400/2.010^7=4.210^{-4}$) was found to be nearly 1300 larger than for Cu^I(TPMA)Br ($K_{ATRP}=k_a/k_d=3.8$ M^{-1}s^{-1}/1.210^7 M^{-1}s^{-1}=3.210^{-7}) (*91*). The large difference in K_{ATRP} values can be attributed mostly to an increase in the activation rate constant (k_a, 8400 M^{-1}s^{-1} v.s. 3.8 M^{-1}s^{-1}), indicating that Cu^I(TPMA*3)Br should be much more active in ATRP, as confirmed by recently published study (*91*).

Table 4. Stability Constants for Copper Triflate Complexes with TPMA Based ligands in Dimethylformamide at 25 °C.

Ligand[a]	β^I	β^{II}	$log\ (\beta^{II}/\beta^I)$	$\beta_L^{II}\ /\ \beta_{TPMA}^{II}$
TPMA	1.3×10^{13}	1.3×10^{18}	5.0	1.0
TPMA*1	2.4×10^{13}	2.0×10^{19}	5.9	15
TPMA*2	1.6×10^{13}	3.0×10^{20}	7.3	2.3×10^2
TPMA*3	3.4×10^{13}	3.0×10^{21}	7.9	2.3×10^3

[a]All values were taken from Ref. [98].

Applications in ATRP

TPMA is a widely used ligand for copper catalyzed ATRP methods ranging from conventional ATRP (*41*, *42*, *102*) to improved protocols that require only ppm amounts of the catalyst (*13*, *40*, *49*, *55–58*, *103–106*). These enhanced synthetic procedures allow for the use of air stable Cu^{II} complexes, often eliminating the need for deoxygenation, and rely on the continuous reduction of Cu^{II} to Cu^I species within the polymerization process. Consequently, additional non-radical (e.g. tin(II) 2-ethylhexanoate = Sn(EH)$_2$, ascorbic acid or hydrazine) or radical (e.g. AIBN or V-70) reducing agents are employed. The selection of appropriate ATRP conditions is reliant on various factors such as monomer, initiator, ligand, solvent, etc. (*59*, *74*) Large K_{ATRP} values require ATRP methods with constant regeneration of Cu^I complex due to early termination reactions that typical occur under normal ATRP conditions (*91*, *107*). Therefore, in the present study, activators regenerated by electron transfer (ARGET) ATRP (*56*) of *n*-butyl acrylate (*n*BA) was targeted utilizing low amounts of Sn(EH)$_2$ as the reducing agent and only 10 ppm of the copper complexes with TPMA, TPMA*1, TPMA*2 and TPMA*3 ligands. As indicated in Table 5, all catalysts showed excellent conversion and good correlation between experimental ($M_{n,exp}$) and theoretical molecular weights ($M_{n,theo}$). However, [Cu^{II}(TPMA*2)Cl][Cl] and [Cu^{II}(TPMA*3)Cl][Cl] showed a significantly narrower molecular weight distributions (M_w/M_n) than the corresponding copper(II) complexes with TPMA and TPMA*1 ligands, indicating better control in the polymerization system. Therefore, based on the straightforward synthesis and a large value for K_{ATRP},

the results presented in this article indicate that in some ARGET ATRP systems copper complexes with TPMA*2 ligand could perform better than the ones with previously reported TPMA*3.

Table 5. Polymerization Results for ARGET ATRP of n-Butyl Acrylate Catalyzed by 10 ppm of $Cu^{II}Cl_2$ Complexes with TPMA Based Ligands.

Ligand[a]	Conv. (%)	$M_{n,exp}$	$M_{n,theo}$	M_w/M_n
TPMA	90.5	19800	18800	2.01
TPMA*1	64.0	13500	13110	1.54
TPMA*2	90.0	19400	18700	1.46
TPMA*3	81.0	17800	16800	1.50

[a] Conditions: $[nBA]_o:[EBiB]_o:[Sn(EH)_2]_o:[TPMA \text{ or } TPMA^{*x}]_o:[Cu^{II}Cl_2]_o=160:1:0.1:0.03:0.016$, EBiB=ethyl 2-bromoisobutyrate, $[nBA]_o=5.6$ M, 20% (v/v) anisole, $[Cu^{II}]_o=10$ ppm, $T=60$ °C, $t=24$ h. Monomer conversion was determined by ^1H NMR spectroscopy using anisole as an internal standard.

Conclusions

In summary, structural and mechanistic aspects of ATRA and ATRP reactions catalyzed by copper complexes with tris(2-pyridylmethyl)amine ligand and its derivatives containing electron donating groups were reviewed. In the solid state, copper(II) complexes with the general formula $[Cu^{II}(TPMA)X][Y]$ (X=Cl⁻, Br⁻ and Y=Cl⁻, Br⁻, ClO₄⁻, BPh₄⁻ or PF₆⁻) were typically distorted trigonal bipyramidal in geometry, and the counterion had negligible effect on the structure of $[Cu^{II}(TPMA)X]^+$ cation. On the contrary, structures of the corresponding Cu^I complexes were strongly dependent not only on the counterion, but also on neutral auxiliary ligands. Typically, partial dissociation of one of the pyridyl arms in TPMA was not observed when small auxiliary ligands such as CH₃CN, Cl⁻ or Br⁻ were coordinated to the copper(I) center, but occurred with the larger ones such as PPh₃ or 4,4′-dipyridyl. Furthermore, depending on the counterion, dimerization in the solid state was also observed. In solution, $Cu^I(TPMA)Br$ and $Cu^I(TPMA)Cl$ complexes were highly symmetrical and monomeric in solution. Dimerization typically occurred with less coordinating counterions such as BPh₄- or ClO₄⁻. On the other hand, in the solid state, Cu^I complexes with TPMA based ligands containing 4-methoxy-3,5-dimethyl substituted pyridine arms (TMPA*1, TPMA*2 and TPMA*3) were found to be distorted tetrahedral in geometry and contained coordinated bromide anions. Pseudo coordination of the aliphatic nitrogen atom to copper(I) center was observed in $Cu^I(TPMA^{*2})Br$ and $Cu^I(TPMA^{*3})Br$ complexes, whereas pyridine arm dissociation occurred in $Cu^I(TPMA^{*1})Br$. All copper(I) complexes with substituted TPMA ligands exhibited high degree of fluxionality in solution. At low temperature, $Cu^I(TPMA^{*1})Br$ was found to be symmetrical and monomeric, while dissociation of either unsubstituted pyridine and/or 4-methoxy-3,5-dimethyl substituted pyridine arms was observed

in $Cu^I(TPMA^{*2})Br$ and $Cu^I(TPMA^{*3})Br$. The geometry of the corresponding copper(II) complexes in the solid state deviated from ideal trigonal bipyramidal, as confirmed by a decrease τ in values ([$Cu^{II}(TPMA^{*1})Br$][Br] (τ=0.92) > [$Cu^{II}(TPMA^{*3})Br$][Br] (τ=0.77) > [$Cu^{II}(TPMA^{*2})Br$][Br] (τ=0.72)). Furthermore, cyclic voltammetry studies indicated a nearly stepwise decrease (E~60 mV) of $E_{1/2}$ values relative to SCE (TPMA (-240 mV)>TPMA^{*1} (-310 mV) > TPMA^{*2} (-360 mV) > TPMA^{*3} (-420 mV)) on going from [$Cu^{II}(TPMA)Br$][Br] to [$Cu^{II}(TPMA^{*3})Br$][Br], confirming that the presence of electron donating groups in the 4 (-OMe) and 3,5 (-Me) positions of the pyridine rings in TPMA increases the reducing ability of the corresponding copper(I) complexes. This increase was mostly the result of a stronger influence of substituted TPMA ligands towards stabilization of the copper(II) oxidation state ($\log\beta^I$=13.4±0.2, $\log\beta^{II}$=19.3 (TPMA^{*1}), 20.5 (TPMA^{*2}) and 21.5 (TPMA^{*3})). Lastly, based on the straightforward synthesis and a large value for K_{ATRP}, the preliminary results indicated that in some ARGET ATRP systems copper complexes with TPMA^{*2} ligand could perform better than the ones with previously reported TPMA^{*3}.

Acknowledgments

References

1. Anderegg, G.; Wenk, F. *Helv. Chim. Acta* **1967**, *50*, 2330–2332.
2. Canary, J. W.; Yank, Y.; Roy, R.; Que, L. J.; Miyake, H. *Inorg. Synth.* **1998**, *32*, 70–75.
3. Robertson, N. J.; Carney, M. J.; Halfen, J. A. *Inorg. Chem.* **2003**, *42*, 6876–6885.
4. Wei, R.-J.; Tao, J.; Huang, R.-B.; Zheng, L.-S. *Inorg. Chem.* **2011**, *50*, 8553–8564.
5. Natrajan, L.; Pécaut, J.; Mazzanti, M.; LeBrun, C. *Inorg. Chem.* **2005**, *44*, 4756–4765.
6. Shin, B.-K.; Kim, M.; Han, J. *Bull. Korean Chem. Soc.* **2007**, *28*, 417–423.
7. Spiropulos, N. G.; Standley, E. A.; Shaw, I. R.; Ingalls, B. L.; Diebels, B.; Krawczyk, S. V.; Gherman, B. F.; Arif, A. M.; Brown, E. C. *Inorg. Chim. Acta* **2012**, *386*, 83–92.
8. Ito, M.; Sakai, K.; Tsubomura, T.; Takita, Y. *Bull. Chem. Soc. Jpn.* **1999**, *72*, 239–247.
9. Tajika, Y.; Tsuge, K.; Sasaki, Y. *Dalton Trans.* **2005**, 1438–1447.
10. Eckenhoff, W. T.; Pintauer, T. *Inorg. Chem.* **2010**, *49*, 10617–10626.
11. Pintauer, T. *Polym. Prepr. (Am. Chem. Soc., Div. Polym. Chem.)* **2008**, *49* (2), 12–13.
12. Karlin, K. D.; Zubieta, J. *Copper Coordination Chemistry: Biochemical and Inorganic Perspectives*; Adenine Press: New York, 1983.
13. Eckenhoff, W. T.; Pintauer, T. *Cat. Rev. Sci. Eng.* **2010**, *52*, 1–59.

14. Bjernemose, J.; Hazell, A.; McKenzie, C. J.; Mahon, M. F.; Nielsena, L. P.; Raithby, P. R.; Simonsen, O.; Toftlund, H.; Wolny, J. A. *Polyhedron* **2003**, *22*, 875–885.

15. Mandon, D.; Machkour, A.; Goetz, S.; Welter, R. *Inorg. Chem.* **2002**, *41*, 5364–5372.

16. Baldwin, M. J.; Ross, P. K.; Pate, J. E.; Tyeklar, Z.; Karlin, K. D.; Solomon, E. I. *J. Am. Chem. Soc.* **1991**, *113*, 8671–8679.

17. Fry, H. C.; Scaltrito, D. V.; Karlin, K. D.; Meyer, G. J. *J. Am. Chem. Soc.* **2003**, *125*, 11866–11871.

18. Karlin, K. D.; Hayes, J. C.; Juen, S.; Hutchinson, J. P.; Zubieta, J. *Inorg. Chem.* **1982**, *21*, 4106–4108.

19. Karlin, K. D.; Nanthakumar, A.; Fox, S.; Murthy, N. N.; Ravi, N.; Huynh, B. H.; Orosz, R. D.; Day, E. P. *J. Am. Chem. Soc.* **1994**, *116*, 4753–4763.

20. Karlin, K. D.; Wei, N.; Jung, B.; Kaderli, S.; Niklaus, P.; Zuberbuhler, A. D. *J. Am. Chem. Soc.* **1993**, *115*, 9506–9514.

21. Tyeklar, Z.; Jacobson, R. R.; Wei, N.; Murthy, N. N.; Zubieta, J.; Karlin, K. D. *J. Am. Chem. Soc.* **1993**, *115*, 2677–2689.

22. Wei, N.; Lee, D.; Murthy, N. N.; Tyeklar, Z.; Karlin, K. D.; Kaderli, S.; Jung, B.; Zuberbuehler, A. D. *Inorg. Chem.* **1994**, *33*, 4625–4626.

23. Wei, N.; Murthy, N. N.; Chen, Q.; Zubieta, J.; Karlin, K. D. *Inorg. Chem.* **1994**, *33*, 1953–1965.

24. Chishiro, T.; Shimazaki, Y.; Tani, F.; Naruta, Y. *Chem. Commun.* **2005**, 1078–1081.

25. Kim, E.; Helton, M. E.; Wasser, I. M.; Karlin, K. D.; Shen, L.; Hong-wei, H.; Moënne-Loccoz, P.; Imcarvito, C. D.; Rheingold, A. L.; Honecker, M.; Kaderli, S.; Zuberbühler, A. D. *Proc. Natl. Acad. Sci. U. S. A.* **2003**, *100*, 3623–3628.

26. Company, A.; Lloret, J.; Gómez, L.; Costas, M. In *Alkane C-H Activation using Single Site Metal Catalysis*; Perez, P., Ed.; Springer: New York, 2012; Vol. 38, p 143.

27. Plietker, B. *Iron Catalysis in Organic Chemistry: Reactions and Applications*; Wiley-VCH: Weinheim, 2008.

28. Yamaguchi, M.; Kousaka, H.; Izawa, S.; Ichii, Y.; Kumano, T.; Masui, D.; Yamagishi, T. *Inorg. Chem.* **2006**, *45*, 8342–8354.

29. Jastrzebski, R.; Weckhuysen, B. M.; Bruijnincx, P. C. A. *Chem. Commun.* **2013**, *49*, 6912–6914.

30. Kojima, T.; Matsuo, H.; Matsuda, Y. *Inorg. Chim. Acta* **2000**, *300-302*, 661–667.

31. Britovsek, G.; England, J.; White, A. *Inorg. Chem.* **2005**, *44*, 8125–8134.

32. Yoon Lee, J.; Peterson, R. L.; Ohkubo, K.; Garcia-Bosch, I.; JHimes, R. A.; Woertink, J.; Moore, C. D.; Solomon, E. I.; Fukuzumi, S.; Karlin, K. D. *J. Am. Chem. Soc.* **2014**, *136*, 9925–9937.

33. Ricardo, C.; Pintauer, T. *Chem. Commun.* **2009**, 3029–3031.

34. Ricardo, C.; Pintauer, T. *Eur. J. Inorg. Chem.* **2011**, 1292–1301.

35. Ricardo, C.; Pintauer, T. *Isr. J. Chem.* **2012**, *52*, 320–327.

36. Ricardo, C.; Pintauer, T. *ACS Symp. Ser.* **2012**, *1100*, 73–98.

37. Berg, R.; Straub, B. F. *Beilstein J. Org. Chem.* **2013**, *9*, 2715–2750.

38. Golas, P. L.; Tsarevsky, N. V.; Sumerlin, B. S.; Matyjaszewski, K. *Macromolecules* **2006**, *39*, 6451–6457.
39. Clark, A. J. *Chem. Soc. Rev.* **2002**, *31*, 1–11.
40. Pintauer, T. *Eur. J. Inorg. Chem.* **2010**, 2449–2460.
41. Matyjaszewski, K.; Xia, J. *Chem. Rev.* **2001**, *101*, 2921–2990.
42. Wang, J.-S.; Matyjaszewski, K. *J. Am. Chem. Soc.* **1995**, *117*, 5614–5615.
43. Xia, J.; Matyjaszewski, K. *Macromolecules* **1999**, *32*, 2434–2437.
44. Balili, M. N. C.; Pintauer, T. *Inorg. Chem.* **2009**, *48*, 9018–9026.
45. Eckenhoff, W. T.; Garrity, S. T.; Pintauer, T. *Eur. J. Inorg. Chem.* **2008**, 563–571.
46. Eckenhoff, W. T.; Pintauer, T. *Inorg. Chem.* **2007**, *46*, 5844–5846.
47. Pintauer, T. *ACS Symp. Ser.* **2009**, *1023*, 63–84.
48. Pintauer, T.; Eckenhoff, W. T.; Ricardo, C.; Balili, M. N. C.; Biernesser, A. B.; Noonan, S. J.; Taylor, M. J. W. *Chem. Eur. J.* **2009**, *15*, 38–41.
49. Pintauer, T.; Matyjaszewski, K. *Chem. Soc. Rev.* **2008**, *37*, 1087–1097.
50. Pintauer, T.; Matyjaszewski, K. *Top. Organomet. Chem.* **2009**, *26*, 221–251.
51. Muñoz-Molina, J. M.; Belderraín, T. R.; Pérez, P. J. *Adv. Synth. Catal.* **2008**, *350*, 2365–2372.
52. Muñoz-Molina, J. M.; Belderraín, T. R.; Pérez, P. J. *Inorg. Chem.* **2010**, *49*, 642–645.
53. Muñoz-Molina, J. M.; Caballero, A.; Díaz-Requejo, M. M.; Trofimenko, S.; Belderraín, T. R.; Pérez, P. J. *Inorg. Chem.* **2007**, *46*, 7725–7730.
54. Balili, M. N. C.; Pintauer, T. *Inorg. Chem.* **2010**, *49*, 5642–5649.
55. Jakubowski, W.; Matyjaszewski, K. *Macromolecules* **2005**, *38*, 4139–4146.
56. Jakubowski, W.; Matyjaszewski, K. *Angew. Chem. Int. Ed.* **2006**, *45*, 4482–4486.
57. Jakubowski, W.; Min, K.; Matyjaszewski, K. *Macromolecules* **2006**, *39*, 39–45.
58. Matyjaszewski, K.; Jakubowski, W.; Min, K.; Tang, W.; Huang, J.; Braunecker, W. A.; Tsarevsky, N. V. *Proc. Natl. Acad. Sci. U. S. A.* **2006**, *103*, 15309–15314.
59. Matyjaszewski, K. *Macromolecules* **2012**, *45*, 4015–4039.
60. Coessens, V.; Pintauer, T.; Matyjaszewski, K. *Prog. Polym. Sci.* **2001**, *26*, 337.
61. Tsarevsky, N. V.; Matyjaszewski, K. *Chem. Rev.* **2007**, *107*, 2270–2299.
62. Matyjaszewski, K.; Tsarevsky, N. V. *Nat. Chem.* **2009**, *1*, 276–288.
63. Tang, W.; Tsarevsky, N. V.; Matyjaszewski, K. *J. Am. Chem. Soc.* **2006**, *128*, 1598–1604.
64. Fischer, H. *J. Am. Chem. Soc.* **1986**, *108*, 3925–3927.
65. Fischer, H. *J. Polym. Sci., Part A: Polym. Chem.* **1999**, *37*, 1885–1901.
66. Fischer, H. *Chem. Rev.* **2001**, *101*, 3581–3610.
67. Goto, A.; Fukuda, T. *Prog. Polym. Sci.* **2004**, *29*, 329–385.
68. Goto, A.; Fukuda, T. *Macromol. Rapid Commun.* **1999**, *20*, 633–636.
69. Matyjaszewski, K.; Paik, H.-j.; Zhou, P.; Diamanti, S. J. *Macromolecules* **2001**, *34*, 5125–5131.
70. Ohno, K.; Goto, A.; Fukuda, T.; Xia, J.; Matyjaszewski, K. *Macromolecules* **1998**, *31*, 2699–2701.

71. Pintauer, T.; Matyjaszewski, K. *Coord. Chem. Rev.* **2005**, *249*, 1155–1184.

72. Pintauer, T.; McKenzie, B.; Matyjaszewski, K. *ACS Symp. Ser.* **2003**, *854*, 130–147.

73. Braunecker, W. A.; Matyjaszewski, K. *Prog. Polym. Sci.* **2007**, *32*, 93–146.

74. Tang, W.; Kwak, Y.; Braunecker, W.; Tsarevsky, N. V.; Coote, M. L.; Matyjaszewski, K. *J. Am. Chem. Soc.* **2008**, *130*, 10702–10713.

75. Tsarevsky, N. V.; Braunecker, W. A.; Matyjaszewski, K. *J. Organomet. Chem.* **2007**, *692*, 3212–3222.

76. Tsarevsky, N. V.; Braunecker, W. A.; Vacca, A.; Gans, P.; Matyjaszewski, K. *Macromol. Symp.* **2007**, *248*, 60–70.

77. Qiu, J.; Matyjaszewski, K.; Thounin, L.; Amatore, C. *Macromol. Chem. Phys.* **2000**, *201*, 1625–1631.

78. Buckingham, D. A.; Sargeson, A. M. In *Chelating Agents and Metal Chelates*; Dwyer, F. P., Mellor, D. P., Eds.; Academic Press: New York, 1964.

79. Lingane, J. J. *Chem. Rev.* **1941**, *29*, 1.

80. Rossotti, F. J. C.; Rossotti, H. *The Determination of Stability Constants*; McGraw Hill: New York, 1961.

81. Vlcek, A. A. *Prog. Inorg. Chem.* **1963**, *5*, 211–384.

82. Navon, N.; Golub, G.; Cohen, H.; Paoletti, P.; Valtancoli, B.; Bencini, A.; Meyerstein, D. *Inorg. Chem.* **1999**, *38*, 3484–3488.

83. Ambundo, E. A.; Deydier, M. V.; Grall, A. J.; Aguera-Vega, N.; Dressel, L. T.; Copper, T. H.; Heeg, M. J.; Ochrymowycz, L. A.; Rorabacher, D. B. *Inorg. Chem.* **1999**, *38*, 4233–4242.

84. Golub, G.; Lashaz, A.; Cohen, A.; Paoletti, P.; Bencini, A.; Valtancoli, B.; Meyerstein, D. *Inorg. Chim. Acta* **1997**, *255*, 111–115.

85. Tsarevsky, N. V.; Tang, W.; Brooks, S. J.; Matyjaszewski, K. *ACS Symp. Ser.* **2006**, *944*, 56–70.

86. Tsarevsky, N. V.; Matyjaszewski, K. *J. Polym. Sci., Part A: Polym. Chem.* **2006**, *44*, 5098–5112.

87. Eckenhoff, W. T.; Biernesser, A. B.; Pintauer, T. *Inorg. Chem.* **2012**, *51*, 11917–11929.

88. Magenau, A. J. D.; Kwak, Y.; Schröder, K.; Matyjaszewski, K. *ACS Macro Lett.* **2012**, *1*, 508–512.

89. Zhang, C. X.; Kaderli, S.; Costas, M.; Kim, E.-I.; Neuhold, Y.-M.; Karlin, K. D.; Zuberbuhler, A. D. *Inorg. Chem.* **2003**, *42*, 1807–1824.

90. Xue, G.; Wang, D.; DeHont, R.; Fiedler, A. T.; Shan, X.; Münck, E.; Que, L, Jr. *Proc. Natl. Acad. Sci. U. S. A.* **2007**, *104*, 20713–20718.

91. Schröder, K.; Mathers, R. T.; Buback, J.; Konkolewicz, D.; Magenau, A. J. D.; Matyjaszewski, K. *ACS Macro Lett.* **2012**, *1*, 1037–1040.

92. Konkolewicz, D.; Schöder, K.; Buback, J.; Bernhard, S.; Matyjaszewski, K. *ACS Macro Lett.* **2012**, *1*, 1219–1223.

93. Ribelli, T. G.; Konkolewicz, D.; Bernhard, S.; Matyaszewski, K. *J. Am. Chem. Soc.* **2014**, *136*, 13303–13312.

94. Ribelli, T. G.; Konkolewicz, D.; X., P.; Matyaszewski, K. *Macromolecules* **2014**, *47*, 6316–6321.

95. Schröder, K.; Konkolewicz, D.; Poli, R.; Matyaszewski, K. *Organometallics* **2012**, *31*, 7994–7999.

96. Hsu, S. C.; Chien, S. S.; Chen, H. H.; Chiang, M. Y. *Chin. Chem. Soc.* **2007**, *54*, 685–692.

97. Maiti, D.; Sarjeant, A. A. N.; Itoh, S.; Karlin, K. D. *J. Am. Chem. Soc.* **2008**, *130*, 5644–5645.

98. Kaur, A.; Schröder, K.; Ribelli, T. G.; Matyaszewski, K. *Inorg. Chem.* **2015**, *54*, 1474–1486.

99. Addison, A. W.; Nageswara Rao, T.; Reedijk, J.; van Rijn, J.; Verschoor, G. C. *J. Chem. Soc., Dalton Trans.* **1984**, 1349–1356.

100. Harrison, W. D.; Kennedy, D. M.; Ray, N. J.; Sheahan, R.; Hathaway, B. J. *J. Chem. Soc., Dalton Trans.* **1981**, 1556–1564.

101. Bortolamei, N.; Isse, A. A.; Di Marco, V. B.; Gennaro, A.; Matyjaszewski, K. *Macromolecules* **2010**, *43*, 9257–9267.

102. Matyjaszewski, K.; Patten, T. E.; Xia, J. *J. Am. Chem. Soc.* **1997**, *119*, 674–680.

103. Min, K.; Jakubowski, W.; Matyjaszewski, K. *Macromol. Rapid Commun.* **2006**, *27*, 594–598.

104. Matyaszewski, K.; Tsarevsky, N. V. *J. Am. Chem. Soc.* **2014**, *136*, 6513–6533.

105. McLeod, D. C.; Tsarevsky, N. V. *Polym. Int.* **2014**, *63*, 868–875.

106. Woodruff, S. R.; Davis, B. J.; Tsarevsky, N. V. *Macromol. Rapid Commun.* **2014**, *35*, 186–192.

107. Wang, Y.; Soerensen, N.; Zhong, M.; Schroeder, H.; Buback, M.; Matyjaszewski, K. *Macromolecules* **2013**, *46*, 683–691.

Chapter 7

Kinetic Studies of Elementary Reactions in SET-LRP / SARA ATRP

Julien Nicolas,[1] Sebastian Perrier,[2,3] and Simon Harrisson[4,*]

[1]Institut Galien Paris-Sud, Univ Paris-Sud, UMR CNRS 8612, Faculté de Pharmacie, 5 rue Jean-Baptiste Clément, F-92296 Châtenay-Malabry cedex, France
[2]Department of Chemistry, The University of Warwick, Gibbet Hill, Coventry, CV4 7AL, United Kingdom
[3]Faculty of Pharmacy and Pharmaceutical Sciences, Monash University, 381 Royal Parade, Parkville, VIC 3052, Australia
[4]Laboratoire des Interactions Moleculaires et de la Reactivité Chimique et Photochimique, UMR CNRS 5623, Université de Toulouse, 31062 Toulouse, France
***E-mail: polyharrisson@gmail.com**

A kinetic scheme for controlled radical polymerization in the presence of copper is developed, first neglecting comproportionation or disproportionation reactions, then taking them into account. Experimental results on the kinetics of the elementary reactions of comproportionation, activation by copper(0) and biradical termination are presented, showing solvent effects on activation and comproportionation reactions and chain length dependence of activation and termination. Unusually high rates of termination are observed in controlled radical polymerizations in the presence of copper; around an order of magnitude faster than in conventional or RAFT polymerizations.

Introduction

The history of metallic copper in radical polymerization begins in 1967, when Otsu et al. reported that radical polymerizations could be initiated by the combination of copper metal and an alkyl halide (*1*). After the development of

atom transfer radical polymerization (ATRP) (*2*, *3*), the effect of copper metal was reexamined, both as an additional component in an ATRP reaction (*4*) and as the sole catalytic species (*4*, *5*). These early works established that copper(0) participated in two key reactions: activation of alkyl (or sulfonyl) halides, and reduction of copper(II) to copper (I) (Scheme 1). The relative significance of these two reactions was an important subject of the ensuing debate over the mechanism of controlled radical polymerization (CRP) in the presence of copper, known variously as Single Electron Transfer Living Radical Polymerization (SET-LRP) (*6*) or Supplemental Activator and Reducing Agent ATRP (SARA ATRP) (*7*).

$$RX \ + \ Cu(0) \ \overset{k_{a0}}{\rightarrow} \ R* \ + \ Cu(I)$$
$$\text{activation}$$
$$Cu(0) \ + \ Cu(II) \ \overset{k_{comp}}{\longrightarrow} \ Cu(I) \ + \ Cu(I)$$
$$\text{comproportionation}$$
$$Cu(I) + Cu(I) \ \overset{k_{disp}}{\longrightarrow} \ Cu(0) + Cu(II)$$
$$\text{disproportionation}$$
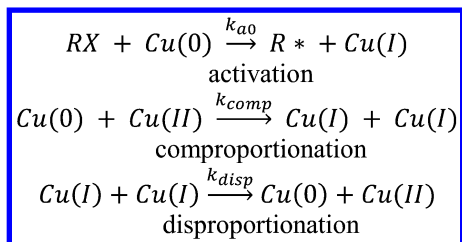
Scheme 1. Reactions of copper metal in atom transfer radical polymerization. Note that Cu(I) and Cu(II) represent all dissolved copper(I) and copper(II) species – the presence of solubilizing ligands is assumed.

Development of copper-based CRP continued through the 2000s, with two schools of thought emerging. With the introduction of ARGET (activator regenerated by electron transfer) ATRP (*8*, *9*) Matyjaszewski and coworkers demonstrated that the addition of copper metal (among other reducing agents) allowed ATRP polymerizations to be carried out at extremely low copper concentrations while continuously regenerating the copper(I) activating species by reduction of copper(II). Meanwhile, Percec and coworkers carried out copper-metal mediated polymerizations of vinyl chloride in biphasic mixtures of water and THF (*10*) and of methyl acrylate and methyl methacrylate in DMSO solution (*6*). The observation of disproportionation of copper(I) salts in water and of copper(I)/ligand complexes in DMSO led this group to propose that in these systems (and many others which had been considered to follow the ATRP mechanism) copper(0) was the primary activating species, and that concentrations of copper(I) were essentially zero as a result of rapid disproportionation. Additionally, the generation of copper(II) was thought to remove the need for build-up of copper(II) deactivating species via the persistent radical effect, thus providing low (or even zero (*11*–*14*)) levels of termination from the beginning of the reaction.

Thus two conflicting mechanisms for CRP in the presence of copper(0) were established – one (ARGET) dominated by comproportionation with copper(I) as the main activating species (*15*), the other (SET-LRP) dominated by disproportionation with activation primarily by copper(0) (Scheme 2). The ARGET mechanism in presence of copper was later renamed SARA, reflecting the role of copper(0) as both Supplemental Activator and Reducing Agent (*7*).
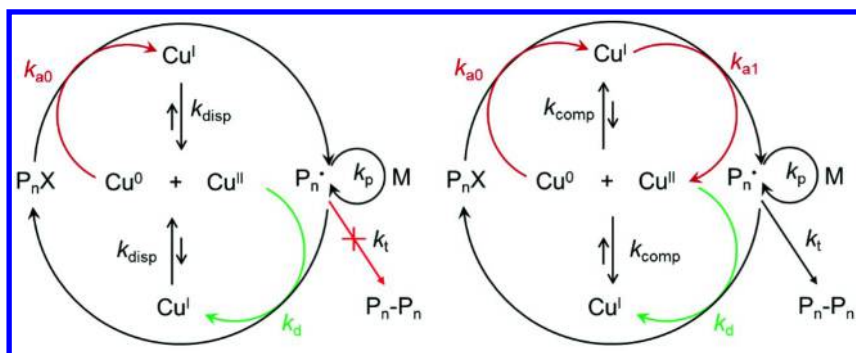
*Scheme 2. SARA (left) and SET (right) mechanisms of polymerization.
Key differences in the mechanisms include: No activation by copper(I) in
SET-LRP; no biradical termination in SET-LRP; comproportionation dominates
disproportionation in SARA ATRP. Note that Cu(I) and Cu(II) represent all
dissolved copper(I) and copper(II) species – the presence of ligands is assumed
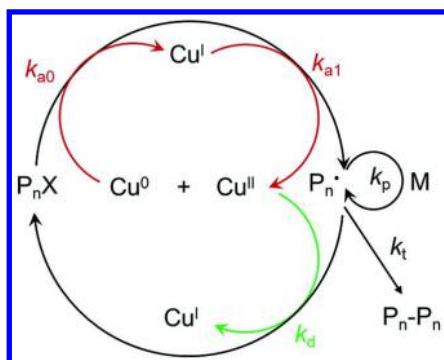and rate constants shown are aggregate rate constants.*

The full story of the development of the two mechanisms is beyond the scope of this contribution, and different viewpoints can be found in recent reviews (*12, 16–18*). The mechanisms are chiefly distinguished by the relative rates of four reactions, viz.: the rates of comproportionation (k_{comp}) and disproportionation (k_{disp}) (in SET-LRP, disproportionation dominates; in SARA ATRP the equilibrium favors comproportionation); the rates of activation by copper(0) (k_{a0}) and copper(I) (k_{a1}) (in SET-LRP, all activation occurs by reaction with copper(0)); and the rate of bimolecular termination (zero or negligible in SET-LRP). The measurement of the rates of these elementary reactions has been a significant focus of our (*19–21*) and other groups' (*22–25*) work in this field.

In this paper, we develop a kinetic scheme for CRP in the presence of copper, first neglecting comproportionation or disproportionation reactions, then taking them into account, and present some experimental results on the kinetics of the elementary reactions of comproportionation, activation by copper(0) and biradical termination.

Results and Discussion

Polymerization in Noncomproportionating, Nondisproportionating Solvents

Comproportionation and disproportionation reactions take place very slowly in nonpolar solvents such as toluene. Thus performing polymerization in the presence of copper(0) in toluene (*19, 26, 27*) is a useful model for SET-LRP or SARA ATRP reactions in solvents that favor disproportionation or comproportionation, as equilibration between copper species can be neglected, leading to the simplified mechanism shown in Scheme 3.

In Controlled Radical Polymerization: Mechanisms; Tsarevsky, et al.;
ACS Symposium Series; American Chemical Society: Washington, DC, 2015.

Scheme 3. SARA/SET-LRP polymerization in toluene. Rates of comproportionation and disproportionation are negligible. Note that Cu(I) and Cu(II) represent all dissolved copper(I) and copper(II) species – the presence of ligands is assumed and rate constants shown are aggregate rate constants.

It is immediately apparent from Scheme 3 that the reaction involves net consumption of copper(0) and generation of dead polymer – indeed it could be summarized as:

$$2.\,Cu(0) + 2.\,P_nX \rightarrow 2.\,CuX + P_nP_n \ (dead \ polymer)$$
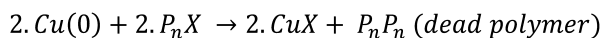
The rates of generation of the various soluble copper species and radicals are given in the equations below (S_{Cu}/V represents the ratio of copper surface area to the total reaction volume):

$$\frac{d[Cu^I]}{dt} = k_{a0}[P_nX]\frac{S_{Cu}}{V} - k_{a1}[P_nX][Cu^I] + k_d[P_n^\bullet][Cu^{II}] \tag{1}$$

$$\frac{d[Cu^{II}]}{dt} = k_{a1}[P_nX][Cu^I] - k_d[P_n^\bullet][Cu^{II}] \tag{2}$$

$$\frac{d[P_n^\bullet]}{dt} = k_{a0}[P_nX]\frac{S_{Cu}}{V} + k_{a1}[P_nX][Cu^I] - k_d[P_n^\bullet][Cu^{II}] - 2.\,k_t[P_n^\bullet]^2 \tag{3}$$

From these equations we can derive two useful identities:

$$\frac{d[Cu^I]}{dt} + \frac{d[Cu^{II}]}{dt} = k_{a0}[P_nX]\frac{S_{Cu}}{V} \tag{4}$$

$$\frac{d[P_n^\bullet]}{dt} = \frac{d[Cu^I]}{dt} + 2.\frac{d[Cu^{II}]}{dt} - 2.\,k_t[P_n^\bullet]^2 \tag{5}$$

It is clear from equation 4 that the total dissolved copper concentration will steadily increase. As this occurs, the rates of activation by copper(I) and deactivation by copper(II) will also increase, causing the ratio of copper(I) to copper(II) to approach the value given by the ATRP equilibrium (*19*) (note that the concentration of copper(II) will always be slightly below the ATRP equilibrium value as a result of the continuing generation of copper(I) from copper(0)):

$$\frac{[Cu^{II}]}{[Cu^{I}]} \rightarrow \frac{k_{a1}[P_nX]}{k_d[P_n^\bullet]} \tag{6}$$

Assuming negligible changes in the radical concentration (the steady state approximation), $[P_nX]$ (low levels of termination) and the copper surface area, we arrive at the following expressions for the steady state radical concentration (equation 8) and the overall rate of polymerization (equation 9):

$$\frac{d[P_n^\bullet]}{dt} = (1+\varphi).\left(\frac{d[Cu^{I}]}{dt} + .\frac{d[Cu^{II}]}{dt}\right) - 2.k_t[P_n^\bullet]^2 = 0 \tag{7}$$

$$[P_n^\bullet] = \sqrt{\frac{(1+\varphi).k_{a0}[P_nX]\frac{S_{Cu}}{V}}{2.k_t}} \tag{8}$$

$$-\frac{d[M]}{dt} = k_p[M][P_n^\bullet] = k_p.[M].\sqrt{\frac{(1+\varphi).k_{a0}[P_nX]\frac{S_{Cu}}{V}}{2.k_t}} \tag{9}$$

where φ represents the fraction of total copper present in the form of copper(II):

$$\varphi = \frac{[Cu^{II}]}{[Cu^{I}]+[Cu^{II}]} \approx \frac{k_{a1}[P_nX]}{k_d[P_n^\bullet]+k_{a1}[P_nX]} = \frac{K_{ATRP}[P_nX]}{[P_n^\bullet]+K_{ATRP}[P_nX]} \tag{10}$$

The value of φ can vary between 0 (very slow activation by copper(I)) and 1 (very rapid activation by copper(I)), so that:

$$\sqrt{\frac{k_{a0}[P_nX]\frac{S_{Cu}}{V}}{2.k_t}} < [P_n^\bullet] < \sqrt{\frac{k_{a0}[P_nX]\frac{S_{Cu}}{V}}{k_t}} \tag{11}$$

Thus the rate of polymerization is primarily determined by the rate of activation of dormant polymer by copper(0), and is proportional to the square roots of the copper surface area and dormant polymer/initiator concentration. Kinetically, the reaction resembles ICAR (initiators for continuous activator regeneration) ATRP (28), with the copper(0)/P_nX couple playing the role of the radical initiator. In ICAR, the rate of reaction is determined by the rate of initiator decomposition, according to the equation below (28):

$$-\frac{d[M]}{dt} = k_p[M][P_n^\bullet] = k_p.\sqrt{\frac{f.k_d[I]}{k_t}} \tag{12}$$

An advantage of SARA ATRP in toluene over ICAR is that the dormant polymer itself serves as the supplementary source of radicals, thus the final polymer is not contaminated by end-groups derived from the supplemental initiator (e.g. cyanoisopropyl groups from AIBN). On the other hand, the copper concentration continually increases as the reaction proceeds, which may result in higher overall levels of copper in the final product.

Polymerization in Comproportionating and/or Disproportionating Solvents

Comproportionation and disproportionation reactions take place more rapidly in polar solvents such as acetonitrile, DMSO and water, and can no longer be neglected.

Disproportionation, according to the proposed SET-LRP mechanism, results in the formation of nanosized 'nascent' copper particles which are assumed to be highly reactive. Thus we assume that the copper(0) produced as a result of disproportionation immediately reacts with dormant polymer to generate a propagating radical and regenerate copper(I) (Scheme 4).

$$Cu(I) + Cu(I) \xrightarrow{k_{disp}} Cu(0)^* + Cu(II)$$
disproportionation
$$Cu(0)^* + P_nX \rightarrow Cu(I) + P_n^\bullet$$
rapid initiation by 'nascent' copper
$$Cu(I) + Cu(I) + P_nX \xrightarrow{k_{disp}} Cu(I) + P_n^\bullet + Cu(II)$$
overall reaction
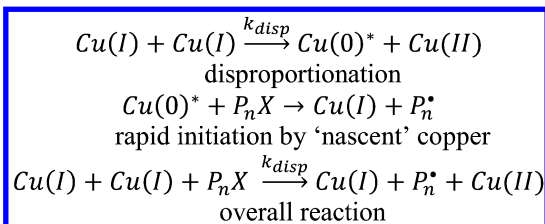
Scheme 4. Rapid activation by 'nascent' copper produced as a result of disproportionation.

If it is assumed that both disproportionation and comproportionation reactions may take place, the equations for the rates of generation of soluble copper species become the following:

$$\frac{d[Cu^I]}{dt} = k_{a0}[P_nX]\frac{S_{Cu}}{V} - k_{a1}[P_nX][Cu^I] + k_d[P_n^\bullet][Cu^{II}] + 2.k_{comp}[Cu^{II}]\frac{S_{Cu}}{V} - k_{disp}[Cu^I]^2 \tag{13}$$

$$\frac{d[Cu^{II}]}{dt} = k_{a1}[P_nX][Cu^I] - k_d[P_n^\bullet][Cu^{II}] - k_{comp}[Cu^{II}]\frac{S_{Cu}}{V} + k_{disp}[Cu^I]^2 \tag{14}$$

$$\frac{d[P_n^\bullet]}{dt} = k_{a0}[P_nX]\frac{S_{Cu}}{V} + k_{a1}[P_nX][Cu^I] - k_d[P_n^\bullet][Cu^{II}] + k_{disp}[Cu^I]^2 - 2.k_t[P_n^\bullet]^2 \tag{15}$$

Note that equation 5 remains valid, while the total change in copper concentration is now equal to

$$\frac{d[Cu^I]}{dt} + \frac{d[Cu^{II}]}{dt} = \left(k_{a0}[P_nX] + k_{comp}[Cu^{II}]\right)\frac{S_{Cu}}{V} \tag{16}$$

and the rate of change in the radical concentration equals:

$$\frac{d[P_n^\bullet]}{dt} = (1+\varphi).\left(k_{a0}[P_nX] + k_{comp}[Cu^{II}]\right)\frac{S_{Cu}}{V} - 2.k_t[P_n^\bullet]^2 \tag{17}$$

with φ now equal to (20, 21)

$$\varphi = \frac{[Cu^{II}]}{[Cu^I]+[Cu^{II}]} \approx \frac{k_{a1}[P_nX]+k_{disp}[Cu^I]}{k_d[P_n^\bullet]+k_{a1}[P_nX]+k_{disp}[Cu^I]} \tag{18}$$

As the concentration of copper(II) species is not constant, equation 17 is difficult to solve, but the radical concentration can be approximated by (20):

$$[P_n^\bullet] \approx \sqrt{\frac{(1+\varphi).\left(k_{a0}[P_nX]+k_{comp}\varphi[Cu^{II}]_0\right)\frac{S_{Cu}}{V}}{2.k_t}}\, e^{\frac{1}{2}.k_{comp}\frac{S_{Cu}}{V}\varphi.t} \tag{19}$$

Significant levels of comproportionation create a feedback loop in which the increasing copper concentration leads to an increased rate of comproportionation. The radical concentration is predicted to increase exponentially, although in reality increased radical generation as a result of comproportionation would be offset by a decrease in the dormant polymer concentration due to high levels of termination. High levels of comproportionation are thus incompatible with a well-controlled polymerization, which probably explains the poor control observed in acetonitrile, a solvent which strongly favors comproportionation.

It is important to note that the polymerization system as described above is not at equilibrium with respect to comproportionation and disproportionation. The reactions of activation by copper(I) (k_{a1}) and biradical termination (k_t) maintain a net flow of copper(I) to copper(II). Thus if the system is at equilibrium before the addition of dormant polymer (e.g. as a result of disproportionation of copper(I) salts), the addition of the dormant polymer will deplete the copper(I) concentration, shifting the equilibrium towards comproportionation. The copper(I) concentration will remain depleted with respect to the equilibrium until all dormant polymer has been converted to dead polymer through biradical termination reactions. This is true regardless of the value of the equilibrium constant of disproportionation, even in solvents such as water in which a large excess of Cu(II) over Cu(I) is typically present at equilibrium.

Simultaneous Measurement of Rates of Comproportionation and Activation by Copper(0)

The preparation of alkoxyamine initiators by reaction of alkyl halides with copper metal in the presence of a nitroxide radical (29, 30) provides an example of the autocatalytic effect of comproportionation (Scheme 5). When the reaction is carried out in acetonitrile an exponential increase in the rate of reaction is observed, as copper(I) generated by the reaction of copper(0) with alkyl halide reacts with a second molecule of alkyl halide to form copper(II), which in turn reacts with copper(0) to regenerate copper(I). Copper(II) is thus both a product and a catalyst for the reaction.
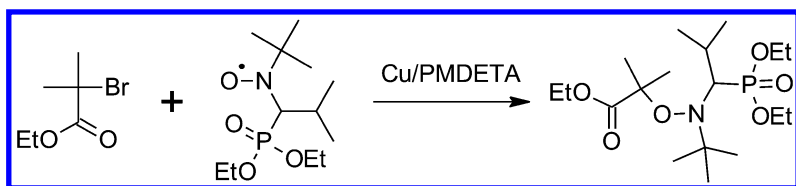
Scheme 5. Preparation of ethyl isobutyryl-SG1 adduct by reaction of ethyl bromoisobutyrate with copper metal in the presence of SG1 and N,N,N',N'',N''-pentamethyl diethylene triamine (PMDETA).

Experiments carried out in a variety of solvents showed autocatalytic effects in acetonitrile, DMF, ethanol and DMSO, while no autocatalysis was observed in toluene, ethyl acetate or a mixture of ethanol and water (Figure 1).

Analysis of the reaction kinetics shows that the initiator conversion is given by (20):

$$\frac{[RBr]_0 - [RBr]}{[RBr]_0} = \frac{2.k_{a0}}{k_{comp} - 2.k_{a0}} \cdot \left(e^{(k_{comp} - 2.k_{a0})\frac{S_{Cu}}{V}.t} - 1\right) \tag{20}$$

Fitting the observed kinetics to equations of the form conversion = A.exp(k.t) allowed the simultaneous determination of k_{a0} and k_{comp}. The results obtained are shown in Table 1.

It is notable that k_{a0} shows relatively little variation (typically 10^{-4}-10^{-3} cm.s^{-1}), while k_{comp} varies across several orders of magnitude. DMSO, the solvent of choice for SET-LRP, exhibits a high k_{a0} and relatively low k_{comp}, while MeCN has a relatively low k_{a0} and high k_{comp}. The significant rate of comproportionation observed in DMSO is in accordance with previous observations that Cu(I) is quite stable towards disproportionation in DMSO in the presence of sufficient Me$_6$tren ligand (31). The ethanol/water mixture and ethyl acetate are characterized by moderate k_{a0} and negligible k_{comp}, suggesting that these solvents are good candidates for rapid, well-controlled polymerizations. Interestingly, activation rate constants of a secondary initiator, methyl 2-bromopropionate, in the presence of Me$_6$tren ligand in DMSO (32) or water (24) have been reported as 1.8×10^{-4} cm.s^{-1} and 1.0×10^{-5} cm.s^{-1}, respectively, indicating that the change from a tertiary to a secondary initiator results in a 5-fold reduction in k_{a0}, and that water is a very poor solvent for the activation reaction, presumably due to the instability of Cu(I) species in aqueous solution. Even the highest values of k_{a0} measured here are slow in comparison to typical rate constants for activation by copper(I) (e.g. 2.7 M^{-1} s^{-1} for ethyl bromoisobutyrate in MeCN/PMDETA at 35°C (33)), which lends support to the SARA mechanism in which most activation of dormant polymer occurs through reaction with copper(I).
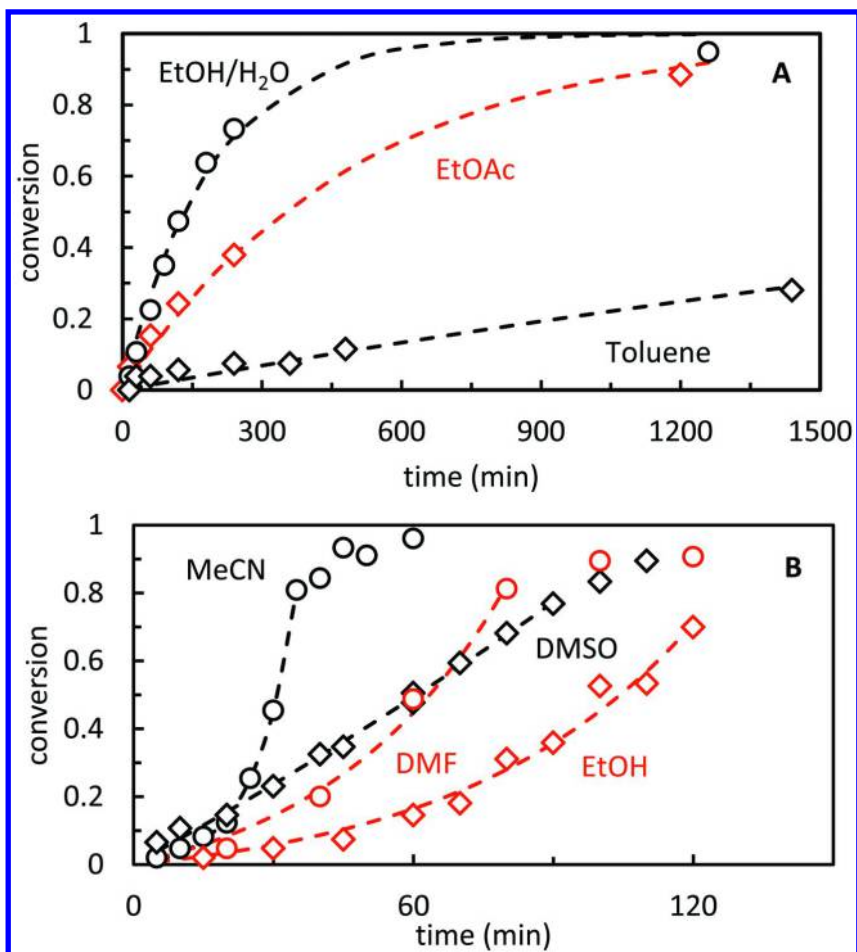
Figure 1. Conversion of ethyl bromoisobutyrate to the SG1 adduct in the presence of copper metal and PMDETA in non-comproportionating (A) and comproportionating (B) solvents, with exponential fits up to 80% conversion. Reproduced with permission from reference (20). Copyright 2012 American Chemical Society.

Table 1. Values of k_{a0} and k_{comp} obtained from kinetic analysis of the preparation of ethyl 2-methyl-2-[*N*-tert-butyl-*N*-(1-diethoxyphosphoryl-2,2-dimethylpropyl)aminoxy]propionate from ethyl bromoisobutyrate and SG1 nitroxide (*N*-tert-butyl-*N*-(1-diethylphosphono-2,2-dimethylpropyl)-*N*-oxyl) in the presence of *N,N,N′,N″,N″*-pentamethyldiethylene triamine.

Solvent	$k_{a0} \times 10^3$ (cm.s^{-1})[a]	$k_{comp} \times 10^3$ (cm.s^{-1})[a]	k_{comp}/k_{a0}
DMSO	1.05	2.8	2.8
EtOH/H$_2$O	0.72	<0.72[b]	—
DMF	0.45	7.8	18
EtOAc	0.28	<0.28[b]	—
MeCN	0.25	32	124
EtOH	0.20	6	30
Toluene	0.03	<0.03[b]	—

[a] Originally published values (*20*) have been corrected for reaction volume (6 mL) and copper surface area (0.36 cm^2).   [b] Negligible relative to k_{a0}.

While the rate constants of disproportionation could not be explicitly determined from these experiments, measured values of the disproportionation equilibrium constants in various solvents (for example in Table 6 of reference (*16*)) suggest that disproportionation is at best slow in DMSO, EtOH, and toluene, and completely negligible in MeCN. Significant disproproportionation cannot be ruled out in DMF ($K_{disp} \sim 2 \times 10^4$) or ethanol/water mixtures. It should be borne in mind that the presence and concentration of ligand has a strong effect on the disproportionation equilibrium (*31*).

Chain Length Dependence of k_t and k_{a0}

The simple model of polymerization kinetics presented above predicts a linear increase in copper concentration with time (equation 4). However, a detailed kinetic study of the polymerization of methyl acrylate in DMSO solution carried out by Percec and coworkers (*11*) showed that the rate of generation of copper decreased as the reaction proceeded. This was not a result of loss of dormant polymer chains through termination, which was less than 4% as estimated by the increase in copper concentration during the reaction (using the principle of halogen conservation (*34*)) and was too small to be measured by NMR (estimated at <0.5% by the authors of the study). To explain these results, we postulated (*21*) that the rate constant of activation by copper is chain length dependent, and could be expressed as:

$$k_{a0} = k_{a0}^1 (DP_n)^\alpha \qquad (21)$$

We further assume that nearly all the copper in solution is present in the form of copper(II) (i.e., $\varphi \approx 1$), justified by the use of a highly active ligand

(Me$_6$tren, $K_{ATRP} = 3 \times 10^{-6}$ in 50% DMSO (35)), and that comproportionation can be neglected due to the low concentration of copper(II) relative to dormant polymer and the relatively slow rate of comproportionation relative to activation in DMSO. As the radical concentration was constant throughout the reaction, the conversion (X) is an exponential function of time, and in a well-controlled polymerization DP$_n$ is proportional to conversion:

$$X = \frac{[P_nX]_0}{[M]_0} DP_n = 1 - e^{-k'.t} \tag{22}$$

$$\frac{d[Cu^{II}]}{dt} \approx k_{a0}[P_nX] = k_{a0}^1 DP_n^\alpha [P_nX] \propto X^\alpha \tag{23}$$

This condition can be fulfilled by representing $[Cu^{II}]$ as:

$$[Cu^{II}] = A \int_0^X \frac{s^\alpha}{(1-s)} ds + c = A.B_X(\alpha + 1,0) + c \tag{24}$$

where the incomplete beta function is defined as:

$$B_x(a,b) = \int_0^x s^{a-1}(1-s)^{b-1} ds \tag{25}$$

Differentiation with respect to time gives:

$$\frac{d[Cu^{II}]}{dt} = \frac{d[Cu^{II}]}{dX}.\frac{dX}{dt} = A\frac{X^\alpha}{1-X}.k'.(1-X) = A.k'.X^\alpha \tag{26}$$

and hence $d[Cu^{II}]/dt$ is proportional to X^α as required. Representation of the integral in terms of the incomplete beta function is convenient as it allows evaluation using commonly used spreadsheets such as EXCEL (36).

This function provides an excellent fit to the experimental $[Cu^{II}]$ data (Figure 2), and allowed the chain length dependence of k_{a0} to be determined as $k_{a0} = 1.25(9) \times 10^{-4}.DP_n^{-0.51(3)}$ cm·s^{-1} (values in parentheses represent the standard error in the last significant digit) (21).

As the radical concentration remained constant throughout the polymerization (evidenced by a constant $d(\ln[M])/dt$), equation 8 indicates that a similar chain length dependence must also be observed for the termination rate constant, k_t^{app}. Again assuming negligible contribution of Cu^I to the total copper concentration, the change in $[Cu^{II}]$ can be represented as:

$$\frac{d[Cu^{II}]}{dt} \approx k_t^{app}[P_n^\bullet]^2 \tag{27}$$

and hence k_t^{app} can be obtained by dividing $d[Cu^{II}]/dt$ by the square of the radical concentration. This procedure gives the chain length dependence of k_t as $k_t = 3.1(1) \times 10^9.DP_n^{-0.49(2)}$ L·mol^{-1}·s^{-1} (21). The values of k_t^{app} thus obtained are higher by an order of magnitude than those obtained in conventional radical or RAFT polymerizations, but are in agreement with measures in other ATRP-type systems (e.g., Zhong et al., $k_t^{app} = 1.4 \times 10^9$ L.mol^{-1}.s^{-1}) (37). The high values of k_t^{app} measured in these systems strongly suggests that an alternative mechanism of termination exists, probably involving interaction with copper metal, as proposed by Zhong et al. (37) While this finding does not negate the claims of high chain

end functionality that have been made for SET-LRP / SARA ATRP, it does imply that better results could be obtained from the same monomers using a reversible deactivation radical polymerization system such as RAFT which gives lower rates of termination.
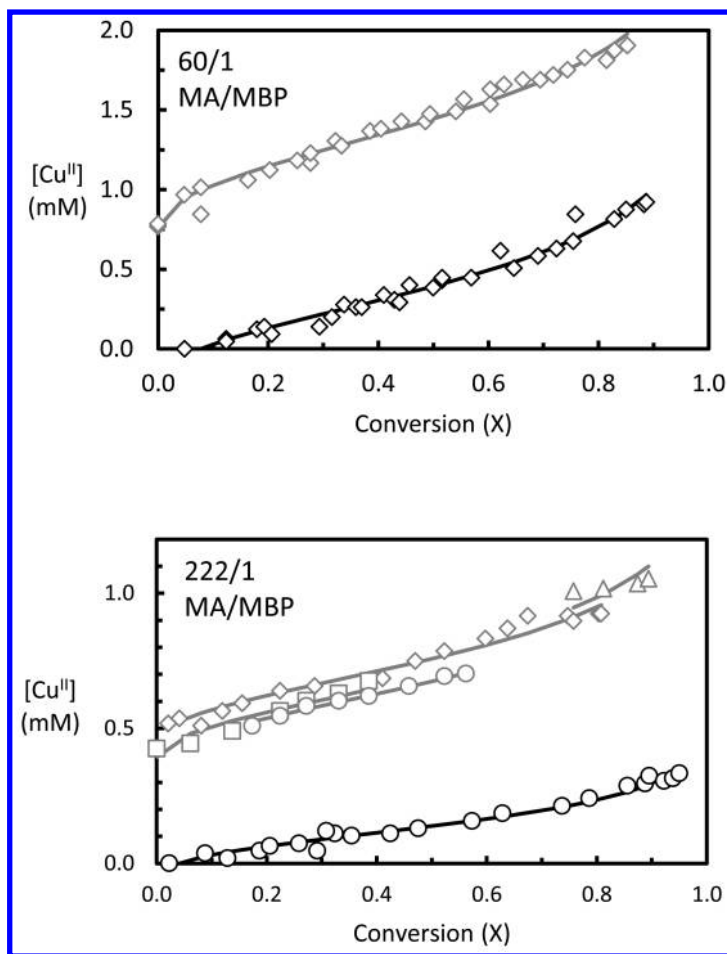
Figure 2. Generation of copper(II) as measured by UV-Vis spectroscopy during SET-LRP of methyl acrylate (MA) in DMSO solution, initiated by methyl 2-bromopropionate (MBP). Solid lines represent best fit to $[Cu^{II}]=A.B_X(\alpha+1,0)+c$, where c represents the initial $[Cu^{II}]$. In the 222/1 MA/MBP series carried out in the presence of initial added copper (gray points), different experiments appeared to have different initial copper concentrations. For this data set, the parameter c was allowed to vary between experiments, while A and α were held constant. Reproduced with permission from reference (21). Copyright 2014 American Chemical Society.

An interesting side effect of the strong chain length dependence of the termination rate constant is that polymerizations carried out in the presence of additional Cu^{II} show an increased fraction of dead chains. Copper(II) salts are frequently added to SET-LRP polymerizations in order to reduce the dispersity of the final polymer (*38–40*). The increased copper(II) concentration leads to faster deactivation and the production of lower molecular weight polymer at the beginning of the reaction. This polymer is especially susceptible to termination reactions, leading to a higher loss of functionality than in systems without initial added copper, despite the apparent improvement in control suggested by the narrower molecular weight distribution. This effect should not be apparent in chain extension reactions, where the chain length of the macroinitiator is already substantial.

Conclusions

In this paper we have developed a simple kinetic treatment for controlled radical polymerization in the presence of copper metal, known as SET-LRP or SARA ATRP, and demonstrated its use in the measurement of a number of elementary rate constants, *viz.*: activation by copper metal (k_{a0}), comproportionation (k_{comp}) and biradical termination (k_t^{app}). Our scheme provides a simple explanation for the observed ½-order dependence of polymerization rate on copper surface area, and provides a unified mechanism for polymerizations in solvents which favor disproportionation (e.g. mixtures of ethanol and water), those that favor comproportionation (e.g. MeCN) and those in which rates of comproportionation and disproportionation are essentially negligible (e.g. toluene). A strong chain length dependence on activation (k_{a0}) and termination (k_t) reactions is observed, which leads to the paradoxical effect that addition of copper(II) to the reaction, while narrowing the chain length distribution, results in lower chain end functionality compared to polymers with broader size distributions synthesized without added copper(II).

Experimental Part

Full experimental details for simultaneous measurement of comproportionation and activation rate constants may be found in reference (*19*). Data for the measurement of chain length dependence on activation and termination rate constants were obtained from Levere et al., reference (*12*). Full details of fitting procedures used in the treatment of these data may be found in reference (*20*).

Acknowledgments

References

1. Otsu, T.; Yamaguchi; Takemura, Y.; Kusuki, Y.; Aoki, A. *J. Polym. Sci., Polym. Lett.* **1967**, *5*, 697–701.
2. Kato, M.; Kamigaito, M.; Sawamoto, M.; Higashimura, T. *Macromolecules* **1995**, *28*, 1721–1723.
3. Wang, J. S.; Matyjaszewski, K. *J. Am. Chem. Soc.* **1995**, *117*, 5614–5615.
4. Matyjaszewski, K.; Coca, S.; Gaynor, S. G.; Wei, M.; Woodworth, B. E. *Macromolecules* **1997**, *30*, 7348–7350.
5. Percec, V.; Barboiu, B.; van der Sluis, M. *Macromolecules* **1998**, *31*, 4053–4056.
6. Percec, V.; Guliashvili, T.; Ladislaw, J. S.; Wistrand, A.; Stjerndahl, A.; Sienkowska, M. J.; Monteiro, M. J.; Sahoo, S. *J. Am. Chem. Soc.* **2006**, *128*, 14156–14165.
7. Zhang, Y.; Wang, Y.; Peng, C. H.; Zhong, M.; Zhu, W.; Konkolewicz, D.; Matyjaszewski, K. *Macromolecules* **2011**, *45*, 78–86.
8. Jakubowski, W.; Min, K.; Matyjaszewski, K. *Macromolecules* **2005**, *39*, 39–45.
9. Jakubowski, W.; Matyjaszewski, K. *Angew. Chem., Int. Ed.* **2006**, *45*, 4482–4486.
10. Percec, V.; Popov, A. V.; Ramirez-Castillo, E.; Monteiro, M.; Barboiu, B.; Weichold, O.; Asandei, A. D.; Mitchell, C. M. *J. Am. Chem. Soc.* **2002**, *124*, 4940–4941.
11. Levere, M. E.; Nguyen, N. H.; Percec, V. *Macromolecules* **2012**, *45*, 8267–8274.
12. Zhang, N.; Samanta, S. R.; Rosen, B. M.; Percec, V. *Chem. Rev.* **2014**, *114*, 5848–5958.
13. Jiang, X.; Rosen, B. M.; Percec, V. *J. Polym. Sci., Part A: Polym. Chem.* **2010**, *48*, 2716–2721.
14. Nguyen, N. H.; Levere, M. E.; Percec, V. *J. Polym. Sci., Part A: Polym. Chem.* **2012**, *50*, 860–873.
15. Matyjaszewski, K.; Tsarevsky, N. V.; Braunecker, W. A.; Dong, H.; Huang, J.; Jakubowski, W.; Kwak, Y.; Nicolay, R.; Tang, W.; Yoon, J. A. *Macromolecules* **2007**, *40*, 7795–7806.
16. Rosen, B. M.; Percec, V. *Chem. Rev.* **2009**, *109*, 5069–5119.
17. Konkolewicz, D.; Wang, Y.; Krys, P.; Zhong, M.; Isse, A. A.; Gennaro, A.; Matyjaszewski, K. *Polym. Chem.* **2014**, *5*, 4396–4417.
18. Konkolewicz, D.; Wang, Y.; Zhong, M.; Krys, P.; Isse, A. A.; Gennaro, A.; Matyjaszewski, K. *Macromolecules* **2013**, *46*, 8749–8772.
19. West, A. G.; Hornby, B.; Tom, J.; Ladmiral, V.; Harrisson, S.; Perrier, S. *Macromolecules* **2011**, *44*, 8034–8041.
20. Harrisson, S.; Couvreur, P.; Nicolas, J. *Macromolecules* **2012**, *45*, 7388–7396.
21. Harrisson, S.; Nicolas, J. *ACS Macro Lett.* **2014**, *3*, 643–647.
22. Wang, Y.; Zhong, M.; Zhu, W.; Peng, C. H.; Zhang, Y.; Konkolewicz, D.; Bortolamei, N.; Isse, A. A.; Gennaro, A.; Matyjaszewski, K. *Macromolecules* **2013**, *46*, 3793–3802.

23. Peng, C. H.; Zhong, M.; Wang, Y.; Kwak, Y.; Zhang, Y.; Zhu, W.; Tonge, M.; Buback, J.; Park, S.; Krys, P.; Konkolewicz, D.; Gennaro, A.; Matyjaszewski, K. *Macromolecules* **2013**, *46*, 3803–3815.

24. Konkolewicz, D.; Krys, P.; Gois, J. R.; Mendonca, P. V.; Zhong, M.; Wang, Y.; Gennaro, A.; Isse, A. A.; Fantin, M.; Matyjaszewski, K. *Macromolecules* **2014**, *47*, 560–570.

25. Wang, Y.; Soerensen, N.; Zhong, M.; Schroeder, H.; Buback, M.; Matyjaszewski, K. *Macromolecules* **2013**, *46*, 683–691.

26. Hornby, B. D.; West, A. G.; Tom, J. C.; Waterson, C.; Harrisson, S.; Perrier, S. *Macromol. Rapid Commun.* **2010**, *31*, 1276–1280.

27. Tom, J.; Hornby, B.; West, A.; Harrisson, S.; Perrier, S. *Polym. Chem.* **2010**, *1*, 420–422.

28. Matyjaszewski, K.; Jakubowski, W.; Min, K.; Tang, W.; Huang, J.; Braunecker, W. A.; Tsarevsky, N. V. *Proc. Natl. Acad. Sci. U. S. A.* **2006**, *103*, 15309–15314.

29. Matyjaszewski, K.; Woodworth, B. E.; Zhang, X.; Gaynor, S. G.; Metzner, Z. *Macromolecules* **1998**, *31*, 5955–5957.

30. Harrisson, S.; Couvreur, P.; Nicolas, J. *Polym. Chem.* **2011**, *2*, 1859–1865.

31. Wang, Y.; Zhong, M.; Zhu, W.; Peng, C. H.; Zhang, Y.; Konkolewicz, D.; Bortolamei, N.; Isse, A. A.; Gennaro, A.; Matyjaszewski, K. *Macromolecules* **2013**, *46*, 3793–3802.

32. Peng, C. H.; Zhong, M.; Wang, Y.; Kwak, Y.; Zhang, Y.; Zhu, W.; Tonge, M.; Buback, J.; Park, S.; Krys, P.; Konkolewicz, D.; Gennaro, A.; Matyjaszewski, K. *Macromolecules* **2013**, *46*, 3803–3815.

33. Tang, W.; Matyjaszewski, K. *Macromolecules* **2007**, *40*, 1858–1863.

34. Wang, Y.; Zhong, M.; Zhang, Y.; Magenau, A. J. D.; Matyjaszewski, K. *Macromolecules* **2012**, *45*, 8929–8932.

35. Wang, Y.; Kwak, Y.; Buback, J.; Buback, M.; Matyjaszewski, K. *ACS Macro Lett.* **2012**, *1*, 1367–1370.

36. The incomplete beta function can be evaluated as follows using EXCEL: Value = BetaDist(x, a, b, true) * Exp(GammaLn(a) + GammaLn(b) - GammaLn(a + b)). This formula returns an error for b = 0, but using small values of b (<0.001) provide a good approximation to the true value of the function.

37. Zhong, M.; Wang, Y.; Krys, P.; Konkolewicz, D.; Matyjaszewski, K. *Macromolecules* **2013**, *46*, 3816–3827.

38. Nyström, F.; Soeriyadi, A. H.; Boyer, C.; Zetterlund, P. B.; Whittaker, M. R. *J. Polym. Sci., Part A: Polym. Chem.* **2011**, *49*, 5313–5321.

39. Anastasaki, A.; Waldron, C.; Wilson, P.; Boyer, C.; Zetterlund, P. B.; Whittaker, M. R.; Haddleton, D. *ACS Macro Lett.* **2013**, *2*, 896–900.

40. Soeriyadi, A. H.; Boyer, C.; Nyström, F.; Zetterlund, P. B.; Whittaker, M. R. *J. Am. Chem. Soc.* **2011**, *133*, 11128–11131.

Visible Light-Induced Atom Transfer Radical Polymerization for Macromolecular Syntheses

Yusuf Yagci,[1,2,*] Mehmet Atilla Tasdelen,[1,3] Baris Kiskan,[1] Mustafa Çiftci,[1] Sajjad Dadashi-Silab,[1] Omer Suat Taskin,[1] and Gorkem Yilmaz[1]

[1]Istanbul Technical University, Faculty of Science and Letters, Department of Chemistry, Maslak, 34469, Istanbul, Turkey
[2]King Abdulaziz University, Faculty of Science, Department of Chemistry, 21589, Jeddah, Saudi Arabia
[3]Yalova University, Faculty of Engineering, Department of Polymer Engineering, 77100, Yalova, Turkey
*E-mail: yusuf@itu.edu.tr

Visible light-induced atom transfer radical polymerization (ATRP) of vinyl monomers are examined by using various photocatalysts systems including *Type I* and *Type II* photoinitiators, dyes, dimanganese decacarbonyl and semiconducting photocatalysts. The influence of various experimental parameters on the polymerization such as type of light sources and photocatalyts, and concentration of metal catalysts are also investigated. Although there currently exist only a few examples, the visible light initiation can be applied to the ATRP process providing a mild and efficient method for the *in situ* generation of Cu(I) activator.

Introduction

Atom transfer radical polymerization (ATRP) is currently one of the most often-used synthetic polymerization methods due to its simplicity and broad applicability, and the ability to prepare previously inaccessible well-defined polymers with complex architecture (*1–4*). The ATRP is a redox process

involving a transition metal complex in which a halide atom (especially Cl or Br) is reversibly transferred between a growing radical and a dormant species. Copper and iron compounds are particularly successful metal catalysts used in ATRP, but there are also studies reporting other transitional metals such as ruthenium, molybdenum and osmium (*5*). During the past years, various initiation techniques involving simultaneous reverse and normal initiated (SR&NI), activators by electron transfer (AGET), activators regenerated by electron transfer (ARGET) (*6*), initiators for continuous activator regeneration (ICAR) (*7*, *8*), and supplementary activator and reducing agent (SARA) ATRP (*9*, *10*), and single electron transfer-living radical polymerization (SET-LRP) have been reported to create some substantial benefits for environmental and practical issues, *i.e.* in the presence of oxygen, at room temperature or the use of catalyst at the level of parts per million (ppm). All of these methods are based on the *in situ* formation of activator via secondary reduction process including (I) the use of various reducing agents (either externally added (*11*) or monomers containing amine (*12*) or epoxide (*13*) groups as intrinsic reducing agents), (II) electrochemically redox processes (*14*), (III) copper-containing nanoparticles (*15*), and (IV) photochemically mediated redox processes (*16–27*).

Light is a particularly fascinating stimulus because it can be precisely modulated in terms of wavelength, polarization direction and intensity, allowing spatial and temporal of the chemical reactions (*28–32*). The use of UV and visible light irradiation for the *in situ* generation of activators for the photoinduced ATRP reaction has been researched extensively (*16*). Many copper (II) salts are light-sensitive compounds and can be photochemically reduced in the presence of the amine ligands. The required Cu(I) catalysts for the ATRP process can be engendered by light directly or indirectly. In the direct system, the polymerization activator, Cu(I) is generated from Cu(II) under UV light without any photoinitiator and the polymerization can be initiated by the reaction of the Cu(I)X with alkyl halide (*27*, *33*, *34*). In the indirect system, the polymerization activators, Cu(I), can be generated from Cu(II) under UV light through the help of photoinitiators. Many UV and visible light free radical photoinitiators are reported to be powerful promoters for photoinduced ATRP (*17–19*, *34*). Recently, studies from this laboratory showed that the spectral sensitivity of the photoinduced ATRP can be extended into the visible light region to avoid hazardous UV light. In the present chapter, we will outline the recent achievements, mechanistic aspects, limitations and opportunities of the visible light-induced ATRP through several examples.

Visible Light-Induced ATRP by Directly Generated Activator

Many copper(II)/ligand complexes are known to be light sensitive and undergo photoredox reactions during UV or visible light irradiation. Earlier spectroscopic studies indicated that Cu(II) complex has three distinct absorption, two of which at UV (around 250 and 300 nm) and one at visible and near infra-red regions (between 650-1000 nm) (*35*, *36*). These bands are highly dependent on the nature of the copper salt and the ligand used and can vary in different systems.

The ATRP of various monomers have been successfully conducted by applying several wavelengths in both UV and visible light regions. Very recently, the photopolymerization of various acrylates mediated by ppm level of Cu catalyst without the use of any photoinitiator or reducing agent was achieved (*20*). A variety of vinyl monomers including poly(ethylene glycol) methyl ether acrylate, *tert*-butyl acrylate, methyl acrylate, ethyl acrylate, methyl methacrylate, and styrene, as well as functional initiators in different solvents were tested. There are three distinct pathways for photochemical (re)generation of Cu(I) activator including (i) direct photochemical reduction of the Cu(II) complexes by excess free amine moieties, (ii) unimolecular reduction of the Cu(II) complex, (iii) photochemical radical generation either directly from the alkyl halide, ligand, or via interaction of the ligand with either monomer or with alkyl halides. Both experimental and simulation results show that the photochemically mediated reduction of Cu(II) complexes by an excess of amine groups is dominant for the (re)generation of Cu(I) activator (*24, 37–42*).

The ability of other transition metals such as iridium (Ir) (*43*), and ruthenium (Ru) (*44*), as alternative to the cupric catalyst system, are investigated to succeed photoinitiated ATRP. Recently Hawker et al. investigated the Ir-based photoredox system that can be utilized in order to control the polymerization of methacrylate monomers (*45*). The *fac*-[Ir(ppy)₃] (ppy =2-pyridylphenyl) complex was used as the photocatalyst which affords photoexcited *fac*-[Ir(ppy)₃]* species upon irradiation under visible light. The photoexcited Ir^III* captured a halogen atom from alkyl halide to form initiating radicals as well as highly oxidized Ir^IV complex. This Ir^IV could then react with the propagating radicals to generate initial Ir^III complex in the ground state. The process is applied to a variety of acrylate monomers including methyl acrylate, ethyl acrylate, *n*-butyl acrylate and *tert*-butyl acrylate. The nature of the *fac*-[Ir(ppy)₃] catalyst tolerates carboxylic acid functionality such as acrylic acid. The block and random copolymers of acrylic acid with other (meth)acrylates can be obtained by either macroinitiator or along the backbone of random copolymer with up to 50 mole percent of acrylic acid (*46*). The process also established spatiotemporal control over the patterning of polymer brushes using the same catalytic system under visible light irradiation (*47, 48*).

Visible Light-Induced ATRP by Using *Type I* Photoinitiators

Recent studies from this laboratory showed that the spectral sensitivity of the photoinduced ATRP could be extended into the visible-light region by commercially available *Type I* photoinitiators. Photochemically mediated reverse and simultaneous reverse and normal initiation (SR & NI) ATRP of various vinyl monomers in the presence of bis(2-methyl-2-propanyl)(phenyl)phosphine oxide (BAPO) as a *Type I* photoinitiator resulted in polymers with relatively molecular weight distributions (*18, 22, 49*). However, the reverse photoinduced ATRP gave uncontrolled molecular weight of polymers with broad molecular weight distributions. This may be due to that the concentration of the propagating

radicals is decreased and normal bimolecular termination becomes significant, which results in loss of control. Another disadvantage of the photoinduced reverse ATRP is related to the loss of the terminal functionality and hence limitation of its use in further block or chain-extension reactions. In order to further prove the living characteristics of polymer obtained by photoinduced reverse ATRP, PMMA ($M_{n,GPC}$ = 67700 g/mol, M_w/M_n = 1.30) was used as a macroinitiator to initiate classical ATRP of MMA. The final polymer curve slightly shifted to higher molecular weights ($M_{n,GPC}$ = 80300 g/mol, M_w/M_n = 1.42) after chain extension. There is an increase in the molecular weight distribution after 2 h and a low-molecular-weight shoulder can be detected in the GPC traces of the final polymer, which suggests that some chains from the macroinitiator failed to initiate the second polymerization. This is a clear indication of poor initiation efficiency of the macroinitiator, which may not be only due to termination reactions, but also side reactions between growing radicals and the copper catalyst (18).

In the photoinduced SR&NI ATRP case, a mixture of an excess amount of alkyl halide and photoinitiator together with Cu(II) catalyst complex is used as a dual initiator for the ATRP process. In this way, not only handling problems can be avoided but also the molecular weight distribution and chain end functionality of the polymers can be improved (Scheme 1).
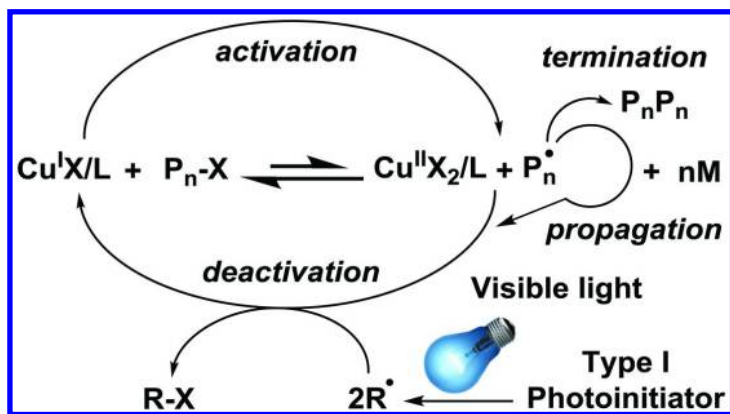
Scheme 1. Proposed mechanism for the photoinduced SR&NI and ICAR ATRP.

When the polymerization is performed with a photoinitiator, two photogenerated radicals induce chain growth propagation in addition to Cu(I) (re)generation. The molecular weight of the polymers obtained by this system are in good agreement with the theoretical values and show very narrow-molecular-weight distributions, ranging from 1.11–1.18. One can note that the photoinduced SR&NI ATRP system allowed better control over molecular weight and distribution under the same experimental conditions (Figure 1).
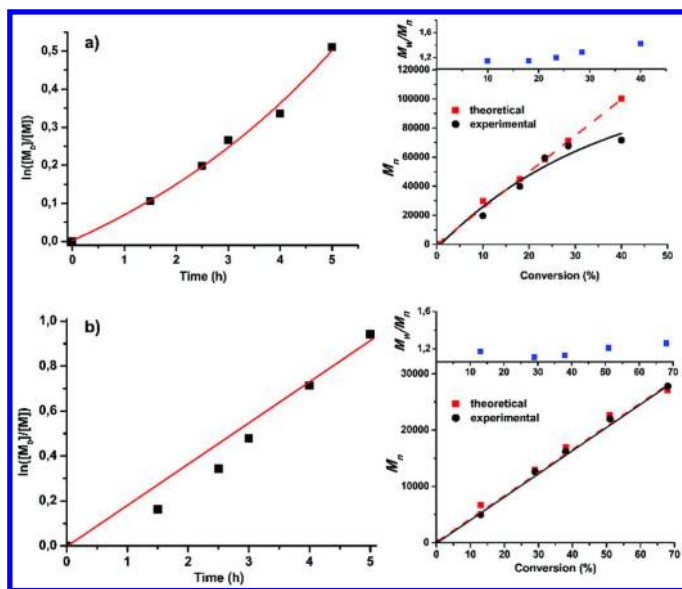
Figure 1. Kinetic plots and molecular weights and distributions of resulting polymers as a function of degree of conversion for photoinduced reverse (a) and SR&NI (b) ATRP. Reproduced with permission from reference 18. Copyright 2011 John Wiley & Sons.

Visible Light-Induced ATRP by Using *Type II* Photoinitiators

In *Type II* photoinitiating systems, the radical photoinitiator like camphorquinone is also active in the range of visible light and is capable of generating radicals via Norrish *Type II* reaction in the presence of a hydrogen donor, such as tertiary amines or alcohols. First step of the process involves electron abstraction from the amine by the excited photoinitiator to produce aminoalkyl and ketyl radicals. These radicals are not only able to add to monomer molecules to initiate growth of polymer chains but also regenerate Cu(I) activator by reducing the Cu(II) species. Notably, the photogenerated ketyl radicals are not reactive enough to activate the vinyl polymerization.

In order to extend the spectral sensitivity of the photoinduced ATRP into the visible-light region, various dyes such as eosin Y and erythrosin B are used in SR&NI ATRP (*18, 49*). The primary photochemical reaction involves the excited dye molecules abstracting an electron from the amine molecules to form radical-cation/radical-anion pairs. After the proton transfer, some of the radicals are in the system. These radicals are not only able to add to monomer molecules to initiate the polymerization but can reduce the Cu(II) to Cu(I), which is used as activator in ATRP. In the dye systems, the molecular weights increase linearly with conversions, which are consistent with the polymerizations proceeding in a controlled fashion (Figure 2). However, the experimental molecular weights are slightly higher than the theoretical values, indicating low initiation efficiency. In dye/amine system, back electron transfer generally limits the efficient generation

of free radicals which directly reduce Cu(II) to Cu(I). The applicability of this system is also extended to other vinyl monomers such as methyl acrylate and styrene. Although visible light induced ATRP represented well-controlled system for the polymerization of methyl acrylate, the system was less controlled toward styrene monomer due to the high quenching rate of the monomer.
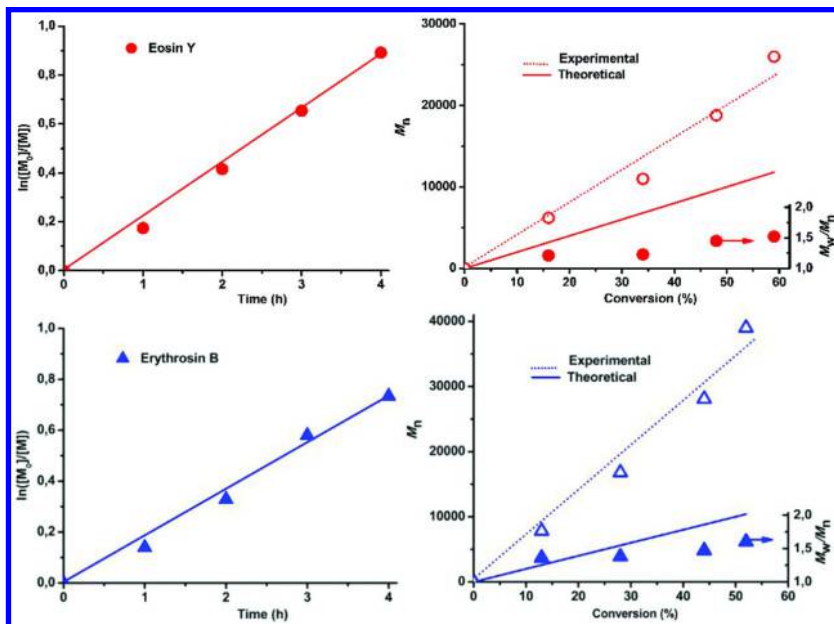
Figure 2. Kinetic plots and molecular weights and distributions of resulting polymers as a function of degree of conversion for eosin and erythrosin B sensitized ATRP of methyl methacrylate. Reproduced with permission from reference 49. Copyright 2012 John Wiley & Sons.
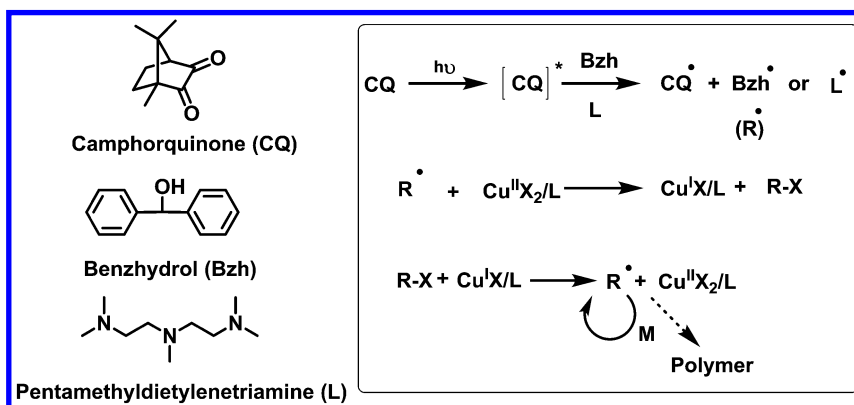
Scheme 2. Mechanistic scheme for photoinduced reverse ATRP using CQ/Bzh.

Quite recently a new photoinduced reverse ATRP approach using camphorquinone/benzhydrol (CQ/Bzh) as an alternative initiating system has been reported (*50*). In this process, triplet state CQ abstracts hydrogen from the ground state Bzh to give two ketyl type radicals, which do not react with the surrounding monomer as a result of its stability and steric hindrance. These radicals, however, reduce the Cu(II) complex to Cu(I) activator and simultaneously generate the alkyl halide (R-X, where X is Cl or Br). In the following step, the R-X compound is responsible for the initiation of photoinduced ATRP of acrylic monomer (Scheme 2).

The main benefit of this approach is that it simultaneously forms alkyl halide initiator by the addition of acid released from the redox process to the monomer. The experimental molecular weights are considerably higher than theoretical values and the obtained polymers showed slightly broad molecular weight distributions ranging from 1.13 to 1.51 in the process. The photoinduced SR&NI ATRP of MMA under the same conditions is also presented and the system leads to a better control of the polymerization as reflected by the improved molecular weight distribution and chain end functionality.

Visible Light-Induced ATRP by Using Dimanganese Decacarbonyl

Dimanganese decacarbonyl ($Mn_2(CO)_{10}$) has a weak Mn–Mn linkage and visible light photolysis provides the $\cdot Mn(CO)_5$ metalloradicals which are not capable of initiating polymerization but abstracting halides from a variety of organohalogen compounds, generating the corresponding carbon centered radicals (Scheme 3). We have previously shown that manganese based radical generation process can successfully be employed in different modes of polymerization processes including radical promoted cationic polymerization (*51*), mechanistic transformation (*52, 53*), radical coupling (*54*), hyper-branching (*55*) and grafting from polyolefines (*56*). Recent studies from our laboratory showed that this chemistry can be used as a photoredox catalyst system for the ATRP of vinyl monomers such as methyl methacrylate, methyl acrylate and styrene (*57*). The polymerizations were performed either by visible- or sunlight in the presence of ppm level of copper catalysts at room temperature. The ease of this novel light induced ATRP comes from the usage of $Mn_2(CO)_{10}$ which was surely responsible for the both initiation and control of the polymerization.

In order to gain a better understanding of the polymerization mechanism several control experiments were performed in the absence of either light, $Mn_2(CO)_{10}$ or $Cu^{II}Br_2$. When the polymerization was performed in the dark (entry 1, Table 1) or in the absence of $Mn_2(CO)_{10}$ (entry 2, Table 1) no polymer was obtained. In the case of no $Cu^{II}Br_2$, polymer with uncontrolled molecular weight was formed *via* free radical polymerization (entry 3, Table 1), due to photogenerated radicals from alkyl halides by classical halogen abstraction reaction. The effect of $Mn_2(CO)_{10}$ concentration on the polymerization was

investigated by changing molar ratio of $Mn_2(CO)_{10}$. At relatively high $Mn_2(CO)_{10}$ concentration (entry 4, Table 1) the reaction showed little control, with a high molecular weight distribution value due to the irreversible radical termination. However, reducing the concentration of the $Mn_2(CO)_{10}$ significantly decreased the molecular weight distribution of the resulting polymers (entries 5 and 6, Table 1). Additionally, even at the ppm level of the catalyst, molecular weight distribution remained narrow and the system still had a good living nature (entry 7, Table 1). In the sunlight induced process (entry 8, Table 1), the polymerization proceeded at a relatively slower rate and showed slightly higher molecular weight distribution due to the broader wavelength spectrum in the sunlight irradiation. Applicability of the method with other vinyl monomers such as methyl acrylate and styrene (entries 10 and 11, Table 1) was also examined. In both cases, control over molecular weight and molecular weight distribution was good.

On the basis of above results, the mechanism was proposed as follows (Scheme 3). First step of the process involves the formation of $^{\bullet}Mn(CO)_5$ radical by homolysis of $Mn_2(CO)_{10}$ under visible- or sun light. These photogenerated $^{\bullet}Mn(CO)_5$ radicals not only abstract halogen atoms from alkyl halides to initiate polymerization but also provide continuous activator regeneration by reducing the excess of Cu(II) deactivator to the Cu(I) activator. Additionally, sunlight induced ATRP of MMA in the presence of commercially available poly(vinyl chloride) (PVC) using $Mn_2(CO)_{10}$ resulted in the formation of PVC-*g*-PMMA copolymers successfully. In the process, chlorine atoms of PVC acted as initiation sites for grafting of MMA.
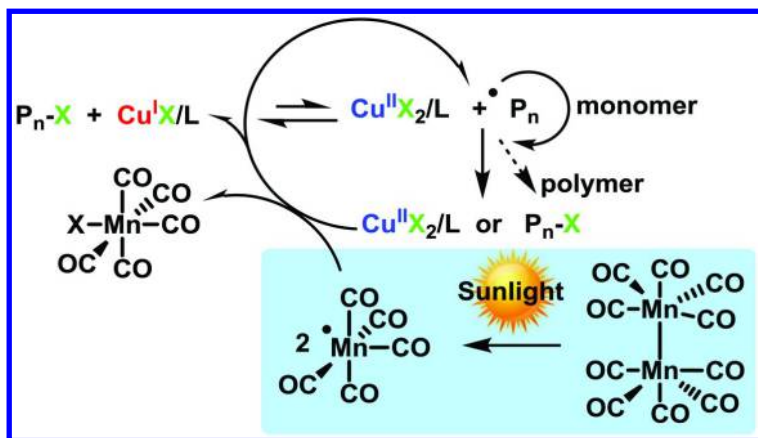
Scheme 3. Mechanistic scheme for sunlight induced ATRP using $Mn_2(CO)_{10}$.

Table 1. Visible light or sunlight induced ATRP of vinyl monomers at room temperature. Reproduced with permission from reference 57. Copyright 2014 Royal Society of Chemistry.

Entry	$[M]_0/[RX]_0/[MtX]_0/[L]_0/[Mn_2(CO)_{10}]_0$	Mon.	Conv. (%)	$M_{n,th}$[a] (g.mol-1)	$M_{n,GPC}$[b] (g.mol-1)	M_w/M_n[b]
1[c]	200/1/0.2/0.2/0.2	MMA	-	-	-	-
2[d]	200/1/0.2/0.2/0.0	MMA	-	-	-	-
3[d]	200/1/0.0/0.2/0.2	MMA	93	18600	74800	2.65
4[d]	200/1/0.2/0.2/0.2	MMA	82	16400	34500	1.82
5[d]	200/1/0.2/0.2/0.1	MMA	54	8500	16500	1.48
6[d]	200/1/0.2/0.2/0.05	MMA	35	7000	8100	1.16
7[d]	200/1/0.01/0.01/0.05	MMA	29	5800	6200	1.21
8[e]	200/1/0.2/0.2/0.05	MMA	28	6200	5600	1.28
9[d]	200/1/0.2/0.2/0.05	MA	21	3600	4100	1.19
10[d]	200/1/0.2/0.2/0.05	St	17	3500	3800	1.23

[a] $M_{n,th}$ = [Monomer]$_0$/([RX]$_0$ × $M_{Wmonomer}$ × conversion);   [b] Number-average molecular weight ($M_{n,GPC}$) and molecular weight distribution (M_w/M_n) were determined by gel permeation chromatography;   [c] Polymerization was performed in the dark, time = 180 min;   [d] Polymerization was performed at visible light irradiation, time = 180 min, light intensity = 45 mW cm-2.   [e] Polymerization was performed with sunlight, time = 180 min, light intensity = 60 mW cm-2.

Visible Light-Induced ATRP by Semiconducting Photocatalysts

There has been an intense research interest in the past decades in developing (nano)engineered materials exhibiting photocatalytic properties in order to actualize catalytic reactions under more environmentally benign conditions and with inexpensive materials.   Owing to their photosensitive properties, semiconductor materials have been extensively utilized as photocatalyst, which can be excited upon photo illumination and provide the required charge carriers to induce reactions by enabling reduction/oxidation processes. Upon photoexcitation of semiconductors, electron-hole pairs are released correspondingly from the conduction and valence band of the semiconductor, which can then promote reduction or oxidation reactions, respectively.   In addition to widely used inorganic semiconductor nanoparticles such as titanium dioxide (TiO_2) or zinc oxide (ZnO), metal-free organic-based polymeric semiconductors have also been developed as inexpensive and efficient energy transducers for photocatalyst purposes. Mesoporous graphitic carbon nitride (mpg-C_3N_4), for instance, has been developed as an efficient photocatalyst in a broad variety of reactions (*58*).

It was previously reported that free radical photopolymerization can be achieved by using mpg-C_3N_4 as the photocatalyst by which the initiating radicals were formed through oxidation reactions induced by the releasing charge carriers from mpg-C_3N_4 under visible light irradiation (59). The applicability of this kind of polymeric photocatalyst has been recently extended to the ATRP system. The required Cu(I) activator can be obtained from air-stable Cu(II) species via electrons released from mpg-C_3N_4 under light (60, 61). The photoinduced ATRP of a variety of vinyl monomers, including methyl methacrylate, methyl acrylate and styrene is investigated by using Cu(II)/PMDETA as the catalyst and mpg-C_3N_4 as the photocatalyst in acetonitrile media. The polymerization conducted under either UV light (λ = 350 nm) or natural sunlight and in both cases the photoinduced ATRP gives well-controlled polymers having molecular weights in good agreement with theoretical values and low molecular weight distributions (1.10-1.16). Kinetics studies reveal a linear relationship between the monomer consumption, $\ln([M]_0/[M])$, and reaction time indicative of the constant concentration of the propagating radicals during the reaction. A linear increase in the molecular weights of the resulting polymers was also observed as conversion increased. Compared with UV light, natural sunlight resulted in a more controllable, efficient process as the polymer chains had narrower molecular weight distributions, and near-quantitative monomer conversion was achieved when irradiated under sunlight. The use of copper catalyst at ppm levels (50 ppm) caused an increase in the rate of reaction and gave slightly broad polymer chains with molecular weight distribution of around 1.28. This was probably due to the low deactivation rate of the propagating radicals. Furthermore, the livingness of the process was proved by ^{1}H NMR and *in situ* chain extension experiments as the resulted polymers exhibited excellent chain end fidelity. The proposed mechanism was based on the perpetual reduction of air-stable Cu(II) species by the releasing electrons from mpg-C_3N_4 furnishing activator Cu(I) catalyst *in situ* to active a dormant chain (P_n-X) (Scheme 4).
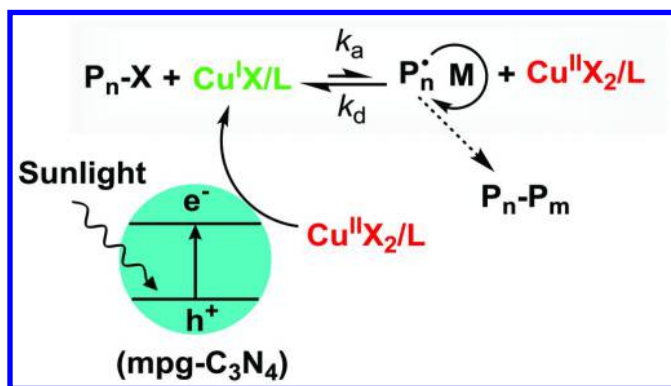
Scheme 4. Proposed mechanism of photoinitiated ATRP by mpg-C_3N_4

Temporal control over the growth of polymer chains is achieved by intermittent light and dark experiments. Exposing the polymerization solution

including mpg-C_3N_4 to the light initiate the polymerization while treating in the dark results in no growth as no conversion is detected during the dark periods and no change in the molecular weight of the polymer is observed.

Similar photomediated ATRP processes have also been achieved by using inorganic semiconductor nanoparticles to afford well-controlled macromolecular architectures. Yagci et al. used ZnO nanoparticles as photocatalyst to initiate ATRP process (*62*). Zhou and co-workers reported surface-initiated ATRP mediated by irradiation of TiO_2 nanoparticles to reduce Cu(II) species (*63*). Although these reactions are accomplished under UV light irradiation, the spectral activity of such systems was extended to visible regions by using dye-sensitized TiO_2 nanoparticles in which dyes acting as visible light-sensitizer were used to excite electrons in the conduction band of TiO_2 (*64*). Mechanistically, photoinduced electron transfer from the dye to the conduction band of the semiconductor leads to a charge separation in TiO_2 and electron release reducing Cu(II). This system is applied to grow polymer brushes of different compositions and architectures from an ATRP initiator-functionalized substrate with a range of water-soluble monomers. An interesting aspect of this system is the ability to gain spatial control over the growth of polymer brushes affording patterned features with desired composition. Scheme 5 shows the mechanism of surface-initiated ATRP by dye-sensitized TiO_2 nanoparticles.
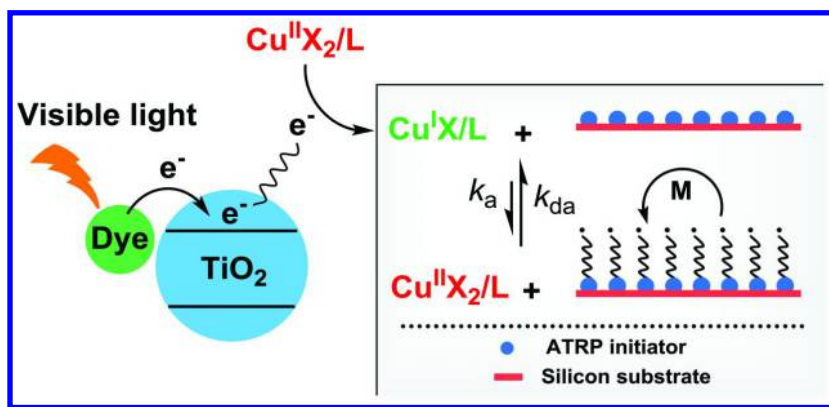
Scheme 5. Schematic illustration of the growth of polymer brush by the photoinitiated ATRP using dye-sensitized TiO_2 nanoparticles

Conclusion

In this contribution, possibilities and limitations of visible light-induced ATRP for the synthesis of well-defined polymers with controlled architecture have been reported with particular references to recent works conducted in the area. The use of environmentally friendly, non-toxic and inexhaustible visible light in photochemical synthesis is a scientific challenge to prepare tailor-made polymers. The visible light-induced ATRP not only enables the easy control of the polymerization under ambient temperature even for heat-sensitive monomers but also tends to minimize side reactions like chain transfer or depolymerization.

Furthermore, this system do not need for high-energy ultraviolet radiation in most photochemical processes, which has limited both the practicality and environmental benefits of photochemical synthesis on industrially relevant scales.

References

1.   Wang, J. S.; Matyjaszewski, K. *J. Am. Chem. Soc.* **1995**, *117*, 5614–5615.
2.   Wang, J. S.; Matyjaszewski, K. *Macromolecules* **1995**, *28*, 7901–7910.
3.   Kato, M.; Kamigaito, M.; Sawamoto, M.; Higashimura, T. *Macromolecules* **1995**, *28*, 1721–1723.
4.   Percec, V.; Barboiu, B. *Macromolecules* **1995**, *28*, 7970–7972.
5.   di Lena, F.; Matyjaszewski, K. *Prog. Polym. Sci.* **2010**, *35*, 959–1021.
6.   Jakubowski, W.; Min, K.; Matyjaszewski, K. *Macromolecules* **2006**, *39*, 39–45.
7.   Dong, H. C.; Tang, W.; Matyjaszewski, K. *Macromolecules* **2007**, *40*, 2974–2977.
8.   Jakubowski, W.; Kirci-Denizli, B.; Gil, R. R.; Matyjaszewski, K. *Macromol. Chem. Phys.* **2008**, *209*, 32–39.
9.   Zhu, G. H.; Zhang, L. F.; Zhang, Z. B.; Zhu, J.; Tu, Y. F.; Cheng, Z. P.; Zhu, X. L. *Macromolecules* **2011**, *44*, 3233–3239.
10. Abreu, C. M. R.; Mendonca, P. V.; Serra, A. C.; Popov, A. V.; Matyjaszewski, K.; Guliashvili, T.; Coelho, J. F. J. *ACS Macro Lett.* **2012**, *1*, 1308–1311.
11. Matyjaszewski, K.; Jakubowski, W.; Min, K.; Tang, W.; Huang, J.; Braunecker, W. A.; Tsarevsky, N. V. *Proc. Natl. Acad. Sci. U.S.A.* **2006**, *103*, 15309–15314.
12. Dong, H.; Matyjaszewski, K. *Macromolecules* **2008**, *41*, 6868–6870.
13. Woodruff, S. R.; Davis, B. J.; Tsarevsky, N. V. *Macromol. Rapid Commun.* **2014**, *35*, 186–192.
14. Magenau, A. J. D.; Strandwitz, N. C.; Gennaro, A.; Matyjaszewski, K. *Science* **2011**, *332*, 81–84.
15. Matyjaszewski, K.; Tsarevsky, N. V.; Braunecker, W. A.; Dong, H.; Huang, J.; Jakubowski, W.; Kwak, Y.; Nicolay, R.; Tang, W.; Yoon, J. A. *Macromolecules* **2007**, *40*, 7795–7806.
16. Dadashi-Silab, S.; Tasdelen, M. A.; Yagci, Y. *J. Polym. Sci., Part A: Polym. Chem.* **2014**, *52*, 2878–2888.
17. Tasdelen, M. A.; Uygun, M.; Yagci, Y. *Macromol. Rapid Commun.* **2011**, *32*, 58–62.
18. Tasdelen, M. A.; Uygun, M.; Yagci, Y. *Macromol. Chem. Phys.* **2011**, *212*, 2036–2042.
19. Tasdelen, M. A.; Ciftci, M.; Uygun, M.; Yagci, Y. Possibilities for Photoinduced Controlled Radical Polymerizations. In *Progress in Controlled Radical Polymerization: Mechanisms and Techniques*; Matyjaszewski, K., Sumerlin, B. S., Tsarevsky, N. V., Eds.; American Chemical Society: Washington, DC, 2012; Vol. 1100, pp 59–72.

20. Konkolewicz, D.; Schroeder, K.; Buback, J.; Bernhard, S.; Matyjaszewski, K. *ACS Macro Lett.* **2012**, *1*, 1219–1223.
21. Ciftci, M.; Tasdelen, M. A.; Li, W.; Matyjaszewski, K.; Yagci, Y. *Macromolecules* **2013**, *46*, 9537–9543.
22. Yagci, Y.; Tasdelen, M. A.; Jockusch, S. *Polymer* **2014**, *55*, 3468–3474.
23. Zhang, T.; Chen, T.; Amin, I.; Jordan, R. *Polym. Chem.* **2014**, *5*, 4790–4796.
24. Mosnacek, J.; Ilcikova, M. *Macromolecules* **2012**, *45*, 5859–5865.
25. Murtezi, E.; Yagci, Y. *Macromol. Rapid Commun.* **2014**, *35*, 1782–1787.
26. Doran, S.; Yagci, Y. *Polym. Chem.* **2015**, *6*, 946–952.
27. Tasdelen, M. A.; Uygun, M.; Yagci, Y. *Macromol. Chem. Phys.* **2010**, *211*, 2271–2275.
28. Yagci, Y.; Jockusch, S.; Turro, N. J. *Macromolecules* **2010**, *43*, 6245–6260.
29. Tasdelen, M. A.; Yagci, Y. *Angew. Chem. Int. Ed.* **2013**, *52*, 5930–5938.
30. Tasdelen, M. A.; Yagci, Y. *Tetrahedron Lett.* **2010**, *51*, 6945–6947.
31. Tasdelen, M. A.; Yilmaz, G.; Iskin, B.; Yagci, Y. *Macromolecules* **2012**, 45, 56–61.
32. Guillaneuf, Y.; Bertin, D.; Gigmes, D.; Versace, D. L.; Lalevee, J.; Fouassier, J. P. *Macromolecules* **2010**, *43*, 2204–2212.
33. Mosnáček, J.; Ilčíková, M. *Macromolecules* **2012**, *45*, 5859–5865.
34. Konkolewicz, D.; Schröder, K.; Buback, J.; Bernhard, S.; Matyjaszewski, K. *ACS Macro Lett.* **2012**, *1*, 1219–1223.
35. Giuffrida, S.; Condorelli, G. G.; Costanzo, L. L.; Fragala, I. L.; Ventimiglia, G.; Vecchio, G. *Chem. Mater.* **2004**, *16*, 1260–1266.
36. Hayase, K.; Zepp, R. G. *Environ. Sci. Technol.* **1991**, *25*, 1273–1279.
37. Ribelli, T. G.; Konkolewicz, D.; Pan, X.; Matyjaszewski, K. *Macromolecules* **2014**, *47*, 6316–6321.
38. Ribelli, T. G.; Konkolewicz, D.; Bernhard, S.; Matyjaszewski, K. *J. Am. Chem. Soc.* **2014**, *136*, 13303–13312.
39. Anastasaki, A.; Nikolaou, V.; Zhang, Q.; Burns, J.; Samanta, S. R.; Waldron, C.; Haddleton, A. J.; McHale, R.; Fox, D.; Percec, V.; Wilson, P.; Haddleton, D. M. *J. Am. Chem. Soc.* **2014**, *136*, 1141–1149.
40. Anastasaki, A.; Nikolaou, V.; Simula, A.; Godfrey, J.; Li, M.; Nurumbetov, G.; Wilson, P.; Haddleton, D. M. *Macromolecules* **2014**, *47*, 3852–3859.
41. Anastasaki, A.; Nikolaou, V.; Pappas, G. S.; Zhang, Q.; Wan, C.; Wilson, P.; Davis, T. P.; Whittaker, M. R.; Haddleton, D. M. *Chem. Sci.* **2014**, *5*, 3536–3542.
42. Wenn, B.; Conradi, M.; Carreiras, A. D.; Haddleton, D. M.; Junkers, T. *Polym. Chem.* **2014**, *5*, 3053–3060.
43. Telitel, S.; Dumur, F.; Telitel, S.; Soppera, O.; Lepeltier, M.; Guillaneuf, Y.; Poly, J.; Morlet-Savary, F.; Fioux, P.; Fouassier, J.-P.; Gigmes, D.; Lalevee, J. *Polym. Chem.* **2015**, *6*, 613–624.
44. Vargas Alfredo, N.; Espinosa Jalapa, N.; Lopez Morales, S.; Ryabov, A. D.; Le Lagadec, R.; Alexandrov, L. *Macromolecules* **2012**, *45*, 8135–8146.
45. Fors, B. P.; Hawker, C. J. *Angew. Chem., Int. Ed.* **2012**, *51*, 8850–8853.
46. Treat, N. J.; Fors, B. P.; Kramer, J. W.; Christianson, M.; Chiu, C.-Y.; Alaniz, J. R. d.; Hawker, C. J. *ACS Macro Lett.* **2014**, *3*, 580–584.

47. Poelma, J. E.; Fors, B. P.; Meyers, G. F.; Kramer, J. W.; Hawker, C. J. *Angew. Chem., Int. Ed.* **2013**, *52*, 6844–6848.
48. Fors, B. P.; Poelma, J. E.; Menyo, M. S.; Robb, M. J.; Spokoyny, D. M.; Kramer, J. W.; Waite, J. H.; Hawker, C. J. *J. Am. Chem. Soc.* **2013**, *135*, 14106–14109.
49. Tasdelen, M. A.; Ciftci, M.; Yagci, Y. *Macromol. Chem. Phys.* **2012**, *213*, 1391–1396.
50. Taskin, O. S.; Yilmaz, G.; Tasdelen, M. A.; Yagci, Y. *Polym. Int.* **2014**, *63*, 902–907.
51. Yagci, Y.; Hepuzer, Y. *Macromolecules* **1999**, *32*, 6367–6370.
52. Acik, G.; Kahveci, M. U.; Yagci, Y. *Macromolecules* **2010**, *43*, 9198–9201.
53. Kahveci, M. U.; Acik, G.; Yagci, Y. *Macromol. Rapid Commun.* **2012**, *33*, 309–313.
54. Iskin, B.; Yilmaz, G.; Yagci, Y. *Macromol. Chem. Phys.* **2013**, *214*, 94–98.
55. Bektas, S.; Ciftci, M.; Yagci, Y. *Macromolecules* **2013**, *46*, 6751–6757.
56. Ciftci, M.; Batat, P.; Demirel, A. L.; Xu, G.; Buchmeiser, M.; Yagci, Y. *Macromolecules* **2013**, *46*, 6395–6401.
57. Ciftci, M.; Tasdelen, M. A.; Yagci, Y. *Polym. Chem.* **2014**, *5*, 600–606.
58. Wang, Y.; Wang, X.; Antonietti, M. *Angew. Chem. Int. Ed.* **2012**, *51*, 68–89.
59. Kiskan, B.; Zhang, J. S.; Wang, X. C.; Antonietti, M.; Yagci, Y. *ACS Macro Lett.* **2012**, *1*, 546–549.
60. Dadashi-Silab, S.; Tasdelen, M. A.; Kiskan, B.; Wang, X.; Antonietti, M.; Yagci, Y. *Macromol. Chem. Phys.* **2014**, *215*, 675–681.
61. Dadashi-Silab, S.; Kiskan, B.; Antonietti, M.; Yagci, Y. *RSC Adv.* **2014**, *4*, 52170–52173.
62. Dadashi-Silab, S.; Tasdelen, M. A.; Asiri, A. M.; Khan, S. B.; Yagci, Y. *Macromol. Rapid Commun.* **2013**, *35*, 454–459.
63. Yan, J. F.; Li, B.; Zhou, F.; Liu, W. M. *ACS Macro Lett.* **2013**, *2*, 592–596.
64. Li, B.; Yu, B.; Zhou, F. *Macromol. Rapid Commun.* **2014**, *35*, 1287–1292.

Chapter 9

Pushing Monomer Conversions High in Bulk ATRP: The Effects of ICAR Agent Concentrations on the System Livingness and Polymer Molecular Weight Control

Ali Mohammad Rabea and Shiping Zhu*

Department of Chemical Engineering, McMaster University, Hamilton, Ontario, Canada L8S 4L7
***Tel.: 1(905) 525-9140 ext 24962; Fax: 1(905) 521-1350; E-mail: zhuship@ mcmaster.ca**

Controlled radical polymerization often loses control over polymer molecular weight at high monomer conversions due to diffusion-controlled reactions. This is particularly true for bulk polymerization systems. In this work, bulk atom transfer radical polymerization (ATRP) of methyl methacrylate (MMA) was carried out by employing an initiator for continuous activator regeneration (ICAR) method. Binary systems of ICAR agents, that is, low temperature azobisisobutyronitrile (AIBN) and high temperature tert-butyl peroxybenzoate (TBPB) or tert-butyl peroxide (TBP) were used. The polymerization was run at 70 °C at the beginning and completed at an elevated temperature. The objective was to investigate the effects of ICAR agent concentration on the system livingness and control at high conversions. It was found that both ICAR agents significantly affected the rate of catalyst regeneration and consequently the rate and control of polymerization. By optimizing the concentrations of the ICAR agents and employing step temperature profile, MMA was polymerized with 50 ppm $CuBr_2$ up to 98% conversion in less than 5 hours. The final products had dispersity (Đ) about 1.3.

Introduction

Controlled radical polymerization (CRP), mostly nitroxide-mediated polymerization (NMP) (*1*), atom transfer radical polymerization (ATRP) (*2*, *3*), and reversible addition fragmentation chain transfer (RAFT) polymerization (*4*), have provided great potential for synthesis of functional polymers with predetermined molecular weight and narrow molecular weight distribution (MWD). The number of publications on the CRP methods, ATRP in particular, has increased dramatically in the recent decade (*5*), but their commercial exploitation is rather limited (*6*, *7*). Among many others, high catalyst loading and limited conversion represent two significant challenges. The high catalyst loading gives deep color to the final ATRP products and makes the post purification costly (*8*). The high conversion in bulk causes diffusion control problem for those reactions involving chain species and loss of control of the reaction (*9*). Solution polymerization is often employed. However, both solvent and residual monomer are costly in terms of separation and purification and have environmental concern as well. With numerous efforts, the catalyst loading problem has been solved to some extent by catalyst supporting or by introducing new ATRP methods, such as the activator regenerated by electron transfer (ARGET ATRP) and the initiator for continuous activator regeneration (ICAR ATRP) (*10–12*), as shown in Scheme 1. In contrast, the problem associated with high conversion has not been addressed thoroughly. The high conversion problem is attributed to diffusion-controlled reactions, which cause "gel effect" and "glass effect" and make the system suffer from loss of control and result in high dispersity (Đ) (*9*, *13*, *14*).
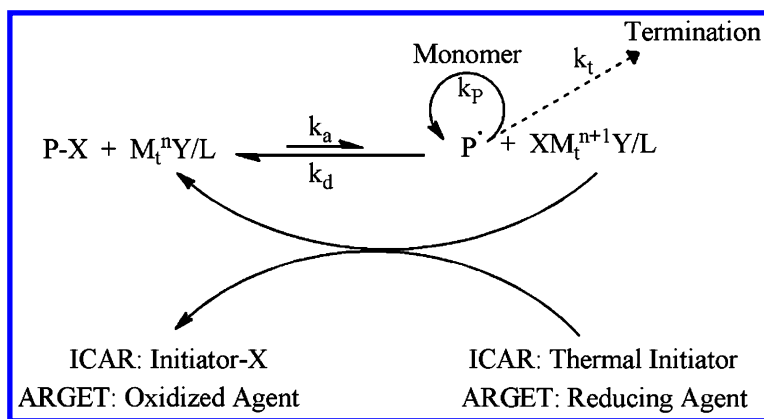
Scheme 1. ATRP with the activator regenerated by electron transfer (ARGET ATRP) and the initiator for continuous activator regeneration (ICAR ATRP).

Recently, we launched a research program aiming to tackle the problems that limit commercial exploitation of controlled radical polymerization processes. One of the objectives is to push monomer conversion high in the most challenging bulk systems. Polymerization up to a complete conversion but still living and controlled serves as an ultimate target. On the fundamental side, we tried to

investigate the effects of diffusion-controlled reactions on bulk polymerization in order to develop strategies to keep system livingness and control up to high conversions. In our first study (*9*), the effect of deactivator concentration (CuBr$_2$), from 50 to 250 ppm, on the bulk ICAR ATRP of methyl methacrylate (MMA) was examined. Two thermal initiators (azobisisobutyronitrile (AIBN) and tert-butyl peroxybenzoate (TBPB)) were employed as the ICAR agents. The polymerization runs were performed at 70 ˚C up to the glass state. The results showed good livingness and control at low monomer conversions. However, diffusion-controlled deactivation occurred at medium conversion, causing "gel effect" and loss of control over polymer molecular weight. Loading higher concentration of the deactivator (250 ppm) compensated the loss of control to some extent but decreased the rate of the polymerization. Also, the polymer chains were protected from termination because of the diffusion-controlled termination.

In another study (*15*), the bulk ICAR ATRP of MMA was performed up to high conversions by using AIBN and tert-butyl peroxide (TBP) as the ICAR agents in the presence of 250 ppm catalyst concentration. Temperature profile was employed to postpone the diffusion-controlled deactivation reaction to higher conversion. The results showed that increasing temperature before the onset time of diffusion-controlled deactivation could help to keep the control of polymerization up to higher conversions, while polymer chains were still preserved from termination because of diffusion-controlled termination. This was due to a difference in the onset times between diffusion controlled deactivation and termination. The former involved one chain species with the other small molecule catalyst complex, while the latter involved two chain species and thus became diffusion controlled earlier. Using this method, we obtained polymer products having Ð smaller than 1.3 at about 98% conversion.

It is well known that ICAR agent adjusts the rate and control of polymerization through reducing catalyst of higher oxidation state (deactivator) (mostly CuBr$_2$) to a lower oxidation state (CuBr). When the radical concentration generated through thermal initiator decomposition is low, the regeneration of catalyst is slow as well, causing accumulation of the deactivator and finally stopping the polymerization. On the other side, when the radical concentration is high, most deactivator molecules are reduced to catalyst, increasing the rate of polymerization but at the cost of losing control over polymer molecular weight. Therefore, the deactivator concentration must be precisely regulated through the ICAR reactions for an optimal balance of control and rate of polymerization.

In this work, the effects of concentration of ICAR agents on the control and rate of polymerization are investigated. We focus on high conversions and target to achieve the optimal ICAR concentration for the livingness of polymerization system and the control of polymer molecular weight at high conversions. It must be pointed out that diffusion-controlled reactions at high conversion are very complicated. It is worth of much effort in research to understand their mechanisms. There are so many reactions involved, namely, ATRP initiation, propagation, termination, activation, deactivation, catalyst regeneration and thermal initiator decomposition. Any of the reactions could become diffusion controlled at very high conversions, particularly when the system approaches its

glass stage. The relative onset times and magnitudes of diffusion limitations are very important in determining the system livingness and control. In our program, we make effort to investigate the effects of each of the major parameters on the bulk polymerization, with the final objective of a comprehensive understanding of the high conversion mechanisms and a possible computer model that could be used to design and control the polymerization operation for achieving targeted polymer products. This paper report the result of the effect of ICAR agent type and concentration.

Experimental Section

Materials

Methyl methacrylate (MMA, Aldrich, 99%) was distilled under vacuum. After passing through a column of inhibitor remover, it was stored at -20°C before use. 4,4′-Dinonyl-2,2′-dipyridyl (dNbpy, 97%) as ligand, $CuBr_2$ (99.999%) as deactivator and ethyl (α-bromophenyl)acetate (EBPA) ATRP initiator were purchased from Aldrich and used without any further purification. Initiators for continuous activator regeneration (ICAR agents), tert-butyl peroxybenzoate (TBPB, 98%), tert-butyl peroxide (TBP, 98%) and azobisisobutyronitrile (AIBN, 99%) were purchased from Aldrich and used as received, except for AIBN which was recrystallized from methanol and stored at -20 °C.

Instrumentation

^{1}H NMR spectra were recorded through running diluted polymer-acetone solution in d-chloroform ($CDCl_3$) on a Bruker AV-200 spectrometer at 200 MHz. The intensity ratio of the methoxy group signals of polymer (3.60 ppm) and monomer (3.75 ppm) was employed for estimate of monomer conversions. Gel permeation chromatography (GPC) was used for determining the number average molecular weight (Mn) and dispersity (Đ) relative to a set of narrow polymethyl methacrylate standards. The polymer samples were run through a Waters 2690 autoinjector with three linear columns in series (Waters Styragel HR 2, 3 and 4) and a 2410 RI detector, with THF as effluent at a fixed flow rate of 1 mL/min. The columns and detector were heated to 35 ˚C and 40 ˚C, respectively. Data were recorded by Waters Millennium software package for further manipulation.

Polymerization

The bulk ICAR ATRP runs of MMA with the molar ratios of [MMA]:[EBPA]:[CuBr$_2$]:[dNbpy]:[AIBN]: [TBPB] = 200:1:0.05:0.1:X:Y (X=0.1 and 0.2) (Y=0.075 and 0.2) and [MMA]:[EBPA]:[CuBr$_2$]:[dNbpy]:[AIBN]:[TBP] = 1000:1: 0.05:0.1:0.375:0.5 was carried out as follow. A 25 mL bottom round flask containing a magnetic bar was loaded with appropriate amount of CuBr$_2$ (0.0015 or 0.0075 gr), dNbpy (0.0055 or 0.0275 gr) and AIBN (0.0082,

0.0109 or 0.0219 gr). The sealed reactor was degassed by several cycles of vacuum-nitrogen. Degassed MMA (13.43 gr) was then added to the reactor. Required amount of TBPB (9.6 or 25.5 µL) or TBP (12.3 µL) was added to the flask using a nitrogen-purged syringe. Proper amount of EBPA (23.5 or 117.5 µL) was added to the flask using syringe after the mixture was stirred for an hour at room temperature. The reactor was then placed to an oil bath at 70 °C. The reaction was continued under stirring at the speed of 400 rpm. For the polymerization runs requiring other temperatures, separated oil baths were set to 90 and 120 °C. The reaction was continued by switching oil baths. Ice water was employed to stop the reaction.

Chain Extension Reaction

The sample used for chain extention experiments was prepared with the molar ratio of [MMA]:[EBPA]:[CuBr$_2$]:[dNbpy]:[AIBN]:[TBP] = 1000:1:0.05: 0.1:0.375:0.5. The polymerization was performed for 4.5 hours at 70 ˚C and followed by 10 min at 90 ˚C and 10 min at 120 ˚C. The polymer was purified by passing the polymer solution in acetone through a column of alumina, then was precipitated out in methanol and dried in vacuum oven. The dried polymer was used as macroinitiator for the chain extention with the molar ratios of [MMA]:[PMMA]:[CuBr$_2$]:[dNbpy]:[AIBN]:[TBP] = 1000:0.001:0.05: 0.1:0.375:0.5. Chain extension reaction was carried out at 70 ˚C for 3 hours.

Results and Discussion

Three different concentrations of ICAR agents (AIBN and TBPB) were applied in the following recipe: [MMA]:[EBPA]:[CuBr$_2$]:[dNbpy]:[AIBN]: [TBPB] = 200:1:0.05:0.1:X:Y containing 250 ppm catalyst. Their conversion versus time profiles are shown in Figure 1. It can be seen that the run with a low concentration of the ICAR agents (X=0.1 and Y=0.075) reached only 77% conversion after 12 hours at 70 ˚C. It did not show any "gel effect". Because of the low ICAR concentrations, little catalyst could be regenerated after 12 hours. The conversion did not increase much with time in further reaction. Increasing the ICAR concentrations significantly accelerated the rate of polymerization, with "gel effect" occurred at about 50% conversion. For X=0.2 and Y=0.075, a maximum conversion of 94% was obtained in about 4.5 hours. For X=0.2 and Y=0.2, the rate of polymerization was even faster and the same conversion was achieved in 3 hours. It is clear that both ICAR agents decomposed at 70 ˚C and contributed the rate of polymerization. Lowering the ICAR agents concentrations decreased the concentration of primary radicals, so the rate of CuBr$_2$ reduction to CuBr slowed down, which accumulated the concentration of CuBr$_2$ during the polymerization. When deactivation reaction became diffusion-controlled, the higher deactivator concentration could partly compensate the decreased rate constant of deactivation. As a result, the rate of deactivation remained, to some

extent. At the same time, because of the lower regenerated catalyst (CuBr) concentration, the rate of activation and consequently the rate of polymerization decreased. Therefore, the run with X=0.1 and Y=0.075 did not show "gel effect". Increasing the ICAR agent concentrations led to faster regeneration of catalyst from deactivator. The higher CuBr concentration increased the rate of activation and that of polymerization as well. Furthermore, with the onset of diffusion-controlled deactivation, the concentration of radical chains increased and thus "gel effect" occurred in the system.
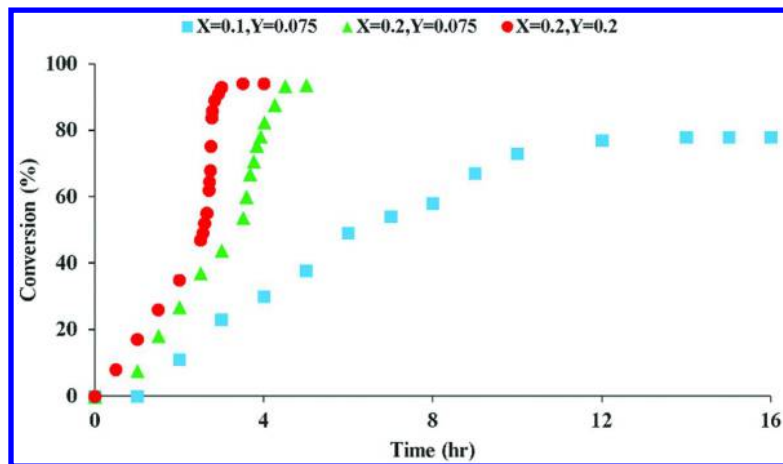
Figure 1. Conversion versus time for the bulk ICAR ATRP of methyl methacrylate with [MMA]:[EBPA]:[CuBr$_2$]:[dNbpy]:[AIBN]:[TBPB] = 200:1:0.05:0.1:X:Y at 70 °C.

Figure 2 shows the number-average molecular weight (Mn) versus conversion data with different concentrations of the ICAR agents. For X=0.1, Y=0.075 and X=0.2, Y=0.075, a good correlation between experimental and theoretical Mn values was observed. With these two recipes, the initiator efficiencies (I$_{eff}$), estimated from the ATRP initiator only, were about 70% at the start and reached over 90% at the end of polymerization. For comparison, with X=0.2 and Y=0.2, the I$_{eff}$ was about 20% at the low conversion and increased to about 80% at the end. Loading higher ICAR agents concentrations increased the catalyst concentration and consequently increased the rate of activation reaction and thus the concentration of radicals, which increased termination and resulted in the lower I$_{eff}$. At the increased conversions, radical termination became diffusion controlled and suppressed, thus improving the initiator efficiency I$_{eff}$. The polymer chains generated from the ICAR agents also contributed the increase in I$_{eff}$ during polymerization.

Figure 3 shows dispersity (Đ) versus conversion for different concentrations of the ICAR agents.
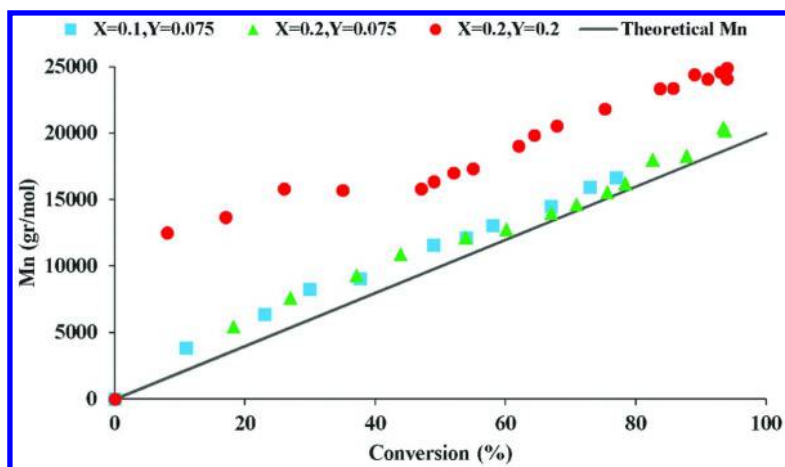
Figure 2. Mn versus conversion for bulk ICAR ATRP of methyl methacrylate with [MMA]:[EBPA]:[CuBr₂]:[dNbpy]:[AIBN]:[TBPB] = 200:1:0.05:0.1:X:Y at 70 °C.
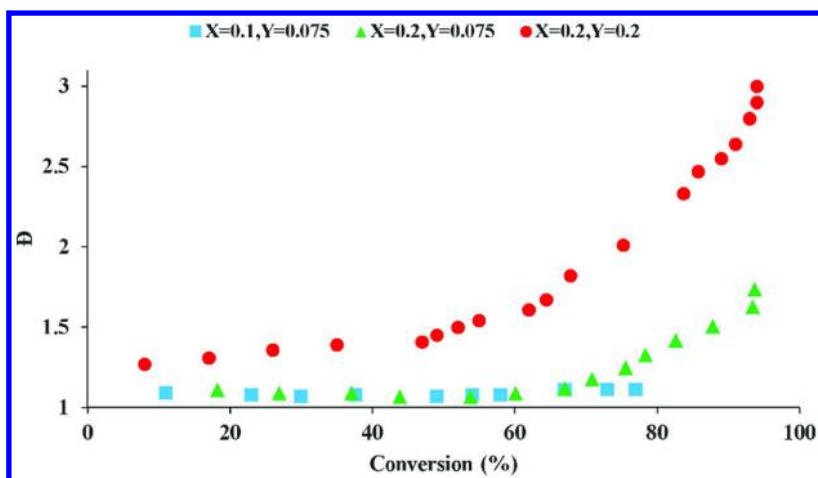
Figure 3. Đ versus conversion for the bulk ICAR ATRP of methyl methacrylate with [MMA]:[EBPA]:[CuBr₂]:[dNbpy]:[AIBN]:[TBPB] = 200:1:0.05:0.1:X:Y at 70 °C.

Decreasing the ICAR concentration improved the control of polymer molecular weight and resulted in lower dispersity's. For X=0.1 and Y=0.075, the Đ was around 1.1 throughout the course of polymerization. For X=0.2 and Y=0.075, there was a good control until about 65% conversion with Đ about 1.1. After that, the system started to lose the control. The Đ value reached to > 1.7 at the end of reaction. For X=0.2 and Y=0.2, the Đ was around 1.3 at low conversion, but increased continuously and reached about 3 at the end. This could be because of some side reactions between TBPB and catalyst, as well (*16*).

In our previous study (*15*), we found that employing two ICAR agents with varying operating temperature could be helpful in regulating rate and control of the polymerization. It allowed us to lower the thermal initiator concentration at each temperature in order to keep the control of polymerization while there was adequate ICAR action to reach to high conversions at an elevated temperature, which postponed diffusion-controlled deactivation and improved the control over polymer molecular weight. As TBPB affected the rate of the polymerization even at 70 ˚C, TBP was employed which had higher decomposition temperature and did not affect the rate of the polymerization at 70 ˚C.

In this work, this temperature elevation method was employed with the following recipe: [MMA]:[EBPA]:[CuBr$_2$]:[dNbpy]:[AIBN]:[TBP] = 1000:1: 0.05:0.1:0.375:0.5. It contained 50 ppm CuBr$_2$ and a ratio of 1000 monomer to ATRP initiator. AIBN and TBP were used as the ICAR agents, which had very different decomposition temperatures. AIBN was mostly responsible for ICAR at 70 ˚C, while TBP for 120 ˚C. Different concentrations for the ICAR agents were evaluated in order to find the optimal values for the control over polymer molecular weight, within a reasonable time duration. Figure 4 shows a representative conversion result. At 70 ˚C and remaining constant, a maximum conversion of 96% was reached in about 6 hours. The "gel effect" occurred after 3.5 hours at around 30% conversion. About 52% conversion was obtained by carrying out the reaction for 4.5 hours at 70 ˚C. Continuing the polymerization for 10 minutes at 90 ˚C led to 78% conversion. Final increasing the temperature to 120 ˚C resulted in more than 98% conversion in about 10 minutes. The temperature elevation significantly shortened the polymerization duration.
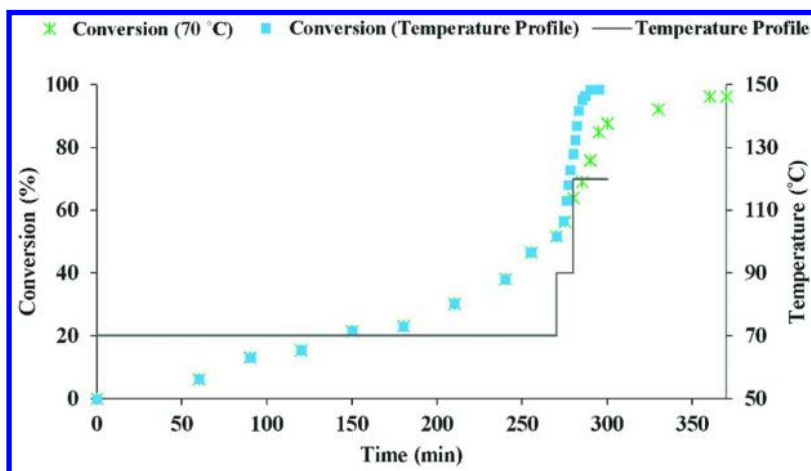
Figure 4. Conversion and adjusted temperature versus time
for the bulk ICAR ATRP of methyl methacrylate with
[MMA]:[CuBr$_2$]:[dNbpy]:[AIBN]:[TBP] = 1000:1:0.05:0.1:0.375:0.5.

Figure 5 shows the corresponding molecular weight and Ð versus conversion data. In both cases of remaining temperature versus varying temperature, there

were good correlations between the experimental molecular weights with their theoretical values. The initiator efficiencies (I_{eff}), based on ATRP initiator only, were higher than 80% at lower conversions and reached to about 115% at the end of polymerization. It is evident that some new chains were generated through ICAR agents, causing I_{eff} over 100%.
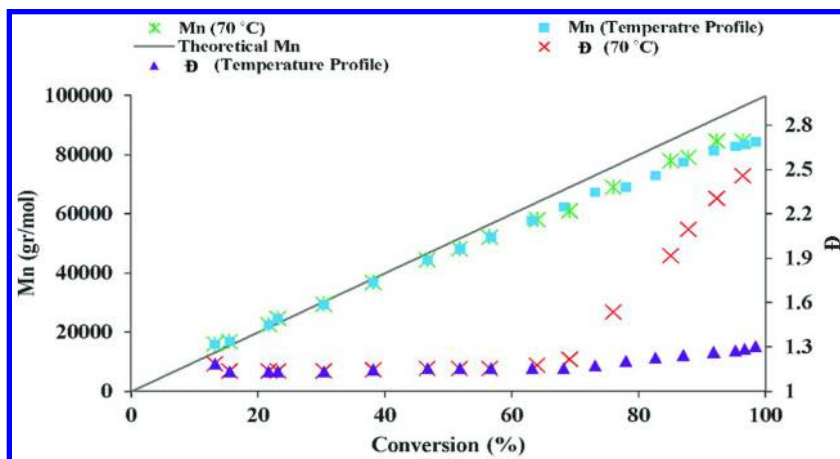
Figure 5. Mn and Đ versus conversion for the bulk ICAR ATRP of methyl methacrylate with [MMA]:[EBPA]:[CuBr₂]:[dNbpy]:[AIBN]:[TBP] = 1000:1:0.05:0.1:0.375:0.5 at 70 ˚C and under temperature profile.

In the case of remaining temperature at 70 ˚C, Đ remained below 1.2 up to 70% conversion. It then started to increase dramatically, because of the diffusion-controlled deactivation. It reached to 2.5 at the end of reaction. In a strong contrast, increasing the temperature from 70 ˚C to 90 ˚C at 52% conversion and continuing the reaction at 90 ˚C for 10 min gave a Đ about 1.2 at 78% conversion. A final push of the temperature to 120 ˚C for another 10 min resulted in a Đ about 1.3 at 98% conversion. It was also found that, if remaining 90 ˚C for 15 min, Đ increased considerably to 1.75 at 95% conversion.

Through a systematical study, we found that by optimizing the concentrations of ICAR agents and temperature profile, it was possible to decrease the deactivator concentration to 50 ppm CuBr₂ but still achieve the good control over polymer molecular weight up to very high conversions in a reasonable time duration.

The polymers collected at 98% conversion were used in chain extension experiments to examine their livingness. The dried purified samples were used as a macroinitiator with the following recipe: [MMA]:[PMMA]:[CuBr₂]:[dNbpy]:[AIBN]:[TBP] = 1000: 0.001:0.05:0.1: 0.375:0.5 run for 3 hours at 70 ˚C and 35% conversion. Figure 6 shows the chain extension result. The molecular weight increased to higher values, which proved livingness for the synthesized polymers collected at very high conversions. Diffusion-controlled termination at high conversions improved the livingness (*9, 15*). Furthermore, GPC curve of the macro initiator showed a very small peak at high molecular weight region, caused by the diffusion-controlled deactivation

in the macro-initiator preparation (*9*), where Đ increased from 1.15 to 1.3. This peak was almost disappeared after the chain extension reaction.
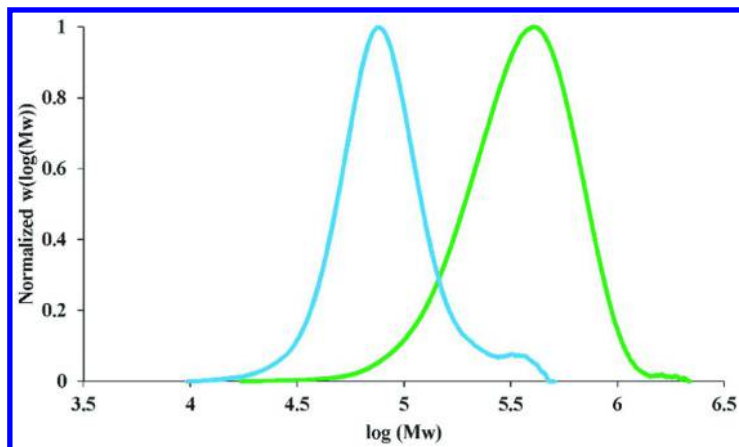
Figure 6. Chain extension result of the polymer collected at 98% conversion and used as macroinitiator. Chain extension recipe was [MMA]:[PMMA]:[CuBr₂]:[dNbpy]:[AIBN]:[TBP] = 1000:0.001:0.05:0.1:0.375:0.5 run for 3 hours at 70 °C.

Conclusion

Bulk ICAR ATRP of MMA at 70 ˚C was carried out up to high conversions with different concentrations of AIBN and TBPB as ICAR agents. The system of low ICAR concentrations (X=0.1, Y=0.075 in [MMA]:[EBPA]:[CuBr₂]:[dNbpy]:[AIBN]:[TBPB] = 200:1:0.05:0.1:X:Y) behaved very well with Đ about 1.1 throughout of the reaction.   However, the maximum conversion was only 77% after 12 hours. Increasing the ICAR agent concentrations improved the rate of polymerization but at the cost of control over polymer molecular weight because of diffusion-controlled deactivation. With X=0.2, Y=0.075, Đ started to increase after 67% conversion and reached to 1.7 at the end of polymerization (94% conversion). With X=0.2, Y=0.2, Đ was around 1.3 at the beginning but continuously increased to 3 at 94% conversion. With [MMA]:[EBPA]:[CuBr₂]:[dNbpy]:[AIBN]:[TBP] = 1000:1:0.05:0.1:0.375:0.5, the monomer to initiator ratio was pushed to 1000, with only 50 ppm CuBr₂. The reaction was first carried out at 70 ˚C for 4.5 hours, followed by a temperature elevation to 90 ˚C for 10 min and to 120 ˚C for another 10 min. The rate of polymerization was improved significantly with the step temperature profile. A conversion of 98% was reached in less than 5 hours. The molecular weight data were very close to their theoretical values. The polymers collected at 98% conversion had Đ about 1.3.   The chains were living, confirmed by a chain extension experiment. This work demonstrated that the ICAR agent concentration plays a critical role in determining the livingness of ATRP system and the control of polymer molecular weight. By optimizing the concentrations and

temperature profile, high conversion bulk ATRP with fast rate and good control becomes feasible. The key is to balance the diffusion controlled reactions such as termination and deactivation, through relaxing the diffusion limitations of various reacting species and regulating the ICAR action.

Acknowledgments

References

1. Georges, M. K.; Veregin, R. P. N.; Kazmaier, P. M.; Hamer, G. K. *Macromolecules* **1993**, *26*, 2987–2988.
2. Wang, J.; Matyjaszewski, K. *J. Am. Chem. Soc.* **1995**, *117*, 5614–5615.
3. Kato, M.; Kamigaito, M.; Sawamoto, M.; Higashimuras, T. *Macromolecules* **1995**, *28*, 1721–1723.
4. Chiefari, J.; Chong, Y. K. B.; Ercole, F.; Krstina, J.; Jeffery, J.; Le, T. P. T.; Mayadunne, R. T. A.; Meijs, G. F.; Moad, C. L.; Moad, G.; Rizzardo, E.; Thang, S. H.; South, C. *Macromolecules* **1998**, *31*, 5559–5562.
5. Matyjaszewski, K. Controlled Radical Polymerization?: State-of-the-Art in 2011. In *Controlled Radical Polymerization: Mechanisms and Techniques*; American Chemical Society: Washington, DC, 2012; pp 1−13.
6. Destarac, M. *Macromol. React. Eng.* **2010**, *4*, 165–179.
7. Jakubowski, W. *ACS Symp. Ser.* **2012**, *1100*, 203–216.
8. Tsarevsky, N. V.; Matyjaszewski, K. *Chem. Rev.* **2007**, *107*, 2270–2299.
9. Mohammad Rabea, A.; Zhu, S. *Ind. Eng. Chem. Res.* **2014**, *53*, 3472–3477.
10. Jakubowski, W.; Matyjaszewski, K. *Angew. Chem.* **2006**, *118*, 4594–4598.
11. Jakubowski, W.; Min, K.; Matyjaszewski, K. *Macromolecules* **2006**, *39*, 39–45.
12. Min, K.; Gao, H.; Matyjaszewski, K. *Macromolecules* **2007**, *40*, 1789–1791.
13. Faucher, S.; Zhu, S. *Ind. Eng. Chem. Res.* **2005**, *44*, 677–685.
14. He, W.; Zhang, L.; Bai, L.; Zhang, Z.; Zhu, J.; Cheng, Z.; Zhu, X. *Macromol. Chem. Phys.* **2011**, *212*, 1474–1480.
15. Mohammad Rabea, A.; Zhu, S. *Macromol. React. Eng.* **2014**, *8*, 771–776.
16. Xia, J.; Matyjaszewski, K. *Macromolecules* **1999**, *32*, 5199–5202.

Chapter 10

Living Radical Polymerizations Using Sodium Iodide and Potassium Iodide as Catalysts

Atsushi Goto,[*] Miho Tanishima, Yuuki Nakajima, Akimichi Ohtsuki, Lin Lei, and Hironori Kaji[*]

Institute for Chemical Research, Kyoto University, Uji, Kyoto 611-0011, Japan
[*]E-mails: agoto@scl.kyoto-u.ac.jp, kaji@scl.kyoto-u.ac.jp

Sodium iodide (NaI) and potassium iodide (KI) were utilized as efficient catalysts for living radical polymerization. The studied monomer was methyl methacrylate (MMA). NaI and KI were dissolved in MMA through the addition of crown ethers and a polyether, i.e., diethylene glycol dimethyl ether (diglyme). The polymer molecular weight and its distribution (M_w/M_n = 1.2–1.4) were well controlled with high conversions (e.g., 80–90%) in reasonably short times (3–6 h) at mild temperatures (60–70 °C) in the MMA polymerizations. The effects of the ethers on the polymerization behavior were systematically studied in this work.

Introduction

Living radical polymerization (LRP) has gained substantial attention, because it allows for the rational design of polymer architectures with predictable molecular weights and narrow molecular weight distributions (*1–12*). Mechanistically, LRP is based on the reversible activation of a dormant species (Polymer-X) to a propagating radical (Polymer•) (Scheme 1a). A sufficiently large number of activation–deactivation cycles are required to achieve low polydispersity (*13–15*).
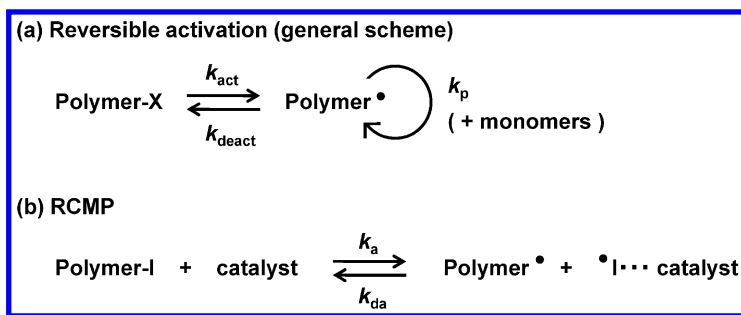
Scheme 1. Reversible activation: (a) General scheme and (b) RCMP.

We have developed new LRP systems using iodine as a capping agent (X) and organic molecules as catalysts. We developed two mechanistically different systems, i.e., reversible chain transfer catalyzed polymerization (RTCP) (*16–21*) and reversible complexation mediated polymerization (RCMP) (*22–27*). In this paper, we focus on RCMP. The catalysts for RCMP include amines such as triethylamine. RCMP involves reversible complexation of Polymer-I with a catalyst (activator) to generate Polymer$^\bullet$ and an $^\bullet$I-catalyst complex (deactivator) (Scheme 1b). Technically, RCMP is similar to normal atom transfer radical polymerization (normal ATRP) (*4–6*) in that both include only a dormant species and an activator.

We recently utilized iodine anion (I$^-$) as a highly reactive catalyst for RCMP, which significantly widened the scope of RCMP (*24*). In these experiments, we utilized organic salts (A$^+$I$^-$) that contain organic counter cations, such as tetrabutylammonium iodide (Bu$_4$N$^+$I$^-$). We suppose the following mechanism. An iodide anion (A$^+$I$^-$) activates Polymer-I, thereby generating Polymer$^\bullet$ and an I$_2$ radical anion (A$^+$I$_2^{\bullet-}$) (Scheme 2a). Because A$^+$I$_2^{\bullet-}$ is not a stable radical, two A$^+$I$_2^{\bullet-}$ species react with each other to produce A$^+$I$^-$ and an I$_3$ anion (A$^+$I$_3^-$), which are stable species (Scheme 2b). A$^+$I$^-$ acts as an activator, whereas A$^+$I$_3^-$ acts as a deactivator (Scheme 2c). Polymer$^\bullet$ can thus be deactivated by either A$^+$I$_2^{\bullet-}$ (Scheme 2a) or A$^+$I$_3^-$ (Scheme 2c).
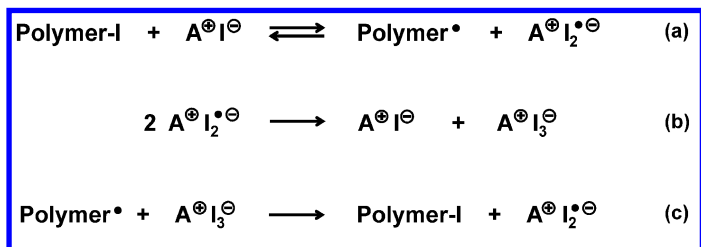
Scheme 2. Possible mechanism of reversible activation with a salt catalyst: (a) Reversible activation of Polymer-I with A$^+$I$^-$, (b) Reaction of two A$^+$I$_2^{\bullet-}$ radicals, and (c) Deactivation of Polymer$^\bullet$ with A$^+$I$_3^-$.

The attractive features of RCMP include no use of special capping agents or expensive catalysts. The catalysts are relatively non-toxic, easy to handle, and amenable to a wide range of monomers, including styrenes, methacrylates, acrylates, acrylonitrile, and those with various functional groups. RCMP can serve as a facile methodology for various applications.

We previously used organic salts that contain organic counter cations. In this work, we attempted to use alkali metal cations as the counter cations. We used sodium iodide (NaI) and potassium iodide (KI) as catalysts for RCMP. These catalysts are not organic catalysts, but they are among the most inexpensive salts and may be suitable for practical use. The studied monomer was methyl methacrylate (MMA). An important issue is the dissolution of these alkali metal iodides in MMA. We used crown ethers and a polyether to solvate the alkali metal iodides (Figure 1) and systematically studied the effects of the ethers on the polymerization behavior.
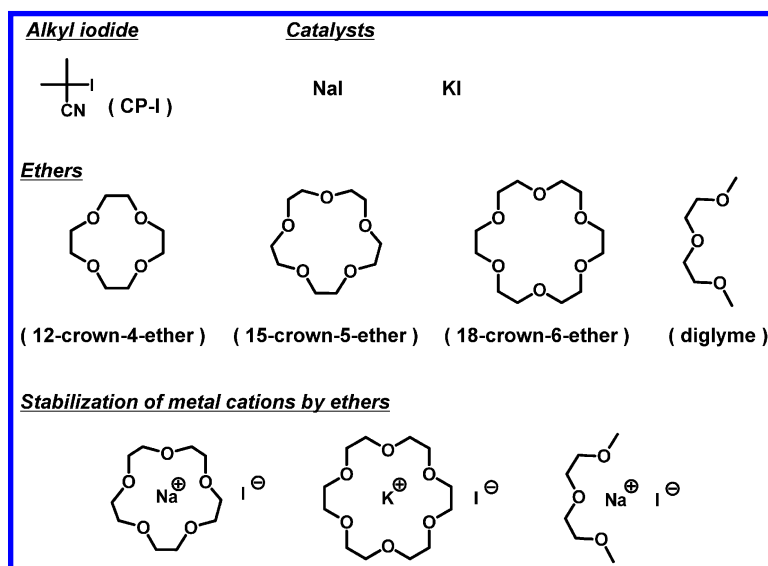
Figure 1. Structures of CP-I, catalysts, and ethers used in this work and illustration of the stabilization of the metal cations by the ethers.

Experimental

Materials

MMA (99%, Nacalai Tesque, Japan) was purified through an alumina column. 2-Cyanopropyl iodide (CP-I) (2-iodo-2-methylpropionitrile, 99%, Tokyo Chemical Industry (TCI), Japan), NaI (99.9%, Wako Pure Chemical, Japan), KI (99.9%, Wako), 18-crown-6-ether (98%, TCI), 15-crown-5-ether (97%, TCI), 12-crown-4-ether (95%, TCI), diethylene glycol dimethyl ether (diglyme) (97%, Wako), azobis(isobutyronitrile) (AIBN) (98%, Wako), and

The structures of CP-I and the ethers are illustrated in Figure 1.

Gel Permeation Chromatography (GPC)

GPC analysis was performed with a Shodex GPC-101 liquid chromatograph (Tokyo, Japan) equipped with two Shodex KF-804L polystyrene mixed gel columns (300 × 8.0 mm; bead size = 7 μm; pore size = 20–200 Å). Tetrahydrofuran (THF) was used as the eluent at a flow rate of 0.8 mL/min (40 °C). Sample detection and quantification were performed with a Shodex differential refractometer RI-101 calibrated with known concentrations of polymer in THF. The monomer conversion was determined from the GPC peak area. The column system was calibrated with standard poly(methyl methacrylate)s.

Polymerization

In a typical run, a Schlenk flask containing MMA (3 mL), CP-I, NaI, and an ether was deoxygenated via argon bubbling and then heated at 70 °C under an argon atmosphere with magnetic stirring. After a prescribed time t, an aliquot (0.1 mL) of the solution was taken out with a syringe, quenched to room temperature, diluted with THF to a known concentration, and analyzed by GPC.

Results and Discussion

NaI with Crown Ethers

We studied the bulk polymerizations of MMA (8 M, 100 equiv) containing CP-I (Figure 1) (80 mM, 1 equiv) as a low-mass dormant species and NaI (40 mM, 0.5 equiv) as an activator at 70 °C. In the absence of an ether, NaI was not completely dissolved in MMA, and the polymerization was slow (monomer conversion reached only 25% after 8 h), as shown in Figure 2 (open triangle). Thus, we added a crown ether (40 mM, same equivalent as NaI). The studied crown ethers (Figure 1) were 12-crown-4-ether (cavity size = 1.2–1.5 Å), 15-crown-5-ether (cavity size = 1.7–2.2 Å), and 18-crown-6-ether (cavity size = 2.6–3.2 Å) (*28*). These ethers have different cavity sizes and tend to coordinate specific metal cations based on atomic sizes (*28–31*). The atomic sizes of Na$^+$ (1.94 Å) and K$^+$ (2.66 Å) particularly match the cavity sizes of 15-crown-5-ether and 18-crown-6-ether, respectively.

Figure 2 (filled symbols) and Table 1 (entries 1-3) present the results with crown ethers. The polymerization was faster after the addition of these ethers than it was without the addition of ethers. The fastest polymerization was achieved using 18-crown-6-ether (not 15-crown-5-ether), in contrast with the expectation based on the above discussion. The reason for this unexpected result is unclear at the moment and will be studied in the future.
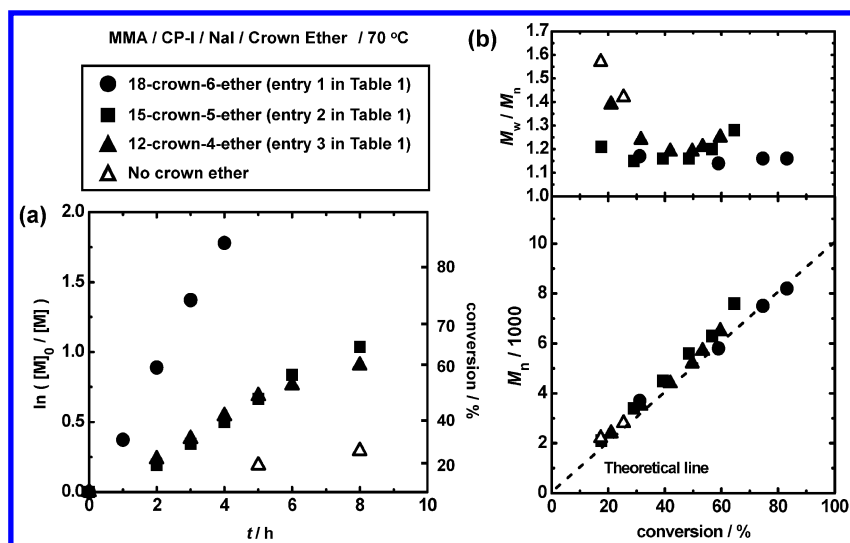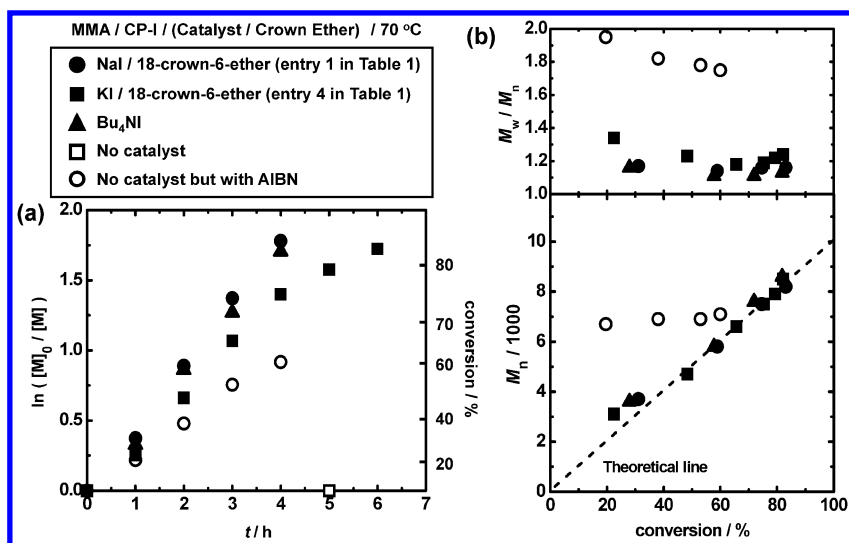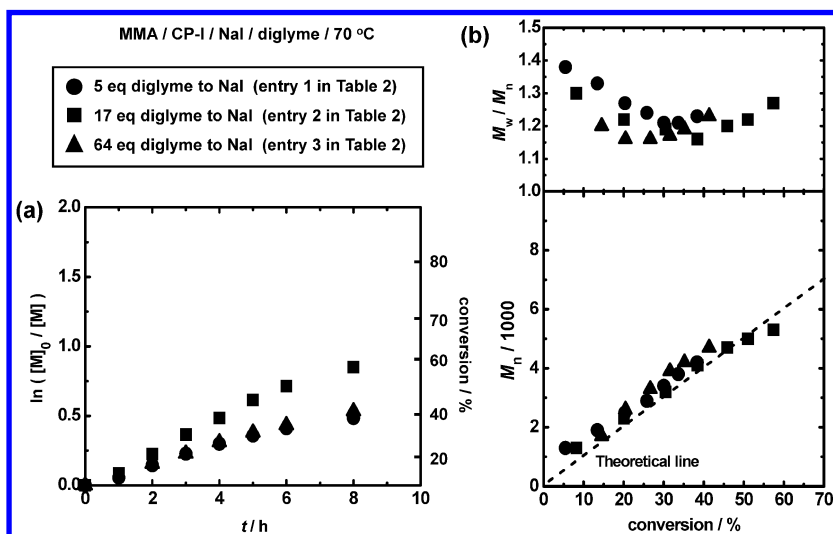
Figure 2. Plots of (a) ln([M]₀/[M]) vs t and (b) M_n and M_w/M_n vs conversion for MMA/CP-I/NaI/crown ether systems (in bulk) (70 °C): $[MMA]_0 = 8$ M; $[CP\text{-}I]_0 = 80$ mM; $[NaI]_0 = 40$ mM; [crown ether]₀ = 0 (open triangle) or 40 mM (filled symbols). The symbols and ethers are indicated in the figure.

Table 1. Bulk polymerizations of MMA (8 M) with CP-I (80 mM), a catalyst (40 mM), and a crown ether (40 mM) at 70 °C.[a]

entry	catalyst	crown ether	t (h)	conv (%)	M_n ($M_{n,theo}$)[b]	PDI
1	NaI	18-crown-6-ether	4	83	8200 (8300)	1.16
2	NaI	15-crown-5-ether	8	65	7600 (6500)	1.28
3	NaI	12-crown-4-ether	8	60	6500 (6000)	1.25
4	KI	18-crown-6-ether	6	82	8500 (8200)	1.24
5	KI	15-crown-5-ether	8	66	7400 (6600)	1.25
6	KI	12-crown-4-ether	8	20	2300 (2000)	2.07

[a] $[MMA]_0/[CP\text{-}I]_0/[catalyst]_0/[crown\ ether]_0 = 100/1/0.5/0.5$. [b] Theoretical M_n calculated with $[MMA]_0$, $[CP\text{-}I]_0$, and conversion.

Using 18-crown-6-ether (Figure 2 (filled circle) and Table 1 (entry 1)), the monomer conversion reached 83% in a relatively short time of 4 h. The first-order plot of the monomer concentration [M] was linear in the studied range of time *t*. The $[MMA]_0/[CP\text{-}I]_0$ ratio was set to 100 in this study, and thus, the degree of polymerization expected at full (100%) monomer conversion was 100. The number-average molecular weight (M_n) agreed with the theoretical value ($M_{n,theo}$), and the polydispersity index (PDI) (= M_w/M_n) was approximately 1.2 from an

early stage of polymerization, where M_w is the weight-average molecular weight. Also importantly, PDI remained small (approximately 1.2) at high conversions, demonstrating the success of the use of NaI as a catalyst.

KI with Crown Ethers

We carried out the same experiments using KI (40 mM) instead of NaI (40 mM). Again, in the absence of an ether, KI was insoluble in MMA and the polymerization was very slow (conversion reached only 4% after 8 h) (Figure 3 (open triangle)). Figure 3 (filled symbols) and Table 1 (entries 4-6) present the results obtained with crown ethers. 12-Crown-4-ether (with the smallest cavity size) did not effectively dissolve KI. The polymerization proceeded smoothly with 15-crown-5-ether and 18-crown-6-ether, resulting in small PDI values. 18-Crown-6-ether led to the fastest polymerization, as expected based on the above discussion.
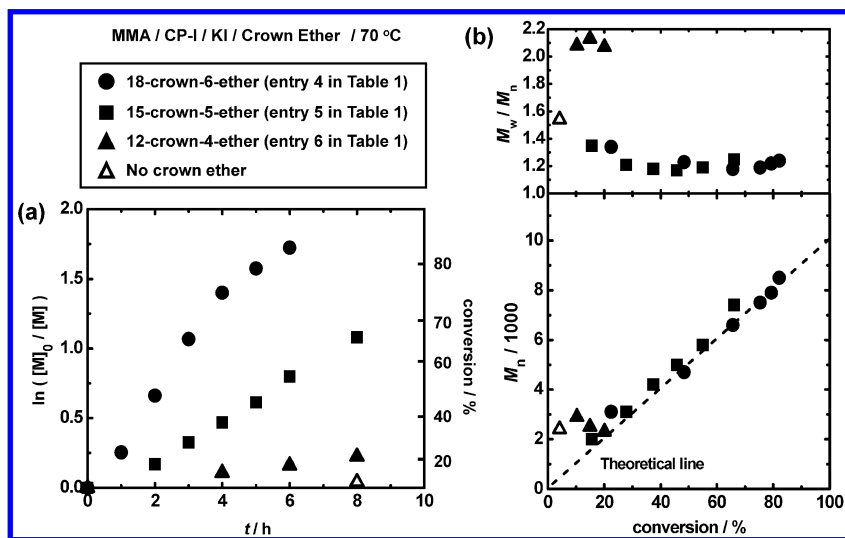
Figure 3. Plots of (a) ln([M]$_0$/[M]) vs t and (b) M_n and M_w/M_n vs conversion for MMA/CP-I/KI/crown ether systems (in bulk) (70 °C): [MMA]$_0$ = 8 M; [CP-I]$_0$ = 80 mM; [KI]$_0$ = 40 mM; [crown ether]$_0$ = 0 (open triangle) or 40 mM (filled symbols). The symbols and ethers are indicated in the figure.

Figure 4 compares the results for NaI (filled circle) and KI (filled square) using 18-crown-6-ether and that with Bu$_4$NI (filled triangle) as a representative organic salt catalyst (*24*) under the same experimental conditions but with different catalysts. NaI and Bu$_4$NI catalysts exhibited very similar polymerization behaviors. This result confirms that the iodine anion plays a catalytic role (Scheme 2a) regardless of the counter cation. KI showed slightly slower polymerization, probably because of the partially undissolved KI and some effects of the counter cation on the catalytic center (iodine anion).

Figure 4. Plots of (a) ln([M]$_0$/[M]) vs t and (b) M$_n$ and M$_w$/M$_n$ vs conversion for MMA/CP-I/(catalyst/crown ether) systems (in bulk) (70 °C): [MMA]$_0$ = 8 M; [CP-I]$_0$ = 80 mM; [NaI]$_0$ = 40 mM and [18-crown-6-ether]$_0$ = 40 mM (filled circle), [KI]$_0$ = 40 mM and [18-crown-6-ether]$_0$ = 40 mM (filled square), [Bu4NI]$_0$ = 40 mM (filled triangle), [AIBN]$_0$ = 10 mM (open circle), or none (open square). The symbols are indicated in the figure.

No polymerization occurred in the absence of a catalyst (Figure 4a (open square)). This result means that the radical was generated because of the reaction of CP-I (and Polymer-I) with the catalyst in RCMP. In RCMP, in a mechanistic point of view, not only reversible complexation (RC) (Scheme 1b) but also degenerative chain transfer (DT) (activation of Polymer-I by Polymer•) occurs in the activation process. However, the contribution of DT is minor. Figure 4 (open circle) shows the pure DT system (iodine transfer polymerization) that did not include a catalyst (RC) but did include AIBN as a radical initiator (DT) (*24*). Only large PDI values (> 1.7) were observed in this pure DT system, which clearly indicates that the regulated polydispersity in RCMP arises primarily from the work of the catalyst (RC) with only a small contribution from DT. In the case of MMA polymerization, the degenerative chain transfer constant is as small as 1.6 at 90 °C (*22*).

Notably, Lacroix-Desmazes et al. obtained low-polydispersity (PDI ≤ 1.2) polymers in reverse iodine transfer polymerization (RITP) of MMA using I$_2$ and AIBN (*32*).

Lacroix-Desmazes et al. successfully utilized NaI as the source of an iodine capping agent in RITP, while PDI > 1.5 in this case (*33–35*). They effectively combined NaI with potassium persulfate (KPS) (acting as an oxidant) to generate I$_2$ in situ in polymerization with excess KPS (acting as a radical source), which then reacted with the monomer and I$_2$ to produce an alkyl iodide dormant species and induced the polymerization (iodine transfer polymerization). In this NaI/KPS

method, NaI is used as a source of the dormant species. In our polymerization (RCMP), NaI is used as a catalyst (activator of the dormant species). The combination of RITP (NaI/KPS method) and RCMP to exploit both roles of NaI would be interesting to study in the future.

NaI and KI with Diglyme

Crown ethers are effective to dissolve NaI, but they are expensive. Thus, we attempted to use diglyme (Figure 1) as an ether. Diglyme is inexpensive and environmentally friendly; therefore, it is widely used as a solvent for radical polymerization in industry. Diglyme is a linear polyether and appears similar to an 18-crown-6-ether structure cut in half.

Figure 5 and Table 2 (entries 1-3) show the results with fixed concentrations of CP-I (80 mM) and NaI (40 mM) and various concentrations of diglyme (5, 17, and 64 equivalents to NaI). The 5, 17, and 64 equivalents of diglyme to NaI correspond to 3, 10, and 30 wt% of diglyme (solvent), respectively, in the polymerization solution. NaI was completely dissolved with 17 equivalents of diglyme at the polymerization temperature of 70 °C. Among the three studied cases, 17 equivalents of diglyme resulted in the fastest polymerization. At 64 equivalents of diglyme, the polymerization was slowed down because of the dilution of CP-I and NaI. The PDI was small (1.2–1.4) in all studied cases, demonstrating the usefulness of diglyme as an ether.

Figure 5. Plots of (a) $ln([M]_0/[M])$ vs t and (b) M_n and M_w/M_n vs conversion for MMA/CP-I/NaI/diglyme systems (70 °C): $[MMA]_0 = 8$ M; $[CP-I]_0 = 80$ mM; $[NaI]_0 = 40$ mM; $[diglyme]_0$ as indicated in the figure. The symbols are indicated in the figure.

Table 2. Polymerizations of MMA (8 M) with CP-I (80 mM), NaI (40 mM), diglyme, and V65.[a]

entry	$[diglyme]_0$ $(mM)^b$	$[V65]_0$ (mM)	T $(°C)$	t (h)	$conv$ $(\%)$	M_n $(M_{n,theo})^c$	PDI
1	200	none	70	8	38	4200 (3800)	1.23
2	660	none	70	8	57	5300 (5700)	1.27
3	1800	none	70	8	41	4700 (4100)	1.23
4	660	none	60	8	25	2900 (2500)	1.15
5	660	20	60	3	94	9000 (9400)	1.14

[a] $[MMA]_0/[CP\text{-}I]_0/[NaI]_0/[diglyme]_0/[V65]_0$ = 100/1/0.5/variable/variable. [b] $[MMA]_0/$ $[diglyme]_0$ = 97/3 (entry 1), 90/10 (entries 2, 4, and 5), and 70/30 (entry 3) wt%.
[c] Theoretical M_n calculated with $[MMA]_0$, $[CP\text{-}I]_0$, and conversion.

Increase in the Polymerization Rate

The polymerization with diglyme was relatively slow even at 17 equivalents of diglyme to NaI, as the conversion reached 57% after 8 h at 70 °C (Figure 5 (square) and Figure 6 (circle), same data in both figures). This slow polymerization was overcome by means of the addition of a small amount of an azo initiator, V65 (Figure 6 (triangle)). Azo initiators have often been used to decrease the deactivator concentration and thus effectively increase the polymerization rate in other LRP systems such as ATRP and nitroxide-mediated polymerization (13–15). As Figure 6 shows, compared with the system without V65 at 70 °C (circle), the addition of V65 dramatically increased the polymerization rate by a factor of approximately five even at the lower temperature of 60 °C (triangle). Compared with the system without V65 at 60 °C, the addition of V65 increased the polymerization rate by a factor of as much as twenty (square vs triangle). The addition of V65 did not significantly affect M_n or PDI despite the significant increase in the polymerization rate. The conversion reached 94% in a relatively short time of 3 h even at the mild temperature 60 °C using diglyme.

Diglyme is among the most inexpensive polyethers. The use of this common polyether as an additive (or solvent) may be attractive for potential practical applications. The small PDI that is achievable even at high conversions may also be attractive for practical use.
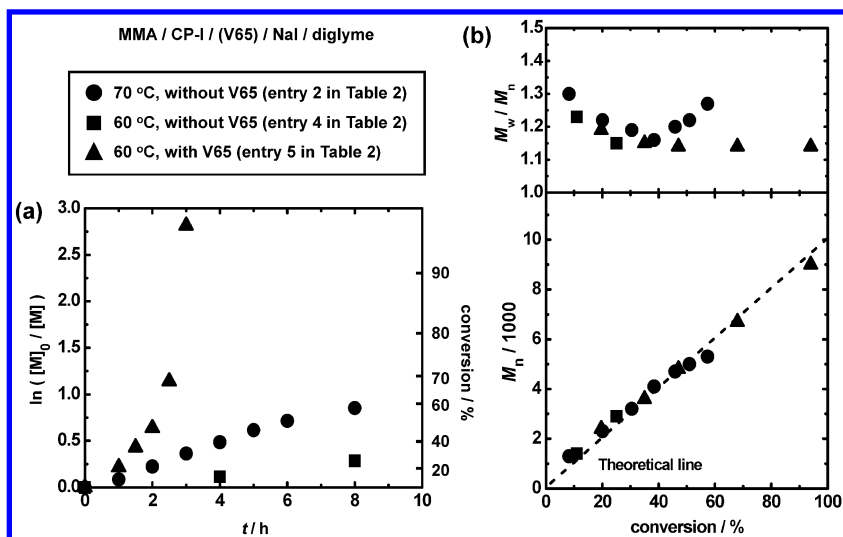
Figure 6. Plots of (a) ln([M]$_0$/[M]) vs t and (b) M$_n$ and M$_w$/M$_n$ vs conversion for MMA/CP-I/(V65)/NaI/diglyme systems: [MMA]$_0$ = 8 M; [CP-I]$_0$ = 80 mM; [V65]$_0$ = 0 (circle and square) or 20 mM (triangle); [NaI]$_0$ = 40 mM; [diglyme]$_0$ = 660 mM ([MMA]$_0$/[diglyme]$_0$ = 90/10 wt%). The symbols and temperatures are indicated in the figure.

Conclusions

NaI and KI were successfully utilized as catalysts in RCMP with the addition of crown ethers and diglyme. Low-polydispersity polymers (PDI = 1.2–1.4) were obtainable with high conversions (e.g., 80–90%) in reasonably short times (e.g., 3–6 h) at mild temperatures (60–70 °C) in MMA polymerizations. These catalysts are easy to handle (insensitive to air), and the NaI/diglyme system is inexpensive. These features may be attractive for practical use. NaI and KI catalysts may be applicable to a wider variety of monomers and higher molecular weight polymers. These possibilities are currently explored in our laboratory and will be reported in future publication.

Acknowledgments

References

1. *Polymer Science: A Comprehensive Reference*; Matyjaszewski, K., Möller, M. Eds.; Elsevier: Amsterdam, 2012.

2. *Fundamentals of Controlled/Living Radical Polymerization*; Tsarevsky, N. V., Sumerlin, B. S., Eds.; Royal Society of Chemistry: London, U.K., 2013.
3. Nicolas, J.; Guillaneuf, Y.; Lefay, C.; Bertin, D.; Gigmes, D.; Charleux, B. *Prog. Polym. Sci.* **2013**, *38*, 63–235.
4. Matyjaszewski, K.; Tsarevsky, N. V. *J. Am. Chem. Soc.* **2014**, *136*, 6513–6533.
5. Ouchi, M.; Terashima, T.; Sawamoto, M. *Chem. Rev.* **2009**, *109*, 4963–5050.
6. Zhang, N.; Samanta, S. R.; Rosen, B. M.; Percec, V. *Chem. Rev.* **2014**, *114*, 5848–5958.
7. Keddie, D. J.; Moad, G.; Rizzardo, E.; Thang, S. H. *Macromolecules* **2012**, *45*, 5321–5342.
8. David, G.; Boyer, C.; Tonnar, J.; Ameduri, B.; Lacroix-Desmazes, P.; Boutevin, B. *Chem. Rev.* **2006**, *106*, 3936–3962.
9. Yamago, S. *Chem. Rev.* **2009**, *109*, 5051–5068.
10. Zetterlund, P. B.; Kagawa, Y.; Okubo, M. *Chem. Rev.* **2008**, *108*, 3747–3794.
11. Satoh, K.; Kamigaito, M. *Chem. Rev.* **2009**, *109*, 5120–5156.
12. Monteiro, M. J.; Cunningham, M. F. *Macromolecules* **2012**, *45*, 4939–4957.
13. Fukuda, T. *J. Polym. Sci., Part A: Polym. Chem.* **2004**, *42*, 4743–4755.
14. Fischer, H. *Chem. Rev.* **2001**, *101*, 3581–3618.
15. Goto, A.; Fukuda, T. *Prog. Polym. Sci.* **2004**, *29*, 329–385.
16. Goto, A.; Zushi, H.; Hirai, N.; Wakada, T.; Tsujii, Y.; Fukuda, T. *J. Am. Chem. Soc.* **2007**, *129*, 13347–13354.
17. Goto, A.; Hirai, N.; Wakada, T.; Nagasawa, K.; Tsujii, Y.; Fukuda, T. *Macromolecules* **2008**, *41*, 6261–6264.
18. Goto, A.; Tsujii, Y.; Fukuda, T. *Polymer* **2008**, *49*, 5177–5185.
19. Vana, P.; Goto, A. *Macromol. Theory Simul.* **2010**, *19*, 24–35.
20. Yorizane, M.; Nagasuga, T.; Kitayama, Y.; Tanaka, A.; Minami, H.; Goto, A.; Fukuda, T.; Okubo, M. *Macromolecules* **2010**, *43*, 8703–8705.
21. Goto, A.; Hirai, N.; Nagasawa, K.; Tsujii, Y.; Fukuda, T.; Kaji, H. *Macromolecules* **2010**, *43*, 7971–7978.
22. Goto, A.; Suzuki, T.; Ohfuji, H.; Tanishima, M.; Fukuda, T.; Tsujii, Y.; Kaji, H. *Macromolecules* **2011**, *44*, 8709–8715.
23. Ohtsuki, A.; Goto, A.; Kaji, H. *Macromolecules* **2013**, *46*, 96–102.
24. Goto, A.; Ohtsuki, A.; Ohfuji, H.; Tanishima, M.; Kaji, H. *J. Am. Chem. Soc.* **2013**, *135*, 11131–11139.
25. Tanishima, M.; Goto, A.; Lei, L.; Ohtsuki, A.; Kaji, H.; Nomura, A.; Tsujii, Y.; Yamaguchi, Y.; Komatsu, H.; Miyamoto, M. *Polymers* **2014**, *6*, 311–326.
26. Lei, L.; Tanishima, M.; Goto, A.; Kaji, H. *Polymers* **2014**, *6*, 860–872.
27. Lei, L.; Tanishima, M.; Goto, A.; Kaji, H.; Yamaguchi, Y.; Komatsu, H.; Jitsukawa, T.; Miyamoto, M. *Macromolecules* **2014**, *47*, 6610–6618.
28. Pedersen, C. J. *Angew. Chem., Int. Ed.* **1988**, *27*, 1021–1027.
29. Pedersen, C. J. *J. Am. Chem. Soc.* **1967**, *89*, 7017–11139.
30. Lehn, J.-M. *Angew. Chem., Int. Ed.* **1988**, *27*, 89–112.
31. Cram, D. J. *Angew. Chem., Int. Ed.* **1988**, *27*, 1009–1020.
32. Lacroix-Desmazes, P.; Villa-Hernandez, A.-M.; Rayeroux, D. *ACS Symp. Ser.* **2012**, *1100*, 317–331.

33. Tonnar, J.; Lacroix-Desmazes, P.; Boutevin, B. *Macromolecules* **2007**, *40*, 6076–6081.
34. Tonnar, J.; Lacroix-Desmazes, P. *Angew. Chem., Int. Ed.* **2008**, *47*, 1294–1297.
35. Tonnar, J.; Lacroix-Desmazes, P. *Soft Matter* **2008**, *4*, 1225–1260.

<center>Chapter 11</center>

Photochemically Enabled Iodine Degenerative Transfer Controlled Radical Homo- and Block Copolymerization of Vinylidene Fluoride at Ambient Temperatures with Mn$_2$(CO)$_{10}$ and Visible Light

Christopher P. Simpson, Olumide I. Adebolu, Joon-Sung Kim, Vignesh Vasu, and Alexandru D. Asandei*

Institute of Materials Science and Department of Chemistry, University of Connecticut, 97 North Eagleville Rd, Storrs, Connecticut 06269-3139
***Ph: 860-486-9062, E-mail: asandei@ims.uconn.edu**

The Mn$_2$(CO)$_{10}$ visible light photomediated polymerization of vinylidene fluoride (VDF) occurs readily in dimethyl carbonate from a variety of alkyl, semi- and perfluorinated halides at 40 °C, in low pressure glass tubes. Perfluoroalkyl iodide initiators also enable a controlled radical polymerization *via* iodine degenerative transfer (IDT) which proceeds with accumulation of the less reactive P$_m$-CF$_2$-CH$_2$-I vs. the P$_n$-CH$_2$-CF$_2$-I chain ends. Their subsequent quantitative activation by Mn$_2$(CO)$_{10}$ affords well-defined PVDF block copolymers.

Introduction

Polymers based on the radical polymerization main chain fluorinated alkenes such as tetrafluoroethylene (CF$_2$=CF$_2$) vinylidene fluoride (VDF, CH$_2$=CF$_2$), hexafluoropropene (CF$_2$=CF(CF$_3$)), trifluorochloroethylene (CF$_2$=CFCl), etc. represent a fundamental class of specialty materials endowed with wide morphological versatility, high chemical, thermal, weather and ageing resistance, as well as low flammability, surface energy, refractive index, and moisture absorption. In addition, certain fluoropolymers, especially poly(vinylidene fluoride) (PVDF) exhibit special electrical responses including piezo- and

ferroelectricity. As such, their applications range from paints and coatings, pipe liners, transmission fluids, O-rings for extreme temperatures, fuel cell membranes, antifouling layers etc., to optical fibers and high power capacitors, transducers, actuators, sensors etc. Thus, their precise synthesis is very relevant. Conversely, all such monomers propagate with very reactive radicals and are also gases under normal conditions (*e.g.* b_p^{VDF} = -83 °C). Indeed, such polymerizations are quite challenging on a laboratory scale, as typical polymerizations are carried out at T > 100-150 °C (*1*), in high-pressure metal reactors. These drawbacks lead to additional levels of difficulty, by comparison with conventional monomers.

As such, though notable progress has been achieved in controlled radical polymerizations (CRPs) over the last two decades (*2–6*), and atom transfer, addition-fragmentation or nitroxide based methods are successful for styrene and acrylates their suitability for the CRP of *side-chain* fluorinated monomers (*e.g.* pentafluoro styrene ($CH_2=CH(C_6F_5)$)), fluorinated (meth)acrylates ($CH_2=CHCOO(CH_2)_nR_F$), and α-trifluoromethyl acrylates ($CH_2=C(CF_3)COOR_{alk}$) remains in its early stages (*1*). Moreover, although potentially industrially significant, their application in the CRP of the *main chain* fluoromonomers (FM) has not been demonstrated.

Consequently, the unavailability of practical chemistry for the CRP of such FMs and for the synthesis of their well-defined complex architectures (blocks, graft, hyperbranched, stars, etc.), has led to a big lag in the study and understanding of their self-assembly and of the properties and applications thereby derived vs. conventional monomers (styrene, acrylates, dienes etc.). As such, development of FM-CRPs and synthesis of intricate fluoropolymer constructs is a worthy, albeit demanding endeavor (*7*, *8*).

In additional contrast with typical monomers, VDF regioselectivity propagation defects generate both Head-Tail (HT) and Head-Head (HH) internal units, where up to one in 10 VDF units is reversed to form the HH $-CH_2-CF_2-CF_2-CH_2-CH_2-CF_2-$, instead of the desired HT $-CH_2-CF_2-CH_2-CF_2-CH_2-CF_2-$ sequence. Such sequence defects also lead to defects in the crystal, and improper arrangement of the units in the β-phase, required for electroactive properties.

Likewise, while carrying out a CRP process, irrespective of the Y "protecting group″, such dual propagation inevitably leads to PVDF containing both $-CF_2-CH_2-Y$ and $-CH_2-CF_2-Y$ chain ends. Clearly, the C-Y bond dissociation energy (BDE) in $-CF_2-CH_2-Y$ is larger than for $-CH_2-CF_2-Y$, thereby rendering the corresponding chain ends *dead*, not dormant, vs. reversible activation. Consequently, the dead chain ends will accumulate with increasing conversion, to broaden the PDI, and eventually will lead to loss of control. Indeed, to date there is no evidence of the reversible activation of the "bad" PVDF-CF_2-CH_2-Y chain ends. In fact, even for the "weaker" $-CH_2-CF_2-Y$ chain end, the corresponding BDE for Y = Cl, Br (*9*) and most likely for RAFT and nitroxides derivatives are also prohibitively high for such polymerizations to proceed at T < 100 °C with any significant rate.

As such, the only current approach to FM-CRP (*1*), remains the iodine degenerative transfer (*3*, *10–15*) (IDT: $P_n^• + P_m\text{-}I \rightleftharpoons P_n\text{-}I + P_m^•$) (*1*, *16*, *20*), an outcome of earlier research on the high temperature (100-230 °C) free radical

VDF telomerization (*17*, *18*) with polyhalides (*19*), especially (per)fluorinated R_F-I iodo chain transfer (CT) agents (*20*) such as CF_3-I, (*21–24*) CF_3-CF_2-I (*25*), CF_3-$(CF_2)_3$-I (*26*, *39*), CF_3-$(CF_2)_5$-I (*22*, *27–29*), $(CF_3)_2CF$-I (*39*), Cl-CF_2-$CFCl$-I (*24*), I-$(CF_2)_{4-6}$-I (*11*, *29*, *30*), and even the less active $HCF_2CF_2CH_2$-I (*27*, *28*), $C_6F_{13}CH_2CF_2$-I (*28*, *31*), and even CH_2I_2 (*32*), R_F-CH_2-CH_2-I (*33*), or CH_3-I (*34*). Modeling (*30*, *35*) and kinetic (*21*, *27*, *28*) investigations have also illustrated the importance of the structure and reactivity of the CT agent (I > Br > Cl~ H and difunctional better than monofunctional), (*11*, *20*) and the contributions of side reactions (transfer to polymer, solvent etc.) and of monomer addition mode (1,2- vs. 2,1-) to the quality of the polymerization control. In fact, IDT is one also of the oldest CRP methods, as a linear dependence of M_n on polymer yield was previously demonstrated (*11*) in the early 80's, and was the first implemented industrially (*11*), taking advantage of the commercial availability of iodine CT agents (*20*, *36*) and its tolerance of emulsion polymerization.

As a classic degenerative process, VDF-IDT-CRPs also requires a free radical initiator source (*e.g.* ᵗbutyl peroxide etc.). While most chains should indeed be derived from the R_F-I chain transfer agent, higher levels of initiator required for higher rate will inevitably lead to a decreased fraction of the R_F-functionalized chains. Moreover, such system are not suitable for the synthesis of well-defined blocks, as PVDF-CF_2-CH_2-I would be hardly activated and would inevitably lead to mixtures of homo- and copolymers. This is a clear shortcoming with respect to the precise synthesis of block or graft copolymers based on FMs. Thus, FM initiation *directly from* a halide (*e.g.* from perfluoroalkyl iodides or any other halides), and mediated by transition metal catalysis is highly desirable.

However, while the propagation rate constant (k_p) of VDF is large enough (*37*) that polymer can be obtained even at room temperature (*38*), only very low telomers (DP = 1-3) result from redox reactions of transition metal complexes and polyhalides, even at high temperatures (> 100 °C) (*1*, *39*, *40*). Furthermore, while the addition R_F-Mt-I (Zn (*41*, *42*), Zn/Cu (*43*)) organometallics to carbonyls and amides, as well as the radical perfluoroalkyl iodination of alkenes with R_F-I derivatives occurs readily with a variety of catalytic systems (Cu (*44*), Zn (*45*), Pd (*46*), $SnCl_2$/CH_3COOAg (*47*), Cp_2TiCl (*48*), etc.), the corresponding metal catalyzed addition of electrophilic R_F• radicals to electrophilic fluorinated alkenes (FMs) at T < 100 °C, and especially at room temperature is not available.

Likewise, due to the gaseous monomer nature, and by contrast to conventional styrene or acrylate CRPs which can be easily sampled from Schlenk tubes on *e.g.* a 1 g scale, kinetic investigation of VDF polymerizations require several one-data-point experiments. This is quite time-consuming and expensive due to the prerequisite large number of costly metal reactors, which moreover require hundreds of grams of monomer.

As such, development of chemistry that enables small-scale, (1 g) polymerizations to proceed at room temperature (rt) in inexpensive, low-pressure glass tubes, would be highly desirable, as it could be enable fast screening of a multiple catalysts and reaction conditions, and allow for photocatalysis. Indeed, the capability to carry out such reactions under mild conditions would be of great synthetic use not only in polymer fluoro-functionalization, or the initiation and CRP of FMs and synthesis of their complex architectures, but also

in perfluoroalkylations and trifluoromethylations that are in increasing demand in organic/medicinal chemistry (*49*). Yet, prior to our recent work (*50–53*), there were no disclosures on metal-mediated FM or VDF polymerizations, let alone VDF-CRP.

Towards this goal, we originally started our investigations by testing VDF polymerization at moderate temperatures (25 °C - 60 °C) in low pressure glass tubes using conventional CRP methods (Cu-ATRP (*54*), nitroxides, RAFT, Cp₂TiCl (*50*, *55*), etc.). Cp_2TiCl However, while polymer could be obtained under similar conditions by the photochemical decomposition of TBPO (*50*), all these attempts were unsuccessful. The reason for failure was a combination of the inability of the particular catalyst to generate radicals reactive enough to add to VDF, and to reactivate the PVDF-Y chain ends at or around rt, and the lack of solvents compatible with both PVDF and the catalyst (*50*).

Indeed, in ATRP, while CuX/L abstracts halides from activated substrates (esters, benzyl, etc.), it hardly does so from perfluoroalkyl derivatives ($k_{act}^{(CH3)2C(COOEt)-Br}$/$k_{act}^{C8F17-Br}$ > 10²) (*56*). Moreover, assuming otherwise identical conditions, DFT calculations (*9*) show that even at 90 °C, and using Br as the ATRP halide, $K_{ATRP}^{Ethylene}$/K_{ATRP}^{VDF}/K_{ATRP}^{MA}/K_{ATRP}^{St}/K_{ATRP}^{MMA} = ~ 2x10⁻⁷/9x10⁻⁷/1/6/30. Similarly, one can estimate (*9*, *57*) the relative ATRP rates of MA and VDF as rate$_{VDF}$/rate$_{MA}$ = (k_p^{VDF} x K_{ATRP}^{PVDF})/(k_p^{MA} x K_{ATRP}^{MA}) = ~ 8.75 x 10⁻⁷. Thus, the conversion obtained in one second of polymerization time for MA would require ~13 days for VDF (Br) and ~ 317 days (Cl). Obviously, this is impractical.

While quantitative iodine-ATRP data are not available, under normal conditions, Cu barely activates the C-I bond of -CF₂-CF₂-I. Thus, only modest activation is expected in the "good" PVDF-CH₂-CF₂-I chain end, and negligible activation of the "bad" PVDF-CF₂-CH₂-I chain end, which explains the inability of ATRP to provide well defined PVDF block copolymers. In addition, activating amine ligands (*4*) react with R$_F$-I initiators to form ammonium iodide salts and/or charge transfer complexes (*58*), and are thus impractical with CuX here.

Conversely, metal mediated radical processes which are successful in other CRPs (Co, Ti, Mo, etc.) (*2*) involving C-Mt bond formation, will likely proceed with *β*-H and especially *β*-F eliminations (*50*). In addition, while we have shown that Cp₂TiCl is an excellent mediator for the CRP of styrene (*59–71*) and dienes (*72*), as well as for the living ring opening polymerization of cyclic esters (*73*, *74*), a solvent compatible with both Cp₂TiCl and PVDF was not found. Thus, as none of the conventional CRP protocols or R-CF₂-I activators tested worked, we decided to investigate alternative, photochemical means of radical generation and trapping (*75*, *76*).

Indeed, high power UV photoinduced *telomerizations* were described for VDF over 50 years ago (*19*, *77*, *78*). Likewise, we have also confirmed (*50*, *79–82*) that VDF free radical polymerization (FRP) occurs readily under UV irradiation at rt in the presence of TBPO. However, before our work (*50–53*), there were no reports on the VDF polymerization using regular *visible* light. Thus, while aiming to maintain an ambient reaction temperature and a relatively low pressure in the glass tubes, and also considering the very poor stability of most organometallic complexes under UV irradiation, we decided to investigate

186
In Controlled Radical Polymerization: Mechanisms; Tsarevsky, et al.;
ACS Symposium Series; American Chemical Society: Washington, DC, 2015.

Publication Date (Web): May 1, 2015 | doi: 10.1021/bk-2015-1187.ch011

photopolymerizations mediated by commercially available transition metal complexes, using low wattage (< 30 W), white light fluorescent bulbs.

As VDF propagates with an extremely reactive radical, successful R-X initiators should also provide highly reactive, alkyl, semifluorinated, or perfluoroalkyl radicals. In turn, the visible light derived $L_nMt^\bullet$ metalloradical activator should be a very good halide (X) abstractor. In addition, for metal mediated reversible deactivation, (*i.e.* metal catalyzed IDT, X = I), L_nMt-X should also be a very good halide donor. Typical examples (*61*, *62*) of transition metal complexes that photolyze radically are $(CO)_nMt$-$Mt(CO)_n$ carbonyl metal dimers, which are clearly similar with the $ClCp_2Ti$-$TiCp_2Cl$ dimer we described earlier for the CRP of styrene (*59*) and isoprene (*60*), but which due to solvent incompatibility, was unsuccessful for VDF (*50*).

Many such systems are commercially available, and were investigated before in both organic reactions and in radical polymerizations. Qualitatively, the order of their ability to abstract halides (*83*) (k_{act} of ATRP) is $Re(CO)_5^\bullet$ > $Mn(CO)_5^\bullet$ > $CpW(CO)_3^\bullet$ > $CpMo(CO)_3^\bullet$ > $CpFe(CO)_2^\bullet$ > $Co(CO)_4^\bullet$. However, while $Re(CO)_5^\bullet$ does indeed abstract Cl from CCl_4 ~65 times faster than $Mn(CO)_5^\bullet$ (*69*, *84*), the stronger Re-Re (*85*) bond dissociation energy and its higher price, render the relatively inexpensive $Mn_2(CO)_{10}$ (*86*, *87*) the most popular reagent in the series (*62*). The dimer is stable at room temperature, in the dark (K_{eq} < 2.4 x 10^{-19}) (*88*), but as the Mn-Mn BDE is relatively small (30-40 kcal/mol) (*62*, *89*, *90*), and further decreased by extra ligands (*91*), $Mn_2(CO)_{10}$ easily dissociate thermally (~ 60-90 °C) (*92*), and respectively, photolytically at rt. Indeed, while UV leads to CO loss to $Mn_2(CO)_9$ and $Mn(CO)_5^\bullet$, near-UV and visible longer wavelength (λ = 366-400 nm, $\lambda_{max}^{Mn2(CO)10}$ = 324 nm) produce the 17e$^-$ paramagnetic $Mn(CO)_5^\bullet$ metalloradical ($\lambda_{max}^{Mn(CO)5}$ = 780-830 nm) (*93*) with reasonable quantum efficiency (*94–96*).

$Mn(CO)_5^\bullet$ easily abstracts hydrides and halide from *e.g.* Bu_3SnH (*97*), and respectively from RX halides with moderate to high BDEs (< 310 kJ/mol) (*98*) such as CCl_4 (*99*), I_2 (*85*), polyhalides (*84*), allyl and benzyl halides (*84*, *85*), and even CH_3I (*100*) and other inactivated alkyl iodides. Remarkably, unlike other radical abstractors, $Mn(CO)_5^\bullet$ reacts faster with primary rather than secondary or tertiary halides, due to the sterics of the CO ligands (*84*). Moreover, prior to our work (*50–53*), there were no examples of $Mn_2(CO)_{10}$ mediated activation of perfluoroalkyl or sulfonyl halides, or trifluoromethylations with CF_3-I or CF_3-SO_2-I.

Mn-alkyls photolyze very easily, and are not considered effective in radical reactions (*76*). Thus, CRPs based on reversible termination with $Mn(CO)_5^\bullet$ are not likely to be effective. Nonetheless, very early reports did propose photo or thermal $Mn_2(CO)_{10}$ or $Re_2(CO)_{10}$ mediated FRPs initiated *via* either H abstraction from the monomer (*101*), addition of the metalloradical to tetrafluoroethylene to initiate its homopolymerization (*102*, *103*) or the MMA (*88*, *104*, *105*) block copolymerization (*106*), as well as the addition to 1,2-disubstituted acetyls and alkenes (*107*). However, while polymerizations initiated by $Mn_2(CO)_{10}$ or $Re_2(CO)_{10}$ and CCl_4 (*108*) or grafting from N-halogenated polyamides (*109*) were carried out in the 60s, $Mn_2(CO)_{10}$ was only recently utilized in the thermal (60-90

°C) (*110*) FRP of MMA, or in PMMA initiation from -CCl$_3$ groups on SiO$_2$ (*111*), chitosan (*112*) or from PSt-Br (*113–115*).

Very recently, Mn$_2$(CO)$_{10}$ was nevertheless employed as a photo-activator of alkyl iodides (IDT) (*116–118*), or RAFT reagents (*119*) in controlled radical photo(co)polymerizations of VAc, acrylates, styrene and alkenes. Here, Mn(CO)$_5$• was shown to irreversibly activate the iodine terminated chains or the initiator (*102*), but the in-situ generated Mn(CO)$_5$-I (*85*) was not involved in the IDT.

Thus, as Mn$_2$(CO)$_{10}$ was never used in CRPs of main chain fluorinated monomers, or with inactivated alkyl halides or perfluoroalkyl iodides, we decided to first assess its scope and limitations as a photoactivator, and demonstrate the initiation of VDF polymerization *directly* from a variety of alkyl and perfluoroalkyl halides (Cl, Br, I) at rt. Second, we set to explore these polymerization kinetically, and investigate the Mn$_2$(CO)$_{10}$ mediated VDF-IDT-CRP. Third, we aimed to demonstrate the first examples of the synthesis of well-defined PVDF block copolymers.

Experimental

Materials

Manganese carbonyl (Mn$_2$(CO)$_{10}$, (Strem chemicals, 98%), vinylidene fluoride (VDF,99.9%), 2-Iodoheptafluoropropane (PFIPI, 97%)), 1-iodononafluorobutane (perfluorobutyl iodide, PFBI, 98%), ethyl bromodifluoroacetate (EBDFA, 99%), 1,1,2-trichlorotrifluoroethane (TCTFE, 99%), 1,1,1,3,3-Pentafluorobutane (99%), 3-Iodo-1,1,2,2-tetrafluoropropane (98%), 1,8-dichloroperfluorooctane (99%), iodotrifluoromethane (CF$_3$I, 99%), 1,6-diiodododecafluorohexane (DIPH, 98%), 1,2-dichloro-1,1,2-trifluoro-2-iodoethane (90+%), hexafluorobenzene (HFBz, 99+%), 1,4-dibromooctafluorobutane (98%), hexafluoropropene (HFP, 99%), chlorotrifluoroethylene (CTFE, 99%), bromotrifluoroethylene (BTFE, 98%), vinyl fluoride (VF, 98%), trifluorometyl trifluorovinyl ether (99%), 1-Chloro-1-fluoroethylene (98%), 1,1-dichloro-2,2-difluoroethylene (90 %) (all from Synquest), ethyl iododifluoroacetate (EIDFA, 97%), heptafluorobenzyl iodide (97%), iodoperfluoro-tert-butane (97%), 1,2-Diiodotetrafluoroethane (97%) (All from Matrix Scientific); 1,3-dibromo-1,1,3,3-tetrafluoropropane (97%), carbon tetrabromide (CBr$_4$, 98%) (both from Alfa Aesar), heptafluorobutyryl chloride (98%), 1,4-diiodoperfluorobutane (98%), chloroform (CHCl$_3$, stabilized with ca. 1% ethanol), 4-methoxybenzenesulfonyl chloride (MBSC, 99%), iodoform (CHI$_3$ 99+%), dimethyl sulfoxide (DMSO, 99.8%), 4-iodoanisole (98%), ethyl 2-bromoisobutyrate (EBIB, 98%), thymol iodide, 1,4-dioxane (Diox, 99.7%), N,N′-dimethylacetamide, (DMAc, 99%), ethylene carbonate (EC, +99%), ε-caprolactone (CL, 99%), benzonitrile (BN, 99%, extra pure), 4-methyl-2-pentanone (reagent ACS), isopropanol (99.5%), vinyl acetate (VAc, 99+%), acrylonitrile (99+%), styrene (99%), methyl acrylate

(MA, 99%) (all from Acros Organics); iodomethane (CH$_3$I, ReagentPlus, 99.5%), bromotrichloromethane (BrCCl$_3$, 99%), 1-Iodohexane (98+%), halocarbon oil 27, methanesolfonyl chloride (≥99.7%) , N-iodosuccinimide (NIS, 95%), hexachloroethane (99%), trifluoromethanesulfonyl chloride (≥99%), α,α,α-trifluorotoluene (TFT, 99%), bromoform (CHBr$_3$, ≥99%), acetonitrile (ACN, 99%), iodoacetonitrile (98%), 1H,1H,7H-dodecafluoroheptyl acrylate (95%), 2-bromopropionitrile (97%), dimethyl carbonate (DMC, ≥ 99% anhydrous), 2-butanone(ACS reagent, ≥99%), trimethyl phosphate (TMP, 99+%), diethyl carbonate (DEC, ≥99%), β-butyrolactone(98+%), γ-butyrolactone (ReagentPlus, ≥99%), propylene carbonate (PC, 99.7%, HPLC grade), methanol (99%), anisole (99.7%), tert-butanol (anhydrous, 99.5%), dichloromethane (anhydrous, > 99.5%), 1,2-dichloroethane (anhydrous, 99.8%), o-cresol (99%), ethyl acetate (anhydrous, 99.8%), cyclopentanone (99%), allyl iodide (98%), 1,1,1,3,3,3-hexafluoro-2-propanol (HFIPA, > 99%), (1-bromoethyl)benzene (BEB, 97%), 2-iodo-2-methylpropane (copper-stabilized, 95%), diethylene glycol dimethyl ether (diglyme, anhydrous 99.5%), 1,3-butadiene (≥99%) (all from Aldrich); allyl bromide (>98%), α,α′-dibromo-p-xylene (DBPX, ≥98%), tetramethylurea (≥99.0%), N-bromosuccinimide (NBS, >95%), poly(ethylene oxide) 2000, vinyl chloride (≥99.5%) (all from Fluka); δ-valerolactone (99%) 1,10-diiododecane (97%), di-tert-butyldicarbonate (99%), allyl chloride (98%), (all from Janssen Chimica); carbon tetrachloride (CCl$_4$,), acetic anhydride (certified A.C.S.), N,N′-Dimethylformamide (DMF, 99.9%), trifluoroacetic anhydride (reagent grade), diethylene glycol monoethyl ether (lab grade), diethylether (anhydrous, 99%), (all from Fisher Scientific); acetone-d$_6$ (Cambridge Isotope Laboratories, Inc., D, 99.9%), tetrahydrofuran (THF, 99%, acetone, 99.9 % both J. T. Baker) were used as received. Ethyl-2-iodoisobutyrate (EIIB), α,α′-diiodo-p-xylene (DIPX) and Mn(CO)$_5$-I were prepared from ethyl-2-bromoisobutyrate (EBIB, 98%, Acros), α,α′-dibromo-p-xylene, (DBPX, ≥98%, Fisher) (*120*) (99%, Fisher) and respectively from Mn$_2$(CO)$_{10}$ (*121*) as described in the literature.

Techniques

^{1}H NMR (500 MHz) and ^{19}F-NMR (400 MHz) spectra were recorded on a Bruker DRX-500 and respectively on a Bruker DRX-400 at 24 ^{0}C in acetone-d$_6$. IR spectra were recorded on a Nicholet 560 spectrometer on KBr plates or pellets. GPC analyses were performed on a Waters gel permeation chromatograph equipped with a Waters 2414 differential refractometer and a Jordi 2 mixed bed columns setup at 80^{0}C. DMAc (Fisher, 99.9% HPLC grade) was used as eluent at a flow rate of 1 mL/min. Number-average (M$_n$) and weight-average molecular weights (M$_w$) were determined from calibration plots constructed with PMMA standards. All reported polydispersities are those of water precipitated samples. While narrower PDIs could be obtained by MeOH precipitation, this may also lead to partial fractionation, especially for lower molecular weight samples.

Polymerizations

VDF Homopolymerization

In a typical reaction (*51*), a 35-mL Ace Glass 8648 # 15 Ace-Thread pressure tube equipped with a bushing, and plunger valve with two O-rings and containing a magnetic stir bar, $Mn_2(CO)_{10}$, (53.6 mg, 0.14 mmol) and solvent (*e.g.* DMC, 3 mL) was degassed with He and placed in a liquid nitrogen bath. Note that it is important to use He for degassing, as N_2 or Ar would condense in the tube in a liquid nitrogen bath. The tube was subsequently opened, and the initiator (*e.g.* CF_3-$(CF_2)_3$-I (PFBI), 0.12 mL, 0.69 mmol) was added, followed by the condensation of VDF (1.1 g, 17.2 mmol), directly into the tube, which was then re-degassed with He. The amount of condensed VDF was determined by weighing the closed tube before and after the addition of the monomer. The tube was then placed in behind a plastic shield, in a thermostated oil bath illuminated with a commercial GE Helical 26 W fluorescent white light Hg spiral bulb, from about 2-4 cm. For polymerization kinetics, identical reactions were set up simultaneously and stopped at different polymerization times. At the end of the reaction, the tube was carefully placed in liquid nitrogen, slowly opened behind the shield, and allowed to thaw to room temperature in the hood, with the concomitant release of unreacted VDF. The contents were poured in water, filtered and dried. The polymer was than dissolved in DMAC, and the residual Mn inorganics (which may interfere with the NMR signals) were removed by column chromatography. The polymer was finally reprecipitated in water, filtered and dried. While precipitation in MeOH is feasible, it will also lead to fractionation and narrowing of the polydispersity by about 0.2, especially on lower molecular weight samples. Thus, all reported GPC results are from water precipitation. The monomer conversion was determined as the ratio of the differences of the tube weight before and after the reaction and respectively before and after VDF charging (*i.e.* $c = (Wt_{after\ VDF\ condensation} - Wt_{after\ VDF\ release})/(Wt_{after\ VDF\ condensation} - Wt_{before\ VDF\ addition})$, as well as the ratio of the dry polymer to the condensed VDF. Both procedures gave conversions within < 5% of each other. In this particular example the reaction time was 16 h, M_n = 4,015, M_w/M_n = 1.31.

Synthesis of PVDF Block Copolymers

An example of the block synthesis (*51*) is as follows: A Schlenk tube containing a DMAC solution of PVDF-I or I-PVDF-I (in this case, I-PVDF-I, M_n = 2,500, PDI = 1.34, with a total halide chain end functionality of F = 95% ($F_{1,Pn-CH2-CF2-I}$ = 0.64 and $F_{2,Pm-CF2-CH2-I}$ = 0.31, 100 mg, 0.05 mmol in 2 mL of DMAC), a second monomer (*e.g.* styrene, 215 mg, 2.1 mmol) and $Mn_2(CO)_{10}$ (36 mg, 0.1 mmol) was degassed under Ar then heated to 110 °C under visible light irradiation for 5 h. The solution was precipitated in MeOH, filtered and dried. M_n = 14,500, PDI = 2.25 conv. = 67%, and composition, VDF/St = 30/70.

Results and Discussion

While alkyl iodides may photodissociate, control experiments revealed no polymerization in the dark, or under irradiation in the absence of $Mn_2(CO)_{10}$ (*51*). Polymerizations were tested at T = 0 °C - 100 °C, but T = 40 °C was eventually selected for all experiments, as a reasonable compromise between rate and a safe pressure inside the tube. In fact, positioning the bottom part of the fluorescent light bulb inside the oil bath helped maintain such temperature, with minimal additional heating from the hotplate (*51*).

Solvent Effect

While typical VDF "solution" polymerizations are carried out in AN (*18*), which is a non-solvent and a weak CT agent, there is very little data (*122–124*) on the solvent effect in VDF polymerizations, and none for photopolymerizations. Nonetheless, previous investigations of PVDF solution properties (*125–130*) have indicated that the best solvents are polar aprotic and H-bonding capable, and that HH sequences decrease solubility (*111*). A common feature of good solvents is the presence H bonding between the weakly acidic Hs of $-CF_2-CH_2-CF_2-$ and the polar Y=O solvent bond (Y = C, S, P). As such, bearing in mind that minimization of chain transfer to solvent and of side reactions with the catalyst outweigh monomer/polymer solubility concerns or a photosensitizing solvent effect, we scanned > 40 polymerization media (*51*). Indeed, when we carried out a similar study using Cp_2TiCl_2, solvents compatible with both $Cp_2TiCl^{\bullet}$ and PVDF could not be found (*50*).

Comparisons were made under the same conditions (VDF/R_F-I/$Mn_2(CO)_{10}$ = 25/1/0.2; VDF/solvent = 1/3 v/v) and revealed that in accordance with the principles outlined above, no polymerization occurred in anisole, α,α,α-trifluorotoluene, diglyme, diethylene glycol monoethyl ether, ethyl ether, THF, dioxane, *o*-cresol, isopropanol, trifluoroacetic anhydride, tetrametyl urea, sulfolane, benzonitrile, cyclopentanone even after 1-3 days. Poor reactions were observed in HMPA, 2-butanone, methyl pentanone, DMF, DMSO, PEO, DMAc, δ-valerolactone, ^{t}BuOH and EtOAc. Slightly faster polymerizations were seen in CH_2Cl_2, acetic anhydride, γ-butyrolactone, 1,2-dichloroethane, trimethyl phosphate, MeOH, pentafluorobutane and C_6F_6, whereas β-butyrolactone, ε-caprolactone, ACN and H_2O displayed medium rates. While much faster polymerizations occurred in diethyl-, di^{t}Bu- and propylene carbonate, the fastest rates were provided by ethylene carbonate, hexafluoroisopropanol, and especially by dimethyl carbonate (DMC).

As such, the known good solvents for PVDF (DMF, DMAc, etc.) are also strong CT agents in VDF radical polymerization, and thus provide very little conversion. However, remarkable trends are observed with carbonates, and especially with DMC, a green solvent (*131*). Indeed, though DMC does not dissolve PVDF at rt, and like ACN, affords a heterogeneous polymerization, it provides by far the fastest reaction rates, at least thrice those obtained in ACN. Here, the conversion, polymerization rate, M_n and PDI were largely insensitive to the amount of DMC, (V_{tube} = 35 mL, 1 g VDF, 1-12 mL DMC). However, the

rate significantly increased with the amount VDF (*i.e.* pressure and monomer concentration in solution, with 1-4 g VDF, 3-12 mL DMC). These features are typical of heterogeneous polymerizations of gaseous monomers (*132*), and resemble precipitation/dispersion polymerization of VDF in scCO₂ (*29, 133*). Possible explanations for the faster rate include a photosensitizing effect or better monomer/polymer solubilization.

As DMC is stable to pyrolysis and photolysis up > 300 °C (*134*), there are no reports on DMC as a photosensitizer. Moreover, no photopolymerization occurs in DMC with VDF alone, VDF/Mn₂(CO)₁₀ or VDF/R_F-I. Thus, while DMC may still be a weak CT agent, it clearly does not generate radicals under visible light. As such, the solvent effect trends represent a combined outcome where the best solvents (alkyl carbonates) display minimum transfer and highest VDF solubilization and PVDF swelling, which also enables better monomer diffusion to the propagating center. These trends are consistent with the use carbonate solvent electrolytes and the swelling of PVDF microporous membranes (*135–137*) in Li-ion batteries (*138*).

Polymerization Mechanism and Initiator Evaluation

The mechanism of Mn₂(CO)₁₀-mediated VDF polymerization is presented in Scheme 1 (*51*). After reversible photodissociation of Mn₂(CO)₁₀ (eq. 1), subsequent irreversible (*102, 103*) halide abstraction from R-X (and later from PVDF-X), which is driven by the formation of high BDE Mn-X (*75, 76, 139*), X = Cl, Br, I, (eq. 2) affords Mn(CO)₅-X and R•, which, if reactive enough, adds to VDF, typically at the CH₂ side, driven by polar effects, initiating polymerization (eq. 3). Due to regioselectivity propagation defects, both 1,2- and 2,1-units, (eq. 4, HT, ~95 % (*21, 109*) and respectively, HH) occur in FRP (eq. 4). Mn(CO)₅ is slowly but continuously generated by the photolysis of the dimer throughout the polymerization, and, by activating R-X and PVDF-X (especially PVDF-CH₂-CF₂-I), compensates for termination reactions and maintains a steady state radical concentration.

With substoichiometric amounts of Mn₂(CO)₁₀, depending on the value of initiator chain transfer (CT) constant to PVDF•, ($CT_{RX}^{PVDF•}$ = $k_{transfer}^{PVDF*to RX}$/$k_{propagation}^{VDF}$), excess RX may act as a chain transfer agent (CTA) towards the propagating chains (eqs. 5, 6). Higher CT values ($CT_{RX}^{PVDF•}$ > 1) and X = I are required for IDT-CRP (*20*), where such initiators are consumed very early in the process to provide iodide terminated polymeric CTAs (*28, 51*). For PVDF, two such chain ends (P_n-CH₂-CF₂-I and P_m-CF₂-CH₂-I), are thus obtained (*20, 27, 28, 31, 51*).

While very few $CT_{RX}^{PVDF•}$ values are known (CCl₃Br = 35, CCl₄ = 0.25, CHCl₃ = 0.06 at 141 °C (*140*), C₆F₁₃-I = 0.8, C₆F₁₃-Br = 0.08, C₆F₁₃-H = 0.0002 in scCO₂ at 120 °C (*29*)), perfluoroalkyl iodides and PVDF-CH₂-CF₂-I have similarly large CT values (C₆F₁₃-I = 7.9, C₆F₁₃-CH₂-CF₂-I = 7.4). By contrast, the "bad" PVDF-CF₂-CH₂I 2,1-chain end is 25 times less active (CT of HCF₂CF₂CH₂I = 0.3 at 75 °C) (*28*). As such, PVDF-CF₂-CH₂• is much more reactive than PVDF-CH₂-CF₂•.

Initiation and Propagation

$$Mn_2(CO)_{10} \underset{}{\overset{h\nu}{\rightleftharpoons}} 2\overset{\bullet}{Mn}(CO)_5 \tag{1}$$

$$R\text{-}X + \overset{\bullet}{Mn}(CO)_5 \underset{X}{\rightleftharpoons} R\bullet + Mn(CO)_5X \tag{2}$$

$$R\bullet \xrightarrow{k_i,\ VDF} R\text{-}VDF^\bullet \xrightarrow{nVDF,k_p} P^\bullet_{n+1} \tag{3}$$

$$P_m\text{-}CH_2\text{-}\overset{\bullet}{C}F_2 \xrightarrow[k_p]{VDF} P_m\text{-}CH_2\text{-}CF_2\text{-}CH_2\text{-}\overset{\bullet}{C}F_2 + P_m\text{-}CH_2\text{-}CF_2\text{-}CF_2\text{-}\overset{\bullet}{C}H_2 \tag{4}$$

Chain Transfer to Initiator

$$P_n\text{-}CH_2\text{-}\overset{\bullet}{C}F_2 + R\text{-}X \xrightarrow{k_{1tr}} P_n\text{-}CH_2\text{-}CF_2\text{-}X + R\bullet \tag{5}$$

$$P_m\text{-}CF_2\text{-}\overset{\bullet}{C}H_2 + R\text{-}X \xrightarrow{k_{2tr}} P_m\text{-}CF_2\text{-}CH_2\text{-}X + R\bullet \tag{6}$$

Iodine Degenerative Transfer

$$P_m\text{-}CH_2\text{-}\overset{\bullet}{C}F_2 + P_n\text{-}CH_2\text{-}CF_2\text{-}I \underset{}{\overset{K_{ex}=1}{\rightleftharpoons}} P_m\text{-}CH_2\text{-}CF_2\text{-}I + P_n\text{-}CH_2\text{-}\overset{\bullet}{C}F_2 \tag{7}$$

$$P_m\text{-}CH_2\text{-}\overset{\bullet}{C}F_2 + P_n\text{-}CF_2\text{-}CH_2\text{-}I \underset{}{\overset{K_{ex}\ll 1}{\rightleftharpoons}} P_m\text{-}CH_2\text{-}CF_2\text{-}I + P_n\text{-}CF_2\text{-}\overset{\bullet}{C}H_2 \tag{8}$$

$$P_m\text{-}CF_2\text{-}\overset{\bullet}{C}H_2 + P_n\text{-}CF_2\text{-}CH_2\text{-}I \underset{X}{\rightleftharpoons} P_m\text{-}CF_2\text{-}CH_2\text{-}I + P_n\text{-}CF_2\text{-}\overset{\bullet}{C}H_2 \tag{9}$$

Bimolecular termination

$$P_m\text{-}CH_2\text{-}\overset{\bullet}{C}F_2 + P_n\text{-}CH_2\text{-}\overset{\bullet}{C}F_2 \longrightarrow P_m\text{-}CH_2\text{-}CF_2\text{-}CF_2\text{-}CH_2\text{-}P_n \tag{10}$$

H Transfer

$$P_m\text{-}CF_2\text{-}\overset{\bullet}{C}H_2 + S\text{-}H \longrightarrow P_m\text{-}CF_2\text{-}CH_2H \tag{11}$$

$$P_n\text{-}CH_2\text{-}\overset{\bullet}{C}F_2 + S\text{-}H \longrightarrow P_n\text{-}CH_2\text{-}CF_2H \tag{12}$$

Scheme 1. Mechanism of $Mn_2(CO)_{10}$-Mediated VDF Polymerization.

To select and classify the proper initiators for VDF FRP and respectively CRP, a wide variety of over 40 halide structures never previously reported with $Mn_2(CO)_{10}$ were subsequently evaluated (*51*). However, no initiation was observed (*51*) from I_2, $^tBu\text{-}I$, $CH_3\text{-}SO_2Cl$, $CH_3O\text{-}Ph\text{-}SO_2Cl$, CH_2Cl_2, CH_2I_2, $CHCl_2\text{-}CHCl_2$, $CHBr_3$, CHI_3, CBr_4, $CH_2{=}CH\text{-}CH_2\text{-}Cl/Br/I$, $Ph\text{-}CH_2\text{-}Cl/Br/I$, $Ph\text{-}CH(CH_3)\text{-}Br$, $Ph(CH_2\text{-}Br/I)_2$, $CH_3\text{-}CH(CN)\text{-}Br$, $CH_2(CN)\text{-}I$, $(CH_3)_2C(COOEt)\text{-}Br/I$, $I\text{-}Ph\text{-}O\text{-}CH_3$ and NBS under a wide variety of conditions. $Mn(CO)_5{}^\bullet$ has a very high halide affinity (*62*), and abstraction is available in all cases. Thus, the lack of initiation is a consequence of the corresponding radicals being more stable than the propagating PVDF$^\bullet$, and thus failing to add at moderate temperatures.

However, very reactive alkyl, polyhalide, as well as semi- and perfluorinated halide analogues such as $CHCl_3$, CCl_4, $CCl_3\text{-}CCl_3$, $CF_3(CF_2)_2CO\text{-}Cl$, $CF_3\text{-}SO_2\text{-}Cl$, $Cl\text{-}CF_2\text{-}CClF\text{-}Cl$, $Cl\text{-}(CF_2)_8\text{-}Cl$, $\text{-}(CF_2\text{-}CFCl)_n\text{-}$, $CCl_3\text{-}Br$, $EtOOC\text{-}CF_2\text{-}Br$, $Br\text{-}(CH_2)_{10}\text{-}Br$, $Br\text{-}CF_2\text{-}CH_2\text{-}CF_2\text{-}Br$, $Br\text{-}(CF_2)_4\text{-}Br$, $CH_3\text{-}I$, $CH_3(CH_2)_5\text{-}I$, $I\text{-}(CH_2)_{10}\text{-}I$, $C_6F_5\text{-}CF_2\text{-}I$, $H\text{-}CF_2\text{-}CF_2\text{-}CH_2\text{-}I$, $EtOOC\text{-}CF_2\text{-}I$, $Cl\text{-}CF_2\text{-}CFCl\text{-}I$, $CF_3\text{-}I$, $CF_3CF_2\text{-}I$, $(CF_3)_2CF\text{-}I$, $(CF_3)_3C\text{-}I$, $CF_3(CF_2)_3\text{-}I$ and $I\text{-}(CF_2)_{4,6}\text{-}I$, all led to polymer formation

(*50*) not only for VDF, but also for $CF_2=CFCl$, $CF_2=CCl_2$, $CF_2=CFBr$, $CH_2=CFH$ and for VDF random copolymers with $CF_2=CF(CF_3)$ and $CF_2=CF(OCF_3)$ (*51*).

Indeed, initiation occurred not only from polyhalides and all R_F-I structures (which allow for IDT and elimination of HH defects), but even from semifluorinated $H-CF_2-CF_2-CH_2-I$ models of the "bad" PVDF chain end or inactivated alkyl iodides such as CH_3-I. These results suggest that the $Mn_2(CO)_{10}$-mediated block or graft VDF copolymerization is feasible, when initiated directly from such halides when anchored on polymeric chains, surfaces, etc.

After initiation, the polymerization type is determined by the combined effect of the $CT_{RX}^{PVDF\bullet}$ values (*i.e.* the C-X BDE of RX) (*18*, *29*), (eqs. 5, 6), the reactivity of fluorinated radicals (*i.e.* more branched, more electrophilic) (*141*), and by the preferential activation of primary vs. secondary or tertiary halides (*84*) with $Mn(CO)_5\bullet$. As such, depending of the amount of $Mn_2(CO)_{10}$ required for activation (*i.e.* the CT values) and the nature of the halide, three initiators classes can be identified, and VDF undergoes FRP or telomerization for R-X (X = Cl, Br, I) and IDT-CRP only for R_F-I. These distinctions are easily identifiable from the features of the halide chain ends in the corresponding PVDF NMRs (Figure 1).

As such, halides with strong R-X bonds only provide initiation but no chain transfer (R_{alk}-I, $CHCl_3$, and R_F-Cl, *i.e.* $Cl-CFCl-CF_2-Cl$, $Cl-(CF_2-CFCl)_{3-6}-Cl$, $CHCl_3$, $CF_3-(CF_2)_2-CO-Cl$, $Cl-CF_2-(CF_2)_6-CF_2-Cl$, CH_3-I, $CH_3-(CH_2)_4-CH_2$-I and $I-CH_2-(CH_2)_8-CH_2$-I). They do not undergo noticeable CT with PVDF$\bullet$, require stoichiometric $Mn_2(CO)_{10}$ for activation, and afford PVDF with no halide chain ends, and with visible HH defects. The lack of polymer halide termini, stems from the very low initiator CT value $CT_{RX}^{PVDF\bullet}$ << 1) and the stoichiometric amount of $Mn_2(CO)_{10}$ required, and leads to VDF-FRP.

Secondly, substrates with weaker R-X bonds (CF_3SO_2-Cl, R-CCl_3, R_F-X, X = Br, I; *i.e.* CF_3-SO_2-Cl, CCl_4, CCl_3Br, CCl_3-CCl_3, $Br-CF_2-CH_2-CF_2$-Br, $Br-CF_2-CF_2-CF_2-CF_2$-Br, $EtOOC-CF_2$-Br), do undergo CT (eqs. 5, 6), require reduced (10 %) amounts of $Mn_2(CO)_{10}$, and thus, provide at least one or both halide functionalized PVDF-X chain ends (*i.e.* -CH_2-CF_2-X and -CF_2-CH_2-X, X = Cl, Br, I, Figure 1). Here, the initiator is an efficient CT agent, but the resulting PVDF halide chain ends are less reactive ($CT_{RX}^{PVDF\bullet} > 1 > CT_{PVDF-CF_2-X}^{PVDF\bullet} \gg CT_{PVDF-CH_2-X}^{PVDF\bullet}$). As such, since the Cl- and Br-DT exchange does not occur, only telomerization or VDF-FRP is available. Likewise, the absence of reversible chain end activation prevents the accumulation of PVDF-CH_2-X. Indeed, both types of propagating chain ends abstract the initiator halide to provide the same typical ~10/1 ratio of "good"/"bad" halide chain ends, as seen in HT *vs.* HH propagation, unless the $CT_{RX}^{PVDF\bullet}$ is so low, that only the more reactive PVDF-$CH_2\bullet$ can abstract. In addition, $Mn(CO)_5\bullet$ could still activate PVDF-X chain ends (X = Cl, Br) throughout the polymerization, and some molecular weight increase could occur, although in a poorly controlled fashion.
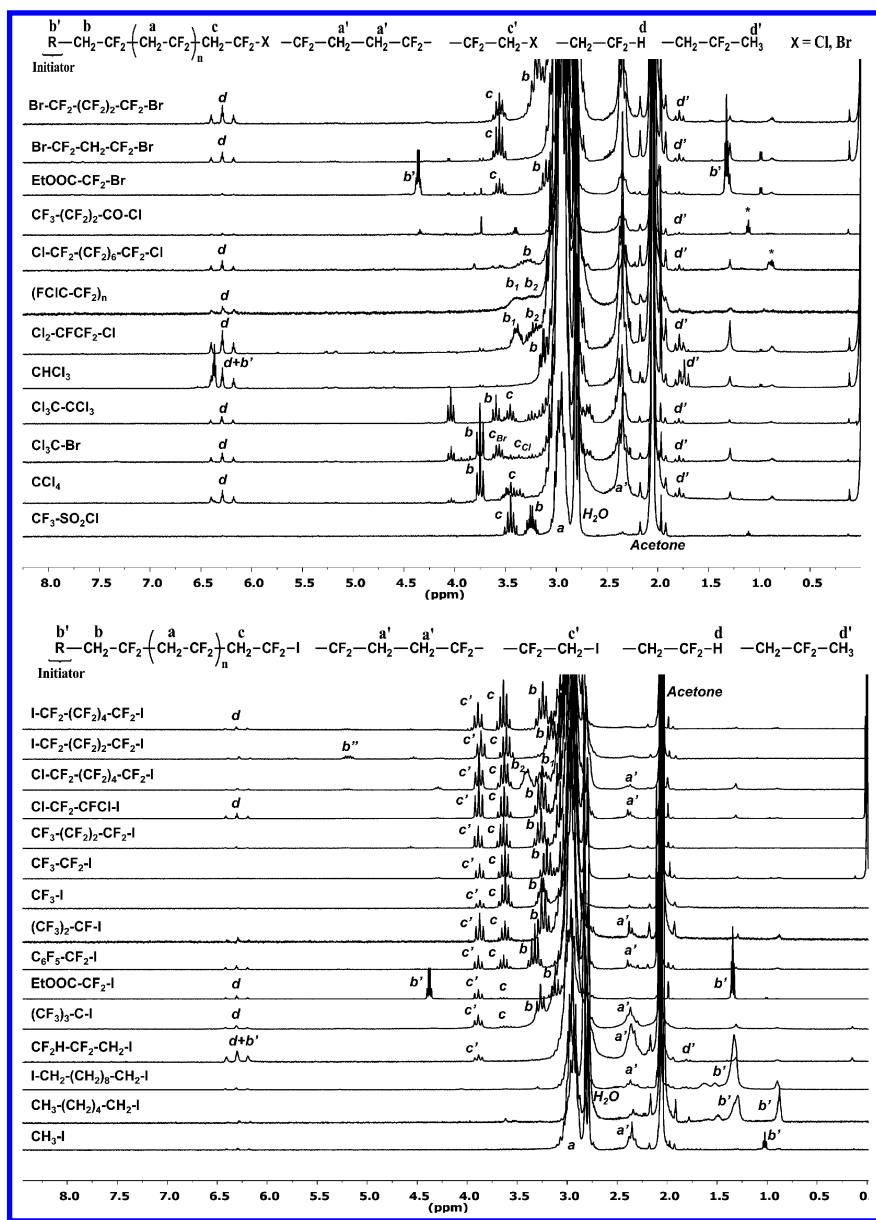
Figure 1. ¹H-NMR spectra of Mn₂(CO)₁₀-photoinitiated PVDF from Cl, Br and I based initiators substrates. Reproduced with permission from reference 51. Copyright 2012 American Chemical Society.

However, the only initiators useful in VDF-IDT-CRP and for the synthesis of PVDF-I with high chain end functionality (CEF), suitable for block copolymer synthesis or other chain end derivatizations, are semi- and perfluoroalkyl iodides. Indeed, while even efficient chain transfer agents based on Cl and Br will at most provide efficient telomerizations (*18*), uncatalyzed halide DT-CRP occurs only for iodine (*16–20*). Here, although HCF$_2$-CF$_2$-CH$_2$-I or (CF$_3$)$_3$C-I afford a less efficient IDT due to $CT_{RI}^{PVDF\bullet} \sim CT_{PVDF-CH2-I}^{PVDF\bullet} \ll 1$ and respectively Mn(CO)$_5^\bullet$ slower reaction with tertiary halides, all other activated perfluoroalkyl iodides (CF$_3$-CF$_2$-I $\sim$ (CF$_3$)$_2$CF-I < C$_6$F$_5$-CF$_2$-I, EtOOC-CF$_2$-I < Cl-CF$_2$-CFCl-I < CF$_3$-(CF$_2$)$_2$-CF$_2$-I < CF$_3$-I, < I-(CF$_2$)$_{4,6}$-I) provide not only both types of iodine chain ends, but remarkably, dramatic suppression of the HH propagation defects, and of termination by H transfer (-CF$_2$-H and -CH$_2$-H), to below 1 % via the very efficient competition of degenerative transfer $CT_{RF-I}^{PVDF\bullet} \sim CT_{C6F13-I}^{PVDF\bullet} = 7.9$ (*28*), with both propagation and termination. These high CT R$_F$-I initiators suitable for VDF-IDT (*20*), are then converted to macromolecular PVDF-I CT agents (*28*), where the terminal P$_m$-CF$_2$-CH$_2$-I (*20–31*) 2-1 unit is about 25 times less reactive towards IDT than the isomeric P$_n$-CH$_2$-CF$_2$-I 1,2-unit (*28*).

After the consumption of the R$_F$-I initiator by chain transfer, no *new* PVDF-I chains are generated, and the only productive, thermodynamically neutral, uncatalyzed, reversible iodine degenerative exchange/transfer (IDT), is the equilibrium between equally reactive, propagating and dormant P$_n$-CH$_2$-CF$_2^\bullet$ and P$_m$-CH$_2$-CF$_2$-I terminal 1,2-units (eq. 7, K$_{equil\,(ex1)}$ = 1). Here, the exchange constant, $C_{ex}^1 = k_{1,exchange}^{PVDF-CF2\bullet,\ PVDF-CF2-I}/k_{propagation,12-addition}^{PVDF-CF2\bullet,\ VDF} \gg 1$, and therefore, the exchange is favored over propagation and termination. However, the much stronger -CH$_2$-I bond, pushes the cross-IDT between the 1,2- and 2,1- units (eq. 8) towards the irreversible buildup of P$_n$-CF$_2$-CH$_2$-I chain ends. Finally, the IDT of the 2,1-terminal units is kinetically irrelevant (eq. 9) (*27, 28*).

Nonetheless, the IDT equilibrium from eqs. 7 and 8 still supports the Mn$_2$(CO)$_{10}$ mediated photo-CRP over a wide range of molecular weights IDT-CRP, as proven (*51*) (Figure 2) by the expected linear dependence of M$_n$ on conversion and by reasonable PDI values. While this does represent the first example of metal mediated VDF-CRP and the first example of visible light mediated VDF-CRP, mechanistically, with the exception of iodide chain end reactivation by Mn(CO)$_5^\bullet$ to compensate for termination, it remains a conventional IDT. Indeed, while IDT catalysis by Mn complexes would decrease PDI (*3, 10*), control experiments (*51*) show that, similar to the IDT of VAc (*102, 103*), Mn(CO)$_5$-I is photochemically inactive (*142, 143*) and unable to donate iodine.

In addition, although perfluoroalkyl manganese derivatives R$_F$-Mn(CO)$_5$ (R$_F$ = CH$_2$F, CF$_2$H) (*128*) are available, potential organometallic CRP mediation *via* reversible C-Mn bond homolysis in PVDF-Mn(CO)$_5$ is discounted based on the observed iodine not -H or -Mn(CO)$_5$ chain ends, the successful CRP with only *catalytic* Mn$_2$(CO)$_{10}$ *vs.* R$_F$-I, and in view of the relative order of the BDEs (kcal/mol) of R$_F$-Mn(CO)$_5$ (34) (*27*) < (CO)$_5$Mn-Mn(CO)$_5$ (38) (*125*) < R$_F$-I (48) (*144*) < I-Mn(CO)$_5$ (54) (*125*).

Finally, difunctional I-R$_F$-I initiators are especially appropriate for VDF-IDT, since the availability of two functional chain ends per chain (*11*), still enables the

molecular weight to continue to grow, even if one of them is lost to termination. Indeed activation by the continuously photogenerated Mn(CO)$_5^{\bullet}$ (*145*, *146*) (eq. 2), compensates for termination by radical coupling or transfer (*11*) and helps maintain a steady state radical concentration (*51*). As such, termination is not as pronounced for polymerizations initiated by I-R$_F$-I as it is for those from monofunctional R$_F$-I, as dimerization of two propagating I-PVDF$^{\bullet}$ radicals still provides I-(PVDF)$_2$-I, while H transfer affords I-PVDF-H. Consequently, while the number of chains decreases, the iodine chain end functionality is retained, can be reactivated by Mn(CO)$_5^{\bullet}$ and thus can continue to propagate and even undergo additional dimerizations. Therefore the concentration of -CH$_2$-H or -CF$_2$-H chain ends is substantially diminished while the lifetime of the chains is greatly extended. This significantly improves the livingness of the polymerization, lowers the PDI values and helps maintain a reasonably high iodine chain end functionality.
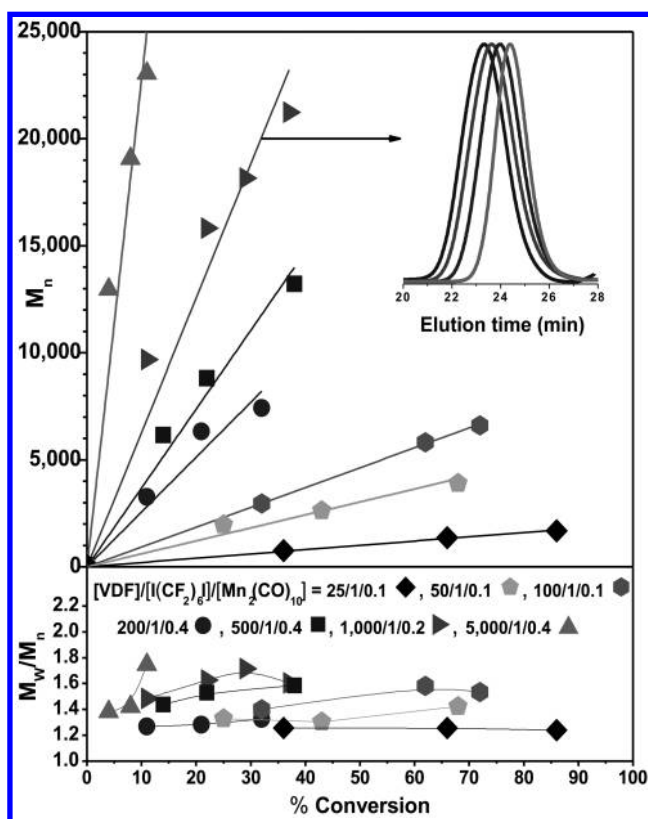
Figure 2. Dependence of M_n and M_w/M_n on conversion in Mn$_2$(CO)$_{10}$-photomediated VDF-IDT-CRP. Reproduced with permission from reference 51. Copyright 2012 American Chemical Society.

Effect on Conversion on Chain End Functionality and HH Units in IDT

Careful NMR analysis of the PVDF chain ends reveals that in IDT, the HH defects ($\delta = 2.3$-2.4 ppm) are strongly decreased (Figure 1). Obviously, IDT does not control the regioselectivity of propagation, and the 2,1-addition is just apparently prevented by CT to R_F-I. In reality, the reverse unit of the propagating chain is intercepted as the terminal P_m-CF_2-CH_2-I (*51*), which due to the very low reactivity is less likely to be activated again, and thus no longer able to propagate, transfer or terminate. Nonetheless, some reactivation if using excess $Mn(CO)_5$ ·, or much slower by IDT with ~PVDF-CF_2-CH_2·, may still provide an internal HH unit. Thus, the HH units of VDF-FRP are observed as the terminal, inactive PVDF-CF_2-CH_2-I in VDF-IDT. Since ~PVDF-CF_2-CH_2· is more reactive than ~PVDF-CH_2-CF_2· ($k_{p,21} > k_{p,12}$), the lowering of the concentration of the HH and of the terminal -CH_2-H and -CF_2-H units, is due to the faster chain transfer to R_F-I initiators by comparison to propagation ($CT_{RX}^{PVDF-CH2*} > CT_{RX}^{PVDF-CF2*} > 1$), dimerization, or H abstraction.

Consequently, the IDT-unreactive PVDF-CH_2-I chains accumulate (Figure 3) (*51*), to afford a lower molecular weight population than the dormant PVDF-CF_2-I, which can still propagate. As in VAc-IDT (*102*, *147*), their buildup leads to PDI broadening. Moreover, their reactivation will demand stronger halide abstractors than the 1,2- PVDF-CF_2-I unit (*51*). Conversely, the activators will form an even stronger bond with the halide, and the process will not be reversible.

Thus, IDT catalysis by $Mn(CO)_5$·/$Mn(CO)_5$-I would have prevented accumulation of P_n-CF_2-CH_2-I, but this was not observed. Indeed, these chain ends are rather unreactive in free radical initiated IDT or most metal mediated or organic chain end derivatizations (*27*). The continuous increase in the concentration of PVDF-CF_2-CH_2-I, indicates that at high conversions, most chains are pseudo-dead species. However, since in IDT from difunctional initiators, the total (-CF_2-CH_2-I + -CF_2-CH_2-I) iodine chain end functionality still remains > 90 % (Figure 3), block copolymers could still be synthesized if both chain ends can be activated. Indeed, this is the case with stoichiometric $Mn(CO)_5$·.

Quantitative Activation of PVDF-CF_2-CH_2-I and PVDF-CF_2-CH_2-I Chain Ends and Synthesis of Well-Defined PVDF Block Copolymers

Earlier attempts at the synthesis of PVDF blocks (*148*) included VDF initiation from macromolecular R_F-I CT agents using free radical initiators (*31*, *149*, *150*) (which inherently produces PVDF homopolymer), or simply assuming that the chain ends of PVDF-X (*136*, *151–153*) would be radically activated by Cu/ATRP (*137–139*) or thermal IDT (*136*) for the initiation of another monomer, or that both chain ends could be converted to azide groups, which is not the case (*154–156*). As described earlier, CuX/L hardly activates perfluoroalkyl halides ($k_{abstr}^{(CH3)2C(COOEt)-Br}$ / $k_{abstr}^{C8F17-Br}$ ~10^2) (*157*), and thus, would barely initiate from -CF_2CF_2-I, let alone from -CH_2CF_2-I, and especially from the unreactive -CF_2-CH_2-I chain end.
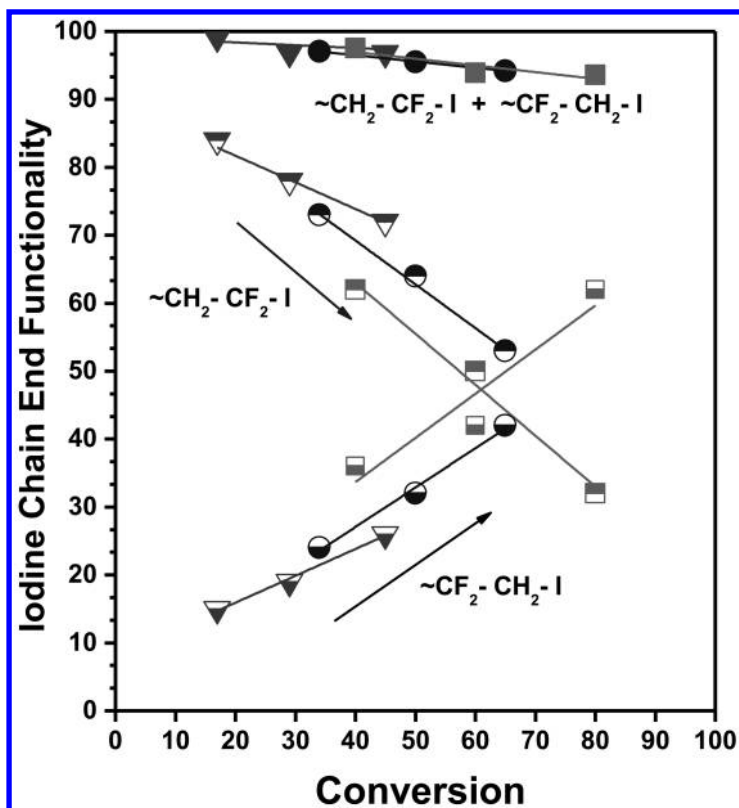
Figure 3. Dependence of the iodide chain end functionality on conversion in the $Mn_2(CO)_{10}$ photomediated VDF-IDT-CRP. $[VDF]/[I(CF_2)_6I]/[Mn_2(CO)_{10}] = 50/1/0.1$ (▾), $50/1/0.2$ (●), $50/1/0.4$ (■). Filled symbols = total functionality, top filled = $\sim CH_2$-CF_2-I, bottom filled = $\sim CF_2$-CH_2-I. Reproduced with permission from reference 51. Copyright 2012 American Chemical Society.

Most importantly, the dependence of the chain end functionality on conversion was never studied and acknowledged. Thus, with one exception (*136*), no details on the PVDF-X halide chain ends were provided, or the fact that mixtures are actually produced, was recognized and understood. Indeed, as we have shown (*51*), the concentration of the inactive PVDF-CH$_2$-I chain end increases with conversion. Thus, all high conversion PVDF-I samples previously used, were most likely > 80 % "bad" chain ends. Similarly, radical ethyleneation (*36*, *158*, *159*), or azidation (*160*) are only available for the -CH$_2$-CF$_2$-I chain end, and only at high temperature (150-200 °C), or under microwave irradiation.

It is thus clear that, due to the failure to activate the stronger and dominant -CF$_2$-CH$_2$-X termini, all previous endeavors were futile and fundamentally incomplete, and that all so-called "blocks" were in fact always ill-defined mixtures of PVDF-CH$_2$-I with PVDF-block copolymers. Thus, clean synthesis of "pure", well-defined PVDF block copolymers requires *complete* activation of both PVDF chain ends, especially of $\sim CF_2$-CH$_2$-X.

As seen in Figure 3, while the concentration of the "good" -CH$_2$-CF$_2$-I chain ends decreases, and that of the "bad" -CF$_2$-CH$_2$-I increases with conversion (*51*), the *total* (-CH$_2$-CF$_2$-I + -CF$_2$-CH$_2$-I) iodine chain functionality (CEF) remains at least 90 %, even at larger levels of Mn$_2$(CO)$_{10}$ (*51*). Such CEF is satisfactory for block copolymer synthesis, on condition that both halide chain ends are activated. This is where the Mn(CO)$_5$• proves to be a useful catalyst not only for IDT, but especially as a stoichiometric activator for block synthesis.

Indeed, Mn(CO)$_5$• enables activation not only of ~CF$_2$-I initiators, but also of the inactive CH$_3$-I, CH$_3$-(CH$_2$)$_5$-I, and H-CF$_2$-CF$_2$-CH$_2$-I PVDF-CF$_2$-CH$_2$-I models. As ~CF$_2$-CH$_2$-I and ~CH$_2$-CF$_2$-I are easier to activate than regular alkyl iodides, Mn(CO)$_5$• should afford quantitative activation of *both* PVDF chain ends. Thus, regardless of VDF-IDT conversion, *i.e.* ratio of the two iodine chain ends, they are *both* viable initiating sites in the presence of Mn(CO)$_5$•. However, while PVDF~CH$_2$-CF$_2$-I is a very good chain transfer agent that can be activated even with catalytic Mn(CO)$_5$•, PVDF~CF$_2$-CH$_2$-I requires stoichiometric activation. This is illustrated in Figure 4, for a VDF chain extension onto PVDF-I, using catalytic, and respectively, stoichiometric Mn$_2$(CO)$_{10}$.

Here, in the spectrum of the starting PVDF-I, similar to Figure 1, besides acetone and water (δ = 2.05 ppm and 2.84 ppm), the HT -CF$_2$-[C*H$_2$*-CF$_2$]$_n$-CH$_2$-, (a), and HH, -CF$_2$-C*H$_2$*-C*H$_2$*-CF$_2$- (a′) PVDF linkages (*36*, *161*) are seen (*27*) at δ = 2.8-3.1 ppm and δ = 2.3-2.4 ppm. Resonance **b** (δ = 3.25 ppm) confirms the R$_F$-C*H$_2$*-CF$_2$- connectivity with the first polymer unit, while the 1,2-C*H$_2$*-CF$_2$-I (**c**) and 2,1-CF$_2$-C*H$_2$*-I (**c′**), iodine chain ends are seen(*27*) at δ = 3.62 ppm and δ = 3.87 ppm. Trace termination by H transfer to PVDF• (eq. 11, 12), (*i.e.* -CH$_2$-CF$_2$-*H* and -CF$_2$-C*H$_3$*, peaks **d**, **d′**) is seen at δ = 6.30 ppm and δ = 1.80 ppm (*147*). Subsequently, upon using catalytic Mn$_2$(CO)$_{10}$, selective activation of only PVDF~CH$_2$-CF$_2$-I (disappearance only of δ ~ 3.65 ppm) is observed, while stoichiometric Mn$_2$(CO)$_{10}$ activates both chain ends (disappearance of both δ ~ 3.65 ppm, and δ ~ 3.85 ppm ~C*H$_2$*-CF$_2$-I and ~CF$_2$-C*H$_2$*-I).

Conversely, treatment of PVDF-I with stoichiometric Mn(CO)$_5$• in a solvent prone to chain transfer (DMAC), results in the complete radical activation of *both* iodide chain ends, and the deactivation of the PVDF• radicals by H abstraction from the solvent, to afford the corresponding PVDF-H chain ends. This is demonstrated by the disappearance of the **c** and **c′** peaks, (top Figure 5) and by the dramatic increase in the **d** and **d′** peaks, and the more resolved -CH$_2$-CF$_2$-C*H$_2$*-CF$_2$-H **d′′**, δ = 2.77 ppm (*50*, *147*).

Finally, quantitative activation of both PVDF iodide chain ends in the presence of radically polymerizable alkenes, leads to the first examples of well-defined, AB or ABA-type PVDF block copolymers (Figure 5) with styrene (St, **e, e′**), butadiene (BD, **f, f′, f′′, f′′′**), vinyl chloride (VC, **g, g′**), vinyl acetate (VAc, **h, h′**), methyl acrylate (MA, **i, i′, i′′**), and acrylonitrile (AN, **j, j′**). While here Mn$_2$(CO)$_{10}$ only performs irreversible halide activation, and there is no IDT, control of the block copolymerization can be established by other CRP methods. The characterization (*51*) of the blocks is summarized in Table 1 (*51*).
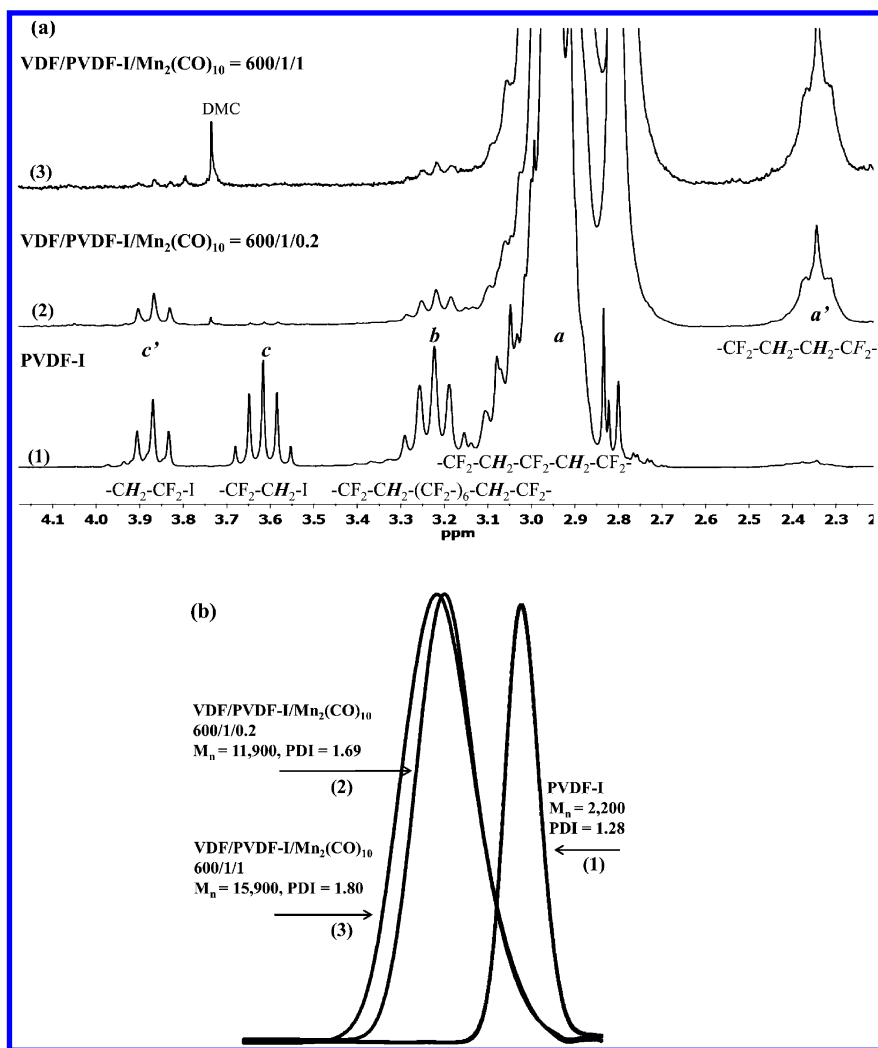
Figure 4. PVDF Chain extension from I-PVDF-I. (a) 500 MHz ^1H NMR, (b) GPC traces. (1) I-PVDF-I macroinitiator, (2) [VDF]/[I-PVDF-I]/[Mn$_2$(CO)$_{10}$] = 600/1/0.2, and (3) [VDF]/[I-PVDF-I]/[Mn$_2$(CO)$_{10}$] = 600/1/1.
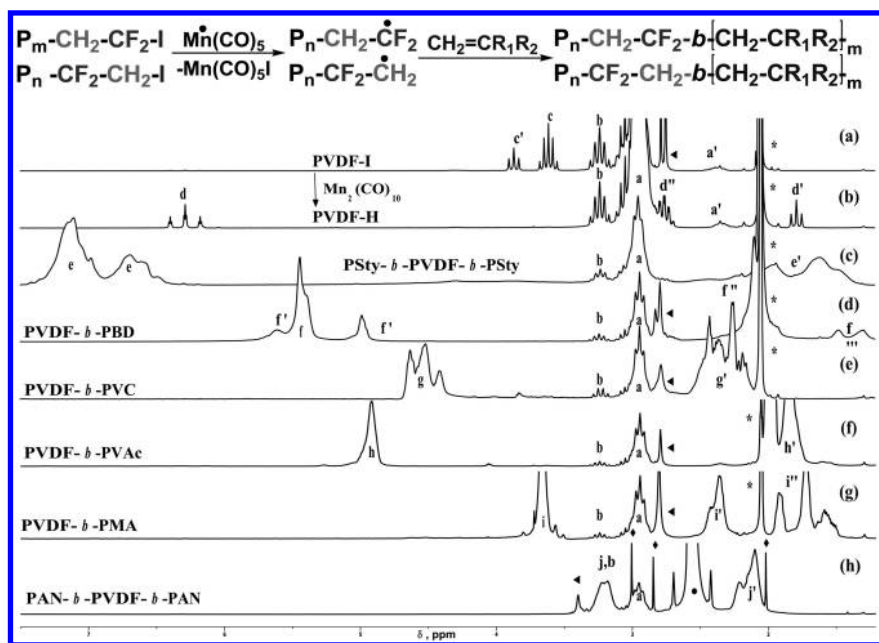
Figure 5. 500 MHz 1H-NMR spectra of PVDF-I, PVDF-H and various PVDF block copolymers. ◄ = H₂O, * = acetone, ♦ = DMAC, ● = DMSO. Reproduced with permission from reference (51). Copyright 2012 American Chemical Society.

Table 1. Mn₂(CO)₁₀ Photomediated Synthesis of PVDF Block Copolymers.[a] Adapted with permission from reference 51. Copyright 2012 American Chemical Society.

Exp	M	PVDF-I or I-PVDF-I		[M]/ [PVDF-I]/ [Mn₂(CO)₁₀]	Conv (%)	Blocks		
		M_n	PDI			Comp-osition M/VDF	M_n	PDI
1	St[b,c]	2,500	1.34	60/1/2	67	70/30	14,500	2.25
2	BD[c]	1,400	1.48	200/1/1	25	62/38	4,700	2.00
3	VC[d]	1,800	1.29	100/1/1	35	77/23	20,100	1.52
4	VA	1,500	1.49	100/1/0.2	30	65/35	11,000	1.70
5	MA	2,300	1.52	75/1/4	40	72/28	9,000	2.46
6	AN[b]	2,100	1.31	50/1/1	25	74/26	25,800	2.33

[a] T = 40 °C and solvent = DMAC except where noted.   [b] Block copolymers from I-PVDF-I samples.   [c] Polymerization was carried out at 110 °C,   [d] in dioxane.

Conclusions

Using a photochemical approach based on the visible light, dissociation of $Mn_2(CO)_{10}$ to $Mn(CO)_5^\bullet$, we have shown that by contrast to high pressure, high temperature reactions carries out in metal reactors, the metal catalyzed initiation of the polymerization of main chain fluorinated gaseous monomers including VDF, can easily be accomplished at ambient temperatures, by direct activation of wide variety of alkyl, semifluorinated and perfluoroalkyl halides (Cl, Br, I) in low pressure glass tubes, and employing dimethyl carbonate and solvent.

Moreover, perfluorinated alkyl iodides, especially difunctional I-R_F-I species, are most suitable for the iodine degenerative transfer (IDT) mechanism, which enables controlled radical polymerizations of VDF with very high (> 95 %) iodide chain end functionality and < 1% HH defects.

In addition, although the concentration of active -CH_2-CF_2-I decreases and that of unreactive -CF_2-CH_2-I PVDF chain ends increases with conversion, their sum remains relatively constant, and their subsequent quantitative activation with $Mn_2(CO)_{10}$ affords well-defined PVDF block copolymers with a variety of monomers.

The synthetic advantages afforded by this photochemistry (direct halide VDF initiation, VDF-IDT-CRP and the quantitative iodide chain ends activation), open up novel strategies for the synthesis of pure and well-defined, architecturally complex fluoromaterials. Indeed, main chain fluorinated monomers can be now easily be block copolymerized or grafted from substrates containing halide initiators, and respectively, the polymerization of other monomers can be initiated quantitatively from the halide chain ends of such fluoropolymers, without mixture formation. Moreover, using multifunctional initiators, star and hyperbranched fluoropolymers can also be envisioned. Finally, the R_F-I/$Mn_2(CO)_{10}$ procedure is also applicable in radical trifluoromethylation/perfluoroalkylation reactions which are in great demand in organic/medicinal chemistry (*49*).

Acknowledgments

References

1. Ameduri, B. *Macromolecules* **2010**, *43*, 10163–10184.
2. Lena, F.; Matyjaszewski, K. *Prog. Polym. Sci.* **2010**, *35*, 959–1021.
3. *Handbook of Radical Polymerization*; Matyjaszewski, K., Davis, T. P., Eds.; Wiley: New York, 2002.
4. Braunecker, W. A.; Matyjaszewski, K. *Prog. Polym. Sci.* **2007**, *32*, 93–146.
5. Goto, A.; Fukuda, T. *Prog. Polym. Sci.* **2004**, *29*, 329–385.
6. Fukuda, T. *J. Polym. Sci., Part A: Polym. Chem.* **2004**, *42*, 4743–4755.
7. Ameduri, B. *Chem. Rev.* **2009**, *109*, 6632–6686.
8. Hansen, N. M. L.; Jankova, K.; Hvilsted, S. *Eur. Polym. J.* **2007**, *43*, 255–293.

9. Gillies, M. B.; Matyjaszewski, K.; Norrby, P. O.; Pintauer, T.; Poli, R.; Richard, P. *Macromolecules* **2003**, *36*, 8551–8559.

10. Fukuda, T.; Goto, A.; Tsujii, Y. Kinetics of Living Radical Polymerization. In *Handbook of Radical Polymerization*; Matyjaszewski, K., Davis, T. P., Eds.; Wiley: New York, 2002; pp 407−462.

11. Oka, M.; Tatemoto, M. Vinylidene fluoride-hexafluoropropylene copolymer having terminal iodines. In *Contemporary Topics in Polymer Science*; Bailey, W. J., Tsuruta, T., Eds.; Plenun Press: New York, 1984; Vol. 4, pp 763−781.

12. Tatemoto, M. *Int. Poly. Sc. Tech.* **1985**, *12*, 85–98.

13. Tatemoto, M. In *Polymeric Materials Encyclopedia*; Salamone, J. C., Ed.; CRC Press: Boca Raton, FL, 1996; Vol. 5, pp 3847−3862.

14. Tatemoto, M.; Shimizu, T. Thermoplastic Elastomers. In *Modern Fluoropolymers*; Scheirs, J., Ed.; Wiley: New York, 1997; pp 565−576.

15. Tatemoto, M.; Nakagawa, T. U.S. Patent 4,158,678, 1979.

16. Gaynor, S. G.; Wang, J. S.; Matyjaszewski, K. *Macromolecules* **1995**, *28*, 8051–8056.

17. Boutevin, B. *J. Polym. Sci., Part A: Polym. Chem.* **2000**, *38*, 3235–3243.

18. Ameduri, B.; Boutevin, B. *Top. Curr. Chem.* **1997**, *192*, 165–233.

19. Ameduri, B.; Boutevin, B.; *Well Architectured Fluoropolymers: Synthesis, Properties and Applications*; Elsevier: Amsterdam, 2004; pp 1−99.

20. David, G.; Boyer, C.; Tonnar, J.; Ameduri, B.; Lacroix-Desmazes, P.; Boutevin, B. *Chem. Rev.* **2006**, *106*, 3936–3962.

21. Ameduri, B.; Ladavière, C.; Delolme, F.; Boutevin, B. *Macromolecules* **2004**, *37*, 7602–7612.

22. Montefusco, F.; Bongiovanni, R.; Priola, A.; Ameduri, B. *Macromolecules* **2004**, *37*, 9804–9813.

23. Cape, J. N.; Greig, A. C.; Tedder, J. M.; Walton, J. C. *J. Chem. Soc., Faraday Trans. 1: Phys. Chem. Condens. Phases* **1975**, *71*, 592–601.

24. Hauptschein, M.; Braid, M.; Lawlor, F. E. *J. Am. Chem. Soc.* **1958**, *80*, 846–851.

25. Soueni, A. E.; Tedder, J. M.; Walton, J. C. *J. Fluorine Chem.* **1978**, *11*, 407–417.

26. Combes, J. R.; Guan, Z.; DeSimone, J. M. *Macromolecules* **1994**, *27*, 865–886.

27. Boyer, C.; Valade, D.; Sauguet, L.; Ameduri, B.; Boutevin, B. *Macromolecules* **2005**, *38*, 10353–10362.

28. Boyer, C.; David, V.; Lacroix-Desmazes, P.; Ameduri, B.; Boutevin, B. *J. Polym. Sci., Part A: Polym. Chem.* **2006**, *44*, 5763–5777.

29. Imran-ul-haq, M.; Förster, N.; Vukicevic, R.; Herrmann, K.; Siegmann, R.; Beuermann, S. *ACS Symp. Ser.* **2009**, *1024*, 233–243.

30. Apostolo, M.; Arcella, V.; Storti, G.; Morbidelli, M. *Macromolecules* **2002**, *35*, 6154–6166.

31. Valade, D.; Boyer, C.; Ameduri, B.; Boutevin, B. *Macromolecules* **2006**, *39*, 8639–8651.

32. MacMurray, N.; Tedder, J. M.; Vertommen, L. L. T.; Walton, J. C. *J. Chem. Soc., Perkin Trans.* **1976**, *2*, 63–69.

33. Hung, M. H. U.S. Patent 5,231,154, 1993.

34. Low, H. C.; Tedder, J. M.; Walton, J. C. *J. Chem. Soc., Faraday Trans. 1: Phys. Chem. Condens. Phases* **1976**, *72*, 1707–1714.

35. Apostolo, M.; Arcella, V.; Storti, G.; Morbidelli, M. *Macromolecules* **1999**, *32*, 989–1003.

36. Ameduri, B.; Boutevin, B. *J. Fluorine Chem.* **1999**, *100*, 97–116.

37. Siegmann, R.; Drache, M.; Beuermann, S. *Macromolecules* **2013**, *46*, 9507–9514.

38. Zhang, Z. C.; Chung, T. C. *Macromolecules* **2006**, *39*, 5187–5189.

39. Balague, J.; Ameduri, B.; Boutevin, B.; Caporiccio, G. *J. Fluorine Chem.* **1995**, *70*, 215–223.

40. Balague, J.; Ameduri, B.; Boutevin, B.; Caporiccio, G. *J. Fluorine Chem.* **2000**, *102*, 253–268.

41. Yang, Z. Y.; Burton, D. J. *J. Org. Chem.* **1991**, *56*, 1037–1041.

42. Tsunoi, S.; Ryu, I.; Fukushima, H.; Tanaka, M; Komatsu, M.; Noburu, S. *Synlett* **1999**, *5*, 1249–1252.

43. Benefice-Malouet, S.; Blancou, H.; Commeyras, A. *J. Fluorine Chem.* **1993**, *63*, 217–226.

44. Nguyen, B. V.; Yang, Z. Y.; Burton, D. J. *J. Org. Chem.* **1998**, *63*, 2887–2891.

45. Li, A. R.; Chen, Q. Y. *J. Fluorine Chem.* **1997**, *81*, 99–101.

46. Chen, M. Y.; Yang, Z. Y.; Zhao, C. X.; Qiu, Z. M. *J. Chem. Soc., Perkin Trans. I* **1988**, *3*, 563.

47. Metzerg, J. O.; Linker, U. *Liebigs Ann. Chem.* **1992**, *3*, 209–216.

48. Hu, C. M.; Qiu, Y. L. *J. Chem. Soc., Perkin Trans. 1.* **1992**, *13*, 1569–1572.

49. Pham, P. V.; Nagib, D. A.; MacMillan, D. W. C. *Angew. Chem., Int. Ed.* **2011**, *50*, 1–5.

50. Asandei, A. D.; Adebolu, O. I.; Simpson, C. P. *ACS Symp. Ser.* **2012**, *1106*, 47–63.

51. Asandei, A. D.; Adebolu, O. I.; Simpson, C. P. *J. Am. Chem. Soc.* **2012**, *134*, 6080–6083.

52. Asandei, A. D.; Adebolu, O. I.; Simpson, C. P.; Kim, J. S. *Angew. Chem., Int. Ed.* **2013**, *52*, 10027–10030.

53. Asandei, A. D.; Adebolu, O. I.; Simpson, C. P. In *Handbook of Fluoropolymer Science and Technology*; Smith, D. W., Iacono, S. T., Iyer, S. S., Eds.; John Wiley & Sons Inc.: Hoboken, NJ, USA, 2014; Ch. 2., pp 21−42.

54. Asandei, A. D.; Simpson, C. P.; Adebolu, O.; Chen, Y. *Polym. Prepr.* **2011**, *52*, 728–729.

55. Asandei, A. D.; Simpson, C. P.; Adebolu, O.; Chen, Y. *Polym. Prepr.* **2011**, *52*, 554–555.

56. Sauguet, L.; Boyer, C.; Ameduri, B.; Boutevin, B. *Macromolecules* **2006**, *39*, 9087–9101.

57. Siegmann, R.; Drache, M.; Beuermann, S. *Macromolecules* **2013**, *46*, 9507–9514.

58. Messina, M. T.; Metrangolo, P.; Resnati, G. *ACS Symp. Ser.* **1999**, *746*, 239–254.

59. Asandei, A. D.; Moran, I. W. *J. Am. Chem. Soc.* **2004**, *126*, 15932–15933.

60. Asandei, A. D.; Saha, G. *Macromolecules* **2006**, *39*, 8999–9009.
61. Asandei, A. D.; Chen, Y. *Macromolecules* **2006**, *39*, 7459–7554.
62. Asandei, A. D.; Moran, I. W.; Saha, G.; Chen, Y. *ACS Symposium Ser.* **2006**, *944*, 125–139.
63. Asandei, A. D.; Moran, I. W.; Saha, G.; Chen, Y. *J. Polym. Sci., Part A: Polym. Chem.* **2006**, *44*, 2156–2165.
64. Asandei, A. D.; Moran, I. W.; Saha, G.; Chen, Y. *J. Polym. Sci., Part A: Polym. Chem.* **2006**, *44*, 2015–2026.
65. Asandei, A. D.; Moran, I. W. *J. Polym. Sci., Part A: Polym. Chem.* **2006**, *44*, 1060–1070.
66. Asandei, A. D.; Saha, G. *J. Polym. Sci., Part A: Polym. Chem.* **2006**, *44*, 1106–1116.
67. Asandei, A. D.; Moran, I. W. *J. Polym. Sci., Part A: Polym. Chem.* **2005**, *43*, 6039–6047.
68. Asandei, A. D.; Moran, I. W. *J. Polym. Sci., Part A: Polym. Chem.* **2005**, *43*, 6028–6038.
69. Asandei, A. D.; Chen, Y.; Saha, G.; Moran, I. W. *Tetrahedron* **2008**, *64*, 11831–11838.
70. Asandei, A. D.; Chen, Y.; Moran, I. W.; Saha, G. *J. Organomet. Chem.* **2007**, *692*, 3174–3182.
71. Asandei, A. D.; Moran, I. W.; Saha, G; Chen, Y. *Mater. Res. Soc. Symp. Proc.* **2005**, *856E*, BB11.9.1–BB11.9.6.
72. Asandei, A. D.; Simpson, C. P.; Yu, H. S.; Adebolu, O. I.; Saha, G.; Chen, Y. *ACS Symp. Ser.* **2009**, *1024*, 149–166.
73. Asandei, A. D.; Chen, Y.; Adebolu, O. I.; Simpson, C. P. *J. Polym. Sci., Part A: Polym. Chem.* **2008**, *46*, 2869–2877.
74. Asandei, A. D.; Saha, G. *Macromol. Rapid Commun.* **2005**, *26*, 626.
75. Rowlands, G. J. *Tetrahedron* **2009**, *65*, 8603–8655.
76. Gilbert, B. C.; Parsons, A. *J. Chem. Soc., Perkin Trans. 2* **2002**, *3*, 367–387.
77. Haszeldine, R. N.; Steele, B. R. *J. Chem. Soc.* **1954**, 923–925.
78. Saint-Loup, R.; Ameduri, B. *J. Fluorine Chem.* **2002**, *116*, 27–34.
79. Asandei, A. D.; Chen, Y. *Polym. Mater.: Sci. Eng.* **2008**, *98*, 346–347.
80. Asandei, A. D.; Chen, Y. *Polym. Prepr.* **2007**, *48*, 452–453.
81. Asandei, A. D.; Chen, Y. *Polym. Mater.: Sci. Eng.* **2007**, *97*, 270–271.
82. Asandei, A. D.; Chen, Y. *Polym. Prepr.* **2005**, *46*, 633.
83. Abrahamson, H.; Wrighton, M. S. *J. Am. Chem. Soc.* **1977**, *99*, 5510–5512.
84. Meckstroth, W. K.; Walters, R. T.; Waltz, W. L.; Wojcicki, A.; Dorfman, L. M. *J. Am. Chem. Soc.* **1982**, *104*, 1842–1846.
85. Fawcett, J. P.; Poe, A.; Sharma, K. R. *J. Chem. Soc., Dalton Trans.: Inorg. Chem.* **1979**, *12*, 1886–90.
86. Brimm, E. O.; Lynch, M. A., Jr.; Sesny, W. J. *J. Am. Chem. Soc.* **1954**, *76*, 3831–3835.
87. Treichel, P. M. Manganese Carbonyls and Manganese Carbonyl Halides. In *Comprehensive Organometallic Chemistry II*; Abel, E. W., Stone, F. G. A., Wilkinson, G., Casey C., Eds.; Elsevier: 1995; Vol. 6, Manganese group, pp 1–19.

88. Tenhaeff, S. C.; Covert, K. J.; Castellani, M. P.; Grunkemeier, J.; Kunz, C.; Weakley, T.; Koenig, T.; Tyler, D. R. *Organometallics* **1993**, *12*, 5000–5004.
89. Martinho Simoes, J. A.; Beauchamp, J. A. *Chem. Rev.* **1990**, *90*, 629–688.
90. Friestad, G. K.; Qin, J. *J. Am. Chem. Soc.* **2001**, *123*, 9922–9923.
91. Jackson, R. A.; Poe, A. *Inorg. Chem.* **1978**, *17*, 997–1003.
92. Fawcett, J. P.; Poe, A.; Sharma, K. R. *J. Am. Chem. Soc.* **1976**, *98*, 1401.
93. Rothberg, L. J.; Cooper, J. N.; Peters, K. S.; Vaida, V. *J. Am. Chem. Soc.* **1982**, *104*, 3536–3537.
94. *Comprehensive Organometallic Chemistry III*; Robert, H. C., Michael, P., Eds.; Elsevier: Providence, RI, 2007; Vol. 5; pp 440−746.
95. Zhang, J. Z.; Harris, C. B. *J. Chem. Phys.* **1991**, *95*, 4024–4032.
96. Sarakha, M.; Ferraudi, G. *Inorg. Chem.* **1999**, *38*, 4605–4607.
97. Sullivan, R. J.; Brown, T. L. *J. Am. Chem. Soc.* **1991**, *113*, 9155–9161.
98. Gilbert, B. C.; Kalz, W.; Lindsay, C. I.; McGrail, P. T.; Parsons, A. F.; Whittaker, D. T. E. *J. Chem. Soc., Perkin Trans. 1* **2000**, 1187–1194.
99. Gilbert, B. C.; Lindsay, C. I.; McGrail, P. T.; Parsons, A. F.; Whittaker, D. T. E. *Synth. Commun.* **1999**, *29*, 2711–2718.
100. Hallock, S. A.; Wojcicki, A. *J. Organomet. Chem.* **1979**, *182*, 521–35.
101. Bamford, C. H.; Mahmud, M. U. *J. Chem. Soc., Chem. Commun.* **1972**, *13*, 762–3.
102. Bamford, C. H.; Mullik, S. U. *Polymer* **1973**, *14*, 38–39.
103. Bamford, C. H.; Mullik, S. U. *Polymer* **1976**, *17*, 225–30.
104. Aliwi, S. M.; Bamford, C. H.; Mullik, S. U. *J. Polym. Sci., Polym. Symp.* **1975**, *50*, 33–50.
105. Bamford, C. H.; Mullik, S. U. *J. Chem. Soc., Faraday Trans. 1* **1975**, *71*, 625–636.
106. Bamford, C. H.; Mullik, S. U. *Polymer* **1976**, *17*, 94–95.
107. Bamford, C. H.; Mullik, S. U. *J. Chem. Soc., Faraday Trans. 1* **1976**, *72*, 368–375.
108. Bamford, C. H.; Denyer, R. *Nature* **1968**, *217*, 59–60.
109. Bamford, C. H.; Duncan, F. J.; Reynolds, R. J. W.; Seddon, J. D. *J. Polym. Sci., Part C: Polym. Symp.* **1968**, *23*, 419–432.
110. Bamford, C. H.; Dyson, R. W.; Eastmond, G. C. *J. Polym. Sci., Part C* **1967**, *16*, 2425–2234.
111. Jiang, M.; Wang, S.; Jin, X. *J. Mater. Sci. Lett.* **1990**, *9*, 1239–1240.
112. Jenkins, D. W.; Hudson, S. M. *Macromolecules* **2002**, *35*, 3413–3419.
113. Eastmond, G. C.; Parr, K. J.; Woo, J. *Polymer* **1988**, *29*, 950–957.
114. Eastmond, G. C.; Richardson, J. E. *Macromolecules* **1991**, *24*, 3189–3200.
115. Iskin, B.; Yilmaz, G.; Yagci, Y. *Macromol. Chem. Phys.* **2013**, *214*, 94–98.
116. Koumura, K.; Satoh, K.; Kamigaito, M. *Macromolecules* **2008**, *41*, 7359–7367.
117. Koumura, K.; Satoh, K.; Kamigaito, M. *J. Polym. Sci.: Part A: Polym. Chem.* **2009**, *47*, 1343–1353.
118. Koumura, K.; Satoh, K.; Kamigaito, M. *Macromolecules* **2009**, *42*, 2497–2504.
119. Kimura, K.; Satoh, K; Kamigaito, M. *Polym. J.* **2009**, *41*, 595–603.

120. Curran, D. P.; Bosch, E.; Kaplan, J.; Newcomb, M. *J. Org. Chem.* **1989**, *54*, 1826–1831.
121. Wrighton, M. S.; Ginley, D. S. *J. Am. Chem. Soc.* **1975**, *97*, 2065–2072.
122. Doll, W. W.; Lando, J. B. *J. Appl. Polym. Sci.* **1970**, *14*, 1767–73.
123. Russo, S.; Behari, K.; Chengji, S.; Pianca, M.; Barchiesi, E.; Moggi, G. *Polymer* **1993**, *22*, 4777–478134.
124. Duc, M.; Ameduri, B.; Boutevin, B.; Kharroubi, M.; Sage, J.-M. *Macromol. Chem. Phys.* **1998**, *199*, 1271–1289.
125. Galin, M.; Maslinkot, L. *Macromolecules* **1985**, *18*, 2192–2196.
126. Galin, J. C.; Lutringer, G.; Galin, M. *J. Appl. Polym. Sci.* **1989**, *37*, 487–498.
127. Lutringer, G.; Meurer, B.; Weill, G. *Polymer* **1991**, *32*, 884–891.
128. Kutringer, G.; Weill, G. *Polymer* **1991**, *32*, 877–883.
129. Bottino, A.; Campanelli, G.; Munari, S.; Turturro, A. *J. Polym. Sci., Part B: Polym. Phys.* **1988**, *26*, 785–794.
130. Lee, W. H. In *Chemistry of Nonaqueous Solvents*; Lagowski, J. J., Ed.; Academic Press: New York, 1976; Vol. 4, p 167.
131. Tundo, P.; Selva, M. *Acc. Chem. Res.* **2002**, *35*, 706–716.
132. Odian, G. *Principles of Polymerization*, 4th ed.; Wiley: 2004; pp 292−298.
133. Ahmeda, T. S.; DeSimone, J. M.; Roberts, G. W. *Chem. Eng. Sci.* **2010**, *65*, 651–659.
134. Gordon, A. S.; Norris, W. P. *J. Phys. Chem.* **1965**, *69*, 3013–17.
135. Burchill, M. T. *Prog. Batteries Battery Mater.* **1998**, *17*, 144–156.
136. Saunier, J.; Alloin, F.; Sanchez, J. Y.; Barriere, B. *J. Polym. Sci., Part B: Polym. Phys.* **2004**, *42*, 532–543.
137. Saunier, J.; Alloin, F.; Sanchez, J. Y.; Barriere, B. *J. Polym. Sci., Part B: Polym. Phys.* **2004**, *42*, 544–552.
138. Freunberger, S. A.; Chen, Y.; Peng, Z.; Griffin, J. M.; Hardwick, L. J.; Barde, F.; Novak, P.; Bruce, P. G. *J. Am. Chem. Soc.* **2011**, *133*, 8040–8047.
139. Drago, R.; Wong, N. M.; Ferris, D. C. *J. Am. Chem. Soc.* **1992**, *114*, 91–98.
140. Duc, M.; Ameduri, B.; Ghislain, D.; Boutevin, B. *J. Fluorine Chem.* **2007**, *128*, 144–149.
141. Dolbier, W. R., Jr. *Top. Curr. Chem.* **1997**, *192*, 97–163.
142. Pan, X.; Philbin, C. E.; Castellani, M. P.; Tyler, D. R. *Inorg. Chem.* **1988**, *27*, 671–676.
143. Martinho-Simoes, J. A.; Beauchamp, J. L. *Chem. Rev.* **1990**, *90*, 629–688.
144. Okafo, E. N.; Whittle, E. *Int. J. Chem. Kinet.* **1975**, *7*, 287–300.
145. Sarakha, M.; Ferraudi, G. *Inorg. Chem.* **1999**, *38*, 4605–4607.
146. Hughey, J. L.; Anderson, C. P.; Meyer, T. J. *J. Organomet. Chem.* **1977**, *125*, C49–C52.
147. Koumura, K.; Satoh, K.; Kamigaito, M. *Macromolecules* **2006**, *39*, 4054–4061.
148. Voet, V. S.; Brinke, G.; Loos, K. *J. Polym. Sci., Part A: Polym. Chem.* **2014**, *52*, 2861–2877.
149. Gelin, M.; Ameduri, B. *J. Polym. Sci., Part A: Polym. Chem.* **2003**, *41*, 160–171.
150. Laruelle, G.; Nicol, E.; Ameduri, B.; Tassin, J. F; Ajellal, N. *J. Polym. Sci., Part A: Polym. Chem.* **2011**, *49*, 3960–3969.

151. Ming, E.; Tsang, W.; Shi, Z.; Holdcroft, S. *Macromolecules* **2011**, *44*, 8845–8857.
152. Yang, Y.; Shi, Z.; Holdcroft, S. *Macromolecules* **2004**, *37*, 1678–1681.
153. Jol, S.; Lee, W.; Ahn, B.; Park, K.; Paeng, I. *Polym. Bull.* **2000**, *44*, 1–8.
154. Vukicevic, R.; Vukovic, I.; Stoyanov, H.; Korwitz, A.; Pospiech, D.; Kofod, G.; Loos, K.; ten Brinke, G.; Beuermann, S. *Polym. Chem.* **2012**, *3*, 2261–2265.
155. Vukicevic, R.; Schwadtke, U.; Schmucker, S.; Schafer, P.; Kuckling, D.; Beuermann, S. *Polym. Chem.* **2012**, *3*, 409–414.
156. Voet, V. S. D.; Gert, O. R.; Alberda, G. O. R.; van Ekenstein, G. O. R. A.; Niels, L.; Meereboer, N. L.; Anton, H.; Hofman, A. H.; ten Brinke, G.; Loos, K. *Polym. Chem.* **2014**, *5*, 2219–2230.
157. Sauguet, L.; Boyer, C.; Ameduri, B.; Boutevin, B. *Macromolecules* **2006**, *39*, 9087–9101.
158. Manseri, A.; Ameduri, B.; Boutevin, B.; Kotora, M.; Caporiccio, G. *J. Fluorine Chem.* **1997**, *81*, 103–113.
159. Balague, J.; Ameduri, B.; Boutevin, B.; Caporiccio, G. *J. Fluorine Chem.* **2000**, *102*, 253–268.
160. Vukicevic, R.; Beuermann, S. *Macromolecules* **2011**, *44*, 2597–2603.
161. Wormald, P.; Ameduri, B.; Harris, R. K.; Hazendonk, P. *Polymer* **2008**, *49*, 3629–3638.

Chapter 12

RAFT Polymerization – Then and Now

Graeme Moad*

CSIRO Manufacturing Flagship, Bayview Ave, Clayton, Victoria 3168, Australia
***E-mail: graeme.moad@csiro.au**

Publication Date (Web): May 1, 2015 | doi: 10.1021/bk-2015-1187.ch012

RAFT Polymerization is currently one of the most versatile and most used methods for implementing reversible deactivation radical polymerization (RDRP) otherwise known as controlled or living radical polymerization. This paper will briefly trace the historical development of RAFT with reference to the kinetics and mechanism of the process. It will also highlight the most recent developments in our laboratories at CSIRO during the period 2011-2014 specifically covering such areas as kinetics and mechanism, RAFT agent development, end-group transformation, RAFT crosslinking polymerization, monomer sequence control and multi-block copolymer synthesis, and high throughput RAFT polymerization.

Introduction

The historical development of RAFT (reversible addition-fragmentation chain transfer) polymerization at CSIRO (*1–3*) and the parallel development of MADIX (macromolecular design via interchange of xanthates) at Rhodia (*4, 5*) has been described in a number of recent reviews. The invention of RAFT at CSIRO should be seen against a background of research into defining and understanding polymer structures and on controlling the outcome of radical polymerization that had commenced more than two decades earlier. By the mid-nineties this work had already led to significant developments in control of polymer structure using chain transfer processes, to the invention of nitroxide mediated polymerization (NMP), and to the establishment of a Strategic Alliance with DuPont to further these goals (*3, 6*). The discovery of RAFT was aided by a research environment that allowed the rapid shifting of priorities necessary to follow up sometimes serendipitous observations without rigorous justification.

Published 2015 by the American Chemical Society

In Controlled Radical Polymerization: Mechanisms; Tsarevsky, et al.;
ACS Symposium Series; American Chemical Society: Washington, DC, 2015.

In the early 1980s radical polymerization was seen as a mature technology with little scope for technological improvement. The 20 years has seen a remarkable transformation such that radical polymerization is now one of the most active and fertile fields for research into polymer synthesis. This turnaround is largely attributable to the development of techniques for reversible deactivation radical polymerization (RDRP) (*7*), often called living or controlled radical polymerization, which impart living character to the polymerization. These techniques include NMP (*3*, *8*, *9*), Atom Transfer Radical Polymerization (ATRP) (*10–13*) and RAFT polymerization (*1–3*, *14–18*). Papers relating to these methods now account for more than two-thirds of all papers on radical polymerization (*19*).

In conventional radical polymerization (non-RDRP) (*19*), chains are initiated by radicals formed from an initiator adding to monomer (Scheme 1). These chains ($P_n\cdot$, $P_m\cdot$) propagate by sequential addition of monomer. Chain termination occurs when the propagating radicals self-react by combination or disproportionation. Initiation and termination occur continuously to provide a steady-state radical concentration of only ~10^{-7} M such that the lifetime of an individual chain is typically ~5-10 seconds in an overall reaction span of several hours. For a conventional radical polymerization carried out in the absence of chain transfer agents, the average length of the chains formed initially is high and, not withstanding auto-acceleration through the gel or Trommsdorf effect, will decrease with conversion because of monomer depletion (*20*). The breadth of the molecular weight distribution is governed by statistical factors. The dispersity (*Đ*), the ratio of weight to number average molecular weights (M_w/M_n), is ideally 2.0, if termination occurs by disproportionation or chain transfer, or 1.5, if termination is by combination (*20*).
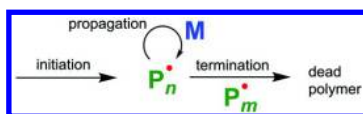
Scheme 1. Simplified mechanism for radical polymerization

In an ideal living polymerization (*21–23*), all chains are initiated at the commencement of the process, grow at a similar rate and all survive the polymerization. There is no chain death by termination or irreversible chain transfer. Thus, long as the rate of initiation is rapid with respect to that of propagation, the molar mass distribution of chains will be narrow (*Đ* less than 1.1) and chains can be extended indefinitely with the provision of monomer.

Radical polymerization is applicable to a vast range of monomers. The technique is compatible with unprotected functionality in monomer and solvent and with a wide variety of reaction conditions. Living (anionic) polymerization is applicable only to a limited number of monomers and demands stringent control over process conditions to achieve the outcomes mentioned. The use of conventional radical polymerization imposes severe constraints on the degree of control that can be asserted over molar mass distributions, copolymer

compositions and macromolecular architectures. However, the relative simplicity and low cost of implementation saw the technique widely adopted for the commercial production of high molecular weight polymers (*19*).

In a radical polymerization, the propensity of radicals to undergo self-termination means that all chains cannot be simultaneously active. Thus, a living radical polymerization as per the IUPAC definition is not possible. The concept of living radical polymerization was introduced by Otsu and coworkers in 1982 (*24*, *25*). They recognized that living attributes might be displayed in the presence of reagents that are capable of reversibly deactivating active chains (propagating radicals, $P_n\bullet$), such that the majority of living chains are maintained in a dormant form (P_n-X), and reaction conditions that support a rapid equilibrium between active and dormant chains. Such reversible deactivation may occur by a coupling-dissociation mechanism (Scheme 2) or by degenerative chain transfer (Scheme 3).
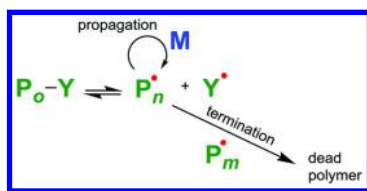
Scheme 2. Simplified mechanism for reversible deactivation radical polymerization with reversible disassociation
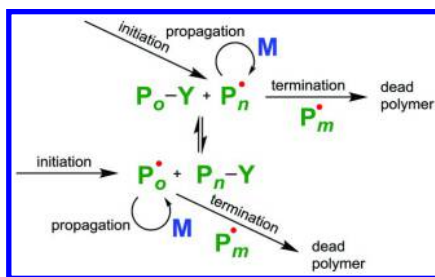
Scheme 3. Simplified mechanism for reversible deactivation radical polymerization with degenerate chain transfer

Addition-Fragmentation Chain Transfer

The discovery of RAFT came out of studies on control of polymerization using chain transfer processes. The best known mechanism for chain transfer is the homolytic substitution process (Scheme 4). Some typical transfer agents in this context are thiols (Y=H, X=S) and halocarbons (Y=halogen, X=CR″$_2$).
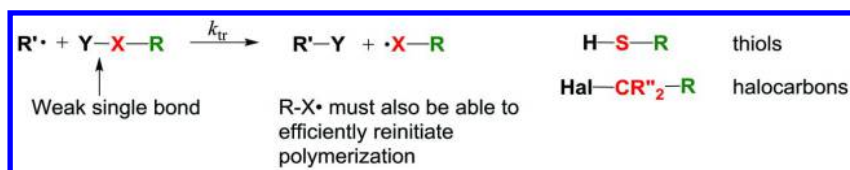
Scheme 4. Mechanism for chain transfer by homolytic substitution

Radical addition-fragmentation processes have been known in synthetic organic chemistry since the early 1970's (Scheme 5) (*26–28*). Allyl transfer reactions with allyl stannanes (*29*) and the Barton-McCombie deoxygenation process with xanthates (*30*) are just two examples of reactions known to involve a S_H2' mechanism. However, the first reports of addition-fragmentation transfer agents in polymerization appeared in the late 1980's (*17, 31–33*). The transfer agents studied in the CSIRO work included benzyl vinyl ethers, (X=CH$_2$, A=O) (*34*) allyl sulfides (X=CH$_2$, A=CH$_2$, R=SR′) (*35, 36*), thionoesters (X=S, A=O) (*37*) (Figure 1) and methacylate macromonomers (Figure 2, *vide infra*) (*38, 39*).
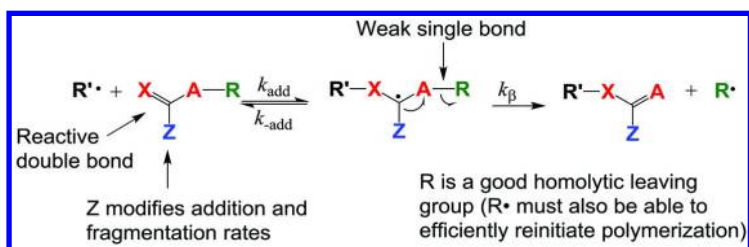
Scheme 5. Mechanism for chain transfer by addition-fragmentation
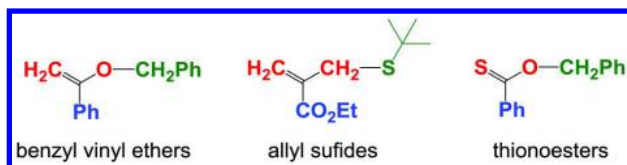
Figure 1. Structures of addition-fragmentation transfer agents

Figure 2. Structure of methyl methacrylate "macromonomer"

As long as reinitiation is rapid relative to propagation, the occurrence of chain transfer should not affect polymerization kinetics. This follows if the concentration of radicals is not affected by the process.

A transfer constant ($C_{tr}=k_{tr}/k_p$) of 1.0 has been called "ideal" because the ratio of monomer to transfer agent, and thus the molecular weight, should remain constant throughout the polymerization (*40*). Many addition-fragmentation transfer agents, such as the benzyl vinyl ethers, allyl sulfides and methacrylate macromonomers have $C_{tr}\sim 1$. If the transfer constant is >1.0 the molecular weight will increase linearly with monomer conversion. Irrespective of chain transfer constant, statistical factors dictate that in polymerization with irreversible chain transfer as the dominant process for chain termination the molecular weight dispersity ($Đ = M_w/M_n$) will be 2.0.

Macromonomer RAFT Polymerization

RAFT polymerization as form of RDRP to produce low dispersity homopolymers and block copolymers was first reported (*41*, *42*) in 1995 and applied in polymerization methacrylate monomers with so-called macromonomer chain transfer agents. The acronyms "RAFT" and "RDRP" were not used at the time. The properties of the macromonomers in copolymerization and as addition-fragmentation transfer agents had been reported a decade earlier (*38*).

The mechanism for reversible addition-fragmentation with a macromonomer transfer agent is shown in Scheme 6. Macromonomer RAFT polymerization is most effective with methacrylate monomers (*41–43*). However, the transfer constants of the methacylate macromonomers are low ($C_{tr} \sim 0.5$ for $n >2$) (*38*, *44–46*), which necessitates the use of starved feed conditions to achieve low dispersities. With monosubstituted monomers (*e.g.* St, acrylates) transfer constants are higher, but macromonomer copolymerization to from graft copolymers is a significant "side reaction", which can be mitigated though not eliminated by the use of higher reaction temperatures (*42*).
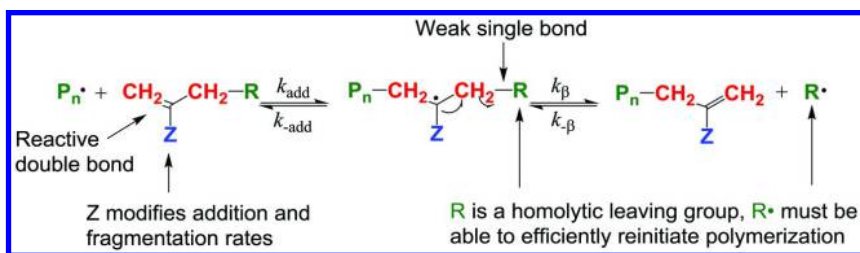
Scheme 6. Mechanism for reversible addition-fragmentation with a macromonomer transfer agent

Block copolymer synthesis using macromonomer RAFT polymerization is illustrated by the starved feed emulsion polymerization of butyl methacrylate (BMA) in the presence of a methyl methacrylate (MMA) macromonomer (M_n 2300, Đ 1.5) to form a low dispersity poly(butyl methacrylate)-*block*-poly(methyl methacrylate) (see Figure 3) (*41*).
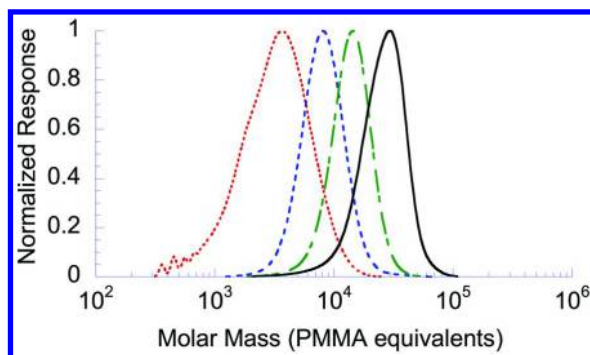
Figure 3. Evolution of the molecular weight distribution for polyMMA-block-polyBMA during starved feed RAFT emulsion polymerization of BMA mediated by MMA macromonomer RAFT agent. Molecular weights determined by size exclusion chromatography are in polystyrene equivalents. Adapted from reference (41). Copyright 1995 American Chemical Society.

The process can be seen to have some advantages over thiocarbonylthio RAFT polymerization in that no potentially undesirable end-groups are introduced and reagent costs are low. However, as a RDRP, the method only has limited applicability over a narrow range of monomers and reaction conditions.

Thiocarbonylthio RAFT Polymerization

The acronym RAFT was first used in our paper (*47*) disclosing RAFT polymerization with thiocarbonylthio compounds as RAFT agents (Scheme 7).
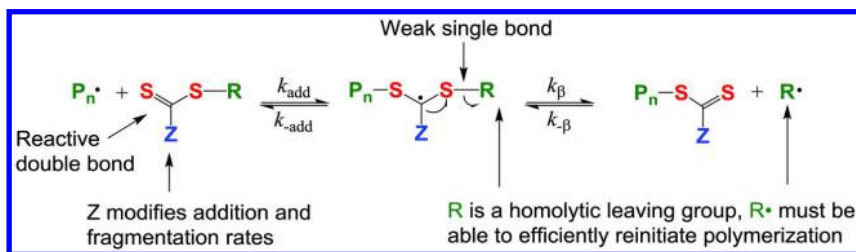
Scheme 7. Mechanism for reversible addition-fragmentation with a thiocarbonylthio transfer agent

Often the RAFT process with thiocarbonylthio compounds simply requires adding a source of radicals to a monomer (M) and a RAFT agent. Chains are continuously initiated, propagate, and die (the same number as in conventional polymerization). However, there are more chains ([chains] = [RAFT agent] + [initiating radicals]). With appropriate choice of RAFT agent and reaction conditions, on average, all chains grow simultaneously to provide a narrow

molecular weight distribution and the polymer end-groups (R and Z-CS$_2$) are largely preserved.

In Scheme 8, conventional radical polymerization, the initiating radical sequentially adds 46 monomer units before termination to form a chain of 46 units. In Scheme 9, RAFT polymerization, the initiating radical also adds 46 monomer units before terminating. However, during this time, 9 chains each of length ~5 are formed. Of these, 8 of the chains are dormant species (macro-RAFT agents) which could be reactivated and extended in the presence of a radical source and further monomer.
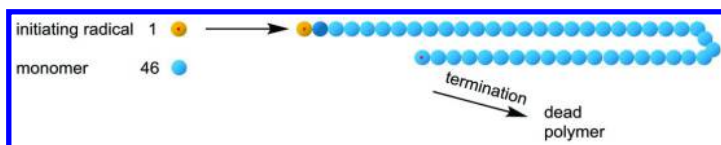
Scheme 8. Simplified scheme for formation of an individual chain during conventional radical polymerization.
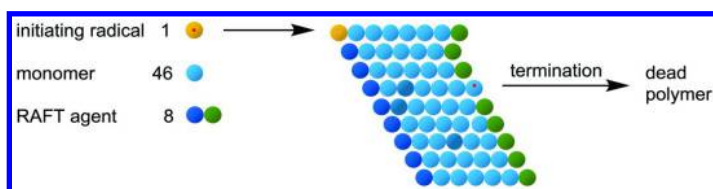
Scheme 9. Simplified scheme showing chains formed from an individual initiating radical during for RAFT polymerization.

A large number of thiocarbonylthio compounds have been described for use in RAFT polymerization (*48*). The effectiveness of the RAFT agent depends on the monomer being polymerized and is strongly influenced by the properties of the homolytic leaving group 'R' and the activating group Z.

The 'Z' group should be selected to convey appropriate reactivity to the thiocarbonyl double bond of the RAFT agent and the intermediate species formed by radical addition (Figure 4) (*49*).
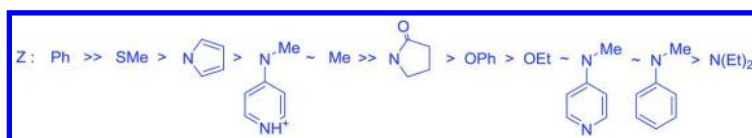
Figure 4. Relative effectiveness of 'Z' activating groups in RAFT agents (Z-C(=S)S-R) for various polymerizations. Addition rates and transfer constants decrease and fragmentation rates increase from left to right. Adapted from reference (1). Copyright 2005 CSIRO.

The properties of the major classes of RAFT agent can be summarized as follows:

- Dithiobenzoates (Z=aryl). Very high transfer constants. Preferred RAFT agents for batch or solution polymerization of 1,1-disubstituted MAMs (methacrylates, methacrylamides). Prone to hydrolysis. May give substantial retardation when used in high concentrations. Inhibition or strong retardation with most LAMs.
- Trithiocarbonates (Z=S-alkyl or S-aryl). Readily synthesized. High transfer constants. Preferred RAFT agents for monosubstituted MAMs, e.g., acrylates, acrylamides, styrenes. Less retardation and more hydrolytically stable than dithiobenzoates. Inhibition or strong retardation with most LAMs.
- Xanthates (Z=O-alkyl or O-aryl). Lower transfer constants. Poor control over MAMs. Effective control over LAMs, e.g., vinyl esters, vinyl amides. Made more active by electron-withdrawing substituents on oxygen.
- Dithiocarbamates (Z=heteroaryl or N-alkyl-N-aryl-). Activity strongly dependent on substituents on nitrogen. N-heteroaryl dithiocarbamates effective with MAMs; activity similar to trithiocarbonates. N-aryl-N-alkyl dithiocarbamates effective with LAMs; activity similar to xanthates. The N-methyl-N-(4-pyridinyl)dithiocarbamate **1** is switchable such that, in neutral form, its activity is similar to dithiocarbamate **3** providing good control over the polymerizations of LAMs (refer Figure 5). In protonated form (**2**) it provides effective control over the polymerization of MAMs (*50–53*).
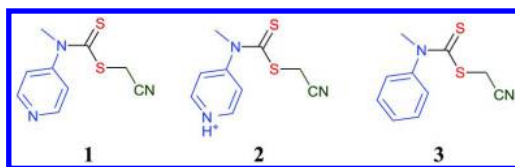
Figure 5. Structures of N-methyl-N-aryldithiocarbamate RAFT agents

The 'R' group should be selected to be a good homolytic leaving group with reference to the propagating radicals and such that the radical R is capable of efficiently reinitiating polymerization (Figure 6). Transfer constants decrease in the series where the homolytic leaving group R is tertiary >> secondary > primary; where α-substituent on R is CN ~ Ph >> CO_2R >> alkyl; where chain length of R is > 2 >> 1.

R : $\quad\overset{CH_3}{\underset{CH_3}{\mid}}$ —CN ~ $\overset{CH_3}{\underset{CH_3}{\mid}}$ —Ph > $\overset{H}{\underset{CN}{\mid}}$ —Ph > $\overset{CH_3}{\underset{CH_3}{\mid}}$ —COOEt >> $\overset{CH_3}{\underset{CH_3}{\mid}}$ —CH₂ $\overset{CH_3}{\underset{CH_3}{\mid}}$ —CH₃ ~ $\overset{CH_3}{\underset{H}{\mid}}$ —CN $\overset{H}{\underset{CH_3}{\mid}}$ —Ph > $\overset{CH_3}{\underset{H}{\mid}}$ —CH₃ ~ $\overset{H}{\underset{H}{\mid}}$ —CN ~ $\overset{H}{\underset{H}{\mid}}$ —Ph
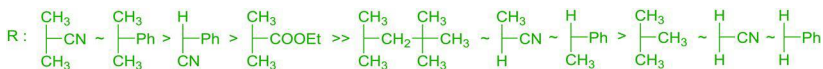
Figure 6. Relative effectiveness of 'R' activating groups in RAFT agents (Z-C(=S)S-R) for various polymerizations. Addition rates and transfer constants decrease and fragmentation rates increase from left to right. Adapted from reference (1). Copyright 2005 CSIRO.

The impact of the transfer constant on the molecular weight and dispersity can be appreciated by examining Figure 7. The degree of polymerization is simply the ratio of [monomer consumed]:[RAFT agent consumed]. The figure shows that a higher degree of polymerization than that predicted for complete utilization of the transfer agent simply indicates a low C_{tr} and reflects incomplete conversion of initial RAFT agent to macro-RAFT agent (*54*). Low dispersities require $C_{tr} >$ 2. $C_{tr} > 10$ are required to achieve the significantly narrowed molecular weight distributions associated with RDRP and molecular weights that are predictable from reagent concentrations and increase linearly with conversion. The most effective RAFT agents have $C_{tr} >> 50$.
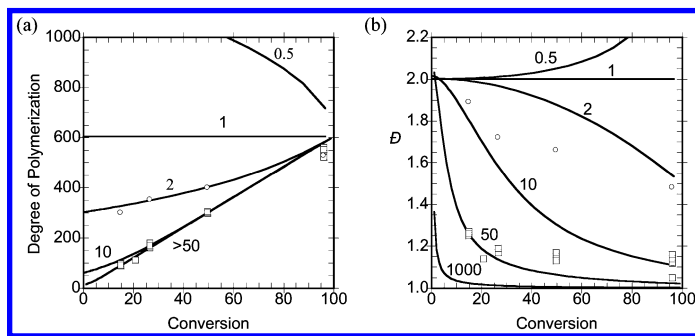
Figure 7. Predicted dependence of (a) the degree of polymerization and (b) the dispersity (Đ) on conversion in polymerizations involving reversible chain transfer as a function of the chain transfer constant (C_{tr}). Predictions are based on equations proposed by Müller et al. (55, 56) with a $=10^{-7}$ (the concentration of active species), β (the transfer constant) as indicated and γ=605 (the ratio of monomer to transfer agent). Experimental data points are for methyl methacrylate (7.02 M) polymerization in presence of dithiobenzoate esters (0.0116 M) where R = C(Me)₂CO₂Et (○) and C(Me)₂Ph (□). Reproduced from reference (57). Copyright 2003 American Chemical Society.

A major advantage of RAFT polymerization over most other forms of RDRP is that is amenable to being performed in aqueous media (homogeneous, emulsion, miniemulsion) (*58–60*). The significance of this area is such that of the ~5000 journal publications relating to RAFT polymerization (Figure 8), ~ 1000 of these are also associated with the terms "aqueous" and/or "water" (Scifinder®). The percentage of papers per annum on aqueous RAFT has remained at consistently at ~20% for the last 10 years. This can be in part attributed to the significance of the bioapplications field (*61*) and the industrial significance of RAFT in emulsion and other forms of heterogeneous media.
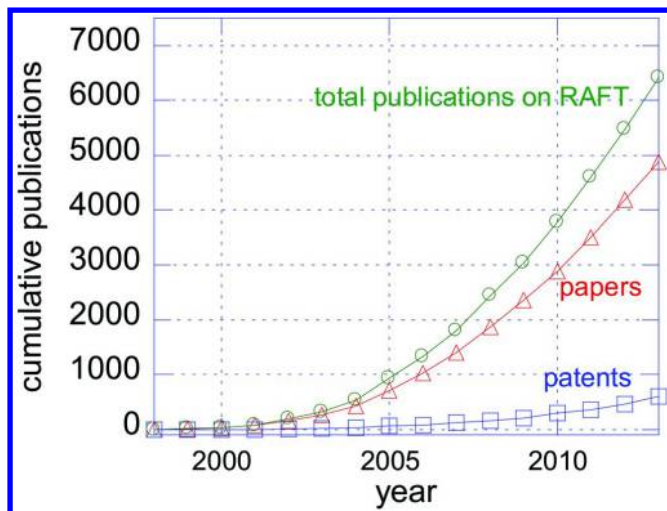
Figure 8. Total publications, papers, and patents on RAFT polymerization based on SciFinder® search of terms "RAFT Polymerization", "Reversible Addition Fragmentation (Chain) Transfer" & "radical", "MADIX" & "radical". The term "papers" includes journal articles, communications, letters and reviews but excludes conference abstracts.

Recent (2011-2014) Applications of RAFT Polymerization at CSIRO

The paper focuses on the early development of RAFT and on CSIRO research over the last 3 years (2011-2014). In having this focus, it is not intended to in any way diminish the importance of the often substantial contributions made by other research groups to the development and application RAFT. Publication on RAFT polymerization with thiocarbonylthio RAFT agents has continued unabated within the period 2011-2014 with approximately one third of papers (~2500 new journal papers and ~350 patent or applications thereto) appearing (Figure 8). Only a small number of these have emanated from CSIRO. A more comprehensive survey of RAFT chemistry is provided in our periodic reviews published in the *Australian Journal of Chemistry* (*1*, *15*, *16*, *18*). A fourth update to this series is currently in preparation.

Many reviews on RAFT polymerization have appeared during the period 2011-14. General reviews include those by Moad, Rizzardo and Thang (*14*, *15*, *62–65*) Destarac (*66*), and Barner-Kowollik *et al.* (*67*). Reviews devoted to RAFT or RAFT polymerization in specific areas include those on the origins of RAFT polymerization (*3*), the design and synthesis of RAFT agents (*48*), advances in Switchable RAFT agents (*68*, *69*), dithiobenzoate-mediated RAFT polymerization (*70*), RAFT chemistry using xanthates (*4*, *71*), RAFT polymerization of vinyl esters (*72*), RAFT crosslinking polymerization (*73*), RAFT polymerization in microemulsion (*74*), RAFT polymerization induced self-assembly (*75*, *76*), the synthesis of block copolymers (*77*), the synthesis of star polymers and other complex architectures (*78–81*), block copolymers based on amino acid-derived monomers (*82*), end group removal and transformation (*83–86*), the synergistic use of RAFT polymerization and ATRP (*87*), microwave-assisted RAFT polymerization (*88*, *89*), silica nanoparticles (*90*), polymer nanocomposites (*91*, *92*), the use of RAFT-synthesized polymers in gene-delivery (*93*), drug delivery and bioapplications (*79*, *94–98*), personal care applications (*99*) block and star copolymers as rheology control agents (*100*), and optoelectronic applications (*101*). There are additionally many more reviews which deal more general with RDRP but which, nonetheless, have a substantial section on RAFT polymerization. Some of those that include significant mention of RAFT polymerization include general reviews on RDRP (*102*), RDRP mechanisms and reagent design (*103*, *104*), click chemistry (*105–109*), photo-initiated RDRP (*110*) synthesis of telechelics (*111*), polymerization of carbazole-containing monomers (*112*), *N*-vinyl-1,2,3-triazoles (*113*), *N*-vinyl heterocycles (*114*), glycomonomers (*115*, *116*), synthesis of metallopolymers (*117*), conjugated block copolymers (*118*), dye-functionalized polymers (*119*), stimuli responsive polymers (*120–122*), complex architectures (*123*), biopolymer-polymer conjugates and bioapplications (*97*, *124–129*), polysaccharide modification (*130*), polymerization in heterogeneous media (*131*), microwave-assisted polymerization (*132*, *133*) and industrial prospects for RDRP (*134*).

Developments in Kinetics and Mechanism, New RAFT Agents

Methods of RAFT Agent Synthesis

RAFT agents, as mentioned above, in addition to having an optimal C_{tr} (in most circumstances higher is better), should exhibit minimal likelihood for retarding polymerization or undergoing side reactions. The RAFT agent should possess end-group functionality appropriate for the intended application. In this light we have critically evaluated the various methods that have been used for RAFT agent synthesis (*48*). These methods include: reaction of a carbodithioate salt with an alkylating agent, various thioacylation procedures, thiation of a carboxylic acid or ester, the ketoform reaction, thiol exchange, radical substitution of a bis(thioacyl) disulfide and radical-induced R-group exchange (Scheme 10). We also consider methods for synthesis of functional RAFT agents and the preparation of macro-RAFT agents by modification of or conjugation to existing RAFT agents. The most used methods involve esterification of a

carboxy-functional RAFT agent, azide-alkyne 1,3-dipolar cycloaddition, the active ester-amine reaction and RAFT single unit monomer insertion. While some of these processes are described as "click reactions" most stray from that ideal. The synthetic method of choice is strongly dependent on the specific features of the desired RAFT agent.
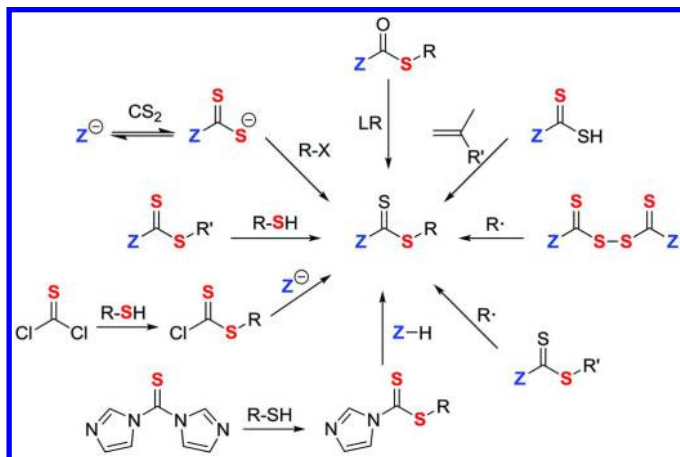
Scheme 10. Processes for RAFT Agent Synthesis (Reproduced from (48) © American Chemical Society). RX = alkylating agent, LR = Lawesson's reagent or equivalent. Reproduced from reference (48). Copyright 2012 American Chemical Society.

Dithiobenzoate RAFT Agents

Dithiobenzoates remain amongst the most popular agents for implementing reversible addition-fragmentation chain transfer (RAFT) polymerization (Scheme 11) (*70*). This can be attributed to the fact that, in RAFT polymerization of methacrylates and methacrylamides, their use can offer better control over molecular weight and molecular weight distribution and end-group fidelity than most alternative RAFT agents. However, the use of dithiobenzoates in controlling polymerization of styrenes, acrylates and acrylamides has diminished with time, mainly in favor of trithiocarbonate RAFT agents, because of issues relating to retardation and to the hydrolytic and thermal instability of the dithiobenzoate group. In 2006 the IUPAC task group, "Towards a Holistic Mechanistic Model for RAFT Polymerizations: Dithiobenzoates as Mediating Agents", published a so-called "dilemma paper" entitled "Mechanism and kinetics of dithiobenzoate-mediated RAFT polymerization" (*135*) which reviewed the relevant literature on dithiobenzoate RAFT agents. That paper stated the then current situation and drew attention to an apparent dilemma relating to the kinetics and mechanism of retardation. We have now critically assessed developments in the understanding of the mechanism and kinetics of dithiobenzoate-mediated RAFT polymerization over the period 2006-2013 with specific reference to choice

of reagents and polymerization conditions, reagent and product stability, side reactions and factors that lead to retardation (*70*).
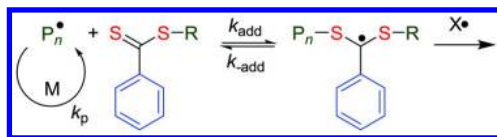
Scheme 11. Mechanism of RAFT with dithiobenzoate RAFT agents

While it cannot be said there is a now clear, universally accepted, resolution to the dilemma posed in the 2006 IUPAC paper (*135*), once "avoidable causes" of retardation are eliminated, the evidence for some form of intermediate-radical termination being the primary cause for retardation in dithiobenzoate-mediated RAFT polymerization now appears overwhelming.

RAFT Single Unit Monomer Insertion (SUMI) and Monomer Sequence Control

Zard and coworkers (*136*) first performed selective single unit monomer insertion (SUMI) in the late 80s for an *N*-alkylmaleimide or a vinyl sulfone into a xanthate. They (*137–142*) have subsequently provided many examples of this chemistry mainly in the context of organic synthesis.

Selective initialization, the complete conversion of an initial low molecular weight RAFT agent to a species incorporating a single monomer unit is common to many well-behaved RAFT polymerizations (*143–149*) including those of styrene (*143*, *146*), methyl acrylate (*145*, *148*), *N*-vinylpyrrolidone (*147*) and vinyl acetate (*147*).

Recently, reports of the synthesis of multiblock copolymers based on (meth)acrylates or acrylamides by sequential RAFT (*150–153*) (or atom transfer radical polymerization (ATRP (*154*))) steps have appeared. In that a single unit can be considered a block with length unity, many of the factors important to the success of multiblock synthesis are also important in achieving multiple SUMI steps. However, an additional criteria for successful SUMI is a very high transfer constant for the RAFT agent for the monomer being inserted (*155*).

We have explored RAFT (reversible addition-fragmentation chain transfer) SUMI into trithiocarbonate (*155*) and dithiobenzoate RAFT agents (*156*). In principle, higher selectivities for single unit insertion of MAMs might be expected with dithiobenzoates because of their higher transfer constants in RAFT polymerization (*49*, *70*). In the more recent work (*156*) styrene and *N*-isopropylacrylamide (NIPAm) were successfully inserted into 2-cyanopropan-2-yl dithiobenzoate (Scheme 12). Attempted SUMI of methyl methacylate (MMA) provided only an oligomeric insertion product from multiple monomer insertion due to the relatively low transfer constant of the dithiobenzoate in MMA polymerization. A very low SUMI yield with maleic anhydride (MAH) reflects the low reactivity of MAH towards 2-cyanopropan-2-yl radicals. We also examined insertion of MAH, styrene and NIPAm into the styrene SUMI

product (Scheme 13). Insertion of MAH was rapid and apparently quantitative no doubt reflecting the high reactivity of MAH towards the 2-phenylethyl radical. SUMI with styrene and NIPAm was selective but slow, which is attributed both to the low monomer concentrations used and the poor leaving group ability of the propagating species. The SUMI with NIPAm was complicated by initiator-derived by-products.
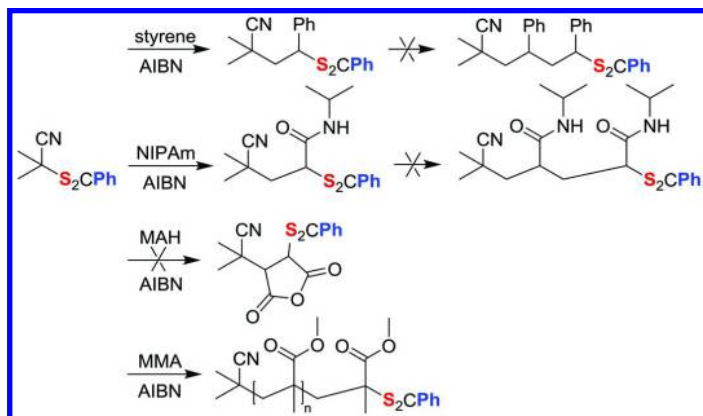
Scheme 12. RAFT SUMI with 2-cyanoprop-2-yl dithiobenzoate
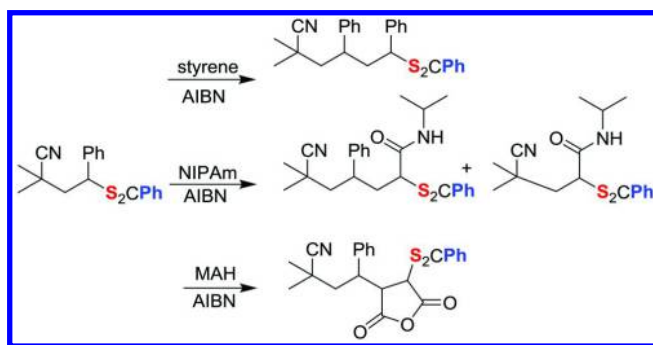
Scheme 13. RAFT SUMI with mono-styrene dithiobenzoate

Another approach to monomer sequence control by RAFT makes use of template polymerization and complementary nucleobase interactions (*157*). One challenge associated with this methodology relates to the synthesis of parent polymers and relates to the very low solubility of the monomers and the derived polymers in most solvents. We have recently reported (*158*) that the alternating, nucleobase-containing, copolymer, low dispersity poly(MAH-*alt*-StyThy), can be synthesized in high conversion through the use of a fluorinated solvent (hexafluoroisopropanol – Scheme 14). Investigations into the use of this

methodology for the preparation of templates for the synthesis of designed daughter polymers comprising the complementary nucleobase are underway.
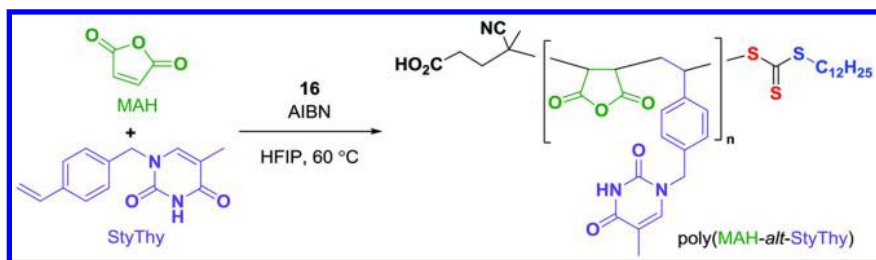
Scheme 14. Synthesis of the 1:1 alternating, nucleobase-containing, polymer poly(MAH-alt-StyThy, by RAFT polymerization in hexafluoroisopropanol (HFIP)

Switchable RAFT Agents, RAFT Polymerization of N-Vinylcarbazole

With appropriate selection of 'R', Many xanthates (*159*), certain dithiocarbamates (e.g., **7**, **11**) (*52*, *160*), "F-RAFT" (*94*, *95*) can provide control over polymerization of both LAMs and MAMs. However, the level control is less than that required to give very low dispersities and complete reagent utilization with the full range of monomers.

Switchable *N*-methyl-*N*-(4-pyridinyl)dithiocarbamate RAFT agents were introduced to provide a viable synthesis of low dispersity polyMAM-*block*-polyLAM (*50*, *51*, *68*). Developments in this area have now been reviewed (*69*). In more recent work, we demonstrated the effectiveness of switchable RAFT in aqueous media (*53*), and explored the use of *N*-aryl-*N*-(4-pyridinyl)dithiocarbamates (*52*). The latter RAFT agents are more active with MAMs in protonated (switched) form and more active with LAMS in non-protonated (unswitched) form.

N-vinylcarbazole (NVC) has long been regarded as a "difficult monomer" for RDRP. Our work with *N*-Aryl-*N*-4-pyridinyl dithiocarbamate switchable RAFT agents (*52*), which showed that best control over NVC polymerization (lowest *Đ* values) was achieved with the most active RAFT agents of the type, led us to question whether NVC should be considered a LAM. High throughput RAFT polymerization of NVC was conducted with a series of cyanomethyl RAFT agents (dithiobenzoate (**4**), trithiocarbonate (**5**), xanthate (**6**), switchable dithiocarbamate (**1, 7**) (refer Figure 9) (*161*). This study showed that RAFT polymerization of NVC is best controlled with a trithiocarbonate RAFT agent, which allows for the synthesis of homopolymers with very narrow molar mass distributions (e.g., *Đ* ~ 1.10) and block copolymers with MAMs.

Thus, contrary to popular belief, NVC does not behave as a typical LAM and should be classified as an intermediate activity monomer (IAM).
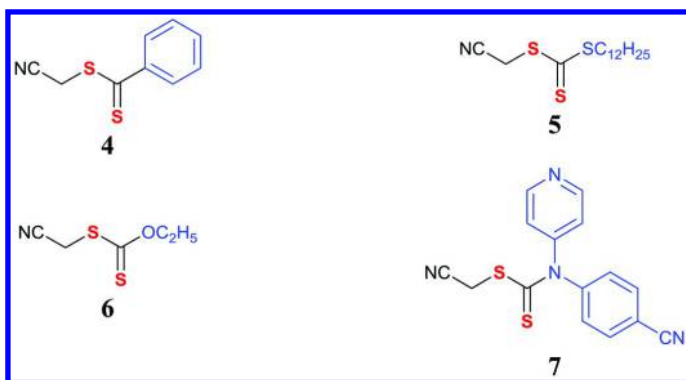
Figure 9. Structures of RAFT agents

Commercial Availability of RAFT Agents

A range of RAFT agents are have been commercially available in research quantities form Strem (*64*) and Sigma-Aldrich (*164*) since 2010. The industrial scale-up has been reported of the xanthate, Rhodixan-A1 (**8**), by Rhodia (*162*) and trithiocarbonates, CTA-1 (**9**) and Blocbuilder DB (**10**), by Lubrizol (*107*, *108*) and Arkema (*163*) respectively (Figure 10).
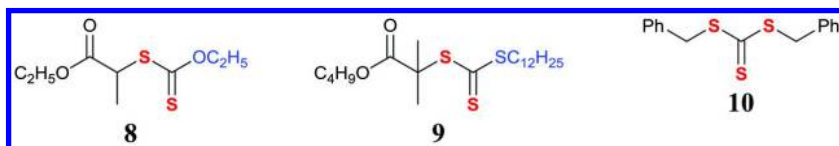
Figure 10. Structures of Rhodia's Rhodixan-A1 (162), Lubrizol's CTA-1 RAFT agents (107, 108). and Arkema's Blocbuilder DB (163)

Boron Molecular has now (2014) made a larger range of RAFT agents (including **3**, **10**, **11-20**) available in commercial quantities (Figure 11) (*165*). The range includes the dithiocarbamate (**3**; good control over LAMs), pyrazole dithiocarbamates (**11**, **12**; moderate control over LAMs, good control over MAMs), a switchable dithiocarbamate (**13**; good control for LAMs and MAMs with switching) and trithiocarbonates (**10**, **14-20**; good control over MAMs). Note that both the 'R' and 'Z' groups need to be chosen to provide good control.

End-Group Transformation

A wide variety of methods are now available for removing or transforming the thiocarbonylthio-groups in RAFT-synthesized polymers (Scheme 15) (*83*). All have advantages and limitations depending on the intended application. The thiocarbonyl functionality present in RAFT-synthesized polymers, once seen as a limitation to the wide-spread adoption of RAFT polymerization is now seen as an

enabling functionality in addressing the needs of the biomedical, optoelectronic, nanotechnology and other sectors.

Many procedures involve initially converting the thiocarbonylthio functionality into a thiol end-group through reaction with nucleophiles. A variety of thiol transformation reactions, many of them erroneously referred to as "click" processes (*109*), can then be used to further transform the thiol end-group. These include the processes as shown in Scheme 16 (*83*).
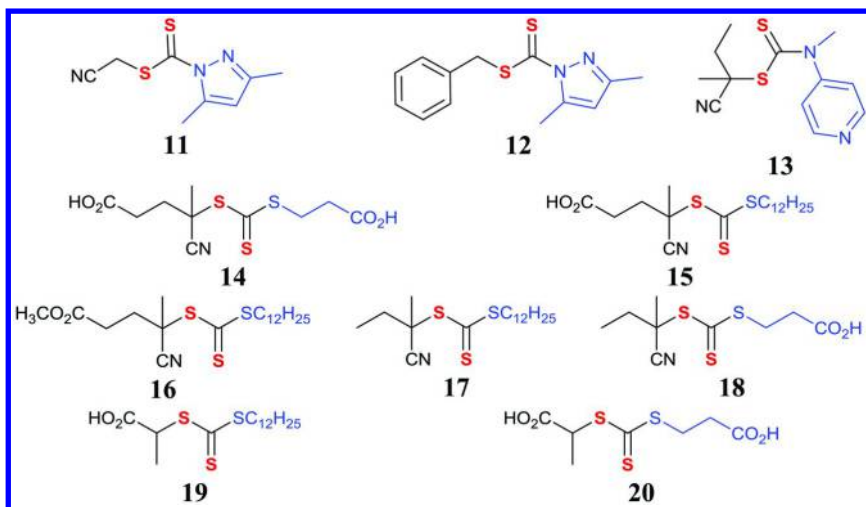
Figure 11. Structures of RAFT agents available from Boron Molecular (165)
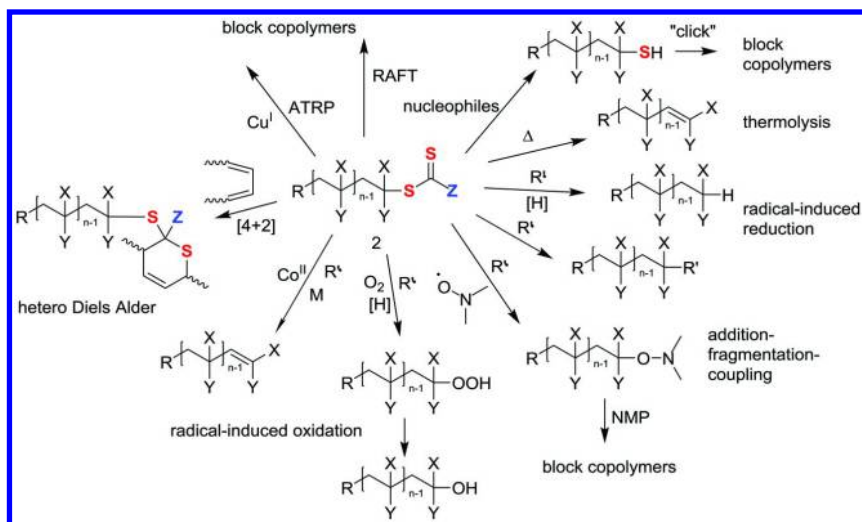
Scheme 15. Processes for RAFT End-group Transformation. Reproduced from reference (83). Copyright 2011 Society of Chemical Industry. R'·= radical, [H] = hydrogen atom donor, M = monomer.
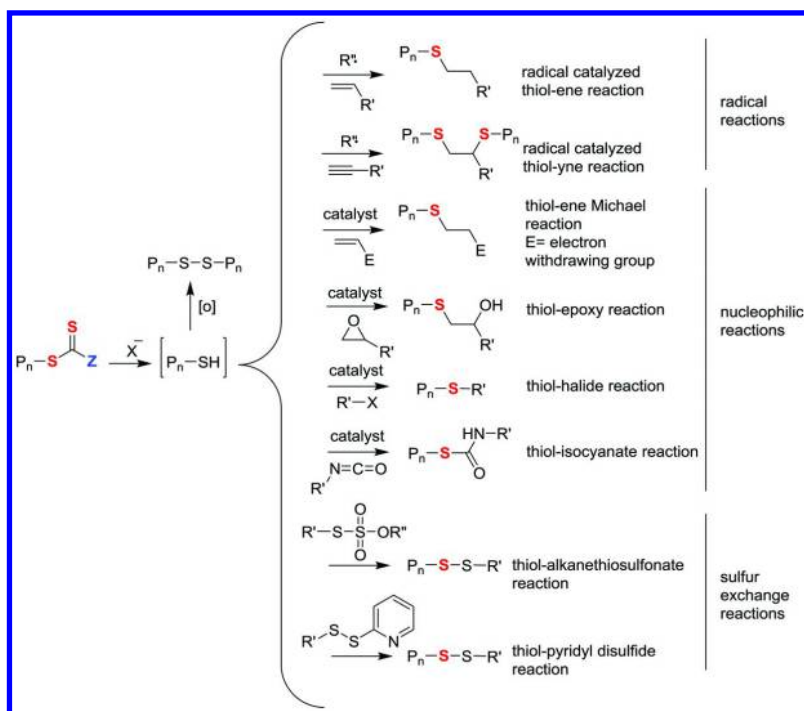
Scheme 16. Reactions of RAFT end-group with nucleophiles with trapping of the thiol end-group formed. Reproduced from reference (83). Copyright 2011 Society of Chemical Industry.

Two recently published US patents address the issue of by-product removal following RAFT end-group transformation (Scheme 17, Scheme 18) (*166, 167*).
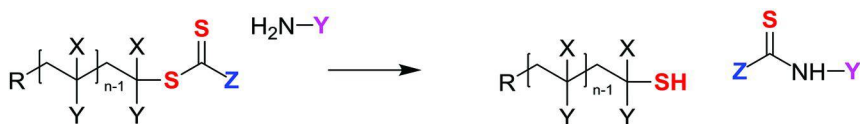
Scheme 17. Processes for RAFT End-group Transformation based on use of a functional reagent to facilitate by-product removal (166).

Scheme 18. Processes for RAFT End-group Transformation based on use of a functional RAFT agent to facilitate by-product removal (167).

RAFT Crosslinking Polymerization

Synthesis of Polymer Networks

The use of RAFT (reversible addition-fragmentation chain transfer)-crosslinking (co)polymerization of multi-olefinic monomers to produce three-dimensional polymer networks has been reviewed with reference to differences between the RAFT and the conventional process, between RAFT and other forms of RDRP (reversible-deactivation radical polymerization such as ATRP and NMP), and the dependence of the polymerization process and network properties on RAFT agent structure (*73*). This knowledge is important in network optimization for applications as dynamic covalent polymers (in self healing polymers), as porous polymer monoliths or gels (used as chromatographic media, flow reactors, controlled release media, drug delivery vehicles and in molecular imprinting) and as coatings.

There are two distinct forms of RAFT crosslinking polymerization (a) making use of mono-RAFT agents, R-SC(=S)Z, and (b) with 'Z'-connected bis-RAFT agents, R-SC(=S)[Z′C(=S)]$_n$-S-R; with n=0 the latter correspond to symmetrical trithiocarbonates, R-SC(=S)-S-R.

In case (a) a "sol" is formed during the initial phase of (co)polymerization, which comprises linear chains, branched chains containing a limited number of crosslinks, and cycle containing chains, all possessing a number of pendant double bonds (Figure 12). With an efficient RAFT agent, the RAFT process should ensure that linear chains are of similar degree of polymerization (n) (whether or not they contain rings) and that branched chains have degree of polymerization $x \times n$ (where x is the number of crosslinks). Notwithstanding that some imperfections will be introduced by termination, all chains should possess RAFT agent functionality at chain ends and branched chains can possess multiple (x) RAFT agent groups.
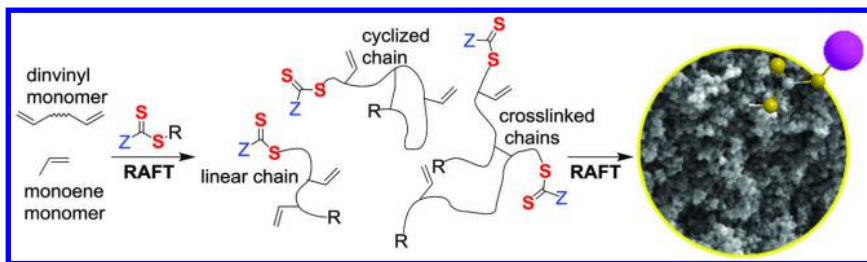
Figure 12. Structure of "sol" formed with RAFT agents R-SC(=S)Z. Adapted from reference (73). Copyright 2015 Society of Chemical Industry.

In a later stage of polymerization, this sol fraction is further crosslinked to form the overall network. Even though crosslinks do not equilibrate, the resulting network is likely to possess a less heterogeneous microstructure than that formed in the conventional process (without control agent). At the end of the process, the RAFT agent functionality remains pendant to the network at the terminus of all chains and can be used for surface-initiated RAFT polymerization. The network

structure is similar to that produced by other RDRP methods such as NMP or ATRP.

In case (b) a "sol" is formed during the initial phase of (co)polymerization, which again comprises linear chains, branched chains containing a limited number of crosslinks, and cycle containing chains, all possessing a number of pendant double bonds (Figure 13). An efficient RAFT agent should again ensure that linear chains are of similar degree of polymerization (n) (whether or not they contain rings) and that branched chains have degree of polymerization $x \times n$ (where x is the number of crosslinks). The main difference is that the RAFT agent functionality is contained within the network structure. It is possible for chains attached to different RAFT functionalities to exchange and for the link between crosslinks (or the size of rings), when they contain at RAFT group, to expand.
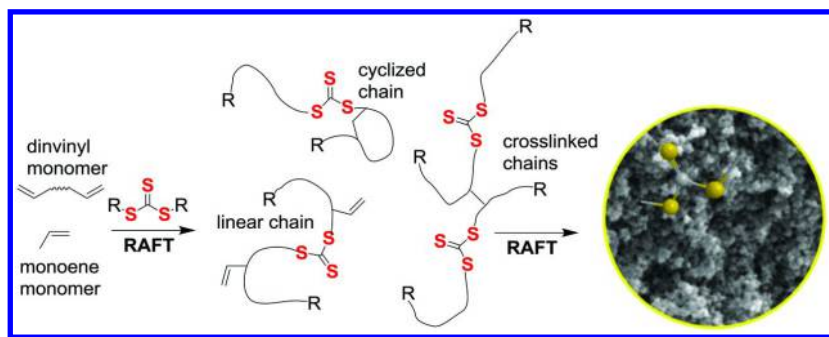
Figure 13. Structure of "sol" formed with RAFT agents R-SC(=S)-S-R. Adapted from reference (73). Copyright 2015 Society of Chemical Industry.

In the later stage, this sol fraction is crosslinked to form the overall network. The resultant network will possess a more homogeneous microstructure than that formed in the conventional process (without control agent). The RAFT agent functionality remains within the network structure. Even in the final structure network, the crosslinks that contain RAFT functionality may equilibrate. This provides capacity for self-healing and for stress relaxation within the network (*168–171*). RAFT agent functionality can also be incorporated into polymer networks formed by thiol-ene chemistry (*172*) or other processes to form similar structures. The presence of the thiocarbonylthio linkages within the network also means that the network is intrinsically unstable and can be degraded by reagents that cleave the thiocarbonylthio linkage (*83*). While the thiocarbonylthio groups in these networks can still be transformed to provide new functionality, such a process is intrinsically more complicated since most such transformation processes will cleave the thiocarbonylthio group thereby degrading the network. This type of network produced with 'Z'-connected bis-RAFT agents cannot be easily formed using other RDRP methods such as NMP or ATRP (note that bis-ATRP or NMP initiators correspond to 'R'-connected RAFT agents).

We have reported a new method for the preparation of porous functional poly(styrene-*co*-divinylbenzene) monoliths by use of RAFT crosslinking

polymerization (Scheme 19) (*173, 174*). The method, exemplified by styrene-divinylbenzene copolymerization in the presence of 2-cyano-2-propyl dodecyl trithiocarbonate, provides control over polymerization kinetics, monolith morphology and surface functionality. Retention of the thiocarbonylthio group within the monolith structure in an active form for surface-functionalization of the polymeric monoliths was demonstrated by the successful RAFT "grafting from" polymerization of (4-vinylphenyl)boronic acid (*173*) or *P*-(4-vinylphenyl)diphenylphosphine (Scheme 20) (*175*). These functional monoliths have potential applications in chromatography and in flow chemistry.
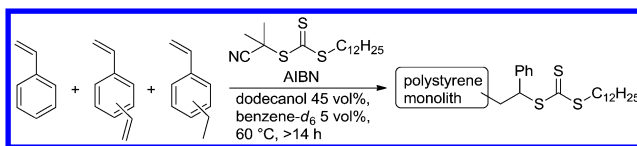
Scheme 19. Synthesis of polystyrene-based monolith in the presence of a RAFT agent. Reproduced from reference (173). Copyright 2014 Royal Society of Chemistry.
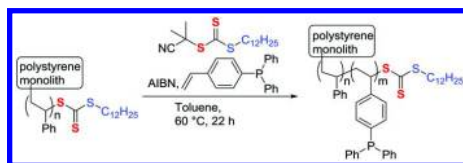
Scheme 20. Functionalization of polystyrene-based monolith by RAFT polymerization.

Star Polymer Synthesis (Core-Crosslinked Stars, Star-Nanogels)

In crosslinking copolymerization, unless crosslinker concentrations are very high, linear chains are formed first and most branching events (reaction with a pendant double bond) occur at a later stage of the polymerization. Work by Sherrington and others (*176, 177*) has found empirically that, as long as the ratio of [crosslinker] to [initiator or transfer agent] is < 1, then a soluble species (hyperbranched polymer, microgel, nanogel) might be obtained even at high monomer conversion. Early work by Flory showed that even with as few as 0.5 branch points per chain the product is likely to be a crosslinked gel. This theoretical prediction and the experimental findings can be reconciled if a significant fraction of pendant double bonds are consumed in intramolecular cyclization reactions rather than intermolecular branching (*178*).

The historical development of 'arm-first' star polymers, also known as core crosslinked star polymers or star-nanogels, has been reviewed by Blencowe *et al*. (*179*), Chen *et al*. (*180*), and Gao and Matyjaszewski (*181*). In the arm-first

process considered here, star assembly and crosslinking take place in a single step involving (co)polymerization of a multi-olefinic monomer mediated by macro-RAFT agent. The processes were first described in patent applications that appeared during 1999-2000 by Solomon *et al.* (*182*) and Berge *et al.* (*183*). They should be distinguished from other arm-first processes that involve crosslinking of micellar species in a subsequent reaction step, the linking of arm polymers to a multifunctional core, and various hybrid strategies.

Mikto-arm star copolymers containing three different arm compositions (hydrophobic (butyl methacrylate – BMA)), hydrophilic (oligo(ethylene glycol) methacrylate – OEGMA) and cationizable (2-(dimethylamino)ethyl methacrylate – DMAEMA) were successfully synthesized by using an arm-first approach involving copolymerization of a dimethacrylate mediated by a mixture of macroRAFT agents (Scheme 21) (*184*). The hydrophilic–hydrophobic balance of the arms appears critical to obtaining good control. The breadth of the molar mass distribution of the stars was found to depend on the proportion of the hydrophobic arms and the amount of crosslinker used in their synthesis. An increase in either parameter lead to an increase in molar mass and dispersity. Our work demonstrated that the proposal (*185*, *186*) that the crosslinker and comonomers used should be incompatible with the polymerization medium to achieve good control was neither a necessary nor a sufficient condition for low dispersity stars. The P(DMAEMA) arms were quaternized with methyl iodide to provide quaternized star polymers with potential as carriers in drug delivery (*187*, *188*).

An alternative method of star-nanogel synthesis is the core-first approach. In a recent study on the preparation of a new family of nanocarriers for protein antigen delivery (*189*), two variants were exploited. In the first, a hyperbranched core was formed by copolymerization of BMA and 2-(*N,N*-diethylamino)ethyl methacrylate) (DEAEMA) was mediated by an "inimer" RAFT agent. In the second, a crosslinked core was formed by RAFT crosslinking copolymerization of the same monomers with diethylene glycol dimethacrylate (EGDMA) – this method is analogous to the arm-first process above except that a low molecular weight RAFT agent is used to mediate the polymerization. The two cores (and a linear copolymer) were then used as macro-RAFT agents to control copolymerization of dimethyl acrylamide (DMA) and pyridyl disulfide methacrylamide (PDSMA) to produce star-nanogels (Scheme 22). This work (*189*) demonstrated that the architecture of pH-responsive, endosomolytic polymers can have a dramatic effect on intracellular antigen delivery, and indicated a promising strategy for enhancing CD8$^+$ T cell responses to protein-based vaccines.

The arm-first approach to star nanogel synthesis has the advantage of allowing full characterization of the arms prior to star synthesis and is readily adapted to mikto-arm star synthesis. Conversely the core-first approach allows characterization of the core, allows the preparation of a library of polymers of different arm structure with identical cores and more suitable for the synthesis stars with a very high arm density.

High Throughput RAFT Polymerization

RAFT in Continuous Flow

Over the past few years, continuous flow chemical processing has found a widespread uptake in organic chemistry laboratories for translation from discovery to production. In this context we (*190–195*) and others (*196, 197*) have examined RAFT polymerization in continuous flow reactors. Recent research at CSIRO in this area has involved developing processes for monomer degassing prior to polymerization (*192*), block copolymer synthesis (*193*), RAFT end-group removal (*191, 194, 195*), and sequential RAFT polymerization and end-group removal by, for example, thermolysis (*194*) or aminolysis (Scheme 23) (*195*).
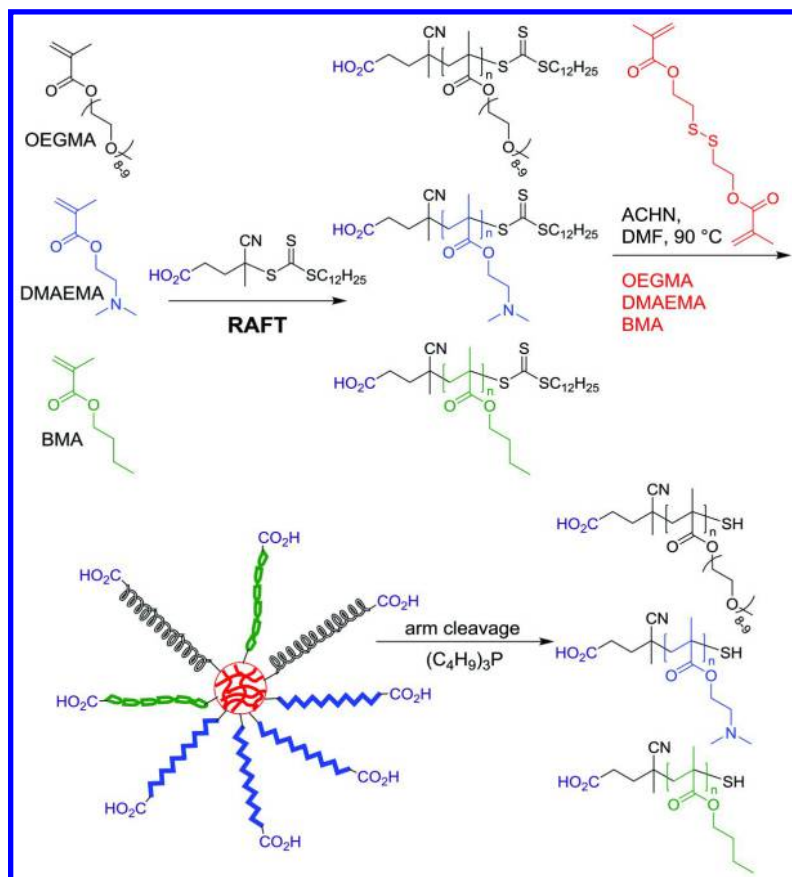
Scheme 21. Synthetic approach used to prepare redox-cleavable mikto-arm star polymers by RAFT polymerization and arm-cleavage by disulfide reduction with tributylphosphine.
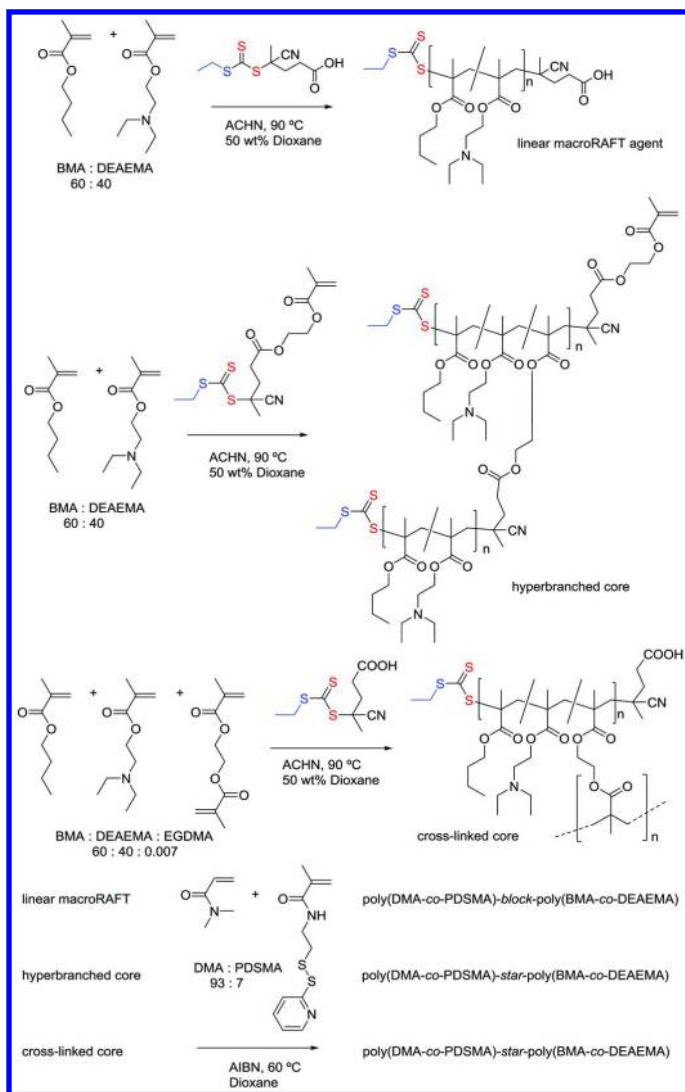
Scheme 22. Synthesis of poly(DMA-co-PDSMA)-block-poly(BMA-co-DEAEMA) of linear or "core –first" star architecture with either a hyperbranched or a cross-linked core.

In Controlled Radical Polymerization: Mechanisms; Tsarevsky, et al.;
ACS Symposium Series; American Chemical Society: Washington, DC, 2015.
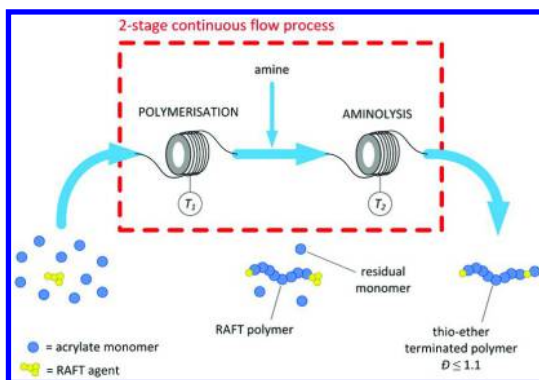
Scheme 23. Process for sequential RAFT polymerization and end group removal involving two continuous reactor units in series in which the residual monomer from the polymerization acts as the Michael acceptor to cap the thiol by aminolysis. Reproduced from reference (195). Copyright 2014 American Chemical Society.

High Throughput RAFT Polymerization

High throughput RAFT polymerization in an automated synthesizer has been developed to provide polymer libraries through the synthesis of di- tri- and higher order multi-block copolymers in a 'hands-free' operation (*150*, *151*, *198*, *199*). Recent work has seen the implementation of freeze-thaw degassing procedures (*200*) and the application of the methodology to determine RAFT agent activity (*52*, *53*, *161*) and copolymerization reactivity ratios (*201*).

The synthesis of a quasi-pentablock copolymer libraries (PDEGMA-*qb*-PMMA-*qb*-PBMA-*qb*-PMMA-*qb*-PDEGMA) by one-pot sequential RAFT polymerization starting with a *bis*-RAFT agent is illustrated in Figure 14 and Figure 15 (*151*). The pentablock library is formed by withdrawing samples at hourly intervals during the last polymerization step. When monomer conversions were limited to <70% in the synthesis of the methacrylate homopolymer and quasi-triblock the extent of termination, as evidenced by the development of a bimodal molecular weight distribution was minimal. For high k_p monomers (acrylates, acrylamides) much higher conversions ($\geq 99\%$) can be targeted.
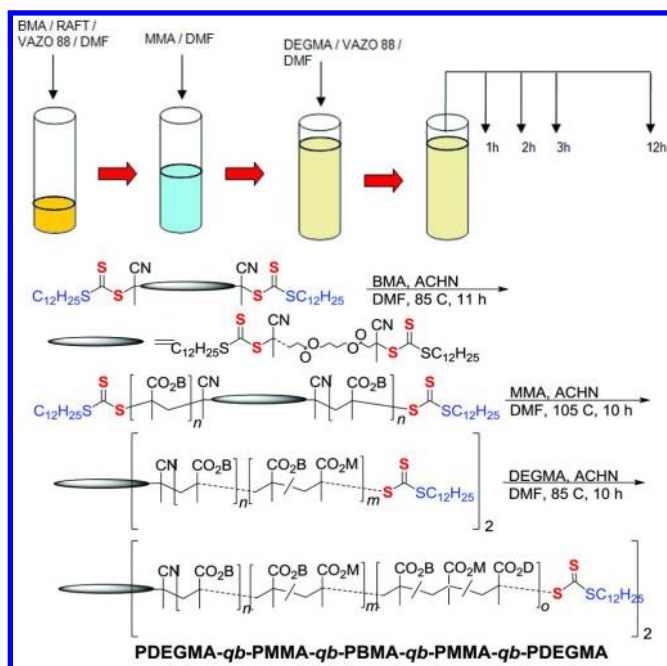
Figure 14. Representation of the automated parallel synthesis of a quasi-pentablock copolymer library by one-pot sequential RAFT polymerization starting with a bis-RAFT agent; B, M and D are the butyl, methyl and diethylene glycol monomethyl ether substituents for BMA, MMA and DEGMA respectively. Reproduced from reference (151). Copyright 2014 Royal Society of Chemistry.
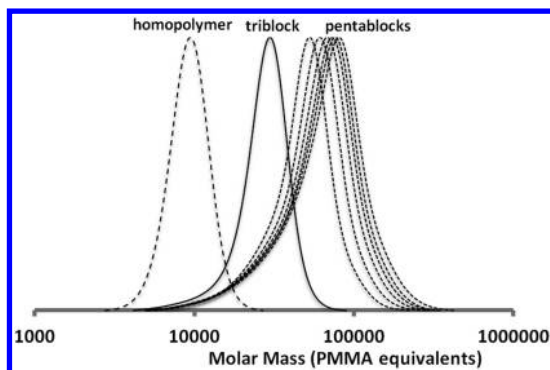
Figure 15. SEC traces demonstrating the chain extension of a bis-macro-RAFT agent homopolymer to a quasi-triblock, then to a library of PDEGMA-qb-PMMA-qb-PBMA-qb-PMMA-qb-PDEGMA quasi-pentablocks –only every 2ⁿᵈ member of the library is shown. Reproduced from reference (151). Copyright 2014 Royal Society of Chemistry.

RAFT Applications

Some recent applications of RAFT were highlighted in our recent review, *RAFT Polymerization and Some of its Applications* (*14*). These will not be recounted in detail here. Significant developments have been made in electroactive and optoelectronic polymers (*101*) (organic semiconductors (*202–205*), materials for organic light emitting diodes (*204*), photochromics (*206*)), the biomedical field (therapeutic delivery (*184, 187–189, 207–209*), surfaces (*210, 211*) personal care (*212*)), and industrial applications (rheology control agents (*213*), surface functionalized membranes (*214*)) and many other areas.

Conclusions

RAFT Polymerization provides unprecedented access to polymers of various size, shape and composition. Polymer chemists in collaboration with biologists, physicists, material scientists and others are developing a vast range of very exciting (many potential, some actual) new materials. Multidisciplinary teams are essential for success so there is a strong incentive to collaborate.

Acknowledgments

References

1. Moad, G.; Rizzardo, E.; Thang, S. H. *Aust. J. Chem.* **2005**, *58*, 379–410.
2. Moad, G.; Rizzardo, E.; Thang, S. H. *Acc. Chem. Res.* **2008**, *41*, 1133–1142.
3. Rizzardo, E.; Solomon, D. H. *Aust. J. Chem.* **2012**, *65*, 945–969.
4. Quiclet-Sire, B.; Zard, S. Z. *Pure Appl. Chem.* **2011**, *83*, 519–551.
5. Zard, S. Z. *Aust. J. Chem.* **2006**, *59*, 663–668.
6. Solomon, D. H. *J. Polym. Sci., Part A: Polym. Chem.* **2005**, *43*, 5748–5764.
7. Jenkins, A. D.; Jones, R. I.; Moad, G. *Pure Appl. Chem.* **2010**, *82*, 483–491.
8. Hawker, C. J.; Bosman, A. W.; Harth, E. *Chem. Rev.* **2001**, *101*, 3661–3688.
9. Bertin, D.; Gigmes, D.; Marque, S. R. A.; Tordo, P. *Chem. Soc. Rev.* **2011**, *40*, 2189–2198.
10. Matyjaszewski, K.; Xia, J. *Chem. Rev.* **2001**, *101*, 2921–2990.
11. Matyjaszewski, K. *Macromolecules* **2012**, *45*, 4015–4039.

12. Kamigaito, M.; Ando, T.; Sawamoto, M. *Chem. Rev.* **2001**, *101*, 3689–3745.
13. Ouchi, M.; Terashima, T.; Sawamoto, M. *Chem. Rev.* **2009**, *109*, 4963–5050.
14. Moad, G.; Rizzardo, E.; Thang, S. H. *Chem. Asian J.* **2013**, *8*, 1634–1644.
15. Moad, G.; Rizzardo, E.; Thang, S. H. *Aust. J. Chem.* **2012**, *65*, 985–1076.
16. Moad, G.; Rizzardo, E.; Thang, S. H. *Aust. J. Chem.* **2009**, *62*, 1402–1472.
17. Moad, G.; Rizzardo, E.; Thang, S. H. *Polymer* **2008**, *49*, 1079–1131.
18. Moad, G.; Rizzardo, E.; Thang, S. H. *Aust. J. Chem.* **2006**, *59*, 669–692.
19. Moad, G.; Solomon, D. H. *The Chemistry of Radical Polymerization*, 2nd ed.; Elsevier: Oxford, 2006; pp 1−9.
20. Moad, G.; Solomon, D. H. *The Chemistry of Radical Polymerization*, 2nd ed.; Elsevier: Oxford, 2006; pp 233−278.
21. Szwarc, M. *Nature* **1956**, *178*, 1168–1169.
22. Szwarc, M.; Levy, M.; Milkovich, R. *J. Am. Chem. Soc.* **1956**, *78*, 2656–2657.
23. Szwarc, M. *J. Polym. Sci., Part A: Polym. Chem.* **1998**, *36*, IX–XV.
24. Otsu, T.; Yoshida, M. *Makromol. Chem., Rapid Commun.* **1982**, *3*, 127–132.
25. Otsu, T.; Yoshida, M.; Kuriyama, A. *Polym. Bull.* **1982**, *7*, 45–50.
26. Lewis, S. N.; Miller, J. J.; Winstein, S. *J. Org. Chem.* **1972**, *37*, 1478–1485.
27. Giese, B. *Radicals in Organic Synthesis: Formation of Carbon-Carbon Bonds*; Pergamon Press: Oxford, 1986.
28. Motherwell, W. B.; Crich, D. *Free Radical Chain Reactions in Organic Synthesis*; Academic Press: London, 1992.
29. Keck, G. E.; Enholm, E. J.; Yates, J. B.; Wiley, M. R. *Tetrahedron* **1985**, *41*, 4079–4094.
30. Barton, D. H. R.; McCombie, S. W. *J. Chem. Soc., Perkin Trans. 1* **1975**, 1574–1585.
31. Meijs, G. F.; Rizzardo, E.; Le, T. P. T. *Polym. Int.* **1991**, *26*, 239–244.
32. Rizzardo, E.; Meijs, G. F.; Thang, S. H. *Macromol. Symp.* **1995**, *98*, 101–123.
33. Moad, G.; Rizzardo, E.; Thang, S. H. Radical Addition–Fragmentation Chemistry and RAFT Polymerization. In *Polymer Science: A Comprehensive Reference*; Krzysztof, M., Martin, M., Eds.; Elsevier: Amsterdam, 2012; pp 181−226.
34. Meijs, G. F.; Rizzardo, E. *Makromol. Chem.* **1990**, *191*, 1545–1553.
35. Meijs, G. F.; Rizzardo, E.; Thang, S. H. *Macromolecules* **1988**, *21*, 3122–3124.
36. Meijs, G. F.; Morton, T. C.; Rizzardo, E.; Thang, S. H. *Macromolecules* **1991**, *24*, 3689–3695.
37. Meijs, G. F.; Rizzardo, E.; Le, T. P. T.; Chong, Y. K. *Macromol. Chem. Phys.* **1992**, *193*, 369–378.
38. Cacioli, P.; Hawthorne, D. G.; Laslett, R. L.; Rizzardo, E.; Solomon, D. H. *J. Macromol. Sci., Chem.* **1986**, *A23*, 839–852.
39. Rizzardo, E.; Harrison, D.; Laslett, R. L.; Meijs, G. F.; Morton, T. C.; Thang, S. H. *Prog. Pacific Polym. Sci.* **1991**, *2*, 77–88.
40. Corner, T. Free radical polymerisation. The synthesis of graft copolymers. In *Initiators — Poly-Reactions — Optical Activity*; Springer: Berlin, Heidelberg: 1984; Vol. 62, pp 95−142.

41. Krstina, J.; Moad, G.; Rizzardo, E.; Winzor, C. L.; Berge, C. T.; Fryd, M. *Macromolecules* **1995**, *28*, 5381–5385.

42. Krstina, J.; Moad, C. L.; Moad, G.; Rizzardo, E.; Berge, C. T.; Fryd, M. *Macromol. Symp.* **1996**, *111*, 13–23.

43. Moad, G.; Ercole, F.; Johnson, C. H.; Krstina, J.; Moad, C. L.; Rizzardo, E.; Spurling, T. H.; Thang, S. H.; Anderson, A. G. *ACS Symp. Ser.* **1998**, *685*, 332–360.

44. Moad, C. L.; Moad, G.; Rizzardo, E.; Thang, S. H. *Macromolecules* **1996**, *29*, 7717–7726.

45. Hutson, L.; Krstina, J.; Moad, C. L.; Moad, G.; Morrow, G. R.; Postma, A.; Rizzardo, E.; Thang, S. H. *Macromolecules* **2004**, *37*, 4441–4452.

46. Chiefari, J.; Jeffery, J.; Krstina, J.; Moad, C. L.; Moad, G.; Postma, A.; Rizzardo, E.; Thang, S. H. *Macromolecules* **2005**, *38*, 9037–9054.

47. Chiefari, J.; Chong, Y. K.; Ercole, F.; Krstina, J.; Jeffery, J.; Le, T. P. T.; Mayadunne, R. T. A.; Meijs, G. F.; Moad, C. L.; Moad, G.; Rizzardo, E.; Thang, S. H. *Macromolecules* **1998**, *31*, 5559–5562.

48. Keddie, D. J.; Moad, G.; Rizzardo, E.; Thang, S. H. *Macromolecules* **2012**, *45*, 5321–5342.

49. Chiefari, J.; Mayadunne, R. T. A.; Moad, C. L.; Moad, G.; Rizzardo, E.; Postma, A.; Skidmore, M. A.; Thang, S. H. *Macromolecules* **2003**, *36*, 2273–2283.

50. Benaglia, M.; Chen, M.; Chong, Y. K.; Moad, G.; Rizzardo, E.; Thang, S. H. *Macromolecules* **2009**, *42*, 9384–9386.

51. Benaglia, M.; Chiefari, J.; Chong, Y. K.; Moad, G.; Rizzardo, E.; Thang, S. H. *J. Am. Chem. Soc.* **2009**, *131*, 6914–6915.

52. Keddie, D. J.; Guerrero-Sanchez, C.; Moad, G.; Mulder, R.; Rizzardo, E.; Thang, S. H. *Macromolecules* **2012**, *45*, 4205–4215.

53. Keddie, D. J.; Guerrero-Sanchez, C.; Moad, G.; Rizzardo, E.; Thang, S. H. *Macromolecules* **2011**, *44*, 6738–6745.

54. Moad, G.; Barner-Kowollik, C. The Mechanism and Kinetics of the RAFT Process: Overview, Rates, Stabilities, Side Reactions, Product Spectrum and Outstanding Challenges. In *Handbook of RAFT Polymerization*; Barner-Kowollik, C., Ed.; Wiley-VCH: Weinheim, Germany, 2008; pp 51−104.

55. Müller, A. H. E.; Litvenko, G. *Macromolecules* **1997**, *30*, 1253–1266.

56. Müller, A. H. E.; Zhuang, R.; Yan, D.; Litvenko, G. *Macromolecules* **1995**, *28*, 4326–4333.

57. Chong, Y. K.; Krstina, J.; Le, T. P. T.; Moad, G.; Postma, A.; Rizzardo, E.; Thang, S. H. *Macromolecules* **2003**, *36*, 2256–2272.

58. Lowe, A. B.; McCormick, C. L. *Prog. Polym. Sci.* **2007**, *32*, 283–351.

59. Smith, A. E.; Xu, X.; McCormick, C. L. *Prog. Polym. Sci.* **2010**, *35*, 45–93.

60. York, S. E.; York, A. W.; McCormick, C. L. *ACS Symp. Ser.* **2010**, *1053*, 49–63.

61. Boyer, C.; Bulmus, V.; Davis, T. P.; Ladmiral, V.; Liu, J.; Perrier, S. *Chem. Rev.* **2009**, *109*, 5402–5436.

62. Moad, G.; Rizzardo, E.; Thang San, H. Fundamentals of RAFT Polymerization. In *Fundamentals of Controlled/Living Radical*

Polymerization; Tsarevsky, N. V., Sumerlin, B. S., Eds.; Royal Society of Chemistry: Cambridge, 2013; pp 205−249.

63. Moad, G.; Bicciocchi, E.; Chen, M.; Chiefari, J.; Guerrero-Sanchez, C.; Haeussler, M.; Houshyar, S.; Keddie, D.; Rizzardo, E.; Thang, S.; Tsanaktsidis, J. Some Recent Developments in RAFT Polymerization. In *Progress in Controlled Radical Polymerization: Mechanisms and Techniques*; Matyjaszewski, K., Sumerlin, B. S., Tsarevsky, N. V., Eds.; American Chemical Society: Washington, DC, 2012; Vol. 1100, pp 243−258.

64. Moad, G.; Rizzardo, E.; Thang, S. H. *Strem Chemiker* **2011**, *25*, 2–10.

65. Moad, G.; Rizzardo, E.; Thang, S. H. Radical Addition-Fragmentation Chemistry and RAFT Polymerization. In *Polymer Science: A Comprehensive Reference*, 2nd ed.; Matyjaszewski, K., Möller, M., Eds.; Elsevier BV: Amsterdam, 2012; Vol. 3, pp 181–226.

66. Destarac, M. *Polym. Rev. (Philadelphia, PA, U. S.)* **2011**, *51*, 163–187.

67. Barner-Kowollik, C.; Blinco, J. P.; Destarac, M.; Thurecht, K. J.; Perrier, S. Reversible addition fragmentation chain transfer (RAFT) polymerization: mechanism, process and applications. In *Encyclopedia of Radicals in Chemistry, Biology and Materials*; Chatgilialoglu, C., Studer, A., Eds.; John Wiley & Sons: Chichester, U.K., 2012; Vol. 4, pp 1895−1929.

68. Moad, G.; Benaglia, M.; Chen, M.; Chiefari, J.; Chong, Y., K.; Keddie, D., J.; Rizzardo, E.; Thang, S. H. Block Copolymer Synthesis through the Use of Switchable RAFT Agents. In *Non-Conventional Functional Block Copolymers*; Theato, P., Kilbinger, A. F. M., Coughlin, E. B., Eds.; American Chemical Society: Washington, DC, 2011; Vol. 1066, pp 81−102.

69. Moad, G.; Keddie, D.; Guerrero-Sanchez, C.; Rizzardo, E.; Thang, S. H. *Macromol. Symp.* **2015**, doi:10.1002/masy.201400022.

70. Moad, G. *Macromol. Chem. Phys.* **2014**, *215*, 9–26.

71. Quiclet-Sire, B.; Zard, S. Z. *Chimia* **2012**, *66*, 404–412.

72. Harrisson, S.; Liu, X.; Ollagnier, J.-N.; Coutelier, O.; Marty, J.-D.; Destarac, M. *Polymers* **2014**, *6*, 1437–1488.

73. Moad, G. *Polym. Int.* **2015**, *64*, 15–24.

74. O'Donnell, J. M. *Chem. Soc. Rev.* **2012**, *41*, 3061–3076.

75. Sun, J.-T.; Hong, C.-Y.; Pan, C.-Y. *Polym. Chem.* **2013**, *4*, 873–881.

76. Warren, N. J.; Armes, S. P. *J. Am. Chem. Soc.* **2014**, *136*, 10174–10185.

77. Keddie, D. J. *Chem. Soc. Rev.* **2013**, *2014*, 496–505.

78. Boyer, C.; Stenzel, M. H.; Davis, T. P. *J. Polym. Sci., Part A: Polym. Chem.* **2011**, *49*, 551–595.

79. An, Z.; Qiu, Q.; Liu, G. *Chem. Commun.* **2011**, *47*, 12424–12440.

80. Barner-Kowollik, C.; Blinco, J. P.; Perrier, S. Macromolecular engineering via RAFT chemistry: from sequential to modular design. In *Synthesis of Polymers: New Structures and Methods*; Schluter, A. D., Hawker, C. J., Sakamoto, J., Eds.; Wiley-VCH: Weinheim, Germany, 2012; Vol. 2, pp 601−626.

81. Gregory, A.; Stenzel, M. H. *Prog. Polym. Sci.* **2012**, *37*, 38–105.

82. Mori, H.; Endo, T. *Macromol. Rapid Commun.* **2012**, *33*, 1090–1107.

83. Moad, G.; Rizzardo, E.; Thang, S. H. *Polym. Int.* **2011**, *60*, 9–25.

84. Harvison, M. A.; Roth, P. J.; Davis, T. P.; Lowe, A. B. *Aust. J. Chem.* **2011**, *64*, 992–1006.

85. Harvison, M. A.; Lowe, A. B. *Macromol. Rapid. Commun.* **2011**, *32*, 779–800.

86. Roth, P. J.; Boyer, C.; Lowe, A. B.; Davis, T. P. *Macromol. Rapid. Commun.* **2011**, *32*, 1123–1143.

87. Nicolaÿ, R.; Kwak, Y. *Israel J. Chem.* **2012**, *52*, 288–305.

88. Brooks, W. L. A.; Sumerlin, B. S. *Israel J. Chem.* **2012**, *52*, 256–263.

89. Brooks, W. L. A.; Sumerlin, B. S. *ACS Symp. Ser.* **2012**, *1100*, 277–291.

90. Moraes, J.; Ohno, K.; Maschmeyer, T.; Perrier, S. *Chem. Commun.* **2013**, *49*, 9077–9088.

91. Zengeni, E.; Samakande, A.; Hartmann, P. C. Polymer-clay nanocomposites prepared in miniemulsion using the RAFT process. In *Polymer Nanocomposites by Emulsion and Suspension Polymerization*; Mittal, V., Ed.; Royal Society of Chemistry: Cambridge, U.K., 2011; pp 244−268.

92. Beija, M.; Marty, J.-D.; Destarac, M. *Prog. Polym. Sci.* **2011**, *36*, 845–886.

93. Ahmed, M.; Narain, R. *Prog. Polym. Sci.* **2013**, *38*, 767–790.

94. Gregory, A.; Stenzel, M. H. *Expert Opin. Drug Delivery* **2011**, *8*, 237–269.

95. Smith, D.; Holley, A. C.; McCormick, C. L. *Polym. Chem.* **2011**, *2*, 1428–1441.

96. Bulmus, V. *Polym. Chem.* **2011**, *2*, 1463–1472.

97. Chu, D. S. H.; Schellinger, J. G.; Shi, J.; Convertine, A. J.; Stayton, P. S.; Pun, S. H. *Acc. Chem. Res.* **2012**, *45*, 1089–1099.

98. Sumerlin, B. S. *ACS Macro Lett.* **2011**, *1*, 141–145.

99. Haeussler, M.; Chiefari, J.; Moad, G.; Rizzardo, E. Controlled Synthesis of Multifunctional Polymers by RAFT for Personal Care Applications. In *Polymers for Personal Care and Cosmetics*; American Chemical Society: Washington, DC, 2013; Vol. 1148, pp 157−172.

100. Laschewsky, A.; Herfurth, C.; Miasnikova, A.; Stahlhut, G.; Weiss, J.; Wieland, C.; Wischerhoff, E.; Gradzielski, M.; Malo de Molina, P. Stars and Blocks: Tailoring Polymeric Rheology Modifiers for Aqueous Media by Controlled Free Radical Polymerization. In *Polymers for Personal Care and Cosmetics*; American Chemical Society: Washington, DC, 2013; Vol. 1148, pp 125−143.

101. Moad, G.; Chen, M.; Häussler, M.; Postma, A.; Rizzardo, E.; Thang, S. H. *Polym. Chem.* **2011**, *2*, 492–519.

102. Shipp, D. A. *Polym. Rev.* **2011**, *51*, 99–103.

103. Coote, M. L. Ab initio kinetic modeling of free-radical polymerization. In *Rate Constant Calculation for Thermal Reactions*; DaCosta, H., Fan, M., Eds.; John Wiley & Sons: Hoboken, NJ, 2012; pp 283−304.

104. Fukuda, T.; Goto, A. Controlled and Living Radical Polymerization – Principles and Fundamentals. In *Polymer Science: A Comprehensive Reference*; Matyjaszewski, K., Möller, M., Eds.; Elsevier: Amsterdam, 2012; pp 119−157.

105. Fu, R.; Fu, G.-D. *Polym. Chem.* **2011**, *2*, 465–475.

106. Slavin, S.; Burns, J.; Haddleton, D. M.; Becer, C. R. *Eur. Polym. J.* **2011**, *47*, 435–446.

107. Lowe, A. B. *Polym. Chem.* **2010**, *1*, 17–36.

108. Akeroyd, N.; Klumperman, B. *Eur. Polym. J.* **2011**, *47*, 1207–1231.

109. Barner-Kowollik, C.; Du Prez, F. E.; Espeel, P.; Hawker, C. J.; Junkers, T.; Schlaad, H.; Van Camp, W. *Angew. Chem., Int. Ed. Engl.* **2011**, *50*, 60–62.

110. Yamago, S.; Nakamura, Y. *Polymer* **2013**, *54*, 981–994.

111. Tasdelen, M. A.; Kahveci, M. U.; Yagci, Y. *Prog. Polym. Sci.* **2011**, *36*, 455–567.

112. Nakabayashi, K.; Mori, H. *Int. J. Polym. Sci.* **2012**, *2012*, 170912.

113. Beghdadi, S.; Miladi, I. A.; Addis, D.; Romdhane, H. B.; Bernard, J.; Drockenmuller, E. *Polym. Chem.* **2012**, *3*, 1680–1692.

114. Green, M. D.; Allen, M. H., Jr.; Dennis, J. M.; Salas-de la Cruz, D.; Gao, R.; Winey, K. I.; Long, T. E. *Eur. Polym. J.* **2011**, *47*, 486–496.

115. Yang, Q. Block glycopolymers and their self-assembly properties. In *Engineered Carbohydrate-Based Materials for Biomedical Applications*; Narain, R., Ed.; John Wiley & Sons: Hoboken, NJ, 2011; pp 119−141.

116. Becer, C. R. *Macromol. Rapid. Commun.* **2012**, *33*, 742–752.

117. Hardy, C. G.; Ren, L.; Zhang, J.; Tang, C. *Isr. J. Chem.* **2012**, *52*, 230–245.

118. Stefan, M. C.; Bhatt, M. P.; Sista, P.; Magurudeniya, H. D. *Polym. Chem.* **2012**, *3*, 1693–1701.

119. Beija, M.; Charreyre, M.-T.; Martinho, J. M. G. *Prog. Polym. Sci.* **2011**, *36*, 568–602.

120. Cayre, O. J.; Chagneux, N.; Biggs, S. *Soft Matter* **2011**, *7*, 2211–2234.

121. Lutz, J.-F. *Adv. Mater.* **2011**, *23*, 2237–2243.

122. Flores, J. D.; Abel, B. A.; Smith, D.; McCormick, C. L. Stimuli-Responsive Polymers Via Controlled Radical Polymerization. In *Monitoring Polymerization Reactions*; John Wiley & Sons: 2013; pp 45−58.

123. Kakwere, H.; Perrier, S. *Polym. Chem.* **2011**, *2*, 270–288.

124. Broyer, R. M.; Grover, G. N.; Maynard, H. D. *Chem. Commun.* **2011**, *47*, 2212–2226.

125. Dehn, S.; Chapman, R.; Jolliffe, K. A.; Perrier, S. *Polym. Rev.* **2011**, *51*, 214–234.

126. Barz, M.; Luxenhofer, R.; Zentel, R.; Vicent, M. J. *Polym. Chem.* **2011**, *2*, 1900–1918.

127. Xu, F. J.; Yang, W. T. *Prog. Polym. Sci.* **2011**, *36*, 1099–1131.

128. Tucker, B. S.; Sumerlin, B. S. *Polym. Chem.* **2014**, *5*, 1566–1572.

129. Wallat, J. D.; Rose, K. A.; Pokorski, J. K. *Polym. Chem.* **2014**, *5*, 1545–1558.

130. Malmstrom, E.; Carlmark, A. *Polym. Chem.* **2012**, *3*, 1702–1713.

131. Charleux, B.; D'Agosto, F.; Delaittre, G. Preparation of Hybrid Latex Particles and Core−Shell Particles Through the Use of Controlled Radical Polymerization Techniques in Aqueous Media. In *Hybrid Latex Particles*; van Herk, A. M., Landfester, K., Eds.; Springer: Berlin, 2011; Vol. 233, pp 125−183.

132. Ebner, C.; Bodner, T.; Stelzer, F.; Wiesbrock, F. *Macromol. Rapid Commun.* **2011**, *32*, 254–288.

133. Kempe, K.; Becer, C. R.; Schubert, U. S. *Macromolecules* **2011**, *44*, 5825–5842.

134. Grishin, D.; Grishin, I. *Russ. J. Appl. Chem.* **2011**, *84*, 2021–2028.

242

In Controlled Radical Polymerization: Mechanisms; Tsarevsky, et al.;
ACS Symposium Series; American Chemical Society: Washington, DC, 2015.

135. Barner-Kowollik, C.; Buback, M.; Charleux, B.; Coote, M. L.; Drache, M.; Fukuda, T.; Goto, A.; Klumperman, B.; Lowe, A. B.; Mcleary, J. B.; Moad, G.; Monteiro, M. J.; Sanderson, R. D.; Tonge, M. P.; Vana, P. *J. Polym. Sci., Part A: Polym. Chem.* **2006**, *44*, 5809–5831.

136. Delduc, P.; Tailhan, C.; Zard, S. Z. *J. Chem. Soc., Chem. Commun.* **1988**, 308–310.

137. Zard, S. Z. *Angew. Chem., Int. Ed. Engl.* **1997**, *36*, 672–685.

138. Quiclet-Sire, B.; Zard, S. Z. *Top. Curr. Chem.* **2006**, *264*, 201–236.

139. Quiclet-Sire, B.; Zard, S. Z. *Chem. Eur. J.* **2006**, *12*, 6002–6016.

140. Quiclet-Sire, B.; Zard, S. Z. *Org. Lett.* **2008**, *10*, 3279–3282.

141. Lebreux, F.; Quiclet-Sire, B.; Zard, S. Z. *Org. Lett.* **2009**, *11*, 2844–2847.

142. Quiclet-Sire, B.; Revol, G.; Zard, S. Z. *Tetrahedron* **2010**, *66*, 6656–6666.

143. McLeary, J. B.; Calitz, F. M.; McKenzie, J. M.; Tonge, M. P.; Sanderson, R. D.; Klumperman, B. *Macromolecules* **2004**, *37*, 2383–2394.

144. McLeary, J. B.; Calitz, F. M.; McKenzie, J. M.; Tonge, M. P.; Sanderson, R. D.; Klumperman, B. *Macromolecules* **2005**, *38*, 3151–3161.

145. McLeary, J. B.; McKenzie, J. M.; Tonge, M. P.; Sanderson, R. D.; Klumperman, B. *Chem. Commun.* **2004**, 1950–1951.

146. McLeary, J. B.; Tonge, M. P.; Klumperman, B. *Macromol. Rapid Commun.* **2006**, *27*, 1233–1240.

147. Pound, G.; McLeary, J. B.; McKenzie, J. M.; Lange, R. F. M.; Klumperman, B. *Macromolecules* **2006**, *39*, 7796–7797.

148. van den Dungen, E. T. A.; Matahwa, H.; McLeary, J. B.; Sanderson, R. D.; Klumperman, B. *J. Polym. Sci., Part A: Polym. Chem.* **2008**, *46*, 2500–2509.

149. van den Dungen, E. T. A.; Rinquest, J.; Pretorius, N. O.; McKenzie, J. M.; McLeary, J. B.; Sanderson, R. D.; Klumperman, B. *Aust. J. Chem.* **2006**, *59*, 742–748.

150. Haven, J. J.; Guerrero-Sanchez, C.; Keddie, D. J.; Moad, G. *Macromol. Rapid Commun.* **2014**, *35*, 492–497.

151. Haven, J. J.; Guerrero-Sanchez, C.; Keddie, D. J.; Moad, G.; Thang, S. H.; Schubert, U. S. *Polym. Chem.* **2014**, *5*, 5236–5246.

152. Vandenbergh, J.; de Moraes Ogawa, T.; Junkers, T. *J. Polym. Sci., Part A: Polym. Chem.* **2013**, *51*, 2366–2374.

153. Gody, G.; Maschmeyer, T.; Zetterlund, P. B.; Perrier, S. *Macromolecules* **2014**, *47*, 639–649.

154. Anastasaki, A.; Waldron, C.; Wilson, P.; Boyer, C.; Zetterlund, P. B.; Whittaker, M. R.; Haddleton, D. *ACS Macro Lett.* **2013**, *2*, 896–900.

155. Houshyar, S.; Keddie, D.; Moad, G.; Mulder, R.; Saubern, S.; Tsanaktsidis, J. *Polym. Chem.* **2012**, *3*, 1879–1889.

156. Moad, G.; Guerrero-Sanchez, C.; Haven, J. J.; Keddie, D. J.; Postma, A.; Rizzardo, E.; Thang, S. H. RAFT for the Control of Monomer Sequence Distribution – Single Unit Monomer Insertion (SUMI) into Dithiobenzoate RAFT Agents. In *Sequence-Controlled Polymers: Synthesis, Self-assembly and Properties*; Lutz, J.-F., Ouchi, M., Sawamoto, M., Meyer, T., Eds.; American Chemical Society: Washington, DC, 2014; Vol. 1170, pp 133−147.

157. Kang, Y.; Lu, A.; Ellington, A.; Jewett, M. C.; O'Reilly, R. K. *ACS Macro Lett.* **2013**, *2*, 581–586.

158. Williams, E. G. L.; Thang, S.; Mulder, R. J.; Moad, G.; Fairbanks, B. D.; Rizzardo, E. *Polym. Chem.* **2015**, *6*, 228–232.

159. Destarac, M.; Taton, D.; Zard, S. Z.; Saleh, T.; Six, Y. *ACS Symp. Ser.* **2003**, *854*, 536–550.

160. Malepu, V.; Petruczok Christy, D.; Tran, T.; Zhang, T.; Thopasridharan, M.; Shipp Devon, A. *ACS Symp. Ser.* **2009**, *1024*, 37–47.

161. Keddie, D. J.; Guerrero-Sanchez, C.; Moad, G. *Polym. Chem.* **2013**, *4*, 3591–3601.

162. Destarac, M. *Macromol. React. Eng.* **2010**, *4*, 165–179.

163. Couvreur, L.; Guerret, O.; Laffitte, J.-A.; Magnet, S. *Polym. Prepr. (Am. Chem. Soc., Div. Polym. Chem.)* **2005**, *46*, 219–220.

164. Moad, G.; Rizzardo, E.; Thang, S. H. *Mater. Matters* **2010**, *5*, 2–5.

165. BoronMolecular. RAFT Agents. http://www.boronmolecular.com/RaftAgents.

166. Moad, G.; Rizzardo, E.; Thang, S. H. Process for synthesizing thiol terminated polymers. US8283436, E. I. du Pont de Nemours and Company, USA, 2012.

167. Moad, G.; Thang, S. H.; Rizzardo, E. Process for transforming the end groups of polymers. US8569441, Commonwealth Scientific and Industrial Research Organisation, Australia. 2013.

168. Nicolaÿ, R.; Kamada, J.; Van Wassen, A.; Matyjaszewski, K. *Macromolecules* **2010**, *43*, 4355–4361.

169. Amamoto, Y.; Kamada, J.; Otsuka, H.; Takahara, A.; Matyjaszewski, K. *Angew. Chem., Int. Ed. Engl.* **2011**, *50*, 1660–1663.

170. Amamoto, Y.; Otsuka, H.; Takahara, A.; Matyjaszewski, K. *ACS Macro Lett.* **2012**, *1*, 478–481.

171. Leung, D.; Bowman, C. N. *Macromol. Chem. Phys.* **2012**, *213*, 198–204.

172. Fenoli, C. R.; Wydra, J. W.; Bowman, C. N. *Macromolecules* **2014**, *47*, 907–915.

173. Barlow, K. J.; Hao, X.; Hughes, T. C.; Hutt, O. E.; Polyzos, A.; Turner, K. A.; Moad, G. *Polym. Chem.* **2014**, *5*, 722–732.

174. López-Domínguez, P.; Hernández-Ortiz, J. C.; Barlow, K. J.; Vivaldo-Lima, E.; Moad, G. *Macromol. React. Eng.* **2014**, *8*, 706–722.

175. Barlow, K. J.; Hao, X.; Hughes, T. C.; Hutt, O. E.; Polyzos, A.; Turner, K. A.; Moad, G. *Polym. Chem.* **2015**, to be submitted.

176. Isaure, F.; Cormack, P. A. G.; Graham, S.; Sherrington, D. C.; Armes, S. P.; Butun, V. *Chem. Commun.* **2004**, 1138–1139.

177. O'Brien, N.; McKee, A.; Sherrington, D. C.; Slark, A. T.; Titterton, A. *Polymer* **2000**, *41*, 6027–6031.

178. Rosselgong, J.; Armes, S. P. *Macromolecules* **2012**, *45*, 2731–2737.

179. Blencowe, A.; Tan, J. F.; Goh, T. K.; Qiao, G. G. *Polymer* **2009**, *50*, 5–32.

180. Chen, Q.; Cao, X.; Xu, Y.; An, Z. *Macromol. Rapid. Commun.* **2013**, *34*, 1507–1517.

181. Gao, H.; Matyjaszewski, K. *Prog. Polym. Sci.* **2009**, *34*, 317–350.

182. Solomon, D. H.; Qiao, G. G.; Abrol, S. Process for microgel preparation. WO9958588A1, The University of Melbourne, 1999.

183. Berge, C. T.; Fryd, M.; Johnson, J. W.; Moad, G.; Rizzardo, E.; Scopazzi, C.; Thang, S. H. Microgels and process for their preparation. WO2000002939A1, Du Pont, CSIRO, 2000.

184. Wei, X.; Moad, G.; Muir, B. W.; Rizzardo, E.; Rosselgong, J.; Yang, W.; Thang, S. H. *Macromol. Rapid Commun.* **2014**, *35*, 840–845.

185. Ferreira, J.; Syrett, J.; Whittaker, M.; Haddleton, D.; Davis, T. P.; Boyer, C. *Polym. Chem.* **2011**, *2*, 1671–1677.

186. Shi, X.; Zhou, W.; Qiu, Q.; An, Z. *Chem. Commun.* **2012**, *48*, 7389–7391.

187. Wei, X.; Gunatillake, P.; Moad, G.; Rizzardo, E.; Rosselgong, J.; Yang, W.; Thang, S. *Sci. China: Chem.* **2014**, *57*, 1–7.

188. Rosselgong, J.; Williams, E. G.; Le, T. P.; Grusche, F.; Hinton, T. M.; Tizard, M.; Gunatillake, P.; Thang, S. H. *Macromolecules* **2013**, *46*, 9181–9188.

189. Wilson, J. T.; Postma, A.; Keller, S.; Convertine, A. J.; Moad, G.; Rizzardo, E.; Meagher, L.; Chiefari, J.; Stayton, P. S. *AAPS J.* **2015**, *17*, 358–369.

190. Hornung, C. H.; Guerrero-Sanchez, C.; Brasholz, M.; Saubern, S.; Chiefari, J.; Moad, G.; Rizzardo, E.; Thang, S. H. *Org. Proc. Res. Dev.* **2011**, *15*, 593–601.

191. Hornung, C. H.; Postma, A.; Saubern, S.; Chiefari, J. *Macromol. React. Eng.* **2012**, *6*, 246–251.

192. Hornung, C. H.; Nguyen, X.; Dumsday, G.; Saubern, S. *Macromol. React. Eng.* **2012**, *6*, 458–466.

193. Hornung, C. H.; Nguyen, X.; Kyi, S.; Chiefari, J.; Saubern, S. *Aust. J. Chem.* **2013**, *66*, 192–198.

194. Hornung, C. H.; Postma, A.; Saubern, S.; Chiefari, J. *Polymer* **2014**, *55*, 1427–1435.

195. Hornung, C. H.; von Känel, K.; Martinez-Botella, I.; Espiritu, M.; Nguyen, X.; Postma, A.; Saubern, S.; Chiefari, J.; Thang, S. H. *Macromolecules* **2014**, *47*, 8203–8213.

196. Vandenbergh, J.; de Moraes Ogawa, T.; Junkers, T. *J. Polym. Sci., Part A: Polym. Chem.* **2013**, *51*, 2366–2374.

197. Diehl, C.; Laurino, P.; Azzouz, N.; Seeberger, P. H. *Macromolecules* **2010**, *43*, 10311–10314.

198. Guerrero-Sanchez, C.; O'Brien, L.; Brackley, C.; Keddie, D. J.; Saubern, S.; Chiefari, J. *Polym. Chem.* **2013**, *4*, 1857–1862.

199. Hinton, T. M.; Guerrero-Sanchez, C.; Graham, J. E.; Le, T.; Muir, B. W.; Shi, S.; Tizard, M. L. V.; Gunatillake, P. A.; McLean, K. M.; Thang, S. H. *Biomaterials* **2012**, *33*, 7631–7642.

200. Guerrero-Sanchez, C.; Keddie, D. J.; Saubern, S.; Chiefari, J. *ACS Comb. Sci.* **2012**, *14*, 389–394.

201. Guerrero-Sanchez, C.; Harrisson, S.; Keddie, D. J. *Macromol. Symp.* **2013**, *325-326*, 38–46.

202. Chen, M.; Haeussler, M.; Moad, G.; Rizzardo, E. *Org. Biomol. Chem.* **2011**, *9*, 6111–6119.

203. Bicciocchi, E.; Chen, M.; Rizzardo, E.; Ghiggino, K. P. *Polym. Chem.* **2013**, *4*, 53–56.

204. Adhikari, R.; Postma, A.; Li, J.; Arima, K.; Hirai, T.; Shimizu, H.; Ueno, K. *J. Inst. Image Inform. Televis. Eng.* **2012**, *66*, 370–376.

205. Chen, M.; Moad, G.; Rizzardo, E.; Evans, R. A.; Haeussler, M. Conducting and Semiconducting Organic Materials. US8501889, CSIRO, 2013.

206. Ercole, F.; Harrisson, S.; Davis, T. P.; Evans, R. A. *Soft Matter* **2011**, *7*, 2687–2696.

207. Williams, C. C.; Thang, S. H.; Hantke, T.; Vogel, U.; Seeberger, P. H.; Tsanaktsidis, J.; Lepenies, B. *ChemMedChem* **2012**, *7*, 281–291.

208. Ercole, F.; Thissen, H.; Tsang, K.; Evans, R. A.; Forsythe, J. S. *Macromolecules* **2012**, *45*, 8387–8400.

209. Chong, J. Y. T.; Mulet, X.; Postma, A.; Keddie, D. J.; Waddington, L. J.; Boyd, B. J.; Drummond, C. J. *Soft Matter* **2014**, *10*, 6666–6676.

210. Ameringer, T.; Ercole, F.; Tsang, K. M.; Coad, B. R.; Hou, X.; Rodda, A.; Nisbet, D. R.; Thissen, H.; Evans, R. A.; Meagher, L.; Forsythe, J. S. *Biointerphases* **2013**, *8*, 16.

211. Fairbanks, B. D.; Thissen, H.; Maurdev, G.; Pasic, P.; White, J. F.; Meagher, L. *Biomacromolecules* **2014**, *15*, 3259–3266.

212. Haeussler, M.; Moad, G.; Rizzardo, E.; Chiefari, J. *AustralAs. J. Cosmet. Sci.* **2012**, *25*, 22–25.

213. Brzytwa, A. J.; Johnson, J. *Polym. Prepr. (Am. Chem. Soc., Div. Polym. Chem)* **2011**, *52*, 533–534.

214. Stenzel, M. H.; Godoy-Lopez, R.; Harrisson, S.; Rizzardo, E. Production of functionalized thin film composite polyamide membranes. US8544658, Polymers CRC Limited, Australia, 2013.

Chapter 13

Catalyst-Free Visible Light-Induced RAFT Photopolymerization

**Jiangtao Xu,* Sivaprakash Shanmugam,
Nathaniel Alan Corrigan, and Cyrille Boyer***

**Centre for Advanced Macromolecular Design (CAMD) and Australian
Centre for NanoMedicine, School of Chemical Engineering,
UNSW Australia, Sydney, NSW 2052, Australia
*E-mail: cboyer@unsw.edu.au; j.xu@unsw.edu.au**

In contrast to thermoinitiated polymerization techniques, photoinitiated systems offer more attractive benefits, such as spatio-temporal control and polymerization rate control through a modulation of light intensity and wavelength. Until recently, there were very few living/controlled polymerization techniques which could be activated by visible light. In this contribution, we investigate the photolysis of different thiocarbonylthio compounds, including 4-cyano-4-[(dodecylsulfanylthiocarbonyl)sulfanyl]pentanoic acid (CDTPA), 2-(dodecylthiocarbonothioylthio)-2-methylpropionic acid (DDMAT), 4-cyanopentanoic acid dithiobenzoate (CPADB), and 2-(*n*-butyltrithiocarbonate) propionic acid (BTPA), under visible lights (typically, 5W) to initiate a reversible addition-fragmentation chain transfer (RAFT) polymerization. This is the first report which shows successful polymerizations of methacrylate monomers under visible LED light. Successful polymerization were obtained in the presence of CDTPA under blue and green LED light. A good control of the molecular weight as well as a low molecular weight distribution was achieved under green light.

Introduction

Living radical polymerization techniques, including atom transfer radical polymerization (ATRP) (*1–6*), reversible addition-fragmentation chain transfer polymerization (RAFT) (*7–9*), nitroxide mediated polymerization (NMP) (*10*) and iodine transfer polymerization (*11, 12*) have changed polymer chemistry by providing capability to engineer functional macromolecules to yield well-defined complex architectures, which could find applications in thermoplastic elastomers, coatings, surfactant dispersants, water remediation, and biomedical applications including drug delivery and tissue engineering, etc. However, so far the majority of these polymerization techniques are triggered and mediated by the thermal decomposition of initiator, which thus do not afford a spatial or temporal control of polymerization behavior. As a matter of fact, one of the earliest examples of pseudo-'controlled/living' radical polymerization (*13*) was reported in 1982 by Otsu and co-workers (*14, 15*) using iniferter (initiator-transfer agent-terminator) compounds, including xanthogene, thiuram, and dithiocarbamate derivatives. In this seminal work, Otsu and co-workers (*14, 16, 17*) have demonstrated that tetraethylthiuram disulfide and other thiurams could act as initiator, chain transfer agent and termination agent under ultraviolet (UV) light irradiation. This process paved the way to produce block copolymers with a relative good control over molecular weights, although the polydispersities were relatively high (typically, greater than 1.5) (*16*).

Recently, with the emergence of RAFT polymerization technique (*8, 18–21*), thiocarbonylthio compounds were employed for photocontrolled radical polymerization in the presence or absence of photoinitiator under UV light. Early papers have reported successful RAFT polymerizations triggered by high energy UV light via photolysis of thiocarbonylthio compound, such as dithiobenzoate (*22*), trithiocarbonate (*23–25*), dithiocarbamate (*26–28*), xanthate (*29, 30*) or disulfide (*31*). For instance, Johonston and co-workers (*24*) have prepared thermoresponsive hydrogels by exposure of a bis-norbornene trithiocarbonate to sunlight or long wavelength UV light. However, the use of UV light presents several limitations due to the slow degradation of RAFT agents (*21, 22, 32–34*), which generally lead to less control, especially at high monomer conversions. In addition, the presence of UV light absorbance for most organic compounds undesirably results in the side reactions associated with photochemical reactions conducted with high energy UV light. To overcome this drawback, Cai (*32, 35–37*), Kamigaito (*38*) and co-workers have demonstrated the use of photoinitiator to induce RAFT polymerization under visible light.

Since 2012, new polymerization techniques initiated or activated by visible light have been intensively developed by Haddleton (*39–41*), Hawker (*42–46*), Matyjaszewski (*28, 47–49*), Yagci (*50–56*), Lalevee (*31, 57–60*) and others (*61–75*). In this area, we have also developed a polymerization technique which utilizes photoredox catalysts to activate a photoinduced electron transfer (PET) process (*76–79*) and a simultaneous RAFT process under light (Scheme 1A), named PET-RAFT polymerization (*80–84*). In this technique, thiocarbonylthio compound acts as an initiator repeatedly reduced by excited photocatalyst via PET process and a chain transfer agent. In this condition, thiocarbonylthio compound

plays the role of an "iniferter", which avoids the use of external initiator. Several photoredox catalysts and biocatalysts, such as *fac*-[Ir(ppy)₃] (*80*), Ru(bpy)₃Cl₂ (*81*), eosin Y (*83*), chlorophyll a (*84*), etc., were successfully employed for the polymerization of large range of monomers, including styrene, (meth)acrylates, (meth)acrylamides, vinyl esters, etc. During the investigation of this project, we discovered that several specific thiocarbonylthio compounds can be unexpectedly photolyzed, and subsequently, activated radical polymerization in the absence of photoredox catalyst under visible light, especially under blue and green LED lights (Scheme 1B). In this contribution, we investigated the photolysis of four thiocarbonylthio compounds (Scheme 2) commonly used as RAFT agent under blue, green and red LED lights to initiate and control the polymerization of methacrylates and acrylates. This is the first report which shows successful polymerization of MMA under LED light in the absence of photoinitiator/thermal initiator or photoredox catalyst.
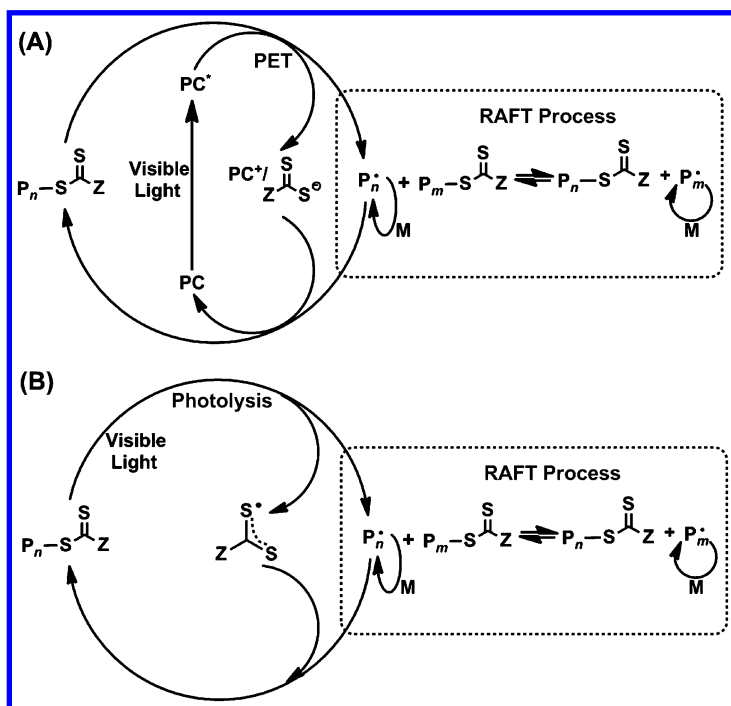
Scheme 1. Comparison of proposed mechanism for PET-RAFT (A) and RAFT photopolymerization in this study (B). Note: PC, photoredox catalyst.
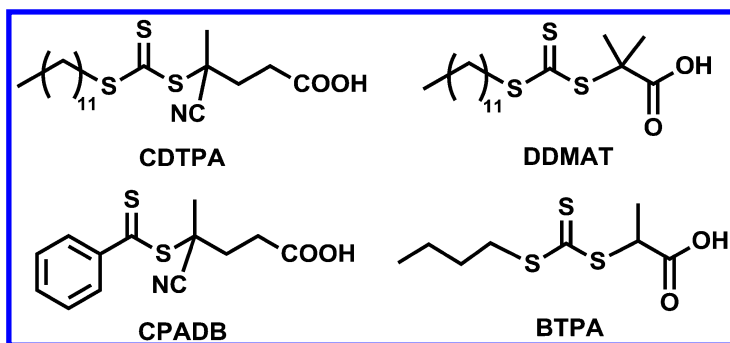
Scheme 2. Thiocarbonylthio compounds investigated in this study.

Experimental Section

Materials

Methyl methacrylate (99%), methy acrylate (99%), 4-Cyano-4-[(dodecylsulfanylthiocarbonyl)sulfanyl] pentanoic acid (CDTPA), and 2-(Dodecylthiocarbonothioyl- thio)-2-methylpropionic acid (DDMAT) were all purchased from Aldrich and used as received. *N,N*-dimethylformamide (DMF, 99.8%,), dimethyl sulfoxide (DMSO), acetonitrile (MeCN), toluene and 1,4-dioxane were purchased from Ajax Chemicals and also used as received. Chain transfer agent, 4-cyanopentanoic acid dithiobenzoate (CPADB) and 2-(n-butyltrithiocarbonate)-propionic acid (BTPA) were synthesized according to literature procedures (*1*).

Instrumentation

Gel Permeation Chromatography (GPC)

Gel permeation chromatography (GPC) was performed using tetrahydrofuran (THF) or dimethylacetamide (DMAc) as the eluent. The GPC system was a Shimadzu modular system comprising an auto injector, a Phenomenex 5.0 μm beadsize guard column (50 × 7.5 mm) followed by three Phenomenex 5.0 μm bead-size columns (10^5, 10^4, and 10^3 Å), and a differential refractive-index detector. The system was calibrated with narrow molecular weight distribution polystyrene standards with molecular weights of 200 to 10^6 g mol^{-1}.

Nuclear Magnetic Resonance (NMR) Spectroscopy

Nuclear magnetic resonance (NMR) spectroscopy was carried out on a Bruker DPX 300 spectrometer operating at 300.17 MHz for ^{1}H and 75.48 MHz for ^{13}C using CDCl$_3$ and DMSO-d_6 as solvents and tetramethylsilane (TMS) as

a reference. Data was reported as follows: chemical shift (δ) measured in ppm downfield from TMS; multiplicity; proton count. Multiplicities were reported as singlet (s), broad single (bs), doublet (d), triplet (t), and multiplet (m).

On-Line Fourier Transform Near-Infrared (FTNIR) Spectroscopy

On-line Fourier Transform Near-Infrared (FTNIR) spectroscopy was used for determination of monomer conversion by mapping the decrement of the vinylic C-H stretching overtone of the monomer at ~ 6200 cm^{-1}. A Bruker IFS 66/S Fourier transform spectrometer equipped with a tungsten halogen lamp, a CaF$_2$ beam splitter and liquid nitrogen cooled InSb detector was used. Polymerizations in blue or red LED lights were carried out using FT-NIR quartz cuvette (1 cm × 2 mm). A spectrum composed of 16 scan with a resolution of 4 cm^{-1} was collected in the spectral region between 7000-4000 cm^{-1} by manually placing the sample into the holder at time intervals of 5, 10, or 30 minutes. The total collection time per spectrum was about 10 seconds and analysis was carried out with OPUS software.

UV-Vis Spectroscopy

UV-vis Spectroscopy spectra were recorded using a CARY 300 spectrophotometer (Varian) equipped with a temperature controller.

Photopolymerization (*24*)

Photopolymerization was carried out in the reaction vessel where the reaction mixtures are irradiated by RS Component PACK LAMP RGB blue, green and red LED lights (5 W, λ_{max} = 461 nm (blue), 530 nm (green), 635 nm (red)) shown below. The distance of the samples to light bulb was 6 cm. The RGB multi-coloured LED light bulb with remote control was purchased from RS Components Australia.

General Procedure for the Synthesis of Methyl Methacrylate (MMA) via RAFT Photopolymerization

Photopolymerization of MMA was carried out in a 5mL glass vial with a rubber septum in the presence of DMSO (0.5 mL), MMA (0.47 g, 4.7 mmol), and CDTPA (9.5 mg, 0.0236 mmol). The glass vial was wrapped with aluminium foil and degassed with nitrogen for 20 minutes. The degassed mixture was then irradiated in blue LED light (5 W, λ_{max} = 461 nm) at room temperature. After 5 hours of irradiation, the reaction mixture was removed from the light source to be analysed by ^{1}H NMR (CDCl$_3$) and GPC (DMAc) to determine the conversions, number-average molecular weights (M_n) and polydispersities (M_w/M_n).

General Procedures for Kinetic Studies of RAFT Photopolymerization of Methyl Methacrylate (MMA) with Online Fourier Transform Near-Infrared (FTNIR) Spectroscopy

A reaction stock solution consisting of DMSO (0.5 mL), MMA (0.47 g, 4.7 mmol), and CDTPA (9.5 mg, 0.0236 mmol) was prepared in a glass vial. Approximately 700 μL of stock solution was transferred into a 1 mL FTNIR quartz cuvette (1 cm × 2 mm) covered with aluminium foil. The reaction mixture in the cuvette was degassed for 20 minutes with nitrogen and then irradiated in blue LED light (5 W, λ_{max} = 461 nm) at room temperature. The cuvette was transferred to a sample holder manually for FTNIR measurements every 20 minutes. After 5 seconds of scanning, the cuvette was transferred back to the irradiation source. Monomer conversions were calculated by taking the ratio of integrations of the wavenumber area 6250-6150 cm^{-1} for all curves at different reaction times to that of 0 minutes. Aliquots of reaction samples were taken at specific time points during the reaction to be analysed by ^{1}H NMR (CDCl$_3$) and GPC (DMAc) to determine the conversions, number average molecular weights (M_n) and polydispersities (M_w/M_n).

For other polymerization kinetics under different light sources (green or red LED light) or different intensity light sources (1 W or 3 W), and in different solvents, the formulations are kept the same as above, except for the solvents, light sources, and light intensities.

Results and Discussion

1. Screening of Thiocarbonylthio Compounds and Light Sources

Four thiocarbonylthio compounds with different activation groups (Z group) and leaving groups (R group) (Scheme 1), including 4-cyano-4-[(dodecylsulfanylthiocarbonyl)sulfanyl]pentanoic acid (CDTPA), 2-(dodecylthiocarbonothioylthio)-2-methylpropionic acid (DDMAT), 4-cyanopentanoic acid dithiobenzoate (CPADB), and 2-(*n*-butyltrithiocarbonate) propionic acid (BTPA), were investigated for photolysis to initiate polymerization of methyl methacrylate under blue, green and red LED lights. The choice of these compounds was motivated to compare two different families of RAFT agents, i.e. dithiobenzoate (CPADB) and trithiocarbonate (CDTPA, DDMAT and BTPA). In addition, the fragmentation rates of leaving groups of these thiocarbonylthio were chosen to present different reactivity to conduct RAFT polymerization. These thiocarbonylthio can be ranked according to the following order: CDTPA ~ CPADB > DDMAT (tertiary carbon) > BTPA (secondary carbon) (*18*, *21*). Moreover, these RAFT agents present different visible absorption from 432 nm to 513 nm (Figure 1).
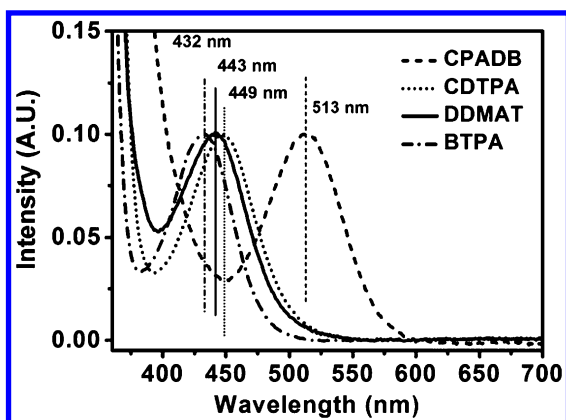
Figure 1. Visible absorption of the RAFT agents employed in this study.

To screen the thiocarbonylthio compounds and light sources, the photopolymerization was initially carried out using the molar ratio of [monomer]:[thiocarbonylthio compounds] = 200:1 at room temperature in dimethyl sulfoxide (DMSO), employing two commonly used monomers, methyl acrylate (MA) and methyl methacrylate (MMA). In the first part, MMA was tested with the four thiocarbonylthio compounds under three LED lights (λ_{max} = 461 ±20 (blue), 530 ±20 (green) and 635 ±20 nm (red)). The choice of these wavelengths was motivated by the different absorption of RAFT agent. Indeed, CDTPA, BTPA and DDMAT present a strong absorption in the region between 430 to 450 which corresponds to the blue light, while CPADB shows a strong absorption at 513 nm corresponding to green light. In addition, CPADB shows a weak absorption in the blue region (i.e., ~430 nm). The polymerization results with these various RAFT agents were shown in Table 1. In order to exclude the possible effect of self-initiation of monomer under light irradiation, the control experiment of MMA in the absence of thiocarbonylthio compounds was examined. No monomer conversions were detected for all the lights (Table 1, # 1). Taking no account of the possible diversity of light from different manufacturers, this result appeared consistent with the data reported by Haddleton (*41*), Hawker (*42*) and co-workers. The polymerization of MMA in the presence of CPADB (Table 1, # 2) and BTPA (Table 1, # 5) showed very low monomer conversion (~10 %) after 24 h blue light irradiation, suggesting of sluggish photopolymerization, which could be attributed to slow photolysis of the RAFT agents. In the case of CPADB is expected as a very low absorption was observed in the blue region. For BTPA, the slow fragmentation could be attributed to the stability of C-S bond between R and trithiocarbonate. Previous reports (*22–25, 85*) support these results and recommended the use of UV light to activate the polymerization of these thiocarbonylthio compounds. In addition, BTPA leads, as expected, to uncontrolled polymerization of MMA due to the difference between the initiating radical from leaving group of RAFT agent (secondary carbon) and the propagating radical (tertiary carbon), which was previously described for conventional RAFT polymerization (*18*).

Table 1. Photopolymerization of MMA and MA in the presence of different thiocarbonylthio compounds under LED light irradiation.[a]

#	RAFT Agent	Monomer	Time (h)	α [b] (%)			$M_{n, th.}$ [c] (g/mol)	$M_{n,GPC}$ [d] (g/mol)	M_w/M_n [d]
				Red	Green	Blue			
1	none	MMA	24	0	0	0	0	-	-
2	CPADB	MMA	24	-	-	10[e]	2600	5050	1.26
3	CDTPA	MMA		~2 (24 h)	83.3 (12 h)	59.6 (3 h)	17060 (Green) 12320 (Blue)	15310 (Green) 12690 (Blue)	1.10 (Green) 1.30 (Blue)
4	DDMAT	MMA		-	0 (24 h)	65.7 (5 h)	13500	43460	1.80
5	BTPA	MMA	24	-	-	11	2130	436800	1.78
6	none	MA	18	-	-	0	0	-	-
7	CPADB	MA	18	-	-	0	0	-	-
8	CDTPA	MA	6	-	-	40.4	7350	6810	1.20
9	DDMAT	MA	6	-	-	33.9	6190	7990	1.29
10	BTPA	MA	6	-	-	0	0	-	-

[a] The polymerizations were performed using the ratio of [monomer]:[thiocarbonylthio] = 200:1 in the absence of oxygen at room temperature in dimethylsulfoxide (DMSO) using 5 W LED light (red, λ_{max} = 635 nm; green, λ_{max} = 530 nm; blue, λ_{max} = 461 nm). [b] Monomer conversion was determined by ^{1}H NMR spectroscopy. [c] Theoretical molecular weight was calculated using the following equation: $M_{n,th}$ = [M]$_o$/[thiocarbonylthio]$_0$ × MW^M × α + MW^{thiocarbonylthio}, where [M]$_o$, [thiocarbonylthio]$_0$, MW^M, α, and MW^{thiocarbonylthio} correspond to initial monomer concentration, initial thiocarbonylthio compoubnd concentration, molar mass of monomer, conversion determined by ^{1}H NMR, and molar mass of thiocarbonylthio compoubnd. [d] Molecular weight and polydispersity were determined by GPC analysis (DMAc as eluent) based on poly(methyl methacrylate) standards. [e] Average of triplicate measurements.

In the case of CDTPA and DDMAT, under blue light (λ_{max} = 461 nm, 5 W), high conversions (59.6% for CDTPA in 3 h and 65.7% for DDMAT in 5 h, Table 1, # 3 and # 4) was obtained, which was attributed to a weaker C-S bond between leaving group and trithiocarbonate group compared to that of BTPA. This result is also in accord with their strong absorbances in blue region. CDTPA presented a controlled molecular weight and low polydispersity (M_w/M_n = 1.30), whereas DDMAT showed a poor control over both molecular weight and polydispersity (M_w/M_n = 1.80) under blue light. After these 'successful' attempts, we decided to test the polymerization under green light (λ_{max} = 530 nm, 5 W), CDTPA reached a monomer conversion around 83% after 12 h light irradiation with good control over molecular weight and polydispersity (M_w/M_n = 1.10), while DDMAT showed no conversion under green light even after 24 h irradiation. This result indicated a stronger C-S bond energy of DDMAT than that of CDTPA, which appears consistent with the order of leaving group and with their absorption. Indeed, CDTPA presents a weak absorption at 520 nm (with λ_{max} = 449 nm), while DDMAT shows a λ_{max} at 443 nm. Finally, the MMA polymerizations with the four thiocarbonylthio compounds were tested under red light, which yielded very low monomer conversion (< 2 % after 24 h). Such results are expected as all RAFT agents present no absorption at 630 nm.

Compared to MMA, MA possesses higher propagation rate and faster polymerization. The initial photopolymerization tests of MA with the four thiocarbonylthio compounds were conducted for 6 and 18 h. The control experiment in the absence of thiocarbonylthio compounds gave no conversions even after 18 h (Table 1, # 6), which is consistent with previous reports (*39–41, 45*). The photopolymerizations of MA with CPADB (Table 1, # 7) and BTPA (Table 1, # 10) presented no conversion after 18 h and 6 h, respectively. The slow photolysis of these two thiocarbonylthio compounds under blue light irradiation observed for MMA was suppressed in the case of MA. This was attributed to a slow photolysis rate of MA-S(C=S)-Z adducts compared to MMA-S(C=S)-Z. However, CDTPA and DDMAT could initiate the polymerization of MA under blue light. The monomer conversion reached 40.4 % and 33.9 % conversion for CDTPA (Table 1, # 8) and DDMAT (Table 1, # 9) after 6 h, respectively. However, we observed a poor polymerization control, with a broad PDI (PDI >1.2) for both thiocarbonylthio compounds. In this case, these compounds were acting as initiator but the exchange transfer between chains was not efficient. These results are consistent with previous publications for DDMAT. Indeed, Bai (*33*) and co-workers have suggested that DDMAT could polymerize MA in the absence of photoinitiator under long-wave UV irradiation. Unfortunately under blue and green LED lights, the photopolymerizations of MA with CDTPA and DDMAT are not practical due to their slow kinetics and poor control. Consequently, in the rest of this study, we focus our investigation on the polymerization of MMA in the presence of CDTPA under blue and green LED light.

2. MMA Polymerization Mediated by CDTPA under Blue and Green Light Irradiation

The kinetics of RAFT photopolymerization of MMA in the presence of CDTPA under 5 W blue, green and red LED lights were intensively investigated with the aid of online Fourier transform near-infrared (FTNIR) spectroscopy. The vinylic stretching signal of MMA at 6250 cm^{-1} ~ 6100 cm^{-1} decreased gradually with the reaction time, which was utilized to determine monomer conversion based on signal intensity as described in previous publications (81, 83, 86). Ln($[M]_0/[M]_t$) derived from the monomer conversion was plotted against exposure time, as shown in Figure 2A. In contrast to conventional RAFT and PET-RAFT polymerization, the evolution of ln($[M]_0/[M]_t$) versus time is not linear (upward curvature), which suggests an increase of radical concentration. This could be attributed to a slow initiation of thiocarbonylthio compound under visible light. We measured the slope at low monomer conversion to determine the apparent propagation rate constant ($k_p{}^{app}$). Similar to the pre-test results in Table 1, blue light gave the highest polymerization rate ($k_p{}^{app} = 9.3 \times 10^{-3}$ min^{-1}, based on assumption and estimation of linear kinetic plotting) and shortest induction period (60 min), while green light gave $k_p{}^{app}$ equal to 3.5×10^{-3} min^{-1} with 220 min induction period, whereas $k_p{}^{app}$ for red light was close to zero. The induction period observed in the polymerization can be attributed to stable and long lifetime intermediate of radical addition product in the RAFT process, which was observed in conventional RAFT polymerization and proved by other research groups (33, 87).

The experimental molecular weights for the polymerizations performed under both blue and red lights deviated from the theoretical ones, especially for the low monomer conversion values for blue light (Figure 2B and 2E). This was attributed to a slow initiation of CDTPA (and a low transfer constant between thiocarbonylthio compounds) which results by the formation of oligomer with higher molecular weights. Such behaviour has been previously reported in thermally initiated RAFT polymerization of MMA (88). We confirmed this hypothesis by monitoring the consumption of RAFT agent during the polymerization using gel permeation chromatography (GPC) equipped with an UV detector. Figure 3 reveals a gradual consumption of CDTPA versus exposure time and monomer conversions until 83.3%. In addition, the polydispersities (M_w/M_n) were greater than 1.2 under blue light and increased slightly with monomer conversion, which indicates a poor control. In contrast, under green light, M_w/M_n decreased from 1.3 to 1.1, which is in good accord with a living radical polymerization (89). The high end group fidelity (> 95 %) was confirmed by ^{1}H NMR (Figure 4).

As expected, GPC analysis for blue light (Figure 2C) showed broader molecular weight distributions than that for green light (Figure 2F). The poor control under blue light was attributed to higher energy source leading to a partial degradation of RAFT agents. Indeed, CDTPA is photosensitive and should be stored under -20 °C according to manufacturer manual.
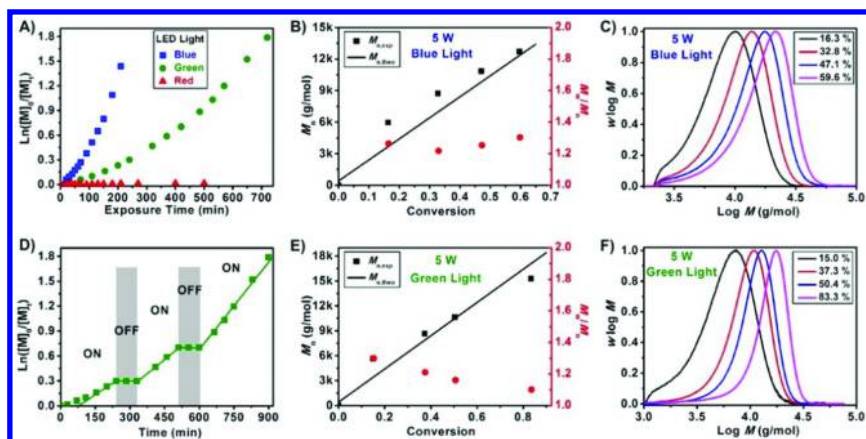
Figure 2. Kinetic study of photopolymerization of MMA under blue, green and red LED light irradiation in the presence of CDTPA. (A) Ln([M]$_0$/[M]$_t$) versus exposure time under different light irradiation; (B) M$_n$ and M$_w$/M$_n$ versus monomer conversion for polymerization under 5 W blue light; (C) Molecular weight distributions at different monomer conversions for polymerization under 5 W blue light; (D) "ON/OFF" study for polymerization under 5 W green light; (E) M$_n$ and M$_w$/M$_n$ versus monomer conversion for polymerization under 5 W green light; (C and F) Molecular weight distributions at different monomer conversions for polymerization under 5 W green light. (see color insert)
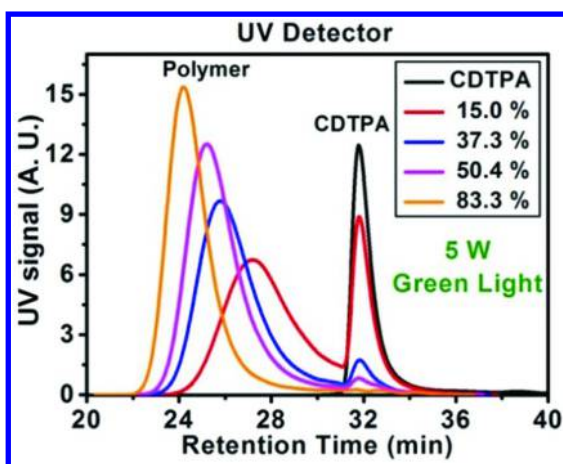
Figure 3. GPC curves recorded by UV detector for polymerization of MMA in the presence of CDTPA under 5 W green LED light irradiation. (see color insert)
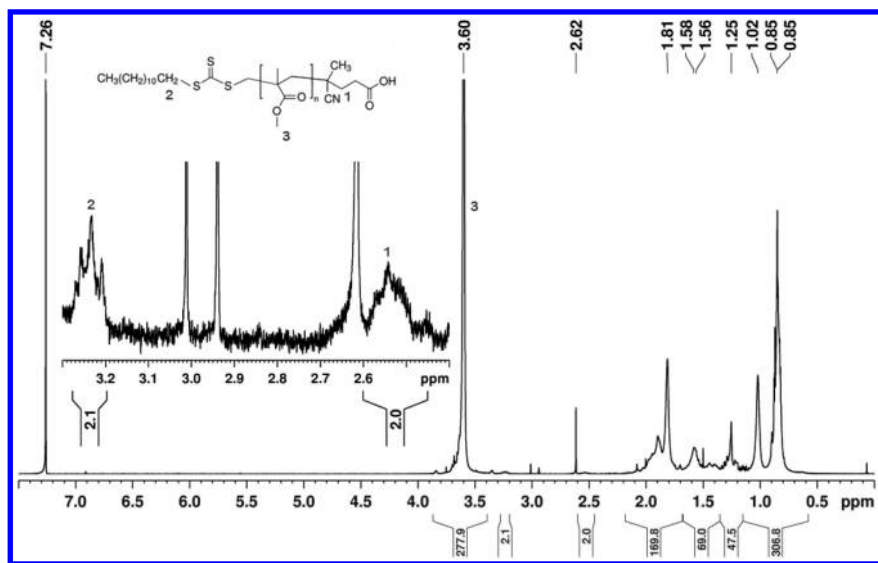
Figure 4. ¹H NMR spectrum for purified PMMA prepared by photopolymerization of MMA mediated by CDTPA under 5 W green light irradiation. $M_{n, GPC} = 10$ 530 g/mol; $M_{n, NMR} = 9660$ g/mol, $M_w/M_n = 1.16$.

Subsequently, to demonstrate temporally controlled polymerization behavior, the polymerization of MMA under green light (Figure 2D) was exposed to an alternating light "ON" and "OFF" environment. In the absence of light ("OFF"), no monomer conversion was recorded, whereas when the light is "ON", the polymerization proceeded as expected.

Next, we investigated the kinetic behavior of RAFT polymerization of MMA in the presence of CDTPA under varied intensity (1, 3 and 5 W) green LED light using online FTNIR measurement. The kinetic plotting of $\ln([M]_0/[M]_t)$ (derived from monomer conversion) versus exposure time (Figure 5) demonstrated that higher light intensity (5 W) lead to higher apparent propagating rates ($k_p^{app} = 3.5 \times 10^{-3}$ min^{-1}), compared to 3 W ($k_p^{app} = 2.7 \times 10^{-3}$ min^{-1}) and 1 W ($k_p^{app} = 2.0 \times 10^{-3}$ min^{-1}). Accordingly, shorter induction period (220 min) against 240 min (3 W) and 440 min (1 W) was observed. The evolution of molecular weights and molecular weight distributions for the polymerization kinetics at 3 and 1 W light intensities (Figure 6) revealed similar trends with those at 5 W. The molecular weights (Figure 6A and C) increased mostly linearly with monomer conversion and polydispersities decreased from 1.3 to 1.1. The molecular weight distributions (Figure 6B and D) displayed monomodal peaks. Additionally, the UV ($\lambda = 305$ nm) and RI signals for molecular weight distributions were in good agreement, which demonstrated that all the chains contained a trithiocarbonate group. Indeed, trithiocarbonate presents a strong absorption at 305 nm (*90*). All the results demonstrated the good control of RAFT polymerization mediated by CDTPA under various green light intensities, although a slow photolytic initiation of RAFT agent was shown at lower intensity.
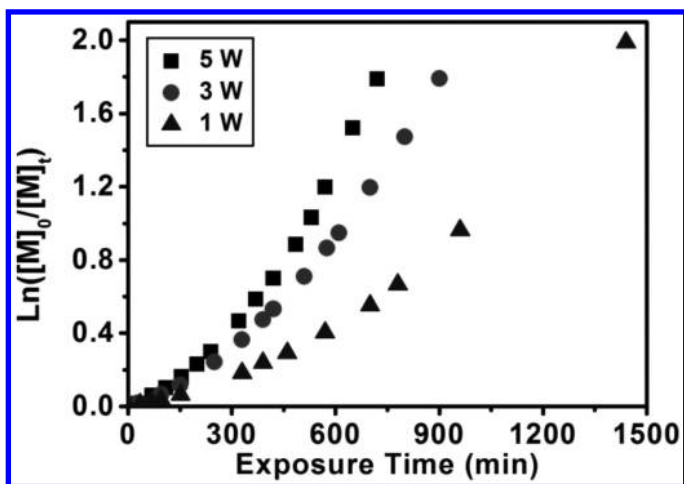
Figure 5. Kinetic plotting of ln([M]$_0$/[M]$_t$) versus exposure time for photopolymerization of MMA in the presence of CDTPA under varied intensity (1, 3 and 5 W) green LED light irradiation. $k_p^{app} = 3.5 \times 10^{-3}$ min^{-1} (5 W); 2.7×10^{-3} min^{-1} (3 W) and 2.0×10^{-3} min^{-1} (1 W).
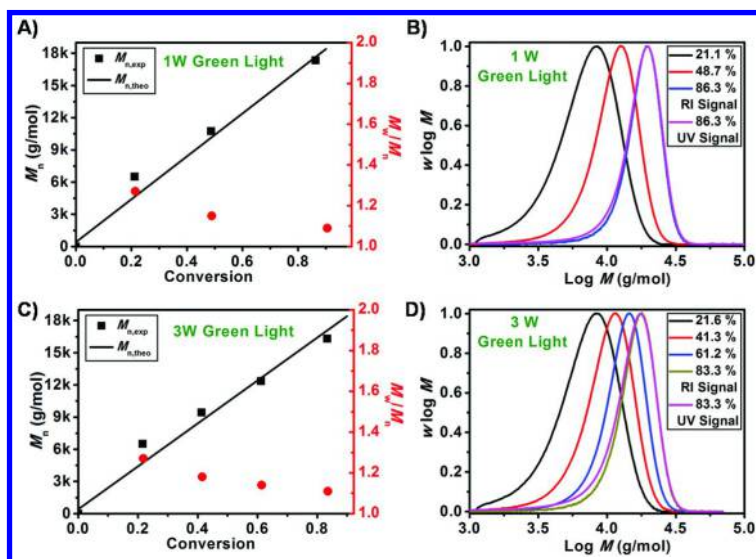
Figure 6. Kinetic study of photopolymerization of MMA in the presence of CDPTA under different intensity green LED light irradiation. (A, C) M_n and M_w/M_n versus monomer conversion for polymerization under 3 and 1 W green light; (B, D) Molecular weight distributions with refractive index (RI) and UV signals at different monomer conversions for polymerization under 3 and 1 W green light. (see color insert)

3. MMA Polymerization Mediated by CDTPA in Other Solvents (DMF, MeCN, Dioxane and Toluene)

Subsequently, the solvent effects were examined to demonstrate the versatility of this approach. Commonly used organic solvents including DMSO, *N,N*-dimethylformamide (DMF), acetonitrile (MeCN), 1,4-dioxane and toluene were evaluated for RAFT polymerization of MMA mediated by CDTPA under 5 W green LED light. The kinetic study was investigated by online FTNIR and aliquot samples were withdrawn for GPC analysis at different exposure times to measure molecular weights and polydispersities. The kinetic plotting of $\ln([M]_0/[M]_t)$ against exposure time for different solvents (Figure 7) presented comparable apparent propagating rates (k_p^{app}) around 1.5×10^{-3} min^{-1} (1.5×10^{-3} min^{-1}, 1.0×10^{-3} min^{-1}, 1.7×10^{-3} min^{-1}, and 1.4×10^{-3} min^{-1} for DMF, MeCN, Dioxane and toluene, respectively.)
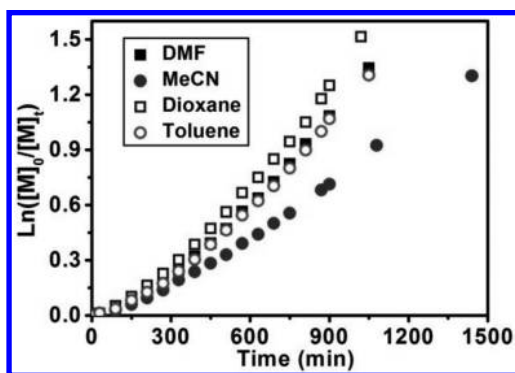
Figure 7. Kinetic plotting of ln([M]$_0$/[M]$_t$) versus exposure time for polymerization of MMA in different solvents: DMF (solid square), MeCN (solid circle), 1,4-dioxane (open square) and toluene (open circle) under 5 W green LED light irradiation. k_p^{app} = 1.5 × 10^{-3} min^{-1} (DMF); 1.0 × 10^{-3} min^{-1} (MeCN); 1.7 × 10^{-3} min^{-1} (Dioxane); 1.4 × 10^{-3} min^{-1} (toluene).

The experimental molecular weights for all investigated solvents increased linearly with monomer conversions (Figure 8A, D, G and J), although the ones at low conversions were higher than theoretical ones due to a slow photolytic initiation of CDTPA as observed in DMSO. The evolution of GPC curves recorded by UV detector versus monomer conversions (Figure 8C, F, I and L) showed a slow consumption of CDTPA. The polydispersities stayed lower than 1.2 at high monomer conversions. The molecular weight distributions (Figure 8B, E, H and K) for all solvents at comparable monomer conversions presented similar characteristics.
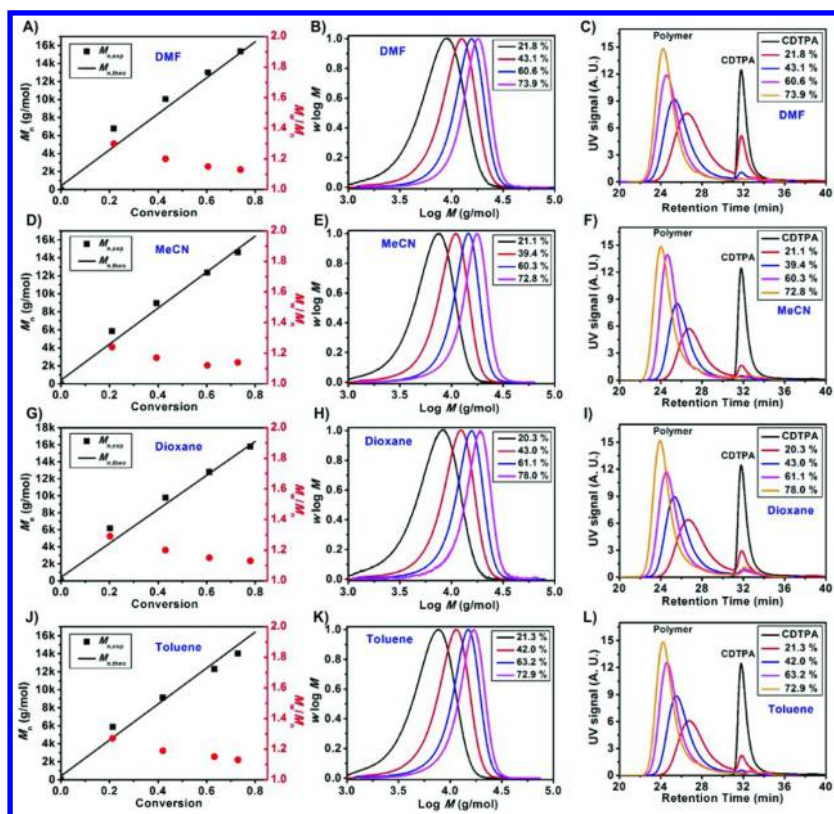
Figure 8. Kinetic study of photopolymerization of MMA in the presence of CDTPA in different solvents DMF (A, B, C), MeCN (D, E, F), Dioxane (G, H, I) and toluene (J, K, L) under 5 W green LED light irradiation. (A, D, G, J) M_n and M_w/M_n versus monomer conversion; (B, E, H, K) Molecular weight distributions at different monomer conversions; (C, F, I, L) GPC curves recorded by UV detector. (see color insert)

4. Photopolymerization of a Variety of Monomers Mediated by CDTPA in DMSO

Three functional methacrylate monomers, glycidyl methacrylate (GMA), 2-hydroethyl methacrylate (HEMA) and *N,N*-dimethylaminoethyl methacrylate (DMAEMA), were explored for photopolymerization mediated by CDTPA using 5 W green LED light as light source. All the polymerization rates were greater than MMA, for instance 89 % monomer conversion was achieved in 5 h for GMA (Table 2). Although the experimental molecular weights (especially for DMAEMA and HEMA) deviated from the theoretic ones, the polydispersities remained less than 1.25 (except for GMA at low monomer conversion.) The kinetic plotting of $\ln([M]_0/[M]_t)$ against exposure time was shown in Figure 9. The kinetics show a similar trend as reported with MMA.

Table 2. Photopolymerization of different functional monomers in the presence of CDTPA under green LED light irradiation.[a]

#	Monomer	Time (h)	α [b] (%)	$M_{n,\,th}$[c] (g/mol)	$M_{n,\,GPC}$[d] (g/mol)	M_w/M_n[d]
1	GMA	1	25	7510	9720	1.43
2	GMA	5	89	25700	26220	1.25
3	DMAEMA	3	26	8510	9350	1.30
4	DMAEMA	5	61	19510	13730	1.24
5	HEMA	2	20	5610	14780	1.31
6	HEMA	3	47	12640	19420	1.26

[a] The polymerizations were performed using the ratio of [monomer]:[RAFT agent] = 200:1 in the absence of oxygen at room temperature in dimethylsulfoxide (DMSO) using 5 W green LED light (λ_{max} = 530 nm). [b] Monomer conversion was determined by ^{1}H NMR spectroscopy. [c] Theoretical molecular weight was calculated using the following equation: $M_{n,th}$ = [M]$_o$/[RAFT] × MW^M × α + MW^{RAFT}, where [M]$_o$, [RAFT]$_o$, MW^M, α, and MW^{RAFT} correspond to initial monomer concentration, initial RAFT concentration, molar mass of monomer, conversion determined by ^{1}H NMR, and molar mass of RAFT agent. [d] Molecular weight and polydispersity were determined by GPC analysis (DMAc as eluent) based on poly(methyl methacrylate) standards.
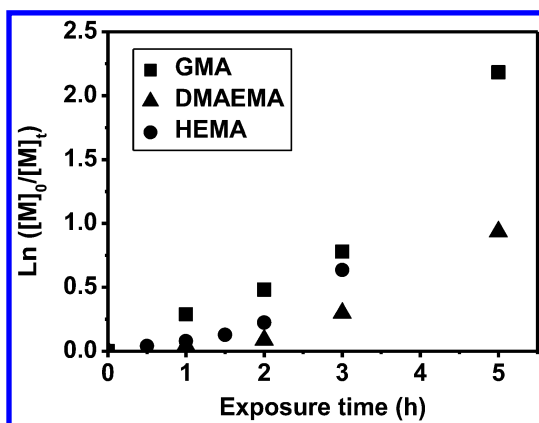
Figure 9. Kinetic plotting of ln([M]$_0$/[M]$_t$) versus exposure time for photopolymerization of different functional monomers: GMA (square), HEMA (circle), and DMAEMA (triangle) in the presence of CDTPA under 5 W green LED light irradiation.

5. Diblock Copolymers by Photopolymerization

Chain extensions of PGMA and PDMAEMA were performed to prove the livingness of the resultant polymer chains prepared by RAFT photopolymerization (Figure 10). PGMA was used as the macroinitiator for chain extension in the

presence of GMA (Figure 10A and 10D) and MMA (Figure 10C and 10F). PDMAEMA was employed for chain extension in the presence of DMAEMA (Figure 10B and 10E). All the diblock copolymers were synthesized at room temperature in DMSO under 5 W green LED light irradiation. The ratios of monomers to macroinitiators ([monomer]: [macroinitiator]) were 500:1. GPC analysis indicated a complete shift of macroinitiators to high molecular weights at different time points. For the chain extension of PGMA in the presence of MMA, high monomer conversion caused broad polydispersity and long tailing. Additionally, the RI and UV signals for resultant diblock polymers were in good agreement, which suggests a good retention of RAFT end-groups.
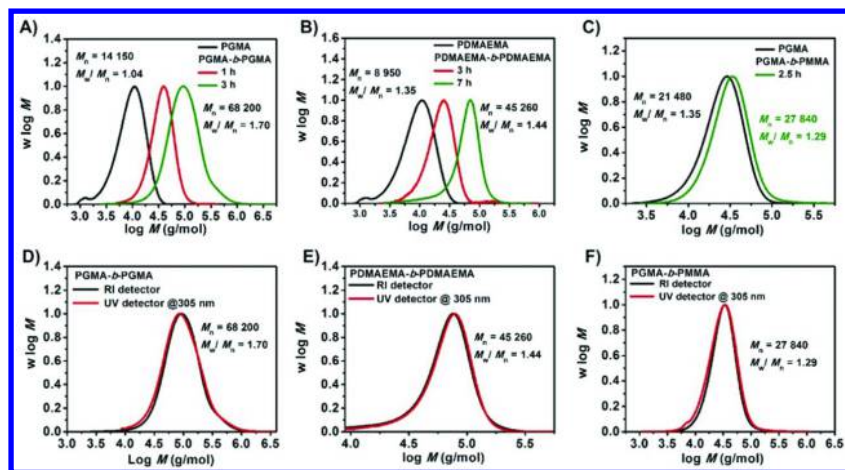
Figure 10. Molecular weight distributions for PGMA and PDMAEMA macroinitiators and their diblock copolymers prepared by RAFT photopolymerization mediated by CDTPA under 5 W green LED light irradiation at room temperature in DMSO: (A) PGMA macromoinitiator and PGMA-b-PGMA; (B) PDMAEMA macromoinitiator and PDMAEMA-b-PDMAEMA; (C) PGMA macromoinitiator and PGMA-b-PMMA; (D) RI and UV signals of PGMA-b-PGMA; (E) RI and UV signals of PDMAEMA-b-PDMAEMA; (F) RI and UV signals of PGMA-b-PMMA. (see color insert)

Conclusion

In this work, we demonstrate, for the first time, that specific thiocarbonylthio compounds (more specifically, CDTPA and DDMAT) can act as iniferter under low wattage visible lights (typically, 5 W). Under blue or green light, the C-S bond between the leaving group and thiocarbonylthio group can be photo-cleaved to generate free radical and subsequently initiate a RAFT polymerization. Out of four different thiocarbonylthio compounds, CDTPA appears to be the best candidate as it achieved high monomer conversion with a good control of molecular as well as a low polydispersity (PDI) under green light (λ_{max} = 530

nm) for the polymerization of MMA. The proposed mechanism was hypothesized to be (Scheme 1B): the thiocarbonylthio compound was photolyzed to generate free radical and subsequently drive the RAFT polymerization. The radical in the other fragment could be localized in the thiocarbonylthio structure, which has the potential to capture the propagating radical to yield dormant species and finish the cycle. In addition, CDTPA can also efficiently initiate and control the polymerization of MMA and functional monomers, including DMAEMA, HEMA and GMA, in different solvents. The successful chain extension of homopolymers prepared by this process demonstrates good end group fidelity of trithiocarbonate, although a slight increase of PDI was noted. Unfortunately, this process is limited to methacrylates and work well only with one class of thiocarbonylthio compound, i.e. CDTPA. In comparison to PET-RAFT process, RAFT photopolymerization produces polymers with a broader molecular weight distribution.

References

1. Matyjaszewski, K.; Xia, J. *Chem. Rev.* **2001**, *101*, 2921–2990.
2. Rosen, B. M.; Percec, V. *Chem. Rev.* **2009**, *109*, 5069–5119.
3. Matyjaszewski, K. *Macromolecules* **2012**, *45*, 4015–4039.
4. Kamigaito, M.; Ando, T.; Sawamoto, M. *Chem. Rev.* **2001**, *101*, 3689–3746.
5. Zhang, N.; Samanta, S. R.; Rosen, B. M.; Percec, V. *Chem. Rev.* **2014**, *114*, 5848–5958.
6. Percec, V.; Guliashvili, T.; Ladislaw, J. S.; Wistrand, A.; Stjerndahl, A.; Sienkowska, M. J.; Monteiro, M. J.; Sahoo, S. *J. Am. Chem. Soc.* **2006**, *128*, 14156–14165.
7. Chiefari, J.; Chong, Y. K.; Ercole, F.; Krstina, J.; Jeffery, J.; Le, T. P. T.; Mayadunne, R. T. A.; Meijs, G. F.; Moad, C. L.; Moad, G.; Rizzardo, E.; Thang, S. H. *Macromolecules* **1998**, *31*, 5559–5562.
8. Moad, G.; Chong, Y. K.; Postma, A.; Rizzardo, E.; Thang, S. H. *Polymer* **2005**, *46*, 8458–8468.
9. Moad, G.; Rizzardo, E.; Thang, S. H. *Aust. J. Chem.* **2009**, *62*, 1402–1472.
10. Hawker, C. J.; Bosman, A. W.; Harth, E. *Chem. Rev.* **2001**, *101*, 3661–3688.
11. Matyjaszewski, K.; Gaynor, S.; Wang, J.-S. *Macromolecules* **1995**, *28*, 2093–2095.
12. David, G.; Boyer, C.; Tonnar, J.; Ameduri, B.; Lacroix-Desmazes, P.; Boutevin, B. *Chem. Rev.* **2006**, *106*, 3936–3962.
13. Matyjaszewski, K. *Macromol. Rapid Commun.* **2005**, *26*, 135–142.
14. Otsu, T.; Yoshida, M.; Tazaki, T. *Makromol. Chem., Rapid Commun.* **1982**, *3*, 133–140.
15. Otsu, T.; Yoshida, M. *Makromol. Chem., Rapid Commun.* **1982**, *3*, 127–132.
16. Otsu, T. *J. Polym. Sci., Part A: Polym. Chem.* **2000**, *38*, 2121–2136.
17. Otsu, T.; Yamashita, K.; Tsuda, K. *Macromolecules* **1986**, *19*, 287–290.
18. Moad, G.; Chong, Y. K.; Mulder, R.; Rizzardo, E.; Thang San, H. In *Controlled/Living Radical Polymerization: Progress in RAFT, DT, NMP &*

In Controlled Radical Polymerization: Mechanisms; Tsarevsky, et al.;
ACS Symposium Series; American Chemical Society: Washington, DC, 2015.

OMRP; American Chemical Society: Washington, DC, 2009; Vol. 1024, pp 3−18.

19. Moad, G.; Rizzardo, E.; Thang, S. H. *Acc. Chem. Res.* **2008**, *41*, 1133–1142.

20. Moad, G.; Rizzardo, E.; Thang, S. H. *Chem. - Asian J.* **2013**, *8*, 1634–1644.

21. Moad, G.; Barner-Kowollik, C. In *Handbook of RAFT Polymerization*; Wiley-VCH Verlag GmbH & Co. KGaA: 2008, pp 51−104.

22. Quinn, J. F.; Barner, L.; Barner-Kowollik, C.; Rizzardo, E.; Davis, T. P. *Macromolecules* **2002**, *35*, 7620–7627.

23. Ran, R.; Wan, T.; Gao, T.; Gao, J.; Chen, Z. *Polym. Int.* **2008**, *57*, 28–34.

24. Zhou, H.; Johnson, J. A. *Angew. Chem., Int. Ed.* **2013**, *52*, 2235–2238.

25. Lu, L.; Yang, N.; Cai, Y. *Chem. Commun.* **2005**, 5287–5288.

26. Lalevée, J.; Blanchard, N.; El-Roz, M.; Allonas, X.; Fouassier, J. P. *Macromolecules* **2008**, *41*, 2347–2352.

27. Yasutake, M.; Andou, Y.; Hiki, S.; Nishida, H.; Endo, T. *Macromol. Chem. Phys.* **2004**, *205*, 492–499.

28. Kwak, Y.; Matyjaszewski, K. *Macromolecules* **2010**, *43*, 5180–5183.

29. Khan, M. Y.; Cho, M.-S.; Kwark, Y.-J. *Macromolecules* **2014**, *47*, 1929–1934.

30. Ham, M.-k.; HoYouk, J.; Kwon, Y.-K.; Kwark, Y.-J. *J. Polym. Sci., Part A: Polym. Chem.* **2012**, *50*, 2389–2397.

31. Lalevée, J.; El-Roz, M.; Allonas, X.; Fouassier, J. P. *J. Polym. Sci., Part A: Polym. Chem.* **2007**, *45*, 2436–2442.

32. Zhang, H.; Deng, J.; Lu, L.; Cai, Y. *Macromolecules* **2007**, *40*, 9252–9261.

33. Wang, H.; Li, Q.; Dai, J.; Du, F.; Zheng, H.; Bai, R. *Macromolecules* **2013**, *46*, 2576–2582.

34. Lu, L.; Zhang, H.; Yang, N.; Cai, Y. *Macromolecules* **2006**, *39*, 3770–3776.

35. Liu, G.; Shi, H.; Cui, Y.; Tong, J.; Zhao, Y.; Wang, D.; Cai, Y. *Polym. Chem.* **2013**, *4*, 1176–1182.

36. Shi, Y.; Gao, H.; Lu, L.; Cai, Y. *Chem. Commun.* **2009**, 1368–1370.

37. Shi, Y.; Liu, G.; Gao, H.; Lu, L.; Cai, Y. *Macromolecules* **2009**, *42*, 3917–3926.

38. Koumura, K.; Satoh, K.; Kamigaito, M. *Polym. J* **2009**, *41*, 595–603.

39. Anastasaki, A.; Nikolaou, V.; Pappas, G. S.; Zhang, Q.; Wan, C.; Wilson, P.; Davis, T. P.; Whittaker, M. R.; Haddleton, D. M. *Chem. Sci.* **2014**, *5*, 3536–3542.

40. Anastasaki, A.; Nikolaou, V.; Simula, A.; Godfrey, J.; Li, M.; Nurumbetov, G.; Wilson, P.; Haddleton, D. M. *Macromolecules* **2014**, *47*, 3852–3859.

41. Anastasaki, A.; Nikolaou, V.; Zhang, Q.; Burns, J.; Samanta, S. R.; Waldron, C.; Haddleton, A. J.; McHale, R.; Fox, D.; Percec, V.; Wilson, P.; Haddleton, D. M. *J. Am. Chem. Soc.* **2014**, *136*, 1141–1149.

42. Fors, B. P.; Hawker, C. J. *Angew. Chem., Int. Ed.* **2012**, *51*, 8850–8853.

43. Fors, B. P.; Poelma, J. E.; Menyo, M. S.; Robb, M. J.; Spokoyny, D. M.; Kramer, J. W.; Waite, J. H.; Hawker, C. J. *J. Am. Chem. Soc.* **2013**, *135*, 14106–14109.

44. Leibfarth, F. A.; Mattson, K. M.; Fors, B. P.; Collins, H. A.; Hawker, C. J. *Angew. Chem., Int. Ed.* **2013**, *52*, 199–210.

45. Treat, N. J.; Fors, B. P.; Kramer, J. W.; Christianson, M.; Chiu, C.-Y.; Alaniz, J. R. d.; Hawker, C. J. *ACS Macro Lett.* **2014**, *3*, 580–584.

46. Treat, N. J.; Sprafke, H.; Kramer, J. W.; Clark, P. G.; Barton, B. E.; Read de Alaniz, J.; Fors, B. P.; Hawker, C. J. *J. Am. Chem. Soc.* **2014**, *136*, 16096–16101.

47. Konkolewicz, D.; Schröder, K.; Buback, J.; Bernhard, S.; Matyjaszewski, K. *ACS Macro Lett.* **2012**, *1*, 1219–1223.

48. Ribelli, T. G.; Konkolewicz, D.; Bernhard, S.; Matyjaszewski, K. *J. Am. Chem. Soc.* **2014**, *136*, 13303–13312.

49. Ribelli, T. G.; Konkolewicz, D.; Pan, X.; Matyjaszewski, K. *Macromolecules* **2014**, *47*, 6316–6321.

50. Mehmet Atilla, T.; Mustafa, Ç.; Mustafa, U.; Yusuf, Y. In *Progress in Controlled Radical Polymerization: Mechanisms and Techniques*; American Chemical Society: Washington, DC, 2012; Vol. 1100, pp 59−72.

51. Ciftci, M.; Tasdelen, M. A.; Yagci, Y. *Polym. Chem.* **2014**, *5*, 600–606.

52. Tasdelen, M. A.; Ciftci, M.; Yagci, Y. *Macromol. Chem. Phys.* **2012**, *213*, 1391–1396.

53. Tasdelen, M. A.; Uygun, M.; Yagci, Y. *Macromol. Rapid Commun.* **2011**, *32*, 58–62.

54. Ciftci, M.; Tasdelen, M. A.; Li, W.; Matyjaszewski, K.; Yagci, Y. *Macromolecules* **2013**, *46*, 9537–9543.

55. Dadashi-Silab, S.; Atilla Tasdelen, M.; Yagci, Y. *J. Polym. Sci., Part A: Polym. Chem.* **2014**, *52*, 2878–2888.

56. Murtezi, E.; Yagci, Y. *Macromol. Rapid Commun.* **2014**, *35*, 1782–1787.

57. Lalevée, J.; Blanchard, N.; Tehfe, M.-A.; Peter, M.; Morlet-Savary, F.; Fouassier, J. *Polym. Bull.* **2012**, *68*, 341–347.

58. Lalevée, J.; Peter, M.; Dumur, F.; Gigmes, D.; Blanchard, N.; Tehfe, M.-A.; Morlet-Savary, F.; Fouassier, J. P. *Chem. - Eur. J.* **2011**, *17*, 15027–15031.

59. Lalevée, J.; Tehfe, M.-A.; Dumur, F.; Gigmes, D.; Blanchard, N.; Morlet-Savary, F.; Fouassier, J. P. *ACS Macro Lett.* **2012**, *1*, 286–290.

60. Xiao, P.; Dumur, F.; Zhang, J.; Gigmes, D.; Fouassier, J. P.; Lalevee, J. *Polym. Chem.* **2014**, *5*, 6350–6357.

61. Yamago, S.; Ukai, Y.; Matsumoto, A.; Nakamura, Y. *J. Am. Chem. Soc.* **2009**, *131*, 2100–2101.

62. Miyake, G. M.; Theriot, J. C. *Macromolecules* **2014**, *47*, 8255–8261.

63. Zhao, Y.; Yu, M.; Zhang, S.; Liu, Y.; Fu, X. *Macromolecules* **2014**, *47*, 6238–6245.

64. Benedikt, S.; Moszner, N.; Liska, R. *Macromolecules* **2014**, *47*, 5526–5531.

65. Ohtsuki, A.; Goto, A.; Kaji, H. *Macromolecules* **2012**, *46*, 96–102.

66. Nakamura, Y.; Arima, T.; Tomita, S.; Yamago, S. *J. Am. Chem. Soc.* **2012**, *134*, 5536–5539.

67. Nakamura, Y.; Arima, T.; Yamago, S. *Macromolecules* **2014**, *47*, 582–588.

68. Zhang, G.; Song, I. Y.; Ahn, K. H.; Park, T.; Choi, W. *Macromolecules* **2011**, *44*, 7594–7599.

69. Wolpers, A.; Vana, P. *Macromolecules* **2014**, *47*, 954–963.

70. Li, B.; Yu, B.; Zhou, F. *Macromol. Rapid Commun.* **2014**, *35*, 1287–1292.

71. Chuang, Y.-M.; Ethirajan, A.; Junkers, T. *ACS Macro Lett.* **2014**, *3*, 732–737.

72. Wenn, B.; Conradi, M.; Carreiras, A. D.; Haddleton, D. M.; Junkers, T. *Polym. Chem.* **2014**, *5*, 3053–3060.
73. Zhang, T.; Chen, T.; Amin, I.; Jordan, R. *Polym. Chem.* **2014**, *5*, 4790–4796.
74. Jiang, X.; Wu, J.; Zhang, L.; Cheng, Z.; Zhu, X. *Macromol. Rapid Commun.* **2014**, *35*, 1879–1885.
75. Mosnáček, J.; Kundys, A.; Andicsová, A. *Polymers* **2014**, *6*, 2862–2874.
76. Prier, C. K.; Rankic, D. A.; MacMillan, D. W. C. *Chem. Rev.* **2013**, *113*, 5322–5363.
77. Yoon, T. P.; Ischay, M. A.; Du, J. *Nat. Chem.* **2010**, *2*, 527–532.
78. Narayanam, J. M. R.; Stephenson, C. R. J. *Chem. Soc. Rev.* **2011**, *40*, 102–113.
79. Tucker, J. W.; Stephenson, C. R. J. *J. Org. Chem.* **2012**, *77*, 1617–1622.
80. Xu, J.; Jung, K.; Atme, A.; Shanmugam, S.; Boyer, C. *J. Am. Chem. Soc.* **2014**, *136*, 5508–5519.
81. Xu, J.; Jung, K.; Boyer, C. *Macromolecules* **2014**, *47*, 4217–4229.
82. Xu, J.; Jung, K.; Corrigan, N. A.; Boyer, C. *Chem. Sci.* **2014**, *5*, 3568–3575.
83. Xu, J.; Shanmugam, S.; Duong, H. T.; Boyer, C. *Polym. Chem.* **2015**.
84. Shanmugam, S.; Xu, J.; Boyer, C. *Chem. Sci.* **2015**, *6*, 1341–1349.
85. Gruendling, T.; Kaupp, M.; Blinco, J. P.; Barner-Kowollik, C. *Macromolecules* **2010**, *44*, 166–174.
86. Darcos, V.; Monge, S.; Haddleton, D. M. *J. Polym. Sci., Part A: Polym. Chem.* **2004**, *42*, 4933–4940.
87. Perrier, S.; Barner-Kowollik, C.; Quinn, J. F.; Vana, P.; Davis, T. P. *Macromolecules* **2002**, *35*, 8300–8306.
88. Han, X.; Fan, J.; He, J.; Xu, J.; Fan, D.; Yang, Y. *Macromolecules* **2007**, *40*, 5618–5624.
89. Goto, A.; Fukuda, T. *Prog. Polym. Sci.* **2004**, *29*, 329–385.
90. Skrabania, K.; Miasnikova, A.; Bivigou-Koumba, A. M.; Zehm, D.; Laschewsky, A. *Polym. Chem.* **2011**, *2*, 2074–2083.

Simultaneous Control over Monomer Sequence and Molecular Weight Using the RAFT Process

Niels ten Brummelhuis[1],* and Marcus Weck[2]

[1]Department of Chemistry, Humboldt-Universität zu Berlin, Brook-Taylor-Str. 2, 12489 Berlin, Germany
[2]Molecular Design Institute and Department of Chemistry, New York University, 29 Washington Place, New York, New York 10003, United States
***E-mail: niels.ten.brummelhuis@hu-berlin.de**

A simultaneous control over molecular weight and monomer sequence is highly desirable since they strongly influence the properties of polymers. The reversible addition-fragmentation chain-transfer (RAFT) process is ideally suited to provide control over molecular weight for a wide range of copolymerizations because of the tolerance of the RAFT process towards functional groups and reaction conditions. Here we highlight that RAFT can be used to prepare polymers with well-defined alternating or periodic monomer sequences and controlled, narrowly distributed, molecular weight.

Introduction

The controlled radical polymerization techniques that have been developed over the last two decades provide an excellent means to control the molecular weight, dispersity and architecture of polymers and can be applied to a wide range of different monomers (*1*). Though highly important for many applications, molecular weight, dispersity and architecture are only some of the properties of polymers that influence its properties. The microstructure of polymers, *i.e.* tacticity (*2*) and, for copolymers, monomer sequence (*3–6*) are two other factors.

These properties strongly influence the macroscopic properties of materials such as T_g, crystallinity, *etc* (*7*).

Control over monomer sequence has become of increasing interest since a plethora of novel properties might come within reach if it can be efficiently controlled (*3–6*). Whereas step-growth polymerizations can be adopted towards sequence control with relative ease (*e.g.* using solid-phase synthesis (*8–11*) or the ligation of oligomers (*12, 13*)), the development of methods suitable for chain-growth polymerization are scarce, and real sequence control is currently limited to the synthesis of alternating or AAB-periodic copolymers (*vide infra*).

Despite the modest degree of control currently possible over monomer sequence, such polymerizations have nevertheless attracted significant attention since they already introduce novel properties and provide a first step towards more complex structures. Of particular interest is the simultaneous control over both molecular weight and monomer sequence. This chapter focuses on the simultaneous control of molecular weight and monomer sequence using reversible addition-fragmentation chain-transfer (RAFT) (co)polymerization.

It is worth mentioning that the advent of controlled-radical polymerization techniques has also made new strategies of controlling monomer sequence possible, and should therefore not be seen as a techniques to 'merely' control molecular weight. Though it will not be covered in the main body of this publication because atom-transfer radical polymerization (ATRP) and nitroxide-mediated polymerization (NMP) rather than RAFT were used, the work by Lutz and coworkers shows that single monomers can be placed at fairly well-defined positions in a polymer chain by the timed addition of electron-deficient monomers (maleimide derivatives) during the controlled radical polymerization of electron-rich monomers (styrene or derivatives thereof) (*14, 15*). This is made possible by the fact that the growth of all polymer chains is initiated more or less simultaneously, and that variations in monomer composition (*e.g.* caused by the fast copolymerization of maleimides with styrenes as compared to the homopolymerization of styrene) are therefore recorded in the polymer chain.

Control over Alternating Copolymerization Using RAFT

The simplest examples of periodic copolymers are alternating copolymers, in which two monomers are incorporated in an alternating fashion. Such polymers are in most instances prepared using a combination of electron-rich and -deficient monomers (*16*), but can also be prepared by copolymerizing non-homopolymerizable (*e.g.* because of sterics), supplied in large excess, with a second monomer (*17*).

Shortly after its establishment as an effective way of controlling molecular weight and dispersity (*18*), RAFT has also been used to control the molecular weight for polymerizations for which alternating copolymerizations were known to occur in free-radical polymerizations (FRP).

The most thoroughly investigated example of such a copolymerization is the copolymerization of styrene (an electron-rich monomer) and maleic anhydride or maleimides (electron-deficient monomers), for which RAFT could effectively be used to control the molecular weight of the copolymerization (*19–22*).

A variety of different conditions can be used to control the molecular weight and dispersity of copolymers of styrene and maleic anhydride (*19, 21, 22, 31*). Polymerizations were performed in a range of solvents, using dithiobenzoate or trithiocarbonates chain-transfer agents (CTAs). Mostly, thermal initiation using AIBN was used at temperatures around 60-80°C. For 1:1 ratios of styrene and maleic anhydride, dispersities (Đ) between 1.06 (using 2-cyanoprop-2-yl dithiobenzoate as the CTA) and 1.2 (for other CTAs) were achieved. Chernikova *et al.* showed that Đ tended to be lower when using an excess of styrene and quenching the polymerization before or at full conversion of the maleic anhydride (as low as 1.1 in that study) (*22*). In all cases styrene and maleic anhydride were incorporated in a 1:1 ratio, indicating that the alternating sequence is maintained in the RAFT process.

You *et al.* presented the alternating RAFT copolymerization of styrene and maleic anhydride at room temperature (using the spontaneous copolymerization of the monomers in the presence of dibenzyl trithiocarbonate in THF) and achieved Đ as low as 1.19. This illustrates one of the major advantages of RAFT over *e.g.* NMP, where high temperatures are required to facilitate efficient polymerization (*23*). In the case of the copolymerization of styrene and maleic anhydride the temperatures required (> 100°C) compromise the near perfect alternating sequence (*24, 25*). Attempts to use ATRP for this copolymerization failed due to undesired reactions between copper-ligands and maleic anhydride (*26*).

The RAFT process also provides a highly efficient way of preparing block copolymers. Block copolymers in which one of the blocks consisted of the alternating copolymer of maleic anhydride and styrene could be prepared using a Kraton L-1203 derived macro-CTA (*19*) or by extension of an alternating polymer of styrene or maleic anhydride with a second block (*27–30*). Alternatively, the strongly enhanced rate of polymerization for the alternating copolymerization of maleic anhydrides and styrene (or derivatives thereof) compared to the rate of homopolymerization of styrene could be used to prepare block copolymers. An excess of styrene was used that was incorporated as a homopolymer block after all maleic anhydride monomer was consumed in an alternating block (*31*), a feature that can only be achieved using (relatively) low polymerization temperatures. Though technically a gradient-copolymer was formed, the gradient in such a copolymer is very steep.

Not only the copolymerization of styrene with maleic anhydride is known to be proceed in a highly alternating fashion; many derivatives of these monomers display similar behavior. A wide variety of maleimides can be copolymerized with styrene to yield alternating copolymers, but also many styrene derivatives have been used. RAFT copolymerizations for such systems have been described (*31–43*), among others for the synthesis of polyampholytes, thermo- and photoresponsive polymers and graft-copolymers. Examples of the maleimides and styrene derivatives that were used are displayed in Figure 1B and C, respectively.
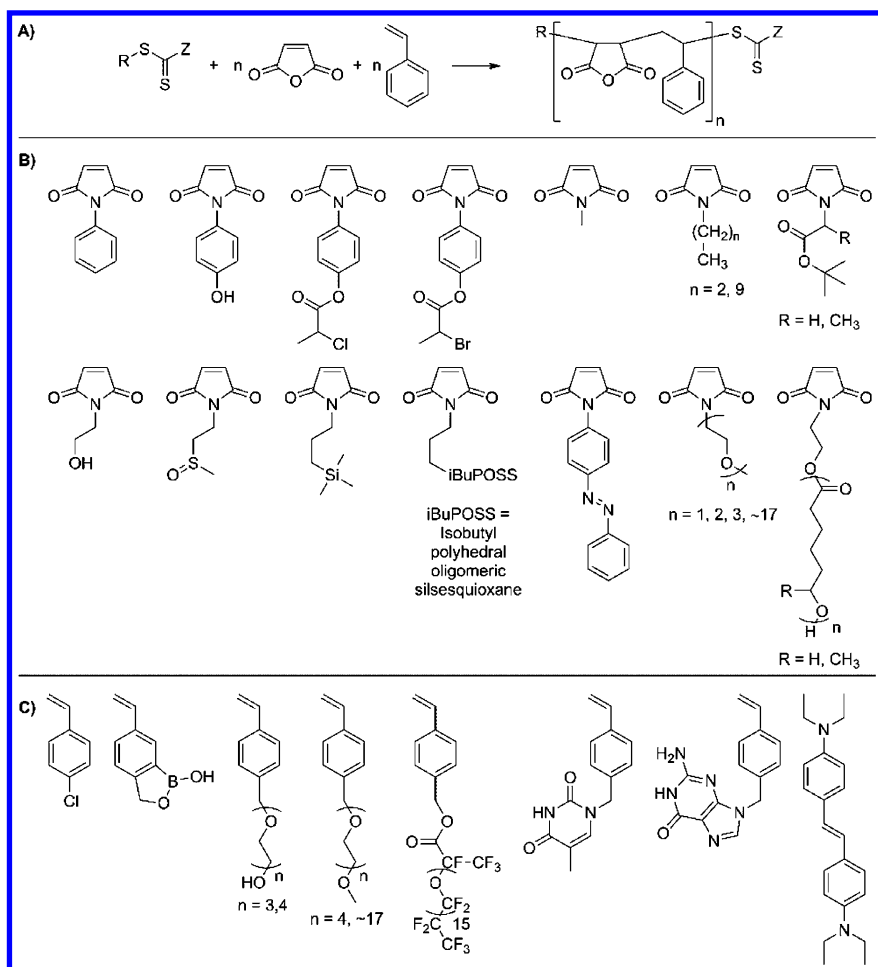
Figure 1. A) The alternating copolymerization of maleic anhydride and styrene controlled by RAFT. B) Examples of maleimides and C) styrene derivatives (including a stilbene derivative) successfully copolymerized into alternating copolymers using RAFT polymerization.

The RAFT copolymerization of maleic anhydride/maleimides with styrene derivatives has also been used to prepare polymers with crown-ether-like cyclic side-chains in cyclo(co)polymerizations. In cyclopolymerizations bi- (or multi-) functional monomers are used. Both polymerizable groups are incorporated into the same polymer chain, thereby introducing cyclic side-chains. Jia *et al.* presented the cyclocopolymerization of various bifunctional styrene monomers containing PEG linkers with maleic anhydride (Figure 2A) (*44*). To prevent cross-linking, the authors were forced to use at least a 2.5-fold excess of maleic anhydride relative to the amount of styrene moieties in solution.
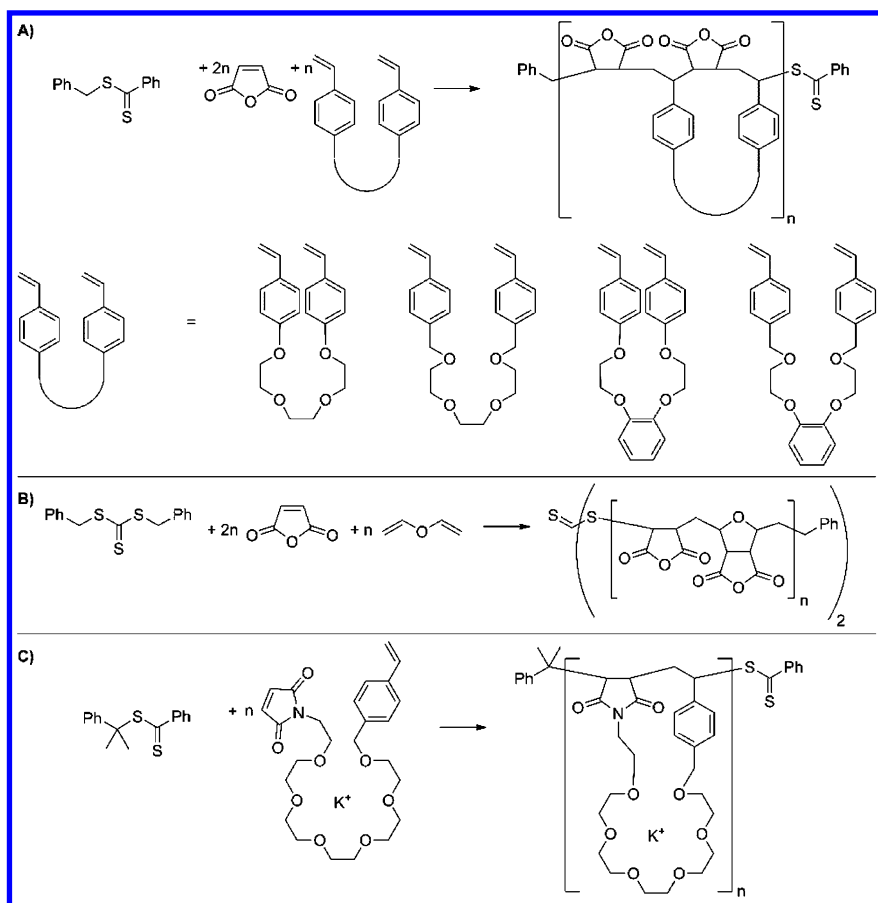
Figure 2. A) RAFT cyclocopolymerization of bifunctional styrene monomers with maleic anhydride (44). B) RAFT cyclopolymerization of divinylether with maleic anhydride (45). C) Potassium-cation templated RAFT cyclopolymerization of a heterobifunctional monomer containing a styrene and a maleimide moiety (46).

Very similar is the alternating cyclocopolymerization of divinylether and maleic anhydride that yields a backbone with tetrahydrofurane rings (Figure 2B) (*45*).

Zou *et al.* presented the cyclopolymerization of a series of heterobifunctional monomers containing both styrene- and maleimide-moieties, separated by a PEG linker (Figure 2C). The molecular weight and dispersity could be controlled using RAFT. Furthermore, a templating effect of potassium cations was observed: potassium cations were efficiently bound by monomers containing ethylene glycol hexa- and heptamer linkers in a crown-ether-like complex thereby bringing the styrene and maleimide moieties into close proximity, making intramolecular polymerization (cyclopolymerization) more favorable (*46*).

Though alternating copolymers containing maleimides have primarily been prepared using styrene derivatives, other electron-rich monomers can be employed. An example is ethyl α-ethylacrylate, the RAFT copolymerization of which with unsubstituted maleimide or *N*-phenyl maleimide resulted in predominantly alternating copolymers (*47*, *48*).

N-Vinyl pyrrolidone (*N*-VP) can also be used. Hu *et al.* studied the copolymerization of a ternary mixture of styrene, maleic anhydride and *N*-VP. They found that this copolymerization yields a polymer in which every second monomer is a maleic anhydride residue, separated by styrene or *N*-VP residues. S and *N*-VP are incorporated in a gradient where *N*-VP is incorporated predominantly at the start of the polymerization and S mostly later on (*49*).

Many other monomer pairs also polymerize in an alternating fashion, such as *N*-vinylnaphthalimide (*50*) or *N*-vinyl phthalimide (*51*) with *N*-isopropyl acrylamide, the copolymerization of which could effectively be controlled using a dithiocarbamate-type CTA, or of *N*-VP with 1,1,1,3,3,3-hexafluoroisopropyl-α-fluoroacrylate (*52*).

For the systems that were thus far mentioned, no influence of the RAFT process on the monomer sequence distribution was reported. Zaitsev *et al.* determined reactivity ratios for the FRP and RAFT copolymerization of *N*-VP and 1,1,1,3,3,3-hexafluoroisopropyl-α-fluoroacrylate (HFA), and though in both cases predominantly alternating sequences are obtained, the reactivity ratios differed somewhat: in the FRP $r_{N-VP} = 0.02$ and $r_{HFA} = 0.05$ were found, where in RAFT $r_{N-VP} = 0.15$ and $r_{HFA} = 0.00$. Though no explanation for this observation was provided, it is an indication that the RAFT process can indeed influence the monomer sequence.

For many applications functional side-groups are required. In principle two ways of preparing polymers with functional side-chains are available: the (co)polymerization of monomers that contain the desired functional groups or the (co)polymerization of functionalizable monomers followed by a post-polymerization functionalization step to introduce the desired functional groups (*53*). The copolymerization of styrene derivatives with maleimides in most cases results in the formation of alternating copolymers, but this nevertheless needs to be confirmed for each functional monomer. A post-polymerization functionalization strategy poses a more modular way to achieve the same goal since a single precursor polymer, with the desired monomer sequence, can be used to prepare a library of functional polymers in which the functional groups are presented in a predefined pattern.

Ten Brummelhuis and Weck presented the first system where such a strategy was investigated. The copolymerization of alkyne containing styrene derivatives with 2,3,4,5,6-pentafluorostyrene (PFS) was used (*54*, *55*). For the copolymerization of S with PFS it is known that a modest degree of alternation is achieved (*56*, *57*). For the FRP of various alkyne containing styrene derivatives with PFS it could be shown that the linker between the S-moiety and the propargyl group strongly influenced the copolymerization behavior by influencing the electron-density of the vinyl group of the S derivative. Electron withdrawing moieties (*e.g.* an ester) lead to a random copolymerization (r_S ? $r_{PFS} = 0.99$), whereas an enhanced degree of alternation was achieved using electron-donating

moieties (ether or tertiary amine groups $r_S \cdot r_{PFS}$ = 0.17 and 0.02 respectively). Functional groups could be introduced in the corresponding random or alternating copolymers in a post-polymerization functionalization step: the alkyne moiety present in the styrene derivatives could efficiently be functionalized with an azide containing functional group in a copper-catalyzed cycloaddition, whereas the PFS residue could be functionalized using thiols in a nucleophilic *para*-substitution reaction (Figure 3).
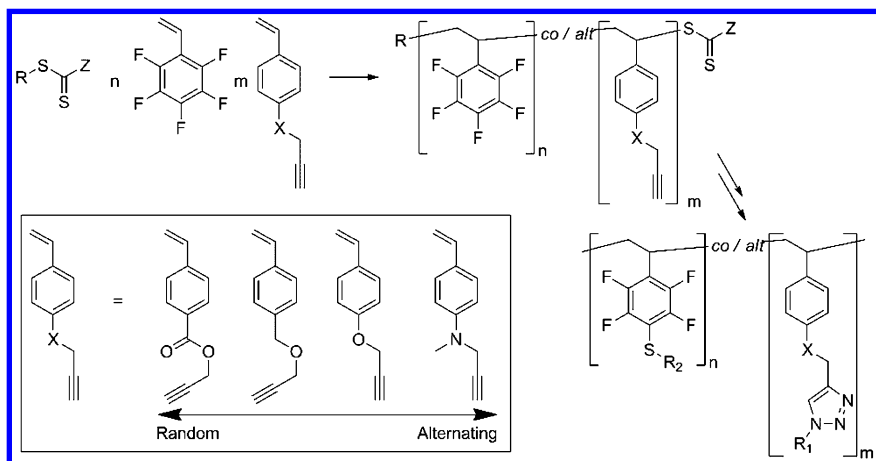
Figure 3. The RAFT copolymerization of various styrene derivatives with 2,3,4,5,6-pentafluorostyrene, resulting in random till alternating copolymers depending on the linker between the styrene moiety and the propargyl group, and the subsequent post-polymerization functionalization with azides and thiols (37, 38).

RAFT copolymerization could be used to gain simultaneous control over molecular weight and monomer sequence. Molecular weight could effectively be controlled using all three tested CTAs (a trithiocarbonate: $Đ$ = 1.31, a dithiobenzoate: $Đ$ = 1.17, and a dithiocarbamate: $Đ$ = 1.19) at 65°C, using AIBN as the initiator, in 1,4-dioxane. The polymerization could also be controlled at room temperature where the degree of alternation is further enhanced, likely because of more pronounced complexation of S and PFS residues. The reactivity ratios found in free-radical polymerization and in the RAFT process were similar under similar conditions, but could be manipulated by changing solvent. In toluene (which can disrupt any stacking interactions between the electron-rich and -deficient monomers) PFS proved less reactive, resulting in larger r_S and lower r_{PFS} values. A very similar system, though prepared by ATRP, has recently been used for catalysis (*58*).

Promotion of Alternating Copolymerization Using Lewis Acids

Polymerizations that are typically not strictly alternating, such as the copolymerization of styrene and methyl methacrylate (MMA), which normally

proceeds with only a very slight tendency towards alternation ($r_S \sim 0.5$, $r_{MMA} \sim 0.5$ (*59*)) can be manipulated such that alternating copolymers are attained. To this end, Lewis acids are added to the polymerization mixture that bind to the carbonyl group of the acrylate monomer. Though the exact mechanism has not been unequivocally determined, the electron-withdrawing property of the Lewis acid likely reduces the electron density on the vinyl group of the acrylate monomers, so that in combination with an electron-rich monomer (such as S) alternating sequences are predominantly formed. Matyjaszewski and coworkers used this strategy for the simultaneous control of molecular weight, using RAFT, and monomer sequence, where the simple addition or omission of Lewis acids determines whether alternating or more or less random monomer sequences are incorporated (*60–62*).

Initial studies focused on the copolymerization of S and MMA in the presence of diethylaluminum chloride (Et$_2$AlCl), where it could be shown that the fraction of S-MMA-S triads in the polymer could be enhanced from 52% in the absence of Et$_2$AlCl to 87% in its presence, which is similar to the percentage found for the corresponding FRP. The control over $Đ$ was slightly compromised by the presence of Et$_2$AlCl ($Đ$ = 1.38 instead of 1.14 for normal RAFT) (*43*).

In later work the application of other controlled-radical polymerization techniques, *i.e.* ATRP, NMP and iodide degenerative transfer polymerization (IDTP) were attempted, but polymerization in the presence of a Lewis acid proceeded in a strongly exothermic (even explosive) and uncontrollable fashion for the former two methods, and polymers with higher $Đ$ were formed using IDTP, making RAFT the sole viable method of controlling both monomer sequence and molecular weight using Lewis acids (*44*). Additionally, also tin(IV) chloride, zinc chloride and ethylaluminum sesquichloride (EASC) were used as Lewis acids, but control over molecular weight only proved possible using EASC (at 40°C) while a similar control over the monomer sequence as for Et$_2$AlCl was attained (*44*). The lack of control using the other Lewis acids is likely due to decomposition of the CTA as qualitatively observed by the disappearance of the characteristic color of the CTA. Alternating copolymers could similarly be prepared using S and *n*-butyl methacrylate (*44*).

Copolymerization with Non-Homopolymerizable Monomers

In recent years an increasing number of reports concerning the alternating and periodic copolymerization with non-conjugated olefin monomers have emerged. The non-conjugated olefin monomers do not homopolymerize in radical polymerizations under typical reaction conditions. Cross-propagation, especially with electron-deficient monomers, is therefore strongly enhanced.

Lu and coworkers presented the alternating RAFT copolymerization of *β*-pinene with acrylonitrile (ACN), for which $r_{pinene} = 0$ and $r_{ACN} = 0.66$ were determined. Only upon the addition of a Lewis acid (Et$_2$AlCl) were nearly perfect alternating copolymers obtained though, while $Đ$ around 1.2 were achieved thanks to the addition of a CTA (*63*). The group continued to study the copolymerization of *β*-pinene with various *N*-substituted maleimides (*64*). In these studies strong penultimate effects were observed, *i.e.* the last two rather than the last monomer

alone (as in the terminal model) determines the kinetics of addition of the two monomers to the growing chain-end. In all cases, approximately a 2:1 ratio of maleimide to β-pinene was found in the copolymer, which indicates the formation of a periodic copolymer with predominantly AAB-monomer sequences (Figure 4A). This conclusion was confirmed by the reactivity ratios that could be determined assuming the rate of homopolymerization of β-pinene is negligible. Control over molecular weight through RAFT is possible to some degree ($Đ \sim$ 1.4) for *N*-phenyl maleimide, whereas conversions of less than 25% were reached using the copolymerization of β-pinene with *N*-methyl maleimide and *N*-ethyl maleimide.
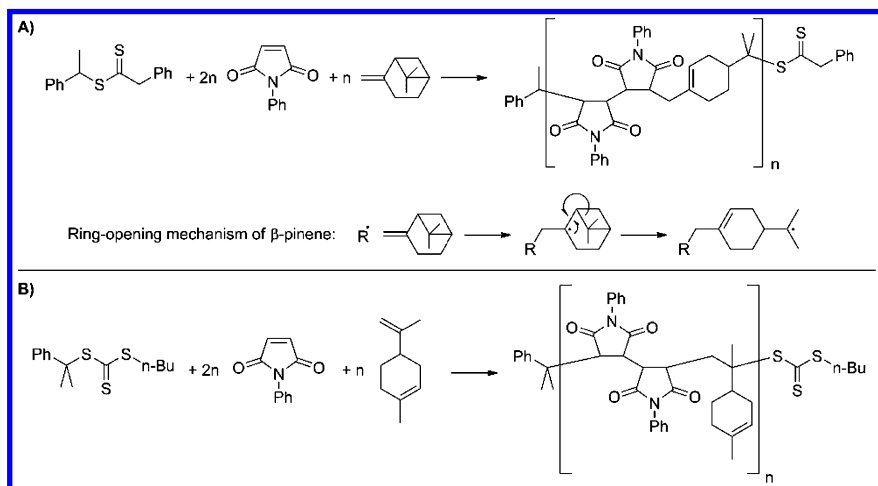
Figure 4. Periodic AAB-copolymerization of β-pinene (A) and (+)-limonene (B) with maleimides controlled by RAFT (47–49).

Further examples where periodic AAB-monomer sequences were attained were reported by the group of Kamigaito (*65*, *66*), who presented the copolymerization of maleimides (primarily *N*-phenyl maleimide, but also *N*-cyclohexyl maleimide and *N*-ethyl maleimide) with (+)-limonene in the presence of a fluoroalcohol (PhC(CF₃)₂OH) in a RAFT copolymerization with a nearly perfect control over the AAB-periodic monomer sequence as well as molecular weight ($Đ$ 1.1 - 1.2) (Figure 4B). The fluoroalcohol serves to decrease the tendency of the maleimide to homopolymerize, similar as the effect found for (inorganic) Lewis acids.

Though RAFT copolymerization was not shown in these examples the FRP of maleimides with other non-conjugated olefins was also shown to result in periodic copolymers, though less bulky olefins typically exhibit a sequence with more errors, likely due to alternating rather than periodic sequences (*49*).

Alternative Methods of Controlling Monomer Sequence

Not only the reactivity of the olefin, influenced by additives or not, but also interactions between monomers, *e.g.* through hydrogen bonding, can be used

In Controlled Radical Polymerization: Mechanisms; Tsarevsky, et al.;
ACS Symposium Series; American Chemical Society: Washington, DC, 2015.

to influence the monomer sequence. The higher relative concentration of the complementary monomer results in the preferred alternating copolymerization of monomer with complementary H-bonding motives, such as adenine and thymine containing methacrylate monomers (AMA and TMA respectively) (*67*). Since the solvent strongly influences the H-bonding between the monomers, strong influences of the solvent on the copolymerization is observed. In DMF, where H-bonding is very weak (binding constant at 60°C ~ 1 M^{-1}) a random copolymer is formed (r_{AMA} = 0.88, r_{TMA} = 0.89), whereas in chloroform, where strong H-bonds are formed (binding constant ~ 20 M^{-1} at 60°C), predominantly alternating monomer sequences are observed (r_{AMA} = 0.17, r_{TMA} = 0.23).

Another method by which an apparent control over monomer sequence is exerted is provided by ring-opening polymerizations. An example is presented by Mori and coworkers, who reported the radical ring-opening polymerization of 10-methylene-9,10-dihydroanthryl-9-spirophenylcyclopropane, as well as its *p*-bromo, *p*-chloro and pyridine derivatives, which could be controlled with RAFT (*68*, *69*). The resulting polymer contains alternating sequences of anthracene and styrene (derived) moieties (Figure 5).
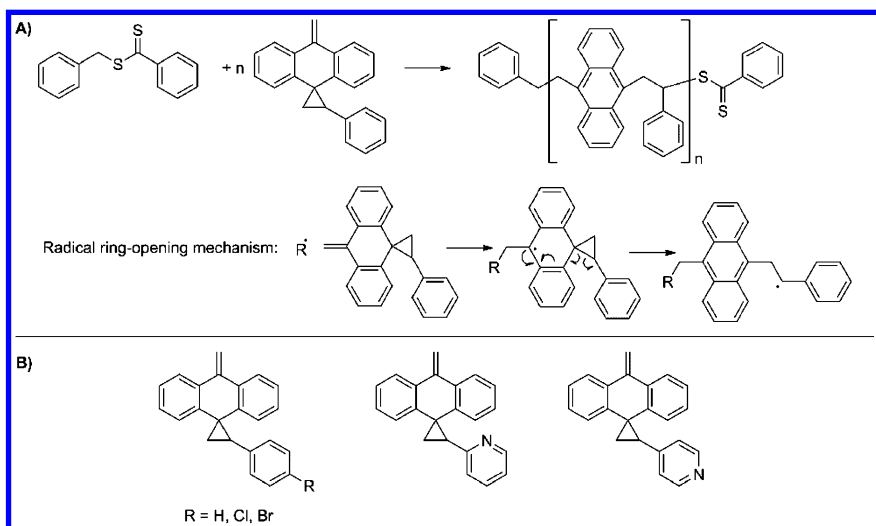
Figure 5. A) The RAFT controlled radical ring-opening polymerization of 10-methylene-9,10-dihydroanthryl-9-spirophenylcyclopropane derivatives resulting in pseudo-alternating copolymers. B) Alternative monomers that can be used in this polymerization (51, 52).

Though its applicability to the synthesis of higher molecular weight sequence controlled polymers is yet to be proven, Moad and coworkers (*70*) and, more recently, Junkers and coworkers presented the preparation of sequence controlled dimers and tetramers respectively by stepwise single-monomer addition in a RAFT process (*71*). The procedure by Junkers and coworkers relied on the addition of a single monomer (on average) to the CTA by using 10 equivalents of a monomer to the CTA in the presence of a small amount of AIBN and heating the solution

for a short time. The desired product was isolated in an automated recycling size-exclusion chromatograph, and subsequently used for further additions. In the subsequent steps only a single equivalent of monomer was used because of the faster insertion. By repetition of this cycle of addition and purification, a tetramer of *e.g.* *n*-butyl acrylate, *tert*-butyl acrylate, 2-ethylhexyl acrylate and *n*-butyl acrylate could be prepared with the CTA functional end-groups intact. The yield of each subsequent step decreased steadily though: whereas a yield of 55% was obtained in the first step, only a 10-15% yield was achieved in the last, making the method highly inefficient.

Conclusion and Outlook

A wide variety of different types of polymerizations that provide control over monomer sequence, ranging from copolymerizations of electron-rich and deficient monomers, affecting the copolymerization with Lewis acids, to radical ring-opening polymerizations have successfully been performed under RAFT conditions that provide a high degree of control over the molecular weight of the resulting sequence-defined polymers. Despite reports that the RAFT process can influence the monomer sequence, as was shown for the copolymerization of MMA/S, methyl acrylate/S and MMA/*n*-butyl acrylate (*72*), in most cases only a negligible effect is observed. Likely such effects are only relevant at very low molecular weight.

ATRP and NMP, the main two other established CRP strategies, are, though applicable in some cases, less versatile than RAFT, thanks to the fact that RAFT is highly compatible with a wide variety of conditions and functional groups. RAFT therefore provides an ideal platform for the simultaneous control over molecular weight and monomer sequence, and will likely play a large role in future work in this direction.

Acknowledgments

References

1. Braunecker, W. A.; Matyjaszewski, K. *Prog. Polym. Sci.* **2007**, *32*, 93–146.
2. Satoh, K.; Kamigaito, M. *Chem. Rev.* **2009**, *109*, 5120–5156.
3. Lutz, J.-F.; Ouchi, M.; Liu, D. R.; Sawamoto, M. *Science* **2013**, *341*–1238149.
4. Badi, N.; Lutz, J.-F. *Chem. Soc. Rev.* **2009**, *38*, 3383–3390.

5. Ouchi, M.; Badi, N.; Lutz, J.-F.; Sawamoto, M. *Nature Chem.* **2011**, *3*, 917–924.
6. Lutz, J.-F. *Polym. Chem.* **2010**, *1*, 55–62.
7. Yokota, K. *Prog. Polym. Sci.* **1999**, *24*, 517–563.
8. Franz, N.; Kreutzer, G.; Klok, H.-A. *Synlett* **2006**, *12*, 1793–1815.
9. Seeberger, P. H.; Werz, D. B. *Nature* **2007**, *446*, 1046–1051.
10. Ponader, D.; Wojcik, F.; Beceren-Braun, F.; Dernedde, J.; Hartmann, L. *Biomacromolecules* **2012**, *13*, 1845–1852.
11. Zuckermann, R. N.; Kerr, J. M.; Kent, S. B. H.; Moos, W. H. *J. Am. Chem. Soc.* **1992**, *114*, 10646–10647.
12. Zhang, C.; Ling, J.; Wang, Q. *Macromolecules* **2011**, *44*, 8739–8743.
13. Kushner, A. M.; Guan, Z. *Angew. Chem., Int. Ed.* **2011**, *50*, 9026–9057.
14. Pfeiffer, S.; Lutz, J.-F. *J. Am. Chem. Soc.* **2007**, *129*, 9542–9543.
15. Lutz, J.-F. *Acc. Chem. Res.* **2013**, *46*, 2696–2705.
16. Rzaev, Z. M. O. *Prog Polym. Sci.* **2000**, *25*, 163–217.
17. Braun, D.; Hu, F. *Prog. Polym. Sci.* **2006**, *31*, 239–276.
18. Moad, G.; Rizzardo, E.; Thang, S. H. *Aust. J. Chem.* **2009**, *62*, 1402–1472.
19. De Brouwer, H.; Schellekens, A. J.; Klumperman, B.; Monteiro, M. J.; German, A. L. *J. Polym. Sci., Part A: Polym. Chem.* **2000**, *38*, 3596–3603.
20. Du, F.-S.; Zhu, M.-Q.; Guo, H.-Q.; Li, Z.-C.; Li, F.-M. *Macromolecules* **2002**, *35*, 6739–6741.
21. You, Y.-Z.; Hong, C.-Y.; Pan, C.-Y. *Eur. Polym. J.* **2002**, *38*, 1289–1295.
22. Chernikova, E.; Terpugova, P.; Bui, C.; Charleux, B. *Polymer* **2003**, *44*, 4101–4107.
23. Hawker, C. J.; Bosman, A. W.; Harth, E. *Chem. Rev.* **2001**, *101*, 3661–3688.
24. Benoit, D.; Hawker, C. J.; Huang, E. E.; Lin, Z.; Russell, T. P. *Macromolecules* **2000**, *33*, 1505–1507.
25. Seymour, R. B.; Garner, D. P. *Polymer* **1976**, *17*, 21–24.
26. Chen, G.-Q.; Wu, Z.-Q.; Wu, J.-R.; Li, Z.-C.; Li, F.-M. *Macromolecules* **2000**, *33*, 232–234.
27. Fan, D.; He, J.; Xu, J.; Tang, W.; Liu, Y.; Yang, Y. *J. Polym. Sci., Part A: Polym. Chem.* **2006**, *44*, 2260–2269.
28. Ma, J.; Cheng, C.; Sun, G.; Wooley, K. L. *Macromolecules* **2008**, *41*, 9080–9089.
29. Yu, Y.; Zhan, X.; Zhang, Q.; Chen, F. *Polym. Eng. Sci.* **2011**, *51*, 1041–1050.
30. Yao, Z.; Zhang, J.-S.; Chen, M.-L.; Li, B.-J.; Lu, Y.-Y.; Cao, K. *J. Appl. Polym. Sci.* **2011**, *121*, 1740–1746.
31. Zhu, M. Q.; Wei, L. H.; Li, M.; Jiang, L.; Du, F. S.; Li, Z. C.; Li, F. M. *Chem. Commun.* **2001**, 365–366.
32. Fang, Y.; Cao, Y.; Zhang, A.; Zhai, G.; Kong, L.; Zhang, D. *Acta Polym. Sin.* **2010**, *1*, 51–58.
33. Davies, M. C.; Dawkins, J. V.; Hourston, D. J. *Polymer* **2005**, *46*, 1739–1753.
34. Mao, M.; Turner, S. R. *J. Am. Chem. Soc.* **2007**, *129*, 3832–3833.
35. Shi, Y.; Fu, Z.; Yang, W. *J. Polym. Sci., Part A: Polym. Chem.* **2006**, *44*, 2069–2075.
36. Xue, X.; Zhu, J.; Zhang, Z.; Zhou, N.; Zhu, X. *React. Funct. Polym.* **2010**, *70*, 456–462.

37. Weiss, J.; Li, A.; Wischerhoff, E.; Laschewsky, A. *Polym. Chem.* **2012**, *3*, 352–361.
38. Li, S.; Ye, C.; Zhao, G.; Zhang, M.; Zhao, Y. *J. Polym. Sci., Part A: Polym. Chem.* **2012**, *50*, 3135–3148.
39. Kim, H.; Kang, Y. J.; Jeong, E. S.; Kang, S.; Kim, K. T. *ACS Macro Lett.* **2012**, *1*, 1194–1198.
40. Moughton, A. O.; Sagawa, T.; Gramlich, W. M.; Seo, M.; Lodge, T. P.; Hillmyer, M. A. *Polym. Chem.* **2013**, *4*, 166–173.
41. Jiang, X.; Shao, W.; Jiang, K.; Zhang, M.; Liu, H.; Ye, C.; Zhao, Y. *Polym. Chem.* **2013**, *4*, 3272–3281.
42. Zhang, Z.; Hong, L.; Gao, Y.; Zhang, W. *Polym. Chem.* **2014**, *5*, 4534–4541.
43. Williams, E. G. L.; Fairbanks, B.; Moad, G.; Mulder, R. J.; Rizzardo, E.; Thang, S. H. *Polym. Chem.* **2015**, *6*, 228–232.
44. Jia, Y.; Liu, L.; Lei, B.; Li, J.; Zhu, X. X. *Macromolecules* **2011**, *44*, 6311–6317.
45. Serbin, A. V.; Karaseva, E. N.; Dunaeva, I. V.; Krut'ko, E. B.; Talyzenkov, Y. A.; Filatova, M. P.; Chernikova, E. V. *Polym. Sci., Ser. B* **2011**, *53*, 116–124.
46. Zou, L.; Liu, J.; Zhang, K.; Chen, Y.; Xi, F. *J. Polym. Sci., Part A: Polym. Chem.* **2014**, *52*, 330–338.
47. Ren, Y.; Zhu, Z.; Huang, J. *J. Polym. Sci., Part A: Polym. Chem.* **2004**, *42*, 3828–3835.
48. Wei, J.; Zhu, Z.; Huang, J. *J. Appl. Polym. Sci.* **2004**, *94*, 2376–2382.
49. Hu, Z.; Zhang, Z. *Macromolecules* **2006**, *39*, 1384–1390.
50. Maki, Y.; Mori, H.; Endo, T. *Macromolecules* **2008**, *41*, 8397–8404.
51. Maki, Y.; Mori, H.; Endo, T. *Macromol. Chem. Phys.* **2010**, *211*, 1137–1147.
52. Zaitsev, S. D.; Semchikov, Y. D.; Chernikova, E. V. *Polym. Sci., Ser. B* **2009**, *51*, 84–88.
53. Günay, K. A.; Theato, P.; Klok, H.-A. *J. Polym. Sci., Part A: Polym. Chem.* **2013**, *51*, 1–28.
54. Ten Brummelhuis, N.; Weck, M. *ACS Macro Lett.* **2012**, *1*, 1216–1218.
55. Ten Brummelhuis, N.; Weck, M. *J. Polym. Sci., Part A: Polym. Chem.* **2014**, *52*, 1555–1559.
56. Pryor, W. A.; Huang, T.-L. *Macromolecules* **1969**, *2*, 70–77.
57. Pugh, C.; Tang, C. N.; Paz-Pazos, M.; Samtan, O.; Dao, A. H. *Macromolecules* **2007**, *40*, 8178–8188.
58. O'Shea, J.-P.; Solovyeva, V.; Guo, X.; Zhao, J.; Hadjichristidis, N.; Rodionov, V. O. *Polym. Chem.* **2014**, *5*, 698–701.
59. Greenley, R. Z. In *Polymer Handbook*, 4th ed.; Brandrup, J., Immergut, E. H., Grulke, E. A., Eds.; John Wiley & Sons, Inc.: New York, NY, 1999.
60. Kirci, B.; Lutz, J.-F.; Matyjaszewski, K. *Macromolecules* **2002**, *35*, 2448–2451.
61. Lutz, J.-F.; Kirci, B.; Matyjaszewski, K. *Macromolecules* **2003**, *36*, 3136–3145.
62. Kirci-Denizli, B.; Lutz, J.-F.; Okrasa, L.; Pakula, T.; Guner, A.; Matyjaszewski, K. *J. Polym. Sci., Part A: Polym. Chem.* **2005**, *43*, 3440–3446.

63. Li, A.-L.; Wang, Y.; Liang, H.; Lu, J. *J. Polym. Sci., Part A: Polym. Chem.* **2006**, *44*, 2376–2387.

64. Wang, Y.; Chen, Q.; Liang, H.; Lu, J. *Polym. Int.* **2007**, *56*, 1514–1520.

65. Satoh, K.; Matsuda, M.; Nagai, K.; Kamigaito, M. *J. Am. Chem. Soc.* **2010**, *132*, 10003–10005.

66. Matsuda, M.; Satoh, K.; Kamigaito, M. *J. Polym. Sci., Part A: Polym. Chem.* **2013**, *51*, 1774–1785.

67. Kang, Y.; Lu, A.; Ellington, A.; Jewett, M. C.; O'Reilly, R. K. *ACS Macro Lett.* **2013**, *2*, 581−586.

68. Mori, H.; Tando, I.; Tanaka, H. *Macromolecules* **2010**, *43*, 7011–7020.

69. Nakabayashi, K.; Inoue, S.; Abiko, Y.; Mori, H. *Macromolecules* **2013**, *46*, 4790–4798.

70. Houshyar, S.; Keddie, D. J.; Moad, G.; Mulder, R. J.; Saubern, S.; Tsanaktsidis *J. Polym. Chem.* **2012**, *3*, 1879–1889.

71. Vandenbergh, J.; Reekmans, G.; Adriaensens, P.; Junkers, T. *Chem. Commun.* **2013**, *49*, 10358–10360.

72. Feldermann, A.; Toy, A. A.; Phan, H.; Stenzel, M. H.; Davis, T. P.; Barner-Kowollik, C. *Polymer* **2004**, *45*, 3997–4007.

Chapter 15

Aqueous RAFT/MADIX Polymerization of Vinylphosphonic Acid under Microwave Irradiation

Olivier Coutelier,[1] Issam Blidi,[1] Stéphanie Reynaud,[2] Bruno Grassl,[2] and Mathias Destarac[*],[1]

[1]Université Paul Sabatier, Laboratoire des Intéractions Moléculaires et de la Réactivité Chimique et Photochimique, UMR-CNRS 5223, 118 route de Narbonne, 31062 Toulouse cedex 9, France
[2]Université de Pau et des Pays de l'Adour, Institut des Sciences Analytiques et de Physico-Chimie pour l'Environnement et les Matériaux, UMR-CNRS 5254, Hélioparc Pau Pyrénées, 2 av. du Président Angot, 64053 Pau Cedex 09, France
[*]E-mail: destarac@chimie.ups-tlse.fr

RAFT/MADIX polymerization of vinylphosphonic acid (VPA) is the technology of choice for the direct synthesis of polymers containing phosphonic acid functions with control of molar masses and dispersity, and to access more complex structures such as block copolymers with one polyphosphonate block. However, the low polymerizability of VPA and its long polymerization times are severe limitations to the development of precision polymers based on this monomer. In this chapter, we investigate the use of microwave heating as an alternative to conventional heating to accelerate the polymerization rate without affecting the quality of the control of the RAFT/MADIX polymerization of VPA.

Introduction

Phosphonic acid- containing polymers are of increasing interest for a wide range of applications such as scale inhibition for water treatment (*1*), dental adhesive compositions (*2*), metal adhesion promoters (*3*), proton conductors for fuel cell membranes (*4*), regenerative medicine (*5*) and

drug delivery (*6*).   These polymers are mostly produced by free-radical polymerization of functional styrene (*7*), (meth)acrylate (*8*), (meth)acrylamide (*2*) and vinyl derivatives (*9*) bearing either a free phosphonic acid group a phosphonic ester, followed by post-polymerization deprotection.   In recent years, the advent of reversible deactivation radical polymerization (RDRP) (*10*) opened many opportunities for the synthesis of phosphonic acid-functional polymers with controlled architectures.   Nitroxide-mediated polymerization (NMP) of dimethyl *p*-vinylbenzylphosphonate (*11*) with TEMPO was the first example of a RDRP polymerization of a phosphonated monomer. Soon after, diisopropyl *p*-vinylbenzylphosphonate (*12*) was polymerized by atom transfer radical polymerization (ATRP) in a controlled manner.   More recently, reversible addition fragmentation chain transfer polymerization/ macromolecular design by interchange of xanthates (RAFT/MADIX) (*13*) has been established as the most robust strategy to yield controlled phosphonated polymers.   For instance, Canniccioni et al.   (*14*) successfully controlled RAFT polymerization of dimethyl(methacryloyloxy)methyl phosphonate in the presence of dithiobenzoates. Graillot et al. (*15*) described the trithiocarbonate-mediated RAFT polymerization of a phosphorus-based acrylamide monomer, namely diethyl-2-(acrylamido)ethylphosphonate and its incorporation into thermoresponsive block copolymers with N-isopropylacrylamide.   Few studies dealt with the use of a *p*-vinylbenzyl phosphonic acid dialkyl ester monomer in RAFT polymerization.   Lacroix-Desmazes and co-workers (*16*) synthesized gradient copolymers from diethyl-*p*-vinylbenzylphosphonate and 1,1,2,2-tetrahydro perfluorodecyl acrylate by means of a dithiobenzoate RAFT agent.   Our group studied the dibenzyl trithiocarbonate-mediated homopolymerization of dimethyl-*p*-vinylbenzyl phosphonate and its statistical and block copolymerization with styrene (*17*).   Most importantly, RAFT polymerization allows the direct polymerization of monomers bearing unprotected phosphonic acid group. Recently, we reported the first example of RDRP of a PO_3H_2-functional monomer, namely vinylphosphonic acid (VPA) which could be efficiently polymerized in a controlled manner in water by RAFT/MADIX polymerization in the presence of a watersoluble xanthate transfer agent (*18*).   This rendered possible the direct aqueous synthesis of poly(acrylic acid)-poly(vinylphosphonic acid) diblock copolymers (*18*). However, due to the low reactivity of VPA and limited kinetic length of PVPA chains, incomplete polymerizations (75-80% conversion) were obtained after 24h of polymerization with controlled M_n in the 1000-5000 g mol^{-1} range.

In order to tackle these limitations, we decided to explore the aqueous RAFT/ MADIX polymerization of VPA under microwave (MW) irradiation.

Experimental

Materials

All reagents were used without further purification.   Vinylphosphonic acid 97% (VPA), was purchased from Aldrich.   2,2′-azobis(isobutyramidine)

dihydrochloride 98% (AIBA) was purchased from Acros.   2-[(ethoxythio-carbonyl)thio]propionic acid (X1) was prepared according to procedure described elsewhere (*19*).

Instrumentation

For PVPA samples, size exclusion chromatography (SEC) was performed on an Agilent 1100 HPLC system, a 18 angle Multi-Angle Light Scattering (MALS) DAWN-Heleos-II (Wyatt Technology), an OptilaRex Refractometer (Wyatt Technology) and a set of 2 columns (Shodex SB-806M and SB-802.5) thermostated at 30°C. Number-average molar masses ($M_{n\ MALS}$) and dispersities Đ (=M_w/M_n) were determined with the SEC-RI-MALS line described above. Water (NaCl 100 mmol.L^{-1}, NaH$_2$PO$_4$ 25 mmol.L^{-1}, Na$_2$HPO$_4$ 25 mmol.L^{-1}, buffer solution at pH=7) was used as eluent with a flow rate of 1.0 mL.min^{-1}.
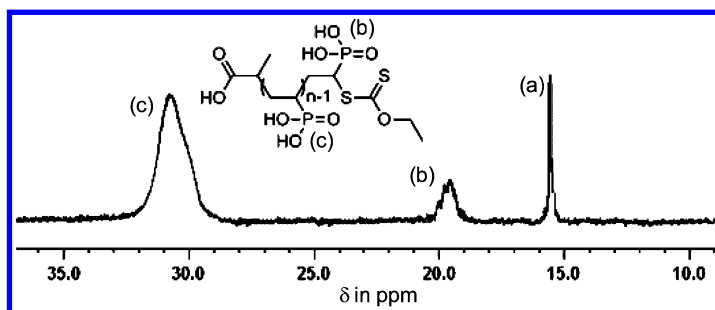
Figure 1. ^{31}P NMR analysis of crude PVPA obtained after X1-mediated RAFT/MADIX polymerization of VPA. Signal (a) correspond to residual VPA, and signals (b) and (c) correspond to the terminal monomer unit and main chain monomer units of PVPA respectively. VPA conversion (%)=(b+c)/(a+b+c) and $M_{n\ NMR}=[b/(b+c)]*M_{VPA}+M_{X1}$

General Procedure for the RAFT/MADIX Polymerization of VPA under Microwave Irradiation

RAFT polymerizations were performed in a Discover single-mode microwave synthesizer (CEM Corp.) equipped with both online IR temperature sensor and optical fiber and compressed air cooling system. Experiments were done using the EMS (Enhanced Microwave Synthesis) mode, that corresponds to a microwave irradiation with a simultaneous air cooling allowing the reaction to receive more energy compared to a classical microwave irradiation. The maximal irradiation power was 300W in all experiments. In a 10 mL microwave reaction vessel, was introduced 5 mL of an aqueous solution of VPA (7.52 mol.L^{-1}), AIBA (56 mmol.L^{-1}) and xanthate X1 (1007 or 290 mmol.L^{-1}). The solution was degassed with nitrogen, and heated at 65°C under microwave irradiation controlled by optical fiber. At different time intervals, the reaction mixture was analyzed by NMR (^{1}H and ^{31}P) and SEC-RI-MALS to access VPA conversion and average molar masses $M_{n\ MALS}$ of the PVPAs. $M_{n\ NMR}$ was calculated by ^{31}P NMR by comparing the

signal intensities of VPA units of the main chain (29-32 ppm) to that of the terminal monomer unit in the alpha position to the thiocarbonylthio group (19-20 ppm), assuming that all the chains are capped with the dithiocarbonate group (Figure 1).

Results and Discussion

Microwave irradiation as an alternative heat source can be beneficial to chemical reactions in many ways, e.g. by a change of selectivity and generation of lower amounts of by-products, and enhancement of reaction rates (*20, 21*). In addition to the well-established advantages of fast and homogeneous heating, non thermal MW effects due to specific heating of polar intermediates can enable reactions that cannot proceed through conventional heating (CH). The last ten years have witnessed major progress in the field of polymerization reactions under MW (*22*). Many studies have been devoted to free radical homo- (*23*) and statistical copolymerization, with unsuccessful attempts to modify reactivity ratios under MW in the latter case (*24*). Numerous examples of RDRP under MW irradiation can be found in the literature (*22, 25–27*). The interpretation of the enhancement in rates of polymerization based on MW or purely thermal effects remains a subject of intense debate. It is difficult to compare results found in different published works because of the differences found in reaction volumes, types of oven, modes of irradiation and control of temperature (*28*). As reviewed by Kappe et al., the accurate measurement of reaction temperature in microwave oven is far from being trivial and requires both a basic understanding of microwave dielectric heating effect and use of appropriate temperature monitoring devices (*29*). In the case of RAFT polymerization, several examples in the literature illustrate the benefits of MW irradiation on the rate of polymerization. In 2007, Perrier and co-workers (*30*) demonstrated exceptional enhancement of rates of polymerization for both polar (e.g. vinyl acetate) and non-polar monomers (e.g. styrene) via monomodal MW irradiation compared to CH. This was later confirmed by Roy et al. for a broader range of vinyl esters (*31*), acrylamides and acrylates (*32*) using a trithiocarbonate RAFT agent. By means of modeling and simulations using the Predici software, Perrier and co-workers proposed that the rate enhancement was due to MW-induced acceleration of propagation and addition to the RAFT moiety by an order of magnitude (*33*). Very few reports can be found on aqueous RAFT polymerization under MW irradiation. Hawker and co-workers described the facile preparation of nanostructured hydrogels and double hydrophilic block copolymers by RAFT polymerization of NIPAM (*34*). Argawal et al. (*35*) explored the ring-closing RAFT cyclopolymerization of diallyldimethylammonium chloride (DADMAC). The authors observed a dramatic increase in the rate of polymerization (up to 520%) at each time interval that they attributed to a MW effect. In the following section, we present our results on the RAFT/MADIX polymerization of VPA in water under MW irradiation.

In order to evaluate the effect of MW heating on the rate of polymerization, we first investigated the free radical polymerization of VPA (7.52 mol.L^{-1}) in water at 65°C in the presence of AIBA (56 mmol.L^{-1}) as initiator, and compared the results with the ones obtained in our earlier study (*18*) using a CH process.

A 4-fold increase in the initial rate of polymerization was observed when MW heating was applied to a conventional radical polymerization of VPA, but over the course of the polymerization, the type of heating had a less marked effect on the rate of VPA consumption (Figure 2). After 2h under MW irradiation, the VPA conversion reached 73% and no longer increased with time (77% after 8h) while with CH, a VPA conversion of only 48% was obtained after 2h, and 8h were necessary to reach 74% VPA conversion (Figure 2). The observed differences in rates of polymerization could be ascribed to a larger flux of radicals in the early stages of polymerization due to more homogeneous and faster heating under MW conditions. This higher initial radical concentration could explain as well why the reaction practically stopped after 2h. M_n of PVPAs obtained after 8h under MW heating were lower than those obtained by CH (M_n=4900 and 8980 g mol^{-1}, respectively). Dispersities were similar with Đ=1.85 for MW heating and 1.78 for CH. This difference in molar mass could be related to the higher radical concentration in the reaction medium under MW irradiation, creating more chains and thus leading to lower M_n.
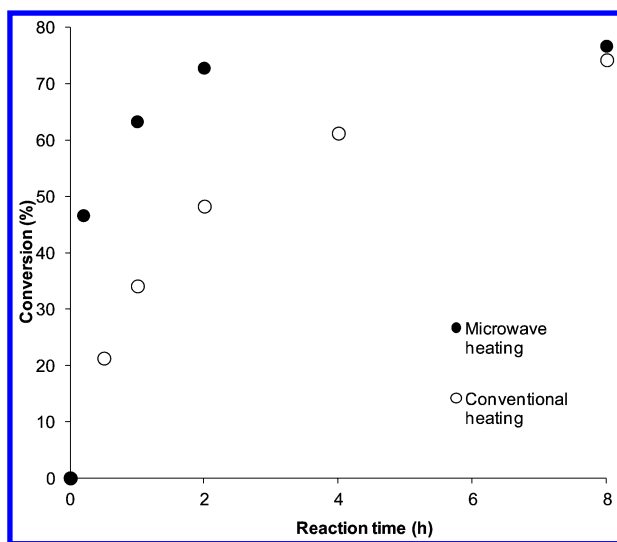
Figure 2. Evolution of VPA conversion during a free radical polymerization under microwave heating and conventional heating. [VPA]$_0$ = 7.52 mol.L^{-1}, [AIBA]$_0$ = 56 mmol.L^{-1}, T = 65°C.

As the M_n of PVPA did not exceed 4900 g.mol^{-1} under MW irradiation, we decided to explore the effect of MW heating on the RAFT/MADIX polymerization of VPA, targeting M$_n$ of 1000 and 3000 g.mol^{-1} in the presence of xanthate X1 (Scheme 1) and compared the polymerization results to those obtained by CH.
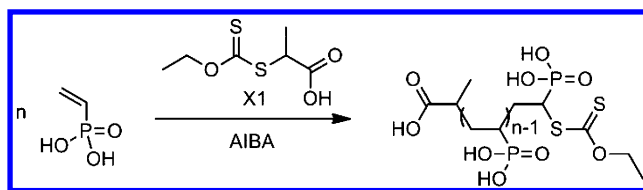
Scheme 1. Aqueous RAFT/MADIX polymerization of VPA mediated by xanthate X1.

During our previous study on the RAFT/MADIX polymerization of VPA (*18*), we observed that the presence of X1 slightly reduced the rate of polymerization of VPA (Figure 3).
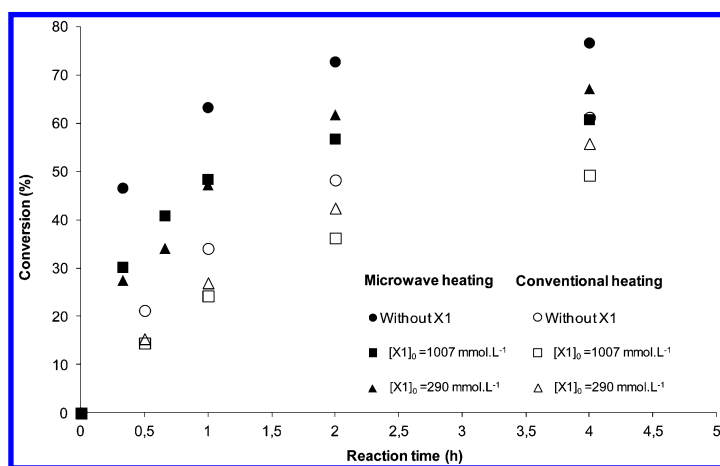
Figure 3. Evolution of VPA conversion with time for different concentrations of xanthate X1 for conventional and microwave heating. T=65°C.

VPA was polymerized in water at 65°C in the presence of AIBA (56 mmol.L^{-1}) as initiator, and two different concentrations of X1 (1007 and 290 mmol.L^{-1}), corresponding to PVPA with $M_{n\ th}$ values of 1000 and 3000 g.mol^{-1}, respectively. Polymerizations were stopped at different times and analyzed by NMR to determine VPA conversion and $M_{n\ NMR}$, and SEC to obtain $M_{n\ MALS}$ (Table 1, entries 9-18). Results of MW polymerizations of VPA were compared with previously published (*18*) data obtained with CH (Table 1, entries 1-8). As previously observed for CH, polymerization of VPA under MW heating is slowed down in the presence of X1. However, the xanthate concentration does not affect the rate of polymerization; nearly identical polymerization kinetics are observed in the presence of two different concentrations of xanthate (Figure 3 and Table 1).

Table 1. RAFT/MADIX polymerization of VPA by conventional heating and under microwave irradiation. $[VPA]_0 = 7.52$ mol.L^{-1}, $[AIBA]_0 = 56$ mmol.L^{-1}, $T = 65°C$. Conventional heating (entries 1-8) and microwave irradiation (entries 9-18)

Entry	$X1$ (mmol.L^{-1})	t (h)	Conv.[a] (%)	$M_{n\ th}$[b] (g mol-1)	$M_{n\ NMR}$[c] (g mol-1)	$M_{n\ MALS}$[d] (g mol-1)	Đ
1		1	24.3	250	400	1340	1.09
2	1007	4	49.3	500	550	1420	1.19
3		8	61.7	650	650	1460	1.17
4		24	74.3	750	750	1600	1.16
5		1	27	850	850	1780	1.27
6	290	4	55.9	1700	1800	2300	1.32
7		8	63.2	1950	2150	2880	1.30
8		24	78.4	2400	2700	3420	1.30
9		0.33	30.2	300	430	980	1.20
10		0.66	40.9	410	490	1290	1.35
11	1007	1	48.4	485	540	1550	1.18
12		2	56.8	570	670	1650	1.22
13		4	60.8	610	670	1610	1.20
14		0.33	27.5	825	950	1000	1.87
15		0.66	34.1	1020	1190	1630	1.49
16	290	1	47.3	1420	1640	2120	1.50
17		2	61.8	1850	2180	2340	1.42
18		4	67.2	2020	2220	2460	1.40

[a] Determined by ^{31}P NMR.   [b] $M_{n\ th} = ([VPA]_0/[X1]_0))*Conv*M(VPA)+ M(X1)$.
[c] Determined by ^{31}P NMR.   [d] Determined by SEC-RI-MALS

As we expected, the rate of RAFT/MADIX polymerization of VPA is faster under MW irradiation, even to a conventional (xanthate-free) polymerization by CH (Figure 3). Concerning the molar mass control, MW heating gave similar results than those obtained for CH conditions, with molar masses of PVPA regulated by $[VPA]_0/[X1]_0$ ratio and VPA conversion. SEC traces were narrower and monomodal in the presence of X1 and shifted towards higher elution times when the concentration of X1 in the reaction was increased (Figure 4).
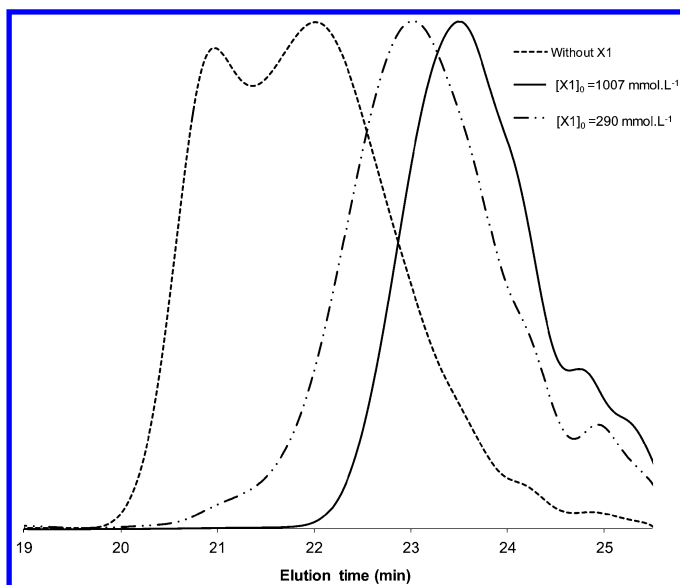
Figure 4. Overlay of SEC traces for different concentrations of xanthate X1 after 4h of polymerization. Conditions of Figure 3 and Table 1.

In a similar fashion to CH conditions, $M_{n\ NMR}$ values (for details of determination of $M_{n\ NMR}$, see Figure 1) obtained for RAFT polymerization of VPA under MW irradiation evolved linearly with conversion, and perfectly fitted the theoretical values calculated for a controlled polymerization for the two initial X1 concentrations that we considered (Figure 5). These results indicate that for both heating methods, X1 was totally consumed in the early stages of the polymerization with no degradation of the xanthate chain-end during the polymerization.

However, at this stage, no evidence was given that the polymer chains grow according to a reversible transfer process. In order to confirm that the polymerization proceeds according to a RAFT/MADIX mechanism, we determined M_n values by SEC-RI-MALS. The evolution of SEC traces with time shows a shift towards higher molar masses over the course of the polymerization, supporting the controlled character of VPA polymerization (Figure 6).

$M_{n\ MALS}$ values increase with VPA conversion and are also virtually identical whatever the heating process (Figure 7). Dispersities are slightly higher under MW irradiations (Figure 7), in particular during the first half of the reaction. This is a result of the large flux of radicals generated at the beginning of the reaction through MW irradiation, leading to the formation of a greater proportion of dead chains compared to CH conditions.
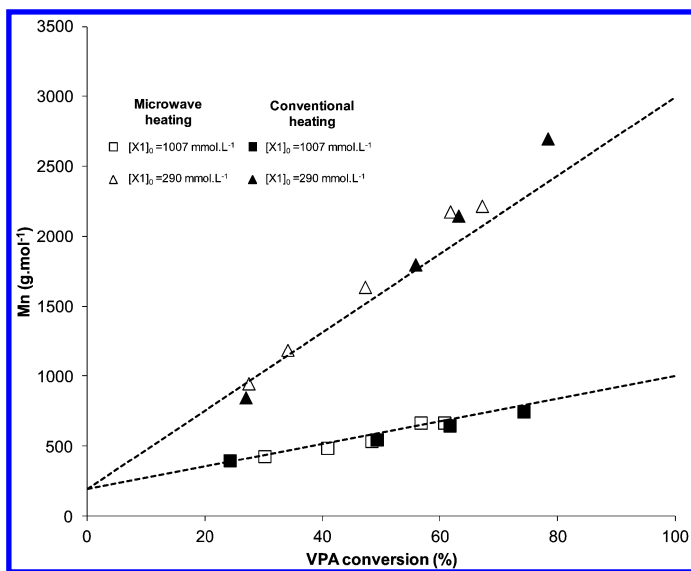
Figure 5. Evolution of $M_{n\ NMR}$ with VPA conversion for $[X1]_0 = 1007$ mmol.L^{-1} and 290 mmol.L^{-1}. Conditions of Figure 3 and Table 1.
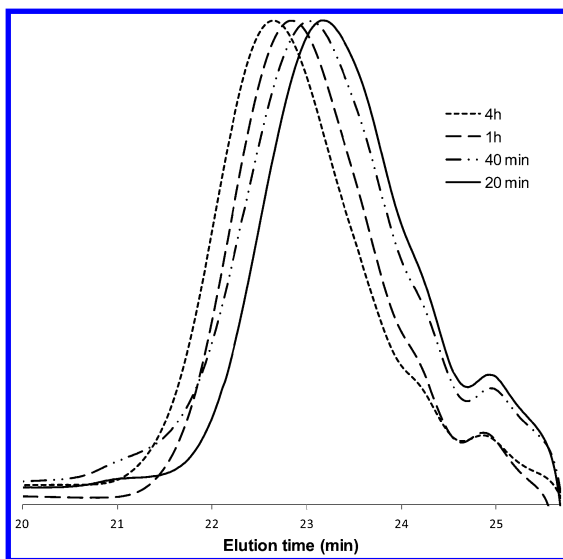
Figure 6. Evolution of SEC traces with time for $[X1]_0 = 290$ mmol.L^{-1} under microwave irradiation (Table 1, entries 14, 15, 17, 18).
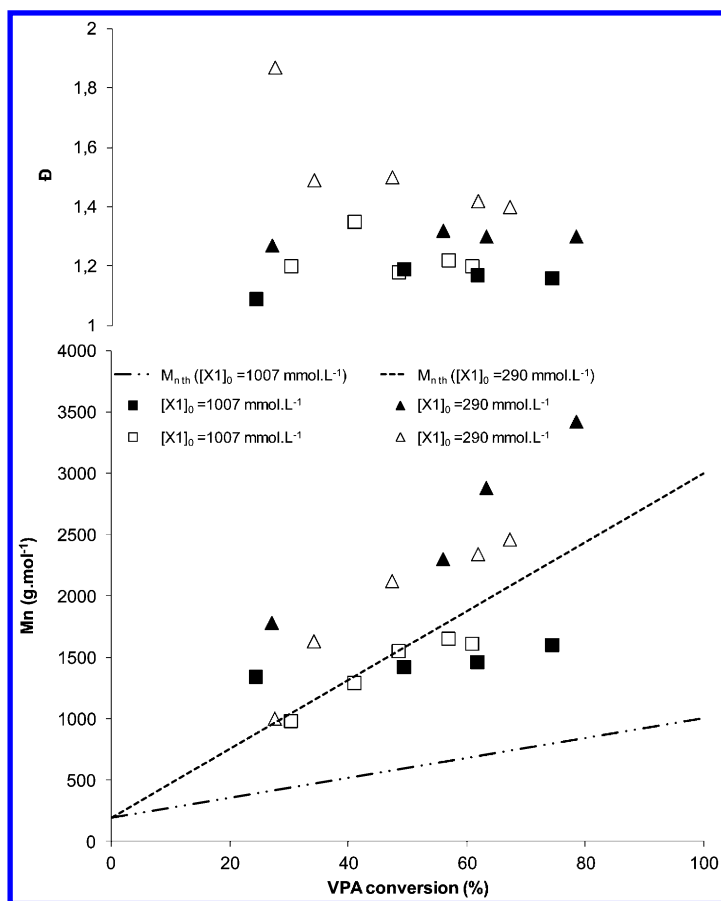
Figure 7. Dependence of $M_{n\,MALS}$ and dispersity of PVPA on VPA conversion for $[X1]_0 = 1007$ mmol.L^{-1} and 290 mmol.L^{-1}. Plain and hollow markers represent conventionnal heating and microwave heating, respectively.

Conclusion

The use of microwave irradiation resulted in an initial 4-fold acceleration of the free radical polymerization of VPA in water at 65°C under microwave irradiation compared to the same polymerization under conventional heating. Although the reasons for this acceleration are not well understood at this point, observations of a faster initial rate of polymerization and a lower molecular weight PVPA indicate that a higher initial radical concentration is present during VPA polymerization under MW irradiation compared to CH. When applied to the RAFT/MADIX polymerization of VPA in the presence of a watersoluble xanthate, MW heating caused a 3-fold increase of the initial rate of polymerization compared with CH. Under MW irradiation, the presence of xanthate caused a slight retardation effect, as observed for CH. However, the polymerizations were still found to be faster than the xanthate-free experiment under CH, with

no negative impact on the macromolecular parameters of PVPA as both M_n and Đ were nearly identical whatever the heating process used. These results indicate that the RAFT/MADIX polymerization kinetics and mechanism are not influenced by MW irradiation.

Acknowledgments

References

1. Oz, N.; Akar, A *J. Appl. Polym. Sci.* **2000**, *78*, 870–874.
2. Altin, A.; Akgun, B.; Bilgici, Z. S.; Turker, S. B.; Avci, D. *J. Polym. Sci., Part A: Polym. Chem.* **2014**, *52*, 511–522.
3. Koehler, J.; Kuehne, A.; Piermattei, A.; Qiu, J.; Keul, H.; Dirks, T.; Keul, H.; Möller, M. *J. Mater. Chem. B* **2015**, *3*, 804–813.
4. Lee, S.-I.; Yoon, K.-H.; Song, M.; Peng, H.; Page, K. A.; Soles, C. H.; Yoon, D. Y. *Chem. Mater.* **2012**, *24*, 115–122.
5. Watson, B. M.; Kasper, F. K.; Mikos, A. G. *Biomed. Mater.* **2014**, *9*, 025014, doi:10.1088/1748-6041/9/2/025014.
6. Kretlow, J. D.; Hacker, M. C.; Klouda, L.; Ma, B. B.; Mikos, A. G. *Biomacromolecules* **2010**, *11*, 797–805.
7. Boutevin, B.; Hervaud, Y.; Boulahna, A.; El Hadrani, E. M. *Polym. Int.* **2002**, *51*, 450–457.
8. Price, D.; Cunliffe, L. K.; Bullet, K. J.; Hull, T. R.; Milnes, G. J.; Ebdon, J. R.; Hunt, B. J.; Joseph, P. *Polym. Adv. Technol.* **2008**, *19*, 710–723.
9. Macarie, L.; Ilia, G. *Prog. Polym. Sci.* **2010**, *35*, 1078–1092.
10. Jenkins, A.; Jones, R. G.; Moad, G. *Pure Appl. Chem* **2010**, *82*, 483–491.
11. Boutevin, B.; Hervaud, Y.; Boulahna, A.; El Asri, M. *Macromolecules* **2002**, *35*, 6511–6516.
12. Jiang, F. J.; Kaltbeitzel, A.; Meyer, W. H.; Pu, H. T.; Wegner, G. *Macromolecules* **2008**, *41*, 3081–3085.
13. Barner-Kowollik, C. *Handbook of RAFT Polymerization*; Barner-Kowollik, C., Ed.; Wiley-VCH: Weinheim, 2008.
14. Canniccioni, B.; Monge, S.; David, G.; Robin, J. J. *Polym. Chem.* **2013**, *4*, 3676–3685.
15. Graillot, A.; Monge, S.; Faur, C.; Bouyer, D.; Robin, J. J. *Polym. Chem.* **2013**, *4*, 795–803.
16. Ribaut, T.; Lacroix-Desmazes, P.; Fournel, B.; Sarrade, S. *J. Polym. Sci., Part A: Polym. Chem.* **2009**, *47*, 5448–5460.
17. Blidi, I.; Coutelier, O.; Destarac, M. *J. Polym. Sci., Part A: Polym. Chem.* **2014**, *52*, 2616–2624.
18. Blidi, I.; Geagea, R.; Coutelier, O.; Mazières, S.; Violleau, F.; Destarac, M. *Polym. Chem.* **2012**, *3*, 609–612.

19. Fleet, R.; McLeary, J. B.; Grumel, V.; Weber, W. G.; Matahwa, H.; Sanderson, R. D. *Macromol. Symp.* **2007**, *255*, 8–19.

20. Kappe, C. O.; Dallinger, D.; Murphree, S. S. *Practical microwave synthesis for organic chemist – Strategies, intruments, and protocols*; John Wiley & Sons: Weinheim, 2009.

21. Kappe, C. O.; Dallinger, D. *Chem. Rev.* **2007**, *107*, 2563–2591.

22. Hoogenboom, R.; Schubert, U. S. *Macromol. Rapid Commun.* **2007**, *28*, 368–386.

23. Wiesbrok, F.; Hoogenboom, R.; Schubert, U. S. *Macromol. Rapid Commun.* **2004**, *25*, 1739–1764.

24. Fellows, C. M. *Central Eur. J. Chem.* **2005**, *3*, 40–52.

25. Rigolini, J.; Grassl, B.; Billon, L.; Reynaud, S.; Donard, O. F. X. *J. Polym. Sci., Part A: Polym. Chem.* **2009**, *47*, 6919–6931.

26. Brooks, W. L. A.; Sumerlin, B. S. *Chem. Isr. J. Chem.* **2012**, *52*, 256–263.

27. Brooks, W. L. A.; Sumerlin, B. S. In *Progress in Controlled Radical Polymerization: Mechanisms and Techniques*; ACS Symposium Series 1100; Americal Chemical Society: Washington, DC, 2012; pp 277−291.

28. Kappe, C. O. *Chem. Soc. Rev* **2008**, *37*, 1127–1139.

29. Kappe, C. O. *Chem. Soc. Rev* **2013**, *42*, 4977–4990.

30. Brown, S. L.; Rayner, C. M.; Graham, S.; Cooper, A.; Rannard, S.; Perrier, S. *Chem. Commun.* **2007**, 2145–2147.

31. Roy, D.; Sumerlin, B. *Polymer* **2011**, *52*, 3038–3045.

32. Roy, D.; Ullah, A.; Sumerlin, B. S. *Macromolecules* **2009**, *42*, 7701–7708.

33. Zetterlund, P. B.; Perrier, S. *Macromolecules* **2011**, *44*, 1340–1346.

34. An, Z.; Shi, Q.; Tang, W.; Tsung, C-K.; Hawker, C. J.; Stucky, G. D. *J. Am. Chem. Soc.* **2007**, *129*, 14493–14499.

35. Assem, Y.; Greiner, A.; Agarwal, S. *Macromol. Rapid Commun.* **2007**, *28*, 1923–1928.

294

In Controlled Radical Polymerization: Mechanisms; Tsarevsky, et al.;
ACS Symposium Series; American Chemical Society: Washington, DC, 2015.

Chapter 16

Organotellurium-Mediated Radical Polymerization under Photo Irradiation

Yasuyuki Nakamura, Mengmeng Yu, Yu Ukai, and Shigeru Yamago*

Institute for Chemical Research, Kyoto University, Uji 611-0011, Japan
E-mail: yamago@scl.kyoto-u.ac.jp

Photophysical properties of organotellurium chain transfer agents and synthetic scope of photo-induced oganotellurium-mediated radical polymerization (Photo-TERP) were investigated. All organotellurium chain transfer agents and organotellurium-living polymers possessed characteristic UV-vis absorption corresponding to n(Te)-σ*(C-Te) transition. Irradiation of this band induced C-Te bond homolysis with high quantum yield (0.84). Photo-TERP proceeds under mild conditions, such as below room temperature, under irradiation of low-intensity light and gave structurally well controlled polymers. Synthetic advantages of low temperature photo-TERP were demonstrated by acrylate polymerization in minimizing back-biting reaction and polymerization of thermally labile monomers.

Introduction

Controlled/living radical polymerization (LRP) or reversible deactivation radical polymerization has now been recognized as one of the most versatile methods for synthesizing functional polymers with controlled macromolecular structure (*1*, *2*). Among various LRP methods, organotellurium-mediated radical polymerization (TERP) (*3–5*) is characterized by high synthetic versatility in, such as monomer families, block copolymer synthesis (*6–9*), end-group transformation (*10–12*), and functional group compatibility (*13*). Due to the highly synthetic potential as well as high adaptability of large scale synthesis, TERP has already been used in industry for commercial production of high-valued polymer materials (*14*). In addition, TERP is also mechanistically unique, as

two activation mechanisms of an organotellurium dormant species, namely the reversible termination (RT) and the degenerative chain transfer (DT) mechanisms, are involved (Scheme 1), while other LRP methods rely on a single activation mechanism either RT or DT besides cobalt mediated method (*15*).
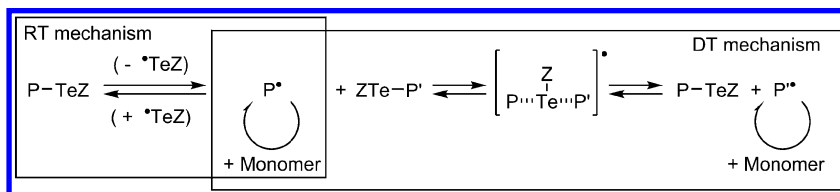
Scheme 1. Two activation mechanisms in TERP

The RT corresponds to homolytic cleavage of the C-Te bond of dormant species P-TeR (P denotes polymer here) generating P radical and the DT is homolytic substitution reaction between P radical and a dormant species. In our early reports (*5*), thermal cleavage of C-Te bond was used for the generation of initiating radicals, and, once the radical was formed, TERP mainly took place by the DT mechanism. While TERP required ~100 °C under this condition, as the thermal cleavage of C-Te bond is the rate determining step, we later found that TERP proceeded under much milder thermal conditions by the addition of azo-initiators (*15*). In such condition, initiating radicals are generated from azo-initiators, and TERP proceeds exclusively by the DT mechanism. This condition is synthetically highly important and has been used in the large scale synthesis in industry, but a drawback is the difficulty in complete control of the α-polymer-end structures and also slight loss in control due to the increase in termination reactions (*16*).

To overcome these difficulties, we have already developed a photo-induced TERP, in which initiating radicals are generated from the organotellurium dormant species by C-Te bond photolysis (*17*, *18*). Furthermore, we already reported several advantages of photochemical conditions, such as highly efficient radical generation by using low-intensity visible light, polymerization at low temperature, and control of the progress of polymerization (*19*). However, photophysical properties of organotellurium compounds, especially structural effects, and synthetic advantages of photochemical conditions have not been fully elucidated in detail. We report here the full details of photophysical properties of organotellurium chain transfer agents and dormant species to clarify structural effects and also detail synthetic applications of photo-induced TERP.

Experimental Section

General

All reaction conditions dealing with oxygen and moisture sensitive compounds were carried out in a dry Pyrex reaction vessel under nitrogen atmosphere. A 500 W high pressure mercury lamp with the combination of a

cutoff filter (Asahi Techno Glass), and 6 W white LED with combination of neutral density filter (Sigma Koki) were used as light sources. The distance between light source and reaction vessel was set to be 10 cm in the photoirradiation experiment. UV-vis absorption spectra were recorded at 25 °C. Fluorospectrometer was used as the source of monochromic light of 352 nm. A standard potassium ferrioxalate actinometer was used for the determination of quantum yield. ^{1}H NMR (400 MHz) and ^{13}C NMR (100 MHz) spectra were measured for a CDCl$_3$ or C$_6$D$_6$ solution of a sample and are reported in ppm (δ) from internal tetramethylsilane or a residual solvent peak. ^{13}C NMR spectra of polymer samples for quantitative analysis of back-biting reaction were measured using gated-decoupling mode with pulse interval of 10.5 sec (*20*). Gel permeation chromatography (GPC) was performed on a machine equipped with polystyrene (PSt) mixed gel columns (two linearly connected Shodex LF-604 or LF-804) at 40 °C using RI and UV detectors. CHCl$_3$ and DMF containing 0.01 mol L^{-1} LiBr were used as eluents. The columns were calibrated with PMMA standards. IR spectra were recorded by using ATR-FTIR instrument.

Materials

Butyl acrylate was washed with 5% aqueous NaOH solution and was distilled over CaH$_2$. 2-Isocyanatoethyl acrylate was heated at 45 °C with CaH$_2$ for 1.5 hours and then distilled under reduced pressure. Ethyl 2-phenyltellanylisobutyrate (**1a**) (*21*), ethyl 2-methyltellanylisobutyrate (**1b**) (*5*), ethyl 2-butyltellanylisobutyrate (**1c**) (*21*) were prepared as reported (Figure 1).
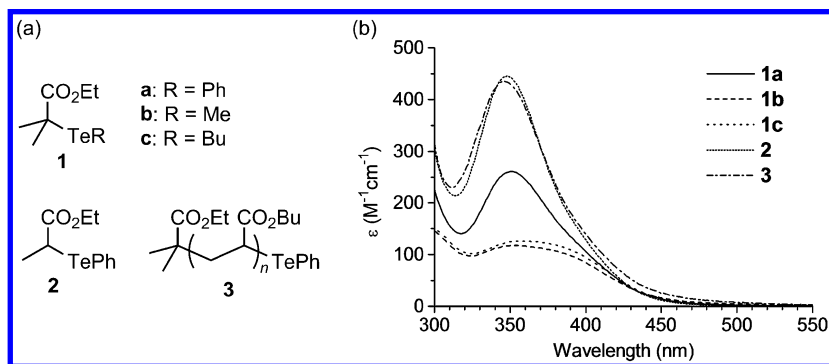
Figure 1. Structure and UV-vis absorption spectra of organotellurium chain transfer agents and living polymers in benzene.

Synthesis of Ethyl 2-phenyltellanylpropionate (2)

Phenyl lithium (50 mL, 1.0 M in cyclohexane and diethyl ether, 50 mmol) was added slowly to a suspension of tellurium powder (6.43 g, 50 mmol) in THF (50 mL) at 0 °C under nitrogen atmosphere, and the resulting solution was stirred at room temperature (rt) for 40 min. To this solution was added ethyl 2-bromopropionate (8.14 g, 45 mmol) at 0 °C, and the mixture was stirred at rt

for 30 min. Degassed water was added, and the aqueous phase was separated under a nitrogen atmosphere. The remaining organic phase was washed with degassed saturated aqueous NH_4Cl solution, dried over $MgSO_4$ and filtered under nitrogen atmosphere. The solvent was removed under reduced pressure followed by distillation (120-125 °C/3 mmHg) to give **2** (4.79 g) in 49% yield. ^{1}H NMR ($CDCl_3$) δ 1.16 (t, J = 7 Hz, 3H), 1.67 (d, J = 7.1 Hz, 3H), 3.93 (q H, J = 7.1 Hz, 1H), 4.06 (q, J = 7.1 Hz, 2H), 7.25 (t, J = 7.4 Hz, 2H), 7.36 (d, J = 7.4 Hz, 1H), 7.86 (d, J = 6.9 Hz, 2H) ppm. ^{13}C NMR ($CDCl_3$) δ 13.9, 17.8, 19.0, 60.7, 111.6, 128.8, 129.1, 140.8, 175.5 ppm.

Reaction of 1a and TEMPO

A solution of **1a** (9.8 μL, 0.04 mmol) and TEMPO (62.4 mg, 0.04 mmol) in 0.60 mL C_6D_6 in a sealed NMR tube under a nitrogen atmosphere was irradiated through a 470 nm short-wavelength cut-off filter at 50 °C for 10 min. The ^{1}H NMR spectra indicated 96% formation of TEMPO adduct **4**, 3% of ethyl methacrylate, and 99% of diphenylditelluride. **4** was isolated by silica-gel column chromatography (hexane). ^{1}H NMR ($CDCl_3$) δ 1.00 (s, 6H), 1.15 (s, 6H), 1.23-1.65 (m, 6H), 1.27-1.33 (t, J = 7.1 Hz, 3H), 1.47 (s, 6H), 4.14-4.25 ppm (q, J = 7.1 Hz, 2H). ^{13}C NMR ($CDCl_3$) 14.3, 17.2, 20.6, 24.6, 33.6, 40.7, 59.6, 60.8, 81.2, 70.5, 176.2 ppm.

Typical Procedure for Photopolymerization of Butyl Acrylate

A solution of butyl acrylate (1.1 mL, 7.8 mmol) and **1a** (17 μL, 0.078 mmol) was irradiated with an Hg lamp through a 470 nm short-wavelength cutoff filter at 50 °C under a nitrogen atmosphere for 2 h. A small portion of the reaction mixture was taken, and the conversion of the monomer (98%) was determined by using ^{1}H NMR spectroscopy. The remaining monomer was removed *in vacuo*. M_n (13,000) and PDI (1.09) were determined by using GPC ($CHCl_3$ eluent).

Typical Procedure for Photopolymerization of 2-Isocyanatoethyl Acrylate

A solution of 2-isocyanoethyl acrylate (1.25 mL, 10.0 mmol) and **1a** (22.6 μL, 0.1 mmol) was irradiated with 500 W Hg lamp equipped with a 470 nm short-wavelength cutoff filter at 50 °C under a nitrogen atmosphere for 1 h. The conversion of the monomer (97%) was determined by ^{1}H NMR spectroscopy, and M_n (20,000) and PDI (1.20) were determined by using GPC (DMF containing 0.01 mol L^{-1} LiBr).

Reaction of Poly(2-isocyanatoethyl)acrylate and Propylamine

Propylamine (196 μL, 1.2 eq to NCO group) was dissolved in 20 mL dried THF in a 100 mL three-neck flask equipped with a dropping funnel, nitrogen inlet

and a stopper. The dropping funnel was filled with 5 mL THF solution of poly(2-isocyanatoethyl)acrylate (282 mg, M_n = 14,000, PDI = 1.20). The reaction mixture was kept under nitrogen atmosphere and was cooled by ice bath. The solution of polymer was added dropwisely within 30 min, and then the reaction mixture was stirred at room temperature for 10 hours. Yellow viscous solid precipitated from the solution which was transferred to another fresh flask. Then the solvent was removed under reduced pressure to give the product. M_n (20,200) and PDI (1.20) were determined by using GPC (DMF containing containing 0.01 mol L^{-1} LiBr).

Poly(2-isocyanatoethyl)acrylate

^{1}H NMR (400MHz, DMSO-d_6) δ (ppm) 1.54, 1.92 (br, 1H, C*H*), 1.68, 2.37 (br, 2H, C*H$_2$*CH), 3.56 (br, 2H, C*H$_2$*NCO), 4.14 (br, 2H, CO$_2$C*H$_2$*). ^{13}C NMR (400MHz, DMSO-d_6) δ (ppm) 34.13 (CH$_2$*C*H), 40.71 (*C*H$_2$CH), 41.90 (CO$_2$CH$_2$*C*H$_2$), 63.59 (CO$_2$*C*H$_2$), 123.53 (N*C*O), 173.70 (*C*OO). IR (FT-IR) 2957.92, 2257.58, 2222.05, 1728.98, 1447.65, 1396.12, 1354.13, 1253.26, 1154.34, 1117.83, 1054.73, 831.20, 798.15 cm^{-1}.

Poly(2-(N′-propylureido)ethyl)acrylate

^{1}H NMR (400MHz, DMSO-d_6) δ (ppm) 0.82 (t, 3H, CH$_3$), 1.36 (m, 2H, CH$_2$C*H$_2$*CH$_3$), 1.36, 1.81 (br, 1H, CH$_2$C*H*), 2.22, 2.59 (br, 2H, C*H$_2$*CH), 2.95 (t, 2H, CONHC*H$_2$*), 3.21 (br, 2H, CO$_2$CH$_2$C*H$_2$*), 3.95 (br, 2H, CO$_2$C*H$_2$*), 6.00 (bs, 1H, CON*H*CH$_2$), 6.03 (bs, 1H, CO$_2$C$_2$H$_4$N*H*CO). ^{13}C NMR (400MHz, DMSO-d_6) δ (ppm) 11.32 (*C*H$_3$), 23.20 (CH$_2$*C*H$_3$), 34.27 (CH$_2$*C*H), 38.16 (CO$_2$CH$_2$*C*H$_2$), 40.81 (*C*H$_2$CH), 41.20 (NH*C*H$_2$CH$_2$), 63.77 (CO$_2$*C*H$_2$), 158.19 (NH*C*ONH), 173.85 (*C*OO). IR (FT-IR) 3323.05, 2962.08, 2871.66, 1730.61, 1630.62, 1557.90, 1446.40, 1382.23, 1240.13, 1156.35, 1059.01 cm^{-1}.

Results and Discussion

Photophysical Properties of Organotellurium Compounds

UV-vis absorption of several organotellurium chain transfer agents **1**-**2** and living poly(butyl acrylate) (PBA) **3** bearing phenyltellanyl group (M_n = 6200, M_w/M_n = 1.14) was summarized in Figure 1 and Table 1. All compounds examined in this study possessed UV-vis absorption at λ_{max} ~350 nm, and the skirts of absorption extended to around 500 nm. The absorption band was assigned as an n(Te)-σ*(C-Te) transition by the time-dependent density functional calculations suggesting the selective C-Te bond cleavage would take place by irradiation to this band (*17*).

Table 1. UV-vis absorption property of organotellurium compounds 1-3 in benzene

Compound	λ_{max} (nm)	ε (M^{-1} cm^{-1})
1a	351	260
1b	353	117
1c	357	126
2	348	445
3	346	435

The absorption coefficient ε were significantly affected by the local structure around the tellurium atom, while absorption maximum (λ_{max}) was rather insensitive to the structure. For example, the coefficient of **1a** (ε = 260 M^{-1} cm^{-1} at λ_{max} = 351 nm) having phenyltellanyl group at the 2-position of ethyl 2-methylpropionate was about two times larger than that of **1b** (ε = 117 M^{-1} cm^{-1} at λ_{max} = 353 nm) having methyltellanyl group, and the results are ascribed to the existence of conjugation between phenyl group and tellurium lone pair. Bulkiness of the α-substituent significantly affected the coefficient, and the chain transfer agent **2** having secondary C-Te bond at the 2-position of ethyl propionate exhibited about 1.7 times stronger absorption than **1a** having tertiary C-Te bond. As poly(butyl acrylate) (PBA) **3** having secondary C-Te bond had virtually identical absorption coefficient to **2** did, the results clearly confirmed the importance of the local structure of organotellurium compounds.

The efficiency of the generation of carbon-centred radicals from organotellurium compounds was determined by using **1a** as a model compound. When a 1:1 mixture of 1a and TEMPO in C$_6$D$_6$ solution was irradiated under the same conditions used in photo-TERP shown below (500 W Hg lamp through a >470 nm cutoff filter) at 50 °C, **1a** was completely consumed within 10 min. Product analysis revealed that carbon-part of **1a** were quantitatively converted to TEMPO adduct **4** (96%) and ethyl methacrylate (4%) and that tellurium part to diphenyl ditelluride (99%) (Scheme 2). **4** and ethyl methacrylate were formed by the reaction of radical **5** generated from **1a** and TEMPO by the coupling reaction (path *a*) and the β-hydrogen abstraction (path *b*), respectively (Scheme 2). The same experiment in the dark required the consumption of **1a** for 94 h even at 100 °C and gave **4** (54%), ethyl methacrylate (45%), and diphenyl ditelluride (91%). The different product ratio (**4**/ethyl methacrylate) between photochemical and thermal conditions is due to thermal instability of **4**, which regenerates radical **5** and TEMPO (*11*). Since the path *b* takes place irreversibly, **4** was slowly converted to ethyl methacrylate during prolonged heating. The results clearly demonstrated the high efficiency of the photochemical condition over the thermal condition in generating the radical species. This difference of radical generation has been recently applied to a switching from TERP to radical coupling reaction for the synthesis of structurally well-controlled symmetrical and/or mid-chain functional polymers (*22, 23*).
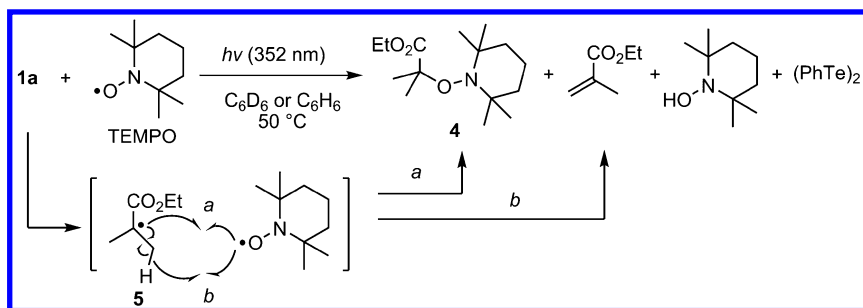
*Scheme 2. Photo reaction of **1a** in the presence of TEMPO.*

The quantum yield of the radical generation from **1a** was determined to be 0.84 by the trapping experiment in the presence of 2 equivalents of TEMPO in C_6H_6. A 352 nm monochromatic light was used to avoid the photochemical activation of diphenyl ditelluride formed as a side product (*24*). The value is considerably higher than those of common photoinitiators such as (2,4,6-trimethylbenzoyl) diphenylphosphine oxide (~0.7). This high quantum yield of **1a** is responsible for the efficient initiation of TERP even under low intensity light.

Conditions and Synthetic Scopes of Photo-TERP

The structural effects of organotellurium CTAs in photo TERP were investigated. The polymerization of butyl acrylate (100 equiv) in the presence of **1a** (1 equiv) was carried out under photoirradiation by 500 W Hg lamp with >470 nm cutoff filter. As the efficiency of photo activation of organotellurium compounds is so high that reduction of light intensity was required when a light source with strong intensity was used (*17*). The monomer conversion reached 98% after 2 h irradiation at 50 ºC, and structurally well-controlled PBA with M_n = 12,500 and PDI = 1.09 was obtained (Table 2, run 1). A weak intensity light, such as 6 W light emitting diode (LED), was sufficiently effective to promote the polymerization (run 2). Polymerization did not proceed in the dark, and the progress or cessation of polymerization could be controlled by turning on or off the light as already reported (*17*, *18*).

Since the radical generation does not require thermal energy, the polymerization could be carried out at low temperature, such as 25 ºC, 0 ºC, and even -30 ºC (runs 3-5). While the longer reaction period was required as the propagation rate decreases as temperature decreases, well-controlled PBAs with narrow molecular weight distributions were obtained in all cases. Since relative reaction rate k_{ex}/k_p (k_{ex} and k_p are rate constant for DT reaction and propagation reaction, respectively) (*25*), which affects the level of PDI control, is rather insensitive to temperature, we believe that the major mechanism at low temperature is the DT reaction.

Table 2. Photo TERP of butyl acrylate (BA) by using various organotelurium CTAs[a]

Run	CTA	Equiv of BA	Temp (°C)	Time (h)	Conv. (%)[b]	M_n (theo)[c]	M_n (exp)[d]	PDI[d]
1	**1a**	100	50-55	2	98	12,500	13,000	1.09
2[e]	**1a**	100	50	2	94	12,000	12,300	1.13
3	**1a**	100	25	2	88	11,300	11,999	1.15
4	**1a**	100	0	4	86	11,000	10,500	1.16
5	**1a**	100	-30	17	81	10,400	11,300	1.13
6[f]	**1a**	500	100	48	90	57,600	50,000	1.31
7	**1a**	500	0	18	86	55,000	54,000	1.16
8	**1a**	1,000	50-55	3	90	119,000	120,800	1.13
9	**1a**	2,000	50-55	5	90	230,400	223,000	1.18
10[g,h]	**1a**	4,000	50	6	65	286,700	302,000	1.26
11[g,h]	**1a**	10,000	50	20	58	742,000	591,000	1.31
12[g,h]	**1a**	20,000	50	20	35	896,000	751,800	1.32
13	**1b**	100	50	2	97	12,400	12,200	1.08
14	**1c**	100	50	2	94	12,200	13,000	1.09
15	**2**	100	50	2	96	12,300	12,900	1.14
16[i]	**2**	100	60	4	81	10,400	9,200	1.24

[a] A solution of organotellurium CTA and butyl acrylate in a Pyrex tube was photoirradiated with a 500 W Hg lamp with >470 nm cutoff filter.   [b] Determined by ^{1}H NMR.   [c] Calculated based on the monomer/CTA ratio and the monomer conversion.   [d] Determined by GPC calibrated with PMMA standards.   [e] 6 W household white LED with 50% neutral density filter was used as a light source.   [f] Polymerization was carried out in the dark.   [g] 0.05 equiv of (PhTe)$_2$ was added.   [h] >580 nm cutoff filter was used.   [i] Polymerization was carried out in the presence of 0.1 equiv of AIBN in the dark.

Low temperature polymerization condition is particularly suitable for the controlled polymerization of acrylates, because back-biting reaction giving branched polymer chains occurs at high temperature (*26*, *27*). Indeed, 2.1% of branching was observed by ^{13}C NMR when the polymerization of BA (500 equiv) was carried out at 100 ºC in the dark, but branching could not be observed (<0.1%) in the polymerization at 0 ºC (run 6 *vs*. 7, Figure 2). Furthermore, the low temperature polymerization also enhanced the PDI control, and PDI of PBA prepared at 0 ºC had lower value than that prepared at 100 ºC (PDI = 1.13 vs. 1.31, Figure 3).
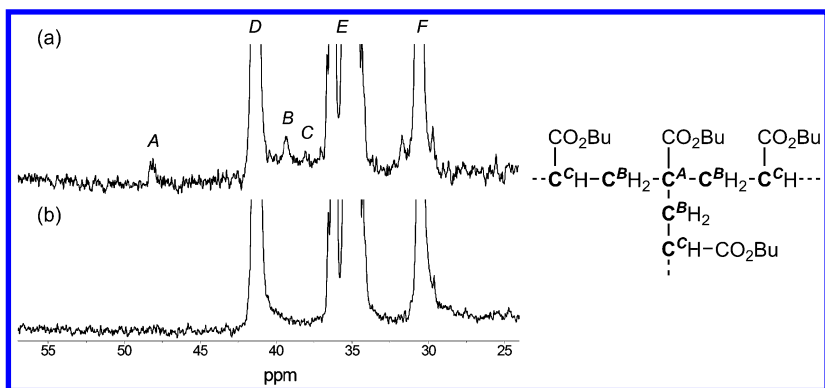
*Figure 2. ¹³C NMR spectra of PBA samples prepared under thermal conditions at 100 °C (a) (Table 1, run 6) or photoirradiation conditions at 0 °C (b) (Table 1, run 7) in the presence of **1**. Signal assignments: A, branch quaternary C; B, CH₂ adjacent to branch; C, CH adjacent to branch; D, main chain CH; E, main chain CH₂; F, CH₂ of OBu (20). Signal intensities are normalized to the maximum peak in this region.*
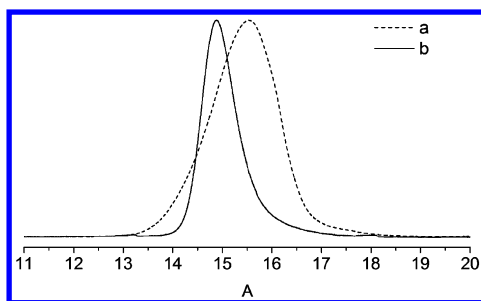
*Figure 3. GPC traces of PBA samples prepared under thermal conditions at 100 °C (a) (Table 1, run 6) and photoirradiation conditions at 0 °C (b) (Table 1, run 7) in the presence of **1a**.*

High molecular weight polymers with narrow polydispersities were also prepared by increasing the monomer/CTA ratio. When the targeted molecular weight was high (M_n > 300,000), monomer conversion became low due to the high viscosity of the reaction media and the use of monomer as a solvent. Under such conditions, PBAs with M_n ranging from 120,000 to 752,000 with low PDIs (<1.32) were prepared under photo irradiation (runs 8-12). While many attempts have been reported for the synthesis of high molecular weight polymers under LRP conditions, successful examples are still limited (*28–33*). Therefore, the current conditions would provide an efficient method to synthesize high molecular weight polymers with narrow molecular weight distributions.

The structural effect of organotellurium CTAs on polymerization control was next examined by using **1b**, **1c**, and **2**. Polymerization of BA by employing methyltellanyl and butyl tellanyl-substituted polymethacrylate mimetic CTAs **1b** and **1c** virtually gave the same results as that using **1a** (runs 13 and 14). Polyacrylate mimetic CTA **2** also afforded structurally well-controlled PBA with narrow PDI under photoirradiation (run 15), while the control slightly dropped in the same polymerization under thermal condition by employing AIBN as a thermal initiator (Run 16). CTAs having polyacrylate end mimetic structure usually show low controllability than those having polymethacrylate due to the low ability in generating the initiating radical species from the CTA under thermal conditions. The almost identical results observed by using **1** and **2** under the photochemical condition suggest that structural variation of CTAs under photochemical condition is much higher than that of thermal condition is.

The advantage of photopolymerization enabling polymerization under low temperature was further explored with a monomer having thermally labile group, i.e., 2-isocyanatoethyl acrylate (ICEA) (Scheme 3). When polymerization of ICEA was carried out at 100 °C in the presence of **1a**, the corresponding polymer **6** with broad PDI of 2.45 was obtained after 6 h (Table 3, run 1 and Figure 4a). Formation of high molecular weight polymers as suggested by GPC trace indicated the occurrence of cross linking reactions involving isocyanate group. The PDI control significantly improved in the polymerization at 60 °C in the presence of AIBN (0.1 equiv), and polymer **6** with narrow molecular weight distribution (PDI = 1.51) was obtained (Table 3, run 2 and Figure 4b). The control was further enhanced under the photoirradiation condition at 50 °C, and highly controlled polymer **6** with narrow dispersity (PDI = 1.20) was obtained (Figure 4c).

The high compatibility of isocyanate group under low temperature conditions enabled the direct synthesis of urea-substituted polyacrylate. The reaction of polymer **6** (M_n = 20,000, PDI = 1.20) with propylamine resulted in propylurea-substituted polyacylate **7** (M_n = 20,200, PDI = 1.20) in quantitative yield by NMR spectrum (Figures 5 and 6). While the molecular weights of **6** and **7** estimated by GPC analyses were the same, this is probably due to the difference of polar interaction between polymer and the stationary phase of the column. In ¹H NMR spectrum (Figure 6a), the signal of CH_2 group adjacent to isocyanate group shifted from 3.56 ppm to 3.21 ppm and two characteristic singlet peaks of NH group were observed at 6.03 ppm and 6.00 ppm after the reaction with propylamine. In ¹³C NMR spectrum (Figure 6b), the peak at 158.19 ppm was assigned to urea carbonyl in polymer **7** and the peak of isocyanate carbon at 123.53 ppm could not be observed. In IR spectrum (Figure 7), the characteristic peak of isocyanate group at 2258 cm⁻¹ completely disappeared and new signals of C=O and N-H group appeared after the reaction. Since the varieties of amines including polymer-end amines are available, the various side-chain modified acrylates including bottle-brush polyacrylates with controlled macromolecular structure would be prepared by low temperature photo-TERP of ICEA and subsequent reaction of isocyanide group and amines.
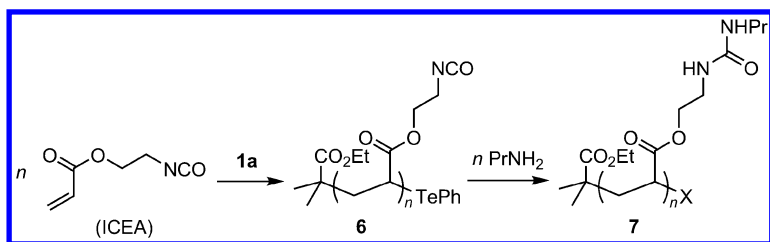
Scheme 3. Polymerization of 2-isocyanatoethyl acrylate (ICEA), and post-polymerization functionalization of polyICEA.

Table 3. Photoinduced polymerization of 2-isocyanatoethyl acrylate in the presence of 1a [a]

Run	Filter (nm)	Temp. (°C)	Time (h)	Conv. (%)[b]	M_n (theo)[c]	M_n (exp)[d]	PDI[d]
1	-[e]	100	6	99	14,100	28,200	2.45
2	-[f]	60	1	90	13,000	18,700	1.51
3	>470	50	1	97	14,000	20,000	1.20

[a] A solution of **1a** and 2-isocyanatoethyl acrylate in a Pyrex tube was conducted the reactions. [b] Determined by ^{1}H NMR. [c] Calculated based on the monomer/CTA ratio and the monomer conversion. [d] Determined by GPC calibrated with PMMA standards. [e] The reaction was carried out by heating in the dark. [f] The reaction was carried out with AIBN (0.1 equiv.) in the dark.
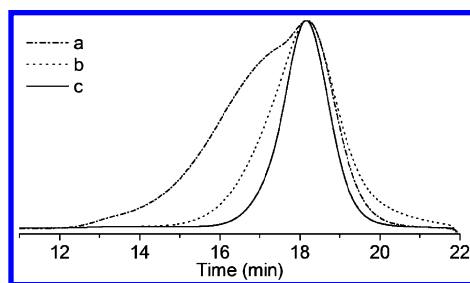
*Figure 4. GPC traces of polyICEA samples prepared by heating at 100 °C (a), with 0.1 equiv. of AIBN at 60 °C (b), or by photoirradiation at 50 °C (c) in the presence of **1a**.*
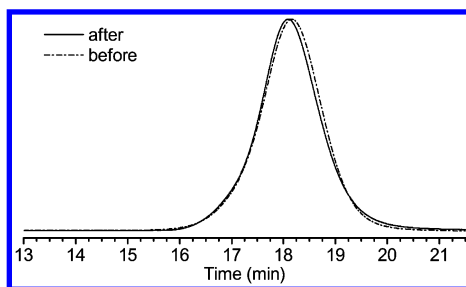
*Figure 5. GPC traces of polymers **6** and **7** before and after the reaction of polyICEA (**6**) with propylamine.*
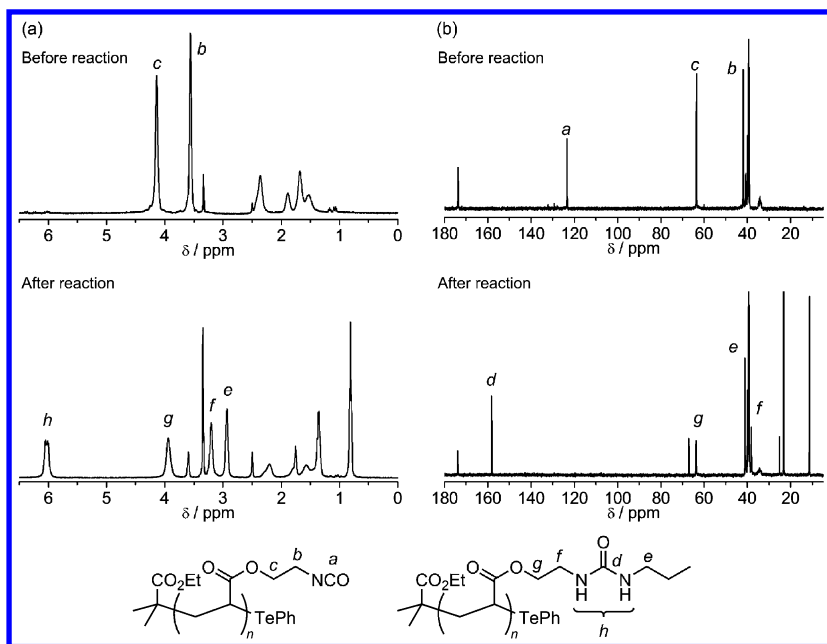
*Figure 6. ^1H NMR (a) and ^{13}C NMR (b) of **6** and **7** before and after the reaction of polyICEA (**6**) with propylamine in DMSO-d_6.*
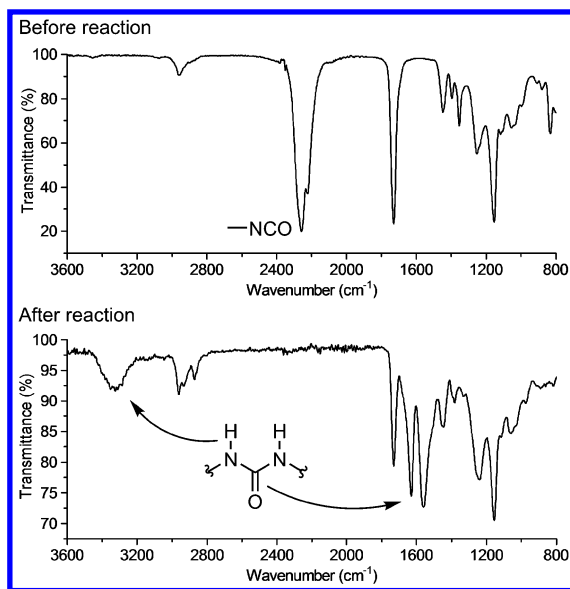
*Figure 7. IR spectra of polymers **6** and **7** before and after the reaction of polyICEA (**6**) with propylamine.*

Conclusion

Photophysical properties of organotellurium compounds and synthetic scopes of photo-TERP have been investigated. All tellurium compounds studied in this work possess broad absorption at λ_{max} ~350 nm corresponding to n(Te)-σ^*(C-Te) transition. Irradiation to this absorption induces C-Te bond homolysis generating the corresponding radical species which initiates a polymerization reaction when monomer is present. Due to high quantum yield of C-Te bond homolysis, a weak-intensity light source was sufficient to initiate the polymerization. Advantages of photo-TERP were illustrated by the low temperature polymerization which avoided undesirable back-biting reaction in acrylate polymerization and enabled the polymerization of monomers possessing thermally labile functional groups. These results clearly reveal the advantage of photochemical conditions for the controlled synthesis of highly functionalized and structurally-controlled living polymers.

Acknowledgments

References

1. *Chain Polymerization of Vinyl Monomers*; Matyjaszewski, K., Möller, M., Eds.; Elsevier BV: Amsterdam, 2012; Vol. 3.
2. *Encyclopedia of Radicals in Chemistry, Biology and Materials*; Chatgilialoglu, C., Studer, A., Eds.; Wiley: Chichester, 2012.
3. Yamago, S. *Chem. Rev.* **2009**, *109*, 5051–5068.
4. Yamago, S.; Iida, K.; Yoshida, J. *J. Am. Chem. Soc.* **2002**, *124*, 2874–2875.
5. Yamago, S.; Iida, K.; Yoshida, J. *J. Am. Chem. Soc.* **2002**, *124*, 13666–13667.
6. Ray, B.; Kotani, M.; Yamago, S. *Macromolecules* **2006**, *39*, 5259–5265.
7. Mishima, E.; Tamura, T.; Yamago, S. *Macromolecules* **2012**, *45*, 2989–2994.
8. Mishima, E.; Tamura, T.; Yamago, S. *Macromolecules* **2012**, *45*, 8998–9003.
9. Mishima, E.; Yamago, S. *Macromol. Rapid Commun.* **2011**, *32*, 893–898.
10. Yamada, T.; Mishima, E.; Ueki, K.; Yamago, S. *Chem. Lett.* **2008**, 650–651.
11. Yamago, S.; Kayahara, E.; Yamada, H. *React. Funct. Polym.* **2009**, *69*, 416–423.
12. Kayahara, E.; Yamada, H.; Yamago, S. *Chem. Eur. J.* **2011**, *17*, 5271–5279.
13. Nakamura, Y.; Nakanishi, K.; Yamago, S.; Tsujii, Y.; Takahashi, K.; Morinaga, T.; Sato, T. *Macromol. Rapid Commun.* **2014**, *35*, 642–648.
14. TERPLUS or Advanced Polymer Synthesized by LRP. Available at: https://www.otsukac.co.jp/en/products/chemical/cat_lr-polymer/.
15. Goto, A.; Kwak, Y.; Fukuda, T.; Yamago, S.; Iida, K.; Nakajima, M.; Yoshida, J. *J. Am. Chem. Soc.* **2003**, *125*, 8720–8721.
16. Nakamura, Y.; Kitada, Y.; Kobayashi, Y.; Ray, B.; Yamago, S. *Macromolecules* **2011**, *44*, 8388–8397.
17. Yamago, S.; Ukai, Y.; Matsumoto, A.; Nakamura, Y. *J. Am. Chem. Soc.* **2009**, *131*, 2100–2101.
18. Yamago, S.; Nakamura, Y. *Polymer* **2013**, *54*, 981–994.
19. Nakamura, Y.; Yamago, S. *Beilstein J. Org. Chem.* **2013**, *9*, 1607–1612.
20. Ahmad, N. M.; Heatley, F.; Lovell, P. A. *Macromolecules* **1998**, *31*, 2822–2827.
21. Kayahara, E.; Yamago, S.; Kwak, Y.; Goto, A.; Fukuda, T. *Macromolecules* **2008**, *41*, 527–529.
22. Nakamura, Y.; Arima, T.; Tomita, S.; Yamago, S. *J. Am. Chem. Soc.* **2012**, *134*, 5536–5539.
23. Nakamura, Y.; Arima, T.; Yamago, S. *Macromolecules* **2014**, *47*, 582–588.
24. Kwak, Y.; Tezuka, M.; Goto, A.; Fukuda, T.; Yamago, S. *Macromolecules* **2007**, *40*, 1881–1885.

25. Kwak, Y.; Goto, A.; Fukuda, T.; Kobayashi, Y.; Yamago, S. *Macromolecules* **2006**, *39*, 4671–4679.
26. Asua, J. M.; Beuermann, S.; Buback, M.; Castignolles, P.; Charluex, B.; Gilbert, R. G.; Hutchinson, R. A.; Leiza, J. R.; Nikitin, A. N.; Vairon, J. P.; val Herk, A. M. *Macromol. Chem. Phys.* **2004**, *205*, 2151–2160.
27. Willemse, R. X. E.; Van Herk, A. M.; Panchenko, E.; Junkers, T.; Buback, M. *Macromolecules* **2005**, *38*, 5098–5103.
28. Jakubowski, W.; Matyjaszewski, K. *Angew. Chem., Int. Ed.* **2006**, *45*, 4482–4486.
29. Kwiatkowski, P.; Jurczak, J.; Pietrasik, J.; Jakubowski, W.; Mueller, L.; Matyjaszewski, K. *Macromolecules* **2008**, *41*, 1067–1069.
30. Arita, T.; Kayama, Y.; Ohno, K.; Tsujii, Y.; Fukuda, T. *Polymer* **2008**, *49*, 2426–2429.
31. Mao, B. W.; Gan, L. H.; Gan, Y. Y. *Polymer* **2006**, *47*, 3017–3020.
32. Percec, V.; Guliashvili, T.; Ladislaw, J. S.; Wistrand, A.; Stjemdahl, A.; Sienkowska, M. J.; Monteiro, M. J.; Sahoo, S. *J. Am. Chem. Soc.* **2006**, *128*, 14156–14165.
33. Simms, R. W.; Cunningham, M. F. *Macromolecules* **2007**, *40*, 860–866.

The Interplay of ATRP, OMRP and CCT in Iron-Mediated Controlled Radical Polymerization

Benjamin R. M. Lake and Michael P. Shaver*

School of Chemistry, University of Edinburgh, Joseph Black Building, David Brewster Road, Edinburgh, Scotland EH9 3FJ
*E-mail: michael.shaver@ed.ac.uk; Phone: +441316504726

Metal-mediated controlled radical polymerization (CRP) is an indispensable tool for the construction of both simple and complicated macromolecules, decorated with an array of functional groups. Whilst this chemistry is dominated by copper, the use of iron complexes as mediators of CRP is becoming increasingly common; not least due to the very low cost of iron and the reduced intensity of its visible absorption spectrum. As a result, significant research effort has been concentrated on the study of iron complexes as catalysts for CRP, which has led to the observation that iron-mediated CRP reactions can be quite complex. They are proposed to be involved in a range of different equilibria, including atom transfer radical polymerization (ATRP), organometallic-mediated radical polymerization (OMRP) and catalytic chain transfer (CCT). An introduction to these equilibria, as well as a discussion of their interplay, particularly with reference to iron-mediated CRP reactions, is provided herein.

Introduction

ATRP, OMRP and CCT

The use of atom transfer radical polymerization (ATRP), a type of reversible deactivation radical polymerization (RDRP), for the synthesis of polymeric

materials with precisely controlled architectures and narrow dispersities has increased rapidly since the seminal reports of Matyjaszewski and co-workers (*1*, *2*) and Sawamoto and co-workers (*3*, *4*). Indeed, ATRP itself is a logical extension of the atom transfer radical addition (ATRA) reaction (*5–8*), which had been known for many years as an efficient carbon-carbon bond forming reaction (*9–12*).

An ATRP reaction depends upon the catalytic metal centre having at least two accessible oxidation states, with a difference of one between the oxidized and reduced states. An equilibrium between the reduced metal complex ([Mt]^x)/ dormant halogen-terminated polymer chain (R$_n$-Hal) and oxidized metal complex (Hal/[Mt]$^{x+1}$)/active radical chain (R$_n$•) can thus be established (Scheme 1), with the position of this equilibrium determining the concentration of active radical chains in solution, and thus the rate of polymerization and degree of control.
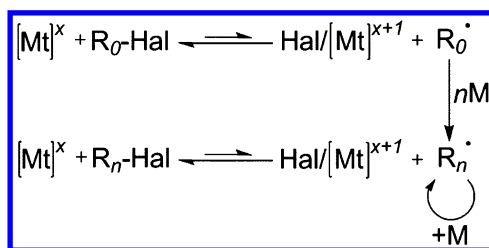
Scheme 1. The mechanism of atom transfer radical polymerization (ATRP)([Mt] = Mt(L)$_n$, Hal = halogen, M = monomer)

The initial radical (R$_0$•) can be generated, and therefore the reaction initiated, in one of two ways. Firstly, as shown in Scheme 1, addition of the reduced metal complex to a suitable alkyl (pseudo)halide can produce the starting radical, a process known as a 'normal' ATRP initiation. Alternatively, a conventional radical initiator (*e.g.* AIBN) can be used to generate the primary radical (R$_0$•) in the presence of an oxidized metal complex ('reverse' ATRP initiation).

However, metal complexes are able to affect the progress of a radical polymerization reaction in other ways, not just by reversibly transferring a halogen to the propagating radical. Indeed, organic radicals are known to interact with transition metal complexes *via* a number of chemically distinct pathways (*13*). Of particular importance to metal-mediated CRP reactions is the ability of the transition metals themselves to act as reversible spin traps, forming labile metal-carbon bonds. The formation and homolytic cleavage of these (typically quite weak) bonds allows the concentration of propagating radicals to be controlled (Scheme 2), which can lead to a more controlled polymerization reaction (*14*). This reversible addition-cleavage type reaction is known as an organometallic-mediated radical polymerization (OMRP) (*15*). Surprisingly, an example of what would later become known as OMRP, was published even earlier than the first observation of ATRP processes. In 1994, Wayland, Fryd and co-workers described the polymerization of methyl acrylate using an organo-Co^{III} porphyrin complex (*16*).
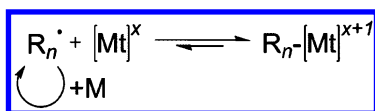
Scheme 2. The OMRP equilibrium

A third process which may occur during a metal-mediated CRP reaction is a catalytic chain transfer (CCT) (*17*). Analogously to (R-)ATRP and OMRP, CCT is an example of a one electron process. The chain transfer is effected through the abstraction of a β-H atom from the radical terminal of a propagating polymer chain, leading to the formation of an alkene-terminated polymer and a transition metal-hydride complex (Scheme 3a). The transfer of a H atom could also occur from an organometallic complex *via* a β-hydride elimination (*18*), providing there are β-H atoms and a vacant site *cis* to the coordinated alkyl group (also shown in Scheme 3a). The metal-hydride complex, once formed, can then transfer the H atom to another monomer, thus initiating the growth of a new polymer chain (Scheme 3b).
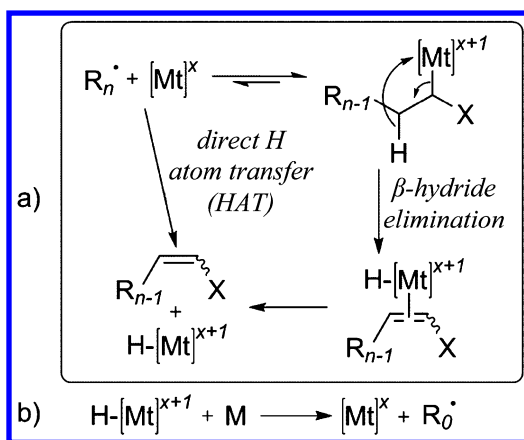
Scheme 3. Catalytic chain transfer (CCT): a) mechanism of formation of alkene-terminated polymer and metal hydride, b) hydrogen transfer to monomer (initiating the growth of a new chain)

The Interplay of ATRP, OMRP and CCT

The interplay between these mechanisms was not apparent until reports on a number of half-sandwich Mo-based systems (**1-4**, Figure 1) (*19–21*), which were shown to be able to control the polymerization of styrene *via* simultaneous ATRP and OMRP mechanisms when the reaction was performed under ATRP conditions. This is able to occur because the reaction equilibrium of an ATRP lies quite significantly to the left (Scheme 1), meaning that a high concentration of the reduced metal complex is typically present in solution. Thus, the spin-trapping of propagating polymer chains *via* reversible metal-carbon bond formation is able to occur efficiently, which can allow an OMRP equilibrium to impart a significant

degree of control over a polymerization process performed under ATRP (or R-ATRP) conditions, by lowering the concentration of radicals in solution and thus reducing the number of bimolecular termination processes.
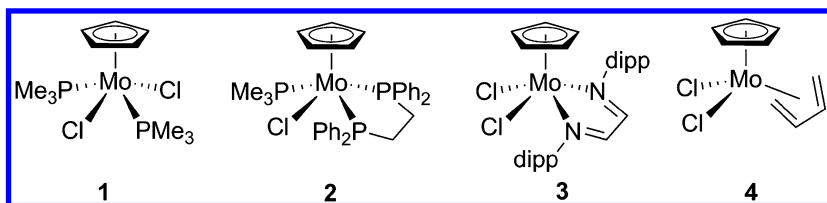
Figure 1. Mo-complexes displaying mechanistic interplay (19–21)

It was found that **1**, **2** and **4** (Figure 1) promote efficient polymerization under OMRP conditions but under ATRP conditions, **4** produces short oligomers with molecular weights independent of conversion. This, and complementary evidence (*e.g.* unsaturated end-groups), strongly suggests the intervention of a CCT mechanism in this system. The difference in reactivity of the phosphine-containing complexes (**1** and **2**) and η^4-butadiene-containing complex (**4**) could be attributed to the somewhat different steric demands of the respective ligands; the phosphines being significantly more sterically demanding than the butadiene. Thus, under ATRP conditions, where there is a high concentration of the reduced metal complex, the propagating radical can approach the metal centre more closely when the metal's coordination sphere contains less bulky ligands. This then facilitates a rapid β-H transfer (which is the rate determining step in CCT) to form an oxidized metal-hydride complex and an oligomeric alkene-terminated polymer.

Since these reports describing the interplay of ATRP, OMRP and CCT in a Mo-based system, others have shown that this interplay may also be operative in Ti- (*22*) and Os-catalyzed (*23*) systems as well. However, iron-mediated CRP reactions are the most studied systems which display mechanistic interplay, and indeed, form the basis of discussion herein.

Results and Discussion

α-Diimine-Supported Iron Complexes

As described above, the use of iron as a mediator of CRP has become an increasingly active area of research (*18*) since the first reports of the use of iron in ATRP, again by the groups of Matyjaszewski and Sawamoto (*24–29*). In 2002, Gibson and co-workers reported the application of an Fe^{II} catalyst bearing an α-diimine ligand for the ATRP of styrene (*30*). It was observed that the complexes derived from α-diimines containing alkyl *N*-substituents (complexes **1a** and **2a**, Figure 2) gave rise to well-controlled ATRP reactions; with relatively

low dispersities (1.27-1.65) that decrease with increasing monomer conversion and molecular weights which agree with calculated values.

(Complexes **1b-9b**, X = Cl)

R^1	R^2	Fe^{II}	Mechanism	k_{obs} (h^{-1})	Fe^{III}
^{t}Bu	H	1a	ATRP	0.27[30]	1b
Cy	H	2a	ATRP	0.25[30]	2b
Cyd	H	3a	ATRP	-	3b
Mes	H	4a	CCT	-	4b
Dipp	H	5a	CCT	-	5b
Cy	4-F-Ph	6a	CCT	0.01-0.03[32]	6b
Cy	4-NMe$_2$-Ph	7a	ATRP	0.72[32]	7b
Cy	4-OMe-Ph	8a	CCT	0.10[32]	8b
Cy	4-Me-Ph	9a	CCT	0.04-0.06[32]	9b

Figure 2. Complexes discussed in this section (Cy = cyclohexyl, Cyd = cyclododecyl, Mes = mesityl, Dipp = diisopropylphenyl)

Furthermore, ^{1}H NMR spectroscopic analysis and halide microanalysis of the resulting polymers illustrated the presence of halogen end-groups, which is strongly suggestive of a well-controlled ATRP-dominated controlled radical polymerization reaction. However, when Fe^{II} complexes derived from aryl-substituted α-diimines (complexes **4a** and **5a**, Figure 2) were applied in the ATRP of styrene, it was observed that M_n was not commensurate with calculated values, and nor did it increase linearly with time. This, along with the semi-linear increase in monomer conversion and the presence of alkene end-groups was postulated as the intervention of a CCT mechanism in a system otherwise set-up for ATRP. Related diamine and diphosphine complexes were also investigated, in a separate study (*31*), for the CRP of styrene and MMA under ATRP conditions. The diamine complex was found to be a reasonably effective ATRP catalyst, albeit giving rise to somewhat slower reaction rates. This was attributed to the relative instability of the Fe^{II}-diamine complex with respect to decomposition to ATRP-inactive species *versus* analogous Fe^{II}-α-diimine complexes. The diphosphine complexes on the other hand were found to be very ineffective ATRP catalysts, possibly due to poor redox reversibility.

In a subsequent paper, the apparent disparity in the catalytic mechanism between alkyl- and aryl-substituted Fe^{II}-α-diimines was examined (*33*). Using methyl methacrylate as the monomer, PMMA bearing all of the characteristics of a well-controlled ATRP reaction was produced using cyclohexyl- and cyclododecyl-substituted Fe^{II}-α-diimines (complexes **2a** and **3a**). Conversely, the characteristics of the PMMA produced by the mesityl- and dipp-containing complexes (complexes **4a** and **5a**) were strongly indicative of mechanistic competition between ATRP and CCT processes. In this case, the difference in reaction mechanism was thought to be a result of the differences in the steric crowding around the respective metal centers, which can be visualized in the crystal structures of the complexes bearing cyclohexyl (*30*) (**2a**) and dipp (**5a**) substituents (*33*). An investigation by Milione and co-workers on the reactivity of a structurally similar ((μ-Cl)$_2$-bridged dimeric) complex to Gibson's cyclohexyl-substituted monomeric Fe^{II}-α-diimine (**2a**) suggested that dimeric complexes were less able to exert control over an ATRP reaction (*34*). Indeed, it was found that the CRP reaction catalyzed by the dimeric complex gave higher values for dispersity than the monomeric complex, and significantly retarded reaction rates (lower values of k_{obs}).

Later work by the Gibson group suggested that the observed polymerization mechanism for the various Fe^{II}-α-diimine complexes can be considered a result of their relative 'halogenophilicities' and 'carbophilicities' (*35*), where the words 'halogenophilic' and 'carbophilic' refer to the relative preference of a given complex to form either a halogen-metal bond or a carbon-metal bond. In order to investigate the origin of the relative halogeno- and carbophilicities of the Fe-α-diimine complexes, and thus their dominant polymerization mechanisms, the synthesis of [Fe(α-diimine)Cl$_3$]-type complexes was performed, since these represent species present in an ATRP equilibrium. It was found that the complexes bearing alkyl *N*-substituents (complexes **1b** and **2b**, Figure 2) displayed solution magnetic moments commensurate with the spin-only value for a 3d^5 high-spin Fe^{III} center (S = 5/2), whereas the complex bearing aryl *N*-substituents (**5b**) possessed a magnetic moment corresponding well with a 3d^5 intermediate-spin Fe^{III} center (S = 3/2). It thus appeared that the preferred polymerization mechanism (ATRP or CCT) and thus relative halogenophilicity or carbophilicity correlated with the spin state of the metal center in the oxidized complex, with high-spin complexes being halogenophilic and giving rise to ATRP-dominated reactions and intermediate-spin complexes being carbophilic and giving rise to CCT-dominated reactions.

This was further illustrated by attempts at forming Fe^{III}-alkyl complexes by reaction of complexes **1b**, **2b** and **5b** with a benzyl-Grignard reagent. Reaction of **1b** or **2b** with the benzyl-Grignard reagent at -78°C led to the formation of bibenzyl as the major organic product, and a [Fe(α-diimine)Cl$_2$]-type complex (**1a** or **2a**). The formation of bibenzyl and a reduced metal complex strongly indicated that the Fe^{III}-benzyl bond was very weak, which allowed the formation of benzyl radicals and their subsequent homocoupling in solution to form bibenzyl. Conversely, toluene was identified as the major organic product following the reaction of complex **5b** with the benzyl-Grignard reagent at -78°C. The toluene is presumably formed following hydrolysis of the putative Fe^{III}-alkyl

complex during work-up. Bibenzyl only becomes the major organic product of the reactions between aryl-substituted complex **5b** and benzyl-Grignard reagents above -30°C (Scheme 4). These reactions suggest only that an OMRP pathway was accessible, not that it is the dominant control mechanism. Furthermore, no Fe^{III}-alkyl complexes could be isolated at room or polymerization temperatures.
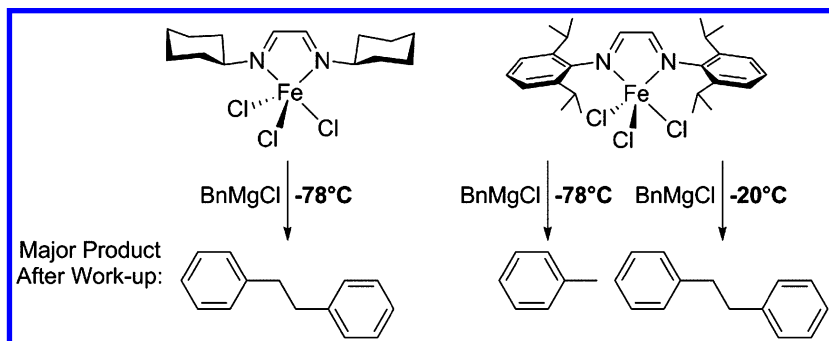
*Scheme 4. Reaction of [Fe(α-diimine)Cl₃] complexes (**2b** and **5b**) with a benzyl-Grignard reagent (35)*

However, this study provided evidence that the Fe^{III}-alkyl bond is somewhat stronger in aryl-substituted complexes than alkyl-substituted complexes, implying that they are better traps of alkyl radicals and thus significantly more carbophilic. This characteristic may allow them to participate in a CCT mechanism during a polymerization reaction performed under ATRP conditions. This synthetic study did not, however, investigate the relative stability of Fe^{III}-hydride complexes nor the rates of possible HAT.

In a desire to both better understand and control this mechanistic interplay, substitution of the hydrogen atoms at the 2- and 3-positions of the α-diimine with *para*-fluorophenyl groups (complex **6a**, Figure 2) was pursued and had a marked effect on polymerization activity. While the Fe^{II} complexes with hydrogen atoms at the 2- and 3-positions of the α-diimine displayed well-controlled ATRP reactivity (*30*), the complexes containing *para*-fluorophenyl groups at the 2- and 3-positions demonstrated sluggish polymerization rates, and produced low molecular weight, olefin-terminated polymers; both of which are characteristic of the intervention of a CCT mechanism. Separate synthesis of the *para*-fluorophenyl-substituted Fe^{III} complexes suggested that these complexes were intermediate-spin (unlike their H-substituted counterparts), which was able to account for their poor CRP performance.

In a key subsequent report (*32*), a range of 2,3-aryl-substituted α-diimines were synthesized, coordinated to Fe^{II} and their activity in an ATRP polymerization examined. It was observed that a strong correlation existed between the electron-donating/withdrawing ability of the 2,3-aryl substituents and the rate of polymerization (k_{obs}, Figure 2) and molecular weights of polymer obtained (Figure 3).
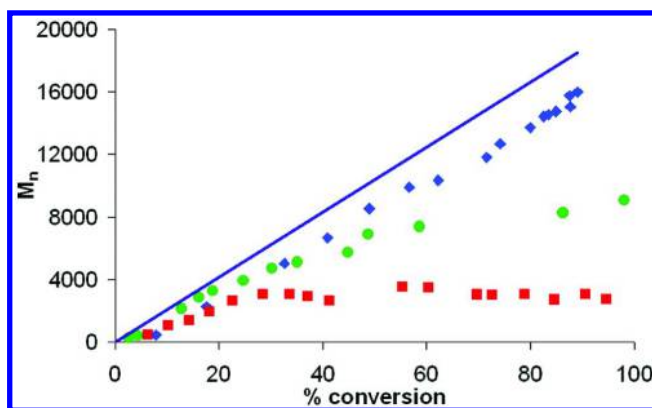
*Figure 3. Molecular weight (M_n) versus % conversion for the polymerization of styrene (conditions: 200 equiv. styrene, 1-PECl initiator, 120°C) by Fe^{II}-α-diimines (complex **9a** ■, **8a** ● and **7a** ◆. Purple line represents $M_{n,(theo.)}$ for comparison). Reproduced from reference (32). Copyright (2007) American Chemical Society.*

Examination of Figure 3 reveals that less electron-rich aromatic substituents (e.g. *para*-methylphenyl, **9a**) significantly retard the rate of polymerization and stunt the polymer growth, while more electron-rich aromatic substituents were found to increase both the rate of polymerization and average molecular weight. Furthermore, it is also clear that by careful selection of the specific Fe^{II}-α-diimine catalyst used, it is possible to control the average molecular weight of the polymer obtained, which is a somewhat unusual property. This permits targeting of alkene-terminated polystyrene polymers with specific average molecular weights.

The majority of the 2,3-aryl-substituted systems studied displayed polymers commensurate with the intervention of a CCT mechanism. However, 2,3-substitution of the α-diimine with strongly electron-donating *para*-dimethylaminophenyl groups (complex **7b**) led to a switching of the reaction mechanism to a one dominated by ATRP, giving rapid reaction rates and high molecular weight polymers. Independent synthesis of the Fe^{III}-complexes derived from these 2,3-aryl-substituted ligands (complexes **6b**, **7b** and **8b**) and interrogation of their solution magnetic moments revealed that, as expected, two of the complexes (**7b** and **8b**) displayed intermediate-spins (hence giving rise to CCT). The other complex (**9b**) was found to be high spin, thus accounting for its preference of an ATRP mechanism. The mechanism of the CCT reaction observed with some of these complexes was also probed using a Grignard reagent containing β-hydrogen atoms. The results of these studies hinted at the CCT reaction occurring *via* a β-hydride elimination and not a direct HAT process, although the evidence was not conclusive.

Attempts were made to investigate the participation of an OMRP equilibrium involving these α-diimine complexes, and to examine whether, for certain complexes, this equilibrium could impose any degree of control over polymerizations performed under ATRP conditions (*36*). All of the complexes

tested under these conditions were found to be poor mediators of OMRP, with high concentrations of complex being required to impart any degree of control over the polymerization (Table 1). For example, at 8 equivalents of complex (**5a**), a moderate value for the dispersity (1.4) could be achieved. However, the reaction rate was extremely slow at this concentration of complex (<10% conversion).

Table 1. OMRP of styrene screening results (conditions: 300 equiv. styrene, 0.5 equiv. AIBN initiator, 120°C, 48 hours) using complex 5a. Adapted from reference (*36*). Copyright (2007) American Chemical Society.

Complex Equiv.	Conversion (%)	$M_{n(exp.)}$	$M_{n(theo.)}$	f ($M_{n(theo.)}/M_{n(exp.)}$)	Đ
1.0	48	16117	14998	0.93	3.7
2.0	31	12001	9686	0.81	2.1
4.0	23	8268	7186	0.87	1.8
8.0	7.5	2190	2333	1.07	1.4

Importantly, the Gibson group linked the concepts of 'halogenophilic' and 'carbophilic' equilibria operating under ATRP conditions to the concentration of radicals present in solution during a polymerization. When strongly halogenophilic complexes are used as catalysts, a high concentration of radicals is present in solution (equilibrium shifts to the right in Scheme 1) and consumption of monomer is rapid. CCT processes are unable to kinetically compete. This is a classic ATRP reaction. As the Fe catalysts become less halogenophilic, the concentration of radicals is reduced in solution (equilibrium begins to shift to the left in Scheme 1). Thus, consumption of monomer is slowed and now CCT is able to kinetically compete with ATRP. It follows then, that a further decrease in halogenophilicity leads to the dominance of CCT, and implies that the relative 'carbophilicity' may not play a role.
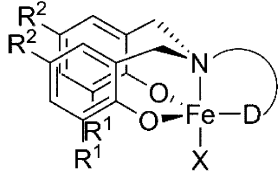
Amine-*Bis*(Phenolate)-Supported Iron Complexes

Amine-*bis*(phenolate) (ABP) ligands have been reported as strong σ- and π-donating ligands (*37*), capable of stabilizing high oxidation state transition metals and lanthanides for applications in catalysis (*38–40*). Kozak and co-workers described the synthesis of Fe[III] complexes of these ligands, and their use as efficient C-C bond-forming catalysts in the coupling of alkyl halides with aryl Grignard reagents (*41*, *42*).

The first application of ABP-supported iron complexes as mediators of CRP was recently reported (*43*). Under R-ATRP conditions, using AIBN as the initiator and 100 equivalents of monomer (styrene), it was found that complexes bearing electron-donating alkyl substituents on the aromatic rings (**10** - **13**, Figure 4) were relatively poor catalysts for the polymerization. Under the reaction

conditions (1 hour, 120°C), significantly higher than calculated molecular weights were obtained, with large dispersity values. However, the addition of electron-withdrawing chloro-substituents to the aromatic ring (**14 - 19**, Figure 4) generally led to exceptionally well-controlled polymerization reactions, with dispersities as low as 1.11. The complexes surveyed in this reaction and the results obtained are provided in Figure 4.

Complex	R^1	R^2	X	D	Conversion (%)	f $(M_{n(theo.)}/M_{n(exp.)})$	Đ
10	^tBu	Me	Cl	CH_2Furf	79	0.53	2.01
11	^tBu	Me	Br	CH_2Furf	48	0.40	1.47
12	^tBu	^tBu	Br	CH_2Furf	86	0.53	2.44
13	^tBu	^tBu	Br	$(CH_2)_2OMe$	50	0.38	1.64
14	Cl	Cl	Cl	$(CH_2)_2NMe_2$	63	0.89	1.19
15	Cl	Cl	Br	$(CH_2)_2NMe_2$	46	0.71	1.12
16	Cl	Cl	Cl	CH_2Furf	54	0.60	1.27
17	Cl	Cl	Cl	CH_2Py	60	0.61	1.11
18	Cl	Cl	Br	CH_2Py	37	0.72	1.16
19	Cl	Cl	Br	$(CH_2)_2OMe$	47	0.83	1.14
20	Me	Me	Cl	$(CH_2)_2NMe_2$	79	0.28	2.17

Figure 4. General structure of Fe^III-amine-bis(phenolate) complex (Furf = tetrahydro-2-furanyl, Py = 2-pyridinyl) and styrene polymerization screening results (conditions: 100 equiv. styrene, AIBN initiator, 120°C, 1 hour). Adapted from reference (43). Copyright (2012) John Wiley and Sons.

Other than the marked effect of aromatic ring substituents (electron-donating/withdrawing) on the polymerisation, the nature of the halide attached to the metal centre also appeared to have an effect. The chloride-containing complexes displayed more rapid polymerisation rates (*e.g.* **14** *vs*. **15** and **17** *vs*. **18**), which manifests in higher % conversions, while the bromide-containing complexes generally provided better control over the polymerisation (lower Đ). Kinetic investigations of the CRP reaction mediated by one of the most efficient complexes in this family (**14**) gave a pseudo first-order rate constant of 1.02 h^{-1} (*44*), which is amongst the highest measured for iron catalysts in styrene polymerization (*32, 45*).

Chlorine end-groups in the purified polymers, as identified by ^{1}H NMR spectroscopy, gave firm support to the occurrence of an R-ATRP mechanism, though the degree of chlorination was not as high as expected. The participation of an OMRP mechanism in these reactions, leading to organometallic-terminated polymers, could potentially account for the lower than expected chlorine content. This is especially in light of the fact that no alkenic end-groups could be observed by ^{1}H NMR spectroscopy, thus decreasing the likelihood that a CCT process is responsible for the reduced halogen content. Hence, it appeared that mechanistic interplay between R-ATRP and OMRP mechanisms could be responsible for the excellent control observed in these systems.

In order to directly probe the OMRP mechanism (in the absence of R-ATRP), the polymerization of styrene using an *in situ* generated Fe^{II} complex and conventional radical initiator (AIBN) was attempted (*44*). The Fe^{II} complex was generated *in situ* since previous attempts at synthesising a stable and isolable Fe^{II}-ABP complex had proved fraught with difficulty. Under these conditions, polymerization was rapid (81% conversion after 1 hour at 120°C) and relatively well-controlled (Đ = 1.32), though the experimentally observed molecular weights were significantly higher than theoretical values ($f = 0.34$). This was suggested as being a result of a high number of termination reactions at the start of the polymerization, which resulted in an increase in the effective monomer concentration. Reducing the temperature (to 100°C) gave an increased initiator efficiency ($f = 0.49$), though the rate of polymerization was somewhat slowed (52% conversion after 1 hour). The slowing of the polymerization rate at lower temperature could be a consequence of the greater persistence of a putative Fe^{III}-R$_n$ complex at the lower temperature, and thus lower concentration of propagating radicals in solution. However, it is likely that the preferred reducing agent, ascorbic acid, would not be able to completely reduce the starting Fe^{III}-Cl to Fe^{II} in the timescale of the reaction, suggesting that this system may more accurately mimic an ARGET ATRP-type polymerization. Unpublished results support this (*46*), with a mechanistic study by Buback and co-workers suggesting that OMRP pathways do not play a significant role in controlling the polymerization, although they may be accessible during the course of the reaction.

Understanding Interplay with Computational Chemistry

Early computational studies (*35*) of the α-diimine system illustrated that the electronic characteristics of the α-diimine substituents could heavily influence the energies of the frontier molecular orbitals (and thus high-spin/intermediate-spin balance). It was also observed that aryl *N*-substituents (*versus* alkyl *N*-substituents) better stabilize Fe^{III} centers with quartet multiplicities, and thus intermediate-spins. Further calculations revealed that for all Fe^{III} systems with quartet multiplicity, carbophilic reactivity was preferred and thus CCT reactions predominated. Meanwhile, Fe^{III} centers possessing sextet multiplicity (high-spin) were more inclined towards halogenophilic behavior and thus well-controlled ATRP reactivity. However, higher level calculations were needed to confirm these early results.

Poli and co-workers recently reported a computational investigation of the mechanism of CRP mediated by this family of Fe^{II}-α-diimines (*47*). In contrast to a previous report (*32*), they found that the ligands themselves do not control the spin-state of the various complexes. Furthermore, it was found that all of the [Fe(α-diimine)Cl$_3$]-type complexes studied computationally possessed high-spin spin-states, contrary to what was observed previously in experimental studies (Figure 5). This discrepancy presumably arises due to the instability of the Fe^{III}-complexes in both the solid-state and solution phase to oxygen, moisture and light, and to decomposition by disproportionation. Thus, the experimentally derived values for the magnetic moments (*32*) may be lower than anticipated due to decomposition of the complexes.
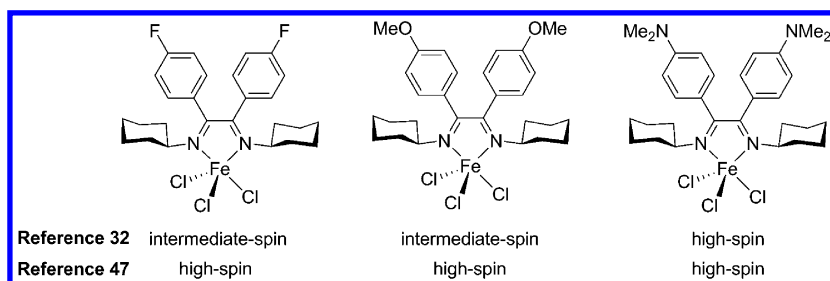
*Figure 5. Experimentally- and computationally-derived spin states of complexes **6b**, **8b** and **7b** (left to right) compared (32, 47)*

These findings were found to accord with those of Johansson and Swart, who also recently published a computational study of this Fe-α-diimine system (*48*). Johansson and Swart also argued that the electron-withdrawing/donating *para*-substituents of the 2,3-diarylated α-diimine complexes act to modulate the relative energies of the ATRP and CCT pathways by charge-transfer effects. However, it is important to note that the OMRP resting state (an Fe^{III}-alkyl complex) was proposed, by Johansson and Swart, to be formed *via* the direct abstraction of an alkyl radical from an alkyl halide, forming a free chlorine atom, along with an ATRP pathway balanced by the formation of Cl$_2$ from two atomic chlorine radicals. This is at complete odds with established mechanistic principles in both CRP, and also more generally in typical one-electron oxidative additions of alkyl halides to transition metal centers. Thus, the interpretation of some of the results obtained should be performed with a significant degree of caution.

Poli and co-workers sought to further explore the intimate mechanism of the CCT reaction observed in certain systems and investigate the origin of the mechanistic differences between various 2,3-diarylated α-diimines (*47*). Contrary to what was suggested in previous work (*36*), where the CCT reaction was proposed to occur *via* a β-hydride elimination pathway from an OMRP resting state, DFT calculations here indicated that a direct H-transfer from the propagating radical is the first step in the CCT mechanism. It was further found that the Fe^{III}-alkyl complex (OMRP resting state) was insufficiently stable to allow Fe^{III}-hydride formation *via* a β-hydride elimination. It was also calculated that

the nature of the *para*-substituent has little/no significant effect on the energetic difference between the sextet and quartet spin-states. Instead, it was found that the *para*-substituents have a relatively small, but important effect on the thermodynamic ATRP activation equilibrium ($\Delta E(ATRP)$). An electron-donating *para*-substituent (*e.g.* $-NMe_2$) acts to reduce $\Delta E(ATRP)$ relative to $\Delta E(CCT)$, thus reducing the participation of a CCT mechanism in the ATRP reaction. When electron-withdrawing *para*-substituents (*e.g.* $-F$) are present, $\Delta E(ATRP)$ is increased substantially relative to $\Delta E(CCT)$, which allows the occurrence of CCT in a system set-up under ATRP conditions. This implies that the balance between ATRP, OMRP and CCT is thus a predominantly kinetic phenomenon.

Poli and co-workers also recently reported a computational study of the behaviour of Fe-ABP complexes (*49*). This work partly focused on examining the superior catalytic activity of the chloro-substituted Fe-ABP complexes *versus* the alkyl-substituted complexes (*43*, *44*). The ATRP/OMRP pathways were also examined with respect to their spin-state changes and activation barriers.

Computational comparison of systems containing 2,4-dimethyl-substituted phenolate ligands with 2,4-dichloro-substituted phenolate ligands indicated that the chloro-substituted ligand afforded more stable ATRP and OMRP dormant species. This was explained as being a result of inductive electron-withdrawal by the chloro-substituents, which acts to reduce the donor strength of the phenolates. As such, the Fe^{III}-containing ATRP active species becomes more destabilized with respect to the Fe^{II}-containing ATRP dormant species, resulting in a higher ATRP activation barrier. Furthermore, where the ABP ligand contains chloro-substituents, the formation of an Fe-C bond (thus giving the OMRP dormant species) was found to be accompanied by a decrease in the calculated Mulliken metal charge, while in the methyl-containing system the calculated Mulliken metal charge was found to increase. Thus, it follows that the formation of the Fe-C bond-containing OMRP dormant species provides a greater degree of stabilization when the ligand contains chloro-substituents. The stabilization of the dormant states of both the ATRP and OMRP equilibria results in an overall lower radical concentration, fewer bimolecular termination processes and therefore a more well-controlled CRP.

Conclusion

This chapter presents an overview of the mechanistic interplay between ATRP, OMRP and CCT through the lens of the two most mechanistically well-studied Fe-based catalytic systems, supported by α-diimine and amine-*bis*(phenolate) ligands. It is apparent, particularly with respect to the Fe-α-diimine-system, that gaining a full understanding of the circumstances under which mechanistic interplay occurs is a far from a trivial matter. The subtleties of ligand sterics and electronics, as well as the varied spin-states of the metal centers, all appear to have significant roles to play in this interplay. What is clear, however, is that when the ATRP equilibrium shifts strongly to favor growing radical chains, polymerization is rapid and CCT is unable to kinetically compete, thus giving rise to extremely well-controlled polymerization reactions with commensurately

low dispersities and polymer molecular weights firmly in agreement with those predicted. Future research efforts, in our group and others, will thus likely be directed towards the development of highly active and versatile (with respect to monomer scope) catalysts. Targeting systems which either explicitly avoid or directly exploit iron's mechanistic interplay between ATRP and OMRP equilibria is important. This will help move iron to the forefront of RDRP research and give rise to a multitude of new polymeric materials formed with inexpensive, non-toxic and low color catalysts.

Abbreviations

ABP	Amine-*bis*(phenolate)
AIBN	Azobisisobutyronitrile
ARGET	Activators regenerated by electron transfer
ATRA	Atom transfer radical addition
ATRP	Atom transfer radical polymerization
CCT	Catalytic chain transfer
CRP	Controlled radical polymerization
Đ	Dispersity
dipp	2,6-Diisopropylphenyl
$\Delta E(ATRP)$	Thermodynamic ATRP activation equilibrium
$\Delta E(CCT)$	Thermodynamic CCT activation equilibrium
f	Initiation efficiency
Furf	Tetrahydro-2-furanyl
Hal	Halogen
HAT	H atom transfer
M	Monomer
MMA	Methyl methacrylate
$M_{n\,(exp.)}$	Number-average molar mass (experimentally-derived)
$M_{n\,(theo.)}$	Number-average molar mass (theoretical)
Mt	'Metal'
OMRP	Organometallic mediated radical polymerization
PMMA	Poly(methyl methacrylate)
Py	2-Pyridinyl
R-ATRP	Reverse atom transfer radical polymerization
RDRP	Reversible deactivation radical polymerization

References

1. Wang, J.-S.; Matyjaszewski, K. *J. Am. Chem. Soc.* **1995**, *117*, 5614–5615.
2. Wang, J.-S.; Matyjaszewski, K. *Macromolecules* **1995**, *28*, 7901–7910.
3. Kato, M.; Kamigaito, M.; Sawamoto, M.; Higashimura, T. *Macromolecules* **1995**, *28*, 1721–1723.
4. Ando, T.; Kato, M.; Kamigaito, M.; Sawamoto, M. *Macromolecules* **1996**, *29*, 1070–1072.
5. Pintauer, T. *Eur. J. Inorg. Chem.* **2010**, *2010*, 2449–2460.

6. Severin, K. *Curr. Org. Chem.* **2006**, *10*, 217–224.
7. Pintauer, T.; Matyjaszewski, K. *Chem. Soc. Rev.* **2008**, *37*, 1087–1097.
8. Muñoz-Molina, J. M.; Belderrain, T. R.; Pérez, P. J. *Eur. J. Inorg. Chem.* **2011**, *2011*, 3155–3164.
9. Bellus, D. *Pure Appl. Chem.* **1985**, *57*, 1827–1838.
10. Hayes, T. K.; Villani, R.; Weinreb, S. M. *J. Am. Chem. Soc.* **1988**, *110*, 5533–5543.
11. Nagashima, H.; Wakamatsu, H.; Ozaki, N.; Ishii, T.; Watanabe, M.; Tajima, T.; Itoh, K. *J. Org. Chem.* **1992**, *57*, 1682–1689.
12. Wallentin, C.-J.; Nguyen, J. D.; Finkbeiner, P.; Stephenson, C. R. J. *J. Am. Chem. Soc.* **2012**, *134*, 8875–8884.
13. Poli, R. *Eur. J. Inorg. Chem.* **2011**, *2011*, 1513–1530.
14. Poli, R. *Angew. Chem., Int. Ed.* **2006**, *45*, 5058–5070.
15. Allan, L. E. N.; Perry, M. R.; Shaver, M. P. *Prog. Polym. Sci.* **2012**, *37*, 127–156.
16. Wayland, B. B.; Poszmik, G.; Mukerjee, S. L.; Fryd, M. *J. Am. Chem. Soc.* **1994**, *116*, 7943–7944.
17. Gridnev, A. A.; Ittel, S. D. *Chem. Rev.* **2001**, *101*, 3611–3660.
18. Poli, R.; Allan, L. E. N.; Shaver, M. P. *Prog. Polym. Sci.* **2014**, *39*, 1827–1845.
19. Le Grognec, E.; Claverie, J.; Poli, R. *J. Am. Chem. Soc.* **2001**, *123*, 9513–9524.
20. Stoffelbach, F.; Poli, R.; Richard, P. *J. Organomet. Chem.* **2002**, *663*, 269–276.
21. Stoffelbach, F.; Poli, R.; Maria, S.; Richard, P. *J. Organomet. Chem.* **2007**, *692*, 3133–3143.
22. Grishin, D. F.; Ignatov, S. K.; Shchepalov, A. A.; Razuvaev, A. G. *Appl. Organomet. Chem.* **2004**, *18*, 271–276.
23. Braunecker, W. A.; Brown, W. C.; Morelli, B. C.; Tang, W.; Poli, R.; Matyjaszewski, K. *Macromolecules* **2007**, *40*, 8576–8585.
24. Matyjaszewski, K.; Wei, M.; Xia, J.; McDermott, N. E. *Macromolecules* **1997**, *30*, 8161–8164.
25. Ando, T.; Kamigaito, M.; Sawamoto, M. *Macromolecules* **1997**, *30*, 4507–4510.
26. Kotani, Y.; Kamigaito, M.; Sawamoto, M. *Macromolecules* **1999**, *32*, 6877–6880.
27. Teodorescu, M.; Gaynor, S. G.; Matyjaszewski, K. *Macromolecules* **2000**, *33*, 2335–2339.
28. Göbelt, B.; Matyjaszewski, K. *Macromol. Chem. Phys.* **2000**, *201*, 1619–1624.
29. Kotani, Y.; Kamigaito, M.; Sawamoto, M. *Macromolecules* **2000**, *33*, 3543–3549.
30. Gibson, V. C.; O'Reilly, R. K.; Reed, W.; Wass, D. F.; White, A. J. P.; Williams, D. J. *Chem. Commun.* **2002**, 1850–1851.
31. O'Reilly, R. K.; Shaver, M. P.; Gibson, V. C.; White, A. J. P. *Macromolecules* **2007**, *40*, 7441–7452.

32. Allan, L. E. N.; Shaver, M. P.; White, A. J. P.; Gibson, V. C. *Inorg. Chem.* **2007**, *46*, 8963–8970.

33. Gibson, V. C.; O'Reilly, R. K.; Wass, D. F.; White, A. J. P.; Williams, D. J. *Macromolecules* **2003**, *36*, 2591–2593.

34. Ferro, R.; Milione, S.; Erra, L.; Grassi, A. *Inorg. Chem. Commun.* **2008**, *11*, 535–538.

35. Shaver, M. P.; Allan, L. E. N.; Rzepa, H. S.; Gibson, V. C. *Angew. Chem., Int. Ed.* **2006**, *45*, 1241–1244.

36. Shaver, M. P.; Allan, L. E. N.; Gibson, V. C. *Organometallics* **2007**, *26*, 4725–4730.

37. Dean, R. K.; Fowler, C. I.; Hasan, K.; Kerman, K.; Kwong, P.; Trudel, S.; Leznoff, D. B.; Kraatz, H.-B.; Dawe, L. N.; Kozak, C. M. *Dalton Trans.* **2012**, *41*, 4806–4816.

38. Kerton, F. M.; Whitwood, A. C.; Willans, C. E. *Dalton Trans.* **2004**, 2237–2244.

39. Tshuva, E. Y.; Goldberg, I.; Kol, M.; Goldschmidt, Z. *Organometallics* **2001**, *20*, 3017–3028.

40. Yang, S.; Nie, K.; Zhang, Y.; Xue, M.; Yao, Y.; Shen, Q. *Inorg. Chem.* **2013**, *53*, 105–115.

41. Chowdhury, R. R.; Crane, A. K.; Fowler, C.; Kwong, P.; Kozak, C. M. *Chem. Commun.* **2008**, 94–96.

42. Reckling, A. M.; Martin, D.; Dawe, L. N.; Decken, A.; Kozak, C. M. *J. Organomet. Chem.* **2011**, *696*, 787–794.

43. Allan, L. E. N.; MacDonald, J. P.; Reckling, A. M.; Kozak, C. M.; Shaver, M. P. *Macromol. Rapid Commun.* **2012**, *33*, 414–418.

44. Allan, L. E. N.; MacDonald, J. P.; Nichol, G. S.; Shaver, M. P. *Macromolecules* **2014**, *47*, 1249–1257.

45. O'Reilly, R. K.; Gibson, V. C.; White, A. J. P.; Williams, D. J. *J. Am. Chem. Soc.* **2003**, *125*, 8450–8451.

46. Buback, M.; Schröder, H.; Shaver, M. P. Private Communication, 2014.

47. Poli, R.; Shaver, M. P. *Chem. - Eur. J.* **2014**, *52*, 17530–17540.

48. Johansson, M. P.; Swart, M. *Dalton Trans.* **2011**, *40*, 8419–8428.

49. Poli, R.; Shaver, M. P. *Inorg. Chem.* **2014**, *53*, 7580–7590.

Subject Index

T

V

W